NON-PERTURBATIVE ASPECTS OF DEEP INELASTIC SCATTERING

Wolodymyr MELNITCHOUK B.Sc.(Hons.)

Thesis submitted for the degree of
Doctor of Philosophy
at
The University of Adelaide
(Department of Physics and Mathematical Physics)
June 1993

Contents

ABSTRACT

This thesis deals with the consistent description of the quark structure of hadrons and nuclei in deep inelastic scattering, with particular emphasis on the non-perturbative region of QCD. Using a novel new approach based on the expansion of the truncated nucleon tensor, we construct a relativistic quark model which enables the nucleon valence quark distributions to be computed. For the sea quarks we scrutinise a model in which the nucleon has an extended structure due to its virtual meson and baryon components, and discuss tests that may reveal such structure experimentally. For scattering from nuclei, we show how structure functions of composite particles can be calculated from the truncated nucleon tensor, and relativistic nucleon—nucleus vertex functions. This allows for a self-consistent treatment of the off-shell properties of bound nucleons. As a result we can understand for the first time the conditions under which the convolution model of deep inelastic scattering can be justified, however, we find that these are generally not satisfied. On the other hand, within our formalism the traditional convolution approach is bypassed altogether. We also calculate the corrections to nuclear structure functions due to shadowing at small Bjorken-x, within a model in which both mesons and partons play distinct roles. Finally, we investigate the possibility of performing (spin-dependent) inclusive hadron leptoproduction experiments as a means of testing directly the relevance of hadronic variables in high energy reactions.

STATEMENT

This work contains no material which has been accepted for the award of any other degree or diploma in any University or other tertiary institution and, to the best of my knowledge and belief, contains no material previously published or written by another person, except where due reference has been made in the text.

I give consent to this copy of my thesis, when deposited in the University Library, being made available for loan and photocopying.

SIGNED: DATE: 30 June 1993

ACKNOWLEDGEMENTS

First and foremost I would like to thank my supervisor, Professor Tony Thomas, for his friendly guidance and assistance which I have had the privilege to enjoy during the last three years. His ever-present enthusiasm, as well as critical and efficient analysis of my work, made for a timely and successful completion of this thesis. Working with him has been an enlightening and thoroughly enjoyable experience, and his influence will be felt for years to come.

Acknowledgement must also be made of the people who in various ways contributed to my understanding and appreciation of theoretical physics: among them I especially would like to thank Bob Carlitz, Carl Carlson, Rod Crewther, Steven Ellis, Manfred Gari, Johann Haidenbauer, Karl Holinde, Angas Hurst, Boris Kopeliovich, Guo Liu, Bonoit Loiseau, Lech Mankiewicz, Andy Rawlinson, Koichi Saito, Tony Signal, Fernando Steffens, Paul Stoler and Stuart Tovey. Deserving particular mention are Andreas Schreiber, Kolya Nikolaev and Ernest Henley, with whom it has been a distinct pleasure to collaborate on some of the work presented here.

I am also indebted to Paul Bickerstaff (Idaho), Bob Carlitz (Pittsburg), Harold Fearing (TRIUMF), Nathan Isgur (CEBAF), Gerry Miller (INT, Seattle), Nimai Mukhopadhyay (Rensellaer), Craig Roberts (Argonne) and Peter Tandy (Kent State) for the hospitality which they showed me during visits to their institutions. Further thanks are extended to the organisers of the First International Spring School on New Frontiers in Nuclear Physics at the University of Tokyo which I was honoured to attend. I am grateful for the support I received from Tony Thomas in helping to make these visits possible.

I also acknowledge financial assistance from the Australian Postgraduate Research Award.

Finally, I would like to thank my family for their tolerance and material support over the last few years, which gave me the freedom to concentrate on physics.

Chapter 1

INTRODUCTION

The main unresolved problem of the Standard Model of particle physics is the description from first principles of the strong interactions. Traditional low energy nuclear physics, where the strong nuclear force acts at relatively large distances, is for the most part successfully described in terms of hadronic variables — mesons and baryons. However, for a complete understanding of the strong interactions, nuclear phenomena must be reconciled with the more fundamental theory of quarks and gluons — Quantum Chromodynamics (QCD).

Historically, the basic interaction which we have sought to explain has been that between protons and neutrons in the atomic nucleus. The original idea of massive particle exchange of Yukawa [1] has been a guiding principle according to which later theories have been formulated. It was pointed out by Wick [2] that this idea fitted in nicely with the Heisenberg Uncertainty principle, whereby the interaction range of the nuclear force is inversely proportional to the mass of the exchanged meson (pion). Over the years a quantitative description of the forces acting between nucleons has been developed within a meson-exchange picture.

Following the experimental confirmation of the pion in 1947, the 1950s and 1960s saw an explosion of newly discovered mesons and baryons, as particle accelerators were able to achieve ever higher energies. To bring some sense of order to the profusion of new particles Gell-Mann [3] and Zweig [4] introduced the idea of quarks, initially seen merely as useful book-keeping devices. Soon after it was realised that a serious problem existed with the simple quark classifications, namely the Δ^{++}. The quark model wavefunction for the Δ^{++} was predicted to be totally symmetric, however it was known that this particle obeyed Fermi-Dirac statistics. A solution to this problem was found by assigning extra colour quantum numbers to the quarks [5], in which baryons would have in addition an antisymmetric colour wavefunction. By imposing local gauge invariance on the colour fields, and including vector gluon exchange as a means by which quarks interact, one obtains the essential elements of QCD [6].

Because QCD is an asymptotically free theory — the effective strong coupling constant decreases at short distances — processes involving large momentum transfers can be calculated using perturbation theory [7, 8]. Perturbative QCD works remarkably well in its region of applicability.

In describing the distribution of hadronic jets in high energy particle collisions, for example, its predictions are in quite spectacular agreement with experiment, even to high orders in the perturbation expansion. Yet despite its successes, we are still unable to extract from QCD sufficient details regarding its long-distance properties. This is because in the infra-red region the strong coupling constant grows, perturbation theory breaks down, and its predictive power becomes rather limited. A closely related problem is that of confinement of individual particles carrying colour quantum numbers. One of the possible ways to circumvent this problem is to solve the QCD equations of motion numerically on a space-time grid. While this is an important pursuit, in reality sufficiently quantitative predictions are still some time away.

It is perhaps the holy grail of the Standard Model to make the leap from QCD to traditional nuclear physics. In a sense it is ironic that the theory which arose out of the desire to understand nuclear forces is able to explain backgrounds in jets, yet unable to answer the fundamental questions of nuclear physics (for a review of the achievements of QCD see, for example, Ref.[9]). Arguing that QCD can in principle explain all hadronic and nuclear phenomena is akin to being satisfied that QED can in principle explain all of the physics of atoms, molecules and condensed matter. One might ask whether it isn't simply a matter of complexity — the fact that there is such a large mismatch in energy scales between nuclear physics (with energies of a few MeV) and the short-distance realm (tens or hundreds of GeV) of QCD. Part of the answer lies in realising that there are still fundamental issues like confinement, chiral symmetry breaking, etc. that will need to be resolved. At this stage the best one can do is construct "QCD-inspired" models which are consistent with the known properties of QCD, but which can be extrapolated into the low energy domain. Then one can hope that experimental input may shed some light on the merits of the various approaches. It would seem sensible, if the aim is to study the frontier between quark and hadron physics, to concentrate on those processes in which both degrees of freedom may be relevant.

One such process in which both large and small scale features of QCD can be studied is deep inelastic scattering (DIS) of leptons from hadrons. Because the Standard Model gives such a good account of electroweak interactions, the scattering of leptons from hadronic targets is a far more elegant method of probing the quark substructure of hadrons than purely hadronic collisions. Indeed, the first experimental evidence for the existence of point-like constituents of the nucleon was obtained through DIS at the Stanford Linear Accelerator Center (SLAC) in the late 1960s [10]. Furthermore, the awarding of the 1990 Nobel prize in physics to Friedman, Kendall and Taylor [11] recognised the important contribution to our understanding of the quark structure of matter that has been made via this method.

Theoretically, in DIS some of the difficulties imposed by confinement can be overcome, since here quarks and gluons (or generically partons) can be treated as if they are (quasi-) free. This is the essence of the Quark Parton Model [12]. The experimental consequence of point-like partons is the non-vanishing of the inelastic structure functions at very large momentum transfers, a phenomenon known as scaling. Actually, this is only the naive expectation — refinement of this model in the

guise of QCD radiative corrections leads to small deviations from exact scaling. It is yet another triumph of QCD that it is able to give a quantitative description of the scaling violations.

In this thesis we will mostly focus on deep inelastic scattering, and what can be learned from this about the quark structure of hadrons and nuclei. In Chapter 2 we briefly outline the formalities and fundamental results of inclusive deep inelastic lepton—nucleon scattering. (The discussion will be restricted to electromagnetic interactions only, although neutrino scattering will be mentioned in Section 6.1.) We introduce the explicit Dirac and Lorentz structure of the truncated nucleon tensor, and use relativistic quark—nucleon vertices to calculate the truncated structure functions explicitly. This will enable us to construct a relativistic, covariant model of the valence quark momentum distributions of the nucleon.

The sea component of the nucleon can of course be generated perturbatively from the QCD evolution equations. On the other, there is some evidence to suggest the existence of a non-perturbative component of the nucleon sea as well, and this is discussed in Chapter 3. In particular, data from the New Muon Collaboration (NMC) at CERN on the proton and deuteron structure functions at very low Bjorken-x suggests a significant violation of the Gottfried sum rule, a plausible explanation of which is an asymmetry in the $\bar{u}$ and $\bar{d}$ sectors of the proton. Such an hypothesis necessarily implies going beyond perturbative QCD. Indeed, if this result is confirmed by future experiments, it would be a case of devout adherence to perturbative QCD leading some physicists astray. We concentrate on one mechanism in particular that can generate a $\bar{u} - \bar{d}$ difference, which is due to the presence of explicit mesonic components in the nucleon wavefunction. Our approach in calculating the scattering from this virtual cloud of mesons is based on time-ordered perturbation theory in the infinite momentum frame. This is particularly advantageous if we wish to use the convolution model, as here off-mass-shell ambiguities in the structure functions of virtual particles are avoided.

The crucial uncertainty in the interpretation of the NMC data is the fact that the neutron structure function is extracted from data taken in DIS experiments with deuterium targets. The extraction is therefore a model-dependent procedure, since it must account for any nuclear effects present in the deuteron. Of particular importance is the region of small Bjorken-x, where the deuteron structure function may be 'shadowed' in comparison with the free nucleon structure function. Because there are potentially significant contributions to the Gottfried sum rule from this region, a thorough examination of the shadowing corrections to the deuteron structure function is of the utmost importance. In Chapter 4 we calculate these corrections using a model which combines aspects of the traditional vector meson dominance model of electromagnetic hadronic interactions, as well as a parton-based approach incorporating the phenomenology of Pomeron exchange from Regge theory.

From DIS experiments on heavy nuclei targets we also know that ratios of nuclear to deuteron structure functions (per nucleon) fall significantly below unity at small x. Using realistic input for the nuclear density distribution, we extend the above model to calculate the shadowing corrections

to structure functions of heavy nuclei as well. We show that a careful analysis can yield quite excellent agreement with recent high-precision data taken at CERN. This serves as a further check on the reliability of the model predictions for shadowing in deuterium.

To understand the differences between nuclear and nucleon structure functions at larger x values, the bound nucleon properties must be properly accounted for. Chapter 5 is devoted to a rigorous reanalysis of the traditional approach to calculating deep inelastic nuclear cross sections. Extending the formalism introduced in Chapter 2, we show how a proper treatment of the truncated nucleon tensor enables the structure functions of any composite particle containing off-mass-shell nucleons to be calculated from a knowledge of relativistic nuclear vertex functions. We verify explicitly that the formalism is gauge invariant, and gives rise to the correct scaling behaviour for the inelastic structure functions, regardless of the production mechanism of the off-shell nucleon. Furthermore, we examine under what conditions can one obtain the convolution model from the fully relativistic calculation, and demonstrate that in general these are not satisfied. The essential reason for the failure of the convolution model is that it omits antiparticles, which of course must be present in any relativistic analysis. This is a rather serious revelation, as the majority of previous calculations of structure functions of composite particles have relied upon the validity of this approach. On the other hand, our new formalism enables direct computation of the scattering process, right from the quark level. In fact, it forbids making the usual short-cut of taking nucleon structure function input and simply smearing it with a nucleon distribution in the nucleus. We illustrate the virtues of the new approach with several examples. Specifically, we calculate the deuteron structure function, and compare against the convolution-type methods. In addition, we estimate the role of off-mass-shell effects in nuclear matter, which will be important in understanding the origin of the EMC effect [13]. Also, we revisit the case of DIS from the nucleon dressed by mesons, where we formally demonstrate the fatal problems associated with the covariant convolution model, and thus implicitly lend weight toward the infinite momentum frame approach of Chapter 3.

Concurrently with the inclusive DIS studies, there exists a wider, more general class of semi-inclusive reactions, where specific hadrons in the final state are tagged. This is a somewhat less explored subject, both theoretically and experimentally, but which has the potential to teach us more about the non-perturbative aspects of quarks physics. Because there exists no formal operator product expansion approach to this problem, our treatment is largely phenomenological. Our main emphasis is on semi-inclusive production of baryons, especially in the target fragmentation region. Firstly, we demonstrate the importance of kinematics for particles produced in this region, and show how ignorance of these can lead to erroneous conclusions about the existence of more exotic effects. Once the kinematics are understood, we can then proceed to study the dynamics of semi-inclusive scattering. We construct a model for the fragmentation of quarks to baryons, and compare its predictions with those of the one-pion-exchange model. As an extra degree of freedom, we examine the possibility of using polarised targets and measuring the spin transfer to the final state hadron as a means of distinguishing the different models. We find that a spin asymmetry of the polarised

baryon (Δ^{++}) yields is particularly sensitive to the production mechanism.

Finally, in Chapter 7 we round off the discussion, and outline potential future directions in which the work presented in this thesis can be taken.

Chapter 2

INCLUSIVE DEEP INELASTIC SCATTERING

Deep inelastic scattering has for 25 years been an extremely useful tool for studying hadronic substructure, providing a wealth of information about the distribution of quarks inside the nucleon and nuclei. In this chapter we shall be concerned with inclusive scattering of unpolarised charged leptons from unpolarised nucleon targets. (The generalisation to weak interactions involving neutrino scattering is straightforward — see Refs.[14, 15].) Firstly, we introduce some notation that will be used in this and later chapters, and then give a brief overview of some of the main results of DIS which will be necessary in our applications. More comprehensive discussions can be found, for example, in Refs. [14–16]. The new work in this chapter is presented in Sections 2.2 and 2.3, where we investigate the truncated nucleon tensor, and then apply our results in a novel calculation of the nucleon valence quark distributions.

2.1 DIS Structure Functions

The process of interest is depicted in Fig.2.1, where the charged lepton (l) of energy E scatters from a target nucleon (N), leaving a final state consisting of the scattered lepton (l') and the hadronic debris (X) of the shattered nucleon: $lN \to l'X$. The observables in this process are the scattered lepton's energy, E', and the angle of lepton scatter, θ. Alternatively, we can use the square of the four-momentum transfer to the nucleon, $Q^2 \equiv -q^2 (\simeq 4EE' \sin^2\theta$ for $m_l \ll E, E')$, and the Bjorken scaling variable $x = Q^2/2p\cdot q$ $(= Q^2/2M\nu$ in the target rest frame, with $\nu = E - E'$ being the energy transferred to the target). In terms of these variables, the inclusive differential cross section (in the target rest frame) in the one photon exchange approximation is given by

$$\frac{d^2\sigma}{dx dQ^2} = \frac{\pi\ \alpha^2}{Q^2 E^2\ M\ x^2}\ L^{\mu\nu}\ W_{\mu\nu}. \tag{2.1}$$

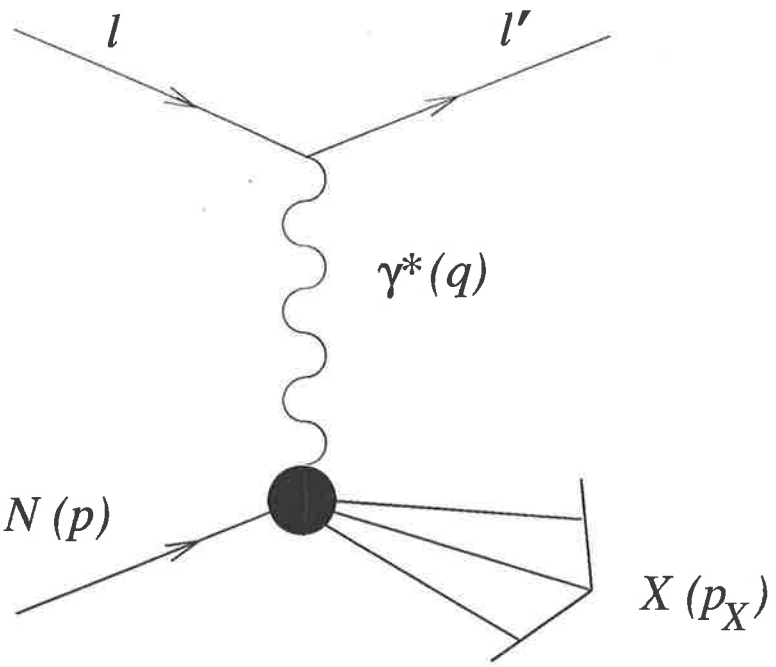

Figure 2.1: Deep inelastic lepton nucleon scattering.

Since we are concerned with unpolarised lepton scattering, we average over the initial, and sum over final, lepton polarisations, in which case the lepton tensor $L^{\mu\nu}$ is given by [1]

$$\begin{aligned} L^{\mu\nu} &= \frac{1}{2}\mathrm{Tr}[(\not{l}' + m_l)\gamma^\mu(\not{l} + m_l)\gamma^\nu] \\ &= 2\left(l'^\mu l^\nu + l'^\nu l^\mu + g^{\mu\nu}\frac{q^2}{2}\right). \end{aligned} \tag{2.2}$$

The hadronic tensor

$$W_{\mu\nu} = \sum_X (2\pi)^3 \delta^4(p + q - p_X)\langle N(p)|J_\mu(0)|X(p_X)\rangle\langle X(p_X)|J_\nu(0)|N(p)\rangle \tag{2.3}$$

contains information on the structure of the target nucleon. Because the unpolarised lepton tensor $L^{\mu\nu}$ is totally symmetric in the Lorentz indices μ and ν, only the symmetric components of $W_{\mu\nu}$ can yield any information on the spin-independent structure of the nucleon.

To ensure Lorentz invariance, the hadronic tensor must be constructed from the quantities $g_{\mu\nu}, p_\mu$ and q_μ. From combinations of these we can form at most four independent tensors (with four independent structure functions),

$$\begin{aligned} W_{\mu\nu}(p,q) &= \mathcal{P}_{T\mu\nu}(p,q)\, W_T(p,q) + \mathcal{P}_{L\mu\nu}(p,q)\, W_L(p,q) \\ &+ \mathcal{P}_{G\mu\nu}(p,q)\, W_G(p,q) + \mathcal{P}_{H\mu\nu}(p,q)\, W_H(p,q). \end{aligned} \tag{2.4}$$

[1] Spinors are normalised such that

$$\sum_s u(p,s)\bar{u}(p,s) = (\not{p} + m)\,\frac{\bar{u}u}{2m}$$

with $\bar{u}u = 2m$

The tensors $\mathcal{P}_{\mu\nu}$ are defined by

$$\begin{aligned}
\mathcal{P}_{T\mu\nu}(p,q) &= \tilde{g}_{\mu\nu} + \frac{\tilde{p}_\mu \tilde{p}_\nu}{\tilde{p}^2}, & \mathcal{P}_{L\mu\nu}(p,q) &= \frac{\tilde{p}_\mu \tilde{p}_\nu}{\tilde{p}^2}, \\
\mathcal{P}_{G\mu\nu}(p,q) &= \frac{q_\mu q_\nu}{q^2}, & \mathcal{P}_{H\mu\nu}(p,q) &= \frac{1}{\sqrt{-q^2\tilde{p}^2}}(\tilde{p}_\mu q_\mu + \tilde{p}_\nu q_\mu),
\end{aligned} \tag{2.5}$$

where $\tilde{g}_{\mu\nu} = -g_{\mu\nu} + q_\mu q_\nu/q^2$ and $\tilde{v}_\mu = v_\mu - q_\mu\ v\cdot q/q^2$, v_μ being any four-vector.

The decomposition in Eq.(2.4) of the nucleon tensor is of course not unique, however it is written in this convenient form because the tensors $\mathcal{P}_{\mu\nu}$ can be used as projectors [17], as they satisfy

$$\begin{aligned}
\mathcal{P}_T^{\mu\nu}(p,q)\ \mathcal{P}_{T\mu\nu}(p,q) &= 2, & \mathcal{P}_L^{\mu\nu}(p,q)\ \mathcal{P}_{L\mu\nu}(p,q) &= 1, \\
\mathcal{P}_G^{\mu\nu}(p,q)\ \mathcal{P}_{G\mu\nu}(p,q) &= 1, & \mathcal{P}_H^{\mu\nu}(p,q)\ \mathcal{P}_{H\mu\nu}(p,q) &= -2,
\end{aligned} \tag{2.6}$$

and are orthogonal, $\mathcal{P}_i^{\mu\nu}\ \mathcal{P}_{j\mu\nu} = 0$ for $i \neq j$. Hence we can project from the hadron tensor the relevant scalar functions: $\mathcal{P}_i^{\mu\nu} W_{\mu\nu} = W_i$ $(i = T, L, G, H)$.

In Eq.(2.4) W_T and W_L are proportional to the transverse and longitudinal structure functions, respectively, which are related to the cross sections for scattering transversely and longitudinally polarised photons from a nucleon,

$$W_T = \left(\frac{K}{4\pi^2\alpha}\right)\sigma_T^{\gamma^* N}, \qquad W_L = \left(\frac{K}{4\pi^2\alpha}\right)\sigma_L^{\gamma^* N}, \tag{2.7}$$

where $K = \sqrt{\nu^2 + Q^2}$ is the flux of incoming virtual photons (in the Gilman convention [18]).

By Nöther's theorem, the requirement that the Lagrangian be invariant under gauge transformations means that the electromagnetic current J_μ is conserved, $\partial^\mu J_\mu = 0$. This has the consequence that for any matrix element of the current operator we have $q^\mu\ \langle f|J_\mu|i\rangle = 0$, which leads to two constraint equations for the hadronic tensor, $q^\mu W_{\mu\nu} = 0 = q^\nu W_{\mu\nu}$. As a result, the functions W_G and W_H must be zero, so that in fact there are only two Lorentz and gauge invariant functions. In more customary notation these are denoted W_1 and W_2, in terms of which the nucleon tensor is

$$W_{\mu\nu}(p,q) = \tilde{g}_{\mu\nu}\ W_1(p,q) + \frac{\tilde{p}_\mu \tilde{p}_\nu}{M^2}\ W_2(p,q). \tag{2.8}$$

The functions W_1 and W_2 are related to the transverse and longitudinal functions by

$$\begin{aligned}
W_1(p,q) &= W_T(p,q) \\
W_2(p,q) &= \left(1 + \frac{\nu^2}{Q^2}\right)^{-1} (W_L(p,q) + W_T(p,q)).
\end{aligned} \tag{2.9}$$

The theoretical result of Bjorken [19, 20] was that in the limit where $Q^2 \to \infty$ but $x = Q^2/2p\cdot q$ is fixed (therefore $p\cdot q = M\nu \to \infty$ also), now referred to as the Bjorken limit, the functions W_1 and νW_2 scale — that is, they become finite functions of only one variable, x. In the Bjorken limit, the scaling functions are usually expressed in terms of the dimensionless structure functions F_1 and F_2,

$$\begin{aligned}
M\ W_1 &= F_1(x) \\
\nu\ W_2 &= F_2(x).
\end{aligned} \tag{2.10}$$

Furthermore, defining $F_L = 2\ x\ M\ W_L$ to be the longitudinal structure function, we have

$$F_L = F_2 \left(1 + \frac{Q^2}{\nu^2}\right) - 2xF_1. \tag{2.11}$$

A consequence of the scaling property of F_1 and F_2 (and the fact that the nucleon's constituents have spin 1/2) is the vanishing of the longitudinal structure function, or equivalently, that $F_2(x) = 2xF_1(x)$ — the famous Callan-Gross relation [21].

The observation of scaling of the inelastic structure functions in the SLAC experiments of the late 1960s [10] was a monumental step forward in our view of quarks as genuine objects, rather than merely convenient mathematical tools, as had been widely believed previously. For one thing, it led directly to Feynman's parton model [12,22–24].

2.1.1 Quark Parton Model

A basic hypothesis of the parton model is that the inelastic scattering from the nucleon can, at a deeper and more fundamental level, be described by elastic scattering from on-shell, point-like, spin 1/2 constituents (partons) in the nucleon. It is more than tempting to associate the partons of DIS with the quarks of the Gell-Mann and Zweig quark model [3, 4].

The validity of this simple picture of deep inelastic scattering relies on the treatment of the interactions of the probe with the partons in impulse approximation. The legitimacy of the impulse approximation rests on two assumptions — that

(i) final state interactions are neglected, and

(ii) the interaction time is less than the lifetime of the virtual state of the nucleon as a sum of its on-shell constituents.

The former seems reasonable since in DIS the energy transferred to the parton is much greater than the binding energy, so that the parton can be viewed as quasi-free (or asymptotically free). Whether the latter is valid or not can best be seen in the infinite momentum frame (IMF) of the target. Here, the momentum of the target nucleon is $p_\mu = (p_L + M^2/2p_L;\ \mathbf{0}_T,\ -p_L)$, with $p_L \to \infty$ (or $\beta \equiv v/c \to 1$), so that the photon's four-momentum must be $q_\mu = (-xp_L(1 - M^2x^2/Q^2) + M\nu/2p_L;\ \mathbf{0}_T,\ xp_L(1 - M^2x^2/Q^2) + M\nu/2p_L)$. As will be seen below, the dominant contributions to the hadronic tensor are those for which $q \cdot \xi \ll 1$ and $\xi_0 \simeq -\xi_L$, where ξ is the space-time distance involved in the DIS process. Therefore $q \cdot \xi \simeq 2M\ \nu\ \xi_0/p_L$, so that the interaction time is $\sim \xi_0 \lesssim p_L/2M\nu$. The lifetime of the virtual state can be obtained by a simple argument as follows: the energy of the virtual nucleon state consisting of on-shell partons with momenta $x_i p_L$ (transverse momentum is irrelevant to the argument) and mass m_i is $\approx \sum_i (x_i p_L + m_i^2/2x_i p_L)$, so that the difference between the energies of the virtual and on-shell nucleons is $\approx (\sum_i m_i^2/x_i - M^2)/2p_L$. Therefore the lifetime of this virtual state is proportional to p_L, and hence the ratio of interaction time to virtual state lifetime $\sim 1/\nu \to 0$ in the Bjorken limit.

The picture is then one of quarks with momentum fraction $x_i = x$ absorbing photons with $x = Q^2/2p \cdot q$, since $\delta((q + x_i p)^2) \to \delta(x - x_i)/2p \cdot q$. It then follows that in the quark parton model,

the structure functions are related to the quark and antiquark momentum distribution functions, $q(x)$ and $\bar{q}(x)$, by

$$F_2(x) \;=\; \sum_q e_q^2\, x(q(x)+\bar{q}(x)) \;=\; 2xF_1(x). \tag{2.12}$$

Note that the structure functions (and to lowest order in QCD corrections, the parton distributions) are Lorentz invariant quantities. It is only the interpretation of $q(x)dx$ as the number of quarks with momentum fraction between x and $x+dx$ that must be seen in the context of the IMF.

2.1.2 Light-Cone Dominance

Having outlined the simple interpretation of the DIS process, we now turn to a more formal analysis of the hadronic tensor, $W_{\mu\nu}$. Using the completeness relation $\sum_X |X\rangle\langle X| = 1$ and translational invariance this can rewritten as

$$W_{\mu\nu} = \frac{1}{2\pi}\int d^4\xi\; e^{iq\cdot\xi}\langle N(p)|J_\mu(\xi)J_\nu(0)|N(p)\rangle. \tag{2.13}$$

In the Bjorken limit $W_{\mu\nu}$ receives the dominant contributions from the light-cone region, $\xi^2 = 0$. This is clear when one writes the argument of the exponential in light-cone coordinates,

$$q\cdot\xi \;=\; \frac{q_+\xi_-}{2} \;+\; \frac{q_-\xi_+}{2} \;-\; \mathbf{q}_T\cdot\xi_T \tag{2.14}$$

where $v_\pm = v_0 \pm v_L$, with v being any 4-vector. The Lorentz scalar $q\cdot\xi$, by definition, takes the same value in any reference frame, so we can choose the target rest frame, in which $q_\mu = \left(\nu;\mathbf{0}_T,-\sqrt{\nu^2+Q^2}\right) \simeq (\nu;\mathbf{0}_T,-\nu-Mx)$, and therefore $q\cdot\xi = -Mx(\xi_0-\xi_L)/2 \;+(2\nu+Mx)(\xi_0+\xi_L)/2$. Obviously the largest contributions to (2.13) will be those for which the exponent oscillates least, namely $q\cdot\xi \simeq 0$. In the Bjorken limit $q_-\xi_+$ will behave like $\nu(\xi_0+\xi_L)$, so that only when $\xi_0 = -\xi_L$ will there be non-negligible contributions to $W_{\mu\nu}$. Thus the DIS cross sections will be controlled by the product of currents $J_\mu(\xi)J_\nu(0)$ near the light cone, $\xi^2 \simeq 0$.

2.1.3 Operator Product Expansion

In quantum field theory products of operators at the same space-time point (composite operators) are not well defined [25]. The short distance operator product expansion (OPE) of Wilson [26], in which the composite operators are expanded in a series of finite local operators multiplied by singular coefficient functions, provides a way of obtaining meaningful results.

Because in DIS it is the $\xi^2 \sim 0$ region that is probed, rather than the $\xi \sim 0$, we need an expansion of the product of currents in Eq.(2.13) that is valid near the light-cone. (This is because at short distances $q\to\infty$, $p\cdot q/q^2 \to 0$, while in DIS the light-cone region corresponds to the Bjorken limit, $-q^2\to\infty$, $p\cdot q/q^2 = O(1)$.) The general form of the light-cone operator product expansion is [27, 28, 14]

$$J(\xi)J(0) \;\sim\; \sum_{i,N} C_i^N(\xi^2)\;\xi_{\mu_1}\cdots\xi_{\mu_N}\;\mathcal{O}_i^{\mu_1\cdots\mu_N}(0) \tag{2.15}$$

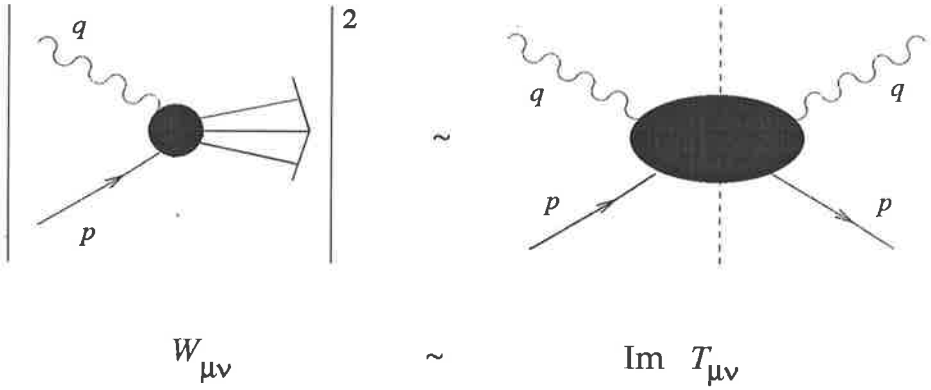

Figure 2.2: Relation between the DIS cross section and the forward virtual Compton scattering amplitude.

where the sum is over different types of operators with spin N (i.e. they transform as tensors of rank N under Lorentz transformations). In DIS the spin N operators $\mathcal{O}_i^{\mu_1\cdots\mu_N}$ represent the soft, or non-perturbative, physics, while the coefficient functions C_i^N describe the hard interaction and are calculable within perturbative QCD.

From Fig.2.2 we can see the similarity between the DIS process described by the tensor $W_{\mu\nu}$ and the forward virtual photon—nucleon Compton scattering amplitude, $T_{\mu\nu}$. We can find the mathematical relation between the two by firstly observing that the product of currents in (2.13) can be expressed as a commutator,

$$W_{\mu\nu} = \frac{1}{2\pi}\int d^4\xi\; e^{iq\cdot\xi}\langle N(p)|\,[J_\mu(\xi), J_\nu(0)]\,|N(p)\rangle \tag{2.16}$$

since the argument in the delta function $\delta^4(q-p+p_X)$ for the combination $J_\nu(0)J_\mu(\xi)$ can never be zero. The reason is that this would require $p_X^2 = M^2 - 2p\cdot q + q^2 = M^2 - Q^2(1+x)/x$, and since the mass of the hadronic debris must be $p_X^2 \geq M^2$, the quantity $Q^2(1+x)/x$ would have to be negative, which is clearly unphysical. Then it is trivial to show that $W_{\mu\nu}$ is related to the imaginary part of $T_{\mu\nu}$ via the optical theorem,

$$W_{\mu\nu} \;=\; \frac{1}{\pi}\,\mathrm{Im}T_{\mu\nu} \tag{2.17}$$

where

$$T_{\mu\nu} \;=\; i\int d^4\xi\; e^{iq\cdot\xi}\;\langle N(p)|T\;J_\mu(\xi)J_\nu(0)\;|N(p)\rangle. \tag{2.18}$$

The formal result of the OPE of the amplitude $T_{\mu\nu}$ is [14, 25]

$$\begin{aligned} T_{\mu\nu} \;=\; \sum_{i,N}\Big\{&\Big(q^2 g_{\mu\mu_1}\tilde{g}_{\nu\mu_2} + q_{\mu_1}(g_{\nu\mu_2}q_\mu - g_{\mu\nu}q_{\mu_2})\Big)\;C_{2,i}^N(Q^2) \\ &-\;\tilde{g}_{\mu\nu}q_{\mu_1}q_{\mu_2}\;C_{L,i}^N(Q^2)\;\Big\}\,q_{\mu_3}\cdots q_{\mu_N}\left(\frac{2}{Q^2}\right)^N\langle N(p)|\mathcal{O}_i^{\mu_1\cdots\mu_N}(0)|N(p)\rangle \end{aligned} \tag{2.19}$$

where the subscripts '2' and 'L' refer to the F_2 and F_L structure functions, and the sums run over the standard set of spin N operators of type i (here, by referring to the longitudinal operators we are pre-empting the discussion in the next section, where renormalisation of the OPE will

be seen to introduce scaling violations, and hence a non-zero F_L). It is useful to categorise the operators according to their flavour properties, namely those that are invariant under SU(N_f) flavour transformations (singlet) and those that are not (non-singlet). Examples of non-singlet quark distributions are $d-\bar{d}$, $u-\bar{u}$, $\eta \equiv (u+\bar{u})-(d+\bar{d})$, while $\Sigma = \sum_q (q+\bar{q})$ is a singlet. In fact, any structure function can be decomposed into a singlet and a non-singlet piece. For example, the electromagnetic structure function of the proton F_{2p} can be written (neglecting contributions from strangeness and charm) as $F_{2p} = \frac{5}{18} x\Sigma + \frac{1}{6} x\eta$.

Since we are dealing with unpolarised processes, the operators must be completely symmetric with respect to interchange of indices $\mu_1 \cdots \mu_N$. Furthermore, in (2.19) we have only written the leading, twist-2, components of the operator expansion, where twist is defined as (mass dimension — spin N) of the operators [29]. Higher twist contributions are suppressed by powers of $1/Q^2$ in the Bjorken limit. For lowest twist (i.e. twist 2), we can construct at most 3 kinds of composite operators. The non-singlet operators must be bilinear in the quark fields,

$$\mathcal{O}_{NS}^{\mu_1 \cdots \mu_N} = \frac{i^{N-1}}{2\,N!}\, \bar{\psi} \left(\gamma^{\mu_1} D^{\mu_2} \cdots D^{\mu_N} \;+\; \mu_i \mu_j \text{ permutations}\right) \vec{\lambda}\, \psi \tag{2.20}$$

where $D^\mu = \partial^\mu + ieA^\mu$ is the covariant derivative and $\vec{\lambda}$ are the eight generators of the flavour SU(N_f) group. The singlet operators are [14, 25]

$$\begin{aligned} \mathcal{O}_{\psi}^{\mu_1 \cdots \mu_N} &= \frac{i^{N-1}}{N!} \bar{\psi} \left(\gamma^{\mu_1} D^{\mu_2} \cdots D^{\mu_N} \;+\; \mu_i \mu_j \text{ permutations}\right) \psi \\ \mathcal{O}_{G}^{\mu_1 \cdots \mu_N} &= \frac{i^{N-2}}{2\,N!} \left(G^{\mu_1 \alpha} D^{\mu_2} \cdots D^{\mu_{N-1}} G_{\alpha}^{\mu_N} \;+\; \mu_i \mu_j \text{ permutations}\right) \end{aligned}$$

for the quark and gluon fields, respectively, where $G^{\alpha\beta}$ is the gluon field strength tensor, and we have suppressed colour indices.

The matrix elements of the operators contain information about the long-distance quark structure of the nucleon, hence they are of particular interest for studying the non-perturbative aspects of hadron physics. On general grounds they can be written as

$$\langle N(p)|\mathcal{O}_i^{\mu_1 \cdots \mu_N}|N(p)\rangle \;=\; \mathcal{A}_i^N\; p^{\mu_1} \cdots p^{\mu_N} \;-\; (g^{\mu_i \mu_j} \text{ terms}). \tag{2.21}$$

The terms containing the $g^{\mu_i \mu_j}$ (the so-called 'trace terms') are necessary to ensure that the matrix elements are traceless (i.e. so that the composite operator has definite spin, N). When contracted with the $q_{\mu_i} q_{\mu_j}$ these give rise to terms that contain smaller powers of ν^2 (i.e. $q^2 = O(\nu)$ instead of $(p\cdot q)^2 = O(\nu^2)$) and therefore are of higher twist (these are also known as target mass corrections, since they go like p^2/q^2). Combining (2.19) and (2.21) we obtain

$$T_{\mu\nu} = \sum_{i,N} \frac{1}{x^N}\, \mathcal{A}_i^N \left\{ \left(-g_{\mu\nu} - \frac{q^2}{(p\cdot q)^2} p_\mu p_\nu + \frac{(p_\mu q_\nu + p_\nu q_\mu)}{p\cdot q} \right) C_{2,i}^N(Q^2) \;-\; \tilde{g}_{\mu\nu} C_{L,i}^N(Q^2) \right\}. \tag{2.22}$$

The expression on the right hand side of (2.22) is convergent only if $1/x < 1$, which is outside the physical region. Since $T_{\mu\nu}$ is an analytic function in the complex $1/x$ plane, with branch cuts along the Re $1/x$ axis for $|1/x| > 1$, we can use Cauchy's theorem to obtain

$$\frac{1}{2\pi i} \oint_C T_{\mu\nu} x^N \;=\; \frac{2}{\pi} \int_1^\infty d(1/x) x^N \mathrm{Im} T_{\mu\nu}$$

Furthermore, using the fact that $\oint_C d(1/x)x^{N-M} = 2\pi i\delta_{M,N-1}$, we can equate both sides for each value of N to obtain the Nth moment, $M^N(Q^2)$, of the structure function:

$$M^N_{2(L)}(Q^2) \equiv \int_0^1 dx\ x^{N-2}\ F_{2(L)}(x,Q^2)\ =\ \sum_i \mathcal{A}^N_i\ C^N_{2(L)i}(Q^2). \tag{2.23}$$

It turns out that it is more convenient to analyse DIS in terms of the moments of structure functions, rather than in terms of the structure functions themselves.

The virtue of the OPE is that we can unambiguously separate the target-dependent (and q^2-independent) part of the moment of the structure function, in the form of the matrix elements $\mathcal{A}^N_i$ of the composite operator, from the target-independent (and q^2-dependent) piece contained in the coefficient functions C^N_i. The former are of course incalculable within perturbative QCD, and represent the main obstacle to the complete description from first principles of the DIS process. For the latter we can use perturbation theory, and can obtain the dependence on q^2 directly from the renormalisation group equations.

2.1.4 Renormalisation Group Equations

In an interacting field theory like QCD quantities such as coupling constants, masses, as well as wavefunctions (operators), must be renormalised. The renormalisation procedure introduces some arbitrary renormalisation scale μ^2 into the theory, although of course the physics itself cannot depend on μ^2.

In DIS the coefficient functions C^N_i depend only on the four-momentum transfer squared Q^2, and as $1/Q^2 \to 0$ in the Bjorken limit, these can be evaluated from perturbative QCD. This will introduce $\ln Q^2$ corrections to the structure functions, which will break the scaling expected from the naive quark-parton model alone.

Let us consider renormalisation of the operator product expansion. Because there are two singlet operators for each spin N ($i = \psi, G$), the renormalisation program will introduce mixing between these operators. There will be no such mixing in the non-singlet sector ($i = NS$), and for our purposes it will be sufficient to examine the renormalisation group equations for this case. (For a renormalisation group analysis of the singlet sector see, for example, Ref.[25].) We shall also refer only to the F_2 structure function, and drop the subscript 'L' and '2', although the generalisation to F_L (or F_1) is straightforward.

Because the unrenormalised matrix elements of the OPE are independent of the renormalisation scale μ, we have

$$\frac{d}{d\mu}\langle N(p)|J_\mu(\xi)J_\nu(0)|N(p)\rangle\ =\ 0. \tag{2.24}$$

Defining the wavefunction renormalisation of the spin N non-singlet operator by $\mathcal{O}^N_{NS\ bare} = Z^N_{NS}\ \mathcal{O}^N_{NS\ ren}$, where Z^N_{NS} is the renormalisation constant, Eq.(2.24) can be rewritten as [14]

$$\left(\mu\frac{\partial}{\partial\mu} + \beta(g)\frac{\partial}{\partial g} - \gamma^N_{NS}\right)\ C^N_{NS}(Q^2/\mu, g) = 0 \tag{2.25}$$

for each spin N. This is the well-known renormalisation group equation for the coefficient functions. In Eq.(2.25), g is the strong coupling constant renormalised at the scale μ^2, γ_{NS}^N is the anomalous dimension of the twist 2 operator $\mathcal{O}_{NS}^N$

$$\gamma_{NS}^N = \mu\frac{\partial}{\partial\mu}(\ln Z_{NS}^N) \tag{2.26}$$

and the β-function is given by

$$\beta(g) = \mu\,\frac{\partial g}{\partial\mu}. \tag{2.27}$$

We have also omitted from (2.25) the anomalous dimension of the current J_μ, since it was shown by Gross [30] to vanish as a result of current conservation.

The solution to (2.25) is

$$C_{NS}^N(Q^2/\mu^2, g^2) = C_{NS}^N(1,\bar{g}^2)\exp\left[-\int_{\bar{g}(\mu^2)}^{\bar{g}(Q^2)} dg'\,\frac{\gamma_{NS}^N(g')}{\beta(g')}\right] \tag{2.28}$$

where $\bar{g}$ is the effective (running) coupling constant, defined by $d\bar{g}^2/dt = \bar{g}\,\beta(\bar{g})$ and $\bar{g}(t=0) = g$, with $t = \ln Q^2/\mu^2$. The calculation of the quantities $C_{NS}^N(\mu^2)$, $\gamma_{NS}^N(g)$ and $\beta(g)$ is straightforward in perturbation theory [7, 8]. Expanding in a series in orders of the coupling constant, they are given by

$$\begin{aligned}
\gamma_{NS}^N(g) &= \gamma_{NS}^{(0)N}\,\frac{g^2}{16\pi^2} + O(g^2)\\
\beta(g) &= -\beta_0\,\frac{g^3}{16\pi^2} + O(g^5)\\
C_{NS}^N(1,\bar{g}^2) &= C_{NS}^{(0)N} + O(g^2).
\end{aligned} \tag{2.29}$$

Note the leading order coefficient $C_{NS}^{(0)N}$ for the longitudinal structure function is zero, so that F_L receives contributions only from higher orders in the coupling constant expansion. Combining Eqs.(2.23), (2.28) and (2.29), we finally obtain the equation governing the Q^2 evolution of the moments of the structure functions (to leading order in g) [31, 32],

$$M_{2,NS}^N(Q^2) = \left[\frac{\alpha_S(Q^2)}{\alpha_S(\mu^2)}\right]^{\gamma_{NS}^{(0)N}/2\beta_0} M_{2,NS}^N(\mu^2) \tag{2.30}$$

where the non-singlet anomalous dimension is [33]

$$\gamma_{NS}^{(0)N} = \frac{8}{3}\left(4\sum_{j=1}^{N}\frac{1}{j} - 3 - \frac{2}{N(N+1)}\right) \tag{2.31}$$

and $\beta_0 = 11 - 2N_f/3$ for N_f active flavours in the evolution. In Eq.(2.30) we have rewritten the strong coupling constant as

$$\alpha_S(Q^2) \equiv \frac{\bar{g}^2(Q^2)}{4\pi} = \frac{4\pi}{\beta_0\ln(Q^2/\Lambda_{QCD}^2)} \tag{2.32}$$

by putting the arbitrariness of the renormalisation scale into the new parameter Λ_{QCD}, known as the QCD scale parameter, $\ln\Lambda_{QCD}^2 = \ln\mu^2 - 16\pi^2/(\beta_0\,\bar{g}^2(\mu^2))$.

The structure function at Q^2 can be obtained from the moments with the help of the inverse Mellin transform,

$$F_{2,NS}(x,Q^2) \;=\; \frac{1}{2\pi i}\int_{N_0-i\infty}^{N_0+i\infty} dN\; x^{1-N}\; M^N_{2,NS}(Q^2). \tag{2.33}$$

In practice it is easier to work with the inverse Laplace transform, which can be obtained from the inverse Mellin transform by a simple change of variables, $t = -\ln x$,

$$F_{2,NS}(x,Q^2) \;=\; \frac{1}{2\pi i}\int_{N_0-i\infty}^{N_0+i\infty} dN\; \exp[(N-1)t(x)]\; M^N_{2,NS}(Q^2) \tag{2.34}$$

and fixing the contour of integration to lie to the right of all singularities of $M^N_{2,NS}(Q^2)$ in the complex N plane.

Once the matrix elements $\mathcal{A}$ (and hence the moments) at μ^2 are known, Eqs.(2.30) and (2.34) can be used to give the moments and structure functions at any other value of Q^2. The challenging task, from the point of view of non-perturbative hadron physics, is to determine $\mathcal{A}$. Attempts at calculating the non-perturbative part of the DIS structure functions from various models of QCD have been made by a numbers of authors [34–42]. The motivation has been the prospect of making a definite connection between the high energy parton picture of DIS on the one hand, and the valence quark models at low energy on the other. If the nucleon behaves like three valence quarks at some low momentum scale $\sim \mu^2$, from the above discussion we see that the nucleon structure function will necessarily evolve with Q^2, and therefore a description in terms of valence quarks will no longer be accurate. An intuitive, and mathematically equivalent picture [43] for this Q^2 evolution is that as Q^2 increases the quarks radiate more and more gluons, which in turn split into pairs of quarks and antiquarks, and so on. In this manner a non-valence (or sea) component of the structure function is generated. However, the underlying philosophy has been that at order μ^2 a purely valence quark model may yield reliable twist two structure functions [35, 44]. These could then be evolved to higher Q^2 to compare with the experimental DIS data.

In Section 2.3 we shall construct a simple, relativistic model of the valence nucleon structure function using some of the phenomenology from the earlier model calculations. Before that, in the next section we set up a formalism, analogous to that of the OPE, that will enable us to clearly separate the q^2-dependent and q^2-independent parts of the *truncated* nucleon tensor, and identify the scaling contributions. We will see in later chapters that this new formalism has extensive uses and applications.

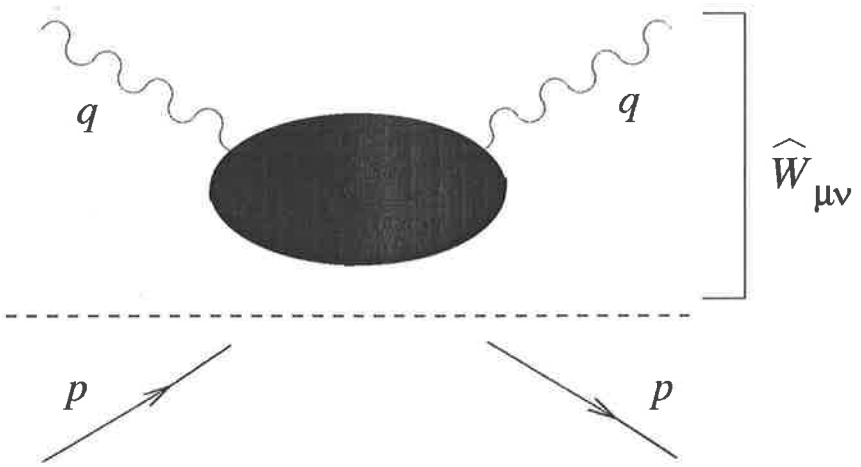

Figure 2.3: Truncated nucleon tensor.

2.2 The Truncated Hadronic Tensor

The Lorentz structure of the nucleon hadronic tensor was given in Eq.(2.4). In this section we delve deeper into the Lorentz and Dirac structure of the truncated nucleon tensor, that is, one which has its fermion legs amputated. Because of the additional spinor degree of freedom the structure of the truncated tensor will necessarily be more complicated than that of the full nucleon tensor, $W_{\mu\nu}$. However, once we identify the relevant structures that contribute to the physical tensor in the Bjorken limit, we will be able to use these in a fully relativistic, covariant calculation of the nucleon structure function. The formalism developed here can also be extended to the case of off-mass-shell nucleons, since the truncated tensor will generally depend upon p^2 as well as q^2 and $p \cdot q$. The application to off-shell nucleon scattering, for example in the calculation of the nuclear structure functions, will be addressed more fully in Chapter 5.

2.2.1 Dirac and Lorentz Structure

We begin by observing that the nucleon tensor can be written [45]

$$M\, W_{\mu\nu}(p,q) \;=\; \frac{1}{2}\mathrm{Tr}\left[(\not{p}+M)\,\widehat{W}_{\mu\nu}(p,q)\right] \tag{2.35}$$

where we have explicitly separated the nucleon spinors from the remaining interaction. This is depicted graphically in Fig.2.3. The tensor $\widehat{W}_{\mu\nu}$ is then related to the truncated virtual photon — nucleon scattering amplitude $\widehat{T}_{\mu\nu}$ via $\widehat{W}_{\mu\nu} \sim \mathrm{Im}\widehat{T}_{\mu\nu}$, where the on-shell Compton amplitude $T_{\mu\nu}$ is given by $T_{\mu\nu}(p,q) = \bar{u}(p)\,\widehat{T}_{\mu\nu}(p,q)\,u(p)$.

In general, the tensor $\widehat{W}_{\mu\nu}$ must be constructed from the Lorentz tensors (Dirac scalars) $g_{\mu\nu}, p_\mu, q_\mu$ and Dirac matrices $I, \gamma_\mu, \sigma_{\mu\nu}, \gamma_\mu\gamma_5$ and γ_5. By parity considerations terms involving $\gamma_\mu\gamma_5$ or γ_5 will not contribute to the spin-averaged tensor. Furthermore, terms with $\sigma_{\mu\nu}$ will not contribute to $W_{\mu\nu}$, but we keep these as they may be relevant for the off-mass-shell tensor in nuclear calculations. Then the tensor with the correct transformation properties under Lorentz and parity

transformations can in general be written in terms of 22 independent functions,

$$\begin{aligned}
\widehat{W}_{\mu\nu}(p,q) &= I\left(\mathcal{P}_{T\mu\nu}\,\widehat{W}_T^0 + \mathcal{P}_{L\mu\nu}\,\widehat{W}_L^0 + \mathcal{P}_{G\mu\nu}\,\widehat{W}_G^0 + \mathcal{P}_{H\mu\nu}\,\widehat{W}_H^0\right) \\
&+ \not{p}\left(\mathcal{P}_{T\mu\nu}\,\widehat{W}_T^1 + \mathcal{P}_{L\mu\nu}\,\widehat{W}_L^1 + \mathcal{P}_{G\mu\nu}\,\widehat{W}_G^1 + \mathcal{P}_{H\mu\nu}\,\widehat{W}_H^1\right) \\
&+ \not{q}\left(\mathcal{P}_{T\mu\nu}\,\widehat{W}_T^2 + \mathcal{P}_{L\mu\nu}\,\widehat{W}_L^2 + \mathcal{P}_{G\mu\nu}\,\widehat{W}_G^2 + \mathcal{P}_{H\mu\nu}\,\widehat{W}_H^2\right) \\
&+ (\gamma_\mu p_\nu + \gamma_\nu p_\mu)\,\widehat{W}^3 + (\gamma_\mu q_\nu + \gamma_\nu q_\mu)\,\widehat{W}^4 \\
&+ \sigma_{\alpha\beta}p^\alpha q^\beta\left(\mathcal{P}_{T\mu\nu}\,\widehat{W}_T^5 + \mathcal{P}_{L\mu\nu}\,\widehat{W}_L^5 + \mathcal{P}_{G\mu\nu}\,\widehat{W}_G^5 + \mathcal{P}_{H\mu\nu}\,\widehat{W}_H^5\right) \\
&+ (\sigma_{\alpha\mu}\,p_\nu + \sigma_{\alpha\nu}\,p_\mu)\,p^\alpha\,\widehat{W}^6 + (\sigma_{\alpha\mu}\,p_\nu + \sigma_{\alpha\nu}\,p_\mu)\,q^\alpha\,\widehat{W}^7 \\
&+ (\sigma_{\alpha\mu}\,q_\nu + \sigma_{\alpha\nu}\,q_\mu)\,p^\alpha\,\widehat{W}^8 + (\sigma_{\alpha\mu}\,q_\nu + \sigma_{\alpha\nu}\,q_\mu)\,q^\alpha\,\widehat{W}^9 \qquad (2.36)
\end{aligned}$$

where each of the functions on the right hand side is a scalar function of q^2, $p\cdot q$ and p^2, $\widehat{W}^i = \widehat{W}^i(p,q) = \widehat{W}^i(p^2, p\cdot q, q^2)$. The projection operators $\mathcal{P}_{\mu\nu}$ are as defined in (2.5).

Substituting (2.36) into (2.35) gives the transverse unpolarised structure function in terms of the functions $\widehat{W}^i(p,q)$,

$$M\,W_T(p,q) = 2\,M\,\widehat{W}_T^0 + 2\,M^2\,\widehat{W}_T^1 + 2\,p\cdot q\,\widehat{W}_T^2. \qquad (2.37)$$

This can be viewed as a definition of W_T. Furthermore, the longitudinal and gauge non-invariant structure functions are

$$M\,W_L(p,q) = 2\,M\,\widehat{W}_L^0 + 2\,M^2\,\widehat{W}_L^1 + 2\,p\cdot q\,\widehat{W}_L^2 - \frac{4\,(p\cdot q)^2}{q^2}\,\widehat{W}^3 \qquad (2.38)$$

$$M\,W_G(p,q) = 2\,M\,\widehat{W}_G^0 + 2\,M^2\,\widehat{W}_G^1 + 2\,p\cdot q\,\widehat{W}_G^2 + \frac{4\,(p\cdot q)^2}{q^2}\,\widehat{W}^3 + 4\,p\cdot q\,\widehat{W}^4 \qquad (2.39)$$

$$M\,W_H(p,q) = 2\,M\,\widehat{W}_H^0 + 2\,M^2\,\widehat{W}_H^1 + 2\,p\cdot q\,\widehat{W}_H^2 + \frac{4\,(p\cdot q)^2}{q^2}\widehat{W}^3 + 2\,p\cdot q\,\widehat{W}^4. \qquad (2.40)$$

Because of gauge invariance the latter two functions must be zero, which means that not all of the functions $\widehat{W}^i(p,q)$ are independent. To check that this is indeed the case requires explicit evaluation of the functions $\widehat{W}^i(p,q)$, which we now do. We shall work in the Bjorken limit, and neglect logarithmic QCD corrections, so that the function W_L should also be zero.

2.2.2 Scaling Properties of the Functions $\widehat{W}$

The diagram we calculate is the 'handbag' diagram depicted in Fig.2.4, which represents the impulse approximation for quarks. [2] As in the operator product expansion, we can separate out the q^2-dependent part of $\widehat{W}_{\mu\nu}$, denoted by $r_{\mu\nu}$, from the q^2-independent, non-perturbative part, which will be described by the function H:

$$\left[\widehat{W}_{\mu\nu}(p,q)\right]_{ab} = \int d\tilde{k}\;\left[r_{\mu\nu}(k,q)\right]_{cd}\;\left[H(k,p)\right]_{dcab} \qquad (2.41)$$

[2] In general the diagram with the 'crossed' photons can also contribute to the structure function in the small x region, however in the subsequent model calculation where we consider only two-quark intermediate states there will be no contribution from this diagram.

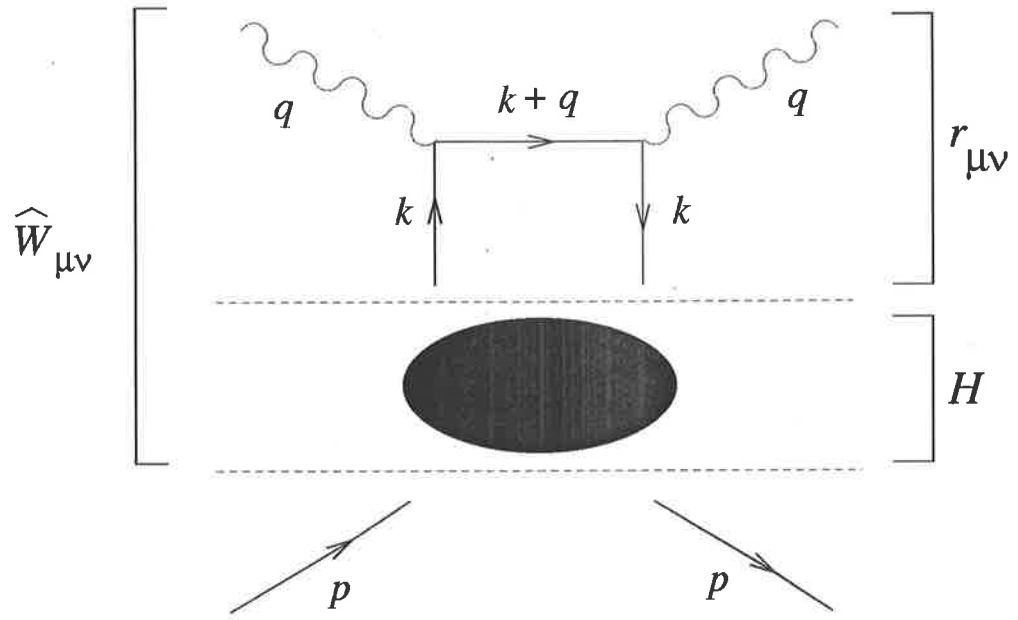

Figure 2.4: Impulse approximation for the truncated nucleon tensor.

where

$$d\tilde{k} = \frac{d^4k}{(2\pi)^4} \frac{(2\pi)\delta([q+k]^2 - m^2)}{(k^2 - m^2)^2} \tag{2.42}$$

and the indices *abcd* are Dirac indices. Here k is the four-momentum of the struck quark, and m its mass.

The tensor $r_{\mu\nu}$ can be evaluated explicitly from the γ_μ coupling of the photon to the struck quark,

$$\begin{aligned} r_{\mu\nu} &= (\not{k} + m)\, \gamma_\mu\, (\not{k} + \not{q} + m)\, \gamma_\nu\, (\not{k} + m) \\ &= R_{\mu\nu} I + R_{\mu\nu\alpha} \gamma^\alpha \end{aligned} \tag{2.43}$$

where

$$\begin{aligned} R_{\mu\nu} &= m \left(q^2 g_{\mu\nu} + 4 k_\mu k_\nu + 2\,(k_\mu q_\nu + k_\nu q_\mu) \right) \\ R_{\mu\nu\alpha} &= R_{\mu\nu} \frac{k_\alpha}{m} + \left(m^2 - k^2 \right) (-q_\alpha\, g_{\mu\nu} + (k+q)_\mu\, g_{\nu\alpha} + (k+q)_\nu\, g_{\mu\alpha}) . \end{aligned} \tag{2.44}$$

Next we take the trace over the indices c, d in (2.41),

$$\mathrm{Tr}\,[r_{\mu\nu}(k,q)\,[H(p,k)]_{ab}] = R_{\mu\nu}(k,q)\,[G(p,k)]_{ab} + R_{\mu\nu\alpha}(k,q)\,[G^\alpha(p,k)]_{ab} \tag{2.45}$$

where G^α and G are 4×4 matrices transforming like a vector and a scalar, respectively. Their most general form is

$$\begin{aligned} G^\alpha &= I\,(p^\alpha f_1 + k^\alpha f_2) + \not{k}\,(p^\alpha f_3 + k^\alpha f_5) + \not{p}\,(p^\alpha f_4 + k^\alpha f_6) + \gamma^\alpha f_7 \\ &+ \sigma^{\beta\alpha} p_\beta\, f_8 + \sigma^{\beta\alpha} k_\beta\, f_9 + p^\beta k^\delta \sigma_{\beta\delta}\, p^\alpha\, f_{10} + p^\beta k^\delta \sigma_{\beta\delta}\, k^\alpha\, f_{11} \\ G &= I\, f_{12} + \not{p}\, f_{13} + \not{q}\, f_{14} + p^a k^b \sigma_{ab}\, f_{15} \end{aligned} \tag{2.46}$$

where the functions $f_1 - f_{15}$ are scalar functions of p and k. We have omitted contributions involving γ_5 to guarantee that G and G^α are even under parity transformations.

To perform the integrations over $d^4k = \frac{1}{2} d^2\mathbf{k}_T dk_+ dk_-$ Eq.(2.41) must be written as a sum of products of k-independent terms containing the indices μ, ν and integrals of k-dependent scalars. In general there will be three types of terms — those involving integration over k_μ, $k_\mu\, k_\nu$ and $k_\mu\, k_\nu\, k_\alpha\, \gamma^\alpha$. These can be expanded as follows:

$$
\begin{aligned}
K^{(1)}_\mu(p,q) \equiv \int d\tilde{k}\; k_\mu &= p_\mu\, P_1^{(1)\mu'} K^{(1)}_{\mu'} \;+\; q_\mu\, P_2^{(1)\mu'} K^{(1)}_{\mu'} \\
K^{(2)}_{\mu\nu}(p,q) \equiv \int d\tilde{k}\; k_\mu k_\nu &= g_{\mu\nu}\, P_1^{(2)\mu'\nu'} K^{(2)}_{\mu'\nu'} \;+\; p_\mu p_\nu\, P_2^{(2)\mu'\nu'} K^{(2)}_{\mu'\nu'} \;+\; q_\mu q_\nu\, P_3^{(2)\mu'\nu'} K^{(2)}_{\mu'\nu'} \\
&+ (p_\mu q_\nu + p_\nu q_\mu)\, P_4^{(2)\mu'\nu'} K^{(2)}_{\mu'\nu'} \\
K^{(3)}_{\mu\nu\alpha}(p,q) \equiv \int d\tilde{k}\; k_\mu k_\nu k_\alpha &= (g_{\mu\nu}p_\alpha + g_{\mu\alpha}p_\nu + g_{\nu\alpha}p_\mu)\, P_1^{(3)\mu'\nu'\alpha'} K^{(3)}_{\mu'\nu'\alpha'} \\
&+ (g_{\mu\nu}q_\alpha + g_{\mu\alpha}q_\nu + g_{\nu\alpha}q_\mu)\, P_2^{(3)\mu'\nu'\alpha'} K^{(3)}_{\mu'\nu'\alpha'} \\
&+ p_\mu p_\nu p_\alpha\, P_3^{(3)\mu'\nu'\alpha'} K^{(3)}_{\mu'\nu'\alpha'} + q_\mu q_\nu q_\alpha\, P_4^{(3)\mu'\nu'\alpha'} K^{(3)}_{\mu'\nu'\alpha'} \\
&+ (p_\mu p_\nu q_\alpha + p_\mu p_\alpha q_\nu + p_\nu p_\alpha q_\mu)\, P_5^{(3)\mu'\nu'\alpha'} K^{(3)}_{\mu'\nu'\alpha'} \\
&+ (q_\mu q_\nu p_\alpha + q_\mu q_\alpha p_\nu + q_\nu q_\alpha p_\mu)\, P_6^{(3)\mu'\nu'\alpha'} K^{(3)}_{\mu'\nu'\alpha'}.
\end{aligned}
$$

Here, the projection operators are

$$
\begin{aligned}
P_1^{(1)\mu} &= \frac{1}{X}\Big\{q^2\, p^\mu \;-\; p\cdot q\; q^\mu\Big\} \\
P_2^{(1)\mu} &= \frac{1}{X}\Big\{-p\cdot q\; p^\mu \;+\; p^2\; q^\mu\Big\},
\end{aligned}
$$

where $X = p^2q^2 - (p\cdot q)^2$, for the k_μ terms. For the $k_\mu\, k_\nu$ terms we have

$$
\begin{aligned}
P_1^{(2)\mu\nu} &= \frac{1}{2\,X}\Big\{X\; g^{\mu\nu} \;-\; q^2\; p^\mu p^\nu \;-\; p^2\; q^\mu q^\nu \;+\; p\cdot q\; (p^\mu q^\nu + p^\nu q^\mu)\Big\} \\
P_2^{(2)\mu\nu} &= \frac{1}{2\,X^2}\Big\{-\,q^2\; X\; g^{\mu\nu} \;+\; 3\; q^4\; p^\mu p^\nu \;+\; (p^2q^2 + 2(p\cdot q)^2)\; q^\mu q^\nu \\
&\qquad -\; 3\; q^2\; p\cdot q\; (p^\mu q^\nu + p^\nu q^\mu)\Big\} \\
P_3^{(2)\mu\nu} &= \frac{1}{2\,X^2}\Big\{-\,p^2\; X\; g^{\mu\nu} \;+\; (p^2q^2 + 2(p\cdot q)^2)\; p^\mu p^\nu \;+\; 3\; p^4\; q^\mu q^\nu \\
&\qquad -\; 3\; p^2\; p\cdot q\; (p^\mu q^\nu + p^\nu q^\mu)\Big\} \\
P_4^{(2)\mu\nu} &= \frac{1}{2\,X^2}\Big\{p\cdot q\; (p^2q^2 - (p\cdot q)^2)\; g^{\mu\nu} \;-\; 3\; q^2\; p\cdot q\; p^\mu p^\nu \;-\; 3\; p^2\; p\cdot q\; q^\mu q^\nu \\
&\qquad +\; (p^2q^2 + 2(p\cdot q)^2)(p^\mu q^\nu + p^\nu q^\mu)\Big\}.
\end{aligned}
$$

Finally, for the $k_\mu k_\nu \not{k}$ terms, the projectors are

$$
\begin{aligned}
P_1^{(3)\mu\nu\alpha} &= \frac{1}{6\,X^2}\Big\{X\; (q^2 B_1^{\mu\nu\alpha} \;-\; p\cdot q B_2^{\mu\nu\alpha}) \;-\; 3\; q^4\; B_3^{\mu\nu\alpha} \\
&\quad +\; 3\; p^2\; p\cdot q\; B_4^{\mu\nu\alpha} \;+\; 3\; q^2\; p\cdot q\; B_5^{\mu\nu\alpha} \;-\; (p^2q^2 + 2(p\cdot q)^2)\; B_6^{\mu\nu\alpha}\Big\} \\
P_2^{(3)\mu\nu\alpha} &= \frac{1}{6\,X^2}\Big\{X\; (-p\cdot q\; B_1^{\mu\nu\alpha} \;+\; p^2\; B_2^{\mu\nu\alpha}) \;+\; 3\; q^2\; p\cdot q\; B_3^{\mu\nu\alpha} \\
&\quad -\; 3\; p^4\; B_4^{\mu\nu\alpha} \;-\; (p^2q^2 + 2\;(p\cdot q)^2)\; B_5^{\mu\nu\alpha} \;+\; 3\; p^2\; p\cdot q\; B_6^{\mu\nu\alpha}\Big\}
\end{aligned}
$$

$$
\begin{aligned}
P_3^{(3)\mu\nu\alpha} &= \frac{1}{2\,X^3}\Big\{X\,(-\,q^4\,B_1^{\mu\nu\alpha}\;+\;q^2\,p\cdot q\,B_2^{\mu\nu\alpha})\;+\;5\,q^6\,B_3^{\mu\nu\alpha}\\
&\quad+\,p\cdot q\,(-3p^2q^2-2(p\cdot q)^2)\,B_4^{\mu\nu\alpha}\;-\;5\,q^4\,p\cdot q\,B_5^{\mu\nu\alpha}\;+\;q^2\,(p^2q^2+4(p\cdot q)^2)\,B_6^{\mu\nu\alpha}\Big\}\\
P_4^{(3)\mu\nu\alpha} &= \frac{1}{2\,X^3}\Big\{X\,(p^2p\cdot q\,B_1^{\mu\nu\alpha}-p^2\,p\cdot q\,B_2^{\mu\nu\alpha})\;+\;p\cdot q\,(-3p^2q^2-2(p\cdot q)^2)\,B_3^{\mu\nu\alpha}\\
&\quad+\,5\,p^6\,B_4^{\mu\nu\alpha}\;+\;p^2\,(p^2q^2+4(p\cdot q)^2)\,B_5^{\mu\nu\alpha}\;-\;5\,p^4\,p\cdot q\,B_6^{\mu\nu\alpha}\Big\}\\
P_5^{(3)\mu\nu\alpha} &= \frac{1}{6\,X^3}\Big\{X\,(3q^2p\cdot q\,B_1^{\mu\nu\alpha}\;-(p^2q^2+2\,(p\cdot q)^2)\,B_2^{\mu\nu\alpha})\;-\;15\,q^4\,p\cdot q\,B_3^{\mu\nu\alpha}\\
&\quad+\,3\,p^2\,(p^2q^2+4(p\cdot q)^2)\,B_4^{\mu\nu\alpha}+\,3\,q^2\,(p^2q^2+4(p\cdot q)^2)\,B_5^{\mu\nu\alpha}+\,3\,p\cdot q\,(-3p^2q^2-2(p\cdot q)^2)\,B_6^{\mu\nu\alpha}\Big\}\\
P_6^{(3)\mu\nu\alpha} &= \frac{1}{6\,X^3}\Big\{X\,(-p^2q^2-2(p\cdot q)^2)\,B_1^{\mu\nu\alpha})\;+\;3\,p^2\,p\cdot q\,B_2^{\mu\nu\alpha}\;+\;3\,q^2\,(p^2q^2+4(p\cdot q)^2)\,B_3^{\mu\nu\alpha}\\
&\quad-\,15\,p^4\,p\cdot q\,B_4^{\mu\nu\alpha}\;+\;3\,p\cdot q\,(-3p^2q^2-2(p\cdot q)^2)\,B_5^{\mu\nu\alpha}+\,3\,p^2\,(p^2q^2+4(p\cdot q)^2)\,B_6^{\mu\nu\alpha}\Big\},
\end{aligned}
$$

where the basis tensors are

$$
\begin{aligned}
B_1^{\mu\nu\alpha} &= p^\mu g^{\nu\alpha}+p^\nu g^{\alpha\nu}+p^\alpha g^{\mu\nu} & B_2^{\mu\nu\alpha} &= q^\mu g^{\nu\alpha}+q^\nu g^{\alpha\nu}+q^\alpha g^{\mu\nu}\\
B_3^{\mu\nu\alpha} &= p^\mu p^\nu p^\alpha & B_4^{\mu\nu\alpha} &= q^\mu q^\nu q^\alpha\\
B_5^{\mu\nu\alpha} &= p^\mu p^\nu q^\alpha+p^\nu p^\alpha q^\mu+p^\alpha p^\mu q^\nu & B_6^{\mu\nu\alpha} &= q^\mu q^\nu p^\alpha+q^\nu q^\alpha p^\mu+q^\alpha q^\mu p^\nu.
\end{aligned}
$$

The result is that the $\widehat{W}^i$ are completely defined in terms of the functions f_1–f_{15}. Furthermore, since the dependence on q^2 is now explicit, their scaling behaviour can be easily determined. The results for the functions $\widehat{W}_T^i$ are as follows:

$$
\begin{aligned}
\widehat{W}_T^0 &= \int d\tilde{k}\left\{\left((m^2-k^2)\,p\cdot q-p\cdot k\,q^2\right)f_1\;-\;\frac{(m^2+k^2)\,q^2}{2}\,f_2\;-\;m\,q^2\,f_{12}\right\}\\
\widehat{W}_T^1 &= \int d\tilde{k}\left\{\left(\frac{(k^2-m^2)\,q^2}{2}+\frac{p\cdot k\,q^4}{2\,p\cdot q}\right)f_3\;+\;\left((m^2-k^2)\,p\cdot q-p\cdot k\,q^2\right)\,f_4\right.\\
&\quad\left.+\left(\frac{(k^2+m^2)\,q^4}{4\,p\cdot q}\right)f_5\;-\;\frac{(k^2+m^2)\,q^2}{2}f_6\;+\;\frac{q^4}{2\,p\cdot q}f_7\;-\;m\,q^2\,f_{13}\;+\;\frac{m\,q^4}{2\,p\cdot q}\,f_{14}\right\}\\
\widehat{W}_T^2 &= \int d\tilde{k}\left\{\left(\frac{p^2\,q^2}{2\,p\cdot q}+p\cdot k\right)\left(m^2-k^2-\frac{p\cdot k\,q^2}{p\cdot q}\right)\,f_3\;-\;\frac{(k^2+m^2)\,q^2}{2\,p\cdot q}\left(p\cdot k+\frac{p^2\,q^2}{2\,p\cdot q}\right)\,f_5\right.\\
&\quad\left.+\left(m^2-k^2-\frac{p^2\,q^4}{2\,(p\cdot q)^2}-\frac{p\cdot k\,q^2}{p\cdot q}\right)\,f_7\;-\;\left(\frac{m\,p^2\,q^4}{2\,(p\cdot q)^2}+\frac{m\,p\cdot k\,q^2}{p\cdot q}\right)\,f_{14}\right\} \qquad (2.47)\\
\widehat{W}_T^5 &= \int d\tilde{k}\left\{\left(k^2-m^2-\frac{p^2\,q^4}{2\,(p\cdot q)^2}-\frac{p\cdot k\,q^2}{p\cdot q}\right)f_8\;+\;\frac{(m^2-k^2)\,q^2}{2\,p\cdot q}f_9\right.\\
&\quad+\left(m^2-k^2-\frac{p\cdot k\,q^2}{p\cdot q}\right)\left(\frac{p^2\,q^2}{2\,p\cdot q}+p\cdot k\right)f_{10}\;-\;\frac{(k^2+m^2)\,q^2}{2\,p\cdot q}\left(\frac{p^2\,q^2}{2\,p\cdot q}+p\cdot k\right)f_{11}\\
&\quad\left.-\left(\frac{m\,p^2\,q^4}{2\,(p\cdot q)^2}+\frac{m\,p\cdot k\,q^2}{p\cdot q}\right)f_{15}\right\}.
\end{aligned}
$$

Since the functions $f_1 - f_{15}$ are q^2-independent, we find that $\widehat{W}_T^0$ and $\widehat{W}_T^1$ are of order 1, and $\widehat{W}_T^2$ (and also $\widehat{W}_T^5$) is of order $1/\nu$ (remember that $d\tilde{k}$ involves a δ-function in q^2). Therefore all three functions $\widehat{W}_T^{0-2}$ contribute in the Bjorken limit to the transverse nucleon structure function, Eq.(2.37).

For the other functions we find that all are of order $1/\nu$, with the exception of $\widehat{W}^7$ and $\widehat{W}^9$, which are of order $1/\nu^2$. This means that some of the terms on the right hand side of (2.38)—(2.40) will be of the some order as W_T. However, because the functions appearing there satisfy the following relations:

$$\begin{aligned}
\widehat{W}_L^2 &= \frac{2\,p\cdot q}{q^2}\,\widehat{W}^3 \\
\widehat{W}_G^2 &= -\frac{2\,p\cdot q}{q^2}\,\widehat{W}^3 - 2\,\widehat{W}^4 \\
\widehat{W}_H^2 &= \widehat{W}_G^2 + \widehat{W}^4 \\
\widehat{W}_L^5 &= \frac{2\,p\cdot q}{q^2}\,\widehat{W}^6 \\
\widehat{W}_G^5 &= -\frac{2\,p\cdot q}{q^2}\,\widehat{W}^6 - 2\,\widehat{W}^8 \\
\widehat{W}_H^5 &= \widehat{W}_G^5 + \widehat{W}^8
\end{aligned} \tag{2.48}$$

the leading (order $1/\nu$) contributions will cancel *exactly* in the Bjorken limit. This is sufficient to guarantee that gauge invariance ($q^\mu W_{\mu\nu}(p,q) = 0$ [3]) and the Callan-Gross relation hold.

Essentially what we have done in the above analysis is temporarily delay calculating the soft part of the complete diagram in Fig.2.4. By doing so we have been able to extract additional information about the q^2-dependent part of the truncated nucleon tensor. The usefulness of this particular result will be made apparent next when we explicitly calculate the 'non-perturbative' functions $f_1 - f_{15}$.

2.3 Relativistic Model of the Nucleon Structure Function

To calculate the transverse structure function of the nucleon requires a description of the soft, non-perturbative physics, which in our case is parameterised by the functions $f_1 - f_{15}$. We observe that because both the nucleon and struck quark inside the nucleon have spin $1/2$, the intermediate spectator state in Fig.2.5 will have either spin 0 or 1. In order to make an overall Lorentz scalar, we therefore need only consider quark–nucleon vertices that transform as scalars or vectors under Lorentz transformations. We shall be more general than is necessary in this section, in keeping p^2 dependence in the nucleon–quark vertex functions. Although for a nucleon p^2 is of course fixed, the full, p^2-dependent vertices will be necessary when discussing scattering from composite targets, such as nuclei, in later chapters.

2.3.1 Relativistic Vertex Functions

It is straightforward to identify the form of the vertices that are allowed by Lorentz, parity and time-reversal invariance, however the specific momentum dependence has to be determined within a model. In general there will be 15 independent scalar ($\Phi^S_{1-4}(k,p)$) and vector ($\Phi^V_{1-11}(k,p)$) vertex functions, given by

[3] Note that the truncated tensor $\widehat{W}_{\mu\nu}(p,q)$ itself need not satisfy $q^\mu \widehat{W}_{\mu\nu}(p,q) = 0$.

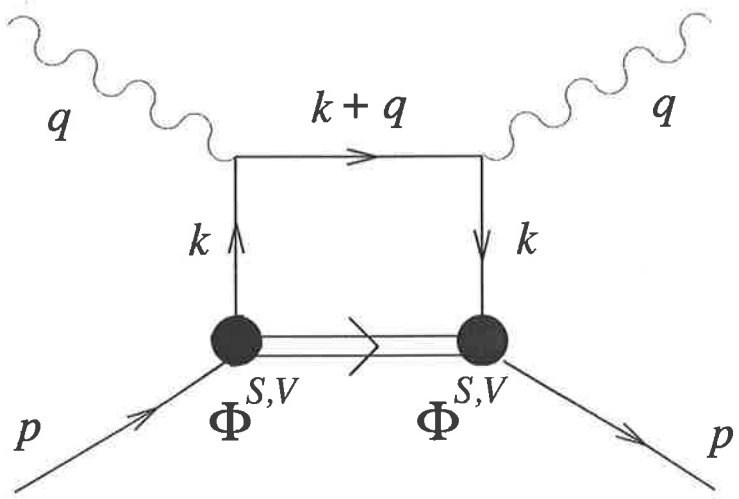

Figure 2.5: Relativistic model of the valence quark distribution, in which the quark–nucleon vertex is described by the vertex function $\Phi^{S,V}$.

$$\mathcal{V}^S = I\,\Phi_1^S + \not{p}\,\Phi_2^S + \not{k}\,\Phi_3^S + \sigma_{\alpha\beta}p^\alpha k^\beta\,\Phi_4^S \tag{2.49}$$

for a scalar vertex, and

$$\begin{aligned}\mathcal{V}_\alpha^V &= \gamma_\alpha\,\Phi_1^V + p_\alpha\,I\,\Phi_2^V + k_\alpha\,I\,\Phi_3^V + \sigma_{\alpha\beta}p^\beta\,\Phi_4^V + \sigma_{\alpha\beta}k^\beta\,\Phi_5^V \\ &+ p_\alpha\,\not{p}\,\Phi_6^V + p_\alpha\,\not{k}\,\Phi_7^V + k_\alpha\,\not{p}\,\Phi_8^V + k_\alpha\,\not{k}\,\Phi_9^V \\ &+ \sigma_{\beta\delta}p^\beta k^\delta\,p^\alpha\,\Phi_{10}^V + \sigma_{\beta\delta}p^\beta k^\delta\,k^\alpha\,\Phi_{11}^V\end{aligned} \tag{2.50}$$

for a vector vertex. (In fact, for DIS from a free nucleon terms involving only the four-vector p will not be present, so the number of independent vertex functions will be reduced.) From these vertex functions the functions $f_1 - f_{15}$ can then be uniquely determined. To see this, let us firstly consider the scalar vertex. The general, non-perturbative, function from Section 2.2.2, $(H(k,p))_{dcab}$, will be proportional to $(\mathcal{V}^S)_{ac}(\mathcal{V}^S)_{db}$.

Using the Fierz theorem the Dirac indices can be rearranged into a form that enables the connection with the functions $f_1 - f_{15}$ to be explicit:

$$\begin{aligned}(\mathcal{V}^S)_{ac}\,(r_{\mu\nu})_{cd}\,(\mathcal{V}^S)_{db} &= \frac{1}{16}\sum_{ij}\mathrm{Tr}[\mathcal{V}^S\Gamma_j\mathcal{V}^S\Gamma_i]\,(\Gamma^i)_{ab}\,(\Gamma^j)_{dc}\,(r_{\mu\nu})_{cd} \\ &= \frac{1}{4}\sum_i\Big(\mathrm{Tr}[\mathcal{V}^S\mathcal{V}^S\Gamma_i]\,R_{\mu\nu} + + \mathrm{Tr}[\mathcal{V}^S\gamma^\alpha\mathcal{V}^S\Gamma_i]\,R_{\mu\nu\alpha}\Big)\,(\Gamma^i)_{ab} \\ &\equiv [G]_{ab}\,R_{\mu\nu} + + [G^\alpha]_{ab}\,R_{\mu\nu\alpha}\end{aligned} \tag{2.51}$$

where the sum over i will include the Dirac matrices $\Gamma_i = I, \gamma_\mu, \sigma_{\mu\nu}$. Equating terms in (2.51) we obtain

$$
\begin{aligned}
f_1 &= 2\,\Phi_1^S\,\Phi_2^S\,\delta, & f_2 &= 2\,\Phi_1^S\,\Phi_3^S\,\delta,\\
f_3 &= \left(2\,\Phi_2^S\,\Phi_3^S + 2\,p\cdot k\,(\Phi_4^S)^2\right)\delta, & f_4 &= \left(2\,(\Phi_2^S)^2 - 2\,k^2\,(\Phi_4^S)^2\right)\delta,\\
f_5 &= \left(2\,(\Phi_3^S)^2 - 2\,p^2\,(\Phi_4^S)^2\right)\delta, & f_6 &= \left(2\,\Phi_2^S\,\Phi_3^S + 2\,p\cdot k\,(\Phi_4^S)^2\right)\delta,\\
f_7 &= \left((\Phi_1^S)^2 - (p\,\Phi_2^S + k\,\Phi_3^S)^2 + (p^2k^2-(p\cdot k)^2)\,(\Phi_4^S)^2\right)\delta, & & \qquad (2.52)\\
f_8 &= -4\,k\cdot(p\,\Phi_2^S + k\,\Phi_3^S)\,\Phi_4^S\,\delta, & f_9 &= 4\,p\cdot(p\,\Phi_2^S + k\,\Phi_3^S)\,\Phi_4^S\,\delta,\\
f_{10} &= 8\,\Phi_2^S\,\Phi_3^S\,\delta, & f_{11} &= 8\,\Phi_3^S\,\Phi_4^S\,\delta,\\
f_{12} &= \left((\Phi_1^S)^2 + p^2(\Phi_2^S)^2 + k^2(\Phi_3^S)^2 + (p^2k^2-(k\cdot p)^2)\,(\Phi_4^S)^2 + 2p\cdot k\,\Phi_2^S\,\Phi_3^S\right)\delta,\\
f_{13} &= 2\,\Phi_1^S\,\Phi_2^S\,\delta, & f_{14} &= 2\,\Phi_1^S\,\Phi_3^S\,\delta, & f_{15} &= 4\,\Phi_1^S\,\Phi_4^S\,\delta,
\end{aligned}
$$

where $\delta \equiv \delta([p-k]^2 - m_R^2)$, and m_R is the mass of on-shell recoil (spectator) quark system. At this stage an objection may be raised about assigning a finite value to the mass of a coloured system of a nucleon with a quark removed. The usual justification for doing this is that because the interaction time in DIS is very short (see Section 2.1.1) this spectator state will not have time to develop into an asymptotic state with infinite mass. For the sake of simplicity we further assume that only valence quarks are present, so that the quark spectator system may be identified with a diquark. In a more refined calculation one could, for example, integrate over diquark masses using some diquark spectral function.

Calculating the functions Φ_{1-4}^S from first principles amounts to solving the relativistic, many-body, bound-state problem. Because present day technology does not yet allow this to be done, one solution could be to try and relate these to quark wavefunctions taken from bag models, or non-relativistic quark models, for example. This, however, implies approximations whose validity can be disputed. Rather than proceed in this direction, we shall choose a single scalar vertex, say $\mathcal{V}^S = I\,\Phi_1^S$, and use phenomenological input to constrain its functional form. For this particular vertex, we find that only f_7 and f_{12} receive contributions,

$$
f_7 = f_{12} = (\Phi_1^S)^2\,\delta([p-k]^2 - m_S^2) \qquad \text{[scalar vertex]}. \qquad (2.53)
$$

For the vector vertex we can repeat the above reduction, this time with many more terms on the right hand side of (2.52), since there are many more combinations of vertex functions (total of $11^2/2+11/2 = 66$ terms!). For simplicity, we choose for the vector vertex a single form, $\mathcal{V}^V = \gamma_\alpha \Phi_V^1$, which makes the following contributions:

$$
f_3 = -f_4 = -f_5 = f_6 = -\frac{2\,f_7}{m_V^2} = \frac{2\,f_{12}}{3\,m_V^2} = -\frac{2\,(\Phi_1^V)^2\delta([p-k]^2 - m_V^2)}{m_V^2} \qquad (2.54)
$$

[vector vertex].

In writing Eq.(2.54) we have assumed that the intermediate vector state has a Lorentz structure $-g_{\alpha\beta} + (p_\alpha - k_\alpha)(p_\beta - k_\beta)/m_V^2$, where m_V is the mass of the vector diquark.

Putting everything together we find that the quark distributions in the nucleon are given by:

$$q_0(x) = \frac{1}{16\pi^2}\int \frac{dk_T^2}{(1-x)}\frac{(\Phi_1^S)^2}{(k^2-m^2)^2}\left\{k_T^2+(m+Mx)^2\right\} \tag{2.55}$$

for a scalar spectator diquark, and

$$\begin{aligned} q_1(x) = \frac{1}{16\pi^2}\int \frac{dk_T^2}{(1-x)}\frac{(\Phi_1^V)^2}{m_V^2\,(1-x)^2\,(k^2-m^2)^2}\Big\{&\left(k_T^2+m^2\right)\left(k_T^2+M^2+2m_V^2\right)\\ &-2\,x\left(k_T^2(M^2+m_V^2+m^2)+m(2M^2m+3Mm_V^2+2mm_V^2)\right)\\ &+x^2\left(k_T^2(M^2+m^2+2m_V^2)+6M^2m^2+2M^2m_V^2+12Mmm_V^2+2m^2m_V^2+m_V^4\right)\\ &-2Mx^3\left(2Mm^2+2Mm_V^2+3mm_V^2\right)+M^2x^4\left(m^2+2m_V^2\right)\Big\} \end{aligned} \tag{2.56}$$

for a vector spectator diquark. In (2.55) and (2.56) we have used the fact that

$$\delta\left([k+q]^2-m^2\right) = \frac{\delta\left(k_+ + q_+\right)}{q_-} \tag{2.57}$$

and

$$\delta\left([p-k]^2-m_R^2\right) = \frac{1}{(M-k_+)}\delta\left(k_- - M - \frac{k_T^2+m_R^2}{k_+-M}\right) \tag{2.58}$$

to fix the values of $k_+ = -q_+$, and $k_- = M + (k_T^2+m_R^2)/(k_+ - M)$. Note that here $q_+ = -Mx$, where $x = -q^2/2p\cdot q = -q_+/p_+$.

In the massless quark limit the quark distributions reduce to the simple forms

$$q_0(x)|_{m=0} = \frac{1}{16\pi^2}\int \frac{dk_T^2}{(1-x)}\frac{(\Phi_1^S)^2}{k^4}\left\{k_T^2+M^2x^2\right\} \tag{2.59}$$

and

$$\begin{aligned} q_1(x)|_{m=0} = &\frac{1}{16\pi^2}\int \frac{dk_T^2}{(1-x)}\frac{(\Phi_1^V)^2}{k^4}\\ &\times\left\{\frac{k_T^4+xm_V^2(2k_T^2+xm_V^2)}{m_V^2(1-x)^2}+\frac{k_T^2\,M^2}{m_V^2}+2k_T^2+2M^2x^2\right\} \end{aligned} \tag{2.60}$$

for scalar and vector spectators, respectively.

2.3.2 Numerical Results

We can easily relate the scalar and vector distributions to the flavour distribution functions in the proton by using an SU(4) symmetric proton wavefunction. DIS from the valence d quark requires that the uu spectators be in a spin 1 — isospin 1 state, while for a valence u quark the spectator can be in either spin 0 — isopin 0 or spin 1 — isospin 1 states,

$$d_V(x) = q_1(x) \tag{2.61}$$

$$u_V(x) = \frac{1}{2}\left(q_1(x)+3q_0(x)\right) \tag{2.62}$$

where the distributions q_0 and q_1 are normalised to unity,

$$\int_0^1 dx\; q_0(x) = \int_0^1 dx\; q_1(x) = 1. \tag{2.63}$$

The k^2-dependence of the functions $\Phi_1^{S,V}$ can most easily be modelled by considering the phenomenology of the nucleon structure function. To obtain the correct large-x behaviour, namely $W_T \sim (1-x)^3$, the leading k^2 dependence in the vertex functions must be $1/k^2$, since the quark four-momentum squared is

$$\begin{aligned} k^2 &= -\frac{k_T^2}{1-x} - \frac{x}{1-x}\left(m_R^2 - (1-x)\,M^2\right) \\ &\sim -\frac{k_T^2 + m_R^2}{1-x} \quad \text{as } x \to 1. \end{aligned} \tag{2.64}$$

This is clear after we also take into account the $\sim 1/k^4$ behaviour in the two quark propagators. Furthermore, since the large-x limit is known to be dominated by u quarks, and as it is only through DIS from valence u quarks that the scalar vertex function enters, we can conclude that Φ_1^S must have a monopole form for its k^2-dependence. The k^2 dependence of the vector vertex function, Φ_1^V, can be fixed by considering the large-x limit of the d_V/u_V ratio, which is known to behave as $\sim (1-x)$ [15]. This requires that the vertex function for DIS from d quarks have $(1-x)^4$, or $(k^2)^{-5/2}$, behaviour (as there is an additional $(1-x)^{-2}$ factor arising from the trace for the vector diquark).

It may now seem reasonable to choose a simple monopole form for the scalar vertex function, and an equivalent one for the vector vertex as was done, for example, in [46]. However, in this naive approach there lurks a problem. At small values of m the quark propagator $(k^2 - m^2)^{-2}$ in (2.42) contains a pole in the physical region of k^2, since the kinematic maximum for k^2 is $(M - m_R)^2$, which occurs when $k_T^2 = 0$ and $x = 1 - m_R/M$. Obviously when the sum of the quark and diquark masses is less than the mass of the nucleon, $m_R + m < M$, the quark propagator becomes singular. This is in fact an indication that the model thus far is incomplete, and the missing ingredient is colour. Without the imposition of confinement, there is nothing in the above to stop the nucleon from decaying into its quark and diquark constituents. One way around this problem is to artificially assign very large masses to the interacting quark and spectator diquark to prevent decay [46]. However, this is not a very attractive solution, since confinement occurs not because the quark mass is large (it is only a few MeV at most), but in a dynamical way due to the nature of the colour interaction. The only place where the information about colour confinement can enter in this model is through the relativistic quark–nucleon vertex function. We can guarantee that the infinite contribution from a deconfined quark is excluded by suitably choosing a numerator in $\Phi_1^{S,V}$ so that the integrand in the structure function is finite at the on-shell point, $k^2 = m^2$.

For the masses of the scalar and vector diquark, m_S and m_V, the only information available to us is that from low energy quark or bag models. There, at a scale of $Q^2 = Q_0^2 \sim$ a few hundred MeV, the diquark masses are expected to be somewhere within the range of 600 to 1100 MeV [47]. Furthermore, from the nucleon–$\Delta(1232)$ mass splitting we would also anticipate that m_V would be some 200 MeV larger than m_S [48].

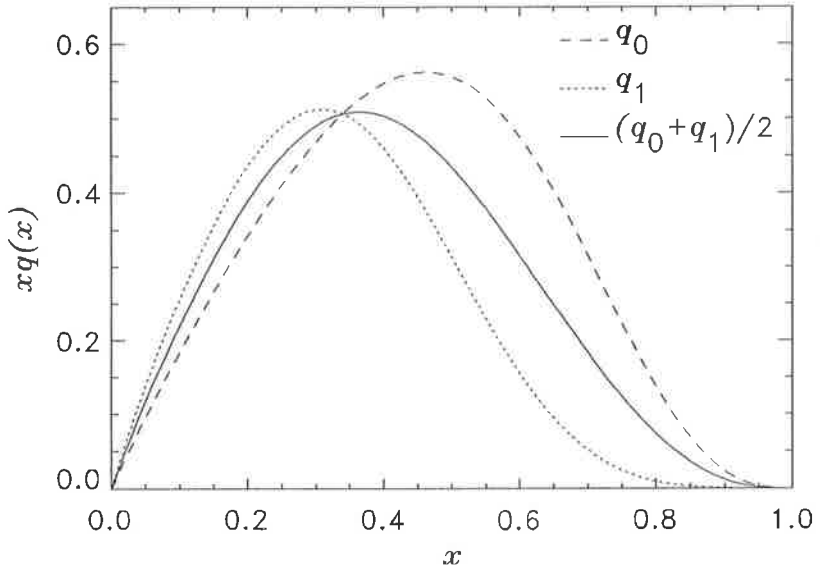

Figure 2.6: Quark distribution functions for scalar and vector spectators.

The final form for the vertex functions that we use is

$$\begin{aligned} \Phi_1^S(k^2) &= N_S \frac{(k^2-m^2)}{(k^2-\Lambda_S^2)^2} \\ \Phi_1^V(k^2) &= N_V \frac{(k^2-m^2)}{(k^2-\Lambda_V^2)^{7/2}} \end{aligned} \tag{2.65}$$

with the constants N_S and N_V determined by the normalisation condition, Eq.(2.63).

As expected with these vertex functions, the quark distribution for a vector spectator is softer than that with a scalar spectator, Fig.2.6. This figure is plotted with diquark masses of $m_S = 850$ MeV and $m_V = 1050$ MeV. Decreasing the diquark masses makes both the scalar and vector distributions harder, as seen in Fig.2.7. Thus smaller masses would imply having to use a lower value of Q_0^2 from which to evolve. There is also some sensitivity to the vertex form factor cut-offs $\Lambda_{S,V}$, with the effect being that the distributions move to larger x with increasing cut-off mass.

As outlined above, on purely theoretical grounds small, or zero, quark masses are preferable in the present context, hence we set $m = 0$ in our calculated distributions. Increasing the interacting quark mass from 0 to 4–5 MeV (as would be appropriate to a current quark mass) has negligible effect. However, large quark masses (~ 300 MeV), as in [46], would make the resulting distributions slightly broader, Fig.2.7.

We find the best fit to the experimental nucleon distributions (as parameterised by Morfin and Tung [50] and Owens [51] at $Q^2 = 4$ GeV^2) for masses $m_S = 850$ MeV and $m_V = 1050$ MeV, and cut-offs $\Lambda_S = 1.2$ GeV and $\Lambda_V = 1.0$ GeV (the curves are evolved from $Q_0^2 = 0.15$ GeV^2 using leading order QCD evolution, with $\Lambda_{QCD} = 250$ MeV [49]). The fits to the $u_V + d_V = 3(q_0 + q_1)/2$ valence quark distribution as well as the valence d_V/u_V are shown in Figs.2.8 and 2.9 respectively. It is remarkable that such a simple model for the vertex functions reproduces the data so well.

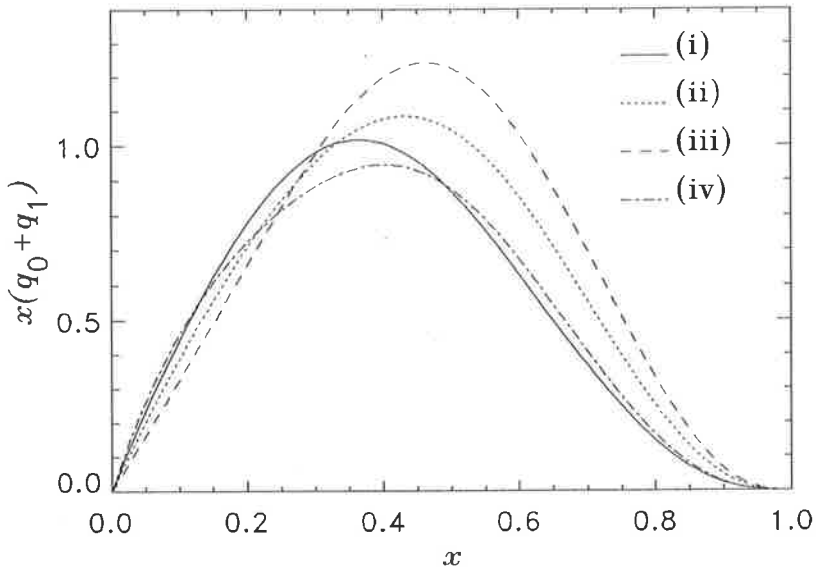

Figure 2.7: Comparison of the total u_V+d_V valence quark distribution, for (i) $\Lambda_{S(V)} = 1.2(1.0)$ GeV, $m_{S(V)} = 850(1050)$ MeV, and $m = 0$; (ii) increasing the vertex function cut-offs to $\Lambda_{S(V)} = 1.5(1.3)$ GeV; (iii) decreasing the spectator masses to $m_{S(V)} = 650(850)$ MeV; (iv) using a very large quark mass $m = 300$ MeV.

To conclude this chapter, let us point out again the new developments that have been made in the calculation of nucleon structure functions. With the expansion of the truncated nucleon tensor we have been able to unambiguously identify the scaling components by calculating the 'handbag' diagram, Fig.2.4. The formalism allows a clear separation of the Q^2-dependent quantities from those which describe the non-perturbative, quark–nucleon interaction. This is consistent with the operator product expansion for the total nucleon tensor. By simple choice for the form of the nucleon–quark vertex and parameterisations of the vertex functions, we have been able to accurately reproduce the experimental valence quark distributions. One element that is missing, however, is the sea distributions. These can of course be generated perturbatively via the QCD evolution equations in Section 2.1.4. However, an interesting possibility is that there may in fact exist a non-perturbative sea component of the nucleon, which cannot be generated by QCD evolution. That is, there may be an intrinsic antiquark component of the nucleon at low Q^2. This will be the subject of the next chapter.

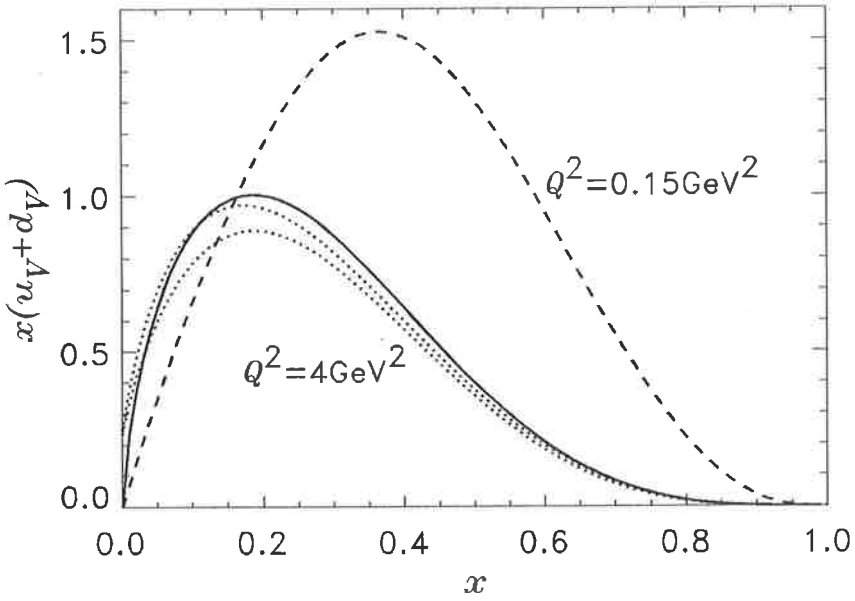

Figure 2.8: Total $u_V + d_V$ valence quark distribution, evolved from $Q_0^2 = 0.15$ GeV^2 (dashed curve) to $Q^2 = 4$ GeV^2 (solid curve). The data (dotted curve) are from recent parameterisations of world data.

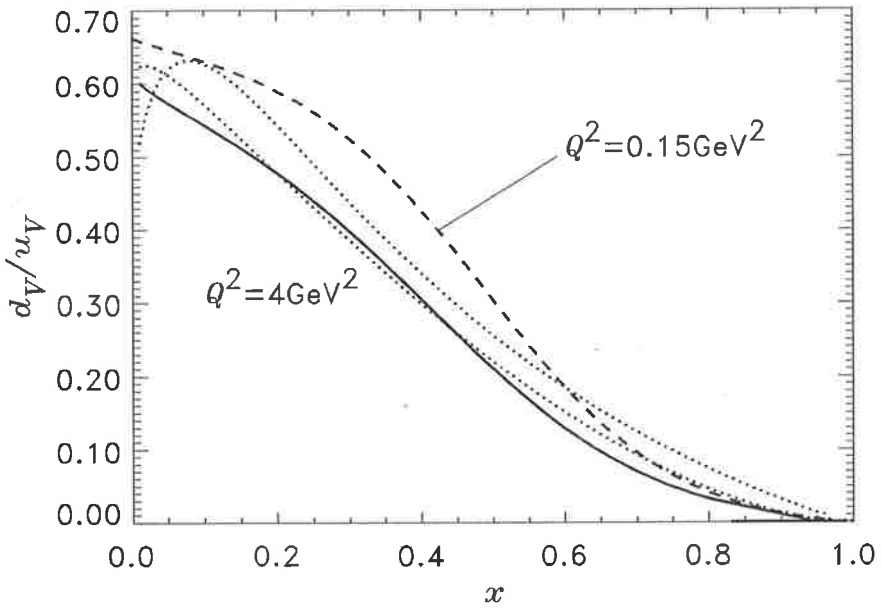

Figure 2.9: Valence d_V/u_V ratio, evolved from $Q_0^2 = 0.15$ GeV^2 (dashed) to $Q^2 = 4$ GeV^2 (solid), and compared with a parameterisations of world data (dotted).

Chapter 3

FLAVOUR CONTENT OF THE PROTON

From the successes of quark models we view many properties of the nucleon as arising from its simple valence quark structure. Models such as the non-relativistic quark model, or the various bag or soliton models can be thought of as describing the valence structure of the nucleon at small momentum scales, $Q \sim$ few hundred MeV. At larger Q^2, however, the total nucleon structure function becomes softer (i.e. grows at small x and becomes smaller at large x). As we saw in Chapter 2, this phenomenon is quite nicely described by perturbative QCD — quarks radiate gluons, which then split into pairs of sea quarks and antiquarks [43]. Therefore the number of quarks increases, but since momentum must be conserved, the average momentum carried by these quarks decreases. Thus, while at low Q^2 valence quarks should carry most (if not all) of the nucleon's momentum (in an infinite momentum frame), at $Q^2 \sim$ few GeV^2 they carry only some 30% of the total momentum, with the remainder residing on the sea quarks (and gluons).

Successful as perturbative QCD is in describing the Q^2 evolution of the quark and antiquark distributions, we are still unable to calculate from first principles the distributions themselves. Some progress in connecting low energy valence quark models with the valence quark distributions in DIS has been made [35–42], although, less is known about how to calculate the sea quark distributions non-perturbatively. While it is possible for all of the sea to be generated via QCD evolution, there are nevertheless a number of good reasons for having a *non-perturbative sea* in the nucleon. It was pointed out by Signal and Thomas [38], using the formalism developed by Jaffe and others [52], that even in a simple model like the MIT bag, there should be a component of the total quark distribution which is non-valence, and that an intrinsic antiquark component should be present as well. Furthermore, some of the properties of this intrinsic sea, such as an asymmetry between the $\bar{d}$ and $\bar{u}$ quark distributions, are very different from those expected from perturbative QCD alone.

In this chapter we discuss a specific model (Section 3.1) in which the physical nucleon is seen as a superposition of bare nucleon and virtual meson and baryon states, the latter which contribute to the non-valence quark distributions. In Sections 3.2 and 3.3 we follow this up with comparisons

of some of the predictions of this model with recent data on the nucleon deep inelastic structure functions, as well as a survey of possible future experiments.

3.1 Mesons in the Nucleon — A Model of the Nucleon Sea

Simply on the basis of the Heisenberg uncertainty principle we know that the long range structure of the nucleon must involve a pion cloud. For example, the non-zero value for the neutron charge radius can be easily understood in terms of the emission from a neutron of a light, negatively charged virtual pion, $n \to p + \pi^-$. Furthermore, from PCAC, and from the tremendous successes of chiral quark models [53–56] we expect that the nucleon should have a pion cloud. In addition, because there is no scale at which chiral symmetry can be ignored, the nucleon properties will have pionic corrections at all Q^2.

The possible relevance of the extended pionic structure of the nucleon in high energy processes, such deep inelastic scattering, was first suggested by Sullivan in the early 1970s [57]. It was shown that the contribution to the inclusive virtual photon—nucleon cross section from pion exchange between the virtual photon and the nucleon scales in the Bjorken limit. The reason for this is that, in contrast to processes such as exclusive pion-production which are suppressed by $O(1/Q^2)$ form factors, here it is the inelastic structure function of the pion itself that is probed.

Using this picture of the physical nucleon, it was later noticed [58] that the pion cloud could be responsible for generating an asymmetry between the $\bar{u}$ and $\bar{d}$ quark content of the proton, through the preferred proton dissociation into a neutron and π^+. Furthermore, deep inelastic scattering data on the momentum fractions carried by antiquarks were used to obtain an upper limit on this non-perturbative pionic component [58, 59]. More recently it has been hypothesised [47,60–63] that this asymmetry could account for some of the apparent discrepancy between the naive parton model prediction for the Gottfried sum rule [64] and its recently determined experimental value [65].

Since it has by far the smallest mass, the pion was the first meson whose contributions to the nucleon structure function were investigated [66, 67]. However, just as other mesons can be included to give corrections to low energy nucleon properties, such as the electromagnetic nucleon form factors or magnetic moments [68], an extended mesonic structure of the nucleon may also be relevant in deep inelastic scattering. This idea has been taken seriously, for example, by Speth and collaborators [62, 69], who have argued that the entire nucleon sea can be understood in terms of DIS from its virtual meson components, even at moderate Q^2.

In this section we shall give a detailed account of the calculation of the virtual meson and baryon contributions to the nucleon structure functions. Furthermore, we will use recent DIS data to examine the extent to which such a picture may be relevant in high energy reactions.

The basic hypothesis of this model, in which the nucleon has internal meson and baryon degrees of freedom, is that the physical nucleon state (in an infinite momentum frame) can be expanded (in

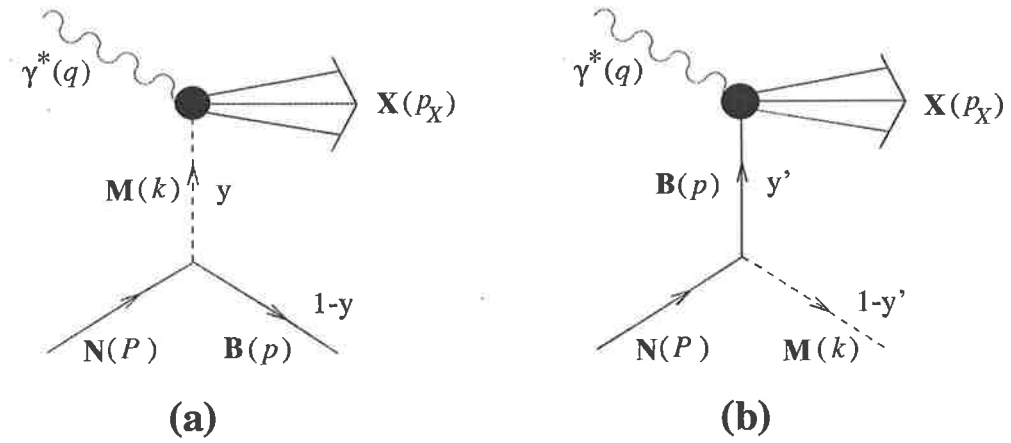

Figure 3.1: Deep inelastic scattering from the virtual (a) meson and (b) baryon components of a physical nucleon.

the one-meson approximation) in a series involving bare nucleon and two-particle meson—baryon states

$$|N\rangle_{\rm phys} = \sqrt{Z}\ \{|N\rangle_{\rm bare} + \sum_{MB}\int dy\ d^2\mathbf{k}_T\ g_{0_{MBN}}\ \phi_{MB}(y,\mathbf{k}_T)\ |M(y,\mathbf{k}_T);B(1-y,-\mathbf{k}_T)\rangle\ \}\,. \tag{3.1}$$

Here, $\phi_{MB}(y,\mathbf{k}_T)$ is the probability amplitude for the physical nucleon to be in a state consisting of a meson M and baryon B, having transverse momenta $\mathbf{k}_T$ and $-\mathbf{k}_T$, and carrying longitudinal momentum fractions y and $1-y$, respectively. Z is the bare nucleon probability. Although we shall work in the one-meson approximation, we shall include higher order vertex corrections to the bare coupling constants $g_{0_{MBN}}$. Illustrated in Fig.3.1 is the deep inelastic scattering of the virtual photon from the two-particle state $|M;B\rangle$. In Fig.3.1(a) the photon interacts with a quark or antiquark inside the exchanged meson, while in Fig.3.1(b) the scattering is from a quark in the baryon component of the physical nucleon.

According to (3.1), the probability to find a meson inside a nucleon with momentum fraction y $(= k\cdot q/p\cdot q = k_+/p_+)$ is (to leading order in the coupling constant)

$$f_{MB}(y) \equiv Z\ g^2_{0_{MBN}}\int d^2\mathbf{k}_T\ |\phi_{MB}(y,\mathbf{k}_T)|^2\,. \tag{3.2}$$

This must also be the probability to find a baryon inside a nucleon with momentum fraction $1-y$. The baryon distribution function, $f_{BM}(y')$, where $y' = p'\cdot q/p\cdot q$, is probed directly through the process in Fig.3.1(b), and should be related to the meson distribution function by

$$f_{MB}(y) = f_{BM}(1-y) \tag{3.3}$$

for all y, if the above interpretation is valid. We also demand equal numbers of mesons emitted by the nucleon, $\langle n\rangle_{MB} = \int_0^1 dy\ f_{MB}(y)$, and virtual baryons accompanying them, $\langle n\rangle_{BM} = \int_0^1 dy'\ f_{BM}(y')$:

$$\langle n\rangle_{MB} = \langle n\rangle_{BM}. \tag{3.4}$$

This is just a statement of charge conservation. Momentum conservation imposes the further requirement that

$$\langle y \rangle_{MB} + \langle y \rangle_{BM} = \langle n \rangle_{MB} \tag{3.5}$$

where $\langle y \rangle_{MB} = \int_0^1 dy\, y\, f_{MB}(y)$ and $\langle y \rangle_{BM} = \int_0^1 dy'\, y'\, f_{BM}(y')$ are the average momentum fractions carried by meson M and the virtual baryon B, respectively. Equations (3.4) and (3.5), and in fact similar relations for all higher moments of $f(y)$, follow automatically from (3.3).

In what follows we shall explicitly evaluate the functions f_{MB} and f_{BM}, and examine the conditions under which (3.3) is satisfied. The results will be used to calculate the contributions to the nucleon structure function from the extended mesonic structure of the nucleon, which are expressed as convolutions of the functions $f(y)$ with the structure functions of the struck meson or baryon:

$$\delta^{(MB)} F_{2N}(x) = \int_x^1 dy\, f_{MB}(y)\, F_{2M}(x_M) \tag{3.6}$$

$$\delta^{(BM)} F_{2N}(x) = \int_x^1 dy'\, f_{BM}(y')\, F_{2B}(x_B) \tag{3.7}$$

with $x_M = x/y$ and $x_B = x/y'$, and $x = -q^2/2p\cdot q$ being the Bjorken variable, Note that Eqs.(3.6) and (3.7) are correct when physical (renormalised) meson—baryon coupling constants are used in the functions f_{MB} and f_{BM} (see Section 3.1.5 for a discussion on this point). By comparing against the experimental structure functions, we will ultimately test the reliability of the expansion in (3.1), and also the relative importance of the states involving heavier mesons compared with the pion states.

3.1.1 Pions – Covariant Formulation

Let us firstly review the previous calculations of the contribution to F_{2N} from the pion cloud. Following the original method of Sullivan, the approach has been to simply treat the diagram in Fig.3.1(a) as a Feynman diagram. With a pseudoscalar πN coupling, $g_{\pi NN}\bar{u}(p)\, i\gamma_5 u(P)$, the contribution from this diagram to the hadronic tensor of the physical nucleon can be written

$$\delta^{(\pi N)} W^{\mu\nu}(P,q) = \int \frac{d^3\mathbf{p}}{(2\pi)^3(2p_0)} \frac{g^2_{\pi NN}(k^2)}{(k^2-m_\pi^2)^2} \frac{1}{2} \mathrm{Tr}\left[(\not{P}+M)\, i\gamma_5\, W_\pi^{\mu\nu}(k,q)\, (\not{p}+M)\, i\gamma_5\right] \tag{3.8}$$

where the hadronic tensor for the virtual pion is expressed as

$$W_\pi^{\mu\nu} = \tilde{g}^{\mu\nu} W_{1\pi} + \frac{\tilde{k}^\mu \tilde{k}^\nu}{m_\pi^2} W_{2\pi} \tag{3.9}$$

and where $g^2_{\pi NN}(k^2)$ is the interaction strength. [1] It is customary to isolate the k^2 dependence of $g^2_{\pi NN}(k^2)$ into the πNN form factor: i.e. $g^2_{\pi NN}(k^2) = g^2_{\pi NN}\, \mathcal{F}_{\pi N}(k^2)$, where $g_{\pi NN}$ is now the

[1] Since only tree order diagrams are ever considered, the pseudoscalar interaction is equivalent to that with a pseudovector coupling $(f_{\pi NN}/m_\pi)\, \bar{u}(p)\, i\gamma_\alpha\gamma_5\, u(P)\, k^\alpha$, providing the coupling constants are related by $f_{\pi NN} = g_{\pi NN}\, (m_\pi/2M)$.

coupling constant at the pion pole ($\mathcal{F}_{\pi N}(-m_\pi^2) = 1$). To get the contributions to the nucleon structure functions W_1 or W_2 we can use the projection operators defined in Chapter 2. Alternatively, and equivalently, we can observe that one obtains the same results for W_1 (and hence W_2 by the Callan-Gross relation) by collecting $\tilde{g}_{\mu\nu}$ (or simply $g^{\mu\nu}$) terms on both sides of (3.8) [70] to obtain an expression like that in (3.6).

Performing the elementary trace gives a factor $2P \cdot p - 2M^2 = -k^2$, so that the distribution function of a virtual pion accompanied by a recoiling nucleon is [58, 67]

$$f_{\pi N}(y) \;=\; \frac{3g_{\pi NN}^2}{16\pi^2}\, y \int_{-\infty}^{k^2_{max}} dk^2\, \frac{\mathcal{F}_{\pi N}^2(k^2)(-k^2)}{(k^2 - m_\pi^2)^2}. \tag{3.10}$$

Here, $k^2 = k^2_{max} - k_T^2/(1-y)$ is the 4-momentum squared of the virtual pion, with a kinematic maximum given by $k^2_{max} = -M^2y^2/(1-y)$, and k_T^2 is the pion transverse momentum squared. We have also included a factor 3 by taking account of the different charge states of the nucleon (namely 2 for the dissociation process $p \to n\pi^+$ and 1 for $p \to p\pi^0$). In a covariant formulation the form factor, $\mathcal{F}_{\pi N}$, parameterising the πNN vertex, at which only the pion is off-mass-shell, can only depend on k^2. In the literature this is most often parameterised by a simple monopole or dipole function,

$$\mathcal{F}_{\pi N}(k^2) \;=\; \left(\frac{\Lambda_{\pi N}^2 - m_\pi^2}{\Lambda_{\pi N}^2 - k^2}\right)^n \tag{3.11}$$

for $n = 1$ and 2, respectively.

Because we integrate over the recoiling particle's momentum, in principle we could also have contributions from processes where a baryon other than a nucleon (e.g. a Δ isobar) is left in the final state in Fig.3.1(a), and which subsequently decays to a nucleon and a pion. It is expected that contributions from the higher mass baryons will be suppressed relative to the nucleon, since the maximum value of k^2 for which energy and momentum can be conserved when a higher mass baryon is produced decreases rapidly as the mass of the baryon increases. Nevertheless, the importance of the Δ-resonance is well known in pion physics. In any quark model the coupling to the N and Δ would enter on the same footing.

The process where the nucleon emits a pion and leaves behind an on-shell Δ was previously calculated in Refs.[59, 63, 71], using the effective interaction $(f_{\pi N\Delta}/m_\pi)\; \bar{u}_\alpha(p)\; k^\alpha\; u(P)$, where $u_\alpha(p)$ is the spin 3/2 Rarita-Schwinger spinor-vector [72], which can be formed by combining the spin 1/2 Dirac spinor $u(p,s)$ with vectors $\epsilon_\alpha(\lambda)$:

$$u_\alpha(p,S) \;=\; \sum_m \left\langle \frac{3}{2} S \middle| 1m, \frac{1}{2} s \right\rangle\; \epsilon_\alpha(m)\; u(p,s). \tag{3.12}$$

The vectors ϵ_α can be parameterised, in a frame where $p = (p_0;\; \cos\varphi \sin\theta\, |\mathbf{p}|,\; \sin\varphi \sin\theta\, |\mathbf{p}|,\; \cos\theta\, |\mathbf{p}|)$, by

$$\begin{aligned}
\epsilon_\alpha(0) \;&=\; \frac{1}{M_\Delta}(|\mathbf{p}|;\; \cos\varphi \sin\theta\; p_0,\; \sin\varphi \sin\theta\; p_0,\; \cos\theta\; p_0) \\
\epsilon_\alpha(\pm 1) \;&=\; \frac{1}{\sqrt{2}}(0;\; \mp\cos\varphi\cos\theta + i\sin\varphi,\; \mp\sin\varphi\cos\theta - i\cos\varphi,\; \pm\sin\theta).
\end{aligned} \tag{3.13}$$

The energy projection operator for the Rarita-Schwinger spinor-vector is [73]

$$\sum_S u_\alpha(p,S)\bar{u}_\beta(p,S) \;=\; \Lambda_{\alpha\beta}(p) \tag{3.14}$$

where

$$\Lambda_{\alpha\beta}(p) \;=\; (\not{p}+M_\Delta)\left(-g_{\alpha\beta}+\frac{\gamma_\alpha\gamma_\beta}{3}+\frac{\gamma_\alpha p_\beta-\gamma_\beta p_\alpha}{3\,M_\Delta}+\frac{2\,p_\alpha p_\beta}{3\,M_\Delta^2}\right). \tag{3.15}$$

Eq.(3.15) can be verified by using the explicit parameterisation in (3.13). Using this projection operator, we can therefore proceed to evaluate the $\pi\Delta$ trace factor, which in this case is

$$\frac{1}{2}\mathrm{Tr}\left[\Lambda_{\alpha\beta}(p)\;k^\alpha k^\beta\;W_\pi^{\mu\nu}(k,q)\;(\not{p}+M)\right] \tag{3.16}$$

and arrive at the distribution function for a pion with a Δ recoil:

$$f_{\pi\Delta}(y)=\frac{4}{3}\frac{f_{\pi N\Delta}^2}{16\pi^2\;m_\pi^2}\;y\int_{-\infty}^{k^2_{max}}dk^2\;\frac{\mathcal{F}^2_{\pi\Delta}(k^2)}{(k^2-m_\pi^2)^2}\frac{\left[(M+M_\Delta)^2-k^2\right]^2\left[(M-M_\Delta)^2-k^2\right]}{6\;M_\Delta^2} \tag{3.17}$$

where now the kinematic upper limit on k^2 is $k^2_{max}=-(M_\Delta^2\;-\;(1-y)\;M^2)\;y/(1-y)$. Note that a dipole function for the $\pi N\Delta$ form factor is necessary to suppress contributions from large $|k^2|$.

Contributions from higher mass baryon resonances can all be computed from the above since the lower lying states all have spin 1/2 or 3/2. For the (spin 1/2) Roper resonance, which with a mass $M_R=1440$ MeV is the next heaviest state after the Δ, the trace factor is

$$\frac{1}{2}\mathrm{Tr}\left[(\not{p}+M)\;i\gamma_5\;(\not{p}+M_R)\;i\gamma_5\right] \;=\; -k^2+(M_R-M)^2. \tag{3.18}$$

With a πNR coupling constant of $g^2_{\pi NR}/4\pi\approx 5.4$ [74] the integral over y of the pion distribution function for a recoil Roper resonance comes to about 10% of that with a nucleon recoil for the same cut-off parameter. Furthermore, the pion distribution function with a Roper recoil appears at somewhat smaller y than $f_{\pi N}$ or $f_{\pi\Delta}$, which means that the convolution in Eq.(3.6) with the Roper distribution function will only be potentially relevant at very small x. Furthermore, because the Roper has the same quantum numbers as the nucleon, its inclusion as an incoherent contribution is somewhat less justified. In what follows we shall therefore restrict ourselves to the nucleon and Δ baryons only.

In order to conserve momentum and charge, we must also allow for the incident photon to scatter from the recoiling N or Δ after a pion has been emitted, Fig.3.1(b). Previous attempts at calculating the contributions from these processes within a covariant framework were made by several authors, including Hwang et al. [62], Mulders et al. [17], and Dmitrašinović et al. [75], although all obtained different results. Partly because there is less phenomenological experience with so-called sideways form-factors (where the nucleon, rather than the pion, is off-mass-shell) some early work [47, 63, 76] simply defined $f_{N\pi}(y')$ through (3.3). However, this is unsatisfactory from a theoretical point of view, and ideally we should be able to verify explicitly that within our model the functions $f_{\pi N}$ and $f_{N\pi}$ satisfy Eq.(3.3). In historical terms, it was the careful examination

of this process that opened up a whole Pandora's box of problems, and led to the realisation of the terminal shortcomings of the covariant convolution model. We shall go more deeply into this issue in Chapter 5, but for now let us briefly summarise the origin of the problem.

Clearly the treatment of deep inelastic scattering from an interacting nucleon is considerably more involved than that from a free nucleon. As we saw in Chapter 2, the truncated nucleon tensor $\widehat{W}_{\mu\nu}$ which enters this calculation can be written as a linear combination of three independent terms. Initial calculations [17] assumed that only the term involving the operator $\not{q}$ was relevant. For pointlike nucleons this operator would indeed be the only one present, just as it is for a point-like quark inside a nucleon [52]. Treating the diagram in Fig.3.1(b) as a Feynman diagram, the contribution to the on-shell nucleon tensor from DIS off the virtual (structured) nucleon with a pion in the final state can be written

$$\begin{aligned} \delta^{(N\pi)}W^{\mu\nu}(P,q) &= g^2_{\pi NN}\int \frac{d^3\mathbf{k}}{(2\pi)^3(2k_0)}\frac{\mathcal{F}^2_{N\pi}(p^2)}{(p^2-M^2)^2} \\ &\quad \times\frac{1}{2}\mathrm{Tr}\left[(\not{P}+M)\,i\gamma_5\,(\not{p}+M)\,\widehat{W}^{\mu\nu}_N(p,q)\,(\not{p}+M)\,i\gamma_5\right] \end{aligned} \tag{3.19}$$

with the tensor $\widehat{W}^{\mu\nu}_N(p,q)$ as defined in (2.36). Using only the operator $\not{q}$ leads to the virtual nucleon distribution function of Ref.[17], namely

$$f_{N\pi}(y') = \frac{3g^2_{\pi NN}}{16\pi^2}\,y'\int_{-\infty}^{p^2_{max}} dp^2\,\frac{\mathcal{F}^2_{N\pi}(p^2)}{(p^2-M^2)^2}\left(-m^2_\pi-\frac{1-y'}{y'}(p^2-M^2)\right) \tag{3.20}$$

where $p^2 = p^2_{max} - p^2_T/(1-y')$ is the 4-momentum squared of the virtual nucleon, with the upper limit now given by $p^2_{max} = M^2y' - m^2_\pi y'/(1-y')$, and p^2_T denotes the nucleon's transverse momentum squared. Apart from possible differences in the form factors, (3.10) and (3.20) are clearly related by an interchange $y' \leftrightarrow 1-y$.

The large-$|p^2|$ suppression for the $N\pi N$ vertex is introduced by the form factor $\mathcal{F}_{N\pi}$, which is usually parameterised by a monopole or dipole function [17, 77, 78]

$$\mathcal{F}_{N\pi}(p^2) = \left(\frac{\Lambda^2_{N\pi}-M^2}{\Lambda^2_{N\pi}-p^2}\right)^n \tag{3.21}$$

for $n = 1$ and 2, respectively. However to satisfy (3.4), the cut-off parameter $\Lambda_{N\pi}$ will in general have to be different from the cut-off $\Lambda_{\pi N}$ regulating the πNN vertex form factor in (3.10), and a different $\Lambda_{N\pi}$ again to satisfy (3.5). Furthermore, because the k^2_T and p^2_T dependence in the form factors in Eqs.(3.11) and (3.21) are clearly different, the calculated distribution functions $f_{\pi N}$ and $f_{N\pi}$ will in general not satisfy (3.3). In Fig.3.2 we plot $f_{\pi N}(y)$ and $f_{N\pi}(1-y)$ for dipole form factors, and cut-offs $\Lambda_{\pi N} = 1$ GeV and $\Lambda_{N\pi} = 1475$ MeV, respectively (to give the same values for $\langle n\rangle_{\pi N}$ and $\langle n\rangle_{N\pi}$, namely ≈ 0.235. Clearly the shapes are quite different, the most obvious difference being that $f_{N\pi}(1-y)$ is finite at $y = 1$.

By using only one operator $\not{q}$ in (3.19) we are of course assuming that the entire structure function of the virtual nucleon can be represented by the function $\widehat{W}^2_T$ in (2.36). As we saw in Section 2.3 in the model calculation of the nucleon structure function, using simple quark–nucleon

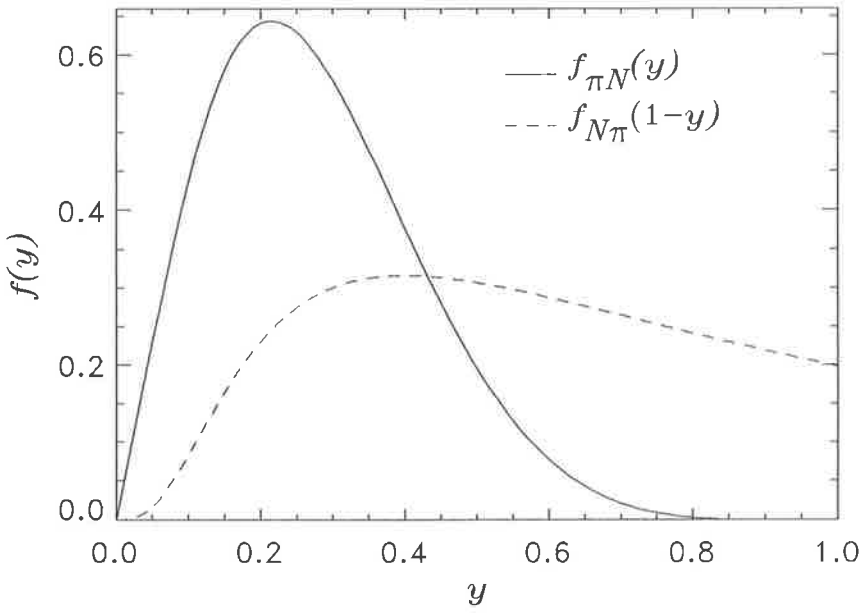

Figure 3.2: Distribution functions $f_{\pi N}(y)$ and $f_{N\pi}(1-y)$ with dipole form factors, and cut-offs $\Lambda_{\pi N} = 1$ GeV and $\Lambda_{N\pi} = 1475$ MeV chosen to give $\langle n \rangle_{\pi N} = \langle n \rangle_{N\pi} = 0.235$.

relativistic vertex functions generally leads to non-zero scaling contributions from other functions as well. For example, for the scalar quark–nucleon vertex considered there, the contribution from the $\widehat{W}_T^1$ term was (for $m = 0$) $\propto 2x^2M^2$, while the $\widehat{W}_T^2$ piece was $\propto k_T^2 - x^2M^2$. Combined, they give the full result, namely $k_T^2 + x^2M^2$, Eq.(2.59). But simply keeping the $\not{q}\widehat{W}_T^2$ term would give non-physical answers at small k_T and large x — negative contributions! In practice, what is usually done is that the experimental nucleon structure function is inserted in (3.7), rather than any calculated function. Furthermore, choosing a different operator form for $\widehat{W}_N^{\mu\nu}$ can also lead to unphysical results. For example, with an operator involving I rather than $\not{q}$ the trace factor in (3.19) is proportional to $-m_\pi^2$ (i.e. negative). This appears to have been done in [75], although in view of this it is rather perplexing that their final result appears positive.

Problems also arise for the emission of scalar mesons, for which the trace factor in $f_{N\sigma}(y')$ for the structure $\not{q}$ is $4M^2 - m_\sigma^2 + (M^2 - p^2)(1-y')/y'$, which is clearly related to the trace in $f_{\sigma N}(y)$ (namely $k^2 + 4M^2$) when written in terms of the transverse momentum squared – apart from the form factor. For an operator I, the trace factor in $f_{N\sigma}(y')$ is $2p^2 + 2M^2 - m_\sigma^2$, which not only violates baryon number conservation but also leads to an unphysical (negative) cross section. For the DIS from a virtual Δ component, these same difficulties will also be present, since the Δ hadronic tensor will have a non-trivial spinor structure, similar to that for the nucleon.

These are the first hints of problems with the covariant approach to calculating DIS processes involving virtual nucleons. Indeed, the convolution formula in (3.7) appears to be a very special case that cannot be easily obtained from the above considerations. The prescription of ignoring some of the structures in $\widehat{W}_N^{\mu\nu}$ is clearly unsatisfactory, as in principle all should be used. Another

important assumption in the covariant convolution model is that the dependence of the virtual meson and baryon structure functions in (3.6) and (3.7) on the particles' invariant mass squared is negligible. The argument usually made is that the vertex form factor suppresses contributions from the far off-mass-shell configurations (i.e. for $|k^2| \gtrsim 10\ M^2$ [63]). However, strictly speaking, in this approach even the identification of the off-shell structure functions themselves is not very clear. Some suggestions about how to relate the off-shell functions to the on-shell ones were made [79, 80] in the context of DIS from nuclei, although these were more *ad hoc* prescriptions rather than theoretical derivations. More importantly, a covariant treatment of DIS from virtual nucleons essentially involves both nucleon and antinucleon degrees of freedom. In contrast to this, the Fock state expansion in (3.1), and in particular the interpretation of $f(y)$ as meson and baryon probability functions, is only meaningful in the IMF. Thus, simply put, the difficulties encountered in trying to obtain sensible results from the covariant calculation of $f(y)$ result from an incompatibility of the covariant formalism with the initial hypothesis that the physical nucleon state can be expanded as in Eq.(3.1).

A full investigation of the off-mass-shell effects in deep inelastic structure functions of composite objects will be the subject of Chapter 5, where we discuss how to calculate structure functions of composite particles in a covariant formalism, without making any on-shell approximations. However, it is clear that a naive application of Feynman rules to the process involving DIS from an off-shell nucleon is highly problematic, and certainly requires great care. The challenge is therefore to formulate the problem self-consistently, using a single formalism. Since we would like to study the relevance of the virtual meson cloud of the nucleon, the most economical solution would be to keep the Fock state expansion in (3.1), and reformulate the rest of the problem in time-ordered perturbation theory (TOPT), where Eq.(3.1) is well defined. In fact, an early calculation of the function $f_{\pi N}(y)$ in TOPT was performed some time ago by Güttner et al. [81], in the context of pion electroproduction. More recently the merits of this approach were expounded by Zoller [82], who demonstrated that the distribution functions for the πN and $\pi\Delta$ states calculated in this fashion could satisfy (3.3).

3.1.2 Pions – TOPT in the IMF

An alternative to the use of covariant Feynman diagrams, in the form of 'old-fashioned' time-ordered perturbation theory in the IMF, was proposed some time ago by Weinberg [83] for scalar particles. This was later extended by Drell, Levy and Yan [84] to the πN system in deep inelastic scattering. The main virtues of this approach are that off-mass-shell ambiguities in the structure functions of virtual particles can be avoided, and that the meson and baryon distribution functions can be shown to satisfy (3.3) exactly. We firstly review the results for the pion cloud, and then compare these with the previous, covariant calculations.

In the time-ordered theory the analogue of Fig.3.1(a) will now involve two diagrams in which the pion moves forwards and backwards in time, Fig.3.3. However, in a frame of reference where

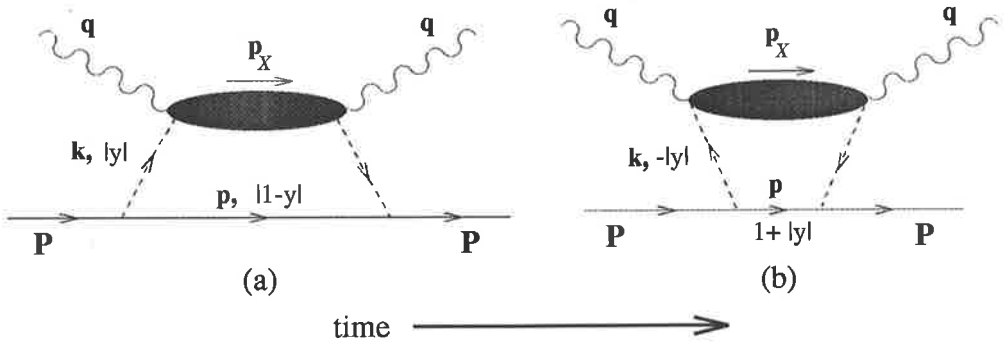

Figure 3.3: Time-ordered diagrams for pions moving (a) forwards and (b) backwards in time. Time is increasing from left to right.

the target nucleon is moving fast in the z direction with longitudinal momentum $P_L(\to \infty)$, only that diagram involving a forward moving pion gives a non-zero contribution. In the IMF the target nucleon of momentum $\mathbf{P} = (0_T, P_L)$ has energy

$$P_0 = P_L + \frac{M^2}{2P_L} + O\left(\frac{1}{P_L^2}\right). \tag{3.22}$$

Following Weinberg [83] we write the pion 3-momentum as

$$\mathbf{k} = y\,\mathbf{P} + \mathbf{k}_T \tag{3.23}$$

where $\mathbf{k}_T \cdot \mathbf{P} = 0$, and conservation of momentum demands that the recoil nucleon momentum be

$$\mathbf{p} = (1-y)\,\mathbf{P} - \mathbf{k}_T. \tag{3.24}$$

Since all particles are on their mass shells the energies of the intermediate meson and baryon must be

$$k_0 = |y|\,P_L + \frac{k_T^2 + m_\pi^2}{2\,|y|P_L} + O\left(\frac{1}{P_L^2}\right) \tag{3.25}$$

$$p_0 = |1-y|\,P_L + \frac{k_T^2 + M^2}{2\,|1-y|P_L} + O\left(\frac{1}{P_L^2}\right). \tag{3.26}$$

For forward moving particles, Fig.3.3(a), y and $1-y$ are positive, and applying the rules of TOPT [83] the contribution to the hadronic tensor of the physical nucleon can be written

$$\begin{aligned}\delta^{(\pi N)}W^{\mu\nu}(P,q) = \int & \frac{d^3\mathbf{k}}{(2\pi)^3(2p_0)(2k_0)^2}\frac{g^2_{\pi NN}(k)}{(P_0-p_0-k_0)^2} \\ & \times\frac{1}{2}\mathrm{Tr}\left[(\not{p}+M)\,i\gamma_5\,W_\pi^{\mu\nu}(p,q)\,(\not{P}+M)\,i\gamma_5\right].\end{aligned} \tag{3.27}$$

The energy denominator in (3.27) can be rewritten as $(P_0 - p_0 - k_0) = (M^2 - s_{\pi N})/2P_L$, where

$$s_{\pi N} = s_{\pi N}(k_T^2, y) = (p_0+k_0)^2 - (\mathbf{p}+\mathbf{k})^2 = \frac{k_T^2+m_\pi^2}{y} + \frac{k_T^2+M^2}{1-y} \tag{3.28}$$

is the centre of mass energy squared of the intermediate πN state. Changing the variables of integration from $d^3\mathbf{k}$ to dy and dk_T^2, all powers of P_L are seen to cancel when combined with

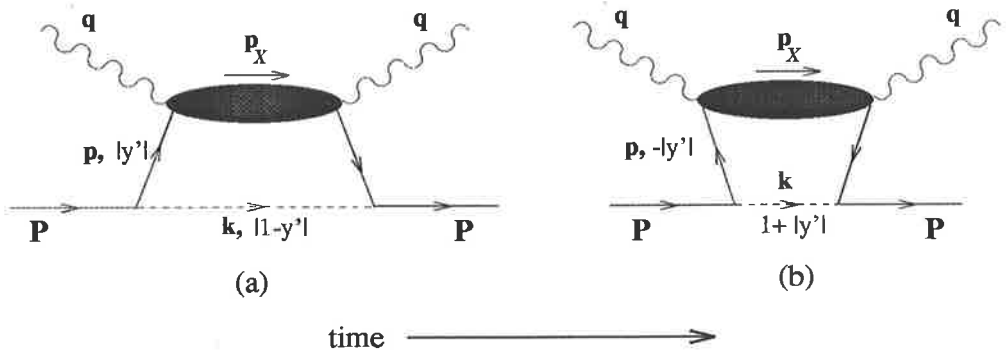

Figure 3.4: Time-ordered diagrams for nucleons moving (a) forwards and (b) backwards in time.

the vertex factors, $(2p_0)^{-1}$ and $(2k_0)^{-2}$, leading to a result that is P_L-independent. Equating coefficients of $g_{\mu\nu}$, we find that the π distribution function with an N recoil is

$$f_{\pi N}(y) = \frac{3g^2_{\pi NN}}{16\pi^2}\int_0^\infty \frac{dk_T^2}{(1-y)}\frac{\mathcal{F}^2_{\pi N}(s_{\pi N})}{y\,(M^2-s_{N\pi})^2}\left(\frac{k_T^2+y^2M^2}{1-y}\right) \tag{3.29}$$

which means that the result of (3.10) is reproduced, form factor aside. Obviously because here all particles are on-mass-shell, we cannot use the same k^2-dependent form factor as in the covariant case. In the time-ordered calculation, it is quite natural to choose the form factor to be a function of the centre of mass energy squared of the πN system, $s_{N\pi}$, as was done by Zoller [82]. For the functional form of $\mathcal{F}_{\pi N}(s_{\pi N})$ we choose a dipole parameterisation,

$$\mathcal{F}_{\pi N}(s_{\pi N}) = \left(\frac{\Lambda^2+M^2}{\Lambda^2+s_{\pi N}}\right) \tag{3.30}$$

normalised so that the coupling constant $g_{\pi NN}$ has its standard value at the pole ($\mathcal{F}(M^2)=1$). Previously, in Refs.[82, 85] an exponential function was used

$$\mathcal{F}_{\pi N}(s_{\pi N}) = \exp\left(\frac{M^2-s_{\pi N}}{\Lambda_e^2}\right) \tag{3.31}$$

although Ref.[82] in addition followed an unconventional normalisation.

For a backward moving meson, Fig.3.3(b), y is negative, and in this case the energy denominator becomes $(P_0-p_0-k_0)=2yP_L+O(1/P_L)$. Therefore in the $P_L\to\infty$ limit this time-ordering is suppressed by a power of $1/P_L^4$, and so does not contribute.

For an interacting nucleon with a pion recoil, Fig.3.4, the contribution to the nucleon hadronic tensor is

$$\delta^{(N\pi)}W^{\mu\nu}(P,q) = \int \frac{d^3\mathbf{p}}{(2\pi)^3(2p_0)^2(2k_0)}\frac{g^2_{\pi NN}(p)}{(P_0-p_0-k_0)^2} \times\frac{1}{2}\mathrm{Tr}\left[(\not{P}+M)\,i\gamma_5\,(\not{p}+M)\,\widehat{W}_N^{\mu\nu}(p,q)\,(\not{p}+M)\,i\gamma_5\right]. \tag{3.32}$$

The kinematics here are similar to those described above, namely the nucleon and pion move with 3-momenta

$$\mathbf{p} = y'\,\mathbf{P}-\mathbf{k}_T \tag{3.33}$$

$$\mathbf{k} = (1-y')\,\mathbf{P}+\mathbf{k}_T \tag{3.34}$$

and have energies

$$p_0 = |y'|\, P_L + \frac{k_T^2 + M^2}{2\,|y'|P_L} + O\left(\frac{1}{P_L^2}\right) \tag{3.35}$$

$$k_0 = |1-y'|\, P_L + \frac{k_T^2 + m_\pi^2}{2\,|1-y'|P_L} + O\left(\frac{1}{P_L^2}\right) \tag{3.36}$$

respectively. Then direct evaluation of the trace in (3.32) gives

$$\begin{aligned} & 2\,(2P\cdot p \;-\; 2M^2)\left[\widetilde{g}^{\mu\nu}\;\left(2M\widehat{W}_T^0 \;+\; 2M^2\widehat{W}_T^1 \;+\; 2p\cdot q\;\widehat{W}_T^2\right) \;+\; \ldots\right] \\ = \;& 2\,(2P\cdot p \;-\; 2M^2)\;\widetilde{g}^{\mu\nu}\;W_{1N}(p,q) \;+\; \cdots \end{aligned} \tag{3.37}$$

where now the exact on-shell nucleon structure function appears, and automatically factorises.

For a backward moving nucleon, Fig.3.4(b), y' is negative, and $2P\cdot p - 2M^2 = -4y'P_L^2 + O(1/P_L)$, so that the numerator becomes large in the $P_L \to \infty$ limit. Technically this is due to the 'badness' of the operator γ_5, which mixes upper and lower components of the nucleon spinors. The energy denominator here is $(P_0 - p_0 - k_0) = 2y'P_L + O(1/P_L)$, and when squared and combined with the $1/P_L^2$ from the integration and vertex factors, the contribution from this diagram vanishes when P_L is infinite. Therefore we need only evaluate the diagram with the forward moving nucleon, Fig.3.4(a), which gives the result

$$f_{N\pi}(y') = \frac{3g_{\pi NN}^2}{16\pi^2}\int_0^\infty \frac{dk_T^2}{(1-y')}\frac{\mathcal{F}_{N\pi}^2(s_{N\pi})}{y'\,(M^2 - s_{N\pi})^2}\left(\frac{k_T^2 + (1-y')^2M^2}{y'}\right) \tag{3.38}$$

with

$$s_{N\pi}(k_T^2, y') = s_{\pi N}(k_T^2, 1-y'). = \frac{k_T^2 + M^2}{y'} + \frac{k_T^2 + m_\pi^2}{1-y'} \tag{3.39}$$

Notice that the integrand is identical to that in (3.20), when p^2 there is written in terms of p_T^2 (or k_T^2), except perhaps for the form factor. It was shown in [82] that within this approach there is an explicit symmetry between the processes in which the intermediate pion and the intermediate nucleon are struck if the form factor in $f_{N\pi}$ is taken to be

$$\mathcal{F}_{N\pi}(s_{N\pi}) = \mathcal{F}_{\pi N}(s_{\pi N}). \tag{3.40}$$

Then as long as the same cut-off mass parameter is used in both vertex functions, Eq.(3.3) is automatically satisfied. [2] In Fig.3.5 we plot the function $f_{\pi N}(y)$ evaluated in the IMF, with both the y-dependent exponential, Eq.(3.31), and dipole, Eq.(3.30), form factors, and compare this with the function evaluated in the covariant approach, with the k^2-dependent dipole form factor in Eq.(3.11). In order to make the comparison meaningful the cut-offs have been chosen to yield the same pion multiplicity $\langle n\rangle_{\pi N}$ ($\simeq 0.235$), for which the cut-offs are $\Lambda_{\pi N} = 1$ GeV, $\Lambda_e = 1380$ MeV and $\Lambda = 1425$ MeV. With the y-dependent exponential form factor $f_{\pi N}(y)$ is a little broader and peaks at around $y = 0.3$, compared with $y \simeq 0.2$ for the covariant convolution model with a dipole

[2] The form factor in Eq.(3.30) may also reduce the number of free parameters in models of NN or $N\overline{N}$ scattering [86], where currently different form factors are necessary for the meson- and baryon-exchange diagrams.

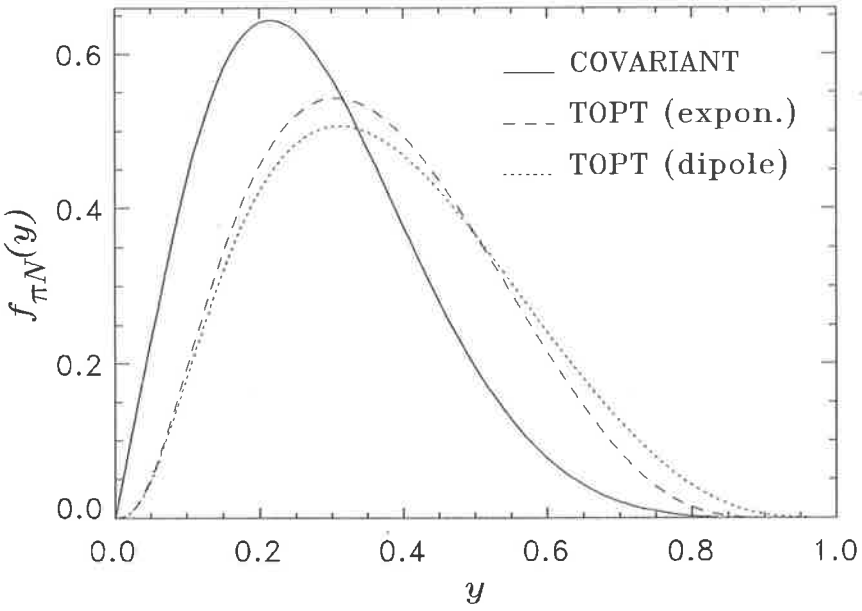

Figure 3.5: Distribution functions $f_{\pi N}(y)$ evaluated using covariant and time-ordered perturbation theory. The covariant function is as in Fig.3.2. The TOPT functions are evaluated with exponential and dipole form factors, with cut-offs $\Lambda_e = 1380$ MeV and $\Lambda = 1425$ MeV, respectively, to give the same value for $\langle n \rangle_{\pi N} = 0.235$.

form factor. The y-dependent dipole form factor yields a distribution which is a little broader still. The consequence of this will be that the convolution of $f_{\pi N}(y)$ with F_{2M} for the y-dependent form factors will have a slightly smaller peak and extend to marginally larger x (see Section 3.1.4).

The processes involving DIS from $\pi\Delta$ states can also be calculated in the IMF, although some care must be taken when describing the $\pi N\Delta$ interaction vertex in TOPT. Namely, in TOPT the relevant vertex is $\bar{u}_\alpha(p)\,(P-p)^\alpha\,u(P)$, rather than $\bar{u}_\alpha(p)\,k^\alpha\,u(P)$ as in the covariant theory, where of course the two are (trivially) identical. Using the same formalism as for calculating $f_{\pi N}$, and with the kinematics as given by Eqs.(3.22) to (3.26), but with $M \to M_\Delta$, we find that the pion distribution function with a Δ left in the final state is

$$f_{\pi\Delta}(y) = \frac{4}{3}\frac{f^2_{\pi N\Delta}}{16\pi^2}\int_0^\infty \frac{dk_T^2}{(1-y)}\frac{\mathcal{F}^2_{\pi\Delta}(s_{\pi\Delta})}{y\,(s_{\pi\Delta}-M)^2} \times \frac{[k_T^2+(M_\Delta-(1-y)M)^2]\,[k_T^2+(M_\Delta+(1-y)M)^2]^2}{6\,M_\Delta^2\,(1-y)^3} \tag{3.41}$$

where $s_{\pi\Delta} = s_{\pi N}(M \to M_\Delta)$, and we take the same functional form for the $\pi N\Delta$ form factor as for the πNN form factor in (3.30).

For an interacting Δ with a pion recoil we need additional information on the truncated Δ hadronic tensor, which in this case will involve additional Lorentz indices stemming from the fact that the Δ has spin 3/2. For an on-shell Δ the hadronic tensor can be represented as [87]

$$W^\Delta_{\mu\nu}(p,q) = \frac{1}{4}\mathrm{Tr}\left[\Lambda^{\alpha\beta}(p)\,\widehat{W}^\Delta_{\mu\nu\alpha\beta}(p,q)\right] \tag{3.42}$$

with $\Lambda^{\alpha\beta}(p)$ the Δ energy projector, Eq.(3.15). Assuming the simplest structure for the truncated

Δ tensor, namely [82]

$$\widehat{W}^{\Delta}_{\mu\nu\alpha\beta}(p,q) \;=\; -g_{\alpha\beta}\,\widehat{W}^{\Delta}_{\mu\nu}(p,q) \tag{3.43}$$

where $\widehat{W}^{\Delta}_{\mu\nu}$ has the same Dirac and Lorentz structure as the truncated nucleon tensor, gives the result

$$W^{\Delta}_{\mu\nu}(p,q) \;=\; 2\left(M_\Delta \widehat{W}^0_\Delta \;+\; M^2_\Delta \widehat{W}^1_\Delta \;+\; p\cdot q \widehat{W}^2_\Delta\right)\,\tilde{g}_{\mu\nu} \;+\; \cdots \tag{3.44}$$

so that by comparing coefficients of $g_{\mu\nu}$ we can use the term in parentheses to define the on-shell Δ structure function. Utilising the form (3.43) for the truncated Δ tensor, we can then evaluate the trace

$$\begin{aligned}
&\frac{1}{2}\mathrm{Tr}\left[(\not{P}+M)\,(P-p)_\alpha\,\Lambda^{\alpha\alpha'}(p)\;\;\widehat{W}_{\mu\nu\alpha\beta}(p,q)\,\Lambda^{\beta'\beta}(p)\;\;(P-p)_\beta\right] \\
&= \;\frac{1}{6\,M^2_\Delta\,y'^3}\left(k_T^2+(M_\Delta-y'M)^2\right)\left(k_T^2+(M_\Delta+y'M)^2\right)^2 \\
&\qquad\cdot\left((2M_\Delta\widehat{W}^0_\Delta+M^2_\Delta\widehat{W}^1_\Delta+p\cdot q\widehat{W}^2_\Delta)\,\tilde{g}_{\mu\nu}\;+\;\cdots\right)
\end{aligned} \tag{3.45}$$

so that the on-shell Δ structure function factorises to give Eq.(3.7), with the virtual Δ distribution function given by

$$\begin{aligned}
f_{\Delta\pi}(y') \;=\; &\frac{4}{3}\frac{f^2_{\pi N\Delta}}{m^2_\pi\;16\pi^2}\int_0^\infty \frac{dk_T^2}{(1-y')}\frac{\mathcal{F}^2_{\Delta\pi}(s_{\Delta\pi})}{y'\;(s_{\Delta\pi}-M)^2} \\
&\times\frac{\left[k_T^2+(M_\Delta-y'M)^2\right]\left[k_T^2+(M_\Delta+y'M)^2\right]^2}{6\;M^2_\Delta\;y'^3}.
\end{aligned} \tag{3.46}$$

Clearly this is related to $f_{\pi\Delta}(y)$ by (3.3) if $\mathcal{F}_{\pi\Delta}(s_{\pi\Delta})=\mathcal{F}_{\Delta\pi}(s_{\Delta\pi})$, where $s_{\Delta\pi}=s_{\pi\Delta}(M\to M_\Delta)$.

In Fig.3.6 we compare the function $f_{\pi\Delta}(y)$, calculated in the IMF, with the function given by Eq.(3.17). The k^2-dependent form factor in the covariant formulation is a dipole form ($\Lambda_{\pi\Delta}=1$ GeV), while the $s_{\pi\Delta}$-dependent form factors are dipole ($\Lambda=1512$ MeV) and exponential ($\Lambda_e=1565$ MeV), with all functions normalised to give the same $\langle n\rangle_{\pi\Delta}(\approx 0.114)$. Whereas for $f_{\pi N}(y)$ the y-dependent form factors produced a slight hardening of the distributions when compared with the covariant form factor, here we see a marked difference between the two calculations, in which the distributions calculated in the IMF are considerably broader and extend to larger y.

Having found a useful method for obtaining the pion distributions in a self-consistent manner, we next apply the TOPT/IMF formalism to non-pseudoscalar mesons. As mentioned above, and in Ref.[69] for example, the difficulties encountered in attempting to compute the contributions from vector mesons make the covariant approach to this problem very problematic, so from a technical point of view we would like to see if the vector mesons can be handled adequately in the IMF. From a physical point of view, our aim will be to test the relevance or otherwise of the higher mass meson states in the physical nucleon. We focus primarily on the vector mesons, but also briefly re-examine the importance of kaons in the time-ordered formalism.

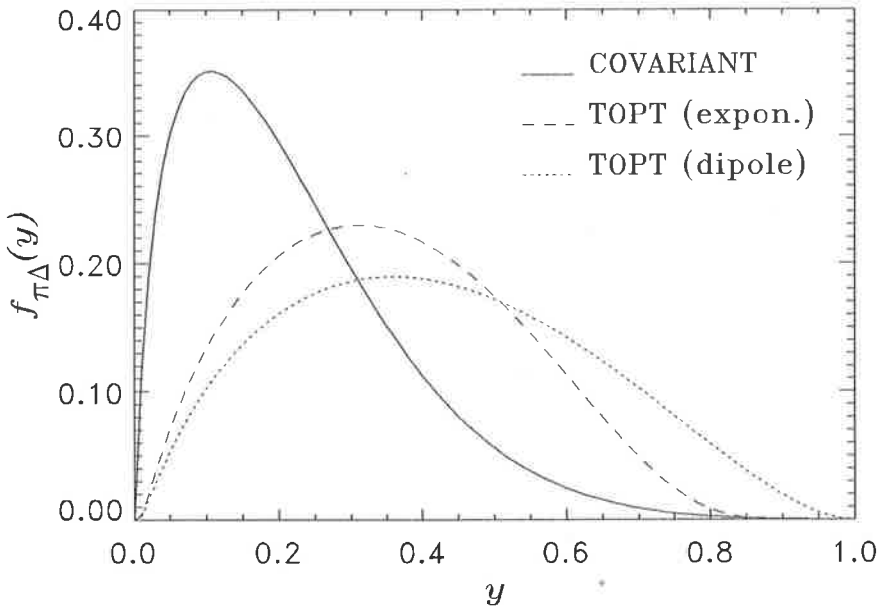

Figure 3.6: Distribution functions $f_{\pi\Delta}(y)$ evaluated using covariant and time-ordered perturbation theory. The covariant function is evaluated with a dipole form factor with cut-off mass $\Lambda_{\pi\Delta} = 1$ GeV. The TOPT functions have exponential and dipole form factors, with cut-offs $\Lambda_e = 1565$ MeV and $\Lambda = 1512$ MeV, respectively, to give the same value for $\langle n \rangle_{\pi N} = 0.114$.

3.1.3 Heavier Mesons

Vector Mesons

The importance of vector mesons in nuclear physics is well known. In the context of meson exchange models of the NN force in nuclear physics, it has long been realised that vector mesons play a vital role [86,88–93]. For example, the isovector ρ meson is needed to provide sufficient cancellation of the tensor force generated by π meson exchange, which would otherwise be too large. On the other hand, the isoscalar ω meson, through its large vector coupling, is responsible for the short range NN repulsive force, and also provides most of the spin-orbit interaction. Traditionally it has been necessary to use hard vector meson—nucleon form factors in order to fit the NN phase shifts [86]. However, alternative approaches have recently been developed in which the NN data can be fitted with quite soft form factors [93–95].

From another direction, the vector meson dominance model of the elastic electromagnetic nucleon form factors, in which an isovector photon couples to the nucleon via a ρ meson, provides a natural explanation of the dipole Q^2 behaviour of the γNN vertex function. Recent analyses [93] have shown that a ρNN vertex parameterised by a soft monopole form factor ($\Lambda_{\text{monopole}} \sim 800$ MeV) provides a good description of the Q^2 dependence of the Dirac and Pauli form factors. The effect of vector mesons upon nucleon electromagnetic form factors has also been explored [68] in the cloudy bag model [54], and in various soliton models [96].

The possible role played by vector (as well as other) mesons in DIS was first investigated by Speth and collaborators [62, 69], who calculated the vector meson distribution functions within

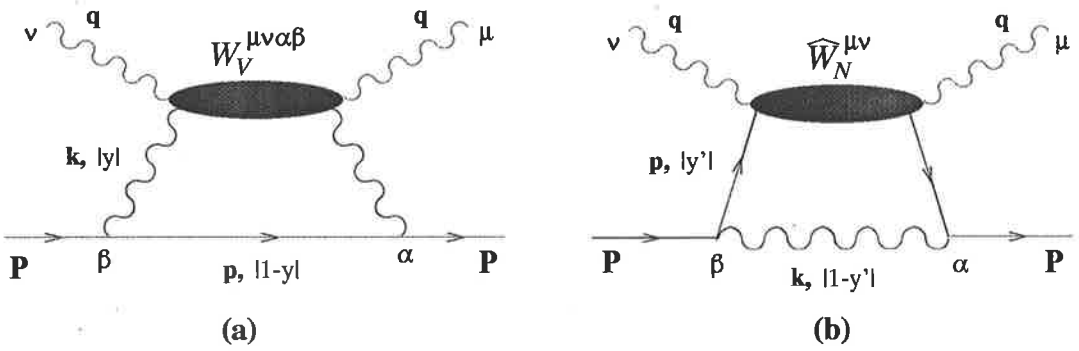

Figure 3.7: Time-ordered diagrams for the DIS from (a) vector mesons and (b) nucleons with recoil vector mesons, that are non-zero in the IMF.

a covariant framework, but with the assumption that the vector meson and nucleon intermediate states were on-mass-shell. In this section we extend the analysis of pions in Section 3.1.2 to the vector meson sector. Specifically, we shall demonstrate that the vector meson functions, calculated within the TOPT/IMF formalism, can be made to satisfy the relation (3.3) exactly.

For the effective VNN interaction we include both a vector, $g_{VNN}\ \bar{u}(p)\gamma^\alpha\epsilon_\alpha u(P)$, and a tensor, $f_{VNN}/(4M)\ \bar{u}(p)\ i\sigma^{\alpha\beta}[(P_\alpha - p_\alpha)\epsilon_\beta - (P_\beta - p_\beta)\epsilon_\alpha]u(P)$, coupling, where $V = \rho$ or ω, and $\epsilon_\alpha(\lambda)$ is the polarisation vector for a spin 1 meson with helicity λ. In the calculation of the vector meson distributions in Ref.[85] the tensor coupling was taken to be $\sim\ \bar{u}(p)i\sigma^{\alpha\beta}k_\alpha\epsilon_\beta u(P)$ [86]. In our treatment of the $\pi\Delta$ states in the previous section, the derivative interaction was constructed from baryon momenta, $P_\alpha - p_\alpha$, rather than from the pion momentum k_α. For overall consistency in calculating contributions from all the meson–baryon states, we therefore use the above interaction for the tensor VNN vertex also [97]. In both cases, however, one can explicitly verify that the probability conservation condition, Eq.(3.3), is satisfied [85].

The contribution from the diagram with backward moving vector mesons is suppressed in the IMF by the energy denominators, just as for pions. Therefore we only need to evaluate the diagram in Fig.3.7(a) with forward moving vector mesons, which gives the following contribution to the nucleon hadronic tensor

$$\begin{aligned}\delta^{(VN)}W^{\mu\nu}(P,q) \;=\; & \int \frac{d^3\mathbf{k}}{(2\pi)^3(2p_0)(2k_0)^2}\,\frac{1}{(P_0 - p_0 - k_0)^2} \\ & \times\frac{1}{2}\sum_{\lambda,\lambda'}\mathrm{Tr}\left[(\not{P}+M)\,\left(g_{VNN}(k)\,\gamma^{\alpha'} + \frac{f_{VNN}(k)}{4M}2i\sigma^{\alpha''\alpha'}\,(P_{\alpha''} - p_{\alpha''})\right)\right. \\ & \cdot(\not{p}+M)\;\epsilon^*_{\alpha'}(\lambda)\epsilon_\alpha(\lambda)\;\;W_V^{\mu\nu\alpha\beta}(k,q)\;\;\epsilon^*_\beta(\lambda')\epsilon_{\beta'}(\lambda') \\ & \left.\cdot\left(g_{VNN}(k)\,\gamma^{\beta'} + \frac{f_{VNN}(k)}{4M}2i\sigma^{\beta''\beta'}\,(P_{\beta''} - p_{\beta''})\right)\right]. \qquad (3.47)\end{aligned}$$

Evaluating the trace gives

$$\left(g^2_{VNN}(k)\;A_{\alpha\beta} \;+\; f^2_{VNN}(k)\;B_{\alpha\beta} \;+\; g_{VNN}(k)\;f_{VNN}(k)\;C_{\alpha\beta}\right) \qquad (3.48)$$

where

$$
\begin{aligned}
A_{\alpha\beta} &= (P-p)^2\, g_{\alpha\beta} \;+\; 2\,(P_\alpha p_\beta \;+\; p_\alpha P_\beta) \\
B_{\alpha\beta} &= (P-p)^2\, g_{\alpha\beta} \;-\; (P_\alpha P_\beta + p_\alpha p_\beta) \;-\; \frac{1}{2}(P_\alpha - p_\alpha)(P_\beta - p_\beta) \;+\; \frac{P\cdot p}{2M^2}(P_\alpha + p_\alpha)(P_\beta + p_\beta) \\
C_{\alpha\beta} &= 2\,(P-p)^2\, g_{\alpha\beta} \;-\; (P_\alpha - p_\beta)\,(P_\beta - p_\alpha)
\end{aligned}
\tag{3.49}
$$

are the VNN vertex trace factors for the vector, tensor and vector–tensor interference couplings, respectively. For an on-mass-shell vector meson, the spin 1 tensor $W_V^{\mu\nu\alpha\beta}$, symmetric under the interchange of $\mu \leftrightarrow \nu$ and $\alpha \leftrightarrow \beta$, is given by

$$
W_V^{\mu\nu\alpha\beta}(k,q) \;=\; \left(\tilde{g}^{\mu\nu}\, W_{1V}(k,q) \;+\; \frac{\tilde{k}^\mu\, \tilde{k}^\nu}{m_V^2}\, W_{2V}(k,q)\right) \tilde{g}^{\alpha\beta}. \tag{3.50}
$$

This form guarantees that the vector current is conserved, $k_{\alpha(\beta)} W_V^{\mu\nu\alpha\beta} = 0 = q_{\mu(\nu)} W_V^{\mu\nu\alpha\beta}$. Furthermore, it reproduces the correct unpolarised on-shell spin 1 tensor when contracted with the meson polarisation vectors ($\epsilon_{\alpha(\beta)}$) and summed over the V helicity, λ [98]:

$$
\begin{aligned}
W_V^{\mu\nu}(k,q) &= \sum_\lambda \epsilon_\alpha^*(\lambda,k)\, \epsilon_\beta(\lambda,k)\, W_V^{\mu\nu\alpha\beta}(k,q) \\
&= \left(-g_{\alpha\beta} + \frac{k_\alpha k_\beta}{k^2}\right) W_V^{\mu\nu\alpha\beta}(k,q) \\
&\propto\; \tilde{g}^{\mu\nu}\, W_{1V}(k,q) \;+\; \frac{\tilde{k}^\mu\, \tilde{k}^\nu}{m_V^2}\, W_{2V}(k,q).
\end{aligned}
\tag{3.51}
$$

In the case of DIS from a vector particle emitted by a nucleon, Fig.3.7(a), contracting the spin 1 tensor $W_V^{\mu\nu\alpha\beta}$ with the VNN vertex trace factors in (3.49) gives for the trace factor in (3.48)

$$
\begin{aligned}
&\left\{ g_{VNN}^2(k) \left(-6\, M^2 + \frac{4P\cdot k\; p\cdot k}{m_V^2} + 2P\cdot p\right)\right. \\
&- f_{VNN}^2(k) \left((P-p)^2 \left(\frac{P\cdot p - 3M^2}{2M^2}\right) - \frac{2}{m_V^2}\left((P\cdot k)^2 + (p\cdot k)^2\right) + \frac{((P+p)\cdot k)^2}{2m_V^2}\left(1 + \frac{P\cdot p}{M^2}\right)\right) \\
&\left. - g_{VNN}(k)\, f_{VNN}(k) \left(4\,(P-p)^2 \;+ \frac{2}{m_V^2}((P-p)\cdot k)^2\right)\right\} W_V^{\mu\nu}(k,q).
\end{aligned}
\tag{3.52}
$$

Equating coefficients of $g_{\mu\nu}$ in (3.47), and using the same IMF kinematics as for the πN system, except with $m_\pi \to m_V$, together with the Callan-Gross relation for the nucleon and vector meson, enables the contribution to F_{2N} from vector mesons to be written as a convolution of the vector meson distribution function $f_{VN}(y)$ with the on-shell vector meson structure function $F_{2V}(x/y)$, as in (3.6), where now

$$
\begin{aligned}
f_{VN}(y) &= \frac{c_V}{16\pi^2} \int_0^\infty \frac{dk_T^2}{(1-y)} \frac{\mathcal{F}_{VN}^2(s_{VN})}{y\,(M^2 - s_{VN})^2} \\
&\times \left\{ g_{VNN}^2 \left(\frac{(k_T^2 + y^2M^2 + m_V^2)\,(k_T^2 + y^2M^2 + (1-y)^2 m_V^2)}{y^2(1-y)m_V^2} + \frac{k_T^2 + y^2M^2}{1-y} - 4M^2\right)\right. \\
&\left. + g_{VNN}\, f_{VNN} \left(-\frac{(k_T^2 + y^2M^2 - (1-y)m_V^2)^2}{2(1-y)^2 m_V^2} + \frac{4\,(k_T^2 + y^2M^2)}{(1-y)}\right)\right.
\end{aligned}
$$

$$+ f_{VNN}^2 \left(\frac{(2-y)^2 \left(k_T^2 + y^2M^2 + (1-y)m_V^2\right)^2 \left(k_T^2 + (4(1-y)+y^2)M^2\right)}{16y^2(1-y)^3M^2m_V^2} \right.$$
$$- \frac{\left(k_T^2 + y^2M^2\right)\left(k_T^2 + (-4(1+y)+y^2)M^2\right)}{4(1-y)^2M^2}$$
$$\left. - \frac{\left(k_T^2 + y^2M^2 + (1-y)^2m_V^2\right)^2}{2y^2(1-y)^2m_V^2} - \frac{\left(k_T^2 + y^2M^2 + m_V^2\right)^2}{2y^2m_V^2} \right) \Bigg\} \qquad (3.53)$$

where $c_V = 1 + 2\delta_{V\rho}$ is the isospin factor (here δ is the Kronecker-δ symbol). The VN centre of mass energy squared is $s_{VN} = s_{\pi N}(m_\pi \to m_V)$, and we take the same form factor for both the vector and tensor couplings, $g_{VNN}(s_{VN}) = g_{VNN}\,\mathcal{F}_{VN}(s_{VN})$ and $f_{VNN}(s_{VN}) = f_{VNN}\,\mathcal{F}_{VN}(s_{VN})$, with $\mathcal{F}_{VN}(s_{VN})$ defined analogously to (3.30).

For the vector meson recoil process, Fig.3.7(b), we evaluate the distribution function $f_{NV}(y')$ using the full spinor structure of $\widehat{W}_N^{\mu\nu}$ in (2.36):

$$\delta^{(NV)}W^{\mu\nu}(P,q) = \int \frac{d^3\mathbf{p}}{(2\pi)^3(2p_0)^2(2k_0)} \frac{1}{(P_0 - p_0 - k_0)^2}$$
$$\times \frac{1}{2}\sum_\lambda \mathrm{Tr}\Big[(\not{p} + M)\left(g_{VNN}(p)\,\gamma^\alpha + \frac{f_{VNN}(p)}{4M} 2i\sigma^{\alpha'\alpha}(P_{\alpha'} - p_{\alpha'})\right)(\not{p} + M)\,\widehat{W}_N^{\mu\nu}(p,q)\,(\not{p} + M)$$
$$\cdot \left(g_{VNN}(p)\,\gamma^\beta + \frac{f_{VNN}(p)}{4M} 2i\sigma^{\beta'\beta}(P_{\beta'} - p_{\beta'})\right)\epsilon_\alpha^*(\lambda)\epsilon_\beta(\lambda)\Big]. \qquad (3.54)$$

Here the trace is given by

$$\left(g_{VNN}^2(p)\,A_{\alpha\beta} + f_{VNN}^2(p)\,B_{\alpha\beta} + g_{VNN}(p)\,f_{VNN}(p)\,C_{\alpha\beta}\right)$$
$$\times\, \tilde{g}^{\alpha\beta}\left(2M\,\widehat{W}^0(p,q) + 2M^2\,\widehat{W}^1(p,q) + 2p\cdot q\,\widehat{W}^2(p,q)\right) \qquad (3.55)$$

where the tensors A, B and C are as in (3.49). Performing the contractions over the indices α, β leads to the convolution integral of Eq.(3.7), with the nucleon distribution function with a vector meson recoil given by

$$f_{NV}(y') = \frac{c_V}{16\pi^2}\int_0^\infty \frac{dk_T^2}{(1-y')}\frac{\mathcal{F}_{NV}^2(s_{NV})}{y'\,(M^2 - s_{NV})^2}$$
$$\times \Bigg\{ g_{VNN}^2 \left(\frac{\left(k_T^2 + (1-y')^2M^2 + m_V^2\right)\left(k_T^2 + (1-y')^2M^2 + y'^2m_V^2\right)}{y'(1-y')^2m_V^2} + \frac{k_T^2 + (1-y')^2M^2}{y'} - 4M^2 \right)$$
$$+ g_{VNN}\,f_{VNN}\left(-\frac{\left(k_T^2 + (1-y')^2M^2 - y'm_V^2\right)^2}{2y'^2m_V^2} + \frac{4\left(k_T^2 + (1-y')^2M^2\right)}{y'} \right)$$
$$+ f_{VNN}^2 \left(\frac{\left(k_T^2 + (1-y')^2M^2 + y'm_V^2\right)^2\left(k_T^2 + (4y' + (1-y')^2)M^2\right)\,(1+y')^2}{16(1-y')^2y'^3M^2m_V^2} \right.$$
$$- \frac{\left(k_T^2 + (1-y')^2M^2\right)\left(k_T^2 + (-4y' + (1-y')^2)M^2\right)}{4y'^2M^2}$$
$$\left. - \frac{\left(k_T^2 + (1-y')^2M^2 + y'^2m_V^2\right)^2}{2(1-y')^2y'^2m_V^2} - \frac{\left(k_T^2 + (1-y')^2M^2 + m_V^2\right)^2}{2(1-y')^2m_V^2} \right) \Bigg\}. \qquad (3.56)$$

and where $s_{NV}(k_T^2, y') = s_{VN}(k_T^2, 1-y')$. Again, we have evaluated only the diagram with forward moving nucleons which is non-zero in the IMF. It is clear therefore from (3.53) and (3.56) that the probability distributions for the VN intermediate states are related by $f_{NV}(y') = f_{VN}(1-y')$.

One should observe that the trace factor inside the braces in $f_{VN}(y)$ is divergent in the limit $y \to 0$. To illustrate one of the problems with the covariant approach to calculating f_{VN}, consider a form factor $\propto \exp\left[y\ (M^2 - s_{VN})\right]$. Since $k^2 = -(k_T^2 + M^2y^2)/(1-y)$, this form factor would correspond to a k^2-dependent covariant form factor $\propto \exp\left[k^2 - m_V^2\right]$. With such a form factor, $\delta^{(VN)}F_{2N}(x)$ would approach a finite value as $x \to 0$, much like a perturbative sea distribution. However, there are several problems with accepting such a result, the most obvious of which is that it would violate charge and momentum conservation very badly, since $f_{NV}(y') \to 0$ for $y' \to 1$ and $\to$ constant as $y' \to 0$ for a form factor $\propto \exp\left[y'(M^2 - s_{NV})\right]$, which in the covariant formalism corresponds to $\exp\left[p^2 - M^2\right]$. Furthermore, it would lead to a gross violation of the Adler sum rule, which integrates the flavour combination $u - \bar{u} - d + \bar{d}$, and such a violation has not been observed in the range $1 < Q^2 < 40$ GeV^2 [99]. This gives further evidence for the preference of the IMF approach together with the y-dependent form factor in (3.30) or (3.31).

To complete our discussion of vector mesons, we give the results for the functions describing the $V\Delta$ states. We saw in the previous section that the contributions from the $\pi\Delta$ states were certainly not negligible in comparison with the πN components of the physical nucleon. For the vector mesons, we would also like to examine whether the Δ isobar is of any importance. Since the ω meson is isoscalar, the only vector meson able to couple to a nucleon and Δ is the ρ, and for this we use a pseudovector coupling [86], $(f_{\rho N\Delta}/m_\rho)\ \bar{u}(P)\ i\gamma_5\gamma^\alpha u^\beta(p)\ ((P-p)_\alpha\epsilon_\beta - (P-p)_\beta\epsilon_\alpha)$. Again, we drop those diagrams which give order $1/P_L^4$ contributions in IMF (i.e. for backward moving ρ mesons or Δ). The contribution from scattering from a ρ meson with a Δ recoil is obtained by evaluating the following trace:

$$\begin{aligned}
&\frac{1}{2}\sum_{\lambda,\lambda'} \mathrm{Tr}\Big[(\not{P}+M)\ i\gamma_5\gamma^\alpha\ \Lambda^{\alpha'\beta'}(p)\ \left((P-p)_\alpha\epsilon^*_{\alpha'}(\lambda)\epsilon_{\alpha''}(\lambda)\ -\ (P-p)_{\alpha'}\epsilon^*_\alpha(\lambda)\epsilon_{\alpha''}(\lambda)\right) \\
&\qquad\qquad \cdot W_\rho^{\mu\nu\alpha''\beta''}(k,q)\ i\gamma_5\gamma^\beta\ \Big((P-p)_{\beta'}\epsilon^*_{\beta''}(\lambda')\epsilon_\beta(\lambda')\ -\ (P-p)_\beta\epsilon^*_{\beta''}(\lambda')\epsilon_{\beta'}(\lambda')\Big)\Big] \\
= \ &\frac{1}{2}\mathrm{Tr}\ \big[(\not{P}+M)\ \{\gamma_5\gamma_{\alpha'}\left(\Lambda_{\alpha\beta'}(p)\ \gamma_5\gamma_\beta\ -\ \Lambda_{\alpha\beta}(p)\ \gamma_5\gamma_{\beta'}\right) \\
&\qquad\qquad -\gamma_5\gamma_\alpha\ \left(\Lambda_{\alpha'\beta'}(p)\ \gamma_5\gamma_\beta\ +\ \Lambda_{\alpha'\beta}(p)\ \gamma_5\gamma_{\beta'}\right)\}\big] \\
&\qquad \times(P-p)^{\alpha'}(P-p)^{\beta'}\ W_\rho^{\mu\nu\alpha\beta}(k,q)
\end{aligned} \tag{3.57}$$

where $W_\rho^{\mu\nu\alpha\beta}$ is the ρ meson structure tensor, as given in (3.50). The resulting probability distribution to find a ρ in the physical nucleon with a Δ recoil is therefore

$$\begin{aligned}
f_{\rho\Delta}(y) \ = \ &\frac{4}{3}\frac{f^2_{\rho N\Delta}}{m_\rho^2\ 16\pi^2}\int_0^\infty \frac{dk_T^2}{(1-y)}\frac{\mathcal{F}^2_{\rho\Delta}(s_{\rho\Delta})}{y\ (M^2 - s_{\rho\Delta})^2} \\
\times\Bigg\{&-\frac{4\ MM_\Delta}{3}\left(2M_\Delta^2 + MM_\Delta + 2M^2\right)\ -\ \frac{4\ MM_\Delta}{3m_\rho^2}((P-p)\cdot k)^2 \\
&-\frac{4}{3m_\rho^2}\left(M_\Delta^2(P\cdot k)^2 + M^2(p\cdot k)^2\right)\ +\ \frac{4\ P\cdot p}{3}\left(2M_\Delta^2 + 4MM_\Delta + M^2\right) \\
&+\frac{4\ P\cdot p}{3m_\rho^2}(p\cdot k)^2\left(1 - \frac{M^2}{M_\Delta^2}\right)\ -\ 4\ (P\cdot p)^2\left(1 - \frac{2P\cdot k\ p\cdot k}{3m_\rho^2 M_\Delta^2} - \frac{P\cdot p}{3M_\Delta^2}\right)\Bigg\}
\end{aligned} \tag{3.58}$$

with the kinematics as given in Eqs.(3.22) through (3.26), except with $m_\pi \to m_\rho$ and $M \to M_\Delta$.

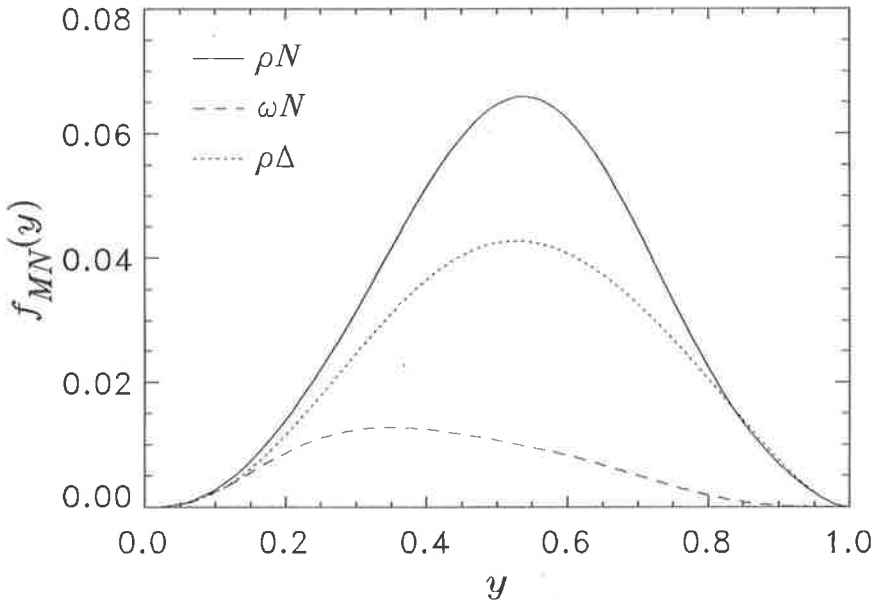

Figure 3.8: Vector meson distribution functions in the nucleon. The (dipole) form factor cut-off is $\Lambda = 700$ MeV for all curves.

For the DIS off a virtual Δ with a ρ meson recoil, we need to evaluate the trace

$$\begin{aligned}
&\frac{1}{2}\sum_{\lambda} \mathrm{Tr}\Big[(\not{P}' + M)\, i\gamma_5\gamma_\alpha \Big((P-p)^\alpha \epsilon^{\alpha'*}(\lambda) - (P-p)^{\alpha'}\epsilon^{\alpha*}(\lambda)\Big) \\
&\qquad \cdot \Lambda_{\alpha'\alpha''}(p)\, \widehat{W}_\Delta^{\mu\nu\alpha''\beta''}(p,q)\, \Lambda_{\beta''\beta'}(p) \\
&\qquad \cdot i\gamma_5\gamma_\beta \Big((P-p)^{\beta'}\epsilon^{\beta}(\lambda) - (P-p)^{\beta}\epsilon^{\beta'}(\lambda)\Big)\Big] \\
= &\left\{ -\frac{4\,MM_\Delta}{3}\left(2M_\Delta^2 + MM_\Delta + 2M^2\right) - \frac{4\,MM_\Delta}{3m_\rho^2}\left((P-p)\cdot k\right)^2 \right. \\
&- \frac{4}{3m_\rho^2}\left(M_\Delta^2 (P\cdot k)^2 + M^2 (p\cdot k)^2\right) + \frac{4\,P\cdot p}{3}\left(2M_\Delta^2 + 4MM_\Delta + M^2\right) \\
&\left. + \frac{4\,P\cdot p}{3m_\rho^2}(p\cdot k)^2\left(1 - \frac{M^2}{M_\Delta^2}\right) - 4\,(P\cdot p)^2\left(1 - \frac{2P\cdot k\; p\cdot k}{3m_\rho^2 M_\Delta^2} - \frac{P\cdot p}{3M_\Delta^2}\right)\right\} W_{\mu\nu}^{\Delta}(p,q).
\end{aligned} \tag{3.59}$$

It's then straightforward to show, using the kinematics of (3.33) to (3.36) that $f_{\Delta\rho}(y') = f_{\rho\Delta}(1-y)$, when the form factors satisfy $\mathcal{F}_{\rho\Delta}(s_{\rho\Delta}) = \mathcal{F}_{\Delta\rho}(s_{\Delta\rho})$.

In Fig.3.8 we plot the vector meson distribution functions $f_{\rho N}$, $f_{\omega N}$ and $f_{\rho\Delta}$ as a function of y, for the dipole form factor of the form in (3.30), with $\Lambda = 700$ MeV in all cases. The dominant contributions come from the tensor (derivative) couplings, which is reflected in the larger ρN and $\rho\Delta$ distributions in comparison with the ωN. Also, the vector distribution functions tend to peak at slightly larger y values ($y \sim 0.5$) in comparison with the πN and $\pi\Delta$ functions.

Strange Mesons

Finally we conclude the discussion of heavy mesons by reinvestigating the DIS process from the kaon cloud of the nucleon using the the time-ordered formalism in the IMF. The role of kaons was first examined by Signal and Thomas [100], however, within a covariant, Feynman diagram

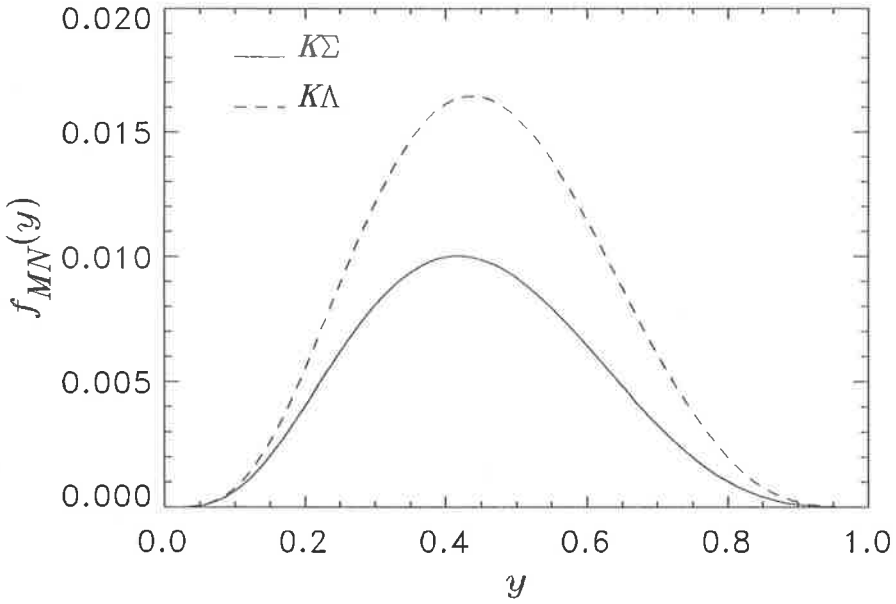

Figure 3.9: Kaon distribution functions in the nucleon, with Σ and Λ recoil. The (dipole) form factor cut-off is $\Lambda = 1.2$ GeV for all curves.

approach. Through the proton dissociation processes $p \to K^0\Sigma^0(\Lambda^0)$ and $p \to K^+\Sigma^-$, the virtual photon will probe the quark structure of the virtual strange mesons and hyperons. Such a process will naturally generate a non-perturbative strange quark component of the nucleon, as well as a different antistrange sea, thereby breaking SU(3) flavour symmetry of the sea in the process.

Taking a pseudoscalar coupling for the KNH vertex, where the hyperon $H = \Sigma$ or Λ, the kaon distribution function is similar to the pion distribution function $f_{\pi N}(y)$, except the mass of the recoil state is now different,

$$f_{KH}(y) = c_H \frac{g^2_{KNH}}{16\pi^2} \int_0^\infty \frac{dk_T^2}{(1-y)} \frac{\mathcal{F}^2_{KH}(s_{KH})}{y\,(M^2 - s_{KH})^2} \times \left(\frac{k_T^2 + y^2M^2 + (M_H - M)(M_H - (1-2y)M)}{1-y} \right) \tag{3.60}$$

where the isospin factor is $c_H = 1 + 2\delta_{H\Sigma}$. Similarly for the DIS from a strange baryon with a spectator K, repeating the calculation of Section 3.1.2, the hyperon distribution function is found to be

$$f_{HK}(y') = c_H \frac{g^2_{KNH}}{16\pi^2} \int_0^\infty \frac{dk_T^2}{(1-y')} \frac{\mathcal{F}^2_{HK}(s_{HK})}{y'\,(M^2 - s_{HK})^2} \times \left(\frac{k_T^2 + (1-y')^2M^2 + (M_H - M)(M_H + (1-2y')M)}{y'} \right) \tag{3.61}$$

In Fig.3.9 we show the strange meson distribution functions, $f_{K\Sigma}(y)$ and $f_{K\Lambda}(y)$, for a dipole form factor with a cut-off $\Lambda = 1.2$ GeV. Notice the scale as compared with Fig.3.8 for the vector mesons and Fig.3.5 for the pions.

The relatively small size of the kaon contributions is also clear from Figs.3.10 and 3.11, where we compare the average number of all mesons considered, $\langle n \rangle_{MB}$, and the average momentum they

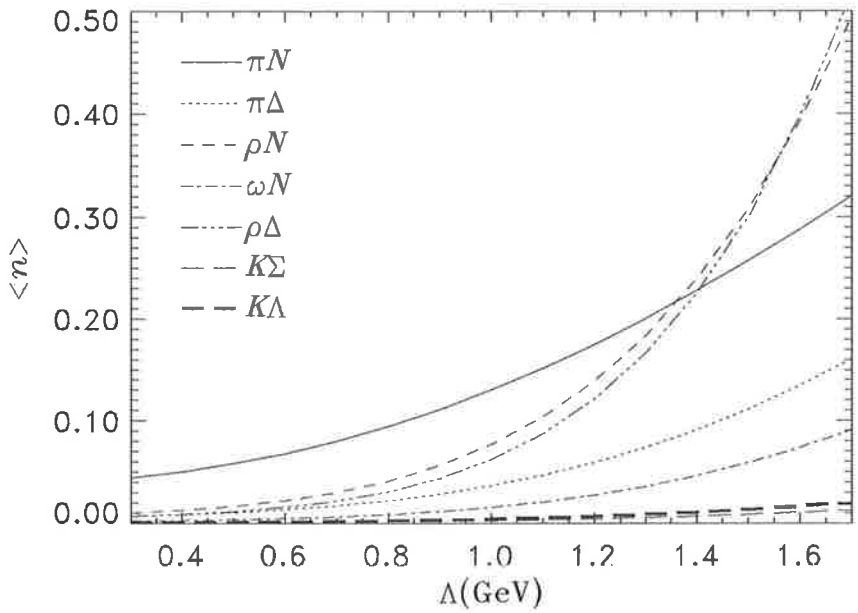

Figure 3.10: Calculated average meson multiplicities in the nucleon, as a function of the (dipole) meson-nucleon form factor cut-off.

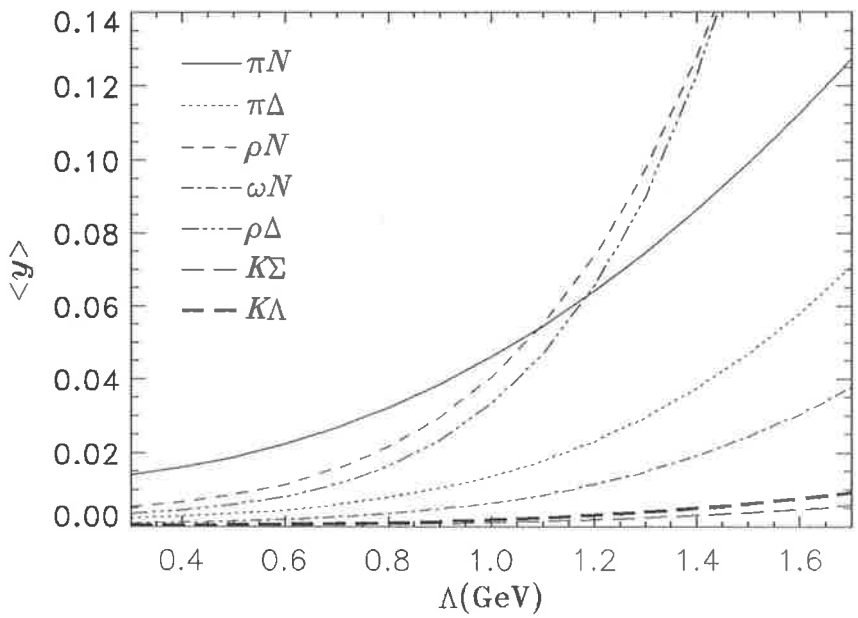

Figure 3.11: Average momentum carried by mesons in the nucleon as a function of the (dipole) form factor cut-off Λ.

carry in an infinite momentum frame, $\langle y\rangle_{MB}$, as a function of the dipole form factor cut-off Λ. For relatively small cut-off masses, $\Lambda \lesssim 0.7$ GeV, the dominant contribution is from the πN component. However, the rapid growth with Λ of the ρ meson multiplicities and momentum fractions means that for large Λ ($\gtrsim 1.2-1.3$ GeV) the vector mesons become as important numerically as pions. In fact, the strong k_T dependence in $f_{\rho N}(y)$ and $f_{\rho\Delta}(y)$ implies that for $\Lambda \gtrsim 1.4$ GeV both $\langle n\rangle_{\rho N}$ and $\langle n\rangle_{\rho\Delta}$ actually exceed $\langle n\rangle_{\pi N}$. (A similar behaviour was found in Ref.[85] with a $\sigma^{\alpha\beta}k_\alpha\epsilon_\beta$ tensor ρNN coupling, in which the dependence on Λ was only marginally weaker.)

Note that for the πN component, $\Lambda = (600, 1000, 1400)$ MeV corresponds to an exponential cut-off $\Lambda_e \simeq (580, 1130, 1360)$ MeV, and a covariant dipole form factor cut-off $\Lambda_{\pi N} \simeq (590, 760, 980)$ MeV for the same $\langle n\rangle_{\pi N}$. In many nuclear physics calculations quite hard form factors of the k^2-dependent type are often used, for example in NN potential models, where cut-offs of the order of 1.5—2 GeV are typical. Clearly such large cut-offs would imply an extremely large number of pions and an even larger number of vector mesons. Whether or not it is reasonable to accept such large heavy meson components in nucleon DIS is debatable, but obviously we would like some data to tell us whether this is so.

Up until now the cut-off Λ has been a free parameter. Indeed, because quantities such as the average number of mesons in the nucleon are not directly (or unambiguously) extracted from experiment, we cannot draw any conclusions about the size of Λ from the functions $f_{MB}(y)$ alone. However, we may be able to restrict the range of allowable values of Λ by comparing the calculated meson and baryon contributions with the experimental structure functions, or quark distributions. This is what we turn our attention to next.

3.1.4 Nucleon Quark Distributions

With the functions f_{MB} and f_{BM} now calculated, we are at last able to compute the contributions to the quark and antiquark distributions of the proton from the DIS from its virtual meson and baryon components. The total contribution to a quark distribution in the proton from this process is

$$\delta q(x) = \sum_{M,B} \left(\delta^{(MB)}q(x) + \delta^{(BM)}q(x)\right) \tag{3.62}$$

and similarly for the antiquark distribution. Using the Clebsch-Gordan coefficients for the various charge states of the meson–baryon combinations we can easily obtain the individual flavour distributions. For DIS from virtual mesons we have the following contributions:

$$\begin{aligned}
\delta^{(\pi/\rho\ N)}u(x) &= \int \frac{dy}{y} f_{\pi/\rho\ N}(y)\left(\frac{1}{3}u^{\pi^0}(x_M) + \frac{2}{3}u^{\pi^+}(x_M)\right) = \int \frac{dy}{y} f_{\pi/\rho\ N}(y)\frac{5}{6}V^M(x/y)\\
\delta^{(\pi/\rho\ N)}\bar{u}(x) &= \int \frac{dy}{y} f_{\pi/\rho\ N}(y)\left(\frac{1}{3}\bar{u}^{\pi^0}(x_M) + \frac{2}{3}\bar{u}^{\pi^+}(x_M)\right) = \int \frac{dy}{y} f_{\pi/\rho\ N}(y)\frac{1}{6}V^M(x_M)\\
\delta^{(\pi/\rho\ N)}d(x) &= \int \frac{dy}{y} f_{\pi/\rho\ N}(y)\left(\frac{1}{3}d^{\pi^0}(x_M) + \frac{2}{3}d^{\pi^+}(x_M)\right) = \int \frac{dy}{y} f_{\pi/\rho\ N}(y)\frac{1}{6}V^M(x_M)\\
\delta^{(\pi/\rho\ N)}\bar{d}(x) &= \int \frac{dy}{y} f_{\pi/\rho\ N}(y)\left(\frac{1}{3}\bar{d}^{\pi^0}(x_M) + \frac{2}{3}\bar{d}^{\pi^+}(x_M)\right) = \int \frac{dy}{y} f_{\pi/\rho\ N}(y)\frac{5}{6}V^M(x_M)
\end{aligned} \tag{3.63}$$

$$
\begin{aligned}
\delta^{(\omega N)}u(x) &= \int \frac{dy}{y} f_{\omega N}(y)\, u^{\omega}(x_M) = \int \frac{dy}{y} f_{\omega N}(y)\, \frac{1}{2} V^M(x_M) \\
\delta^{(\omega N)}\bar{u}(x) &= \int \frac{dy}{y} f_{\omega N}(y)\, \bar{u}^{\omega}(x_M) = \int \frac{dy}{y} f_{\omega N}(y)\, \frac{1}{2} V^M(x_M) \\
\delta^{(\omega N)}d(x) &= \int \frac{dy}{y} f_{\omega N}(y)\, d^{\omega}(x_M) = \int \frac{dy}{y} f_{\omega N}(y)\, \frac{1}{2} V^M(x_M) \\
\delta^{(\omega N)}\bar{d}(x) &= \int \frac{dy}{y} f_{\omega N}(y)\, \bar{d}^{\omega}(x_M) = \int \frac{dy}{y} f_{\omega N}(y)\, \frac{1}{2} V^M(x_M)
\end{aligned}
\tag{3.64}
$$

$$
\begin{aligned}
\delta^{(\pi/\rho\ \Delta)}u(x) &= \int \frac{dy}{y} f_{\pi/\rho\ \Delta}(y) \left(\frac{1}{2} u^{\pi^-}(x_M) + \frac{1}{3} u^{\pi^0}(x_M) + \frac{1}{6} u^{\pi^+}(x_M) \right) = \int \frac{dy}{y} f_{\pi/\rho\ \Delta}(y) \frac{1}{3} V^M(x_M) \\
\delta^{(\pi/\rho\ \Delta)}\bar{u}(x) &= \int \frac{dy}{y} f_{\pi/\rho\ \Delta}(y) \left(\frac{1}{2} \bar{u}^{\pi^-}(x_M) + \frac{1}{3} \bar{u}^{\pi^0}(x_M) + \frac{1}{6} \bar{u}^{\pi^+}(x_M) \right) = \int \frac{dy}{y} f_{\pi/\rho\ \Delta}(y) \frac{2}{3} V^M(x_M) \\
\delta^{(\pi/\rho\ \Delta)}d(x) &= \int \frac{dy}{y} f_{\pi/\rho\ \Delta}(y) \left(\frac{1}{2} d^{\pi^-}(x_M) + \frac{1}{3} d^{\pi^0}(x_M) + \frac{1}{6} d^{\pi^+}(x_M) \right) = \int \frac{dy}{y} f_{\pi/\rho\ \Delta}(y) \frac{2}{3} V^M(x_M) \\
\delta^{(\pi/\rho\ \Delta)}\bar{d}(x) &= \int \frac{dy}{y} f_{\pi/\rho\ \Delta}(y) \left(\frac{1}{2} \bar{d}^{\pi^-}(x_M) + \frac{1}{3} \bar{d}^{\pi^0}(x_M) + \frac{1}{6} \bar{d}^{\pi^+}(x_M) \right) = \int \frac{dy}{y} f_{\pi/\rho\ \Delta}(y) \frac{1}{3} V^M(x_M)
\end{aligned}
\tag{3.65}
$$

$$
\begin{aligned}
\delta^{(K\Sigma)}u(x) &= \int \frac{dy}{y} f_{K\Sigma}(y) \frac{1}{3} u^{K^+}(x_M) = \int \frac{dy}{y} f_{K\Sigma}(y) \frac{1}{3} V^M(x_M) \\
\delta^{(K\Sigma)}d(x) &= \int \frac{dy}{y} f_{K\Sigma}(y) \frac{2}{3} d^{K^0}(x_M) = \int \frac{dy}{y} f_{K\Sigma}(y) \frac{2}{3} V^M(x_M) \\
\delta^{(K\Sigma)}\bar{s}(x) &= \int \frac{dy}{y} f_{K\Sigma}(y) \left(\frac{1}{3} \bar{s}^{K^+}(x_M) + \frac{2}{3} \bar{s}^{K^0}(x_M) \right) = \int \frac{dy}{y} f_{K\Sigma}(y) V^M(x_M)
\end{aligned}
\tag{3.66}
$$

$$
\begin{aligned}
\delta^{(K\Lambda)}u(x) &= \int \frac{dy}{y} f_{K\Lambda}(y)\, u^{K^+}(x_M) = \int \frac{dy}{y} f_{K\Lambda}(y)\, V^M(x_M) \\
\delta^{(K\Lambda)}\bar{s}(x) &= \int \frac{dy}{y} f_{K\Lambda}(y)\, \bar{s}^{K^+}(x_M) = \int \frac{dy}{y} f_{K\Lambda}(y)\, V^M(x_M)
\end{aligned}
\tag{3.67}
$$

where $x_M = x/y$. For simplicity we have assumed here the same meson valence quark distribution $V^M(x_M)$ for all mesons (sea components of the meson distributions themselves are not included),

$$
\begin{aligned}
u^{\pi^+/\rho^+} &= \bar{d}^{\pi^+/\rho^+} = 2u^{\pi^0/\rho^0/\omega} = 2\bar{u}^{\pi^0/\rho^0/\omega} = 2d^{\pi^0/\rho^0/\omega} = 2\bar{d}^{\pi^0/\rho^0/\omega} \\
&= u^{K^+} = d^{K^0} = \bar{s}^{K^+} = \bar{s}^{K^0} = V^M
\end{aligned}
\tag{3.68}
$$

and have used SU(3) flavour symmetry to obtain the others.

In practical applications, for V^M we can use the experimental pion valence distribution, which has been determined from Drell-Yan proton—pion scattering [101, 102]. The pion valence quark distribution was found to be consistent with a behaviour $xV^M(x) \sim x^{0.44}(1-x)^{0.89}$ at $Q^2 \sim 4$ GeV^2 [101]. This is in fairly good agreement with the behaviour expected from large-x ($\sim (1-x)$) counting rules [103] and small-x ($\sim x^{1/2}$) Regge behaviour [104]. It was also found in [105] that the ratio of kaon to pion valence quark distributions was consistent with unity over most of the x range, although dropping slightly at large x, $V^K/V^\pi \sim (1-x)^{0.18\pm0.07}$. Unfortunately, the vector meson valence distribution has not yet been determined experimentally. As a first approximation it may seem reasonable to assume that its x-dependence resembles that of the π meson. Deviations

from this may be expected on theoretical grounds, if one assumes that a spin flip for one of the quarks in a spin 1 meson induces an additional power of $(1-x)$ at large x [103].

For the meson recoil diagrams, the contributions from DIS from a virtual baryon B are as follows:

$$\begin{aligned}
\delta^{(N\,\pi/\rho)}u(x) &= \int \frac{dy'}{y'} f_{N\,\pi/\rho}(y') \left(\frac{1}{3}u^p(x_B) + \frac{2}{3}u^n(x_B)\right) = \int \frac{dy'}{y'} f_{N\,\pi/\rho}(y') \left(\frac{1}{3}u(x_B) + \frac{2}{3}d(x_B)\right) \\
\delta^{(N\,\pi/\rho)}d(x) &= \int \frac{dy'}{y'} f_{N\,\pi/\rho}(y') \left(\frac{1}{3}d^p(x_B) + \frac{2}{3}d^n(x_B)\right) = \int \frac{dy'}{y'} f_{N\,\pi/\rho}(y') \left(\frac{1}{3}d(x_B) + \frac{2}{3}u(x_B)\right)
\end{aligned} \tag{3.69}$$

$$\begin{aligned}
\delta^{(N\omega)}u(x) &= \int \frac{dy'}{y'} f_{N\omega}(y')\, u(x_B) \\
\delta^{(N\omega)}d(x) &= \int \frac{dy'}{y'} f_{N\omega}(y')\, d(x_B)
\end{aligned} \tag{3.70}$$

$$\begin{aligned}
\delta^{(\Delta\,\pi/\rho)}u(x) &= \int \frac{dy'}{y'} f_{\Delta\,\pi/\rho}(y') \left(\frac{1}{2}u^{\Delta^{++}}(x_B) + \frac{1}{3}u^{\Delta^{+}}(x_B) + \frac{1}{6}u^{\Delta^{0}}(x_B)\right) = \int \frac{dy'}{y'} f_{\Delta\,\pi/\rho}(y') \frac{7}{3}d(x_B) \\
\delta^{(\Delta\,\pi/\rho)}d(x) &= \int \frac{dy'}{y'} f_{\Delta\,\pi/\rho}(y') \left(\frac{1}{2}d^{\Delta^{++}}(x_B) + \frac{1}{3}d^{\Delta^{+}}(x_B) + \frac{1}{6}d^{\Delta^{0}}(x_B)\right) = \int \frac{dy'}{y'} f_{\Delta\,\pi/\rho}(y') \frac{2}{3}d(x_B)
\end{aligned} \tag{3.71}$$

$$\begin{aligned}
\delta^{(\Sigma K)}u(x) &= \int \frac{dy'}{y'} f_{\Sigma K}(y') \left(\frac{1}{3}u^{\Sigma^0}(x_B) + \frac{2}{3}u^{\Sigma^+}(x_B)\right) = \int \frac{dy'}{y'} f_{\Sigma K}(y') \frac{5}{6}u(x_B) \\
\delta^{(\Sigma K)}d(x) &= \int \frac{dy'}{y'} f_{\Sigma K}(y') \frac{1}{3}d^{\Sigma^0}(x_B) = \int \frac{dy'}{y'} f_{\Sigma K}(y') \frac{1}{6}u(x_B) \\
\delta^{(\Sigma K)}s(x) &= \int \frac{dy'}{y'} f_{\Sigma K}(y') \left(\frac{1}{3}s^{\Sigma^0}(x_B) + \frac{2}{3}s^{\Sigma^+}(x_B)\right) = \int \frac{dy'}{y'} f_{\Sigma K}(y') \left(\frac{1}{6}u(x_M) + \frac{2}{3}d(x_M)\right)
\end{aligned} \tag{3.72}$$

$$\begin{aligned}
\delta^{(\Lambda K)}u(x) &= \int \frac{dy'}{y'} f_{\Lambda K}(y')\, u^{\Lambda}(x_B) = \int \frac{dy'}{y'} f_{\Lambda K}(y') \frac{1}{2}u(x_B) \\
\delta^{(\Lambda K)}d(x) &= \int \frac{dy'}{y'} f_{\Lambda K}(y')\, d^{\Lambda}(x_B) = \int \frac{dy'}{y'} f_{\Lambda K}(y') \frac{1}{2}u(x_B) \\
\delta^{(\Lambda K)}s(x) &= \int \frac{dy'}{y'} f_{\Lambda K}(y')\, s^{\Lambda}(x_B) = \int \frac{dy'}{y'} f_{\Lambda K}(y') \frac{1}{2}u(x_B)
\end{aligned} \tag{3.73}$$

where $x_B = x/y'$, and all baryon quark distributions have been related to the proton distributions. For the neutron this is trivial if one assumes isospin symmetry. Since the Δ has spin and isospin 3/2, from the SU(6) quark model we expect that the valence spectator diquark in a Δ will have spin and isospin of 1. Using this fact we can relate the valence quark distributions in the Δ to the d quark distribution in the proton (since the spectator uu diquark in the proton has the same quantum numbers), $u^{\Delta^{++}} = \frac{3}{2}u^{\Delta^{+}} = 3d^{\Delta^{+}} = 3d$, with the distributions for the other charge states obtained from isospin symmetry. Similarly for the Σ and Λ hyperons, according to SU(3) flavour symmetry we would expect $s^{\Sigma^+} = d$ and $u^{\Sigma^+} = 2q^{\Sigma^0} = 2q^{\Lambda} = u$.

For our numerical results we use experimentally determined coupling constants, all of which are referred to the nucleon pole. For the πNN coupling we use the recently determined value $g^2_{\pi NN}/4\pi = 13.6$ [106], which is marginally smaller than the 'traditional' value [107]. The vector meson—nucleon couplings are obtained from analyses of πN scattering data, $g^2_{\rho NN}/4\pi = 0.55$,

$f_{\rho NN}/g_{\rho NN} = 6.1$ [108], and $g^2_{\omega NN}/4\pi = 8.1$, $f_{\omega NN}/g_{\omega NN} = 0$ [109]. For the kaon–hyperon–nucleon couplings we use $g^2_{KN\Lambda}/4\pi = 13.1$ and $g^2_{KN\Sigma}/4\pi = 3.7$, as in Ref.[100] (although this $KN\Sigma$ coupling is somewhat larger than the ones determined from KN forward dispersion relations [110] or in some hyperon—nucleon potentials [111], however even so the strange contributions are still very small). Finally, we use the quark model to relate the $\pi N\Delta$ and $\rho N\Delta$ couplings to other experimentally measured ones [112], $f^2_{\pi N\Delta} = (72/25) f^2_{\pi NN}$, and $f^2_{\rho N\Delta} = (f^2_{\pi N\Delta}/f^2_{\pi NN})\, g^2_{\rho NN}\, (m_\rho/2M)^2\, (1 + f_{\rho NN}/g_{\rho NN})^2$.

Apart from the coupling constants, the only other parameters in the model are the meson–baryon form factor cut-offs, Λ. The first suggestion about how one might use DIS data to constrain Λ was made by Thomas [58], who compared $\langle y \rangle_{MB}$ with the measured momentum fractions carried by the antiquarks. Similar analyses were later repeated by Frankfurt et al. [59], Kumano [71] and Hwang et al. [62]. Even more stringent constraints can be achieved by also demanding that the shape of the meson exchange contributions to $\bar{q}(x)$, (i.e. $\delta^{(MB)}\bar{q}(x)$) be consistent with the shape of the experimental antiquark distribution [59, 61].

As mentioned in the previous section, the fact that the old $f_{\pi N}(y)$ calculated in a covariant framework peaked more sharply and at smaller y compared with the $f_{\pi N}$ calculated in the IMF means that the quark distributions in (3.63)—(3.73) will also peak at smaller x for the covariant k^2-dependent form factor. This is evident in Fig.3.12 where the calculated SU(2) antiquark contribution to $\delta^{(\pi N)}F_{2p}(x)$ is compared with some recent empirical data (as parameterised by Morfin and Tung [50], Owens [51], Eichten et al. [15] and Diemoz et al. [113]) for $(\bar{u}+\bar{d})/2$ at $Q^2 = 4$ GeV^2. Because the TOPT/IMF formulation generally gives broader antiquark distributions, the limits on the cut-offs will be more severe than for the covariant case, since at intermediate x ($x \gtrsim 0.2$) the TOPT/IMF distributions are still large compared with the experimental data.

Figure 3.13 shows the contributions to the SU(2) antiquark distribution $x(\bar{u} + \bar{d})/2$ from all of the meson–baryon components of the nucleon, for $\Lambda = 700$ and 900 MeV. Also shown are the calculated results (for $\Lambda = 700$ MeV) for the πN and $\pi N + \pi\Delta$ states alone. Clearly the SU(2) $\bar{q}$ content of the nucleon is well saturated for $\Lambda \approx 700$ MeV in the intermediate-x region when all meson–baryon components are included. The main contributions in this region come from the ρN and $\rho\Delta$ states, since the distribution functions $f_{\rho N(\Delta)}(y)$ generally extend to larger y compared with the pion distributions. As mentioned above, one uncertainty in the treatment of the vector meson contributions arises from the fact the structure function for a spin 1 meson may deviate at large x from the behaviour observed for the pion structure function. In Fig.3.14 we illustrate the effect on the ρN contribution to $x(\bar{u} + \bar{d})/2$ of including an extra power of $(1 - x)$ in the ρ meson structure function. The result is a slightly softer distribution, so that this would allow for a marginally larger cut-off mass when comparing against the data in Fig.3.13. If only the πN states are included, slightly harder form factors could also be accommodated, with around $\Lambda \approx 1$ GeV. In either case, for the πNN vertex this corresponds to a dipole form factor cut-off in the covariant formulation of $\Lambda_{\pi N} \sim 700 - 800$ MeV (to give the same value of $\langle n \rangle_{\pi N} \sim 0.10 - 0.15$), which is still

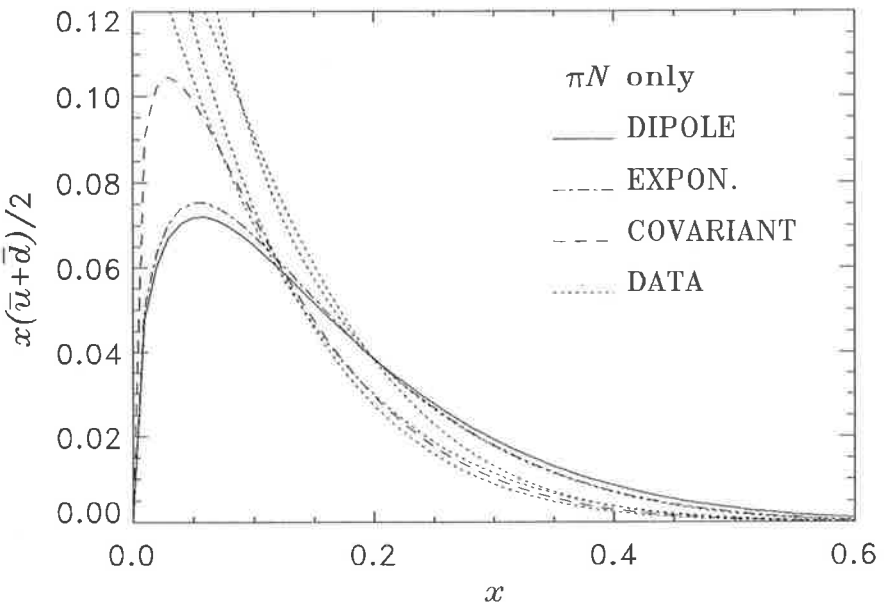

Figure 3.12: Proton SU(2) flavour antiquark distributions for DIS on the πN component of the nucleon, evaluated using different form factors. The values of the cut-off masses are chosen to yield the same average number of pions, $\langle n \rangle_{\pi N}$ ($\simeq 0.175$). For the TOPT/IMF calculation with a dipole form factor $\Lambda = 1000$ MeV; with an exponential form $\Lambda_e = 1240$ MeV; and for a covariant dipole form factor $\Lambda_{\pi N} = 870$ MeV. The dotted curves are parameterisations of the DIS data (see text).

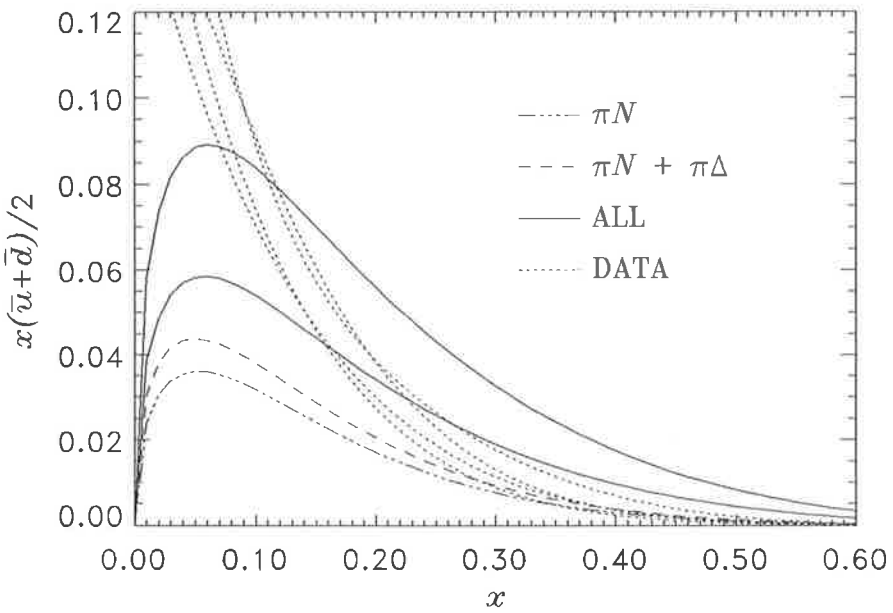

Figure 3.13: Proton SU(2) flavour antiquark distributions for DIS on the various meson–baryon components of the nucleon. The dot-dashed and dashed curves represent the contributions from πN and $\pi N + \pi\Delta$ states, respectively, for $\Lambda = 700$ MeV. The solid curves are the total contributions from all meson–baryon states, for $\Lambda = 700$ MeV (lower curve) and 900 MeV (upper curve). The data are as in Fig.3.12.

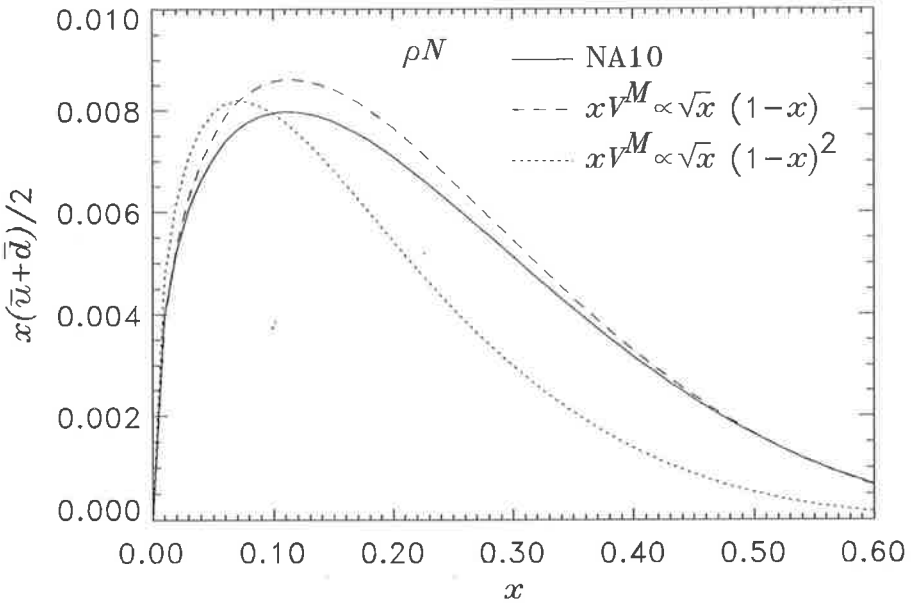

Figure 3.14: Contribution to the antiquark distributions from the ρN states (with $\Lambda = 700$ MeV), for different vector meson valence structure functions.

considerably smaller than that used by many authors.

3.1.5 Renormalisation, Incoherence

A subtle, but nonetheless important, point that needs to be made concerns the renormalisation of the total quark distributions in the presence of mesons. The meson and baryon exchange diagrams in Fig.3.1 describe physical processes (inclusive baryon and meson leptoproduction) whose cross sections involve physical (renormalised) coupling constants. When integrated over the recoil particles' momenta these yield the inclusive DIS cross sections, which are proportional to the total quark (and antiquark) distributions

$$q(x) \;=\; Z\, q_{\rm bare}(x) \;+\; \sum_{M,B} \left(\delta^{(MB)} q(x) \;+\; \delta^{(BM)} q(x) \right). \tag{3.74}$$

Therefore $\delta^{(MB)}q(x)$ and $\delta^{(BM)}q(x)$, and the convolution integrals in (3.6) and (3.7), are expressed in terms of renormalised coupling constants contained in the functions $f_{MB}(y)$ and $f_{BM}(y')$. From (3.74) we also determine the bare nucleon probability

$$Z \;=\; 1 \;-\; \sum_{M,B} \langle n \rangle_{MB} \tag{3.75}$$

by demanding that the valence number and momentum sum rules are satisfied. We emphasise that all quantities in Eqs.(3.74) and (3.75) are evaluated using renormalised coupling constants.

We could, of course, choose to work at a given order in the bare coupling constant, and explicitly verify that the various sum rules are satisfied. For example, to lowest order (g_0^2) the total quark

distributions would be [114]

$$q(x) \;=\; Z\left\{q_{\rm bare}(x) \;+\; \sum_{M,B}\Big(\delta^{(MB)}q_{(0)}(x) \;+\; \delta^{(BM)}q_{(0)}(x)\Big)\right\} \qquad (\text{order } g_0^2) \quad (3.76)$$

with

$$Z \;=\; \left(1+\sum_{M,B}\langle n_{(0)}\rangle_{MB}\right)^{-1} \qquad (\text{order } g_0^2) \quad (3.77)$$

where the subscript (0) indicates that the functions $f(y)$ here are evaluated using bare couplings. Eqs.(3.74) and (3.75) are easily recovered since the bare couplings, to this order, are defined by $g_0^2 = g_{\rm ren}^2/Z$. It would, however, be inconsistent to use (3.76) and (3.77) with renormalised coupling constants, especially with large form factor cut-offs. As long as the form factors are soft, the difference between the bare and renormalised couplings is not very large. However, with large cut-off masses the bare couplings would need to be substantially bigger than the physical ones. (In fact, the form factor cut-off dependence of the bare πN coupling constant in the cloudy bag model [55] showed some 40% difference for very hard form factors — or small bag radii, ~ 0.6 fm.) In addition, with large values of Λ the higher order diagrams involving more than one meson in the intermediate state would become non-negligible, and the initial assumption that the series in (3.1) can be truncated at the one-meson level would be seriously in doubt. Fortunately, we need not consider the multi–meson contributions, since Fig.3.13 clearly demonstrates the difficulty in reconciling the empirical data with quark distributions calculated with such large cut-offs.

Finally, we need to make some additional comments regarding the justification of our calculation in terms of an incoherent summation of cross sections (rather than amplitudes) for the various meson exchange processes. A possible breakdown of incoherence may arise when there are different exchange processes leading to the same final state. For nucleon final states, because of the pseudoscalar nature of the πNN vertex, there will be no interference between π meson and vector meson exchange. Furthermore, no mixing will take place between the ω and ρ exchange configurations due to their different isospins. In fact, all of the meson exchange processes with a recoil N considered in this analysis can be added incoherently. For a Δ recoil, the only mesons coupling to N and Δ are the π and ρ, but since they have different G-parities, interference effects from these will again be excluded. However, the possibility exists in the pion exchange process that the decay products of a Δ recoil, namely π and N, may mix with the state containing an N recoil together with a π from the hadronic debris X of the shattered exchanged pion. Interference between the πN and $\pi\Delta$ states could therefore occur if the π from the debris had very low momentum, enabling the combined system to have an invariant mass squared $\sim M_\Delta^2$. However, as we shall discuss more fully in Chapter 6, the vast majority of semi-inclusive meson events in lepton–nucleon DIS are those with high momentum mesons (slow hadrons are almost exclusively baryons), so that the probability of interference arising from such processes will not be large. A similar argument can be given for the potential interference from hyperon decay into $N\pi$.

For the baryon exchange processes, the requirement of the same recoil meson eliminates interference from most states, except from DIS off N and Δ with π (or ρ) in the final state, and from DIS off a Σ^0 and Λ^0 with a K^+ recoil. For the latter, the different isospin quantum numbers of the $\Lambda(I=0)$ and $\Sigma(I=1)$ rule out interference, just as for the ρN and ωN states. A similar argument can be made for excluding interference contributions from $N(I=1/2)$ and $\Delta(I=3/2)$ exchange. However, as in the meson exchange case, the possibility of vector meson or kaon decay into pions (e.g. $\rho \to 2\pi$, $K^0 \to 2\pi$) may introduce coherent effects when these meson recoil states (with an exchanged N, Δ or hyperon) are added with those containing a π recoil. But the fact that the decay products of the recoil mesons have low momentum, while the pions from the hadronic debris are fast, will again reduce the size of any interference effects here.

Therefore we see that by considering only the lowest lying meson and baryon states (i.e. by excluding resonance having the same quantum numbers as the mesons and baryons considered here) we can avoid potential problems with interference, and certainly for the values of Λ allowed by the data, the only relevant states are those with the lowest masses.

3.2 Flavour Asymmetry in the Proton Sea

From Eqs.(3.63) to (3.73) it is clear that the predicted contributions from DIS off virtual mesons and baryons to the u, d and s quark (and the corresponding antiquark) distributions in the proton will be different. Because the contributions to s and $\bar{s}$ from DIS from kaons and hyperons are very much smaller than those from the non-strange mesons and baryons to the u and d distributions (mainly because $m_K \gg m_\pi$) we see that the meson model produces significant SU(3) flavour symmetry violation. Furthermore, it is apparent that the contributions to the u and d (and $\bar{u}$ and $\bar{d}$) quark distributions themselves are not the same, so that SU(2) flavour symmetry of the proton sea is also broken. In the case of the pion cloud, the simple origin of this is asymmetry is the predominance of the dissociation process $p \to n\pi^+$ over $p \to p\pi^0$. In the former, the π^+ valence quark content is $d\bar{u}$, while in the latter the ratio of $\bar{u}$ to $\bar{d}$ quarks is the same. This process certainly respects isospin symmetry, which simply says that the dissociation $p \to n\pi^+$ is as likely as $n \to p\pi^-$, or at the quark level, $u \to d(u\bar{d})$ is as likely in the proton as $d \to u(d\bar{u})$ in the neutron. But it clearly implies an excess of $\bar{d}$ quarks in the proton, and an equal excess of $\bar{u}$ quarks in the neutron.

If the masses of quarks were identical (i.e. SU(3) flavour symmetry limit) then the ratio of strange to non-strange antiquark distributions in the proton would be 1:2. From neutrino experiments (at $Q^2 \sim 4$ GeV^2) the measured ratio was found to be about 1:4 [115], which can be understood semi-quantitatively from the the heavier mass of the strange quark. On the other hand, because charge symmetry is such a good symmetry in strong interaction physics, it was naively expected that SU(2) flavour symmetry of the sea would be an excellent approximation. Indeed, this expectation has been built into almost all of the analyses of the nucleon structure function data. The main reason was believing this has been the simple picture, motivated by perturbative QCD,

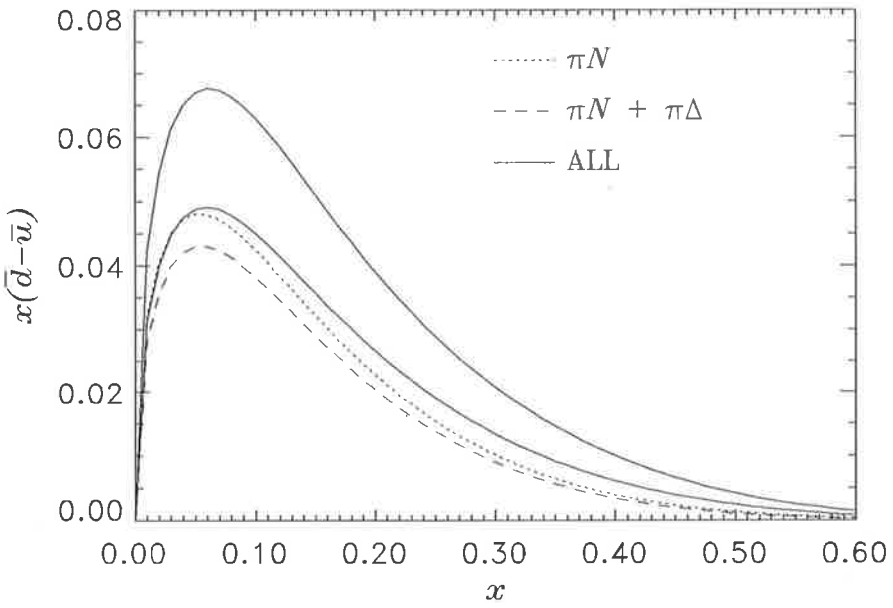

Figure 3.15: Calculated $\bar{d} - \bar{u}$ difference from the various meson-baryon states. For the dotted, dashed and lower solid curves a dipole form factor cut-off of $\Lambda = 700$ MeV is used, while the upper solid curve is calculated with $\Lambda = 900$ MeV.

in which the mechanism for producing antiquarks is gluon splitting into $q\bar{q}$ pairs. However, unless isospin symmetry is genuinely violated (by giving a non-zero mass difference between the u and d quarks), the perturbative process $g \to q\bar{q}$ should be SU(2) flavour symmetric, as the gluons of QCD are flavour–blind. Therefore a $\bar{d} - \bar{u}$ difference cannot be produced by perturbative QCD. Actually, this statement should be qualified by saying that at lowest order in α_S there is no asymmetry. A higher order perturbative QCD calculation of $\bar{d} - \bar{u}$ was performed some time ago by Ross and Sachrajda [116], who found a non-zero result for this difference, although the absolute value was very small. This means that the calculated $\bar{d} - \bar{u}$ difference will be preserved in QCD evolution. But the fact that we get a non-zero $\bar{d} - \bar{u}$ difference in the meson–baryon model is not surprising, since this is a non-perturbative model, and its predictions are not in conflict with QCD, nor with isospin symmetry.

In Figs.3.15 and 3.16 we plot the $\bar{d} - \bar{u}$ difference, and the ratio $(\bar{d} - \bar{u})/(\bar{d} + \bar{u})$, respectively, calculated within the meson-exchange model of the nucleon. Fig.3.15 shows that the inclusion of $\pi\Delta$ states (with $\Lambda = 700$ MeV) eliminates some of the $\bar{d}$ excess, since here the dominant process is $p \to \Delta^{++}\pi^-$, which at the quark level, $d \to u(d\bar{u})$, is seen to produce a $\bar{u}$ excess. However, adding the vector meson components (lower solid curve) restores the original $\bar{d}$ excess at small x, and enhances the excess at larger x. At larger values of Λ ($= 900$ MeV) the $\bar{d} - \bar{u}$ difference is larger still (upper solid curve), although the ratio $(\bar{d} - \bar{u})/(\bar{d} + \bar{u})$ is smaller, Fig.3.16.

On similar grounds the processes $p \to K^0\Sigma^+$ and $p \to K^+\Sigma^0(\Lambda)$ will introduce not only a different strange quark content of the proton than a non-strange, but also a different $\bar{s}$ distribution as well. This is clear from Fig.3.17, where we show both the sum of the calculated xs and $x\bar{s}$

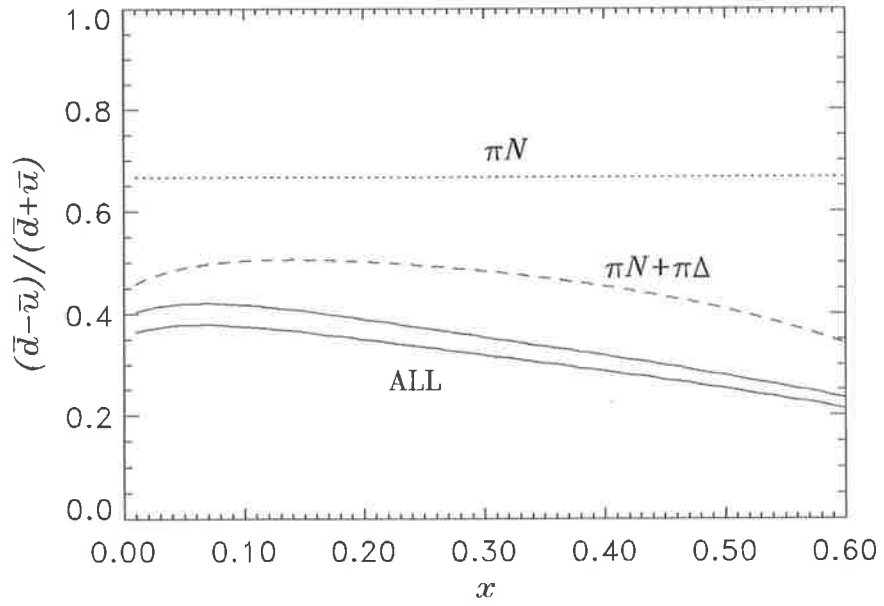

Figure 3.16: Ratio of the difference and sum of the calculated SU(2) antiquark distributions in the proton. The cut-off for the dotted, dashed and upper solid curves is $\Lambda = 700$ MeV, while the lower solid curve is calculated with $\Lambda = 900$ MeV.

distributions and their difference. Although not obvious from the figure, the integral over $s - \bar{s}$ is zero, since the proton has no net strangeness. Since at large x the hyperon structure function is suppressed by about two powers of $(1-x)$ compared with the kaon structure function, the excess of s over $\bar{s}$ is concentrated at very small x ($x \lesssim 0.01$). Although these are quite interesting predictions of the model, because of the very small magnitude of the strange contributions (notice the scale on the vertical axis) it will be difficult for such effects to be observed in DIS experiments in the near future.

Of course the idea of an asymmetric proton sea is not a new one. The earliest, and perhaps most obvious, suggestion for why we should expect $\bar{u} \neq \bar{d}$ was made by Feynman and Field [117]. Because the proton has an unequal number of valence u and d quarks, by the Pauli exclusion principle we would therefore expect creation of additional $q\bar{q}$ pairs inside the proton to be sensitive to the number of quarks of each flavour already in the proton. Since there are 2 valence u quarks in the proton compared with only 1 valence d quark, we therefore expect a larger $\bar{d}$ sea since $u\bar{u}$ pair creation will be suppressed relative to $d\bar{d}$. In [117] the $\bar{d}$ and $\bar{u}$ distributions were parameterised by $x\bar{d} = 0.17(1-x)^7$ and $x\bar{u} = 0.17(1-x)^{10}$, see Fig.3.18. With these, the integrated difference is $\int dx(\bar{d} - \bar{u}) = 0.057$. An early calculation of the u and d sea quark probabilities in the proton, incorporating the effects due to the Pauli principle, was made by Donoghue and Golowich [118] using the MIT bag model nucleon wavefunction. More recently, work by Signal and Thomas [38] on the calculation of quark distribution functions in the MIT bag model suggested a quantitative method of calculating the x-dependence of the Pauli $\bar{d} - \bar{u}$ difference as well. Following the earlier formal analysis by Jaffe of the twist-2 quark and antiquark distributions [52], Signal and Thomas showed

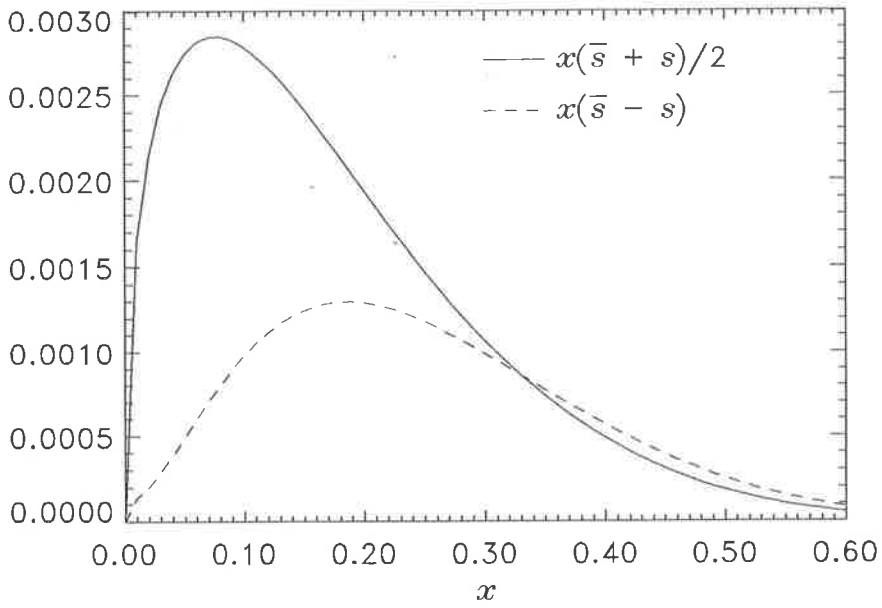

Figure 3.17: Strange & antistrange content of the proton, calculated from DIS off virtual K and hyperon components of the nucleon. The form factor cut-off Λ is 900 MeV.

that the valence quark distributions could be calculated from a sum of distributions representing 2 q, and $3q+1\bar{q}$ intermediate states. On the other hand, the antiquark distributions arose only from 4 q intermediate bag states. Thus the $\bar{d}$ distribution required the intermediate state to consist of 2 u and 2 d quarks, while DIS from a $\bar{u}$ quark implied a $3u+1d$ intermediate state, which, because of the Pauli principle, has a smaller probability. Furthermore, in Ref.[38] the $\bar{d}$ excess associated with the Pauli effect was equal to the d excess and satisfied the condition

$$\int_0^1 dx\ \bar{d}_{\rm excess}(x) = \int_0^1 dx\ (d_{\rm sea}(x) - u_{\rm sea}(x)) = \int_0^1 dx\ p_N(x) \equiv \mathcal{P}_N. \tag{3.78}$$

Here, $p_N(x)$ denotes the piece of the valence quark distribution associated with a four quark intermediate state (all in a $1s$ state), while $1-\mathcal{P}_N$ is the integral over the distribution function associated with a two quark intermediate state. In Ref.[38] the calculated distributions were found to peak at $x \sim 1 - M_{int}/M$, where M_{int} is the mass of the intermediate spectator state. Since the 4-quark intermediate states have mass greater than M, the antiquark distributions will peak at negative x. Therefore in the physical region ($x \geq 0$), $p_N(x)$ should resemble a typical sea quark distribution, namely be finite at $x = 0$ while dropping rapidly to zero by $x \sim 0.2 - 0.3$. For simplicity, we can parameterise the large x behaviour by a $p_N(x) \propto (1-x)^7$ form [15, 63]. On theoretical grounds, we can also expect that due to the lack of Regge $f - A_2$ exchange degeneracy, at small x the $\bar{d} - \bar{u}$ difference should be proportional to $p_N(x) \sim x^\alpha$, where $\alpha(\simeq 0.5)$ is the Regge intercept [119, 104]. The overall normalisation $\mathcal{P}_N$ was calculated in Ref.[47] to be less than about 0.25 for bag radii $R \lesssim 0.8$ fm.

In Fig.3.18 we compare the Feynman & Field parameterisation with the function $p_N(x)$, normalised so that $\mathcal{P}_N = 0.05, 0.15$ and 0.25. Also shown is the effect of using a slightly more singular

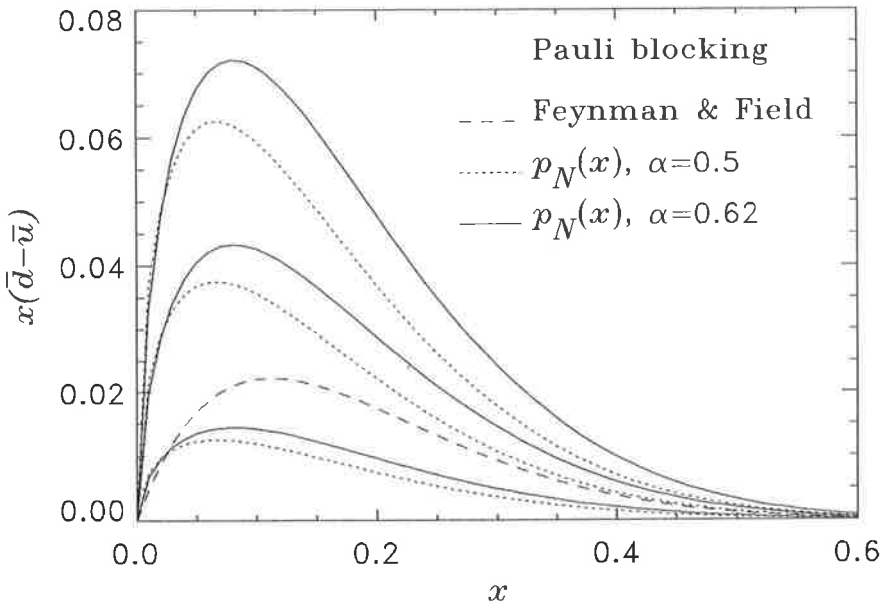

Figure 3.18: Difference between $\bar{d}$ and $\bar{u}$ quark distributions in the proton, for the Feynman and Field parameterisation [117], and a parameterisation of the function $p_N(x) \sim x^{0.62}(1-x)^7$, with normalisation $\mathcal{P}_N = 0.05, 0.15$ and 0.25.

small x behaviour, $\alpha = 0.62$, as suggested by the recent NMC data on $F_{2p} - F_{2n}$ (see Section 3.3).

Apart from the Pauli exclusion principle, and the proton's meson cloud, several other suggestions have been made for possible sources of SU(2) flavour symmetry breaking in the proton sea. One possibility is that isospin symmetry is genuinely violated to a significant extent. Of course in the real world isospin is not a perfect symmetry — it is certainly violated by the electromagnetic interactions. However, since the proton–neutron mass difference is of the order of 0.1% we can expect that its effects on $\bar{u} - \bar{d}$ should be negligible. Furthermore, since the mass of the d quark is believed to be slightly larger than the u quark mass, the sign of $\bar{d} - \bar{u}$ should actually be negative, since in that case the gluon splitting into $d\bar{d}$ pairs would be suppressed relative to $u\bar{u}$ creation.

A curious extension of this idea was put forward by Ma et al. [120] who postulated that isospin may be violated but that flavour SU(2) symmetry could remain unbroken. In such a scenario, one would have $\bar{u}^p = \bar{d}^p$ in the proton, but $\bar{u}^p \neq \bar{d}^n$. However, since the only reason that the $\bar{d}$ content of the neutron differs from the $\bar{u}$ content of the proton is that $m_d > m_u$, it is difficult to imagine how in the proton the same isospin violating mechanism, $g \to q\bar{q}$, can produce equal amounts of $u\bar{u}$ and $d\bar{d}$.

Unfortunately at the present time there are not sufficient data on $\bar{d} - \bar{u}$ to make definitive conclusions about these various mechanisms for SU(2) flavour symmetry breaking. However, there have been a number of interesting suggestions for experiments that could directly probe the light sea quark content of the proton, and we briefly review these now.

Recently it was suggested by Martin, Stirling and Roberts [121] that one could learn about the SU(2) sea by observing the W-boson asymmetries in $p\bar{p}$ collisions, $p\bar{p} \to W^{\pm}X$. The simple

idea is that a $u(d)$ quark in a proton interacts with a $\bar{d}(\bar{u})$ antiquark in an antiproton to produce a $W^+(W^-)$ boson. Because the $u(\bar{u})$ quark in the proton (antiproton) carries more momentum (lies at larger x) than the $d(\bar{d})$ quark, $W^+(W^-)$ bosons will be predominantly produced in the proton (antiproton) direction. However, in addition there will be $W^+(W^-)$-bosons produced by the annihilation of $\bar{d}(\bar{u})$ quarks in the proton with $d(u)$ quarks in the antiproton. Thus at large energies the asymmetry in the W-boson rapidity (y_W) distribution

$$A(y_W) = \frac{\sigma^+ - \sigma^-}{\sigma^+ + \sigma^-} = \frac{u(x_1)d(x_2) + \bar{d}(x_1)\bar{d}(x_2) - d(x_1)u(x_2) - \bar{d}(x_2)\bar{d}(x_1)}{u(x_1)d(x_2) + d(x_1)u(x_2) + d(x_1)u(x_2) + \bar{d}(x_2)\bar{d}(x_1)} \tag{3.79}$$

where $\sigma^\pm = d\sigma/dy_W(W^\pm)$, would be sensitive to the antiquark distributions in the proton. Here, $x_{1,2} = M_W/\sqrt{s}\exp(\mp y)$, s is the centre of mass energy squared, and the W-boson rapidity is defined by $y_W = (1/2)\ \ln(q_-/q_+)$, with q the W-boson momentum. Furthermore, since only left-handed quarks (right-handed antiquarks) couple to W-bosons, in the resulting $W \to e\nu$ decay the electron (positron) distribution will generally follow the direction of the incoming proton (antiproton). It was suggested in [121] that the experimental $e^\pm$ asymmetry, $A(y_e) = (d\sigma/dy_{e^+}(y_{e^+}) - d\sigma/dy_{e^-}(y_{e^-}))/(d\sigma/dy_{e^+}(y_{e^+}) + d\sigma/dy_{e^-}(y_{e^-}))$, could then serve as an independent check on the $\bar{u}$ and $\bar{d}$ distributions in the proton. The claim in Ref.[121] was that their existing parameterisations with no SU(2) flavour asymmetry are consistent with the data on $A_e(y_e)$ taken at the Collider Detector at Fermilab (CDF) [122]. However, the error bars in this experiment are quite large, and the data at present will have difficulty in discriminating between SU(2) flavour symmetric parameterisations, and those with a small $\bar{d} - \bar{u}$ difference, such as that suggested by the meson model in the previous section. On the other hand, a large $\bar{d} - \bar{u}$ difference, such as that arising from the meson model with large form factor cut-offs Λ, may well introduce a detectable difference.

In another experiment, performed some than 10 years ago by the E288 Collaboration at FNAL [123], the slope of the rapidity distribution for proton–nucleus Drell-Yan production was measured, and found to be sensitive to the $\bar{u}/\bar{d}$ ratio. In that experiment, the quantity

$$\frac{d}{dy} \ln \left(s \frac{d^2\sigma}{d\sqrt{\tau} dy} \right)_{y=0} \tag{3.80}$$

was measured as a function of $\sqrt{\tau}$, where $\tau = M^2_{l^+l^-}/s$. It was found that a parameterisation with $\bar{d} > \bar{u}$ improved the quality of the fit [124]. However, since the analysis of this experiment required the quark and antiquark distributions in the nucleus, any conclusions reached about the nucleon sea distributions were obviously dependent upon any nuclear assumptions made. In fact, it was later shown by Ericson and Thomas [125] that a similar improvement in the fit could be made by assuming a small difference between the $\bar{q}$ distributions in the nucleon and in a nucleus.

Proton–nucleus Drell-Yan production was also studied recently by the E772 Collaboration at Fermilab. It was found that by comparing the yield per nucleon in a proton collision with a neutron-rich target such as tungsten with that for an isoscalar nucleus, the resulting ratio would also be sensitive to the $\bar{d} - \bar{u}$ difference. However, it has since been argued by Eichten et al. [126] that this

too may not be a sensitive enough experiment for a small non-zero $\bar{d}-\bar{u}$ difference to be discernable from no difference.

Perhaps the experiment that is most sensitive to the light sea quark distributions was that recently proposed by Ellis & Stirling [127], who suggested measuring the asymmetry between the pn and pp Drell-Yan production (i.e. $pN \to l^+l^-X$) cross sections at zero rapidity, $A_{DY} = (\sigma^{pp} - \sigma^{pn})/(\sigma^{pp} + \sigma^{pn})$, where $\sigma^{pN} \propto d^2\sigma^{pN}/d\sqrt{\tau}dy|_{y=0}$. Neglecting terms involving annihilation of sea quarks in the (beam) proton and (target) nucleon, the cross sections can be written

$$A_{DY} = \frac{(4\lambda_V - 1)(\lambda_S - 1) + (\lambda_V - 1)(4\lambda_S - 1)}{(4\lambda_V + 1)(\lambda_S + 1) + (\lambda_V + 1)(4\lambda_S + 1)} \tag{3.81}$$

where $\lambda_V = u_V/d_V$ and $\lambda_S = \bar{u}/\bar{d}$. The advantage of measuring this ratio is that it would be free from any nuclear dilution effects, and the complete asymmetry could be determined from ratios of valence and sea quark distributions alone. Since the d_V/u_V ratio is well determined, A_{DY} would then serve as an accurate indicator of λ_S. In Fig.3.19 we plot this Drell-Yan asymmetry as a function of $\sqrt{\tau} = \sqrt{Q^2/s}$ with $s \sim 1500$ GeV^2 (corresponding to a proton beam energy of about 800 GeV) calculated using the quark and antiquark distributions of the meson model (with $\Lambda = 700$ MeV). This is compared with the asymmetry arising from the parameterisation of Morfin & Tung [50] for the valence quarks (dotted curve), and from the d_V/u_V ratio fixed at $0.57(1-x)$ [15] (dashed curve), with $\lambda_S = 1$ in both cases. It is clear that even small deviations of $\bar{u}/\bar{d}$ from unity will have a big impact upon A_{DY}.

An extension of this idea was discussed in Ref.[128], where it was argued that one could directly measure the difference $\bar{d} - \bar{u}$ by going to large projectile momentum fractions x_1, but small target fractions x_2. In that case the term in A_{DY} involving the product of projectile sea and target valence distributions could be neglected and the asymmetry reduced to

$$A_{DY} \approx \frac{(4\lambda_V - 1)(\lambda_S - 1)}{(4\lambda_V + 1)(\lambda_S + 1)}. \tag{3.82}$$

Unfortunately, there are as yet no data on A_{DY}, although a proposal has been made [129] for an experiment to measure the Drell-Yan cross sections for hydrogen and deuterium targets. Such data would be eagerly anticipated.

Finally, an interesting observation was made by Levelt, Mulders and Schreiber [130], who found that semi-inclusive charged-hadron production could be used to obtain information on the integrated $\bar{d} - \bar{u}$ difference. Following earlier work by Gronau et al. [131] and Field and Feynman [117] on the parton model for semi-inclusive DIS, Levelt et al. showed that the integrated difference should be proportional to the measured difference between the charged pion and kaon production rates from DIS on protons and neutrons. However, the available data from the EM Collaboration at CERN on semi-inclusive charged-meson production [132] are not yet sufficiently accurate to discriminate between SU(2) flavour symmetry and asymmetry. (For a more detailed discussion of semi-inclusive DIS see Chapter 6.)

However, the most important impact on the question of SU(2) flavour symmetry in the proton sea, and certainly the stimulus for the close attention this question has received in recent times, has

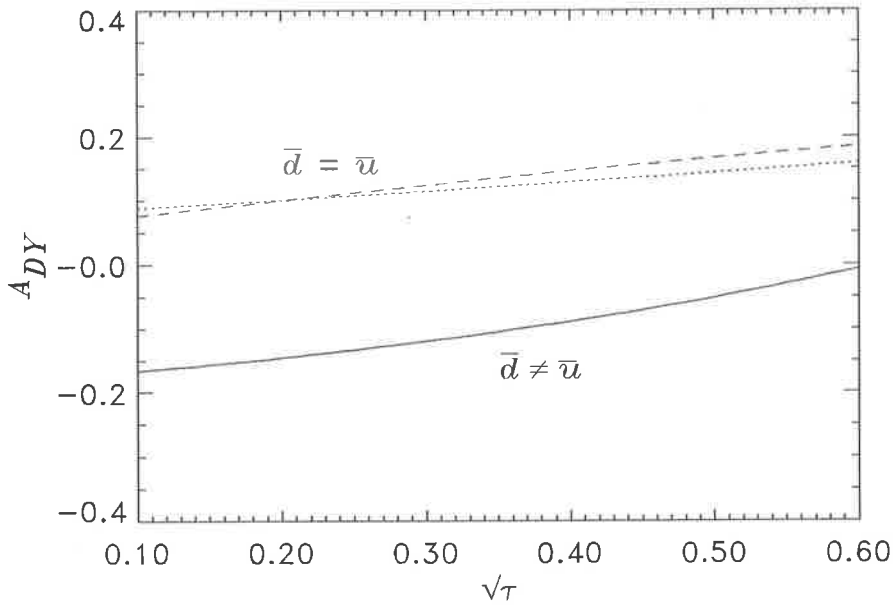

Figure 3.19: Asymmetry for pp and pn Drell-Yan production. The $\bar{u} = \bar{d}$ predictions, with the valence quark parameterisation of Morfin and Tung [50] (dotted) and with a fixed valence ratio $d_V/u_V = 0.57(1-x)$ [15], are compared with the meson model calculation with $\bar{u} \neq \bar{d}$ (for $\Lambda = 700$ MeV).

come from the measurement by the New Muon Collaboration at CERN of the difference between F_{2p} and F_{2n} [65], and the consequent determination of the Gottfried sum rule. We will now discuss the issues involved in this experiment more fully.

3.3 Gottfried Sum Rule

The Gottfried sum rule [64] is perhaps the most famous consequence of SU(2) flavour symmetry of the sea. Because this measures the x-integrated difference between the proton and neutron structure functions, it is sensitive only to the non-singlet SU(2) content of the nucleon. Let us firstly define the quantity

$$S_G(x,1) \;=\; \int_x^1 \frac{dx'}{x'}\left(F_{2p}(x') - F_{2n}(x')\right). \tag{3.83}$$

Relating the proton and neutron structure functions to the quark distributions in the proton (i.e. using charge symmetry), we have

$$S_G(x,1) \;=\; \frac{1}{3}\int_x^1 dx'\left(u(x') + \bar{u}(x') + d(x') + \bar{d}(x')\right) \tag{3.84}$$

$$\;=\; \frac{1}{3}\int_x^1 dx'\left(u_V(x') - d_V(x')\right) \;+\; \frac{2}{3}\int_x^1 dx'\left(\bar{d}(x') - \bar{u}(x')\right) \tag{3.85}$$

where the valence quark distributions are defined by $q_V \equiv q - \bar{q}$. Since the number of valence quarks in a hadron does not change, we obtain the Gottfried sum rule

$$S_G \;\equiv\; S_G(0,1) \;=\; \frac{1}{3} \qquad\qquad \text{[QPM]} \tag{3.86}$$

provided we make the additional assumption $\int_0^1 dx\ \bar{d} = \int_0^1 dx\ \bar{u}$, as would be expected in the quark-parton model (QPM).

The early experimental data for $S_G(x,1)$ did in fact suggest a value lower than 1/3, but with errors large enough to be consistent with it. However, armed with the theoretical expectation of SU(2) flavour symmetry, most authors believed that S_G would tend to 1/3 as the accuracy of the data improved. To the surprise of many, the recent, accurate determination of S_G by the New Muon Collaboration appears to support the idea that $\bar{u} \neq \bar{d}$ [65, 133]. Neglecting nuclear effects, the NMC found

$$S_G(x_{min},1) = 0.229 \pm 0.0157 \tag{3.87}$$

where $x_{min} = 0.004$. Included in (3.87) is an extrapolation from $x = 0.8$ to 1, the contribution from which was estimated to be 0.002 ± 0.001 if a smooth extrapolation of F_{2p}/F_{2n} to 1/4 at $x = 1$ is assumed. From the unmeasured region ($x < 0.004$), using the extrapolation

$$F_{2p}(x) - F_{2n}(x) \longrightarrow \alpha\, x^{\beta} \qquad \text{as } x \to 0 \tag{3.88}$$

with $\alpha = 0.21, \beta = 0.62$, the contribution was found to be $S_G(0,x_{min}) = (\alpha/\beta)\ x_{min}^{\beta} = 0.011$. With the conventional Regge theory assumption that $\beta = 0.5$, $S_G(0,x_{min})$ would be 0.014. The combined integral over the whole range of x was therefore

$$S_G = 0.240 \pm 0.016 \qquad \text{[NMC]} \tag{3.89}$$

with errors added in quadrature.

Although not the only one, the most natural explanation for the smaller than expected value of S_G is that $\bar{d}(x) \neq \bar{u}(x)$ (see later for a discussion of other possibilities). Taken at face value, the NMC result would imply that

$$\int_0^1 dx\ (\bar{d}(x) - \bar{u}(x)) = 0.14 \pm 0.06. \tag{3.90}$$

The various mechanisms discussed in Section 3.2 are then potential candidates for generating such a difference [3]. Before turning to more exotic explanations, it seems more sensible that the simplest possibilities should be exhausted first. The most compelling, and most economical from the theoretical point of view, appear to be those based on the Pauli exclusion principle, and on the presence of a small pion (and perhaps other meson) cloud.

We therefore begin with the meson model, described in Section 3.1. From the mesonic and baryonic corrections to the quark and antiquark distribution functions in Eqs.(3.63)-(3.73), the

[3] In addition to the possibilities discussed there, another explanation for the smaller value of S_G, based in isospin symmetry breaking, was proposed by Walliser and Holzwarth [134]. They showed that within the soliton model the value of S_G deviates from 1/3 by a factor $(M_p - M_n)/(m_u - m_d)$, so that based on current knowledge of the $d-u$ quark mass difference, the sum rule should be some 30% smaller.

total contribution from all mesons to the Gottfried sum can be written

$$S_G = \frac{Z}{3} + \frac{1}{3}\sum_{M,B}\int dx \left(\delta^{(MB)}u + \delta^{(MB)}\bar{u} - \delta^{(MB)}d - \delta^{(MB)}\bar{d} + \delta^{(BM)}u - \delta^{(BM)}d\right)$$
$$= \frac{1}{3}\left(Z - \frac{\langle n\rangle_{N\pi}}{3} - \frac{\langle n\rangle_{N\rho}}{3} + \frac{5\langle n\rangle_{\Delta\pi}}{3} + \frac{5\langle n\rangle_{\Delta\rho}}{3} + \langle n\rangle_{N\omega} + \langle n\rangle_{\Sigma K} + \langle n\rangle_{\Lambda K}\right). \quad (3.91)$$

Note, however, that because the non-strange baryon recoil contributions to the quark and antiquark distributions are related by

$$\delta^{(MB)}u(x) = \delta^{(MB)}\bar{d}(x), \qquad \delta^{(MB)}d(x) = \delta^{(MB)}\bar{u}(x) \qquad [M = \text{non} - \text{strange}] \quad (3.92)$$

the contributions to S_G from DIS from a pion or a vector meson would cancel (see Eq.(3.94) below). The presence of an apparent K and isoscalar ω component in (3.91) should not be misconstrued. When the renormalisation factor Z is expanded; $Z = 1 - \langle n\rangle_{N\pi} - \langle n\rangle_{\Delta\pi} - \langle n\rangle_{N\rho} - \langle n\rangle_{N\omega} - \langle n\rangle_{\Delta\rho} - \langle n\rangle_{\Lambda K} - \langle n\rangle_{\Lambda\Sigma}$, these contributions vanish, so that the total effect upon S_G from mesons can be written as

$$S_G = \frac{1}{3}\left(1 - \frac{4\langle n\rangle_{N\pi}}{3} - \frac{4\langle n\rangle_{N\rho}}{3} + \frac{2\langle n\rangle_{\Delta\pi}}{3} + \frac{2\langle n\rangle_{\Delta\rho}}{3}\right). \quad (3.93)$$

In Fig.3.20 we show the effect of the meson correction on the Gottfried sum rule, and compare with the quoted experimental value. It is clear that the net effect of the virtual meson–baryon states is to decrease S_G. The πN state alone can reproduce the quoted value of S_G for $\Lambda \sim 1.3$ GeV. The addition of $\pi\Delta$ components would require a slightly larger cut-off (since this produces an excess of $\bar{u}$ over $\bar{d}$, which cancels some of the $\bar{d}$ excess generated by the πN states). Including the ρN state however restores, and actually enhances, the $\bar{d}$ excess, although some of this is again cancelled by the $\rho\Delta$ states. With all components included, we find that the NMC value of S_G can be reproduced with $\Lambda \approx 1.1 - 1.2$ GeV. For $\Lambda \lesssim 700$ MeV, as suggested by the antiquark data in the previous section, mesons can generate only about half of the asymmetry required to satisfy the experimental sum rule.

As well as examining the effect of the meson cloud on the Gottfried sum rule, we may be able to learn more by observing its effect upon the shape of the structure function difference $F_{2p}(x) - F_{2n}(x)$. From (3.63)–(3.73) we readily obtain

$$F_{2p}(x) - F_{2n}(x) = \frac{Z}{3}(xu_V(x) - xd_V(x)) + \sum_{M,B}\frac{x}{3}\left(\delta^{(MB+BM)}(u(x) - d(x))\right)$$
$$= \frac{Z}{3}(xu_V(x) - xd_V(x)) + \frac{1}{3}\int_x^1 dy\left(-\frac{1}{3}f_{K\Sigma}(y) + f_{K\Lambda}(y)\right) x_M V^M(x_M)$$
$$+ \frac{1}{3}\int_x^1 dy'\left(-\frac{1}{3}f_{N\pi}(y') - \frac{1}{3}f_{N\rho}(y') + f_{N\omega}(y') + \frac{2}{3}f_{\Sigma K}(y')\right) x_B u(x_B) \quad (3.94)$$
$$+ \frac{1}{3}\int_x^1 dy'\left(\frac{1}{3}f_{N\pi}(y') + \frac{1}{3}f_{N\rho}(y') - f_{N\omega}(y') + \frac{5}{3}f_{\Delta\pi}(y') + \frac{5}{3}f_{\Delta\rho}(y')\right) x_B u(x_B)$$

Note that kaons and ω mesons contribute to the structure functions themselves, even though their contributions cancel when the structure functions are integrated over x. Actually, we include the

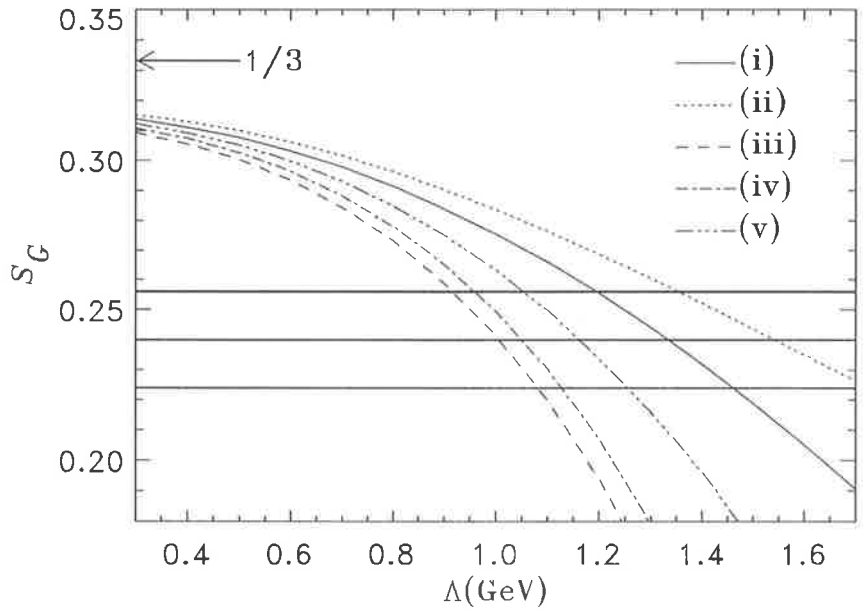

Figure 3.20: Mesonic corrections to the Gottfried sum $S_G(0,1)$, as a function of the dipole cut-off Λ: (i) πN only, (ii) πN and $\pi\Delta$, (iii) πN and ρN, (iv) πN, $\pi\Delta$ and ρN, and (v) πN, $\pi\Delta$, ρN and $\rho\Delta$, compared with the NMC data [65] (thick solid lines, including upper and lower limit of errors).

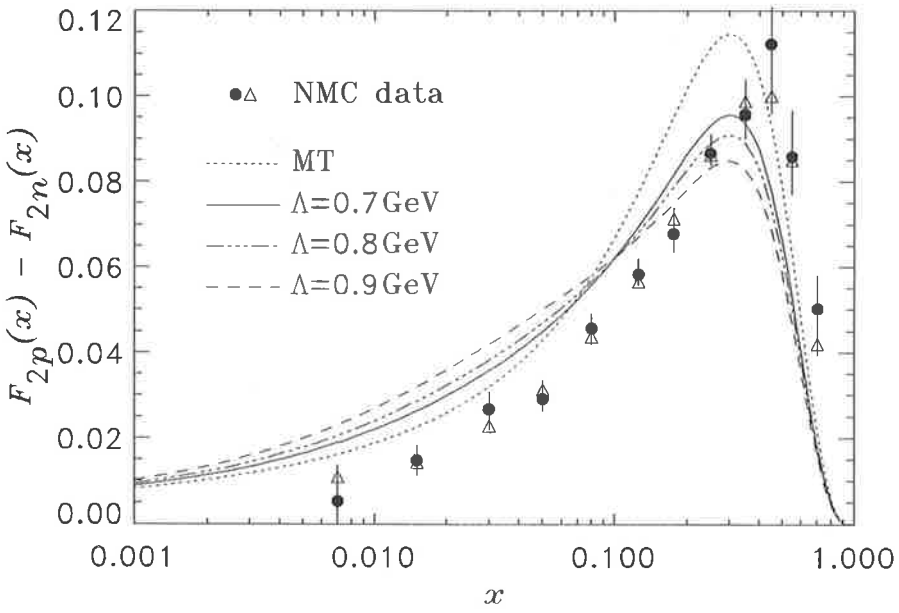

Figure 3.21: Proton—neutron structure function difference for varying meson–baryon form factor cut-off Λ. The dotted curve is the recent (leading order) Morfin and Tung [50] parameterisation of $(u_V - d_V)/3$, in which $\bar{d} = \bar{u}$.

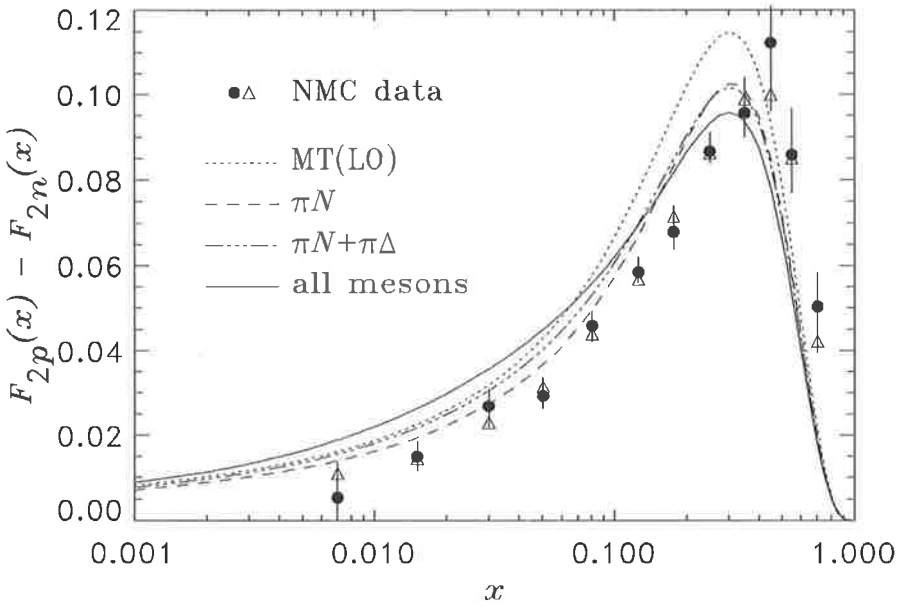

Figure 3.22: Proton—neutron structure function difference as a function of x. Shown is the effect of the πN states alone, $\pi N + \pi\Delta$ states, and all mesons (with $\Lambda = 700$ MeV). The data is as in Fig.3.21.

K and ω contributions only for the sake of completeness. Numerically, we find that dropping them altogether has negligible consequences.

In Fig.3.21 we show the effects on $F_{2p} - F_{2n}$ of including contributions from DIS off the virtual meson–baryon components for varying Λ, and compare with the predictions of existing parameterisations of $(u_V - d_V)/3$ which have $\bar{d} = \bar{u}$. The most noticeable consequence of the meson cloud is a decrease in the peak value of $F_{2p} - F_{2n}$ at $x \sim 0.3$. Since here the parameterisation clearly overestimates the NMC data, the effect of mesons is to move the curve in the right direction. At the same time, however, the structure function difference becomes larger for $x \lesssim 0.1$. Because the parameterisation is already too large in this region compared with the NMC data, it's clear that mesons alone cannot improve the fit at small x.

At large x the meson-corrected curves consistently lie beneath the NMC data points. This is a consequence of the original parameterisation [50] underestimating the NMC $F_{2p} - F_{2n}$ results (in fact most other parameterisations [15, 51] also have this property). If we had a parameterisation which could better reproduce the large-x data, the quality of the fits for the corrected curves would naturally improve. We should add, however, that the NMC did not report much data at $x \gtrsim 0.4$. In any case, the discrepancy between the NMC data and the quark parameterisations at large x is unrelated to the failure of the Gottfried sum rule, and is therefore not our primary concern.

Figure 3.22 shows the effects of the individual meson contributions (for $\Lambda = 700$ MeV). The action of the πN states is to decrease $F_{2p} - F_{2n}$ at small x, while adding the $\pi\Delta$ tends to do the opposite. However, it is only with the addition of the vector mesons that there is an increase over the parameterisation in this region.

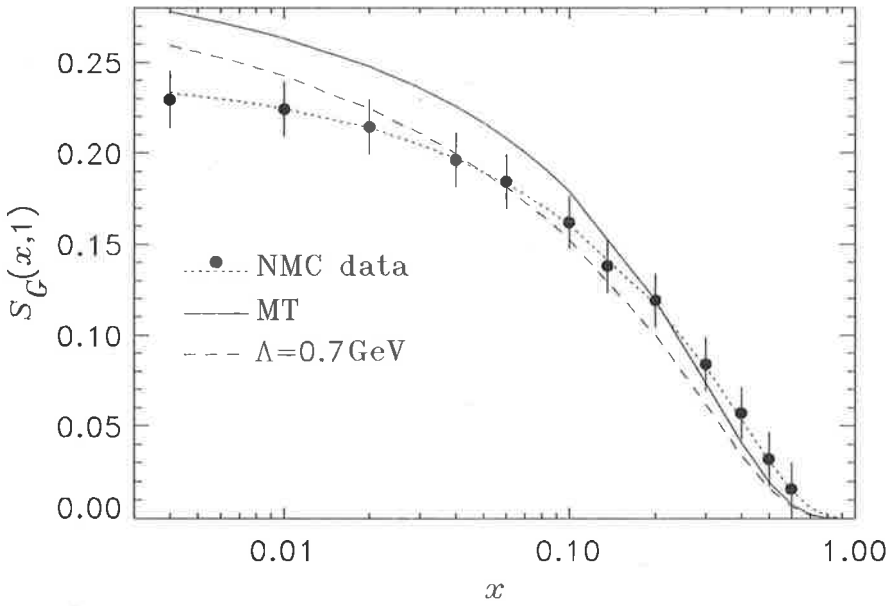

Figure 3.23: Gottfried sum rule integrand, integrated from x to 1. The solid curve is the parameterisation of Morfin & Tung [50] with $\bar{d} = \bar{u}$, while the dashed curve includes mesonic corrections with $\Lambda = 700MeV$. The dotted curve is a best fit to the NMC data.

In Fig.3.23 we show the value of $S_G(x,1)$ as a function of x, for the $\bar{d} = \bar{u}$ parameterisation, and for the meson-corrected curves with $\Lambda = 700$ MeV. The parameterisation (solid curve) is clearly too large for $x \lesssim 0.1$. With the addition of the meson correction (dashed curve), the fit is clearly improved, but still overestimates the NMC data at very small x. To improve the $F_{2p} - F_{2n}$ fit at small x, and at the same time generate the rest of the $\bar{d} - \bar{u}$ asymmetry required to reproduce the NMC S_G value, we must therefore look to other mechanisms. One candidate is the asymmetry generated by the Pauli exclusion principle.

First let us examine the combined effects of the meson cloud and the exclusion principle on the shape of $F_{2p} - F_{2n}$. For the strange mesons and baryons, the Pauli blocking effect should be present in DIS from virtual K^0, K^+ and Σ^+, since these contain unequal numbers of $u(\bar{u})$ and $d(\bar{d})$ quarks. It will not be present in DIS from Σ^0 or Λ^0. This raises the interesting possibility that we may pick up a non-zero strange quark contribution to S_G from the Pauli principle, if the Pauli effect in DIS from K with Σ recoil and in DIS from Σ with K recoil are different (and in principle they should be), which would spoil the cancellation of these components. However, having seen that the role of strange mesons in the DIS process is negligible, we can be fairly confident that by dropping the strange contributions our results will not be significantly affected.

What may be more significant is the possibility that the shape of the Pauli $\bar{d} - \bar{u}$ contribution from DIS off a virtual Δ, with π or ρ recoil (labelled $p_\Delta(x)$) may differ from the shape of the Pauli difference from DIS off a nucleon with a π or ρ recoil, $p_N(x)$. In principle these should be different because the spins of the 4-quark intermediate states (which arise when the $\bar{u}$ or $\bar{d}$ quarks are probed) in the nucleon and Δ are different. This means that, for example, while a quark

inserted into a (spin 1/2) proton can produce a state with spin 0 or 1, one inserted into a (spin 3/2) Δ^+ could produce either a spin 1 or spin 2 intermediate state. One way to make spin 0, 1 or 2 four-quark states is to construct them from spin 0 or spin 1 diquarks, and since a vector diquark is more massive than a scalar diquark (see Section 2.3, and Ref.[48]), and therefore has a softer x-distribution, the result is that the Pauli blocking function $p_\Delta(x)$ should have a softer shape than $p_N(x)$. Furthermore, the integral over $p_\Delta(x)$ (denoted $\mathcal{P}_\Delta$) need not necessarily equal $\mathcal{P}_N$. Having said this, it is probably also true that the uncertainty introduced in taking these to be the same will be much smaller than the overall uncertainty in the absolute normalisation of $\bar{d} - \bar{u}$ due to Pauli blocking in the nucleon.

The final expression for $F_{2p} - F_{2n}$, including meson and Pauli effects, is

$$\begin{aligned} F_{2p}(x) - F_{2n}(x) &= \frac{Z}{3}\left(x u_V(x) - x d_V(x) - 2x p_N(x)\right) \\ &- \frac{1}{9}\int_x^1 dy' \ \left(f_{N\pi}(y') + f_{N\rho}(y') - 3 f_{N\pi}(y')\right)\left(x_B u_V(x_B) - x_B d_V(x_B) - 2 x_B p_N(x_B)\right) \\ &+ \frac{5}{9}\int_x^1 dy' \ \left(f_{\Delta\pi}(y') + f_{\Delta\rho}(y')\right)\left(x_B d_V(x_B) - 2 x_B p_\Delta(x_B)\right) \\ &+ \frac{4}{9}\int_x^1 dy' f_{\Sigma K}(y')\left(\frac{1}{2} x_B u^{\Sigma^+}(x_B) - 2 x_B p_\Sigma(x_B)\right) \\ &- \frac{1}{9}\int_x^1 dy \ \left(f_{K\Sigma}(y) - 3 f_{K\Lambda}(y)\right)\left(x_M V^M(x_M) - 2 x_M p_K(x_M)\right) \end{aligned} \tag{3.95}$$

which, making the above approximations, reduces to

$$\begin{aligned} F_{2p}(x) - F_{2n}(x) &\approx \frac{Z}{3}\left(x u_V(x) - x d_V(x) - 2x p_N(x)\right) \\ &- \frac{1}{9}\int_x^1 dy' \ \left(f_{N\pi}(y') + f_{N\rho}\right)\left(x_B u_V(x_B) - x_B d_V(x_B) - 2 x_B p_N(x_B)\right) \\ &+ \frac{5}{9}\int_x^1 dy' \ f_{\Delta M}(y')\left(x_B d_V(x_B) - 2 x_B p_N(x_B)\right). \end{aligned} \tag{3.96}$$

The resulting x distribution is plotted in Fig.3.24. The Pauli correction is largest in the small x region, for $0.01 \lesssim x \lesssim 0.1$. By reducing the absolute value of $F_{2p} - F_{2n}$ at small x the Pauli correction brings the parameterisation (with $\bar{d} = \bar{u}$) into better agreement with the data in that region. However, for larger x ($0.1 \lesssim x \lesssim 0.3$) the peak in the distributions is still too large to be consistent with the NMC data. On the other hand, when combined with a small mesonic correction (for $\Lambda = 700$ MeV), a very good fit is possible with $\mathcal{P}_N \approx 0.1$.

Integrating the structure function difference between x and 1, we plot in Fig.3.25 the function $S_G(x, 1)$ including both meson and Pauli effects. Clearly the quality of the fit is improved with the addition of Pauli blocking. In particular, the apparent saturation of the sum rule below $x \approx 0.01$ is better fitted by including the Pauli term. (In a more recent experiment, the E665 Collaboration at Fermilab reported an even more dramatic saturation of the Gottfried sum rule for $x \lesssim 0.125$, $\int_{0.001}^{0.125} dx(F_{2p} - F_{2n})/x = -0.07 \pm 0.07$ [135].) In the intermediate-x region ($x \gtrsim 0.3$) the meson-corrected curves appear to underestimate the NMC data. This can be understood from the shape of the original $F_{2p} - F_{2n}$ distributions in Fig.3.24, where for x above ~ 0.3 the curves tend to lie beneath the NMC data points.

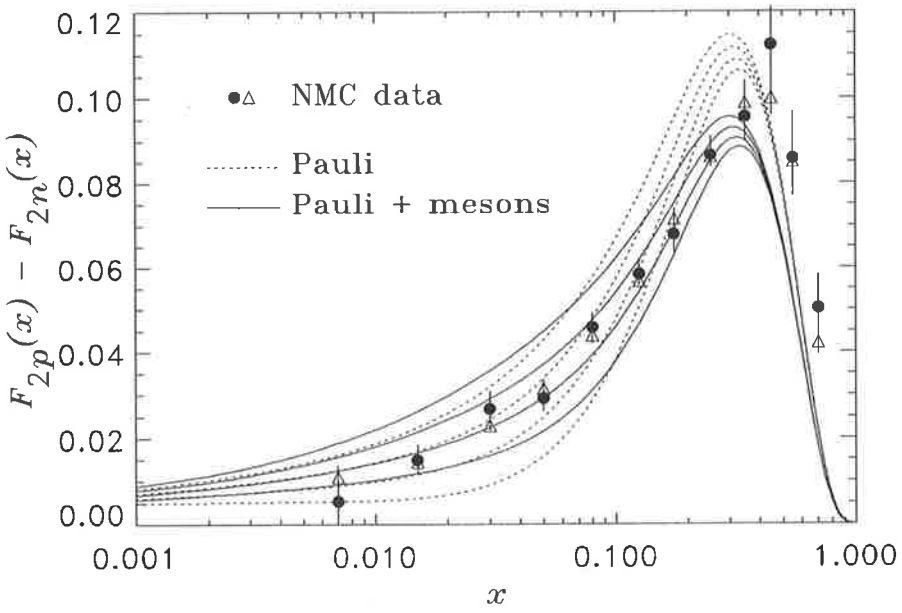

Figure 3.24: Effect of the Pauli exclusion principle on the proton – neutron structure function difference, as a function of x. The dotted (without meson corrections) and solid (with $\Lambda = 700$ MeV meson corrections) curves are for $\mathcal{P} = 0$ (largest curves) 0.05, 0.1, and 0.15 (smallest curves).

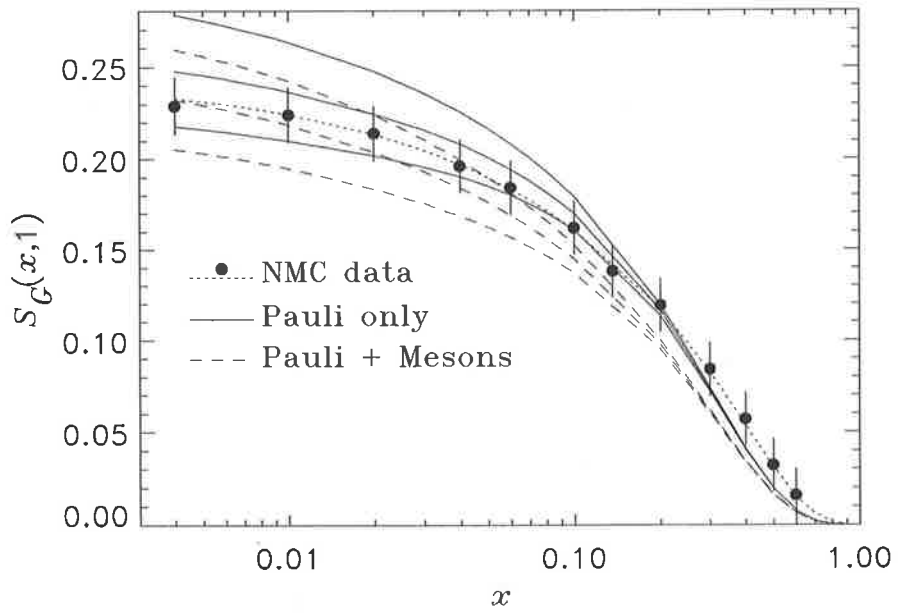

Figure 3.25: Effect of Pauli blocking on the Gottfried sum integrand with no mesons (solid curves), and with mesons for $\Lambda = 700$ MeV (dotted curves). The three curves in each case are for $\mathcal{P}_N = 0$ (largest curves), 0.05 and 0.10 (smallest curves).

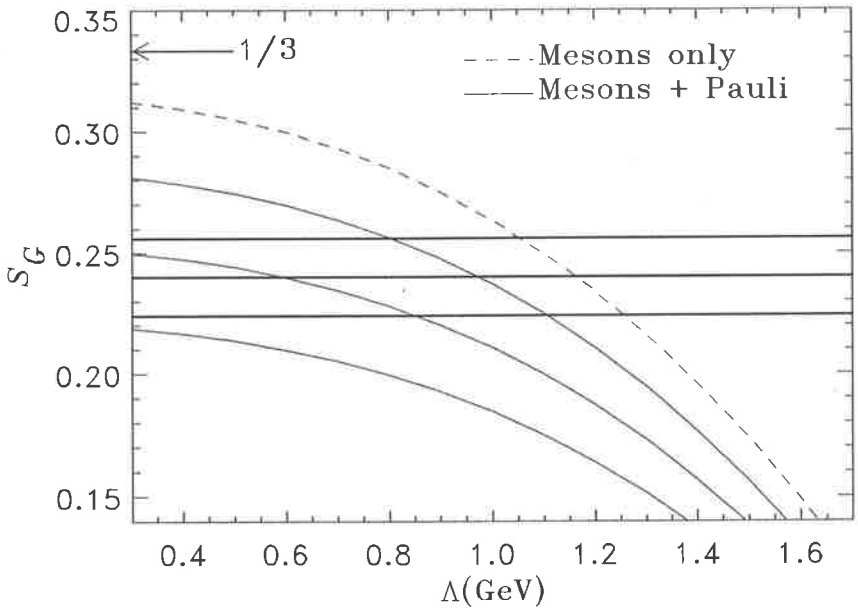

Figure 3.26: Gottfried sum rule with mesonic and Pauli corrections. The solid curves represent Pauli normalisation of $\mathcal{P}_N = 0.05$ (largest), 0.1 and 0.15 (smallest).

For the Gottfried sum, from (3.95) we obtain

$$\begin{aligned} S_G &= S_G^{MB}\ (1 - 2\,\mathcal{P}_N) + \frac{10}{9}(\mathcal{P}_N - \mathcal{P}_\Delta)(\langle n\rangle_{\Delta\pi} + \langle n\rangle_{\Delta\rho}) \\ &+ \frac{2}{9}(3\mathcal{P}_N + \mathcal{P}_K - 4\mathcal{P}_\Sigma)\,\langle n\rangle_{\Sigma K} + \frac{2}{3}(\mathcal{P}_N - \mathcal{P}_K)\,\langle n\rangle_{\Lambda K} \end{aligned} \tag{3.97}$$

where S_G^{MB} is the sum rule with meson/baryon corrections only, as given by Eq.(3.93). Again, dropping the negligible strange contributions, and assuming that the difference between the Pauli blocking in the nucleon and Δ is not large, we obtain

$$S_G \approx S_G^{MB}(1 - 2\,\mathcal{P}_N). \tag{3.98}$$

This last result that the mesonic and Pauli contributions factorise was first presented by Signal, Schreiber and Thomas [47] (although there only the πN and $\pi\Delta$ states were considered). In Fig.3.26 we show the variation of S_G with both Λ and $\mathcal{P}_N$. For $\Lambda \approx 0.7$ GeV, the experimental sum rule can be obtained with $\mathcal{P}_N \approx 0.1$.

To summarise the results of this section, we have seen that the NMC measurement of the Gottfried sum rule suggests a sizeable difference between the $\bar{d}$ and $\bar{u}$ quark distributions in the proton. We have examined two fairly obvious sources of such an asymmetry, namely that arising from the meson cloud of the nucleon, and that due to the Pauli exclusion principle. For consistency with the total antiquark data, as well as the shape of $F_{2p} - F_{2n}$ at small and intermediate x, the value of the meson–nucleon form factor cut-off Λ (determining the size of the meson contributions) needs to be less that about 700 MeV. This is enough to give at most about half of the asymmetry required for agreement with the experimental sum rule. With a small amount of Pauli blocking

($\mathcal{P}_N \approx 0.1$) we find that the combined mechanisms can easily reproduce the NMC result. While it is possible for a larger amount of Pauli blocking ($\mathcal{P}_N \approx 0.15$) to produce the entire sum rule discrepancy, the resulting $F_{2p}(x) - F_{2n}(x)$ is too large at intermediate x, and is underestimated at small x, without any mesonic component. Thus various phenomenological constraints seem to imply the need for both mechanisms.

The fact that our fits do not precisely reproduce the large x data is not very surprising. Apart from the fact that the input valence parameterisation itself disagrees with the NMC data at large x, our own model is not entirely self-consistent. We take as our starting points the valence quark distributions which are parameterised under the assumption of flavour SU(2) symmetry in the sea, which is naturally broken by mesons, as well as by the Pauli effect. A fully consistent approach would be to readjust the full valence distributions, so that with the $\bar{d} - \bar{u}$ corrections included they reproduce the data to which they were originally fitted. However, the effect of this correction is unlikely to be very large. No such ambiguity exists for the integrated distributions, in the Gottfried sum itself.

Before finishing this discussion, we should mention some alternative explanations for the Gottfried sum rule violation. It was suggested by Martin, Stirling and Roberts [121] that there may not be any violation of the quark-parton model S_G prediction at all, if large contributions to the Gottfried integral come from the unmeasured, $x < 0.004$, region. By parameterising their valence quark distributions to be more singular at small x than what would otherwise be expected from Regge theory (namely, $q_V \sim x^{-0.5}$), and also compared with what the NMC used in their $x \to 0$ extrapolation, it was shown in Ref.[121] that a value of 1/3 could be recovered. Although this more singular behaviour seems rather artificial, without data at such small x it remains a possibility. However, one problem with this hypothesis of late onset (in the sense of decreasing x) of Regge behaviour is the data from the E665 Collaboration [135], which suggests early saturation of the Gottfried sum rule, and would therefore tend to rule out this option.

It was also suggested by Kaptari and Umnikov [136] that nuclear effects in deuterium may introduce errors in the extraction of the neutron structure function from the deuteron DIS data. In particular, it was claimed that meson exchange currents in the deuteron could lead to substantial antishadowing corrections, so that F_{2n} extracted in a naive manner would be overestimated. With this correction taken into account, it was argued that a value roughly consistent with 1/3 could again be recovered.

Furthermore, although expected to be small, genuine nuclear shadowing in deuterium could also introduce corrections to the naively-extracted neutron structure function. The nuclear effects thus represent potentially the most significant corrections to the proton–neutron structure function difference, and to the Gottfried sum rule. It is therefore critical for the question of flavour symmetry in the proton sea that we have a reliable estimate of F_{2n}. In the next chapter we shall examine in some detail the nuclear effects in deuterium.

Chapter 4

SHADOWING IN NUCLEAR DIS

We saw at the end of the last chapter that the Gottfried sum rule is sensitive to the small-x behaviour of the neutron structure function, F_{2n}. Unfortunately, the absence of free neutron targets means that deuterium has to be used in order to extract data on F_{2n}. Traditionally in DIS on the deuteron, in which the proton and neutron are held together very weakly, nuclear effects have been ignored, and the total lepton–deuteron cross section assumed to be the sum of the lepton–proton and lepton–neutron cross sections. However, any nuclear effects present in the deuteron would introduce corrections to the F_{2n} extracted under the simple additivity assumption. Furthermore, even a very weak nuclear dependence at small x could have a significant impact upon the proton—neutron structure function difference, and any conclusions about the mechanisms of SU(2) flavour symmetry breaking in the proton sea reached from the naive NMC experimental value of the Gottfried sum rule.

From DIS experiments on heavy nuclei, a deviation from linearity has been observed [137] in the nuclear EMC effect for the ratio of cross sections for scattering from a heavy nucleus and from deuterium (in other words, for a mass number A nucleus, $\sigma_A \neq A\ \sigma_N$). In particular, what those experiments confirmed was a dramatic decrease in the nuclear cross section (or structure function) per nucleon in the region of small x [137, 138], a phenomenon referred to as shadowing. Whether appreciable shadowing exists in *deuteron* DIS will be the primary focus of this chapter. Partly motivated by some conflicting claims in the literature regarding the magnitude of this effect [82, 139, 140], we perform a detailed analysis of the shadowing correction to F_{2D} and examine the sensitivity of the calculation to any model dependent parameters.

Nuclear shadowing is naturally a very interesting and important subject in its own right. (At small x we are of course probing the long-distance structure of the hadronic tensor — see Eq.(2.14).) Furthermore, any realistic model of shadowing in D should, when adequately extended for larger A, be able to predict the shadowing effect in heavy nuclei as well. Following our discussion of the deuteron, we will use the same model to study the small-x dependence of the DIS structure functions of heavy nuclei. We start, though, with a discussion of the physics behind nuclear shadowing, and review some formalism which will be used in the subsequent calculations.

4.1 Physics of Shadowing

Stimulated by earlier work of Bell on the application of the Adler PCAC relation to nuclei [141], Stodolsky was the first to predict shadowing in electromagnetic processes as long ago as 1967 [142]. Generalising the ideas of shadowing applicable to purely hadronic reactions, Stodolsky used an argument based on the vector meson dominance model to show that the real photon—nucleus cross section should deviate from the simple $\propto A$ behaviour.

Since that time, and especially since the experimental discovery of shadowing of virtual photons in nuclear DIS, our understanding of the phenomenon has greatly increased, even though a definitive quantitative description from first principles is still lacking. What is well known is that the essential origin of the deviations from linearity of the nuclear cross section is the finite probability that a projectile scattering from a nucleus can interact with more than one nucleon as it traverses the nuclear medium. Virtually all calculations of shadowing then amount to describing this process, and the model dependence only arises from different treatments of the interaction mechanisms.

The formal way to quantify the shadowing effect in high-energy nuclear processes is the multiple scattering expansion developed by Glauber [143] (see also Sitenko [144]). This was first done by several authors, including Gribov [145], Brodsky & Pumplin [146], Gottfried & Yennie [147], and others (for a review see Ref.[148]).

4.1.1 Glauber Multiple Scattering Formalism

The basic assumption of the multiple scattering formalism is that one can represent the interaction of a high-energy projectile with a nucleus in terms of projectile—nucleon amplitudes. One further makes use of the eikonal approximation, in which the interaction of the projectile with the nucleons is presumed not to affect the projectile's trajectory through the nucleus. This approximation will be valid if, in the target rest frame, the momentum of the projectile is much greater than the momenta of any of the nucleons in the nucleus (or equivalently that the energy transfer is much less than the incident energy [149]).

More formally, we write the elastic scattering amplitude for scattering a high-energy projectile from a target nucleus (A) near the forward direction as

$$\mathcal{F}_A \;=\; \frac{i|\mathbf{q}|}{2\pi}\int d^2\mathbf{b}\;\Gamma_A(\mathbf{b})\;\exp[i(\mathbf{q}-\mathbf{q}')\cdot\mathbf{b}] \tag{4.1}$$

where $\mathbf{q}$ and $\mathbf{q}'$ are the 3-momenta of the incident and scattered particles, and $\Gamma_A(\mathbf{b}) = 1 - \exp[i\chi_A(\mathbf{b})]$ is the profile function, with $\chi_A(\mathbf{b})$ the phase shift associated with impact parameter $\mathbf{b}$. This expression can be obtained by writing the scattering amplitude in a series of spherical harmonics, and expressing the associated Legendre functions for small scattering angles in terms of Bessel functions, and finally replacing the summation over angular momenta by an integral over $\mathbf{b}$ [149]. Eq.(4.1) is valid for small scattering angles, which is a good approximation in high-energy, nearly-forward elastic scattering. In DIS, we can therefore use this scattering amplitude (since

$\mathbf{q} = \mathbf{q}'$) for the virtual photon Compton scattering amplitude (which as we saw in Chapter 2 was related by the optical theorem to the DIS hadronic tensor).

Treating Γ as an operator which we can sandwich between initial and final states, and inserting complete sets of states, we can express (4.1) in terms of the nuclear wavefunctions in coordinate space, $\psi_A(\mathbf{r}_1, ..., \mathbf{r}_A)$,

$$\begin{aligned} \mathcal{F}_A(\mathbf{q}, \mathbf{q}') &= \frac{i|\mathbf{q}|}{2\pi} \int d^2\mathbf{b}\, d^3\mathbf{r}_1 \cdots d^3\mathbf{r}_A\, \psi_A^*(\mathbf{r}_1, ..., \mathbf{r}_A)\, \Gamma_A(\mathbf{b}, \mathbf{r}_1, ..., \mathbf{r}_A)\, \psi_A(\mathbf{r}_1, ..., \mathbf{r}_A) \\ &\quad \times \exp[i(\mathbf{q} - \mathbf{q}') \cdot \mathbf{b}] \end{aligned} \tag{4.2}$$

where $\mathbf{r}_1, ..., \mathbf{r}_A$ denote the coordinates of the nucleons. The next, and crucial, step is to assume that the phase shifts χ_j produced by each nucleon can be added incoherently, so that the total phase shift χ_A accumulated by the projectile as it passes through A can be written

$$\chi_A(\mathbf{b}, \mathbf{r}_1, ..., \mathbf{r}_A) = \sum_{j=1}^{A} \chi_j(\mathbf{b} - \mathbf{s}_j) \tag{4.3}$$

where $\mathbf{s}_j = (\mathbf{r}_j \cdot \hat{b})\, \hat{b}$, with $\hat{b} = \mathbf{b}/|\mathbf{b}|$. The above assumption amounts to admitting only two-body interactions in the scattering process. As a consequence of (4.3), the nuclear profile function can now be written

$$\begin{aligned} \Gamma_A &= 1 - \exp\left[i \sum_j^A \chi_j(\mathbf{b} - \mathbf{s}_j)\right] = \prod_j^A (1 - \Gamma_j) \\ &= \sum_j^A \Gamma_j - \sum_{j<k}^A \Gamma_j \Gamma_k + \sum_{j<k<l}^A \Gamma_j \Gamma_k \Gamma_l - \cdots - (-1)^A \Gamma_1 \cdots \Gamma_A \end{aligned} \tag{4.4}$$

where $\Gamma_j = 1 - \exp[i\chi_j(\mathbf{b} - \mathbf{s}_j)]$ are the nucleon profile functions. With this expansion, Eq.(4.2) now describes all the possible ways that a projectile can be (multiply) scattered from the nucleus. Applying this to DIS, we represent this multiple scattering expansion in Fig.4.1. It's clear that the 1st, 2nd, ... term on the right hand side of (4.4) correspond to the single, double, ... scattering diagrams, respectively. The first term in the series is the impulse approximation for nucleons, and gives the nuclear cross section as a simple sum of nucleon cross sections (aside from Fermi motion effects). The second and subsequent terms introduce deviations from this linearity. Since the contributions from higher order terms are expected to be smaller than the preceding ones, the series is usually truncated after several terms. In calculations of nuclear shadowing, typically only the double scattering diagram is kept. The different models of nuclear shadowing then essentially correspond to different dynamical details of the photon--nucleon 'blob' in the double scattering diagram.

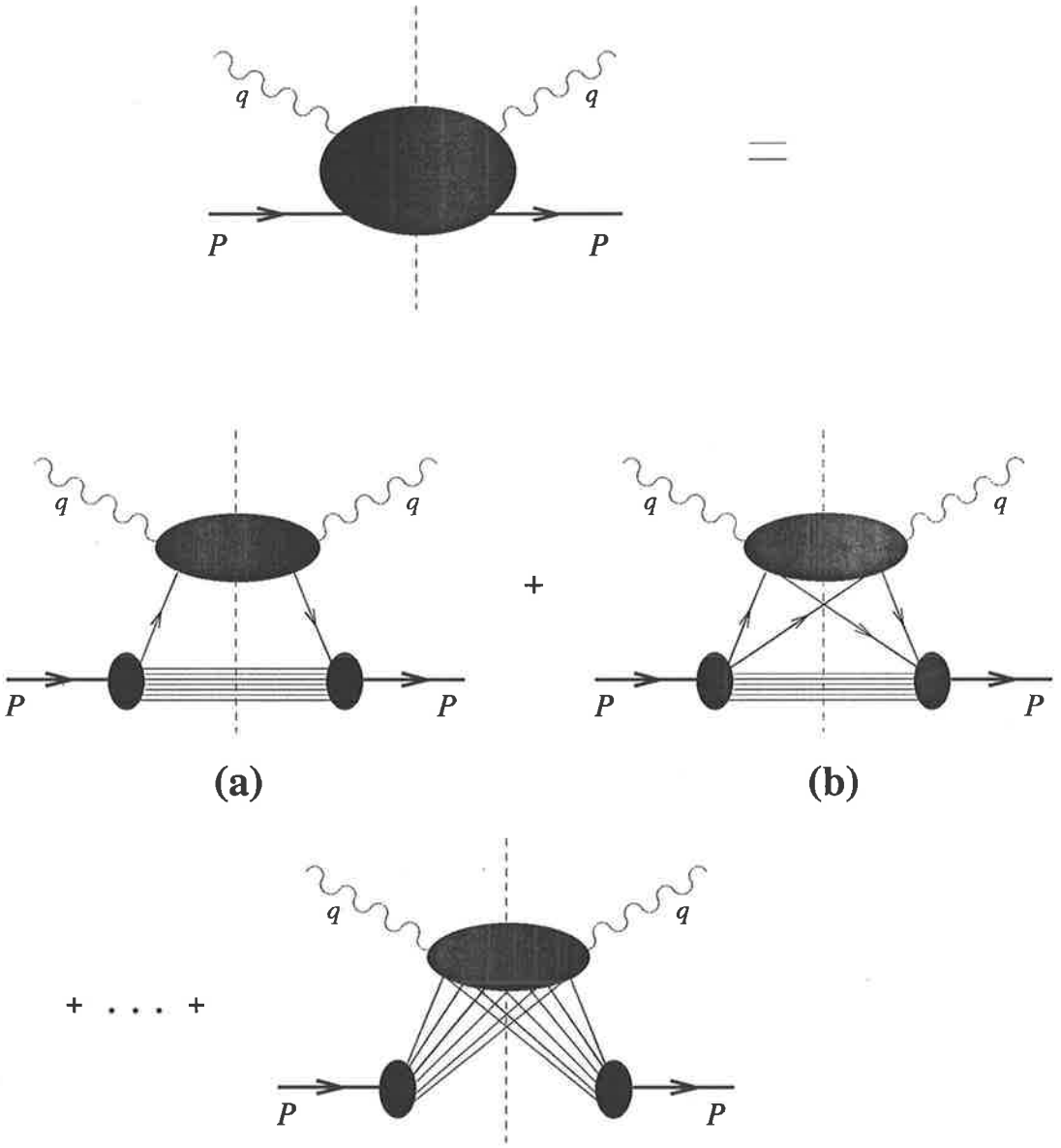

Figure 4.1: Glauber multiple scattering expansion.

4.1.2 Hadronic Structure of γ^*

It has long been established that photon—hadron processes have many remarkable similarities with purely hadronic reactions. The most simple and natural explanation of this phenomenon is that the photon itself has a hadronic structure. In particular, the physical photon state can be considered to be a superposition of a bare photon state and a virtual hadronic component (c.f. Eq.(3.1) for the physical nucleon state in terms of bare nucleon and virtual baryon–meson components). Then the complete photon—hadron process can be viewed as taking place through interaction of the photon's hadronic fluctuations with the target hadron. Since the photon has $J^{PC} = 1^{--}$, the hadronic states with the correct quantum numbers can only be vector mesons, V. Furthermore, by the Heisenberg uncertainty principle, only the lowest mass vector mesons ($V = \rho^0, \omega, \phi$) are expected to play a significant role in low and medium energy processes. This is the basis of the vector meson dominance (VMD) model. The phenomenological successes of this approach are numerous (e.g. the total γN cross section, the copious vector meson photoproduction, etc.), and we refer the reader to the many comprehensive review articles on the subject, for example, Refs. [150–152].

The extension of the VMD idea to virtual photons, such as those in deep inelastic lepton—nucleus scattering, can be made quite easily, although strictly speaking it's incorrect to talk of 'bare' virtual γ states. This is done in the literature because the analysis of γ^* interactions is a simple extension of real γ processes. Thus the VMD hypothesis is that the virtual photon state can be written

$$|\gamma^*\rangle \;=\; \sqrt{Z}\,|\gamma^*_{\rm bare}\rangle \;+\; \sum_{V=\rho^0,\omega,\phi} \frac{\langle V|H_{\gamma^* V}|\gamma^*_{\rm bare}\rangle}{\Delta E}\,|V\rangle \tag{4.5}$$

where Z is the bare photon probability, $\Delta E = \nu - E_V$, with $\nu = \sqrt{\mathbf{q}^2 - Q^2}$ being the energy of the virtual photon and $E_V = \sqrt{\mathbf{q}^2 + M_V^2}$. The Hamiltonian $H_{\gamma^* V}$ describes the electromagnetic interaction between the γ^* and vector meson V. Formally, with this expansion the total γ^*—nucleus amplitude is a sum of two contributions, the bare photon—nucleus amplitude ('one-step' process) and the vector meson—nucleus amplitude ('two-step' process). At high energy, the destructive interference between these two gives the famous result that the one-step amplitude is cancelled by a term in the two-step amplitude [148]. The end result is then proportional to the amplitude for V—nucleus scattering only.

That this is the case can readily be seen if we consider this process in time-ordered perturbation theory in the target rest frame. Here we have two time-ordered diagrams — one in which the photon converts into a vector meson which then interacts with the target (or equivalently, the photon interacts with a vector meson travelling backwards in time after being emitted from the target), and one where the photon interacts with a forward moving V after it has been emitted from the nucleus. The former can be seen as an interaction of the state $|V\rangle$ with the target, while the latter as an interaction between $|\gamma^*\rangle$ and the target. In the target rest frame one can easily show [150] from the structure of the energy denominator in Eq.(4.5) that at high energy ($\nu \to \infty$)

the contribution from the diagram with the forward moving V is of order $1/\nu$ compared with the backward moving V. Hence the conclusion that the state $|\gamma^*\rangle$ is not important in high-energy interactions. (Note that this is the opposite to what occurs in the IMF, as we saw in Chapter 3.)

For the diagram in which the V is produced before the hadronic interaction, the energy denominator is $\Delta E \approx -(Q^2 + M_V^2)/2\nu$. Choosing the normalisation of the state $|V\rangle$ to be $\sqrt{4\pi\alpha}/f_V$, where f_V is the $\gamma^* V$ coupling constant, and excluding non-diagonal vector meson transitions, the total $\gamma^* A$ cross section in the VMD model is

$$\sigma_{\gamma^* A} = \sum_V \frac{4\pi\alpha}{f_V^2} \left(\frac{M_V^2}{M_V^2 + Q^2} \right)^2 \sigma_{VA}. \tag{4.6}$$

Having outlined the basic ideas behind the VMD model, we now turn to its description of shadowing. For real photons the VMD model is known to give a very good description of the shadowing of photoproduction cross sections, which occurs at high photon energies, $\nu \gtrsim 1 - 2$ GeV [153]. This suggests that in deep inelastic scattering, at least at low Q^2, the same mechanism may also be responsible for the shadowing of the inelastic nuclear structure functions.

The physical origin of shadowing in the VMD model can be understood by considering the following space-time picture. When the virtual photon fluctuates into a virtual meson, the propagation distance of the virtual hadronic state is $\Delta d \sim 1/\Delta E \approx 2\nu/(Q^2 + M_V^2)$. If Δd exceeds the inter-nucleon separation, $2R_N \sim 2$ fm, then the hadronic state can interact with two different nucleons as it passes through the nucleus. In terms of the Glauber multiple scattering series, this would correspond to the double scattering diagram in Fig.4.1(b). Furthermore, if the vector meson—nucleon amplitude were purely imaginary, one would automatically obtain a reduction of the total $\gamma^* A$ cross section. For large ν ($\nu \gg M_V$), the propagation length of the hadronic fluctuation becomes $\Delta d \sim (xM)^{-1} \gtrsim 2$ fm, where $x = Q^2/2M\nu$, so that shadowing should start to appear at $x \lesssim x_0 \approx 0.1$.

In the VMD model the correction $\delta\sigma_{\gamma^* A}$ to the total $\gamma^* A$ cross section can be related to the VA shadowing correction, $\delta\sigma_{VA}$, using an expression similar to (4.6). Consequently the vanishing of shadowing at large Q^2 stems directly from the presence of the vector meson propagators $(Q^2 + M_V^2)^{-2}$. Phenomenologically, this is quite important as far as testing models of nuclear shadowing, since in DIS the photon's virtuality can be varied to probe the Q^2 dependence of this effect. Because the study of the small-x behaviour of structure functions in the large-Q^2 region requires very large energy transfers, the early DIS experiments were inconclusive in their results for the Q^2 dependence of shadowing. In the last decade or so, as lepton beams with ever greater energies have become available, nuclear structure functions at small x have been explored at larger Q^2. Indeed, it has become clear that the depletion of the nuclear to nucleon cross section ratios at $x \lesssim 0.1$ does not disappear with Q^2, but rather exhibits scaling behaviour. The inevitable conclusion is that there must be other mechanisms responsible for the large-Q^2 behaviour of shadowing.

The VMD model can be extended by including additional hadronic states (heavier vector mesons), or a $q\bar{q}$ continuum, in the expansion (4.5). Such extensions of the VMD model are

referred to as generalised vector meson dominance (GVMD) [151, 154]. Models of nuclear shadowing based on this approach have been used by several authors, including Bilchak, Schildknecht and Stroughair [155], Piller & Weise [156], and Shaw [157]. Alternatively, it may be preferable when discussing DIS phenomena at high Q^2 to use a partonic description. This is certainly advantageous when describing the scaling behaviour of the inelastic nucleon structure functions, as in the parton model.

4.1.3 Diffractive Scattering from Partons

The description of nuclear shadowing in terms of partons can be understood with the help of a simple physical argument. Consider DIS from a nucleus which is moving with very large speed in the z direction (e.g. one in the IMF). The longitudinal size of the nucleus as seen from the target rest frame will be (by length contraction) $\Delta z_A = \sqrt{1-\beta^2}\ \Delta z_A^*$, where $\Delta z_A^* \approx 2\ R_A$ is the longitudinal length of the nucleus with radius R_A at rest (i.e. the 'proper' length). Here $\beta = 1/\sqrt{1+M_A^2/P_A^2}$, where P_A and M_A are the longitudinal momentum and mass of the nucleus, respectively, which means that $\Delta z_A \approx 2\ R_A\ M_A/P_A$. By the Heisenberg uncertainty principle the longitudinal length (in the IMF) of a parton in the nucleus is $\Delta z = 1/k_z$, where $k_z = xP_A/A$ is the parton's longitudinal momentum (x is the fraction of the target nucleus momentum carried by the parton, normalised to one nucleon). Now, when $\Delta z > \Delta z_A$ the conditions will be just right for partons to overlap spatially in the z-direction inside the nucleus. Furthermore, if the transverse dimensions of the partons $b \sim 1/\sqrt{Q^2}$ are similar, then these may interact and recombine. Specifically, this will occur when $1/x > 2\ R_A\ M_A/A$. In fact, this condition corresponds to complete shadowing, where partons overlap with other partons in the whole nucleus. Incomplete shadowing will occur when partons in one nucleon overlap with partons from only some other nucleons, and the onset of shadowing should occur when partons from neighbouring nucleons only overlap. To determine when shadowing should start to appear, consider the longitudinal size of a nucleon. As seen from the rest frame, this will be $\Delta z_N = 2\ A\ R_N\ M/P_A$. Then partons from adjacent nucleons can overlap whenever $\Delta z_N < \Delta z$, or $x < x_0 = (2\ R_N\ M)^{-1} \approx 0.1$ — precisely the same value as that obtained in the VMD model.

The possibility of antishadowing was also discussed some time ago by Nikolaev & Zakharov [158]. Their argument was based on the hypothesis that the total momentum carried by partons was not changed by parton interactions, but only redistributed. If partons with a given x recombine and annihilate, the overall parton density at this x will be depleted, but the newly created partons will enhance the total parton density at larger x. The onset of antishadowing was also discussed in [158], using an argument similar to the above. Specifically, it was argued that if the parton's longitudinal size Δz exceeded the inter-nucleon separation, Δd_{NN}, then the partons from adjacent nucleons could also overlap spatially and interact. In the IMF (or in the Breit frame [158]), $\Delta d_{NN} = \sqrt{1-\beta^2}\ \Delta d_{NN}^*$, where $\Delta d_{NN}^* \sim 1/m_\pi$ is the average separation between adjacent nucleons in the rest frame of the nucleus. Therefore neighbouring nucleons are contained in the parton localisation

volume when $\Delta z \sim A/(xP_A)$, or $x \lesssim x_0 = Am_\pi/M_A \sim m_\pi/M \sim 0.15$. Then shadowing in a nucleus would be expected to arise when Δz exceeds the nuclear radius, $x \lesssim x_0' = x_0 A^{-1/3}$.

In both of these arguments the value of x_0 (and x_0') is independent of Q^2. The clear implication is that, in contrast to the situation in the VMD model, shadowing and antishadowing should be present at high Q^2. Experimentally this indeed appears to be the case, although the data are not as unambiguous regarding the Q^2 dependence of antishadowing [137, 138].

In the parton model the origin of scaling of the inelastic nucleon structure functions is the direct coupling of the virtual photon to spin 1/2, point-like partons in the nucleon. In other words, scaling depends only on the hard part of the interaction, and is independent of the details of the purely hadronic interaction (which is completely independent of q^2). For this reason the contributions from all of the diagrams in the Glauber scattering series will scale (modulo perturbative QCD corrections).

In the Bjorken limit the parton model description of diffractive ($1/x \gg 1$) deep inelastic processes corresponds to the Regge limit ($s = (p+q)^2 = Q^2(1/x - 1) + M^2 \approx Q^2/x \gg Q^2$). Consequently some phenomenology from Regge theory has been used to describe the small-x behaviour of DIS structure functions. Regge theory was originally developed in the 1960s in order to describe hadronic reactions at high energies. It was found that, for example, the approximate energy-independence of total hadronic cross sections could be accommodated within this formalism. By analytically continuing angular momentum into the complex plane it was discovered that poles in the t-channel partial wave amplitudes could account for the small-t (or forward) elastic scattering (i.e. diffractive) processes. In hadron—nucleon scattering, some of these poles were found to correspond to known mesons. Experimentally, it was also discovered that there existed sequences of mesons having the same quantum numbers, differing only in their spins. Hence it was assumed that all mesons lying on the same mass—spin trajectory were exchanged. Other poles, however, like the Pomeron ($\mathcal{P}$), which had the quantum numbers of the vacuum, did not correspond to known particles. In parton language, it is now generally believed that the Pomeron may really be a system of gluons [159–161] (at least two, in order to construct a spinless object), although there is as yet no QCD-based derivation of the properties of the reactions described by Pomeron exchange. (Some attempts at modelling the properties of the Pomeron have been made, for example, in Ref.[159], where hadron—hadron scattering was described in terms of gluon exchange between MIT bags, while in Ref.[161] gluon-ladder techniques were used to calculate deep inelastic structure functions of hadrons at low x.)

A central result of Regge theory is that the elastic scattering amplitude behaves like $\mathcal{A}(s,t) \sim s^{\alpha(t)}$ at high energy, where $\alpha(t)$ is a function describing the meson trajectory. The amplitude corresponding to forward scattering ($\mathcal{A}(s, t=0)$) then determines (via the optical theorem) the total cross section, $\sigma_{tot} \sim \mathrm{Im}\mathcal{A}/s \sim s^{\alpha(0)-1}$. Now, the intercepts of Regge poles associated with known mesons are generally $\alpha(0) \approx 0.5$, which rules them out as candidates to explain the constancy of total cross sections. However, since the Pomeron has intercept $\alpha_{\mathcal{P}}(0) \approx 1$, it is believed to be

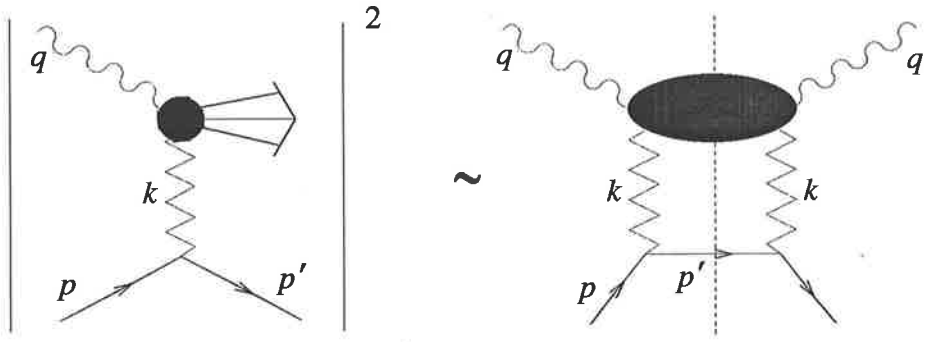

Figure 4.2: Pomeron structure function in diffractive lepton—nucleon scattering.

responsible for the (approximately) energy-independent cross sections.

Applying these ideas to the Regge limit of the total virtual photon—nucleon cross section, we can attribute the (constant) small-x behaviour of the nucleon structure functions (at fixed Q^2) to Pomeron exchange, since $F_{2N} \sim x^{1-\alpha_{\mathcal{P}}(0)}$ ($s \approx Q^2/x$ for $x \to 0$). (The exchange of Regge poles with the ρ meson quantum numbers leads to the $\sim x^{-1/2}$ behaviour of the valence quark distributions.) Thus deep inelastic scattering at small x can be viewed in terms of virtual photon interactions with the Pomeron structure of the nucleon, as depicted in Fig.4.2. If the momentum transfer between the photon and nucleon is small, the nucleon will most likely remain intact, in which case there will only be exchange of vacuum quantum numbers. Such processes can be studied experimentally in semi-inclusive inelastic scattering (see Chapter 6), in which events are 'tagged' by a final state nucleon possessing a large fraction ($\gtrsim 90\%$) of the target nucleon's momentum in the centre of mass frame. Since the virtual photon probes the parton structure of the Pomeron, such processes can actually measure the 'structure function' of the Pomeron, $F_{2\mathcal{P}}$ [162–164], which is defined in terms of the cross section for $\gamma^*\mathcal{P}$ diffractive scattering,

$$F_{2\mathcal{P}} \equiv \frac{Q^2}{4\pi^2\alpha}\sigma_{\gamma^*\mathcal{P}}. \tag{4.7}$$

There have been several attempts to calculate the Pomeron structure function [162–165] (i.e. the $\gamma^*\mathcal{P}$ 'blob' in Fig.4.2). Usually two contributions to $F_{2\mathcal{P}}$ are included, from the quark–antiquark box diagram, Fig.4.3(a), and from the triple Pomeron interaction, Fig.4.3(b)

$$F_{2\mathcal{P}}(x_{\mathcal{P}}, Q^2) = F_{2\mathcal{P}}^{(box)}(x_{\mathcal{P}}, Q^2) + F_{2\mathcal{P}}^{(3\mathcal{P})}(x_{\mathcal{P}}, Q^2) \tag{4.8}$$

and normalised such that

$$F_{2\mathcal{P}} = \left(\frac{16\pi y}{\sigma_{pp}}\right)\left.\frac{d^2F_2^{diff}}{dt\,dy}\right|_{t=0}. \tag{4.9}$$

Here $y = k\cdot q/p\cdot q = x(1 + M_X^2/Q^2) \approx M_X^2/s$ is fraction of the nucleon momentum carried by the Pomeron, $M_X^2 = (k+q)^2$ is the mass of the hadronic debris X, and $x_{\mathcal{P}} \equiv x/y$ is defined to be the fraction of the Pomeron's momentum carried by the struck quark. Also $t \approx -\mathbf{k}^2$, and the function

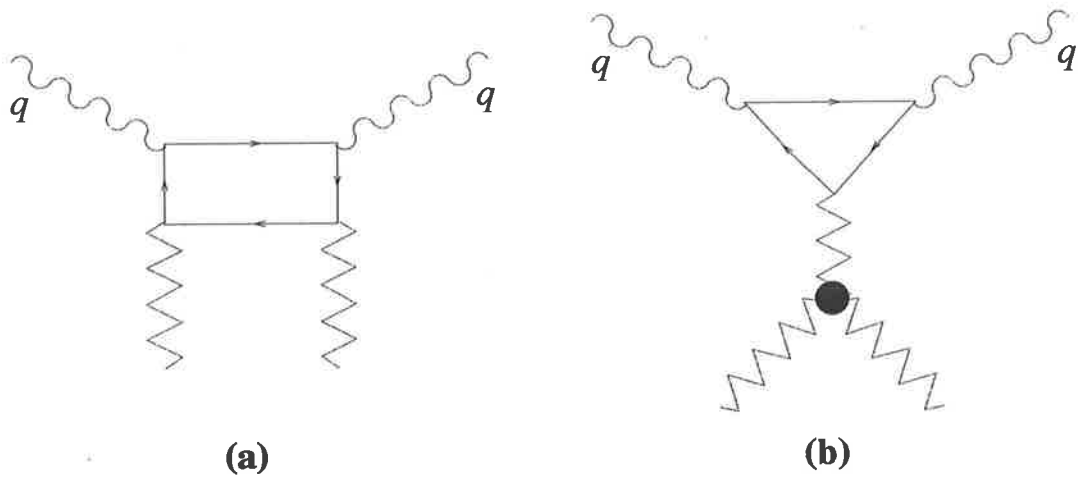

Figure 4.3: Pomeron structure function. (a) quark–antiquark box contribution, (b) triple–Pomeron contribution.

F_2^{diff} is the diffractive structure function, describing semi-inclusive diffractive lepton–nucleon DIS, in which the recoil nucleon and the hadronic state X are separated by a large rapidity [164].

The Pomeron structure function arising from the quark box diagram, $F_{2\mathcal{P}}^{(box)}$, has been calculated by Donnachie and Landshoff [164]

$$F_{2\mathcal{P}}^{(box)}(x_{\mathcal{P}}, Q^2) \;=\; \frac{(12\Sigma_{q^2}\, C)\, \beta_0^2}{\sigma_{pp}}\, x_{\mathcal{P}}(1 - x_{\mathcal{P}}). \tag{4.10}$$

Here, $\beta_0^2 = 3.4\text{GeV}^{-2}$ is the quark—Pomeron coupling constant [166], and we assume the same strength for u, d quark and antiquark—Pomeron couplings, but a weaker coupling to the strange quark: $\Sigma_{q^2} = (10+2\lambda_s)/9$ with $\lambda_s \simeq 0.5$. According to the Particle Data Group [167], the proton—proton total cross section σ_{pp} is approximately 40 mb. The parameter C is determined by the $x \to 0$ behaviour of the nucleon sea distribution, $xq_{sea}(x \to 0) \to Cx^{1-\alpha_{\mathcal{P}}(0)}$. At $Q^2 \approx 4$ GeV^2, recent parameterisations of world DIS, Drell-Yan and prompt photon data [50, 51, 168] give $C \simeq 0.15$. More recently, Nikolaev and Zakharov [165] have calculated the box diagram contribution to $F_{2\mathcal{P}}$, based on a perturbative QCD analysis of $q\bar{q}$ fluctuations of the virtual photon. The $x_{\mathcal{P}}$ dependence of their $F_{2\mathcal{P}}^{(box)}$ parameterisation ($M_X^2/(Q^2+M_X^2)^3$, since $Q^2 + M_X^2 = Q^2/x_{\mathcal{P}}$ from the definition of $x_{\mathcal{P}}$) is the same (despite the conclusions in Ref.[165]) as that in (4.10), providing the same normalisation is used (the normalisations in Ref.[164] and Refs.[165, 169] differ by an overall factor $1 - x_{\mathcal{P}}$).

The triple Pomeron part of the $\mathcal{P}$ structure function,

$$F_{2\mathcal{P}}^{(3\mathcal{P})}(x_{\mathcal{P}}, Q^2) \;=\; \frac{16\pi}{\sigma_{pp}} \left[\frac{y}{\sigma_{hp}} \frac{d^2\sigma_{hp\to hX}}{dtdy}\bigg|_{t=0} \right] F_{2N}^{sea}(x_{\mathcal{P}}, Q^2) \tag{4.11}$$

follows from

$$\frac{1}{F_{2N}^{sea}} \frac{d^2F_2^{diff}}{dtdy}\bigg|_{t=0} \;=\; \frac{1}{\sigma_{hp}} \frac{d^2\sigma_{hp\to hX}}{dtdy}\bigg|_{t=0} \tag{4.12}$$

and the Regge theory expression for the diffractive differential cross section [170]

$$\frac{d^2\sigma_{hp\to hX}}{dtdy} \;=\; \frac{\beta_{h\mathcal{P}}(t)\, \beta_{p\mathcal{P}}^2(t)\, g_{3\mathcal{P}}(t)}{16\pi} y^{1-2\alpha_{\mathcal{P}}(t)} \tag{4.13}$$

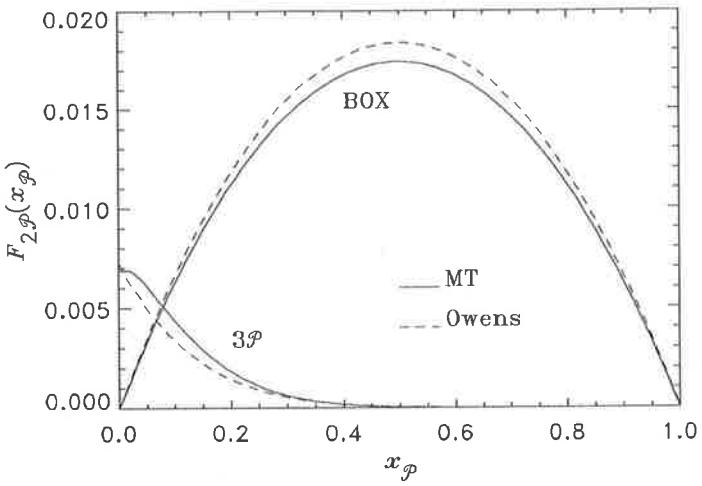

Figure 4.4: Triple–$\mathcal{P}$ and $q\bar{q}$ box contributions to the Pomeron structure function, with the nucleon sea distributions given by the (leading order) parameterisations of Morfin & Tung [50] and Owens [51] at $Q^2 = 4$ GeV^2.

where $\alpha_{\mathcal{P}}(t) \approx 1 + 0.25t$. In the Regge model the total hp cross section is also given in terms of the hadron—Pomeron couplings, $\beta_{h\mathcal{P}}$: $\sigma_{hp} = \beta_{h\mathcal{P}}(0)\ \beta_{p\mathcal{P}}(0)$. It is then evident that the combination

$$\frac{1}{\sigma_{hp}} \frac{d^2\sigma_{hp\to hX}}{dtdy}\bigg|_{t=0} = \frac{\beta_{p\mathcal{P}}(0)\ g_{3\mathcal{P}}(0)}{16\pi y} \tag{4.14}$$

is independent of hadron h. From experiments on the diffractive dissociation of $\pi^{\pm}, K^{\pm}, p$ and $\bar{p}$ on hydrogen, the triple Pomeron coupling constant was found to be $g_{3\mathcal{P}}(0) \simeq 0.364$ mb$^{1/2}$ [171], independent of t, and indeed of the hadron type h.

For the sea part of the nucleon structure function, $F_{2N}^{sea}(x, Q^2) = 5x(u_s + \bar{u} + d_s + \bar{d} + 2(s + \bar{s})/5)/18$, we use recent parameterisations of the data [50, 51]. In Ref.[140], a constant value of 0.3 was used for F_{2N}^{sea} at $Q^2 = 4$GeV^2 together with an empirical low-Q^2 dependence [164]. With the above triple Pomeron coupling constant, Eq.(4.11) gives a $3\mathcal{P}$ component which is about 40% smaller than that obtained in Ref.[82]. However, this is not very significant for the total Pomeron structure function, since $F_{2\mathcal{P}}^{(3\mathcal{P})}$ is very much smaller than the quark–antiquark 'box' contribution, $F_{2\mathcal{P}}^{(box)}$, as illustrated in Fig.4.4.

Quite recently the UA8 Collaboration at the CERN $Sp\bar{p}S$ Collider observed what appears to be a very hard component of the Pomeron structure function [172]. As well as confirming a hard, $(1 - x_{\mathcal{P}})$ structure, in agreement with the above $\mathcal{P}$ structure function, there was also some 30% δ-function like contribution at $x_{\mathcal{P}} \to 1$. However, the effect of such a component would only be noticeable for $x \approx y$, or from the definition of y, at $Q^2 \to \infty$ for finite M_X^2. At finite Q^2, where we will calculate the shadowing corrections for comparison with experiment, $x_{\mathcal{P}}$ will always be less than 1. The exception might be when the mass M_X of the hadronic debris is very small, however for such M_X it is probably more reasonable to describe the scattering in terms of the VMD model.

In the specific calculations which follow, we shall evaluate the double scattering diagram in Fig.4.1(b) using the VMD, as well as the Pomeron exchange mechanisms. A synthesis of the two

approaches is quite sensible if we are to investigate the transition region between small and large Q^2. In the parton picture, the virtual photon interacts with the hadronic target via its fluctuations into $q\bar{q}$ pairs. If the virtuality of the photon is large the fluctuation is short-lived, and a description (in the form of Pomeron interactions) seems appropriate. If the virtuality is smaller, the virtual $q\bar{q}$ pair will have time to evolve into a state which may resemble a vector meson, which would then enable a VMD-based description to be used as an approximation. In this sense our approach is similar to that adopted recently by Badelek & Kwiecinski [140] and Nikolaev & Zoller [139]. A marriage of the VMD and parton descriptions for photon processes was also discussed in some detail recently by Schuler & Sjöstrand [152].

4.2 Shadowing in Deuterium

As well as the potential sensitivity of the Gottfried sum rule to shadowing corrections in deuterium, there are other reasons why a precise determination of the neutron structure function is highly desirable. The extraction of information about the difference between nuclear structure functions and those for the free nucleon from the observed nucleus/deuterium ratios is sensitive to any nuclear effects in D. Conclusions made about nucleon parton distributions based on the nuclear/deuteron structure function ratios (e.g. for the proton antiquark distributions in the Drell-Yan process [173]) at small x may have to be modified once shadowing is taken into account. It is necessary therefore to check for nuclear shadowing effects in deuterium and include this correction in the extraction of F_{2n} from F_{2D}.

We begin our analysis by observing that the Glauber formalism for $\gamma^* D$ scattering involves just the first two diagrams in the multiple scattering series in Fig.4.1. Inserting the first two terms in (4.4) into the $\gamma^* D$ scattering amplitude in (4.2), we obtain

$$\mathcal{F}_{\gamma^* D}(\mathbf{q}-\mathbf{q}') = \frac{i|\mathbf{q}|}{2\pi}\int d^2\mathbf{b}\, d^3\mathbf{r}\, \psi_D^*(\mathbf{r})\left(\Gamma_p(\mathbf{b}+\frac{1}{2}\mathbf{s})+\Gamma_n(\mathbf{b}-\frac{1}{2}\mathbf{s})-\Gamma_p(\mathbf{b}+\frac{1}{2}\mathbf{s})\Gamma_n(\mathbf{b}-\frac{1}{2}\mathbf{s})\right)\psi_D(\mathbf{r}) \times \exp[i(\mathbf{q}-\mathbf{q}')\cdot\mathbf{b}]. \tag{4.15}$$

Taking the Fourier transform of the $\gamma^* N$ amplitude,

$$\Gamma_N(\mathbf{b}) = \frac{1}{2\pi i|\mathbf{q}|}\int d^2\mathbf{q}_T\, \mathcal{F}_{\gamma^* N}(\mathbf{q})\, e^{-i\,\mathbf{b}\cdot\mathbf{q}} \tag{4.16}$$

and defining

$$S_D(\mathbf{k}) = \int d^3\mathbf{r}\, e^{i\mathbf{k}\cdot\mathbf{r}}\, |\psi_D(\mathbf{r})|^2 \tag{4.17}$$

it is then a simple matter to show that for forward scattering ($\mathbf{q}=\mathbf{q}'$)

$$\mathcal{F}_{\gamma^* D}(0) = \mathcal{F}_{\gamma^* p}(0) + \mathcal{F}_{\gamma^* n}(0) + \frac{i}{2\pi|\mathbf{q}|}\int d^2\mathbf{k}_T\, S_D(\mathbf{k})\, \mathcal{F}_{\gamma^* p}(-\mathbf{k})\, \mathcal{F}_{\gamma^* n}(\mathbf{k}) \tag{4.18}$$

since $S_D(0)=1$. The double scattering term, shown in Fig.4.5, then gives rise to shadowing in deuterium.

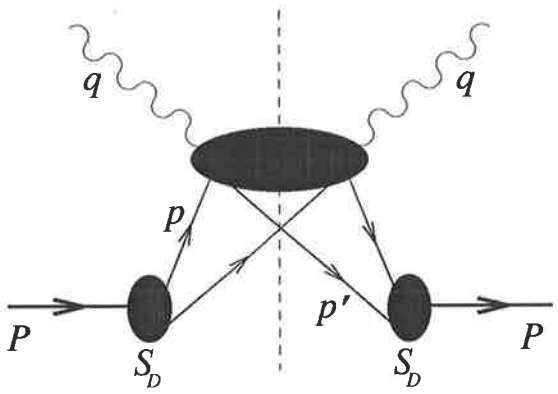

Figure 4.5: Double scattering term gives rise to shadowing in deuterium.

Taking imaginary parts of (4.18) and multiplying by $4\pi/|\mathbf{q}|$, we obtain

$$\sigma_{\gamma^* D} = \sigma_{\gamma^* p} + \sigma_{\gamma^* n} + \frac{2}{\mathbf{q}^2} \int d^2\mathbf{k}_T \; S_D(\mathbf{k}) \; \mathrm{Re}\mathcal{F}_{\gamma^* p}(-\mathbf{k}) \; \mathcal{F}_{\gamma^* n}(\mathbf{k}) \tag{4.19}$$

where we have used the optical theorem,

$$\sigma = \frac{4\pi}{|\mathbf{q}|} \; \mathrm{Im}\mathcal{F}. \tag{4.20}$$

Furthermore, by assuming that $\mathcal{F}_{\gamma^* N}(\mathbf{k}) \approx \mathcal{F}_{\gamma^* N}(0)$ for small $\mathbf{k}$, and that the $\gamma^* N$ amplitude is primarily imaginary, $\mathrm{Re}\mathcal{F}_{\gamma^* N} \ll \mathrm{Im}\mathcal{F}_{\gamma^* N}$, we finally obtain the total $\gamma^* D$ cross section including contributions from single and double scattering,

$$\sigma_{\gamma^* D} = \sigma_{\gamma^* p} + \sigma_{\gamma^* n} + \delta\sigma_{\gamma^* D} \tag{4.21}$$

where

$$\begin{aligned} \delta\sigma_{\gamma^* D} &= -\frac{\sigma_{\gamma^* p}\sigma_{\gamma^* n}}{8\pi^2} \int d^2\mathbf{k}_T \; S_D(\mathbf{k}^2) \\ &= -\frac{\sigma^2_{\gamma^* N}}{4\pi} \int dk \; k \; S_D(\mathbf{k}^2) \end{aligned} \tag{4.22}$$

with $k \equiv |\mathbf{k}|$. The above assumptions are expected to be quite accurate because contributions to $\delta\sigma_{\gamma^* D}$ from large $\mathbf{k}$ will be suppressed by the deuteron form factor $S_D(\mathbf{k})$, and for forward scattering the real part of the amplitude is generally small. We will also assume that S_D is a function of $\mathbf{k}^2$ only (i.e. that it is independent of the azimuthal angle).

4.2.1 Low Mass Contributions

As mentioned in Section 4.1.4, in the low-Q^2 region it seems appropriate to describe the shadowing in terms of the VMD model, see Fig.4.6. Since most of the formalism needed has been developed in the preceding sections, we can simply write down the formula for the shadowing correction to the $\gamma^* D$ cross section in the VMD model. Combining Eqs.(4.6) and (4.22), we find [1]

$$\delta^{(V)}\sigma_{\gamma^* D} = \sum_V \frac{4\pi\alpha}{f_V^2} \frac{1}{(1+Q^2/M_V^2)^2} \; \delta\sigma_{VD}. \tag{4.23}$$

[1] Note that the fine structure constant evaluated at $Q^2 = \mathcal{O}(1\mathrm{GeV}^2)$ is $\alpha \approx 1/130$, although the error introduced by this is probably less than that associated with using f_V^2, which is obtained from the decay of meson v with time-like Q^2, for the coupling to a photon with space-like Q^2.

Writing this in terms of the deuteron structure function [2], F_{2D}, we have

$$\delta^{(V)}F_{2D}(x) = \frac{Q^2}{\pi}\sum_V \frac{\delta\sigma_{VD}}{f_V^2(1+Q^2/M_V^2)^2} \tag{4.24}$$

where now

$$\delta\sigma_{VD} = -\frac{\sigma_{VN}^2}{8\pi^2}\int d^2\mathbf{k}_T\, S_D(\mathbf{k}^2). \tag{4.25}$$

In our numerical calculations, the photon—vector meson coupling constants

$$\frac{f_V^2}{4\pi} = \frac{\alpha^2\, M_V}{3\,\Gamma_{V\to e^+e^-}} \tag{4.26}$$

are equal to 2.28, 26.14 and 14.91 for ρ^0,ω and ϕ, respectively [167]. The total vector meson—nucleon cross sections, σ_{VN}, can be related to the total πN and KN cross sections via the quark model. For $V = \rho^0$ and ω, these are approximately equal to 24 mb, and 14.5 mb for $V = \phi$ (see [174, 175]). The energy dependence of the total cross sections (for $Vp \to X$) was recently parameterised by Donnachie and Landshoff in a way that reflects their origin within Regge theory [176],

$$\begin{aligned}\sigma_{\rho^0 p} \approx \sigma_{\omega p} &\approx \frac{1}{2}(\sigma_{\pi^+ p} + \sigma_{\pi^- p}) \approx 13.63\, s^{\epsilon} + 31.79\, s^{-\eta} \\ \sigma_{\phi p} \approx \sigma_{K^+ p} + \sigma_{K^- p} - \sigma_{\pi^- p} &\approx 10.01\, s^{\epsilon} - 1.51\, s^{-\eta}\end{aligned} \tag{4.27}$$

where $\epsilon \approx 0.0808$ and $\eta \approx 0.4525$. For the range of s in current shadowing experiments, and for the range in which we calculate, the differences between using the s-dependent and constant values are small.

For the deuteron form factor $S_D(\mathbf{k}^2)$ we take the electric monopole body form factor [177]

$$S_D(\mathbf{k}^2) = \int_0^\infty dr \left(u^2(r) + w^2(r)\right) j_0(kr) \tag{4.28}$$

where $u(r), w(r)$ are the S, D-wave deuteron wavefunctions, normalised such that $\int dr\ (u^2(r) + w^2(r)) = 1$, and where j_0 is the spherical Bessel function. The square of the 3-momentum transfer to the interacting nucleon is $\mathbf{k}^2 = (\mathbf{p} - \mathbf{p}')^2 = k_T^2 + k_L^2$, where $k_L^2 = M^2x^2(1 + M_V^2/Q^2)^2$ (since $M_X^2 = M_V^2$). In Fig.4.7 we plot the D form factor using wavefunctions obtained from several realistic NN potential models, namely Paris [90], Bonn (OBEPQ) [86] and Bochum [93]. All of these wavefunctions produce a trough in $kS_D(\mathbf{k}^2)$ at $k \approx 3.5$ fm^{-1} (because the Bessel function is negative at large kr), as well as a rapid fall-off with k for $k \gtrsim 6$ fm^{-1}. Also shown is the model of

[2] In terms of the total cross section for the photo-absorption of virtual photons on an unpolarised deuteron, $\sigma_{\gamma^* D}$, the deuteron structure function is

$$W_{2D} = \frac{K}{4\pi^2\alpha}\frac{Q^2}{Q^2+\nu^2}\sigma_{\gamma^* D}$$

where $K = \sqrt{\nu^2 + Q^2}$ is the flux of incoming virtual photons (in the Gilman convention), so that in the Bjorken limit

$$F_{2D} = \frac{Q^2}{4\pi^2\alpha}\sigma_{\gamma^* D}.$$

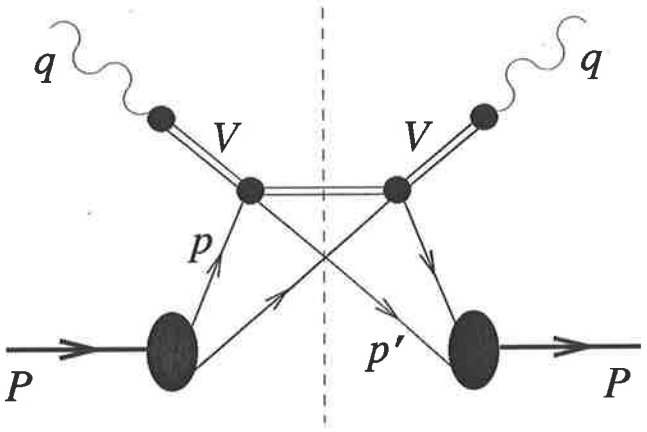

Figure 4.6: Vector meson dominance model of the double scattering mechanism.

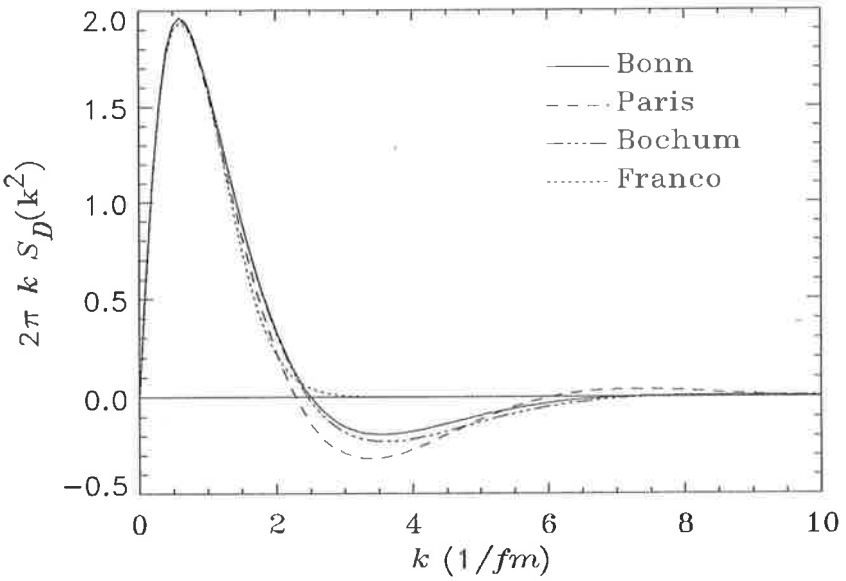

Figure 4.7: Deuteron form factor, as determined from several NN potential models. Also shown is the parameterisation due to Franco & Varma [178] which was used in Refs.[139].

Franco and Varma [178], which was used in [82, 139], for which the form factor, parameterised by a sum of Gaussians, has no large-k tail at all. The differences in the large-k ($\gtrsim 2$ fm^{-1}) behaviour of the form factor arise from the various treatments of the small-r behaviour of $u(r)$ and $w(r)$. In Fig.4.8 we also plot the Fourier transform of the deuteron wavefunctions for the different potential models. At small momenta (large r) there is general agreement between the models, and the differences only start to appear for $p \gtrsim 2$ fm^{-1}. The large variation in $w(p)$ reflects the poor knowledge of the D-wave component.

At $Q^2 = 4$ GeV^2 the VMD model shadowing predictions are given in Fig.4.9 for the various model deuteron form factors. By far the largest contribution ($\approx 80\%$) to $\delta^{(V)}F_{2D}$ comes from the ρ^0 meson. The magnitude of $\delta^{(V)}F_{2D}(x)$ decreases with x because the lower limit of the k-integration in (4.25), $k_{min} = k_L$, is an increasing function of x, and the integrand peaks at small values of k (≈ 0.7 fm^{-1}). It is not surprising to see the differences in the calculated $\delta^{(V)}F_{2D}$ given the

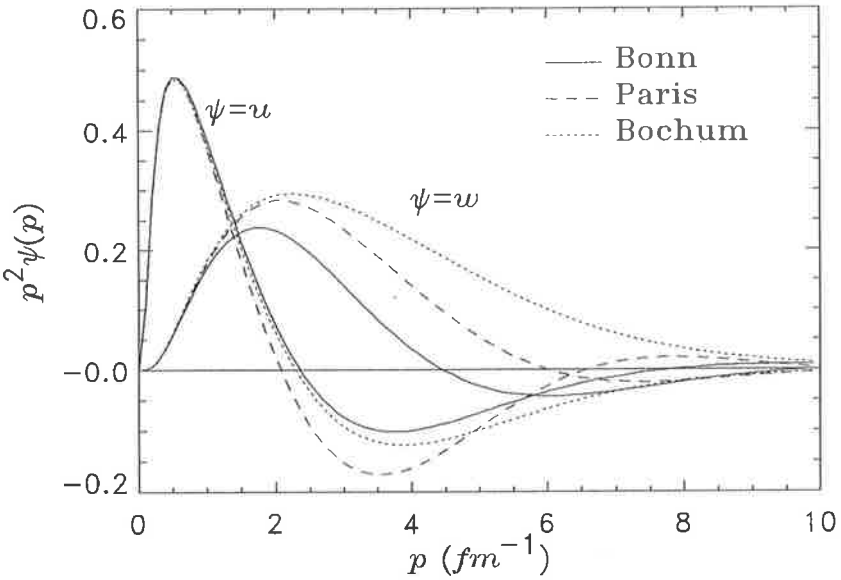

Figure 4.8: Deuteron S and D-wave wavefunctions, from the Paris [90], Bonn (OBEPQ) [86] and Bochum [93] NN potential models.

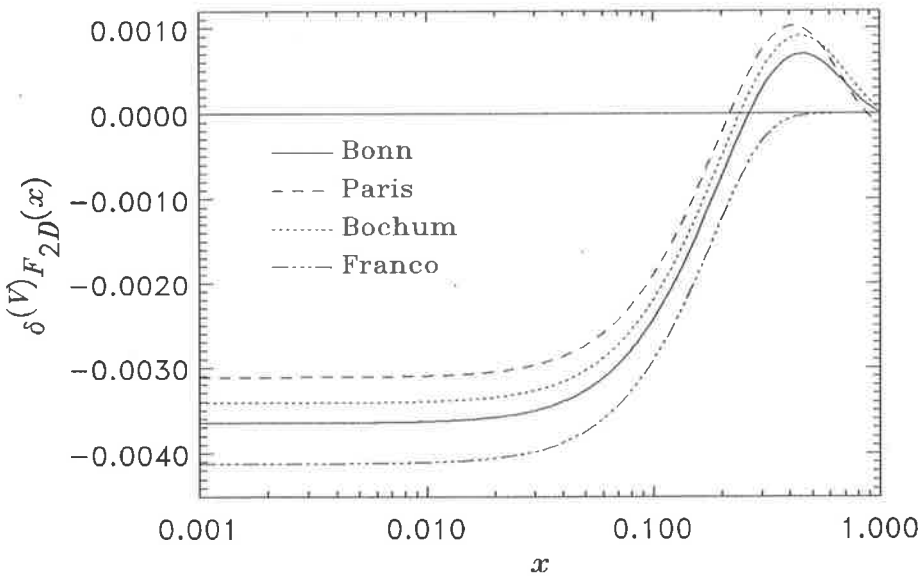

Figure 4.9: Shadowing correction to the deuteron structure function within the VMD model. The curves are evaluated using deuteron form factors from the Bochum, Bonn (OBEPQ) and Paris potential models, as well as the parameterisation of Franco & Varma.

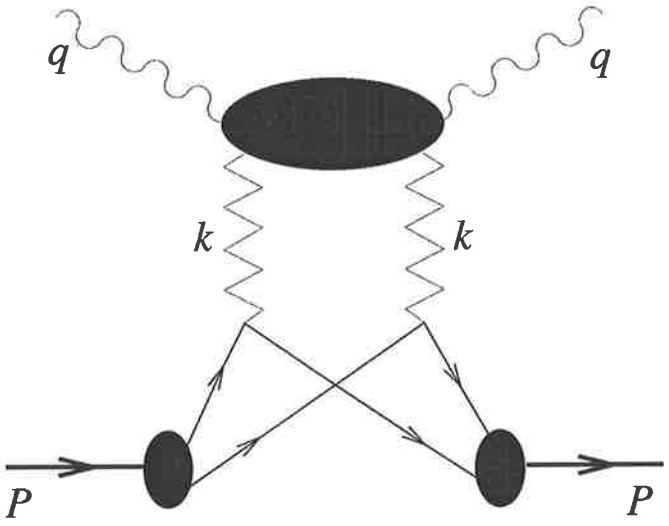

Figure 4.10: Pomeron (zig-zag line) exchange model of the double scattering mechanism which produces shadowing in deuterium.

variation in S_D evident in Fig.4.7. Because the form factor with the Paris wavefunction has the 'deepest' trough, the resultant $\delta^{(V)}F_{2D}$ is $\approx 25\%$ smaller for $x \lesssim 0.01$ than with the Franco and Varma form factor. The trough is also responsible for the antishadowing in the region $x \gtrsim 0.2$.

4.2.2 Pomeron Exchange Contributions

With the VMD model, the spectrum of masses M_X^2 includes only the lowest mass vector mesons. For a complete description of shadowing, the large M_X^2 contributions must also be included. One way to do this is simply to extend the VMD model by including higher mass vector mesons, and the high mass $q\bar{q}$ continuum (as in the GVMD model). However, for reasons outlined in Section 4.1.3, a parton-based description of the double interaction mechanism, in terms of Pomeron exchange (as in Fig.4.10) is more efficient.

The contribution to the F_{2D} structure function from multiple diffractive scattering with $\mathcal{P}$ exchange can be written as a convolution of an exchange-$\mathcal{P}$ function, $f_{\mathcal{P}}(y)$, with the $\mathcal{P}$ structure function of Eq.(4.8),

$$\delta^{(\mathcal{P})}F_{2D}(x) \;=\; \int_{y_{min}}^{2} dy\; f_{\mathcal{P}}(y)\; F_{2\mathcal{P}}(x_{\mathcal{P}}) \tag{4.29}$$

where

$$f_{\mathcal{P}}(y) \;=\; -\frac{\sigma_{pp}}{8\pi^2}\,\frac{1}{y}\int d^2\mathbf{k}_T\; S_D(\mathbf{k}^2) \tag{4.30}$$

and $k_L^2 = M^2y^2$. Note that the function $f_{\mathcal{P}}(y)$ should not be interpreted as a probability distribution function, since there is no probabilistic interpretation of the double scattering diagram from which it arises. Fig.4.11 illustrates the y-dependence of $f_{\mathcal{P}}(y)$, including the $1/y$ divergence for $y \to 0$. The rapid fall off with y is testament to the very small contribution coming from the large-y region.

In formulating a complete description of shadowing which includes more than one mechanism care must be taken to avoid possible double counting. Because of this concern some authors [140]

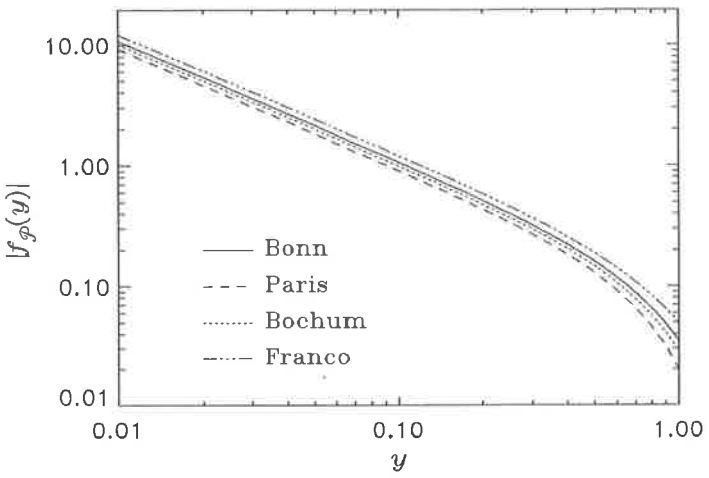

Figure 4.11: y-dependence of the Pomeron function $f_{\mathcal{P}}(y)$ as a function of y, with several different deuteron form factors.

have restricted the Pomeron exchange process to the region of M_X^2 above the highest mass of the vector mesons contributing to the VMD process, $M_X^2 \geq M_{X_0}^2 \simeq 1.5\text{GeV}^2$, and consequently have taken the lower bound on the integral in (4.29) to be $y_{min} = x(1 + M_{X_0}^2/Q^2)$. The VMD contribution, which is essentially a higher twist $(1/Q^2)$ effect, may compete with that part of the diagram in Fig.4.10 which contains low-M_X single particle intermediate states. By keeping only the leading twist piece of the structure function $F_{2\mathcal{P}}$, this contribution can in principle be excluded since it involves extra factors of $1/Q^2$ from the electromagnetic form factors. (Although in practice a decomposition of $F_{2\mathcal{P}}$ in terms of different twist components has not yet been done.) Nevertheless, we can test the sensitivity of the numerical results to the cut-off procedure by varying $M_{X_0}^2$, say from 0 to 2 GeV^2. For low x we find a difference over this range of only some 5% of the total $\mathcal{P}$ exchange contribution to F_{2D}. For larger Q^2 the separation into separate M_X regions becomes irrelevant since $y_{min} \to x$ in the Bjorken limit.

Since the function $f_{\mathcal{P}}(y)$ is independent of Q^2, the scaling behaviour of the $\mathcal{P}$-exchange mechanism will be determined by the scaling behaviour of the $\mathcal{P}$ structure function, and from Eqs.(4.10)—(4.14) it is clear that $\delta^{(\mathcal{P})}F_{2D}$ will be finite as $Q^2 \to \infty$. The individual 'box' and $3\mathcal{P}$ contributions to $\delta^{(\mathcal{P})}F_{2D}$, with the deuteron form factor obtained from the Bochum wavefunction, are shown in Fig.4.12 for $Q^2 = 4$ GeV^2. The dependence of $\delta^{(P)}F_{2D}$ on $S_D(\mathbf{k}^2)$ is illustrated in Fig.4.13. Again, as in the case of the VMD model, the large-k, negative tail of the form factor produces a large (some 30-40%) difference between different models for $x \lesssim 0.05$. For $x \gtrsim 0.2$ the presence or absence of antishadowing will be determined by the model deuteron wavefunction.

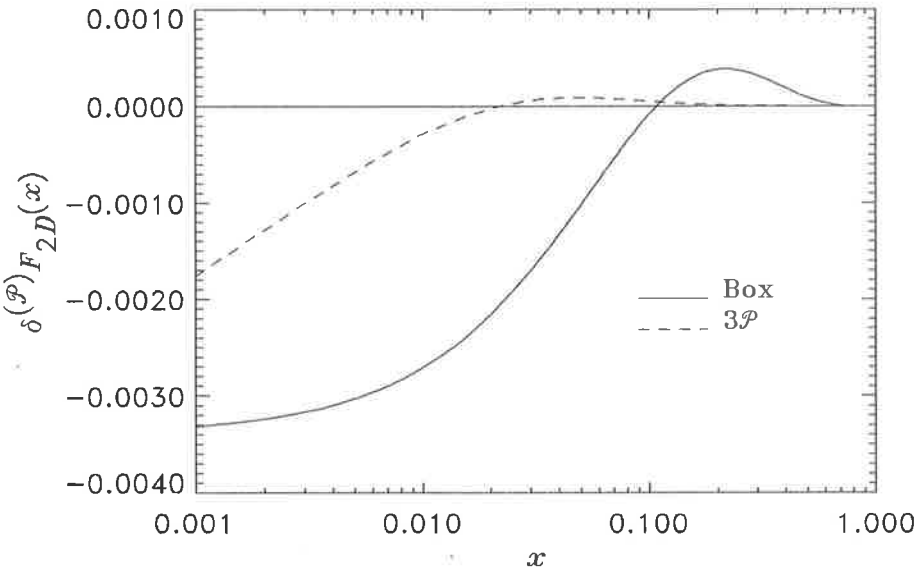

Figure 4.12: Quark–antiquark box and triple–$\mathcal{P}$ contributions to the total deuteron structure function, with the D form factor calculated from the Bochum model wavefunctions.

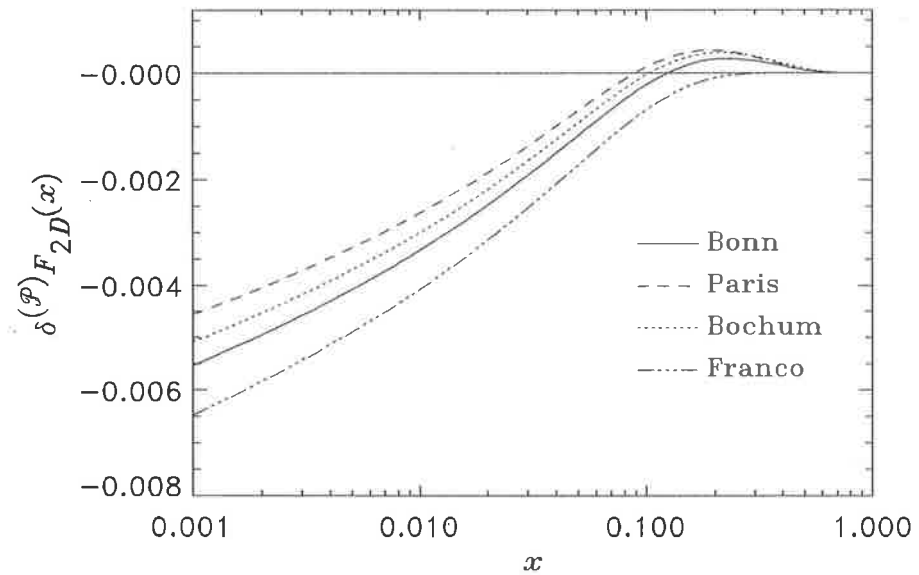

Figure 4.13: Deuteron form factor dependence of the $\mathcal{P}$-exchange contribution to the structure function of the deuteron.

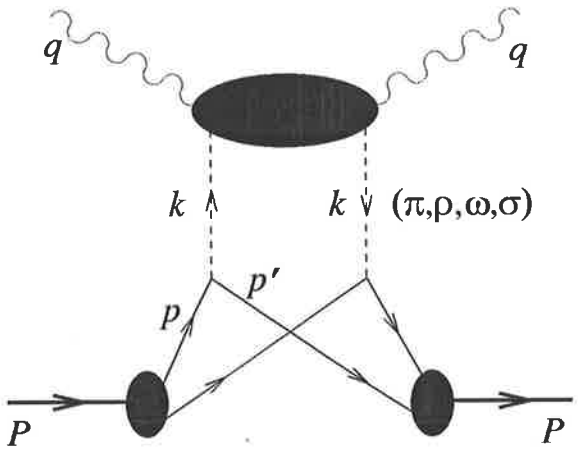

Figure 4.14: Double scattering diagram with meson exchange.

4.2.3 Shadowing by Mesons

Another potential source of shadowing arising from the double scattering mechanism is one which involves the exchange of mesons, Fig.4.14. It has previously been suggested [136] that this can lead to substantial antishadowing corrections to $F_{2D}(x)$, thereby cancelling some of the shadowing produced by the VMD and $\mathcal{P}$-exchange mechanisms. Using a non-relativistic formalism, the total contribution to the deuteron structure function from meson exchange currents is written [179]

$$\delta^{(M)}F_{2D}(x) \;=\; \sum_M \int_x^2 dy\; f_M(y)\; F_{2M}(x_M) \tag{4.31}$$

where $M = \pi, \rho, \omega, \sigma$, and $y = k\cdot q/p\cdot q = (k_0 + k_L)/M$ with $x_M = x/y$. The exchange-meson distribution functions $f_M(y)$ are obtained from the non-relativistic reduction of the nucleon—meson interaction,

$$\begin{aligned} f_M(y) \;=\; & 4c_M\; M\; y \int \frac{d^3\mathbf{p}\; d^3\mathbf{p}'}{(2\pi)^3} \frac{\mathcal{F}^2_{MNN}(k^2)}{(k^2 - m_M^2)^2} \\ & \times \left\{ \frac{1}{3}\sum_{J_z} \Psi^\dagger(\mathbf{p}, J_z)\; \mathcal{V}_{MNN}\; \Psi(\mathbf{p}', J_z) \right\} \delta\left(y - \frac{k_0 + k_L}{M}\right). \end{aligned} \tag{4.32}$$

The deuteron wavefunction is defined by

$$\Psi(\mathbf{p}, J_z) \;=\; \frac{1}{\sqrt{4\pi}} \left(u(p) - w(p)\frac{S_{12}(\hat{p})}{\sqrt{8}} \right)\; \chi_1^{J_z} \tag{4.33}$$

where $u(p)$ and $w(p)$ are its S and D-wave components, normalised so that $\int dp\, \mathbf{p}^2\; (u^2(p) + w^2(p)) = 1$, with $\hat{p} \equiv \mathbf{p}/p$ and $p \equiv |\mathbf{p}|$, and S_{12} is the tensor operator: $S_{12}(\hat{p}) = 3\;\sigma_1\cdot\hat{p}\;\sigma_1\cdot\hat{p} - \sigma_1\cdot\sigma_2$. The deuteron spin wavefunction is denoted by $\chi_1^{J_z}$, where J_z is the total angular momentum projection. In (4.32), $k^2 = k_0^2 - \mathbf{k}^2$, where $k_0 = M_D - \sqrt{M^2 + \mathbf{p}^2} - \sqrt{M^2 + \mathbf{p}'^2}$ is the energy of the off-shell meson, and $\mathbf{k} = \mathbf{p} - \mathbf{p}'$ is its 3-momentum.

In Eq.(4.32) the nucleon—meson interactions are given by [86]

$$\mathcal{V}_{\pi NN} = -\frac{f^2_{\pi NN}}{m^2_\pi}\,\sigma_1\cdot\mathbf{k}\;\sigma_2\cdot\mathbf{k} \tag{4.34}$$

$$\begin{aligned}\mathcal{V}_{\rho NN} &= g^2_{\rho NN}\left[1+\frac{3\mathbf{q}^2}{2M^2}-\frac{\mathbf{k}^2}{8M^2}-\sigma_1\cdot\sigma_2\frac{\mathbf{k}^2}{4M^2}+\frac{\sigma_1\cdot\mathbf{k}\;\sigma_2\cdot\mathbf{k}}{4M^2}\right]\\ &+ \frac{g_{\rho NN}f_{\rho NN}}{2M}\left[-\frac{\mathbf{k}^2}{M}-\sigma_1\cdot\sigma_2\frac{\mathbf{k}^2}{M}+\frac{\sigma_1\cdot\mathbf{k}\;\sigma_2\cdot\mathbf{k}}{M}\right]\\ &+ \frac{f^2_{\rho NN}}{4M^2}\left[-\sigma_1\cdot\sigma_2\;\mathbf{k}^2+\sigma_1\cdot\mathbf{k}\;\sigma_2\cdot\mathbf{k}\right]\end{aligned} \tag{4.35}$$

$$\mathcal{V}_{\omega NN} = g^2_{\omega NN}\left[1+\frac{3\mathbf{q}^2}{2M^2}-\frac{\mathbf{k}^2}{8M^2}-\sigma_1\cdot\sigma_2\frac{\mathbf{k}^2}{4M^2}+\frac{\sigma_1\cdot\mathbf{k}\;\sigma_2\cdot\mathbf{k}}{4M^2}\right] \tag{4.36}$$

$$\mathcal{V}_{\sigma NN} = -g^2_{\sigma NN}\left[1-\frac{\mathbf{q}^2}{2M^2}+\frac{\mathbf{k}^2}{8M^2}\right] \tag{4.37}$$

where $\mathbf{q}=\frac{1}{2}(\mathbf{p}+\mathbf{p}')$. Terms proportional to $\mathbf{S}\cdot\mathbf{k}\times\mathbf{q}$, where $\mathbf{S}=\sigma_1+\sigma_2$, are omitted as they do not contribute to $f_M(y)$.

Evaluation of (4.32) requires the identities

$$\begin{aligned}\frac{1}{3}\sum_{J_z}\Psi^\dagger(\mathbf{p},J_z)\;\Psi(\mathbf{p}',J_z) &= \frac{1}{4\pi}\left[u(p)\;u(p')+w(p)\;w(p')\;P_2(\cos\theta)\;P_2(\cos\theta')\right]\\ &+ \phi\text{ dependent terms}\\ &= \frac{1}{3}\sum_{J_z}\Psi^\dagger(\mathbf{p},J_z)\;\sigma_1\cdot\sigma_2\;\Psi(\mathbf{p}',J_z)\end{aligned} \tag{4.38}$$

$$\begin{aligned}\frac{1}{3}\sum_{J_z}\Psi^\dagger(\mathbf{p},J_z)\;\sigma_1\cdot\mathbf{k}\;\sigma_2\cdot\mathbf{k}\;\Psi(\mathbf{p}',J_z) &= \frac{1}{4\pi}\left\{\frac{1}{3}\left[\mathbf{k}^2-2\;p\;p'\;\sin\theta\;\sin\theta'\;\right]u(p)\;u(p')\right.\\ &-\frac{1}{\sqrt{2}}\left[4\;p\;p'\;\cos\theta\;\cos\theta'\;\sin^2\theta'\;+\;4\;\mathbf{p}'^2\cos^2\theta'\;\sin^2\theta'\right.\\ &\quad-\frac{2}{3}\;(\mathbf{p}^2+\mathbf{p}'^2)\;P_2(\cos\theta')\;+2\;(\mathbf{p}^2\cos^2\theta+\mathbf{p}'^2\cos^2\theta')\;P_2(\cos\theta')\\ &\quad\left.+\;\frac{8}{3}\;p\;p'\;\cos\theta\;\cos\theta'\;P_2(\cos\theta')\right]\;u(p)\;w(p')\\ &-\frac{1}{\sqrt{2}}\left[4\;p'\;p\;\cos\theta'\;\cos\theta\;\sin^2\theta+\;4\;\mathbf{p}^2\cos^2\theta\;\sin^2\theta\right.\\ &\quad-\frac{2}{3}\;(\mathbf{p}'^2+\mathbf{p}^2)\;P_2(\cos\theta)\;+\;2\;(\mathbf{p}'^2\cos^2\theta'+\mathbf{p}^2\cos^2\theta)\;P_2(\cos\theta)\\ &\quad\left.+\;\frac{8}{3}\;p'\;p\;\cos\theta'\;\cos\theta\;P_2(\cos\theta)\right]\;w(p)\;u(p')\\ &-\frac{1}{3}\left[(p\;\cos\theta+p'\;\cos\theta')^2\;P_2(\cos\theta)\;P_2(\cos\theta')\right.\\ &\quad-2\;(\mathbf{p}^2\sin^2\theta+\mathbf{p}'^2\sin^2\theta')\;P_2(\cos\theta)\;P_2(\cos\theta')\\ &\quad+3\;(\mathbf{p}^2\cos^2\theta\;\sin^2\theta+p\;p'\;\cos\theta\;\cos\theta'\;\sin^2\theta)\;P_2(\cos\theta')\\ &\quad+3\;(\mathbf{p}'^2\cos^2\theta'\;\sin^2\theta'+p'\;p\;\cos\theta'\;\cos\theta\;\sin^2\theta')\;P_2(\cos\theta)\\ &\quad\left.\left.+\;\frac{9}{2}\;p\;p'\;\cos\theta\;\cos\theta'\;\sin^2\theta\;\sin^2\theta'\right]\;w(p)\;w(p')\right\}\\ &+\phi\text{ dependent terms.}\end{aligned} \tag{4.39}$$

The terms in (4.38)—(4.39) which depend on the azimuthal angle (ϕ) vanish after integration. The factors c_M are due to isospin, and are equal to 3 for $M = \pi, \rho$, and 1 for $M = \omega, \sigma$.

Note that the functions $f_M(y)$, just like the function $f_{\mathcal{P}}(y)$ in the previous section, are not to be interpreted as meson distribution functions (c.f. the functions f_{MB} in Chapter 3 which were interpreted as virtual meson probability distributions) because a probabilistic interpretation cannot be applied to the double scattering diagram from which they arise. Furthermore, since here we deal with covariant kinematics, the use of the real meson structure function in the convolution formula in (4.31) relies on the assumption of weak k^2 dependence in the function F_{2M}. In the next chapter we shall argue why the convolution formula in a relativistic treatment of DIS from nuclei is invalid. However, since our treatment of the meson-exchange currents is entirely non-relativistic, and the total meson-exchange correction is small anyway, we shall assume that this formula is reliable in this application. For the meson structure function, F_{2M}, we therefore take the parameterisation of the (real) pion structure function from Drell-Yan production [101].

In our non-relativistic approach, we parameterise the MNN vertex form factor $\mathcal{F}_{MNN}(k^2)$ by a dipole form

$$\mathcal{F}_{MNN}(k^2) \;=\; \left(\frac{\Lambda_M^2 - m_M^2}{\Lambda_M^2 - k^2}\right)^2 . \tag{4.40}$$

In non-relativistic NN potential models, the high-momentum cut-offs Λ_M range from $\lesssim 1$ GeV in models with soft form factors [93, 95] to $\sim 1.7 - 2$ GeV when hard form factors are employed [86]. In principle, the meson—nucleon form factor should be universal, and the cut-off Λ_M that is used in the deuteron should be the same as that used in Chapter 3 in the discussion on meson—baryon vertices in lepton—nucleon DIS. However, since different formalisms are used in the two cases, it's not clear what, if any, relation exists between the two sets of form factors. We therefore evaluate the shadowing correction from meson exchange currents for a range of cut-offs.

Fig.4.15 shows the individual meson exchange contributions to $\delta^{(M)}F_{2D}$, for the wavefunction of the Bonn model, and with a universal dipole cut-off of $\Lambda_M = 1.7$ GeV for all mesons. As could be expected, pion exchange is the dominant process. We also include the fictitious σ meson, but with a mass (≈ 800 MeV) that is larger than that used to represent 2π exchange in NN scattering. Both of these produce antishadowing for small x. The exchange of vector mesons (ρ, ω) cancels some of this antishadowing, although the magnitude of these contributions is smaller. In fact, for $\Lambda_M \lesssim 1.3$ GeV all contributions other than that of the pion are totally negligible.

Fig.4.16 shows the dependence of the total $\delta^{(M)}F_{2D}$ on Λ_M for the Bonn model wavefunction. There is approximately a factor of 2 difference between the amount of shadowing with soft ($\Lambda_M = 1$ GeV, lower solid line) and hard ($\Lambda_M = 1.7$ GeV, upper solid line) form factors. We also consider the effect of the model momentum-space deuteron wavefunction on $\delta^{(M)}F_{2D}$. Although the model wavefunctions differ substantially at large momenta ($p \gtrsim 2$ fm^{-1} — see Fig.4.8), this variation will be largely suppressed by the meson—nucleon form factor. The Bochum and Paris wavefunctions are generally larger than the Bonn wavefunction, and this is reflected in a larger $\delta^{(M)}F_{2D}$.

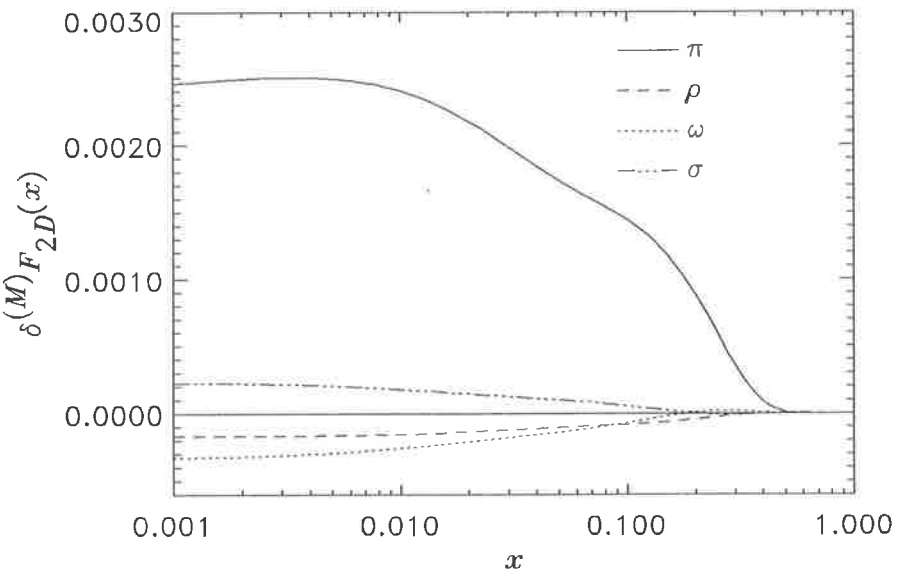

Figure 4.15: Comparison of individual meson exchange contributions to the deuteron structure function, for the Bonn (OBEPQ), Bochum and Paris wavefunctions, with a form factor cut-off of $\Lambda_M = 1.7$ GeV. Note the mass of the effective σ meson is taken to be ≈ 800 MeV.

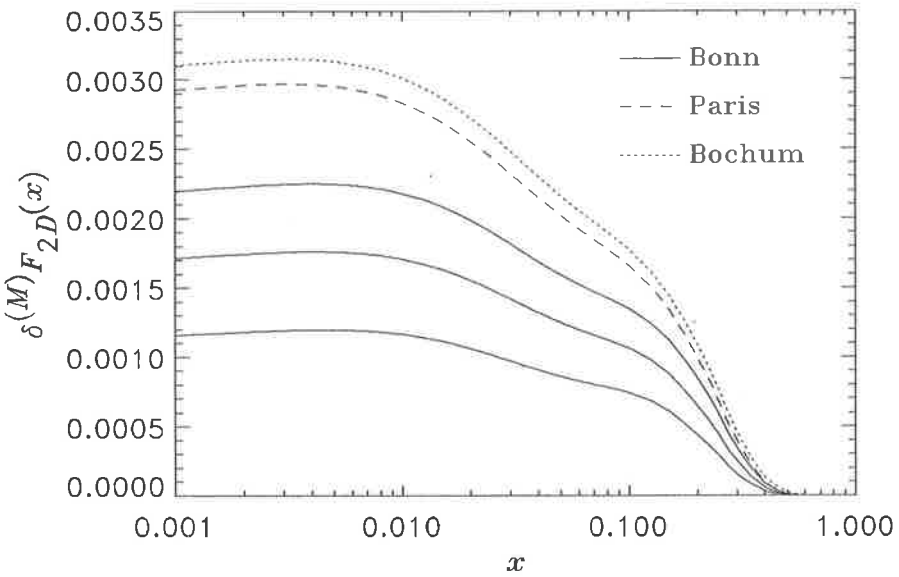

Figure 4.16: Deuteron wavefunction and form factor cut-off dependence of the total meson-exchange correction. The Bochum and Paris curves are evaluated with $\Lambda_M = 1.3$ GeV, while the Bonn (OBEPQ) curves have $\Lambda_M = 1.0, 1.3$ and 1.7 GeV, with the larger cut-offs giving more overall antishadowing.

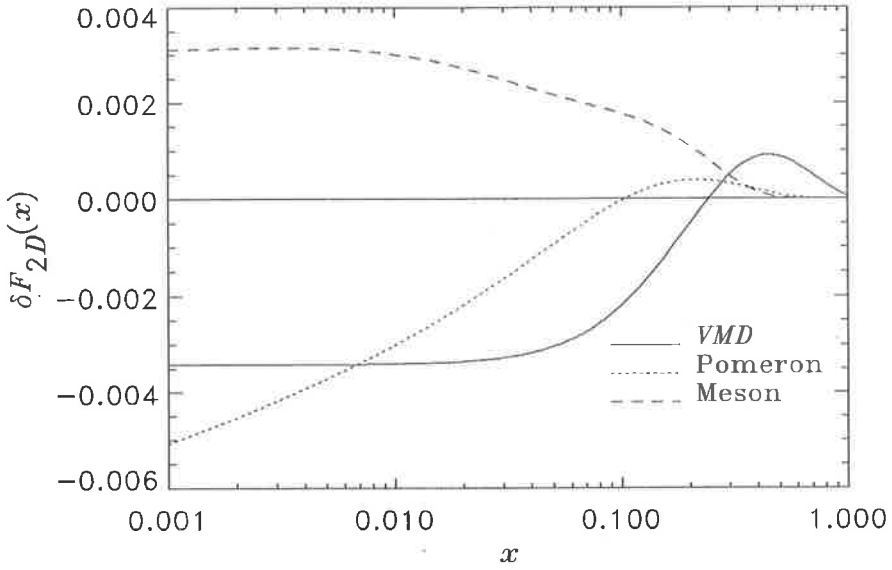

Figure 4.17: Comparison between the VMD, Pomeron and meson exchange corrections to F_{2D} at $Q^2 = 4$ GeV^2. All curves are calculated with the Bochum wavefunction for $\Lambda_M = 1.3$ GeV.

We also comment here on the issue raised in the previous section, namely double counting, this time between the meson exchange and the other mechanisms. It should be clear that since the $\mathcal{P}$ contribution involves the exchange of vacuum quantum numbers, there will be no interference between this and the exchange of pseudoscalar pions or vector mesons. The scalar σ meson, introduced as an effective description of two-pion $N\Delta$ excitations, does not correspond to actual exchange of a spin 0 particle. By restricting the meson structure function to only the leading twist component (our F_{2M} is determined at $Q^2 = 25$ GeV^2 where this assumption seems reasonable) we may view the VMD process as a description of higher twist effects. Still, imposing any low-M_X cut on the meson exchange term has numerically insignificant consequences, largely because $F_{2M}(x/y) \to 0$ as $y \to x$.

4.2.4 Consequences for F_{2n} and the Gottfried Sum Rule

The total deuteron structure function is defined by

$$F_{2D}(x) \;=\; F_{2p}(x) + F_{2n}(x) + \delta F_{2D}(x) \tag{4.41}$$

where the shadowing correction is a sum of the VMD, Pomeron and meson exchange contributions,

$$\delta F_{2D}(x) \;=\; \delta^{(V)} F_{2D}(x) + \delta^{(\mathcal{P})} F_{2D}(x) + \delta^{(M)} F_{2D}(x). \tag{4.42}$$

In Fig.4.17 we compare the contributions to $\delta F_{2D}(x)$ from the three mechanisms considered. For $x \lesssim 0.1$ the magnitude of the (negative) Pomeron/VMD shadowing is larger than the (positive) meson-exchange contribution, so that the total δF_{2D} is negative. The fact that shadowing is present in this region of x does not depend on the model deuteron wavefunction. For larger x ($\approx 0.1 - 0.2$)

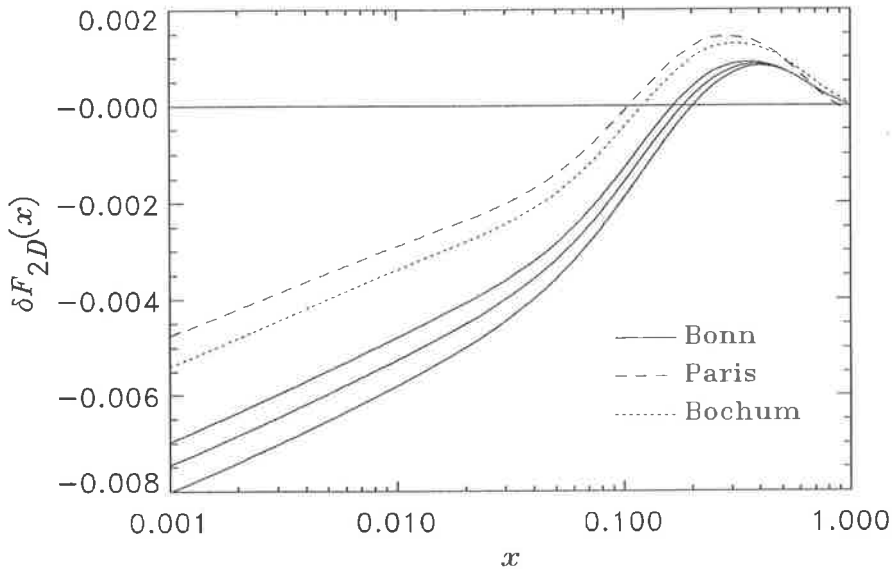

Figure 4.18: Dependence of total shadowing correction on the deuteron wavefunction and the meson—nucleon form factor cut-off Λ_M. For the Bochum and Paris curves $\Lambda_M = 1.3$ GeV, while the Bonn curves are calculated with $\Lambda_M = 1.0, 1.3$ and 1.7 GeV, with the largest cut-off giving the smallest overall shadowing correction.

there is a small amount of antishadowing, which is due mainly to the VMD contribution. The dependence of the total shadowing correction δF_{2D} on the deuteron wavefunction and on the meson—nucleon form factor is shown in Fig.4.18 for $Q^2 = 4$ GeV^2. We point out that the magnitude of δF_{2D} is about 4 times smaller [180] than that obtained in Ref.[82, 139], and about 2 times smaller compared with the result of Ref.[140]. The most important reasons for our smaller results are the inclusion of meson exchange contributions which produce antishadowing at small x, and the use of realistic deuteron wavefunctions which lead to smaller $\mathcal{P}$ exchange and VMD contributions.

Finally we can consider the consequences of the shadowing correction for the neutron structure function. From the NMC measurement of F_{2p} and F_{2D} [65, 181], the neutron structure function was extracted assuming no nuclear effects in D, so that

$$\frac{F_{2D}\,(1-(F_{2D}/F_{2p}-1))}{(1+(F_{2D}/F_{2p}-1))} \;=\; 2F_{2p}-F_{2D} \;\equiv\; (F_{2p}-F_{2n})_{NMC}. \tag{4.43}$$

The actual difference between the p and n structure functions should be, after the shadowing correction is included,

$$F_{2p}-F_{2n} \;=\; (F_{2p}-F_{2n})_{NMC} \;+\; \delta F_{2D} \tag{4.44}$$

and this is shown in Fig.4.19. The dotted line is a best fit to the NMC data, and includes the small-x extrapolation used in [65] (see Eq.(3.88)). The other curves include the shadowing corrections to the NMC data parameterisation. It is not clear whether $F_{2p} - F_{2n}$ will become negative at $x \lesssim 0.004$, and it will be interesting to see whether this cross-over occurs when additional data at smaller x become available.

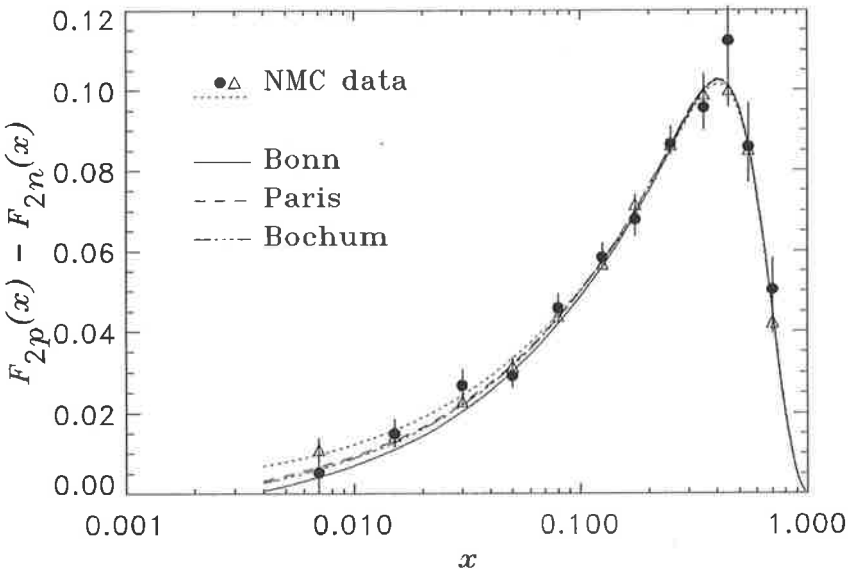

Figure 4.19: Proton—neutron structure function difference with shadowing corrections to the NMC data at $Q^2 = 4$ GeV^2. The dotted line is a parameterisation of the data.

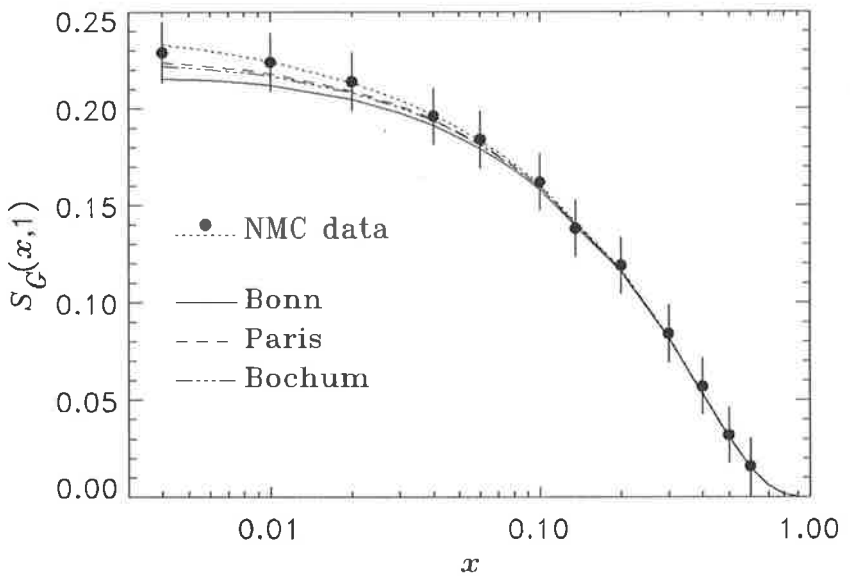

Figure 4.20: Shadowing corrections to the Gottfried integral $S_G(x,1)$. The corrections to the NMC data parameterisation (dotted curve) are for the Bochum, Bonn (OBEPQ) and Paris deuteron wavefunctions, and the meson antishadowing correction is calculated with $\Lambda_M = 1.3$ GeV.

Model	α	β	$S_G(0, x_{min})$	$S_G(x_{min}, 1)$	$S_G(0, 1)$
NMC [65]	0.21	0.62	0.011	0.229	0.240 ± 0.016
	0.109	0.5	0.014		0.243
Bochum ($\Lambda_M = 1.3$GeV)	0.043	0.5	0.005	0.222	0.227
Paris ($\Lambda_M = 1.3$GeV)	0.052	0.5	0.007	0.224	0.230
Bonn ($\Lambda_M = 1.3$GeV)	0.011	0.5	0.001	0.215	0.217
Bonn ($\Lambda_M = 1.0$GeV)	0.002	0.5	0.000	0.214	0.214
Bonn ($\Lambda_M = 1.7$GeV)	0.019	0.5	0.002	0.217	0.219

Table 4.1: Small-x extrapolation parameters for $F_{2p} - F_{2n} (= \alpha x^\beta)$ and the contributions to the Gottfried sum from different x-regions.

The shadowing corrections to the Gottfried integral

$$S_G(x, 1) = \int_{\ln x}^{0} d\,(\log x')\,(F_{2p}(x') - F_{2n}(x')) \tag{4.45}$$

are shown in Fig.4.20 for x down to $x_{min} = 0.004$. The only noticeable effects appear at very small x ($x \lesssim 0.01$), and are largest for the Bonn model wavefunctions.

In Table 4.1 we give the values of S_G including shadowing corrections, and also the $x < x_{min}$ extrapolation parameters ($F_{2p} - F_{2n} \to \alpha x^\beta$). For simplicity we take $\beta = 0.5$, and adjust α to achieve a smooth transition between the $x > x_{min}$ and $x < x_{min}$ regions. The overall correction to the NMC value for $S_G(0, 1)$ is found to be between –0.010 and –0.026. This is to be compared with between –0.07 and –0.088 obtained in [82, 139, 169].

Having obtained the corrected values for S_G, we can now examine the consequences for the question of flavour asymmetry in the proton sea. Despite the model-dependence of the total shadowing correction, we can conclude that the experimental value for S_G should be lowered from 0.24 to ≈ 0.22 when the 'true' neutron structure function is used. Within the model of the previous chapter such a decrease can easily be accommodated by increasing the Pauli blocking correction from $\mathcal{P}_N \approx 0.1$ to ≈ 0.15, if the meson—baryon form factor cut-off is kept at the same value ($\Lambda \approx 0.7$ GeV). Of course a larger Λ could also produce a smaller S_G, but, as we saw in Chapter 3, increasing Λ would also produce a depletion in $F_{2p} - F_{2n}$ at intermediate x, together with an increase at small x. This would be contrary to the behaviour of the shadowing-corrected proton—neutron structure function difference seen in Fig.4.19. A reduction of $F_{2p} - F_{2n}$ at $x \lesssim 0.3$ can only be explained by a larger Pauli blocking correction, such as the one required to reproduce the corrected S_G.

In Fig.4.21 we also show the ratio of neutron structure functions with and without shadowing corrections,

$$\frac{F_{2n}}{(F_{2n})_{NMC}} = 1 - \frac{\delta F_{2D}}{F_{2D}} \left(\frac{1 + (F_{2n}/F_{2p})_{NMC}}{(F_{2n}/F_{2p})_{NMC}} \right) \tag{4.46}$$

where the NMC neutron/proton ratio was defined as $(F_{2n}/F_{2p})_{NMC} \equiv F_{2D}/F_{2p} - 1$. There is an

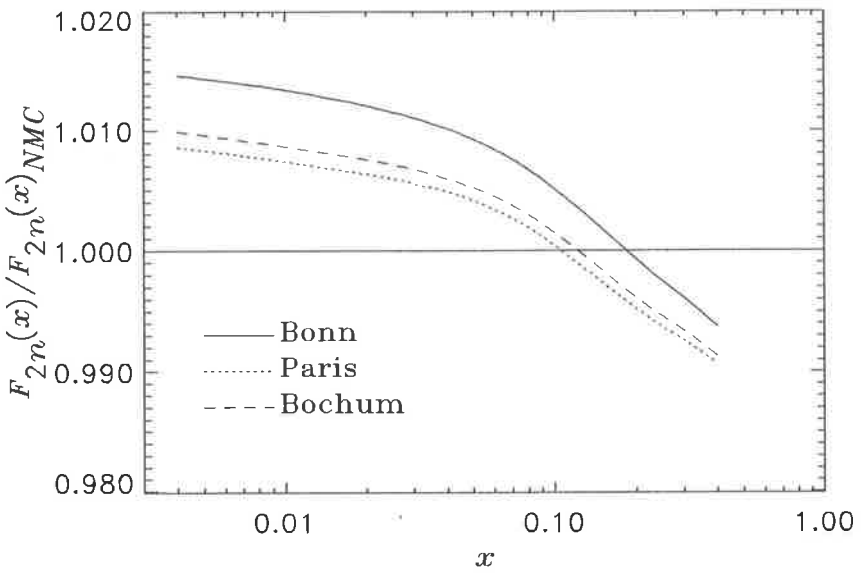

Figure 4.21: Ratio of neutron structure functions with and without shadowing corrections at $Q^2 = 4$ GeV^2. The meson exchange current contribution is evaluated with $\Lambda_M = 1.3$ GeV.

overall $1 - 2\%$ increase in the neutron structure function due to shadowing for $x \lesssim 0.01$. As a fraction of the total $F_{2D}(x)$ [65], the shadowing correction thus amounts to (0.5-1.0%, 0.4-0.8%, 0.0-0.3%) at $x = (0.004, 0.01, 0.1)$, while the antishadowing is less than 0.2% of F_{2D} at $x \approx 0.2$.

Finally, we illustrate in Fig.4.22 the dependence upon Q^2 of the total shadowing correction, $\delta F_{2D}(x, Q^2)$. As expected, the VMD term vanishes rapidly with increasing Q^2, leaving the two scaling contributions from $\mathcal{P}$ and meson exchange to largely cancel each other for $Q^2 \simeq 25$ GeV^2. However, we should add a note of caution about comparing shadowing corrections at very large values of Q^2. In the parton recombination model [182–184] the fusion of quarks and gluons from different nucleons introduces additional terms [182] in the equations governing the Q^2 evolution of the parton distributions. At very small x and large Q^2, such as those attainable at the DESY ep collider HERA, this can lead to significant corrections [140] to the $\delta F_{2D}(x, Q^2)$ evolved without these terms, although the exact magnitude of these is sensitive to the small-x behaviour of the input nucleon gluon distribution. For the moderate range of Q^2 and not too low x values in Fig.4.22, however, we expect the indicated Q^2 behaviour to be reliable.

To summarise, we have estimated the nuclear shadowing in lepton—deuteron DIS from the double scattering mechanism in Fig.4.5. Our approach is similar to that of Refs.[140] and [139], in describing the interaction in terms of the VMD model, together with Pomeron exchange at larger M_X^2. However, we have also included contributions from the exchange of mesons which effectively cancel as much as half of the shadowing from the VMD/$\mathcal{P}$-exchange mechanisms alone. Numerically, there is some dependence on the model deuteron wavefunction, and also on the meson—nucleon form factor for the meson-exchange process. The net effect is a $\lesssim 1\%$ reduction of F_{2D} for $x \sim 0.004$, or equivalently $\lesssim 2\%$ increase in the neutron structure function over the uncorrected F_{2n}.

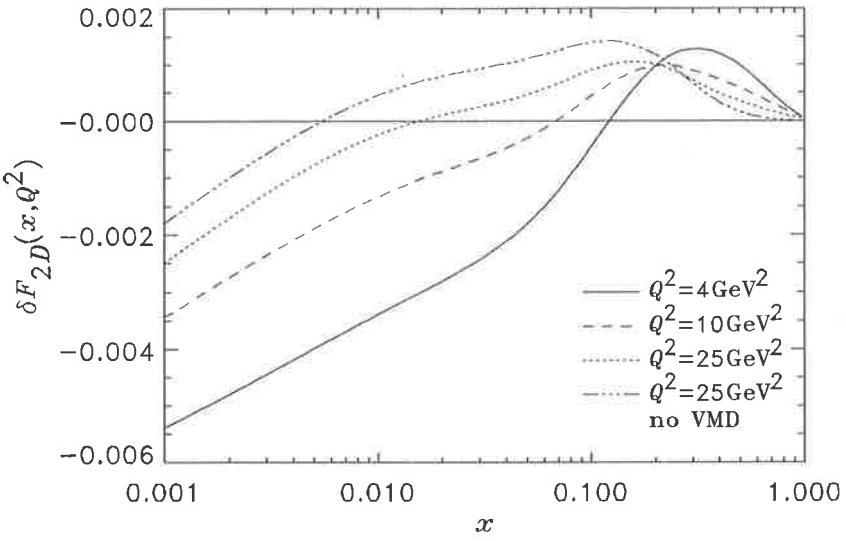

Figure 4.22: Dependence of total shadowing correction on Q^2. The mesonic correction is calculated with the Bochum D wavefunction and $\Lambda_M = 1.3$ GeV.

Consequently, the shadowing correction to the Gottfried sum $S_G(0,1)$ is between −0.010 and −0.026 (or between 4 and 10% of the NMC value), which is about 5 times smaller than in previous estimates, but still not negligible. Nevertheless, it seems clear that the shadowing correction will not alter drastically our conclusions from Chapter 3 about the mechanisms of SU(2) flavour symmetry violation in the proton sea.

To accurately test the descriptions of shadowing in the deuteron it is necessary to obtain model-independent information on the neutron structure function at low x. Even at HERA energies this is not possible with electron scattering alone. However, when combined with high-precision data from neutrino—proton experiments the individual flavour distributions can be determined, and the neutron structure function inferred from charge symmetry. For this to happen, however, the statistics on the neutrino data need to be improved, and the range extended into the smaller-x region. In the meantime, one can still test the validity of the model used in this section by examining other processes, such as shadowing in heavy nuclei. By now a large body of data has been accumulated for the nuclear structure functions, including at small x. In the next section we therefore extend the above model in a calculation of the shadowing corrections to nuclear structure functions, and compare this with the latest high-precision CERN data.

4.3 Shadowing in Heavy Nuclei

With the help of the multiple scattering expansion in Section 4.1.1 one can easily extend the above model, based on the two-phase hadronic (low Q^2) and partonic (high Q^2) picture, to calculate the shadowing corrections to structure functions of heavy nuclei. One obvious difference here is the presence of additional terms in the multiple scattering series, when only two terms existed for deuterium. Another difference is the nuclear wavefunction. For the deuteron this is now fairly well determined, however, for heavy nuclei we are forced to use nuclear matter density functions to describe the distribution of nucleons in the nucleus.

As well as the VMD and Pomeron exchange contributions, in the deuteron we also found that taking into account meson exchange currents produced a non-negligible correction to the total F_{2D}. We may also think of calculating the same meson-exchange contributions to the nuclear structure function, F_{2A}. Models of the nucleus in which meson effects are explicitly taken into account when calculating nuclear structure functions have been considered, for example, by Berger et al. [76], Ericson & Thomas [125], Kaptari et al. [185] and others. In the model of Ref.[125], it was suggested that a larger pion cloud in the nucleus, compared with that associated with a free nucleon, could produce a small enhancement of the nuclear to nucleon structure function ratio in the region $x \sim 0.1$. However, the conclusions there were strongly dependent upon the Landau-Migdal parameter, which characterises the strength of the short-range repulsive NN, $N\Delta$ and $\Delta\Delta$ interactions. In calculating the meson-exchange corrections to nuclear structure functions, one would also need to include such excitations. In view of the difficulty in reliably calculating these effects in nuclei, we shall follow the 'conventional' approach and compute the contributions from VMD and Pomeron-exchange models alone. Since there are now high-statistics data on the shadowing of nuclear structure functions, a failure of these to reproduce the experimental results could then perhaps be seen as evidence for the presence of other mechanisms.

4.3.1 Nuclear Matter Density

The complete Glauber scattering series can be computed if we know all of the n-body nuclear density functions for each n-body scattering diagram, up to and including the diagram in which all A nucleons participate in the scattering. This last term will give a shadowing correction proportional to [186, 156]

$$-A!\ \mathrm{Re} \int d^2\mathbf{b}\ dz_1 ... dz_A\ \rho^{(A)}(\mathbf{b}, z_1, ..., z_A)\ \exp[ik_L(z_1 - z_A)] \tag{4.47}$$

where $\rho^{(A)}(\mathbf{b}, z_1, ..., z_A)$ is the A-body nuclear density function [148]. Following Foldy & Walecka [187], the complete A-body density can be expanded in terms of single body densities $\rho(\mathbf{b}, z_i)$ and two-body correlation functions $\Delta(\mathbf{b}, z_i, z_j)$,

$$\begin{aligned} \rho^{(A)}(\mathbf{b}, z_1, ..., z_A) \equiv |\psi_A|^2 \quad &= \quad \rho(\mathbf{b}, z_1) \cdots \rho(\mathbf{b}, z_A) \ + \sum_{\text{perm}} \Delta(\mathbf{b}, z_1, z_2)\ \rho(\mathbf{b}, z_3) \cdots \rho(\mathbf{b}, z_A) \\ &+ \sum_{\text{perm}} \Delta(\mathbf{b}, z_1, z_2)\ \Delta(\mathbf{b}, z_3, z_4)\ \rho(\mathbf{b}, z_5) \cdots \rho(\mathbf{b}, z_A) \ + \cdots . \end{aligned} \tag{4.48}$$

The two-body correlation function is defined by

$$\Delta(\mathbf{b}, z_i, z_j) \;=\; \rho^{(2)}(\mathbf{b}, z_i, z_j) \;-\; \rho(\mathbf{b}, z_i)\,\rho(\mathbf{b}, z_j) \tag{4.49}$$

where $\rho^{(2)}$ is the two-body density function, normalised so that

$$\int d^3\mathbf{r}_2\; \rho^{(2)}(\mathbf{r}_1, \mathbf{r}_2) \;=\; \rho(\mathbf{r}_1) \tag{4.50}$$

while the single particle density ρ has normalisation

$$\int d^3\mathbf{r}\; \rho(\mathbf{r}) \;=\; \int d^2\mathbf{b}\; dz\; \rho(\mathbf{b}, z) \;=\; 1. \tag{4.51}$$

Keeping only the first term in $\rho^{(A)}$ (i.e. no correlations) corresponds to an independent particle model. In principle the effects of all two-body correlation terms in (4.48) could be included. In previous calculations of scattering from nuclei it has been found that the two-body correlation terms introduce $\lesssim 10\%$ corrections to the single particle density approximation. Although we do not expect the effects of two-body correlations to be large, we shall nevertheless include them in our calculation. However, since we consider nuclei no heavier than ^{40}Ca, we shall neglect terms of order Δ^2. (Essentially nothing is known about the size of the three- and higher-body correlations in real nuclei, although one would reasonably expect that the effects of many-body correlations are not large in comparison with the two-body terms.) In this case we only need to calculate the two-particle density function $\rho^{(2)}$, which we can write in the form [3]

$$\rho^{(2)}(b, z_1, z_2) \;=\; N_C\; \rho(\mathbf{b}, z_1)\,\rho(\mathbf{b}, z_2)\;(1 - C(z_2 - z_1)) \tag{4.52}$$

where the function $C(z_2 - z_1)$ must take into account the short-range repulsion of the NN force,

$$C(r) \longrightarrow \begin{cases} 1 \;\text{ as } r \to 0 \quad \text{and} \\ 0 \;\text{ as } r \to \infty. \end{cases} \tag{4.53}$$

Such a behaviour can be modelled, for example, by

$$C(z_2 - z_1) \;=\; \left(\frac{3j_1(\kappa(z_2 - z_1))}{\kappa(z_2 - z_1)}\right)^2 \tag{4.54}$$

where j_1 is the Bessel function, and $\kappa = 3.6$ fm^{-1} is chosen to reproduce a 'hole' in the two-body density which is ≈ 0.5 fm wide (at 1/2 maximum density).

For the single particle nuclear density, as a first approximation we may consider a constant density function,

$$\rho_C(b, z) \;=\; \rho_C^0\;\theta(r^2 - R_A^2) \tag{4.55}$$

where $r^2 = b^2 + z^2$ and $\rho_C^0 = 3/(4\pi r_0^3\, A)$, and where $R_A = r_0\, A^{1/3}$ is the nuclear radius with $r_0 \approx 1.2$ fm. However, for heavy nuclei ($A \gtrsim 16$) the Woods-Saxon (or Fermi) density is known to be a better approximation,

$$\rho_{WS}(b, z) \;=\; \rho_{WS}^0 \left[1 + \exp\left(\frac{r - R_{WS}}{c}\right)\right]^{-1} \tag{4.56}$$

[3] Equivalently, we may define $\Delta(\mathbf{b}, z_1, z_2) = -\rho(\mathbf{b}, z_1)\rho(\mathbf{b}, z_2)\tilde{C}(z_2 - z_1)$, so that the two-body density becomes $\rho^{(2)} = \rho(\mathbf{b}, z_1)\rho(\mathbf{b}, z_2)(1 - \tilde{C}(z_2 - z_1))$ where $\tilde{C}$ is now related to C by $\tilde{C} = 1 - N_C(1 - C)$.

where $c = 0.57$ fm the surface thickness parameter, and the central density is normalised so that

$$\rho^0_{WS} = \frac{3}{4\pi r_0^3\, A}\left(1 + \frac{\pi^2 c^2}{R^2_{Pb}}\right)^{-1} \tag{4.57}$$

where $R_{Pb} = (207)^{1/3}\, r_0$ is the radius of ^{207}Pb. The Woods-Saxon radius, R_{WS}, is then found by solving the equation

$$f(R_{WS}) = \frac{207}{A}\, f(R_{Pb}) \tag{4.58}$$

where

$$f(R_{WS}) = \left(\frac{3}{4\pi R^3_{WS}}\right)\left(1 + \frac{\pi^2 c^2}{R^2_{WS}}\right)^{-1}. \tag{4.59}$$

This can be solved analytically to give

$$R_{WS} \;=\; \left(\frac{\beta}{2} + \sqrt{\frac{\pi^6 c^6}{27} + \frac{\beta^2}{4}}\right)^{-1/3}\left\{-\frac{\pi^2 c^2}{3} + \left(\frac{\beta}{2} + \sqrt{\frac{\pi^6 c^6}{27} + \frac{\beta^2}{4}}\right)^{2/3}\right\} \tag{4.60}$$

where $\beta = Ar_0^3 + A\pi^2 c^2 r_0/(207)^{2/3}$.

For light nuclei ($A \lesssim 16$) the Woods-Saxon density is not a good approximation, and in this case a harmonic oscillator (shell model) density is more appropriate,

$$\rho_{HO}(b,z) \;=\; \rho^0_{HO}\left(1 + \frac{(A-4)}{6}\frac{r^2}{R_S^2}\right)\exp\left(-r^2/R_S^2\right) \tag{4.61}$$

where the shell model radius is $R_S = \sqrt{2/5}\; R_A$, and the normalisation constant is

$$\rho^0_{HO} \;=\; \frac{4}{A}\left(\sqrt{\pi} R_S\right)^{-3}. \tag{4.62}$$

In Fig.4.23 we show $\rho^{(2)}$ with and without two-nucleon correlations, for an $A = 40$ nucleus. Note that the curves are not to scale, as we merely highlight differences between the shapes.

4.3.2 VMD Model of $\gamma^* A$ Scattering

Because of the finite energy of projectile beams (and hence energy transfer to the nucleus), much of the data on nuclear shadowing at low x taken so far has been at low and intermediate Q^2 (between $\sim$ 0.1 and 10 GeV^2). In this kinematic region we expect that there should be non-negligible contributions from the scattering of vector mesons off nuclei. From the discussions in Sections 4.1.1 and 4.1.2 the contribution to the nuclear structure function from the double scattering diagram in the VMD model is

$$\delta^{(V)} F_{2A}(x) \;=\; \frac{Q^2}{\pi}\sum_V \frac{\delta\sigma_{VA}}{f_V^2(1 + Q^2/M_V^2)^2} \tag{4.63}$$

where from (4.47) we have

$$\delta\sigma_{VA} \;=\; -\frac{A(A-1)\,\sigma^2_{VN}}{2}\int d^2\mathbf{b}\; dz_1\; dz_2\; \theta(z_2 - z_1)\; \rho^{(2)}(\mathbf{b}, z_1, z_2)\; \cos\left[k_L(z_2 - z_1)\right]. \tag{4.64}$$

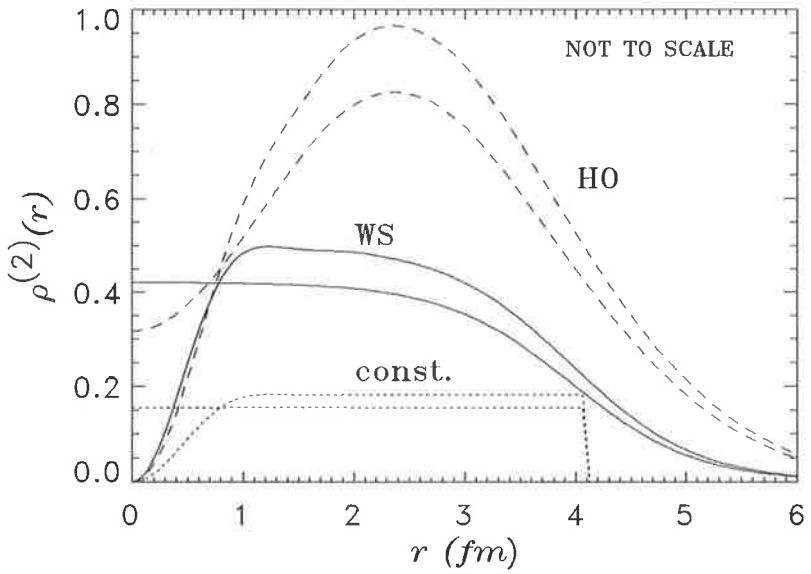

Figure 4.23: Two-particle nuclear density functions, $\rho^{(2)}(r) \equiv \rho^{(2)}(\mathbf{b} = 0, z_1 = 0, z_2 = r)$, for constant (dotted), Woods-Saxon (solid) and harmonic oscillator (dashed) single-particle densities, with and without two-nucleon correlations. The curves for the three densities are in arbitrary units, as we merely emphasise the shapes.

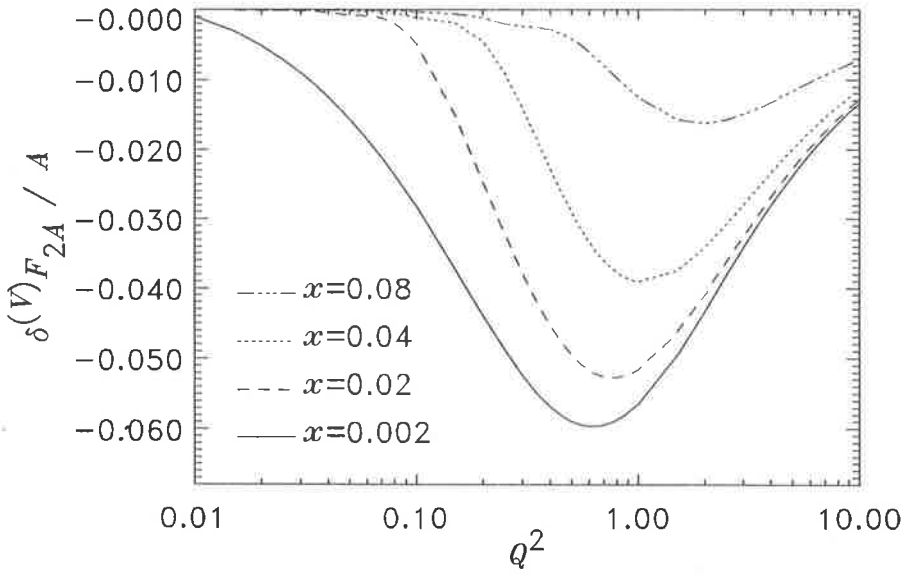

Figure 4.24: Q^2 dependence of the shadowing correction to the nuclear structure function in the VMD model for $A = 40$ and $\rho^{(2)} = \rho_C^2$.

In the model of Ref.[188] the possibility of reabsorption of the vector meson intermediate state while it traverses the nuclear medium was also considered. Classically, one would expect an incident wave to be attenuated according to $\exp\left(-\int dz/L\right)$, where L is the classical mean free path [148]. In [188] the reabsorption in DIS was modelled by introducing an additional exponential factor $\exp\left(-\frac{1}{2}\int_{z_1}^{z_2} dz/L_V\right)$ in Eq.(4.64), where $L_V = (\sigma_{VN}\ \ \rho(b,z))^{-1}$ is the mean free path of the vector meson in the nucleus. Numerically, we find that the inclusion of this contribution has very little effect upon the final nuclear to nucleon structure function ratio, which can be seen as an indication that the higher order rescattering terms in the Glauber series do not contribute significantly.

From Eq.(4.63) it is clear that the vector meson dominance contribution is a non-leading twist effect. To illustrate the strong Q^2-dependence of the shadowing predicted in the VMD model, we plot $\delta^{(V)}F_{2A}$, normalised to one nucleon, in Fig.4.24 for $A = 40$ and $\rho^{(2)} = \rho_C^2$. The VMD model predicts maximum shadowing at $Q^2 \sim 1$ GeV^2. For $Q^2 \to 0$ the shadowing disappears due to the vanishing of the total F_{2A} (as required by gauge invariance — see Eq.(4.67) below). However, for large Q^2, $\delta^{(V)}F_{2A}$ also vanishes due to the presence of the vector meson propagators in (4.63). The amount of shadowing generated via this mechanism dies off fairly rapidly between $Q^2 \sim 1$ and 10 GeV^2, so that for $Q^2 \gtrsim 10$ GeV^2 it is almost negligible. Experimentally, however, the data [138] indicate that the deep inelastic nuclear cross sections are shadowed even at quite large Q^2 (~ 10 GeV^2). Even though the VMD contribution will be important when comparing with the small-Q^2 data, clearly for large Q^2 the VMD model cannot be the whole story.

4.3.3 Pomeron Exchange in Nuclei

In the deuteron, because of the scaling property of the Pomeron structure function, the Pomeron exchange contribution to δF_{2D} was finite in the Bjorken limit. Therefore it is quite likely that the same mechanism is also responsible for the scaling of the nuclear shadowing. The total contribution from $\mathcal{P}$-exchange to the shadowing correction to F_{2A} is

$$\delta^{(\mathcal{P})}F_{2A}(x,Q^2) \;=\; \int_{y_{min}}^{A} dy\ f_A(y)\ F_{2\mathcal{P}}(x_{\mathcal{P}},Q^2) \tag{4.65}$$

where $F_{2\mathcal{P}}(x_{\mathcal{P}},Q^2)$ is the Pomeron structure function, defined in Section 4.1, and $f_A(y)$ is given by [186]

$$f_A(y) \;=\; -\frac{A(A-1)\ 8\pi}{y}\int d^2\mathbf{b}\ dz_1\ dz_2\ \rho^{(2)}(\mathbf{b},z_1,z_2)\ \cos\left[k_L(z_2-z_1)\right]. \tag{4.66}$$

In Ref.[188] the rescattering of the diffractively produced system within the nucleus was modelled by introducing a factor $\exp\left(-\frac{1}{2}\int_{z_1}^{z_2} dz/L_X\right)$, where $L_X = (\sigma_{XN}\ \ \rho(b,z))^{-1}$ is the mean free path of the hadronic state X inside the nucleus. The assumptions made are that, as in the VMD case, the total cross section, σ_{XN}, for the interaction of the state X with a nucleon is independent of the mass M_X, and that non-diagonal transitions are suppressed. For $\sigma_{XN} \approx 20$ mb, as suggested in [188], the effects of this are quite small, and can for practical purposes be neglected.

For fixed ν, the small x region corresponds also to small Q^2. At current energies, this means that probing structure functions at $x \lesssim 0.001$ can only be done for $Q^2 \lesssim 0.1$ GeV^2, which is well

below the scaling region. Since the Q^2 dependence of $F_{2\mathcal{P}}$ is determined by the behaviour with Q^2 of F_{2N}^{sea} (see Eqs.(4.10) & (4.11)), we therefore need to extrapolate the nucleon structure function down to low Q^2. While a rigorous theoretical basis for quark distributions at very small Q^2 is still outstanding, there have been several phenomenological parameterisations of F_{2p} in this region [166, 189, 190]. Clearly any low-Q^2 parameterisation must incorporate the photoproduction limit,

$$\sigma_{\gamma^* N} = \frac{4\pi^2\alpha}{Q^2} F_{2N} \longrightarrow \sigma_{\gamma N} \quad \text{as} \quad Q^2 \to 0. \tag{4.67}$$

The simplest, and most common, way to include this low-Q^2 behaviour is to introduce a factor $(Q^2/(Q^2+M_{\mathcal{P}}^2))^{1+\epsilon}$, with the parameter ϵ taken from Regge theory. More recently, Schuler and Sjöstrand [152] made a detailed study of the low-x and low-Q^2 extrapolation. The low-Q^2 region in their analysis was modelled by demanding an analytical behaviour of the modified distributions in the $x, Q^2 \to 0$ limit for fixed x/Q^2, with the normalisation and the mass parameter $M_{\mathcal{P}}^2$ fixed by matching the photoproduction and deep inelastic regions. For $x > x_0 = 0.0069$, their small-Q^2 extrapolation was taken as

$$x q_{sea}(x,Q^2) \;=\; \left(\frac{1+M_{\mathcal{P}}^2/Q_0^2}{1+M_{\mathcal{P}}^2/Q^2}\right)^{1+\epsilon} x q_{sea}(x,Q_0^2) \tag{4.68}$$

and

$$\begin{aligned} x q_{sea}(x,Q^2) \;=\; & \left(\frac{x}{x_0}\right)^{-\epsilon} \left(\frac{1}{1+M_{\mathcal{P}}^2/Q^2}\right)^{1+\epsilon} \\ & \times \left[N_s \left(1+M_{\mathcal{P}}^2/Q_0^2\right)^{1+\epsilon} x_0 q_{sea}(x_0,Q_0^2) \;+\; 0.044(1-N_s)\, x_0^{-\epsilon}\right] \end{aligned} \tag{4.69}$$

for $x < x_0$, where $N_s = 1-(1-x/x_0)(1-Q^2/Q_0^2)$, and the other parameters are $Q_0^2 = 5$ GeV^2, $M_{\mathcal{P}}^2 = 0.38$ GeV^2 and $\epsilon = -0.08$. In Fig.4.25 we plot $x q_{sea}(x,Q^2)$ (using the input parameterisation from Ref.[51] at large Q^2) as a function of x and Q^2.

The dependence of $\delta^{(\mathcal{P})}F_{2A}$ on Q^2, shown in Fig.4.26, is then solely dependent on the Q^2 dependence of the sea quark distributions. Below $Q^2 \sim 0.5$ GeV^2 the shadowing is almost negligible for all but the very small x values. At higher Q^2, however, the larger nucleon sea quark distribution gives rise to a large shadowing correction, so that above $Q^2 \sim 5$ GeV^2 the $\mathcal{P}$-exchange component exceeds the VMD component (see Fig.4.24), and starts to dominate for $Q^2 \gtrsim 10$ GeV^2.

The combined effect of the VMD and $\mathcal{P}$-exchange mechanisms for Q^2 between ~ 0.5 and 10 GeV^2 is that the total shadowing correction varies little in this region — see Fig.4.27. Calculating the $\mathcal{P}$-exchange contribution at larger Q^2 would give rise to an increasing $\delta^{(\mathcal{P})}F_{2A}$. However, as pointed out at the end of Section 4.2.4, the recombination of partons from different nucleons in the nucleus may modify [182] the QCD evolution equations governing the behaviour of the sea quark distributions with Q^2 (see also Section 2.1.4). At very small x and large Q^2 this can introduce non-negligible corrections [140, 188], although these will also depend on the small-x behaviour of the input gluon distribution in the nucleon. However, since the data on shadowing at small x were taken at low to moderate Q^2 ($\lesssim 10$ GeV^2), the exclusion of this will not play a major role in our region of interest.

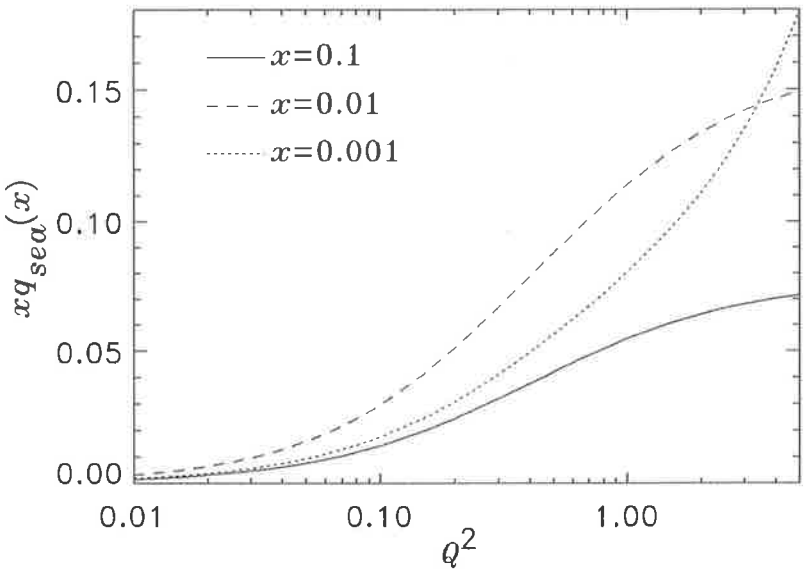

Figure 4.25: Nucleon sea quark distribution as a function of Q^2, for $x = 0.001, 0.01$ and 0.1. The input distribution is from Owens [51], modified to include the small Q^2 extrapolation of Ref.[152].

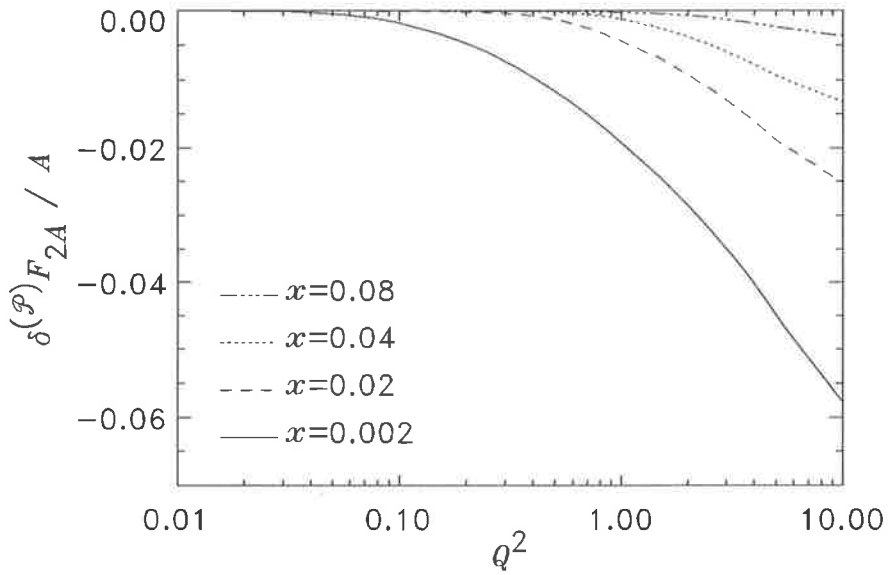

Figure 4.26: Q^2 dependence of the shadowing correction to the nuclear structure function from Pomeron exchange for $A = 40$. The parameters are as in Fig.4.24.

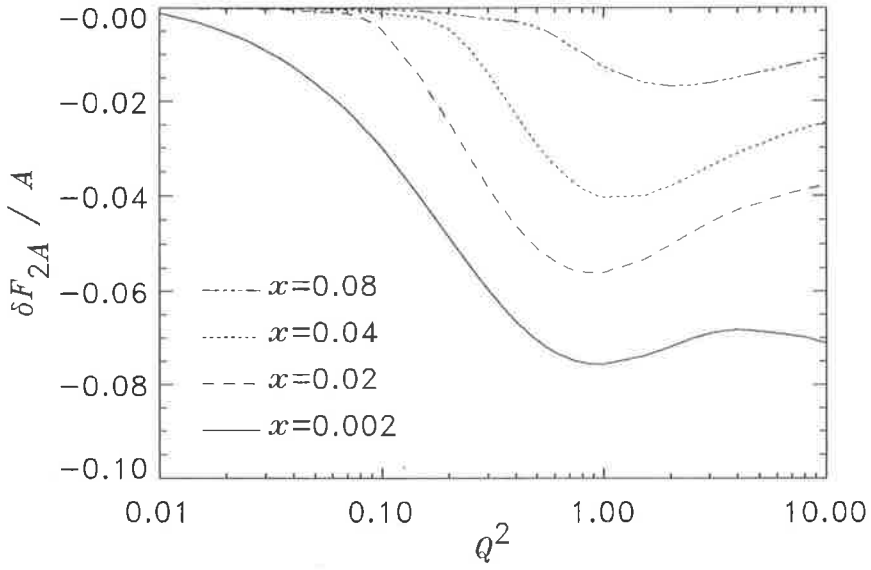

Figure 4.27: Q^2 dependence of the total shadowing correction to the nuclear structure function from VMD and $\mathcal{P}$-exchange, for $A = 40$. The parameters are as in Fig.4.24.

4.3.4 Comparison with Experiment

Finally we can consider the shadowing effect on the ratios of nuclear to deuteron structure functions. Since the magnitude of the shadowing correction to the D structure function was found to be very small (the total correction per nucleon in D, Fig.4.18, is $\sim$ 20 times smaller than that in ^{40}Ca, Fig.4.27) we shall use the isoscalar nucleon structure function in our comparisons,

$$\frac{F_{2A}}{A\ F_{2N}} = \frac{(ZF_{2p} + (A-Z)F_{2n} + \delta F_{2A})}{A\ F_{2N}} \tag{4.70}$$

where $F_{2N} = (F_{2p} + F_{2n})/2$, $F_{2n} \approx F_{2D} - F_{2p}$, and $\delta F_{2A} = \delta^{(V)} F_{2A} + \delta^{(\mathcal{P})} F_{2A}$. In calculating this ratio, for F_{2p} and F_{2D} we use the recent parameterisation from Ref.[191] (valid down to $Q^2 = 0.5$ GeV^2),

$$F_{2p}(x, Q^2) = A(x) \left(\frac{\ln(Q^2/\Lambda^2_{QCD})}{\ln(Q_0^2/\Lambda^2_{QCD})} \right)^{B(x)} \left(1 + \frac{C(x)}{Q^2} \right) \tag{4.71}$$

(and similarly for F_{2D}) where the functions A, B and C are expressed as series in x with the coefficients determined by fitting the combined NMC [191], SLAC [192] and BCDMS [193] data.

Fig.4.28 shows the model predictions for a $Z = 20, A = 40$ nucleus, compared with the high-precision data on the ^{40}Ca to deuteron structure function ratio from the NMC [138], as well as with the previous EMC data [137]. Note that the data at each x are taken at a different average value of Q^2, ranging from $\langle Q^2 \rangle \approx 0.6$ GeV^2 at $x = 0.0035$ to $\langle Q^2 \rangle \approx 10$ GeV^2 at $x = 0.1$, and the curves in Fig.4.28 have been calculated at the specific experimental values. Not surprisingly, at small x the largest contribution is from the scattering of vector mesons, which is about twice as large as the Pomeron exchange contribution. When both mechanisms are included, we find very good agreement between model and experiment over the entire range of x between ≈ 0.004 and

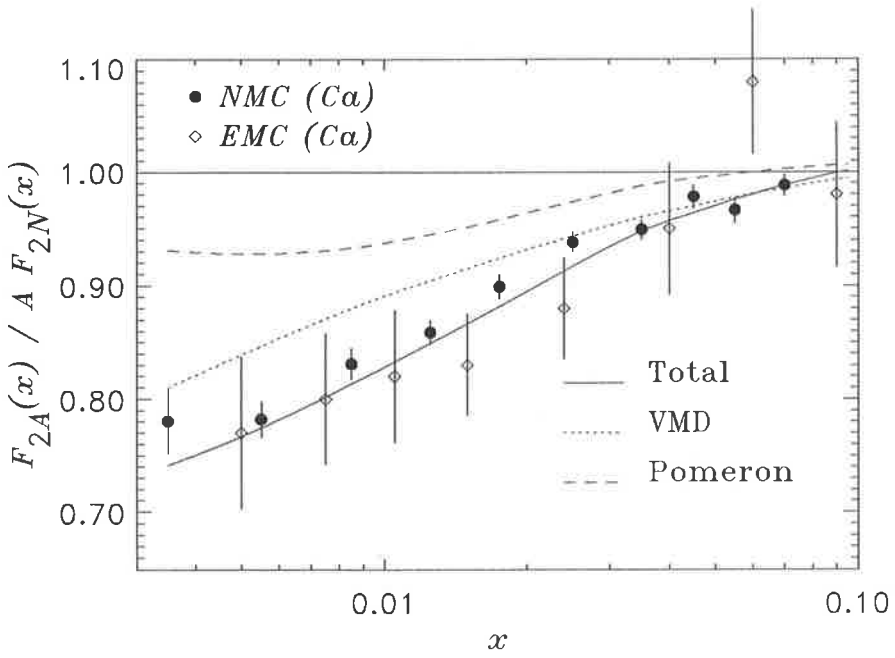

Figure 4.28: Shadowing of the ^{40}Ca structure function. The dashed curve is the $\mathcal{P}$-exchange contribution, while the dotted is the VMD model prediction, and the full curve represents the sum of the two. The data are from the EMC [137] and the NMC [138].

0.1. The curves are calculated using the Woods-Saxon single particle density and the two-particle correlation function in (4.54). To separate the low- and high-M_X^2 regions, and avoid any possibility of double counting between the different mechanisms, we impose a cut of $M_X^2 > M_{X_0}^2 = 1.5$ GeV^2 for the $\mathcal{P}$-exchange contribution, as suggested in [186]. The sensitivity to the cut-off mass $M_{X_0}^2$ is demonstrated in Fig.4.29. At $x \lesssim 0.01$, for no cut-off ($M_{X_0}^2 = 0$) the calculated curve (dashed) lies below the one with a cut-off of $M_{X_0}^2 = 1.5$ GeV^2 (solid), however there is little difference between the curves at larger x. By way of illustration, in Fig.4.29 we also show the effect of using a constant single-particle density rather than a Woods-Saxon shape. With a constant density the amount of shadowing is generally predicted to be some 25–30% larger. It is also evident from Fig.4.29 that the role of two-particle correlations (dotted curve) is not significant for ^{40}Ca. It is apparent that the best fit corresponds to the curve with the most realistic parameters (solid curve).

As mentioned, at the finite values of energy transfer ν, the data at small x necessarily correspond to lower Q^2. Therefore the structure function ratios should be calculated at the experimental Q^2 values. In particular, owing to the non-negligible Q^2-dependence of shadowing at small Q^2, it would seem inappropriate to compare the small-x data points with structure function ratios calculated at some fixed Q^2, as appears to have been done in [169, 153]. Indeed, the results at fixed Q^2 are quite different from those at the correct Q^2 values, as evident from Fig.4.30. Furthermore, it seems puzzling how one can draw conclusions about the merits of models of shadowing from comparing the data with predictions at fixed Q^2 [153].

The NMC also measured the ^{12}C structure function, and this is reproduced in Fig.4.31, together with the model predictions. Again, the VMD model (dotted curve) predicts larger shadowing

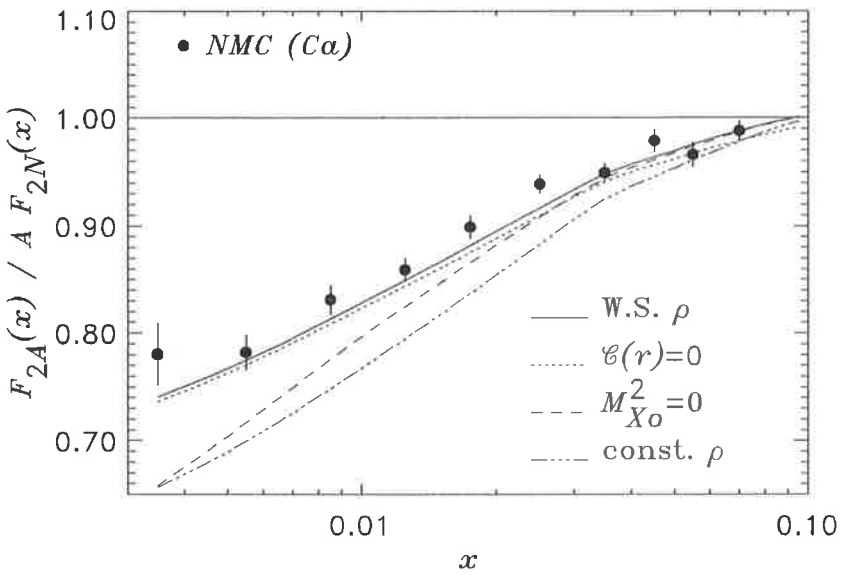

Figure 4.29: Shadowing of the ^{40}Ca structure function. Solid line is the total shadowing correction with the Woods-Saxon single-particle density, including two-particle correlations, and a cut in $M_X^2 > 1.5$ GeV^2 for the $\mathcal{P}$ contribution; dotted curve is with no two-particle correlations; dashed curve is with no M_X^2 cut; and dash-dotted curve is for a constant nuclear density, with correlations and an M_X^2 cut. The data are as in Fig.4.28.

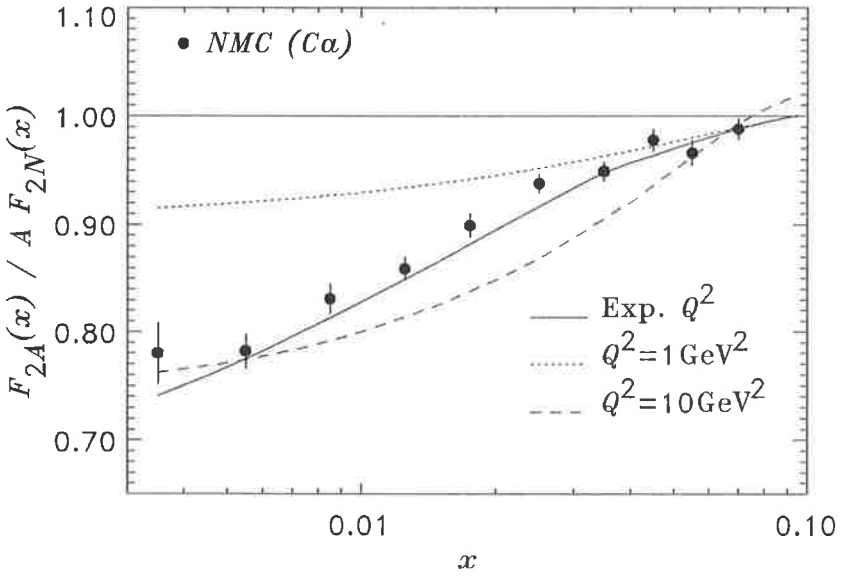

Figure 4.30: Ratio of ^{40}Ca to isoscalar nucleon structure functions, evaluated at fixed values of Q^2 (dashed and dotted curves), and at the experimental Q^2 values (solid curve).

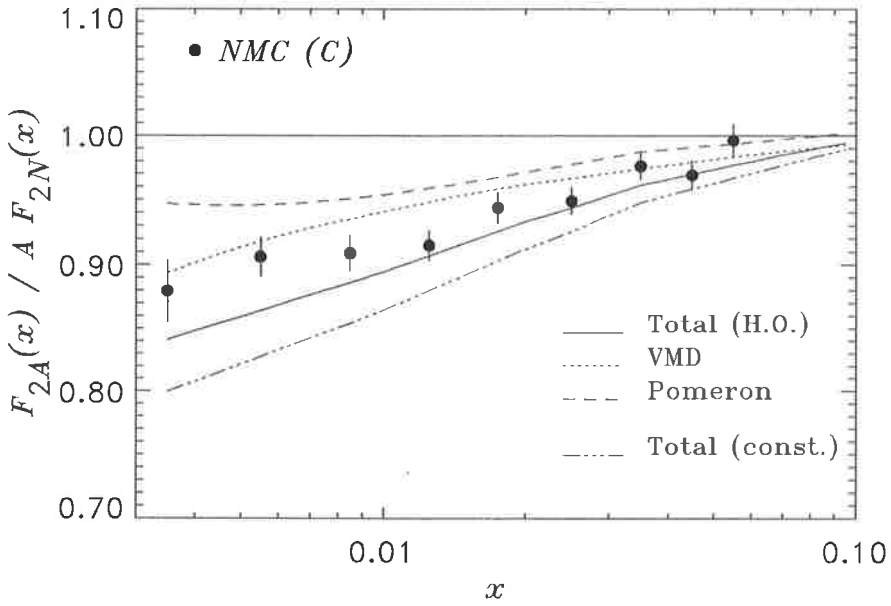

Figure 4.31: Shadowing of the ^{12}C structure function. Solid line is the total shadowing correction with the harmonic oscillator (shell model) single-particle density; dashed and dotted curves are the VMD and $\mathcal{P}$-exchange contributions; and dot-dashed curve is for a constant nuclear density. The data are from Ref.[138].

corrections to F_{2C} than does the $\mathcal{P}$-exchange mechanism (dashed curve). With the combined effects, and with an harmonic oscillator (shell model) single-particle density, the data can be fitted reasonably well (solid curve). With a constant nuclear density (dot-dashed) the model generally predicts too much shadowing. (Note that we use the same radius parameter $r_0 = 1.2$ fm as for ^{40}Ca — increasing this to ≈ 1.4 fm [186] would reduce the magnitude of shadowing to give even better agreement.)

In all, the agreement with the data is very good when both the VMD and $\mathcal{P}$-exchange mechanisms are included. What is also clear is that at low x and low Q^2 most of the observed shadowing comes from the scattering of low-M_X vector mesons, which serves to highlight the importance of hadronic degrees of freedom at small Q^2. We would expect, however, that as the energies of lepton beams increase, and more small-x data taken at larger Q^2, the $\mathcal{P}$-exchange process should become more important. Such data would further enable us to test the relevance of the two mechanisms.

We should also emphasise that the above model of nuclear shadowing has very few adjustable parameters. For the nuclear densities we use the most realistic shapes appropriate to the various nuclei (i.e. Fermi distribution for large A nuclei, shell model for smaller A nuclei). Furthermore, the nuclear radius parameter r_0 is fixed to be ≈ 1.2 fm [194], even though the results could be made smaller (or larger) by increasing (or decreasing) this by a few percent. The other parameter to which our results are sensitive at very small x is the cut-off mass $M_{X_0}^2$. At large Q^2 the cut-off is irrelevant, however at small Q^2 in the small-x region this will be important, and we set this to the value suggested in [186]. All other inputs ($\mathcal{P}$ structure function, total VN cross sections, etc.)

are as specified in Section 4.2 in the discussion on shadowing in D. Therefore the good agreement with the present nuclear data should give us some confidence in the model predictions for δF_{2D}. In particular, our conclusions in the previous chapter, in the analysis of the Gottfried sum rule and the question of flavour asymmetry, should also remain intact.

One word of caution needs to be made about the multiple scattering formalism used in this chapter. Along with the other assumptions inherent in the Glauber theory (i.e. eikonal approximation, additivity of phase shifts, etc.), by assuming that the scattering from a nucleus can be described in terms of scattering from individual free nucleons, this formalism ignores the effects that may arise when the nucleon virtuality is taken into account. While for the deuteron there may be some justification for neglecting the off-shell aspects of bound nucleons, since there the nucleons are only weakly bound, this may not be the case for heavy nuclei. In the next chapter we shall investigate in detail the off-shell properties of nucleons within a relativistic, covariant formalism, and examine the implications for the calculation of nuclear structure functions. In particular, it will be important to understand the consequences of taking into account the nucleons' virtuality in the region of interest for shadowing, namely at small x, although off-shell effects may well be important for all x. We briefly touched on this issue in Chapter 3, in the discussion of DIS from virtual baryon components of a physical nucleon, where our findings forecast potentially serious problems with the usual treatment of DIS from composite particles when relativistic effects are included. In what follows we shall generalise this discussion, and see that a proper treatment of the scattering from off-shell nucleons has far-reaching consequences.

Chapter 5

OFF-SHELL EFFECTS IN DIS FROM COMPOSITE PARTICLES

In the previous chapter we saw how at very small x the nuclear structure function F_{2A} is modified so that it no longer equals the incoherent sum of proton and neutron structure functions. In this chapter we examine how F_{2A} is affected by the fact that the nucleons are bound (and therefore off-mass-shell, $p^2 \neq M^2$). Extending the formalism introduced in Chapter 2, we develop a method of calculating structure functions of composite particles, which will be relevant not only in nuclear DIS, but also in any other process which involves scattering from off-shell nucleons [195].

While it is true that in most calculations of nuclear structure functions the off-shell aspects of the nucleon have been neglected, a few authors have tried to take some of these into account. In the earliest attempts (see, for example, Kusno and Moravcsik [196]) a scheme called 'off-shell kinematics — on-shell dynamics' was used, in which the Lorentz structure of the off-shell nucleon tensor was assumed to be the same as for the on-shell tensor, and in addition the dependence on p^2 was presumed to be negligible. Later, Bodek and Ritchie [79] used a similar method in order to extract the structure function of the neutron from that of the deuteron. To account for the nucleon virtuality, it was suggested there that the on- and off-shell structure functions could be related via a shift in energy transfer, $\nu \rightarrow \nu + (p^2 - M^2)/2$, as long as the structure functions were independent of q^2 and s. In another calculation, Dunne and Thomas [80] used an ansatz in which the matrix elements of the hadronic operators in the operator product expansion were assumed to be independent of p^2. The result was a nucleon structure function that was to be evaluated at a shifted value of $q^2 (\rightarrow \xi(p^2, q^2)q^2$, where ξ is the q^2 rescaling parameter). This result was mathematically equivalent to the dynamical rescaling model of Close, Roberts and Ross [197] and Nachtmann and Pirner [198], in which the shift in q^2 was attributed to a change in confinement radius for nucleons bound inside a nucleus.

Virtually all of the conventional calculations have used, in one form or another, the simple convolution model [52], in which the bound nucleon structure function is folded with the momentum distribution function of the nucleons inside the composite particle. The justification for the convo-

lution approach has been the belief in the validity of the assumption that the form of the off-shell nucleon tensor ($\widehat{W}_{\mu\nu}$) is the same as the on-shell one [199]. However, faced with the findings from Chapter 2 that in the Bjorken limit more than one operator is relevant, we could be excused for having grave fears for this assumption. The appearance of additional operator structures essentially arises from the presence of antiparticle degrees of freedom, which are unavoidable in any relativistic treatment of DIS. Although relativistic calculations have also been attempted in the past, for example by Nakano [200] and Gross and Liuti [201], these too suffer from the fact that critical assumptions need to be made about the nucleon off-shell behaviour in order to derive the convolution model. In fact, to our knowledge, all attempts to derive the simple covariant convolution model result have ultimately resorted to some prescription to account for the fact that the nucleon has $p^2 \neq M^2$. Without performing a full calculation which self-consistently accounts for the nucleon virtuality, all such *ad hoc* prescriptions must remain in doubt.

Of course there do exist alternative, non-covariant, methods which don't suffer from the same off-mass-shell ambiguities that have plagued the covariant formulations. We saw in Chapter 3 that time-ordered perturbation theory in the IMF has advantages when calculating virtual meson and baryon distributions in the nucleon. The instant form of dynamics was also used by Johnson and Speth [202] and Heller and Thomas [203] to calculate structure functions of nuclei (see also Ma [204]). Since nuclear wavefunctions are not known in the IMF, these calculations were necessarily performed in the target rest frame, although in this case the neglect of antinucleons is not strictly valid. Alternatively, for the nuclear EMC effect Berger, Coester & Wiringa [76] used light-front dynamics to calculate the nuclear structure functions. Here all particles are on-mass-shell, transverse momentum and the light-cone variable $p_+ = p_0 + p_L$ are conserved at each vertex, while $p_- = p_0 - p_L$ is not. Although this is an elegant method, its practical use is limited by the fact that nuclear wavefunctions on the light-cone have not been calculated. A review of some of the problems with all these approaches can be found in Refs.[205, 206].

The advantage of the covariant method in nuclear calculations is that Lorentz invariance is manifest. Perhaps the main reason why a proper treatment of the off-shell problem has not been made up to now has been the perceived complexity involved with including the extra antinucleon degrees of freedom. However, having calculated the off-shell tensor $\widehat{W}_{\mu\nu}$ in Chapter 2, we can now use this to describe any process which involves scattering from off-shell nucleons, without making unnecessary off-shell assumptions. In the formalism developed here, all of the soft, non-perturbative, physics will be contained in a set of relativistic quark—nucleon and nucleon—nucleus vertex functions. Of course these are not calculable from first principles, and eventually phenomenological, or model-dependent, input needs to be used to obtain the complete structure function of the physical composite particle. However, regardless of the non-perturbative inputs, we will show that the model is gauge invariant and respects the Callan-Gross relation in the Bjorken limit.

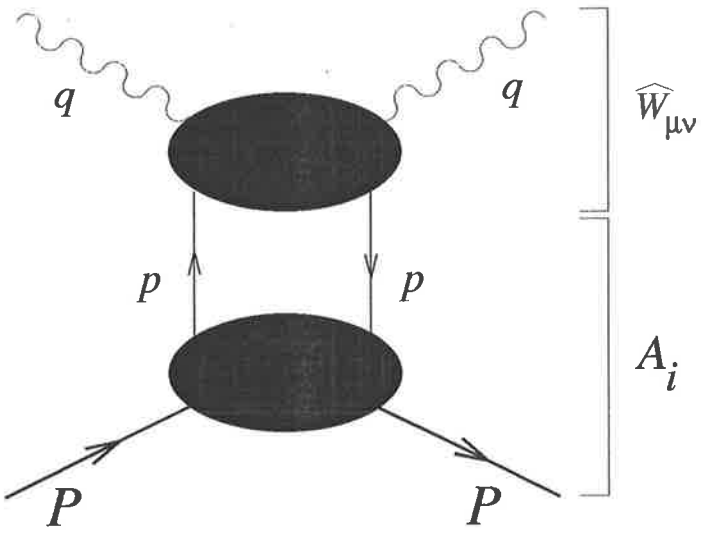

Figure 5.1: Scattering from an off-shell nucleon in a composite target. The functions A_i describe the nucleon—composite target interaction.

5.1 Structure Functions of Composite Particles

The usefulness of the truncated tensor $\widehat{W}_{\mu\nu}$ in calculating deep inelastic structure functions of composite particles will be made apparent in this section. Diagrammatically, the procedure will be simply to attach the truncated (off-shell) nucleon legs to whatever nuclear interaction is being considered, as in Fig.5.1. We will analyse this diagram in detail, with particular emphasis placed on keeping the full p^2 dependence throughout the calculation. Even though this is the simplest diagram out of the multiple scattering series of the previous chapter (i.e. the usual impulse approximation for nucleons), and something that is usually thought to have been well and truly understood, we will see that a rigorous, relativistic treatment of this leads to some surprising results.

Let us begin by writing the full (unpolarised) hadronic tensor for a composite particle, labelled A, with momentum P. Since this tensor can depend only on P_μ, q_μ and $g_{\mu\nu}$, it can be written, in analogy with the hadronic tensor for a free nucleon in Eq.(2.4), in the form

$$\begin{aligned} W^A_{\mu\nu}(P,q) &= \mathcal{P}_{T\mu\nu}(P,q)\, W^A_T(P,q) + \mathcal{P}_{L\mu\nu}(P,q)\, W^A_L(P,q) \\ &+ \mathcal{P}_{G\mu\nu}(P,q)\, W^A_G(P,q) + \mathcal{P}_{H\mu\nu}(P,q)\, W^A_H(P,q) \end{aligned} \tag{5.1}$$

where the functions $W^A_i(P,q)$ are the transverse, longitudinal, and the gauge non-invariant structure functions of the composite particle, for $i = T, L, G$ and H, respectively, and the $\mathcal{P}_{i\mu\nu}$ are the projectors defined in (2.5). Our goal is to identify the combinations of 'truncated' functions $\widehat{W}$ which contribute to these four functions. To do so we first need to relate the Lorentz structure of $\widehat{W}_{\mu\nu}(p,q)$ to that of $W^A_{\mu\nu}(P,q)$. Since the truncated nucleon tensor $\widehat{W}_{\mu\nu}$ has spinor indices, the q^2-independent nucleon—target 'blob' in Fig.5.1 (into which the truncated nucleon legs are inserted) will also be described by a 4×4 matrix in Dirac space. In general, this interaction can be written as

$$I\, A_0(p,P) + \gamma_\alpha\, A^\alpha_1(p,P) + \sigma_{\alpha\beta}\, A^{\alpha\beta}_2(p,P) \tag{5.2}$$

where A_0, A_1 and A_2 are scalar functions of p and P. (Note that since we deal with spin-independent processes we exclude γ_5 terms — these would be zero when contracted with the unpolarised tensor $\widehat{W}_{\mu\nu}$.) The full tensor can then be written

$$M_A\, W^A_{\mu\nu}(P,q) \;=\; \int d\widetilde{p}\; \mathrm{Tr}\left[\Big(I\; A_0(p,P) + \gamma_\alpha\; A_1^\alpha(p,P) + \sigma_{\alpha\beta}\; A_2^{\alpha\beta}(p,P)\Big)\; \widehat{W}_{\mu\nu}(p,q)\right] \qquad (5.3)$$

where M_A and M_R are the masses of the target and target recoil systems, respectively. Implicit in the functions A_0–A_2 is a sum over all excited target recoil states, or equivalently an integration over the masses M_R weighted by some target recoil spectral function. In (5.3) $d\widetilde{p}$ is given by

$$\begin{aligned} d\widetilde{p} \;&=\; \frac{d^4p}{(2\pi)^4}\frac{2\pi\delta\left([P-p]^2 - M_R^2\right)}{(p^2-M^2)^2} \\ &\Rightarrow\; \frac{1}{(2\pi)^3}\frac{dy\; d^2\mathbf{p}_T}{2(1-y)(p^2-M^2)^2} \end{aligned} \qquad (5.4)$$

where $p^2 = p_+p_- - \mathbf{p}_T^2$ is the nucleon's four-momentum squared, $y = p\cdot q/P\cdot q = p_+/P_+$ is its light-cone momentum fraction, and the δ-function has been used to fix $p_- = M_A + (M_R^2+\mathbf{p}_T^2)/(p_+ - M_A)$ upon taking the imaginary part of the Compton amplitude in Fig.5.1.

To see which Dirac structures in $\widehat{W}_{\mu\nu}(p,q)$ are relevant for the structure of the composite particle, we can project from the right hand side of (5.3) the contributions to each of the four structure functions W_i^A, as was done for the on-shell nucleon structure functions in Chapter 2. For this purpose the utility of the projectors $\mathcal{P}_{i\mu\nu}$ becomes apparent — in the Bjorken limit (in which we always work) these projectors also satisfy the relations $\mathcal{P}_i^{\mu\nu}(P,q)\; P_{i\mu\nu}(p,q) = 2, 1, 1$ and -1 for $i = T, L, G$ and H, respectively, for different momenta P and p, and furthermore they are still orthogonal. Therefore, applying the projectors to the truncated nucleon tensor $\widehat{W}_{\mu\nu}(p,q)$ gives the following contributions:

$$\begin{aligned} \frac{1}{2}P_T^{\mu\nu}(P,q)\,\widehat{W}_{\mu\nu}(p,q) \;&=\; \widehat{W}_T^0 + \not{p}\,\widehat{W}_T^1 + \not{q}\,\widehat{W}_T^2 + \sigma_{\alpha\beta}p^\alpha q^\beta\,\widehat{W}_T^5 \\ &\quad + \frac{q^2}{2(p\cdot q)^2}\left(p^2 - 2yp\cdot P + y^2P^2\right)\left[\widehat{W}_L^0 + \not{p}\,\widehat{W}_L^1 + \not{q}\,\widehat{W}_L^2 + \sigma_{\alpha\beta}p^\alpha q^\beta\,\widehat{W}_L^5\right] \\ &\quad + \left[-\not{p} + y\not{P} + \frac{1}{P\cdot q}\left(P\cdot p - yP^2\right)\not{q}\right]\widehat{W}^3 \\ &\quad - \left[y\,P^\alpha + \frac{P\cdot p - y\cdot P^2)}{P\cdot q}q^\alpha\right]\sigma_{\alpha\beta}p^\beta\,\widehat{W}^6 + [p^\alpha - yP^\alpha]\sigma_{\alpha\beta}q^\beta\,\widehat{W}^7 \end{aligned} \qquad (5.5)$$

$$\begin{aligned} \mathcal{P}_L^{\mu\nu}(P,q)\,\widehat{W}_{\mu\nu}(p,q) \;&=\; \widehat{W}_L^0 + \not{p}\,\widehat{W}_L^1 + \not{q}\,\widehat{W}_L^2 + \sigma_{\alpha\beta}p^\alpha q^\beta\,\widehat{W}_L^5 \\ &\quad + \frac{q^2}{(p\cdot q)^2}\left(p^2 - 2yp\cdot P + y^2P^2\right)\left[\widehat{W}_T^0 + \not{p}\,\widehat{W}_T^1 + \not{q}\,\widehat{W}_T^2 + \sigma_{\alpha\beta}p^\alpha q^\beta\,\widehat{W}_T^5\right] \\ &\quad - \frac{2\,p\cdot q}{q^2}\not{q}\,\widehat{W}^3 - \frac{2\,p\cdot q}{q^2}\sigma_{\alpha\beta}p^\alpha q^\beta\,\widehat{W}^6 - 2\,y\,\sigma_{\alpha\beta}P^\alpha q^\beta\,\widehat{W}^7 \end{aligned} \qquad (5.6)$$

$$\begin{aligned} \mathcal{P}_G^{\mu\nu}(P,q)\,\widehat{W}_{\mu\nu}(p,q) \;&=\; \widehat{W}_G^0 + \not{p}\,\widehat{W}_G^1 + \not{q}\,\widehat{W}_G^2 + \frac{2\,p\cdot q}{q^2}\not{q}\,\widehat{W}^3 + 2\,\not{q}\,\widehat{W}^4 \\ &\quad + \sigma_{\alpha\beta}p^\alpha q^\beta\left[\widehat{W}_G^5 + \frac{2p\cdot q}{q^2}\widehat{W}^6 + 2\widehat{W}^8\right] \end{aligned} \qquad (5.7)$$

$$-\frac{1}{2}\mathcal{P}_H^{\mu\nu}(P,q)\,\widehat{W}_{\mu\nu}(p,q) = \widehat{W}_H^0 + \not{p}\,\widehat{W}_H^1 + \not{q}\,\widehat{W}_H^2 + \frac{2\,p\cdot q}{q^2}\not{q}\,\widehat{W}^3 + \not{q}\,\widehat{W}^4 + \sigma_{\alpha\beta}p^\alpha q^\beta\left[\widehat{W}_H^5 + \frac{2p\cdot q}{q^2}\widehat{W}^6 + \widehat{W}^8\right] + \sigma_{\alpha\beta}P^\alpha q^\beta\left[y\,\widehat{W}^7 + \frac{q^2}{P\cdot q}\widehat{W}^9\right]. \tag{5.8}$$

Although there appear to be many functions $\widehat{W}^i$ in the above expressions, having calculated the scaling behaviour of these functions in Chapter 2 we can automatically see which (if any) terms survive in the Bjorken limit. (In fact, as we shall see explicitly below, to leading order in ν only four functions contribute to the transverse structure function of the composite particle, and overall there are no contributions to any of the others.)

The transverse structure function of the composite particle is obtained by taking the trace of the nuclear functions in (5.2) with the 'projected' nucleon tensor in (5.5), and integrating over the four-momentum p of the nucleon,

$$\begin{aligned} M_A\,W_T^A(P,q) &= \frac{M_A}{2}P_T^{\mu\nu}(P,q)\,W_{\mu\nu}^A(P,q) \\ &= 4\int d\widetilde{p}\Big\{A_0(p,P)\,\widehat{W}_T^0(p,q) + p\cdot A_1(p,P)\,\widehat{W}_T^1(p,q) + q\cdot A_1(p,P)\,\widehat{W}_T^2(p,q) \\ &\qquad + (p_\alpha\,q_\beta - p_\beta\,q_\alpha)A_2^{\alpha\beta}(p,P)\,\widehat{W}_T^5(p,q) + O\left(\frac{1}{\nu^2}\right)\Big\}. \end{aligned} \tag{5.9}$$

This result is of particular importance. Compare this with the expression in (2.37) for the on-shell nucleon structure function. It is obvious that in that case a different combination of functions $\widehat{W}^i$ appears to that in (5.9). This is aside from the fact that there are four scaling functions in (5.9) compared with only three in (2.37) — for most vertices only A_0 and A_1 will contribute, while A_2 will arise typically as an interference term when more than one type of vertex is used. Therefore, even for the simplest nucleon–nucleus interactions no part of the right hand side of (5.9) can be be identified with the nucleon structure function, unless of course the functions A_i conspire to give a result proportional to the combination of the $\widehat{W}^i$ which appears in (2.37). This result has significant bearing upon the convolution model of nuclear DIS, which has been a common feature of almost every calculation of structure functions of composite particles until now. In the next section we consider the consequences for the convolution model more fully, and exhaust the possible ways in which this model can be obtained from the full result.

Before we do that it is also important to check that the above formalism is gauge invariant, and that it respects the Callan-Gross relation (vanishing of the longitudinal structure function) in the Bjorken limit. Taking the trace of (5.6) with the nuclear—nucleon interaction in (5.2) we find that the longitudinal structure function is

$$\begin{aligned} M_A\,W_L^A(P,q) &= M_A\,\mathcal{P}_L^{\mu\nu}(P,q)\,W_{\mu\nu}(P,q) \\ &= 4\int d\widetilde{p}\Big\{q\cdot A_1(p,P)\left(\widehat{W}_L^2(p,q) - \frac{2\,p\cdot q}{q^2}\,\widehat{W}^3(p,q)\right) \\ &\qquad + (p_\alpha q_\beta - p_\beta q_\alpha)A_2^{\alpha\beta}(p,P)\left(\widehat{W}_L^5(p,q) - \frac{2\,p\cdot q}{q^2}\widehat{W}^6(p,q)\right) + O\left(\frac{1}{\nu^2}\right)\Big\}. \end{aligned} \tag{5.10}$$

Furthermore, for the non gauge-invariant structure functions, we find

$$\begin{aligned} M_A\, W_G^A(P,q) &= M_A\, \mathcal{P}_G^{\mu\nu}(P,q)\, W_{\mu\nu}(P,q) \\ &= 4\int d\tilde{p}\Big\{q\cdot A_1(p,P)\,\Big(\widehat{W}_G^2(p,q) + \frac{2\,p\cdot q}{q^2}\widehat{W}^3(p,q) + 2\,\widehat{W}^4(p,q)\Big) \\ &\quad + (p_\alpha q_\beta - p_\beta q_\alpha)A_2^{\alpha\beta}(p,P)\Big(\widehat{W}_G^5(p,q) + \frac{2\,p\cdot q}{q^2}\widehat{W}^6(p,q) + 2\,\widehat{W}^8(p,q)\Big) \\ &\quad + O\left(\frac{1}{\nu^2}\right)\Big\} \qquad (5.11) \\ M_A\, W_H^A(P,q) &= -\frac{M_A}{2}\mathcal{P}_H^{\mu\nu}(P,q)\, W_{\mu\nu}(P,q) \\ &= 4\int d\tilde{p}\Big\{q\cdot A_1(p,P)\,\Big(\widehat{W}_H^2(p,q) + \frac{2\,p\cdot q}{q^2}\widehat{W}^3(p,q) + \widehat{W}^4(p,q)\Big) \\ &\quad + (p_\alpha q_\beta - p_\beta q_\alpha)A_2^{\alpha\beta}(p,P)\Big(\widehat{W}_H^5(p,q) + \frac{2\,p\cdot q}{q^2}\widehat{W}^6(p,q) + \widehat{W}^8(p,q)\Big) \\ &\quad + O\left(\frac{1}{\nu^2}\right)\Big\}. \qquad (5.12) \end{aligned}$$

Substituting the relations between the non–transverse functions in (2.48) in the Bjorken limit the right hand sides in Eqs.(5.10)—(5.12) become zero,

$$W_i^A(P,q) \;\to\; 0, \qquad i = L,G,H. \qquad (5.13)$$

Hence the Callan-Gross relation, as well as gauge invariance ($q^\mu W_{\mu\nu}^A = 0$), are assured. This result is true *independent of the production mechanism of the off-shell particle*, or equivalently, independent of A_0–A_2. Hence it confirms the consistency of our model with the operator product expansion of Chapter 2.

5.2 Convolution Model

The most common application of the convolution model has been in calculations of the deep inelastic structure functions of nuclei. In the convolution model of DIS the structure function of a nucleus containing bound nucleons is expressed in terms of a one-dimensional integral, over the nucleon momentum, of the structure function of the bound nucleon with some momentum distribution function of the nucleons in the nucleus [52]. Indeed, its simplicity of interpretation and ease of use made it the standard approach to calculating structure functions of composite particles.

Although it has generally been understood [205] that the convolution model result relies on some critical assumptions about the off-shell behaviour of the nucleon structure function, and the form of the off-shell tensor itself, still the general philosophy has been that without evidence to the contrary, the model could be used as an approximation to the full result. Having obtained the full result in the previous section, we are now in the unique position of being able to critically test for the first time these hypotheses.

Let us outline the usual arguments made in deriving the convolution model. First of all, the assumption is made that the nuclear structure function can be written in factorised form, in terms

of the nucleon structure function, W_T^N, and the nucleon distribution function, φ,

$$W_T^A(x,Q^2) \;=\; \int dy \int d^2\mathbf{p}_T \;\; \varphi(A_0,A_1,A_2) \;\; W_T^N(x/y,Q^2,\mathbf{p}_T). \tag{5.14}$$

Furthermore, to obtain the one-dimensional convolution formula [52], in addition it is assumed that W_T^N is independent of $\mathbf{p}_T$ (or equivalently p^2),

$$W_T^A(x,Q^2) \;=\; \int dy \; \tilde{\varphi}(y) \;\; W_T^N(x/y,Q^2) \tag{5.15}$$

where now the integral over $\mathbf{p}_T$ is absorbed into the definition of $\tilde{\varphi}$. The question is can the factorisation assumptions be justified rigorously? To answer this, let us consider how (5.14) may arise from the full result in (5.9). This can happen if any of the following cases are true:

• CASE (a): If all but one of the functions $\widehat{W}_T^i$ ($i = 0-2,5$) are zero in the Bjorken limit. Most authors adopt this choice, as this corresponds to assuming that the form of the off-shell nucleon tensor is the same as that for a pointlike fermion, where only the $\not{q}\widehat{W}_T^2$ term contributes [52, 17, 199]. However, as was proved in Section 2.1.2, all four functions $\widehat{W}_T^i$ in principle scale in the Bjorken limit, which means that the only way that these can vanish is if some of the functions f in (2.47) are zero. But, as we saw in Section 2.3.1 (Eqs.(2.53) and (2.54)), even the simplest vertex functions lead to a large number of non-zero functions f. In that case, even for massless quarks, there were scaling contributions to both of the functions $\widehat{W}_T^1$ and $\widehat{W}_T^2$. For more complicated q–N vertices, even more of the fs (and hence $\widehat{W}_T^0$ and $\widehat{W}_T^5$ as well) will be non-zero.

• CASE (b): If more than one of the $\widehat{W}_T^i$ is non-zero, but the non-zero ones are proportional to each other. For example, $f_1 = Mf_4$ and all other fs equal to zero would imply $\widehat{W}_T^0 = M\widehat{W}_T^1$, and so (5.14) would be obtained. In general, such a behaviour will not arise from quark–nucleon vertices, as we found in Chapter 2.

• CASE (c): If the non-zero nucleon—target functions A_i multiplying the $\widehat{W}_T^i$ are proportional to each other. An example of this would be if A_0 and A_1 were non-zero and related by $A_0 = p\cdot A_1/M = q\cdot A_1\, M/p\cdot q$, which would then give (5.14). Such an assumption is made for example in Ref.[201]. However, in general this will not be true unless the $p^2 = M^2$ limit is artificially taken inside the functions A_i. (We will give some examples of this when we consider specific processes in the following sections.)

We emphasise that none of the conditions (a) – (c) are generally satisfied in a self-consistent, fully relativistic, calculation. Consequently the *convolution model interpretation of the nuclear structure function in terms of bound nucleon structure functions is inconsistent within the covariant formalism.* This difficulty is intrinsically related to the presence of antinucleon degrees of freedom in the relativistic calculation. While it may have been expected that effects such as final state interactions, higher twists, etc. could also spoil the factorisation property of the convolution model, it was not anticipated that the simplest, impulse approximation, result would also fail to satisfy this.

Furthermore, in the absence of the convolution model, the common practice of extracting *nucleon* structure functions from *nuclear* DIS data is not strictly valid. Indeed, the very concept of a

'bound nucleon structure function' is ill-defined within a covariant formulation. While the failure of the convolution model may appear to be an unwelcome complication, it is clear that in any theoretically self-consistent calculation which takes off-mass-shell effects into account it is an inevitable one. Nevertheless, it should also be clear that what we do have now is a new and powerful method of calculating nuclear structure functions, right down from the quark level. Indeed, this can be seen as a strength of the formalism, since now we are *forced* to consider *quark and nuclear* degrees of freedom in the one calculation.

In the following sections we shall use the relativistic formalism in several applications. Using Eq.(5.9) we will also compare numerically the exact result with that obtained using the convolution model, Eq.(5.15). We should also notice that the functions $\widehat{W}_T^i$ are independent of the nature of the composite target (i.e. there are no P- or y-dependent terms in (5.5) in the Bjorken limit). Therefore by selecting various targets (i.e. by varying $A_0 - A_2$) the relative contributions from the functions $\widehat{W}_T^i$ could be probed, provided, of course, we know the functions $A_0 - A_2$ sufficiently well. Conversely, once the $\widehat{W}_T^i$ have been determined for one process, they may in principle be used for all other processes.

5.3 Deuteron Structure Function

We examine nuclear DIS from a deuteron for several reasons. Firstly, it is critical to know the size of the off-mass-shell corrections to the deuteron structure function if ultimately the nuclear EMC data (which is in the form of ratios of nuclear to deuterium structure functions) is to be used to draw conclusions about the differences between quark distributions in free nucleons and those bound in nuclei. Secondly, in the absence of high-statistics neutrino data, the neutron structure function is often inferred from the deuteron structure function using the naive assumption of additivity of bound proton and neutron structure functions. As was discussed in the previous chapter, the deviations from additivity due to shadowing can introduce small, but nonetheless noticeable, corrections to F_{2n} at $x \to 0$. Of course, due to Fermi motion the deuteron structure function can also extend beyond $x_N = 1$ ($x_N \equiv (M_D/M)\ x$) to $x_N = M_D/M$. In this section we investigate the corrections to F_{2D} due to off-mass-shell effects, which are not restricted to any particular region of x.

The calculation of DIS from the deuteron is more straightforward and reliable than for other nuclei, since the relativistic deuteron–nucleon vertex is reasonably well understood. The treatment of the deuteron recoil state is also simplified by the fact that most of the time this will be an on-shell nucleon (since this can be expected to dominate contributions from processes with a recoil Δ or Roper resonance, or a higher mass state). The structure of the general DNN vertex, with one nucleon on-shell, was first derived by Blankenbecler and Cook [207], $\langle N|\psi_N|D\rangle \propto (\not{p} - M)^{-1}\Gamma^D_\alpha\ \epsilon^\alpha\ \mathcal{C}\bar{u}^T(P-p)$, where the DNN vertex function is [208]

$$\Gamma^D_\alpha(p^2) \;=\; \gamma_\alpha\ F(p) \;+\; \left(\frac{1}{2}P_\alpha - p_\alpha\right)\ G(p) \;+\; \frac{\not{p} - M}{M}\left[H(p)\gamma_\alpha \;+\; \frac{I(p)}{M}\left(\frac{1}{2}P_\alpha - p_\alpha\right)\right] \quad (5.16)$$

and C is the charge conjugation operator. The functions F, G, H and I are related to the ${}^3S_1$,${}^3D_1$,${}^1P_1$ and ${}^3P_1$ deuteron wavefunctions u, w, v_s and v_t, respectively, via the relations [209]

$$\begin{aligned}
F(p) &= \pi\sqrt{2M_D}\,(2E_{\mathbf{p}} - M_D)\left(u(|\mathbf{p}|) - \frac{w(|\mathbf{p}|)}{\sqrt{2}} + \sqrt{\frac{3}{2}}\frac{M}{|\mathbf{p}|}v_t(|\mathbf{p}|)\right) \\
G(p) &= \pi\sqrt{2M_D}\,(2E_{\mathbf{p}} - M_D)\left(\frac{M}{E_{\mathbf{p}}+M}u(|\mathbf{p}|) + \frac{M\,(2E_{\mathbf{p}}+M)}{\mathbf{p}^2}\frac{w(|\mathbf{p}|)}{\sqrt{2}} + \sqrt{\frac{3}{2}}\frac{M}{|\mathbf{p}|}v_t(|\mathbf{p}|)\right) \\
H(p) &= \pi\sqrt{2M_D}\,\frac{E_{\mathbf{p}}M}{|\mathbf{p}|}\,\sqrt{\frac{3}{2}}\,v_t(|\mathbf{p}|) \qquad (5.17) \\
I(p) &= -\pi\sqrt{2M_D}\,\frac{M^2}{M_D}\left(\frac{2E_{\mathbf{p}} - M_D}{E_{\mathbf{p}}+M}u(|\mathbf{p}|) - \frac{(2E_{\mathbf{p}} - M_D)(E_{\mathbf{p}}+2M)}{\mathbf{p}^2}\frac{w(|\mathbf{p}|)}{\sqrt{2}} + \frac{\sqrt{3}M_D}{|\mathbf{p}|}\,v_s(|\mathbf{p}|)\right)
\end{aligned}$$

where $E_{\mathbf{p}} = \sqrt{M^2+\mathbf{p}^2}$. The relativistic deuteron wavefunctions have been calculated, for example, in the model of Buck and Gross [209]. In the numerical work below we use the wavefunctions calculated with a purely pseudovector π exchange interaction (although wavefunctions with pseudoscalar and pseudoscalar–pseudovector combinations were also given in [209]). For the spin-averaged deuteron hadronic tensor we therefore need to evaluate the trace (which appears in Eq.(5.3))

$$\sum_\lambda \epsilon^{*\alpha}(\lambda,P)\,\epsilon^{\beta}(\lambda,P)\,\mathrm{Tr}\left[(\not{P}^T - \not{p}^T + M)\,C\bar{\Gamma}^D_\beta(p^2)\,(\not{p}+M)\,\widehat{W}_{\mu\nu}(p,q)\,(\not{p}+M)\,C\Gamma^D_\alpha(p^2)\right] \quad (5.18)$$

where $\epsilon^\alpha(\lambda,P)$ is the polarisation vector for a deuteron with helicity λ, and $\bar{\Gamma}^D_\beta = \gamma_0\,\Gamma^{D\dagger}_\beta\,\gamma_0$. This yields the following deuteron–nucleon functions A^D_i:

$$\begin{aligned}
A^D_0(p^2) &= M\left\{4\,F^2\left[4\,M^2 + 2\,M_D^2 - \left(p^2-M^2\right)\left(-2+\frac{p^2-M^2}{M_D^2}\right)\right]\right. \\
&- 8\,F\,G\left[4\,M^2 - M_D^2 + \frac{(p^2-M^2)}{4M^2}\left(10\,M^2 - M_D^2 + 2\,p^2 + \frac{3\,M^4 - 2\,M^2p^2 - p^4}{M_D^2}\right)\right] \\
&+ \frac{G^2}{M^2}\left[\left(4\,M^2 - M_D^2\right)^2 - \left(p^2-M^2\right)\left(4\,M_D^2 - 5\,p^2 - 11\,M^2 + \frac{2p^4 - 2M^4}{M_D^2}\right)\right] \\
&- \frac{(p^2-M^2)}{M^2}\left[-12\,H^2\left(p^2-M^2\right) + 4\,F\,H\left(-5M^2 - 2M_D^2 + p^2 + \frac{(p^2-M^2)^2}{M_D^2}\right)\right. \\
&\qquad + \left(p^2 - \frac{(P\cdot p)^2}{M_D^2}\right)\left(\frac{(p^2-M^2)}{M^2}\left(-4\,I^2 + 8\,H\,I\right) + 16\,F\,I\right. \\
&\qquad\left.\left.\left. +16\,G\,H + 8\,G\,I\,\frac{(P\cdot p - M^2 - p^2)}{M^2}\right)\right]\right\} \qquad (5.19) \\
A^D_{1\alpha}(p^2) &= 4\,F^2\left[\left(4\,M^2 + 2\,M_D^2\right)p_\alpha - \left(p^2-M^2\right)\left(\frac{(p^2-M^2)}{M_D^2}p_\alpha + \left(2 - \frac{(p^2-M^2)}{M_D^2}\right)P_\alpha\right)\right] \\
&- 8\,F\,G\left[\left(4\,M^2 - M_D^2\right)p_\alpha + \left(\left(1 - \frac{(p^2-M^2)}{M_D^2}\right)p_\alpha + \frac{P\cdot p}{M_D^2}\right)\right] \\
&+ \frac{G^2}{M^2}\left[\left(4\,M^2 - M_D^2\right)^2 p_\alpha - \left(p^2-M^2\right)\left((M_D^2 - 4\,M^2)\left(2 - \frac{p^2-M^2}{M_D^2}\right)p_\alpha\right.\right. \\
&\qquad\left.\left. -4\left(p^2 - \frac{(P\cdot p)^2}{M_D^2}\right)P_\alpha\right)\right]
\end{aligned}$$

$$
\begin{aligned}
- \; & \frac{(p^2-M^2)}{M^2}\left\{4\,H^2\,(p^2-M^2)\left[p_\alpha-\left(2-\frac{p^2-M^2}{M_D^2}\right)P_\alpha\right]\right. \\
& -4\,I^2\,\frac{p^2-M^2}{M^2}\left(p^2-\frac{(P\cdot p)^2}{M_D^2}\right)[p_\alpha-P_\alpha] \;+\; 8\,H\,I\,(p^2-M^2)\left[p_\alpha-\frac{P\cdot p}{M_D^2}P_\alpha\right] \\
& -8\,F\,H\,M^2\left[2\,p_\alpha+\left(2-\frac{p^2-M^2}{M_D^2}\right)P_\alpha\right] \\
& +4\,F\,I\left[\left(3M^2+p^2-\frac{(p^2-M^2)^2}{M_D^2}\right)p_\alpha-\left(p^2+M^2-\frac{(p^2-M^2)^2}{M_D^2}\right)P_\alpha\right] \\
& +8\,G\,H\left[\left(M^2+p^2-P\cdot p\right)p_\alpha+\left(p^2-\frac{p^2+M^2}{M_D^2}P\cdot p\right)P_\alpha\right] \\
& \left.+8\,G\,I\left(p^2-\frac{(P\cdot p)^2}{M_D^2}\right)[-2p_\alpha+P_\alpha]\right\} \qquad (5.20)
\end{aligned}
$$

$$
A^D_{2\alpha\beta}(p^2) \;=\; 0. \qquad (5.21)
$$

With the nuclear functions A_i^D now determined, we need only one more ingredient in order to calculate the complete DIS process. In Chapter 2 we described DIS from an on-shell nucleon in terms of the truncated nucleon functions $\widehat{W}_T^i$, which in general are functions of $q^2, p\cdot q$ and also p^2, although the p^2 dependence in that case was trivial. For off-shell nucleons we naturally need to know the specific dependence of $\widehat{W}^i$ (and hence of the functions f_i) on p^2. Within the model of Chapter 2 the functions $f_i(p,k)$ were related to the quark—nucleon vertex functions $\Phi_1^{S,V}(k,p)$, whose k^2 dependence was parameterised by a simple form that reflected the phenomenology of nucleon DIS. In the nuclear case, for the quark—off-shell nucleon vertex we need to know in addition the p^2 dependence of the vertex functions. In general this is more difficult to obtain because the p^2 dependence is not restricted to the quark—nucleon vertices alone, but is also be present in the nucleon—nucleus vertices (functions $A_i(p,P)$). This in turn introduces an inherent uncertainty in its determination. Nevertheless, since they are defined within the impulse approximation, the functions $\Phi_1^{S,V}(k,p)$ do not depend on the nuclear target — that information is contained entirely in the functions A_i. This means that if the p^2 dependence in $\Phi_1^{S,V}(p,k)$ could be determined in one process, the results could then be used in all other processes. Since for the deuteron the p^2 dependence of the DNN vertex is known reasonably accurately through (5.18)—(5.21), we can therefore use deuteron DIS data to constrain this universal p^2 dependence of the quark—nucleon vertex functions.

As for the real nucleon case, we restrict our discussion to valence quarks only, and use lepton–deuteron data from NMC, BCDMS and SLAC [191] at intermediate and large x ($x \gtrsim 0.3$), where valence quarks dominate. Because of isospin symmetry ($u^D = d^D$) only a single experimental quantity for the deuteron, namely $F_{2D} = x(4u^D + d^D)/9 = 5x(u+d)/9$, where u^D, d^D and u, d are the up and down quark distributions in the deuteron and proton respectively, can be used to constrain the q–N vertex. Thus we cannot differentiate between the p^2 dependence in Φ_1^S and that in Φ_1^V. (This is in contrast to the nucleon case, where two sources of information, $u+d$ and d/u, could be used to constrain both the scalar and vector q–N vertex functions.) We can therefore

choose a simple monopole form and use the same cut-off mass, Λ_p, in both functions,

$$\Phi_1^S(k^2,p^2) = N'_S \frac{(k^2-m^2)}{(k^2-\Lambda_S^2)^2}\frac{(M^2-\Lambda_p^2)}{(p^2-\Lambda_p^2)} \tag{5.22}$$

$$\Phi_1^V(k^2,p^2) = N'_V \frac{(k^2-m^2)}{(k^2-\Lambda_V^2)^{7/2}}\frac{(M^2-\Lambda_p^2)}{(p^2-\Lambda_p^2)}. \tag{5.23}$$

A detailed comparison between the model and data for $x \lesssim 0.3$ would require separation of the valence and sea components of F_{2D}. Although in principle this could be done by analysing the νD and $\bar{\nu} D$ DIS data, in practice those data suffer from poor statistics. Furthermore, typically only the extracted quark distributions in the nucleon are presented [210], and these depend on the theoretical assumptions made to treat binding and Fermi motion corrections.

Because of the additional p^2 dependence in (5.22) and (5.23), there is no reason for the normalisation constants $N'_{S,V}$ to be the same as those determined by normalising the on-shell nucleon quark distributions, $N_{S,V}$ in (2.65). Note that this would still be true even if the cut-off Λ_p were infinite (which would restore the functional form of $\Phi^{S,V}$ to that for on-shell nucleons), since there is 'implicit' dependence on p^2 coming from the k^2-dependent part,

$$k^2 = k_+k_- - k_T^2 = xM_D\left(p_- - \frac{(\mathbf{p}_T-\mathbf{k}_T)^2+m_R^2}{M_D(y-x)}\right) - k_T^2 \tag{5.24}$$

with p_- as given by the δ-function in Eq.(5.4). Therefore we can also use the deuteron data to fix the overall normalisation constants (e.g. to give baryon number two) for the p^2-dependent scalar and vector vertex functions, although obviously different normalisation constants will be needed for different values of Λ_p. After determining the normalisation constants for a particular Λ_p, in principle the same values may then be used in all other nuclear calculations. In practice, however, the fact that we are only considering the six-valence quark (i.e. two-nucleon) component of the total deuteron wavefunction, and neglecting other Fock states (e.g. with meson components) means that the normalisation will not necessarily be automatic, so that $N'_{S,V}$ will in general need to be modified to give the correct normalisation.

In Fig.5.2 we compare the experimental F_{2D} at $Q^2 = 10$ GeV^2 with the calculated total valence quark distribution in the deuteron, $(5/9)x(u_V+d_V)$, evolved from the same value of $Q_0^2 = 0.15$ GeV^2 (since we use the same spectator diquark masses) as for the free nucleon distributions in Chapter 2. Clearly there is very good agreement between the model calculation (solid curve) and the data for $x \gtrsim 0.3$. (The results obtained using the wavefunctions of the Bochum model [211], in which there is no triplet P state wavefunction, are almost identical to those in Fig.5.2.) The result of the full calculation is virtually independent of the value of Λ_p used, after the normalisation constants for the vertex functions have been determined by the baryon number conservation condition. This is because the p_T distribution is strongly peaked at small transverse momenta, $p_T \sim 25$ MeV, so that modification of the large-p_T (or large-$|p^2|$) behaviour by altering the form factor cut-off is irrelevant. This in turn produces a y-dependence which peaks strongly at around $y = 0.5$, Fig.5.3, which indicates that the deuteron is mostly a two-nucleon system. (We should add that the quality

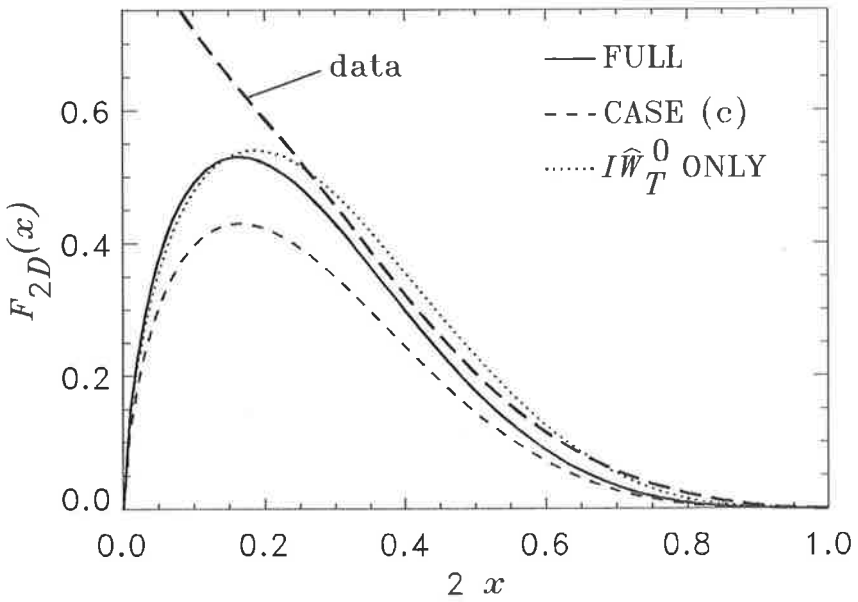

Figure 5.2: Valence part of the deuteron structure function: solid line is the full calculation with $\Lambda_p = \infty$; dashed line is with the $p^2 = M^2$ approximation in A_0, A_1 (with $\Lambda_p = \infty$), with same normalisation constant as in full curve; dotted line is the convolution model using only the $\widehat{W}_T^0$ operator, together with the full nucleon structure function, normalised to baryon number one. The curves have been evolved from $Q_0^2 = 0.15$ GeV^2 to $Q^2 = 10$ GeV^2 for comparison against the experimental $F_{2D}(x, Q^2 = 10\text{GeV}^2)$ [191].

of fit in Fig.5.2 could certainly be improved even more by choosing more sophisticated q–N vertex functions than the very simple parameterisations in (5.22) and (5.23).)

Having calculated the deuteron structure function using the formalism in which the explicit p^2 dependence is kept throughout, we now compare these results with those of earlier calculations that have made use of convolution-like formulas. Firstly we can notice that by taking the on-shell limit ($p^2 \to M^2$) for the kinematic factors in A_0^D and A_1^D in (5.19) and (5.20), we obtain $A_0^D/M = p\cdot A_1^D/M^2 = q\cdot A_1^D/p\cdot q$, thereby satisfying condition (c) in Section 5.2 for the convolution model (although this limit need not be taken in the functions F, G, H, I themselves). The result of this approximation is shown in the dashed curve of Fig.5.2, where we have used the same normalisation constants (for $\Lambda_p = \infty$) as determined in the full calculation. The effect is a reduction in the absolute value of the structure function, without much affect on the shape. By artificially normalising the new distribution so that the final result conserves baryon number, this curve becomes almost indistinguishable from the full result. However, since the $p^2 = M^2$ limit is taken in the nuclear part of the diagram, and thus does not affect the quark—off-shell nucleon vertex, it would seem that in principle the same normalisation as in the full curve should be used.

In other calculations using the convolution model for deuterium, the most common prescription [212, 213] has been to drop all terms but $I\widehat{W}_T^0$ in the expansion of $\widehat{W}_{\mu\nu}$ (in Eq.(5.18)), and to replace $\widehat{W}_T^0$ by the experimental, on-shell structure function of the nucleon. In Fig.5.2 the dotted curve shows the result after renormalisation to ensure baryon number two for the deuteron. It

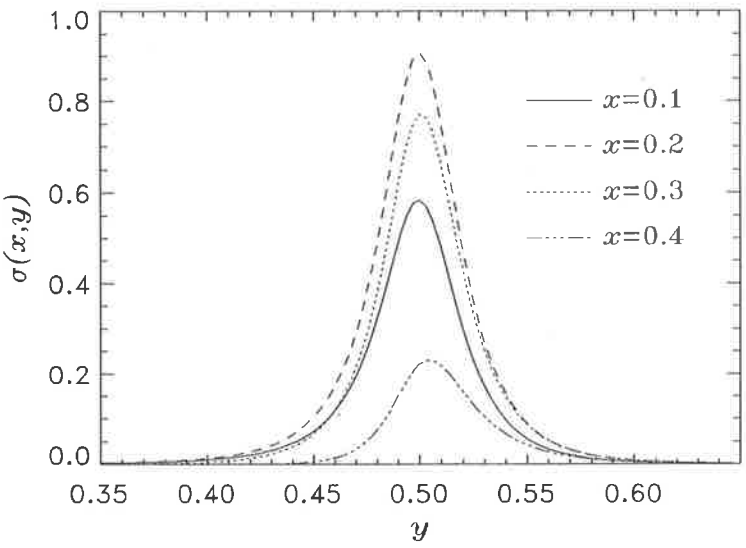

Figure 5.3: Shape of the y-distribution in the deuteron cross section $\sigma(x,y)$ for various x, where $\int dy\ \sigma(x,y) \propto F_{2D}(x)$. (Shown is only the unevolved scalar diquark component, and the vertical axis is in arbitrary units.)

is somewhat surprising that the difference in shape between the full result and this ansatz is as small as it is. Still, a discrepancy of $\sim 20\%$ is quite significant in a system as loosely bound as the deuteron.

Any numerically significant difference between the convolution approach and the exact calculation is of particular importance for the common procedure of extracting the neutron structure function from the deuteron data via the convolution method. Indeed, in view of the problems with the convolution model outlined above, it is rather worrying than our knowledge of F_{2n} is based on this. As seen in Fig.5.2, depending on the approximation or ansatz taken in calculating F_{2D}, the deviation from the full, p^2-dependent result, will vary. Still, although unsatisfactory from a theoretical point of view, by artificially renormalising the deuteron structure function by hand so that it respects baryon number conservation, the differences can be reduced.

A similar situation also arises in calculations of the nuclear EMC effect, in which differences between nuclear and deuteron structure functions are explored. Clearly for any accurate description of this effect we need firstly to have a reliable method of calculating the deuteron structure function. As we have seen, we may compensate for the off-shell effects that are ignored in the deuteron by suitably renormalising the final result. Whether this can also be done in other, heavier nuclei is not clear. Certainly in heavy nuclei we would expect off-shell effects to play some role. To date these have not been adequately treated, and this is what we turn to next.

5.4 Off-Shell Effects in Heavy Nuclei

For any nucleus we can easily repeat the above calculation if we know the relativistic nucleon–nucleus vertex functions. Unfortunately, for heavy nuclei these are presently not at all well known. One solution would be to simply parameterise the vertex functions and make some assumptions about the nuclear recoil state. Alternatively, as is done in most calculations of nuclear structure functions, non-relativistic models could be used for the nucleon distribution within the nucleus. However, in this approach it is not clear how one could then incorporate any effects from off-mass-shell nucleons.

There have been some previous attempts at using a relativistic formalism to calculate structure functions of heavy nuclei. For example, Gross & Liuti [201] considered a model of a spin 0 nucleus, in which it was assumed that the recoil (spin 1/2) nuclear state can be described by a simple fermion propagator (like for the deuteron recoil state). For a scalar nucleon–nucleus vertex function ($\propto I$), the trace factor in (5.3) would be

$$\mathrm{Tr}\left[(\not{p}+M)\,(\not{P}-\not{p}+M_R)\,(\not{p}+M)\,\widehat{W}_{\mu\nu}(p,q)\right] \tag{5.25}$$

which gives the following nucleon–nucleus functions

$$\begin{aligned} A_0^{(S=0)}(p,P) &= \left(M_A^2 - M_R^2 - M^2 + 2MM_R - (p^2-M^2)\left(1-\frac{M_R}{M}\right)\right) M \\ A_{1\alpha}^{(S=0)}(p,P) &= \left(M_A^2 - M_R^2 - M^2 + 2MM_R\right) p_\alpha \;+\; (M^2-p^2)P_\alpha \\ A_{2\alpha\beta}^{(S=0)}(p,P) &= 0. \end{aligned} \tag{5.26}$$

Rather than evaluate the structure function with the full expression in (5.26) it was postulated in [201] that the relativistic density matrix of an off-shell nucleon can be approximated by an on-shell matrix multiplied by some nuclear spectral function. This amounts to inserting the condition $p^2 = M^2$ into (5.26), so that factorisation, and the convolution model, are obtained courtesy of the fact that condition (c) in Section 5.2 is now satisfied. However, while it may be argued from a physical point of view that such an approximation may be valid for light nuclei, where the nuclear binding is not too strong, in heavy nuclei there is little reason for this assumption to remain valid.

For the calculation of F_{2A} in the model of Nakano [200] it was assumed, as usual, that the structure of the off-shell hadronic tensor is the same as that for a real nucleon. Implicit in this model is the assumption that the relevant tensor operator in $\widehat{W}_{\mu\nu}$ is $I\widehat{W}_T^0$, which, as we have already seen, is not the only operator that contributes in the Bjorken limit. Thus, while this model starts with a Feynman diagrammatic formulation, the advantages of the Lorentz covariant treatment are soon lost when the various approximations are taken.

The simplest way to avoid making on-shell approximations is to consider a nucleon embedded in nuclear matter. In this type of calculation the off-shell effects are parameterised in the effective nucleon mass, $M \to M^*$. Experimentally, the effective nucleon mass at nuclear matter density ($\sim 0.15\ \mathrm{fm}^{-3}$) is found to be $\sim 0.7\,M$ [214]. Theoretically, there is a large number of models for nuclear

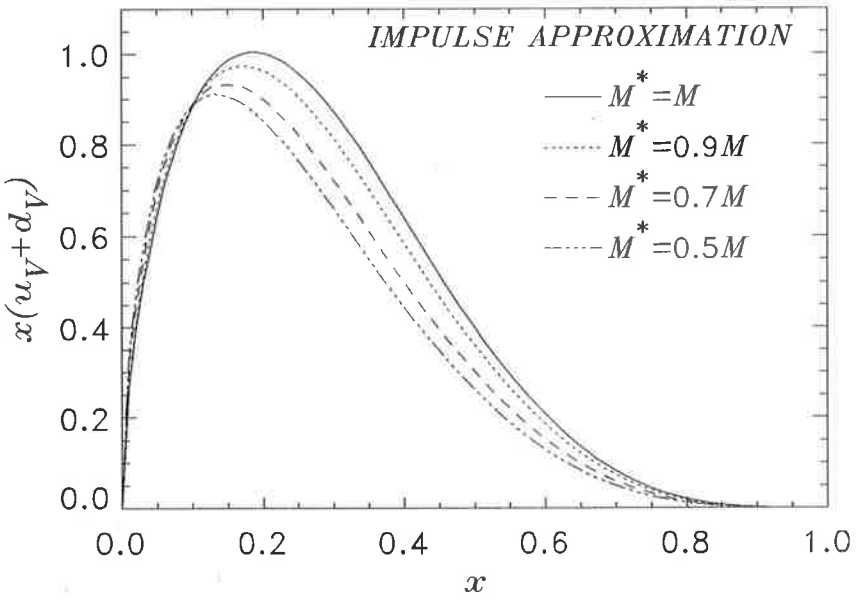

Figure 5.4: Nucleon structure function in nuclear matter in the impulse approximation, for a range of effective nucleon masses, evolved from $Q_0^2 = 0.15$ GeV^2 to $Q^2 = 4$ GeV^2.

matter, which predict a wide range of effective nucleon masses. The Quantum Hadrodynamics model of Walecka and Serot [214], in which pointlike nucleons (in the mean field approximation) are bound by the exchange of scalar (σ) and vector (ω) mesons, predicts rather small effective masses, $M^*/M \simeq 0.56 - 0.6$. Somewhat larger masses are obtained when explicit quark degrees of freedom are introduced. For example, in the Guichon model [215], where the σ and ω mesons are allowed to couple directly to quarks inside the nucleons, the value of M^* is typically $\sim 0.9\ M$. Even larger values are obtained if one includes centre-of-mass corrections and self-coupling of the scalar fields [216, 217]. Rather than choose a specific model for nuclear matter, we let M^* be a parameter and examine the effect of its variation upon the nucleon structure function, defined in Eq.(2.37).

Because the quark–nucleon vertex function will now also depend on the effective mass, it would be inappropriate to use the same normalisation constants in (5.22) and (5.23) as those determined by normalising the on-shell nucleon distributions, Eq.(2.65). Therefore the normalisation constants in this case must be determined by normalising the calculated quark distributions in nuclear matter, for $p^2 = M^{*2}$, so that their first moments are unity.

In Fig.5.4 we show the isoscalar (valence) nucleon structure function, $F_{2N^*} \equiv F_{2N}(x, p^2 = M^{*2})$ $\propto x\,(u_V(x, p^2 = M^{*2}) + d_V(x, p^2 = M^{*2}))$, for a range of effective masses, $M^*/M \sim 0.5 - 1$. There is clearly quite significant softening of the structure function, with the most prominent effects appearing for $0.2 \lesssim x \lesssim 0.5$.

However, before taking these results too seriously, one must realise that they are specific to the impulse approximation within which we have worked thus far. In particular, it was found by

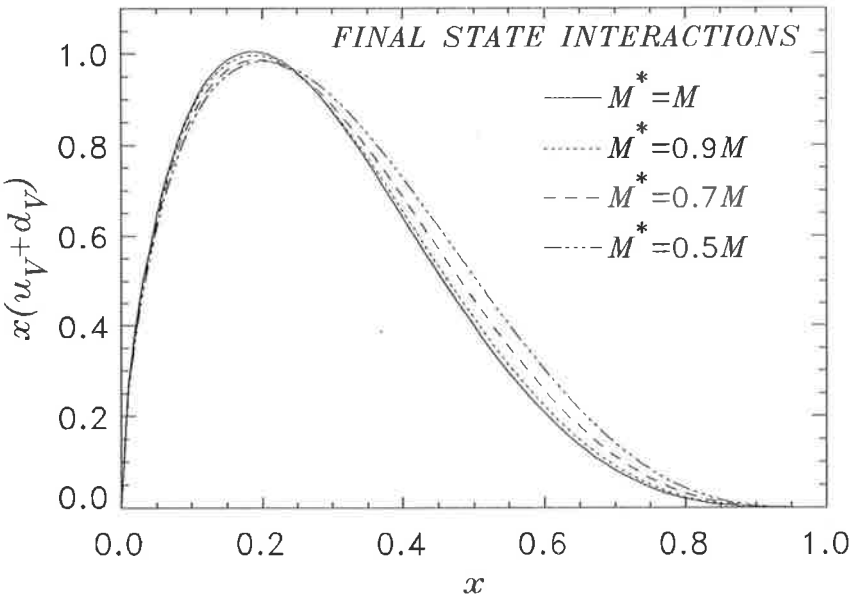

Figure 5.5: As in Fig.5.4, but including the effects of interaction of the spectator diquark with the nuclear medium.

Saito, Michels and Thomas [216] that neglecting interactions between the spectator quarks and the surrounding nucleons leads to a significant overestimate of the suppression of the nuclear valence quark distributions.

A simple means by which effects due to final state interactions can be included is to assume that the scalar and vector potential acts directly on the quarks (therefore the strength of the interaction of the nuclear medium with the diquark is 2/3 that with the nucleon), and is independent of the mass of the diquark. In that case the diquark mass is modified by $m_R \to m_R^*$, where

$$m_R^* = m_R - \frac{2}{3}(M - M^*) \tag{5.27}$$

for both scalar and vector diquarks. The effect of the spectator interactions, shown in Fig.5.5, is to make the quark distributions harder, which more than compensates for the softening produced by the off-shell effects alone. The main differences are then localised in the large x region ($x \gtrsim 0.4$), where the modified distributions (for $M^*/M \approx 0.7$) are up to $\sim 20 - 30\%$ larger than the distributions in a free nucleon. This hardening is even more dramatic if one looks at the ratio $F_{2N^*}(x)/F_{2N}$ as a function of x, Fig.5.6.

We should also comment on the importance of off-shell (and final state interaction) effects in the shadowing region, $x < 0.1$. From Fig.5.7 it can be seen that the impact on the calculated valence quark distributions in nuclear matter is almost negligible at small x. However, since nuclear shadowing is primarily a sea phenomenon, to be sure that these effects do not modify the total nucleon structure function one would need to explicitly calculate the sea quark distributions, using appropriate sea-quark—nucleon vertex functions. Unfortunately, this is beyond the scope of the present model, but such an extension can easily be made in future.

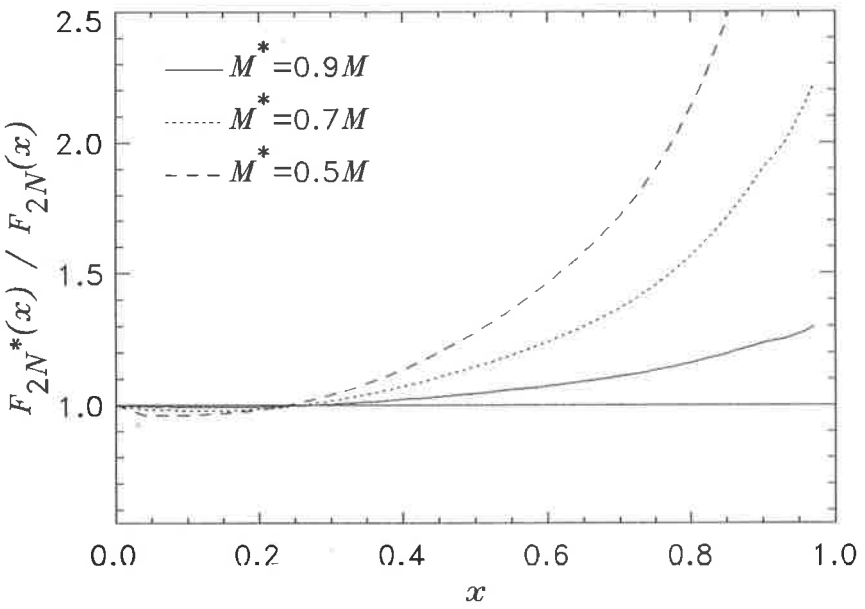

Figure 5.6: Ratio of nucleon valence structure function in nuclear matter to that for a free nucleon. Included are effects due to final state interactions.

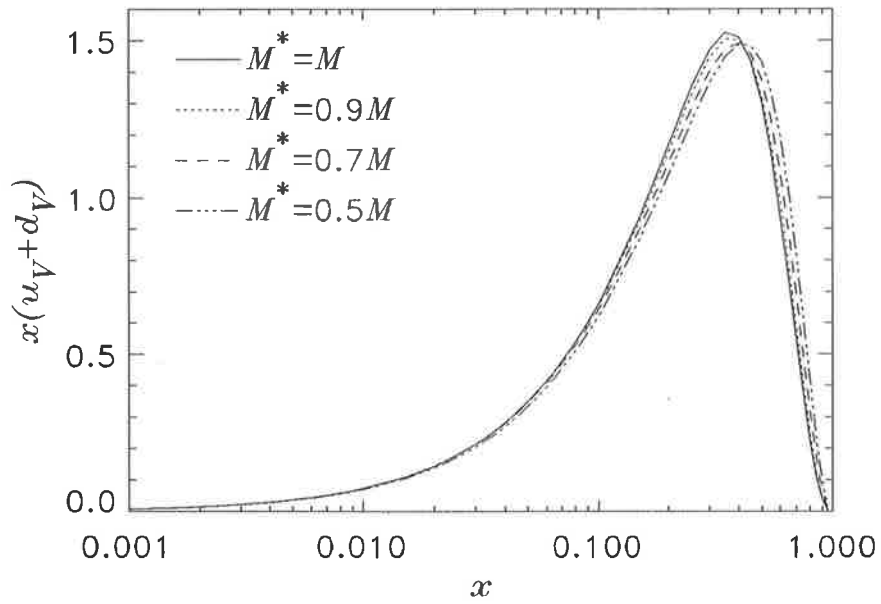

Figure 5.7: Valence quark distribution in nuclear matter at small x for different effective nucleon masses (shown are the unevolved distributions).

5.5 DIS from Dressed Nucleons

Finally, we return to the application of the relativistic formalism to the process discussed in Chapter 2, namely DIS from a virtual baryon component of a physical nucleon. Here we shall restrict ourselves to virtual nucleons and recoil pions, as this will be sufficient to illustrate the problems encountered by combining the covariant formalism with the convolution model.

With a pseudoscalar ($i\gamma_5$) πNN coupling, the relevant trace in Eq.(5.3) for DIS from a virtual nucleon with a pion recoil can be written (see also Eq.(3.19))

$$\mathrm{Tr}\left[(\not{P}+M)\, i\gamma_5 \mathcal{F}_{N\pi}(p^2)\, (\not{p}+M)\, \widehat{W}_{\mu\nu}(p,q)\, (\not{p}+M)\, i\gamma_5 \mathcal{F}_{N\pi}(p^2)\right] \tag{5.28}$$

where the πNN form factor $\mathcal{F}_{N\pi}(p^2)$ is parameterised by a simple monopole form, as in Eq.(3.21), with a cut-off mass $\Lambda_{N\pi} \sim 1.4$ GeV [17]. Rearranging the trace in Eq.(5.28) in the form (5.3), we find that for a pseudoscalar πNN vertex the functions A_i^{ps} are

$$\begin{aligned} A_0^{ps}(p,P) &= g_{\pi NN}^2 \left(-m_\pi^2\, M\right) \mathcal{F}_{N\pi}^2(p^2) \\ A_{1\,\alpha}^{ps}(p,P) &= g_{\pi NN}^2 \left(-m_\pi^2\, p_\alpha + (p^2-M^2)(p_\alpha - P_\alpha)\right) \mathcal{F}_{N\pi}^2(p^2) \\ A_{2\,\alpha\beta}^{ps}(p,P) &= 0. \end{aligned} \tag{5.29}$$

By inserting $p^2 \to M^2$ in $A_{1\alpha}^{ps}$ we can satisfy case (c) in Section 5.2 for the convolution model. However, the structure function in this case is proportional to $-m_\pi^2\, M$ (i.e. negative), which is clearly unphysical.

With a pseudovector ($\gamma_5(\not{p}-\not{P})$) coupling, the functions A_i^{pv} are

$$\begin{aligned} A_0^{pv}(p,P) &= g_{\pi NN}^2 \left(-\frac{m_\pi^2\,(p^2+M^2)}{2M} + \frac{(p^2-M^2)^2}{4M}\right) \mathcal{F}_{N\pi}^2(p^2) \\ A_{1\,\alpha}^{pv}(p,P) &= g_{\pi NN}^2 \left(-m_\pi^2\, p_\alpha + \frac{(p^2-M^2)^2}{4M^2}(p_\alpha - P_\alpha)\right) \mathcal{F}_{N\pi}^2(p^2) \\ A_{2\,\alpha\beta}^{pv}(p,P) &= 0. \end{aligned} \tag{5.30}$$

Again, each of the terms can be made proportional to each other by inserting the $p^2 = M^2$ condition, but at the expense of a negative overall result. Thus great care needs to be taken to ensure that any approximations made do not lead to nonsensical results.

It is naturally of interest to compare the result of the full calculation with the various convolution models used by previous authors, if only to understand the theoretical foundations on which they stand. In previous covariant calculations of this process [47, 60, 63, 71] the same assumptions have been made as for the nuclear calculations, namely factorisation of the bound nucleon structure function, and the lack of any dependence of this on p^2 (or on p_T). In the slightly more formal attempt in Ref.[17] at deriving the convolution model, the assumption was made that the off-shell nucleon tensor is the same as that of a point-like fermion [52], in which case the relevant operator in $\widehat{W}_{\mu\nu}$ is $\not{q}\widehat{W}_T^2$. As we have seen already, this is only part of the complete expression in the Bjorken limit. In fact the model of Ref.[17] can only be obtained from the full result if the following steps are

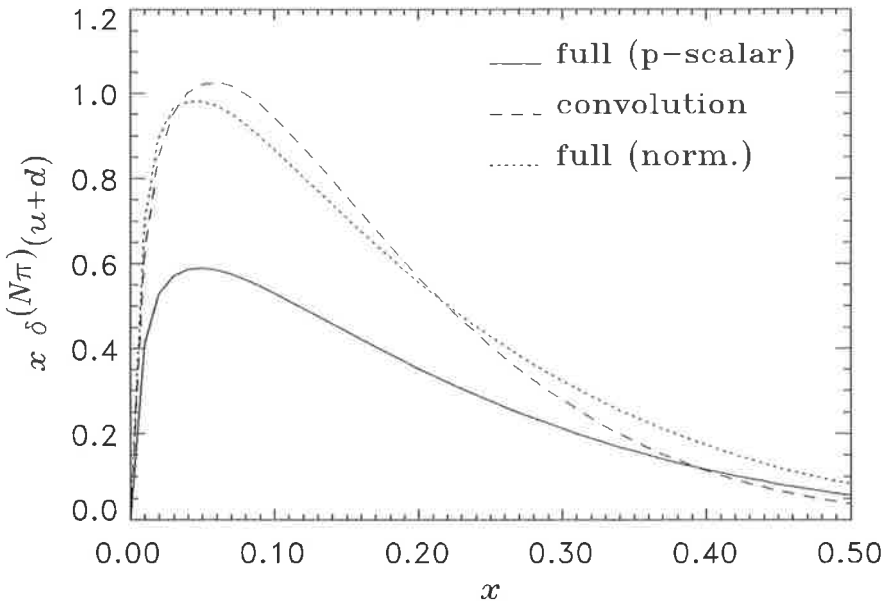

Figure 5.8: Contribution to the structure function of a nucleon from DIS off a virtual nucleon dressed by pions. The convolution model of Ref.[17] (dashed) is compared with the full calculation (for $\Lambda_p = \infty$), using the same normalisation for the off-shell $N - q$ vertex as for the on-shell vertex (solid), and normalising the full result (dotted) to give the same first moment as for the convolution curve. All curves are evolved from $Q_0^2 = 0.15$ GeV^2 to $Q^2 = 4$ GeV^2.

taken: firstly the trace in (5.28) evaluated with the $\not{q}\widehat{W}_T^2$ structure; then to obtain factorisation the limits $\mathbf{p}_T = 0$ and $p^2 = M^2$ taken in the 'nucleon structure function' (i.e. k-dependent) parts; and finally the full structure of the on-shell nucleon function used, as in (2.37), rather than just keeping the $\widehat{W}_T^2$ term. The necessity of the last point is clear, since for the on-shell structure function the individual functions $\widehat{W}_T^i$ are not necessarily positive definite, although the sum is positive of course.

Other authors [75] have implicitly assumed that the relevant operator to be used in the $\widehat{W}_{\mu\nu}$ of (5.28) is $I\widehat{W}_T^0$ (similar to what was done in [200, 212] for the deuteron). However, even with the subsequent replacement of $\widehat{W}_T^0$ by the full on-shell nucleon structure function in the convolution expression, the result (with a pseudoscalar πN coupling) will be proportional to $-m_\pi^2$ since the coefficient of $\widehat{W}_T^0$ is A_0^{ps}. Thus it appears that the result of [75] can only be obtained by taking the modulus of a negative structure function.

In all, it should now be abundantly clear that none of the scenarios described in Section 5.3 (cases (a)—(c)) for obtaining the convolution model are applicable here. As in the deuteron case, the convolution model for dressed nucleons is therefore not derivable from the exact result.

In Fig.5.8 we compare the contribution to the on-shell nucleon structure function from this process, calculated including the full p^2 dependence (with the q–N vertex function evaluated with $\Lambda_p = \infty$), with the result of the convolution model of Ref.[17]. For the full calculation we use the same normalisation constants for the scalar and vector quark—nucleon vertices as determined from the on-shell nucleon. The results indicate that the full, p^2-dependent calculation gives somewhat

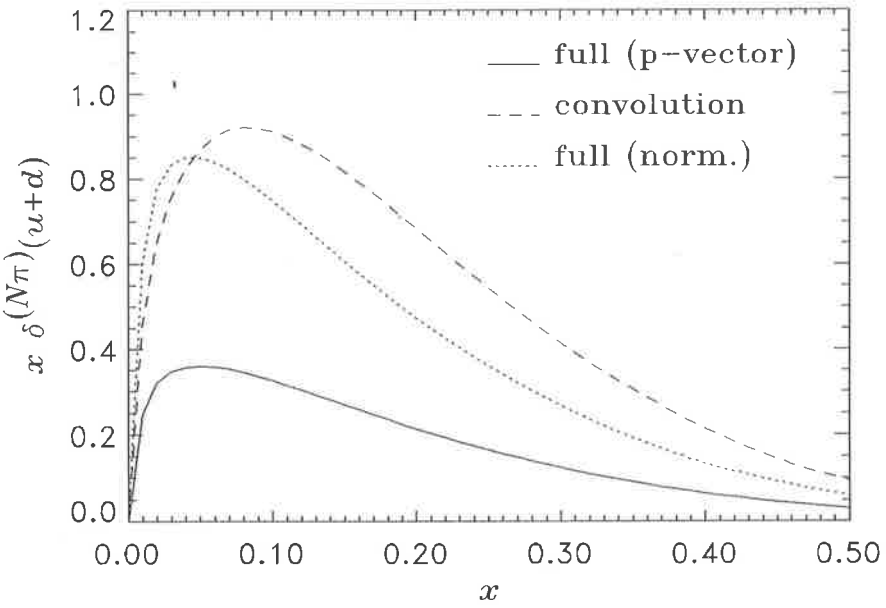

Figure 5.9: Same as in Fig.5.8, except for a pseudovector πN coupling.

smaller results compared with those of the convolution model (although the shapes are quite similar as can be from the dotted curve, where the scalar and vector vertex functions are normalised to the same first moment as in the convolution model). For the pseudovector πNN vertex, we find an even larger difference, Fig.5.9.

Such a difference might have been surprising had the convolution expression been a simple approximation to the full result, in which case we may well have expected small off-shell corrections. Unfortunately, this calculation is more difficult to check since there is no clear normalisation condition for the structure function. Comparing the first moment of the calculated distributions with the average number of pions in the intermediate state, which can be calculated by considering DIS from the virtual pion, is ambiguous due to the presence of antiparticles in the covariant formulation. A convolution formula such as (5.14) can be written for DIS from virtual pions, since there are no spinor degrees of freedom to spoil this factorisation. However, ambiguities in the p^2 dependence of the 'off-shell pion structure function' would still remain. Therefore this fact merely illustrates the absence of a firm foundation for the covariant convolution model for DIS from dressed nucleons, and the preference for the non-covariant approach taken in Chapter 2.

5.6 Summary

Finally, let us reiterate the main findings of this chapter, as these represent perhaps the most significant new developments in the study of structure functions of hadrons which are discussed in this thesis.

Starting with an investigation of the truncated nucleon tensor, $\widehat{W}_{\mu\nu}$, we have been able to put the calculation of structure functions of composite particles on an more solid theoretical footing. This has also enabled us to understand the assumptions that need to go into the derivation of the covariant convolution model of DIS. It has also led to the realisation that even in the impulse approximation a fully relativistic treatment of deep inelastic processes does not yield the convolution model, unless specific on-shell limits are taken at various stages in the derivation. Furthermore, strictly speaking it is incorrect to speak of the 'bound nucleon structure function', as this is an ill-defined quantity within a covariant formulation. This has wide-ranging consequences, as almost all calculations of composite particle structure functions (e.g. nuclei, for the EMC effect) have relied upon the validity of the simple convolution model.

Numerically, we have studied the differences between the full and convolution model results by using models of the relativistic nucleon–quark and nucleon–nucleus vertex functions. In the simplest case of DIS from the deuteron, making various assumptions for the off-shell nucleons naturally introduces deviations from the exact result. However, by suitably renormalising the results to ensure baryon number conservation (as was done in most previous calculations) the differences between the exact results and those of the convolution model can be minimised. Thus, from a phenomenological point of view, the consequences of neglecting the nucleon off-shell effects in the deuteron may not be too great.

Perhaps the most important phenomenological repercussions of neglecting nucleon off-shell effects are found in the structure functions of heavy nuclei. We find quite significant effects in the intermediate x region when the nuclear medium acts to decrease the effective nucleon mass. After including the possibility of interactions of the spectator diquark with the medium, the net effect (for $M^*/M \sim 0.7$) is to make the structure function in nuclear matter some 20-30% harder compared with the on-shell result. (The latter affect is a confirmation of the fact that the usual impulse approximation is a rather poor approximation in nuclear matter.)

The other important application which we examine is DIS from the virtual nucleon component of a physical (or dressed) nucleon, where we also find quite significant differences between the full result and the convolution model. As well as its relevance to the question of flavour asymmetry in the proton sea, this process can also be used to describe the nucleon's spin-dependent structure functions, in particular the neutron spin structure function $g_{1n}(x)$ [114]. Indeed, an obvious extension of the formalism used in this chapter would be to consider next the DIS of polarised leptons from polarised targets. In that case there will naturally be more terms in the general expansion of the polarised truncated nucleon tensor (in fact, $\gtrsim 70$ in all!). Furthermore, we can expect the usual convolution approach to calculating the polarised structure functions of nuclei to break down

as well. This may well be of importance for the extraction of g_{1n} from the polarised deuteron (or helium) structure function g_{1D} ($g_{1\ ^3He}$), and to the whole question of the spin of the proton [218, 219].

In the next chapter we will say more about the spin structure of the nucleon, in the context of semi-inclusive DIS from polarised targets. Having discussed inclusive DIS in some detail in the preceding chapters, we shall examine there semi-inclusive processes, in which specific mesons or baryons are identified out of the complete final hadronic state, with the aim of obtaining additional information on the quark structure of hadrons. For example, we mentioned in the Chapter 4 that in diffractive deep inelastic scattering by 'tagging' final state nucleons carrying a large fraction of the initial nucleon's centre of mass momentum, we could actually measure the structure function of the Pomeron. Furthermore, we may be able to learn more about the nucleon at larger x by searching for low momentum hadrons produced by DIS off the virtual meson or baryon components of the physical nucleon, as in the model of Section 3.1. Because much of the interest in semi-inclusive DIS is in the non-perturbative regime, namely the (long-distance) formation of hadronic states out of quarks and gluons, the discussion there (in contrast to that in this chapter) will be largely phenomenological.

Chapter 6

SEMI-INCLUSIVE DEEP INELASTIC SCATTERING

Much has been learned about the internal structure of the nucleon and nuclei from unpolarised inclusive deep inelastic scattering experiments. Some aspects of the substructure observed in inclusive DIS have been discussed at length in the preceding chapters. In this chapter we will extend those discussions to the case of *semi-inclusive* deep inelastic scattering [220], in which specific hadrons in the final state are observed in coincidence with the scattered lepton. The scaling behaviour of the semi-inclusive cross sections was considered some time ago by Ellis [221] and Stack [222]. As in the case of inclusive structure functions, only higher order QCD effects give rise to any Q^2 dependence of the semi-inclusive structure functions (or 'fragmentation functions').

Central to this process is understanding how quarks fragment to form specific final state mesons and baryons. Because this is a non-perturbative process, describing soft (Q^2-independent) physics, the treatment of hadronisation has necessarily been model-dependent and largely phenomenological. Nevertheless, by testing models of fragmentation we can hope to learn more about long-distance quark physics. We will consider scattering from nucleon targets only, since the dynamics of fragmentation will only be diluted by the greater probability of final state interactions in DIS from nuclei.

In our discussions we will focus attention particularly on the production of baryons. It has been unambiguously demonstrated experimentally [223–225] that the baryon yield is higher by about an order of magnitude for those baryons produced in the backward hemisphere of the probe—target centre of mass frame (so-called *target fragmentation region* (TFR)), than for forward baryons (*current fragmentation region* (CFR)). The CFR baryons have predominantly large laboratory momenta ($\gtrsim$ several GeV), while the baryons produced in the backward centre of mass jet are generally slow. Our concern here will be with such low momentum baryons, and we shall therefore neglect the process which gives rise to the forward baryons (quark $\rightarrow$ baryon fragmentation).

Although their rate of production is generally high, the efficiency with which low momentum baryons can be accurately identified is low [225]. Nevertheless, detection of such particles is possible,

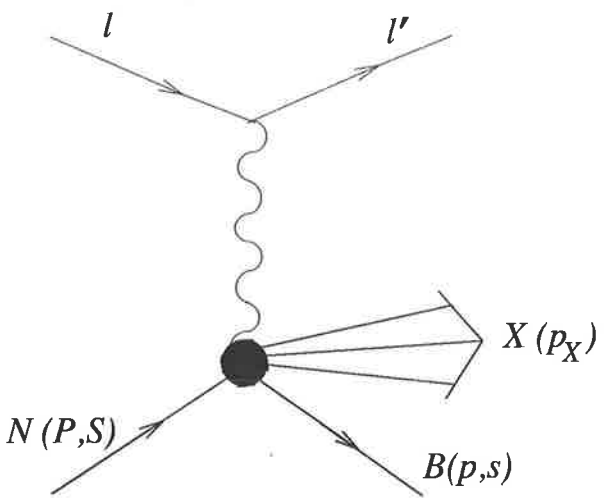

Figure 6.1: Semi-inclusive deep inelastic scattering from a nucleon, with baryon B in the final state.

for example with the CERN EMC spectrometer using muon beams [225], or potentially at CEBAF with a somewhat lower energy electron beam. For scattering by (anti)neutrinos, bubble chambers (such as the Fermilab Freon Bubble Chamber [226]) are employed for hadron identification.

As an extension to unpolarised semi-inclusive scattering, we shall investigate the possibility of obtaining new information from the spin-dependent fragmentation process involving lepton scattering from polarised targets, with subsequent measurement of the recoiling baryon polarisation. The additional spin degrees of freedom may enable differentiation between some models of the fragmentation process, in particular the meson cloud model of the nucleon discussed in Chapter 3.

6.1 Kinematics of Target Fragmentation

Consider the production of baryon B as indicated in Fig.6.1. In semi-inclusive processes we consider the DIS cross sections not only as a function of x, but also a function of the baryon's longitudinal (p_L) and transverse (p_T) momenta. For baryons produced in the TFR these momenta in the target rest frame will generally be small. Consequently, such baryons will be characterised by a small four-momentum transfer squared between the initial and final particles, $t \equiv (p - P)^2 = (-p_T^2 - (1-\zeta)(M_B^2 - M^2\zeta))/\zeta$, where $\zeta = p \cdot q / P \cdot q$ is the light-cone fraction of the target proton's momentum carried by the secondary baryon, and M and M_B are the nucleon and final state baryon masses, respectively. The requirement that the transverse momentum squared of the produced baryon be non-negative, $p_T^2 \geq 0$, leads to a kinematic upper limit on t, namely $t_{max} = -(1-\zeta)(M_B^2 - M^2\zeta))/\zeta$. More specifically, the three-momentum of TFR baryons is given in terms of t by

$$|\mathbf{p}| = \frac{1}{2M}\sqrt{(M^2 + M_B^2 - t)^2 - 4M^2 M_B^2} \tag{6.1}$$

so that the slowest baryons are those for which $t \to 0$, which occurs when $\zeta \to 1$. Clearly as the upper limit on ζ is $1 - x$, slow baryon production also corresponds to the $x \to 0$ limit, and the

slowest possible baryons produced at $\zeta = 1$ (at $x = 0$) have momentum $|\mathbf{p}_{min}| = (M_B^2 - M^2)/2M$. Thus, for example, final state nucleons can be produced with momenta down to 0 MeV, while the slowest Δ isobars have $|\mathbf{p}_{min}| \approx 340$ MeV.

Equivalently, one can observe the spectrum of baryons as a function of the laboratory angle α between the produced baryon and the direction of the probe, which is given by

$$\cos\alpha = \frac{M_B^2 + (1-2\zeta)M^2 - t}{\sqrt{(M_B^2 - M^2 - t)^2 - 4M^2 t}}. \tag{6.2}$$

It is easy to show that α will vary from 0 up to a maximum given by

$$\alpha_{max} = \arccos\left(\frac{1}{M_B}\sqrt{M_B^2 - M^2\zeta^2}\right). \tag{6.3}$$

Thus nucleons can be produced for all angles ($\alpha_{max} = \pi/2$), while the kinematic boundary for Δ isobars is at $\alpha \simeq 50^o$. For a given angle α, the integration limits of t are given by

$$\begin{aligned} t_{min/max}(\alpha) &= \frac{1}{\sin^2\alpha}\left(M_B^2\sin^2\alpha - M^2(1-2x+\cos^2\alpha)\right. \\ &\pm \left. 2M\cos\alpha\sqrt{M^2(1-x)^2 - M_B^2\sin^2\alpha}\right). \end{aligned} \tag{6.4}$$

At small angles baryons are produced over essentially the entire range of t (and therefore ζ), however the number will fall off rapidly as $\alpha \to \arccos\left(\frac{1}{M_B}\sqrt{M_B^2 - M^2(1-x^2)}\right)$ because of the fast convergence of the upper and lower bounds on t, until no particles are produced beyond the kinematic boundary at $t_{max} = t_{min} = -\left(M_B^2(1+x) - M^2(1-x)\right)/(1-x)$.

The importance of the above kinematic restrictions was demonstrated recently in two experiments [226, 227] in which slow proton production was studied in νN and νA scattering. Before we turn to questions of dynamical details of the fragmentation process, we shall describe how the above kinematics is manifested in semi-inclusive leptoproduction of baryons in the TFR. This will serve to illustrate the point that simple things must to be accounted for before one starts invoking more exotic explanations.

In the original experiment performed by the E745 Collaboration [226] a peculiar dependence was observed of the deep inelastic cross section for neutrino scattering off freon gas on the number of secondary protons (or 'stubs') at the interaction vertex. The principle effect seen there was a dramatic softening of the nuclear x-distribution in the stub-containing events. This led to the speculation that an undiluted nuclear EMC effect [228] had in fact been observed (e.g. Kumano & Close [229] and Castorina & Donnachie [230] took this as evidence for a stronger EMC effect for deeply bound nucleons and for νA collisions at small impact parameters).

Following those initial experiments, the BEBC Collaboration [227] demonstrated an even stronger depletion at large x in νH_2 and νD scattering. In Ref.[227] it was correctly concluded that this observation invalidated any nuclear interpretation of the E745 effect. In fact, a careful analysis of the kinematics of target fragmentation in DIS can quantitatively explain the 'nuclear' effect in Ref.[227]. In particular, it can be shown that a softening of the cross section for protons with

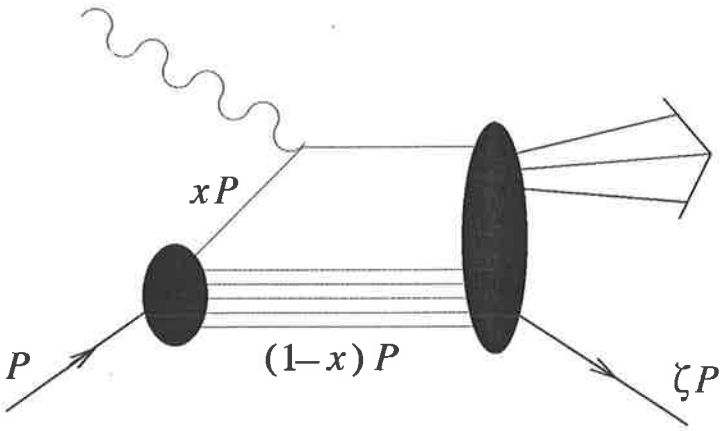

Figure 6.2: Target debris fragmentation into a baryon in the quark parton model.

momentum less than $\mathbf{p}_{max}$ (equal to several hundred MeV in these experiments) arises directly from the absence of interactions at $x > x_{max}$, where

$$x_{max} = 1 - \frac{p_{0max} - |\mathbf{p}_{max}|}{M}. \tag{6.5}$$

This limit can most easily be understood by transforming to the Breit frame, in which the probe (W-boson in this case) of zero energy, but finite three-momentum,

$$q = (0; 0, 0, -q_L), \tag{6.6}$$

scatters from a parton with fraction x of the target proton's momentum, see Fig.6.2. The struck parton has a momentum $q_L/2$ which changes sign after the collision. From the definition of x it follows then that the proton's longitudinal momentum is $P_L = q_L/2x$, so that and the proton's debris carries momentum $P_L - \frac{1}{2}q_L = P_L(1-x)$. In this reference frame (or in an IMF) the spectrum of the fragmentation products can be analysed in terms the light-cone variable z [117, 231],

$$z = \frac{p \cdot q}{(1-x)P \cdot q} = \frac{p_-}{(1-x)P_-} \tag{6.7}$$

which can be interpreted here as the ratio of the produced particle's momentum to that of the nucleon debris. Furthermore, the ratio of the recoiling proton's momentum to that of the target nucleon is $z(1-x) = \zeta$, and since $z \leq 1$, in the laboratory frame (for fixed x) the secondary protons have longitudinal momenta bounded from below,

$$p_L = \frac{M_B^2 - M^2\zeta^2 + p_T^2}{2M\zeta} \geq p_{Lmin} \tag{6.8}$$

where

$$p_{Lmin} = \frac{M_B^2 - M^2(1-x)^2 + p_T^2}{2M(1-x)}. \tag{6.9}$$

Solving this for x, we see that only interactions at

$$x \leq 1 + \frac{p_L - p_0}{M} \tag{6.10}$$

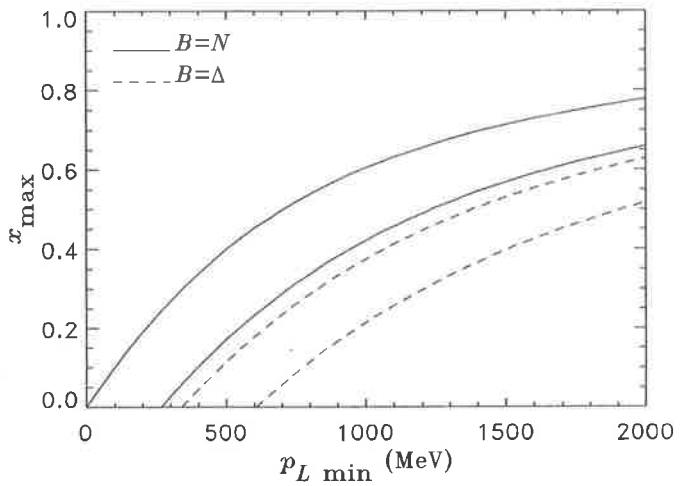

Figure 6.3: Kinematic relation between final state baryon B momentum and maximum value of x allowed. For $B = N$ (solid) and $B = \Delta$ (dashed) the upper and lower curves are for $p_T^2 = 0$ and 0.5 GeV^2, respectively.

where $p_0 = \sqrt{M^2 + \mathbf{p}^2}$ is the proton energy, can contribute to events having protons with momenta below $|\mathbf{p}|$. This is turn introduces significant bias into the x-distribution for the stub-containing events. For example, for $p_T = 0$ this corresponds to $x \leq 0.31$ and 0.45 for the BEBC proton momentum upper cuts of 350 and 600 MeV, respectively. Graphically, this boundary is illustrated in Fig.6.3, where in addition we show the kinematic boundaries for final state Δ baryons.

The above kinematic limits were also discussed in various contexts by Ishii et al. [232] (who in addition tried to account for the E745 nuclear data [226]), Strikman et al. [233], and Bosveld et al. [234]. In the following we demonstrate that the x-dependence of the BEBC effect can be quantitatively attributed to the fragmentation bias in (6.10). The 'nuclear' effect in [226] is likely to be dominated by the diluted BEBC effect [227], the dilution coming from a significant contribution of intranuclear cascading to the production of stubs ('grey tracks' in the experiment) off the nucleus.

Within the quark parton model [12], the differential cross section for $\nu(\bar{\nu})p$ scattering is (in units of $G^2 M E_{\nu(\bar{\nu})}/\pi$) [117, 231]

$$\frac{d^3\sigma^{\nu(\bar{\nu})p}}{dx\ dz\ dp_T^2} = \mathcal{F}_{\nu(\bar{\nu})p}(x)\ \tilde{D}^p_{p-q}(z, p_T^2). \tag{6.11}$$

Here, the neutrino- and antineutrino-proton 'structure functions', integrated over energy transfer ν, are

$$\mathcal{F}_{\nu p} = 2x\left(d(x) + \frac{1}{3}\bar{u}(x)\right) \tag{6.12}$$

and

$$\mathcal{F}_{\bar{\nu}p} = 2x\left(\frac{1}{3}u(x) + \bar{d}(x)\right) \tag{6.13}$$

where $\sin^2\theta_C$ and heavy flavours have been ignored. In writing (6.11) we have assumed factorisation of the primary interaction (x dependence) and fragmentation (z dependence), which is only

spoiled by higher order QCD processes. For simplicity, we have also assumed factorised p_T and z distributions [231, 235], $\tilde{D}^p_{p-q}(z, p_T^2) = D^p_{p-q}(z)\ \varphi(p_T^2)$, where $D^p_{p-q}(z)$ is the target debris (i.e. proton with a quark removed) $\rightarrow$ proton fragmentation function, and $\varphi(p_T^2)$ gives the recoil proton transverse momentum distribution. (The factorisation assumption of the transverse and longitudinal components of the baryon momentum will be subject to further comment in Section 6.2.1 in spin-dependent fragmentation.)

In the IMF (or Breit frame) the fragmentation function $D^B_{p-q}(z)$ gives the probability that once the photon strikes a quark q (with momentum fraction x) in the proton, the remaining spectator system of a proton with a quark removed (with momentum fraction $1-x$) decays to a baryon B carrying a fraction z of the spectator system's momentum, Fig.6.2. At all but very small x, the spectator system will be mostly a diquark. Furthermore, we also take the fragmentation function to be independent of the struck parton.

As mentioned above, fragmentation products emanating from the struck quark (spectator system) are dominant in the W-boson — p center of mass system forward (backward) hemisphere, and the data [223, 224] confirms that protons are predominantly produced in the backward hemisphere. We shall therefore neglect the struck quark $\rightarrow$ proton fragmentation. For estimation purposes we can take a flat fragmentation function

$$D^p_{p-q}(z) \ = \ \frac{\theta(z - z_{min})}{(1 - z_{min})} \tag{6.14}$$

where $z_{min} = \sqrt{M^2 + p_T^2}\ /\ s$ corresponds to the boundary between the forward and backward hemispheres in the centre of mass system, and s is the W-boson — target centre of mass energy squared. Such a fragmentation function is broadly consistent with the EMC data [223, 224], and is also suggested by nucleon fragmentation in hadronic collisions [236]. For comparison, we also consider a quadratic form,

$$D^p_{p-q}(z) = \frac{6\ \theta(z - z_{min})}{(1 - z_{min})^3}(z - z_{min})(1 - z). \tag{6.15}$$

(In Section 6.2 we shall consider more sophisticated fragmentation functions where we will require accurate predictions for the absolute DIS cross sections.)

The transverse momentum distribution function $\varphi(p_T^2)$ can be parameterised by a Gaussian form [235, 237, 238],

$$\varphi(p_T^2) = \frac{\exp(-p_T^2 / < p_T^2 >)}{< p_T^2 >}, \tag{6.16}$$

with $< p_T^2 >$ being the mean transverse momentum squared, typical values of which are of order 0.2—0.3 GeV^2 [235]. For comparison purposes we also consider an exponential parameterisation [237] $\varphi(p_T^2) = \exp(-p_T / < p_T^2 >^{1/2})\ /\ (2 < p_T^2 >)$.

In Fig.6.4 we show the differential cross section $d^2\sigma/dxd|\mathbf{p}|$, divided by the $|\mathbf{p}|$-integrated cross section, for neutrino-proton scattering. The effect of the stub momentum cut-off in (6.10) is unmistakable. Fig.6.5 also shows the absolute differential cross section, in which the large-$|\mathbf{p}|$ tail is

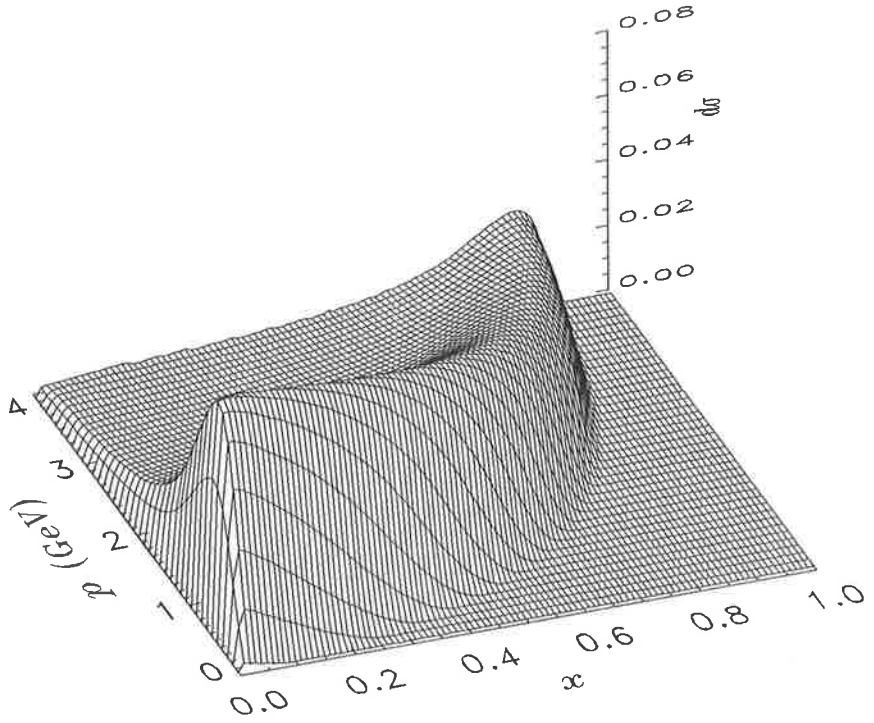

Figure 6.4: Neutrino–proton differential cross section $d\sigma \equiv d^2\sigma/dxdp$ ($p \equiv |\mathbf{p}|$) divided by the p-integrated cross section (with the proton structure function parameterisation from Ref.[15], fragmentation function of (6.14), and Gaussian p_T distribution with $< p_T^2 >= 0.28$ GeV^2).

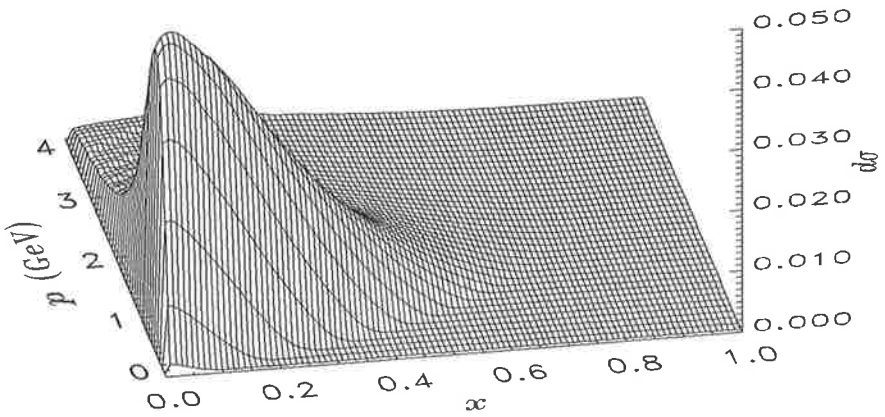

Figure 6.5: Neutrino–proton differential cross section $d\sigma \equiv d^2\sigma/dxdp$.

Structure Function	$< p_T^2 >$ GeV^2	$150 < \|\mathbf{p}\| < 350$MeV	$350 < \|\mathbf{p}\| < 600$MeV	$150 < \|\mathbf{p}\| < 600$MeV
EHLQ	0.28	2.7%	10.3%	13.0%
EHLQ*	0.28	1.3%	8.0%	9.3%
DFLM(0)	0.28	2.7%	10.3%	13.0%
HMRS(B)	0.28	3.4%	11.7%	15.1%
KMRS(B0)	0.28	3.5%	11.9%	15.4%
EHLQ	0.16	4.3%	14.0%	18.3%
EHLQ	0.36	2.2%	8.6%	10.8%
EHLQ	0.28 expon	1.1%	4.2%	5.6%
BEBC experiment		2.3%	7.7%	10%

Table 6.1: Fractions of momentum–restricted to unrestricted neutrino—proton events. In all cases the constant fragmentation function in (6.14) is used, except in that marked (*), for which the quadratic form in (6.15) is taken.

killed off by the structure function at large x (we use the EHLQ parameterisation of the proton structure function [15]). Integration of the differential cross section, Eq.(6.11), subject to cut-offs $150 < |\mathbf{p}| < 350$ MeV and $350 < |\mathbf{p}| < 600$ MeV, gives fractions

$$N^{\nu(\bar{\nu})} = \frac{\sigma^{\nu(\bar{\nu})}(\Delta \mathbf{p})}{\sigma^{\nu(\bar{\nu})}} \tag{6.17}$$

of the proton-, or 'stub'-, containing events, which are given in Tables 6.1 and 6.2. For the quark distributions of Ref.[15], and with the fragmentation function of (6.14), we find (for a Gaussian p_T distribution with $< p_T^2 >= 0.28$ GeV^2) the following ratios: 2.7% (νp), 2.4% ($\bar{\nu} p$), and 10.3% (νp), 9.3% ($\bar{\nu} p$) for the lower and higher momentum cuts, respectively. These numbers are to be compared with the experimental fractions of the stub events found in Ref.[227], namely 2.3% (νp), 2.5% ($\bar{\nu} p$), and 7.7% (νp), 5.7% ($\bar{\nu} p$) for the lower and higher limits.

The fragmentation functions in (6.14) and (6.15) correspond to one proton being present in any final state. In hadronic collisions target protons are known to fragment into neutrons in about 1/3 of all events, with a higher charge exchange probability at large z. After allowance is made for similar $p \to n$ charge exchange in neutrino interactions, there is even better agreement with experiment. Notice that at fixed x, small $|\mathbf{p}|$ corresponds to the limit $z \to 1$ (see Eq.(6.8)). Therefore, for the quadratic fragmentation function of Eq.(6.15) we obtain slightly lower percentages: 1.4% (νp), 1.3% ($\bar{\nu} p$) and 8.1% (νp), 7.3% ($\bar{\nu} p$), respectively, with a greater reduction for lower cuts. There is some obvious kinematic sensitivity to the transverse momentum of the proton — smaller (larger) $< p_T^2 >$ values of $\simeq 0.16$ (0.36) GeV^2 give about a 40% increase (20% decrease) in $N^{\nu(\bar{\nu})}$. Also, an exponential p_T distribution enhances the large p_T tail and gives rise to smaller ($\sim 60\%$) ratios for the same $< p_T^2 >$.

The sensitivity of the integrated cross section to the parton distribution functions is shown in

Structure Function	$< p_T^2 >$ GeV^2	$150 < \|\mathbf{p}\| < 350$MeV	$350 < \|\mathbf{p}\| < 600$MeV	$150 < \|\mathbf{p}\| < 600$MeV
EHLQ	0.28	2.4%	9.3%	11.8%
EHLQ*	0.28	1.2%	7.2%	8.4%
DFLM(0)	0.28	2.5%	9.5%	12.0%
HMRS(B)	0.28	3.3%	11.1%	14.4%
KMRS(B0)	0.28	3.3%	11.1%	14.4%
EHLQ	0.16	3.8%	12.8%	16.7%
EHLQ	0.36	1.9%	7.9%	9.8%
EHLQ	0.28 expon	1.0%	3.8%	4.8%
BEBC experiment		2.5%	5.7%	8%

Table 6.2: Same as in Table 6.1 except for antineutrino—proton events.

Tables 6.1 and 6.2, where several different parameterisations are considered. With the universal fragmentation functions (Eqs.(6.14) and (6.15)), we find that with the DFLM(0) quark distribution [113] $N^{\nu(\bar{\nu})}$ remains virtually unaltered, while with the HMRS(B) [168] and KMRS(B0) [184] distributions the stub ratios are between 20 and 30% larger, compared with the distributions of Ref.[15]. Such a deviation can be simply understood by considering the relative differences in the valence and sea distributions between the various parameterisations. For instance, while the KMRS(B0) and EHLQ valence distributions are comparable, the momentum carried by the SU(2) sea is about 40% larger for the former parameterisation, which gives approximately the difference cited above. In a more sophisticated model one would allow different fragmentation functions for valence and sea quark interactions (see Section 6.2).

The ratio of the normalised x-distributions for events with and without protons in the momentum range $\Delta\mathbf{p}$,

$$R^{\nu(\bar{\nu})}(x) \;=\; \frac{d\sigma/dx(x,\Delta\mathbf{p}) \;/\; \sigma(\Delta\mathbf{p})}{d\sigma/dx(x,1-\Delta\mathbf{p}) \;/\; \sigma(1-\Delta\mathbf{p})} \tag{6.18}$$

is plotted in Figs.6.6—6.8 for various momentum cuts $\Delta\mathbf{p}$ (here $1-\Delta\mathbf{p}$ refers to the complement of the momentum interval $\Delta\mathbf{p}$). The gross features of the experimental data are reproduced fairly well. There is very little effect upon $R^{\nu(\bar{\nu})}(x)$ from varying the mean transverse momentum between $< p_T^2 >= 0.16$ and 0.36 GeV^2, or from using an exponential, rather than Gaussian, p_T distribution. The curves in Figs.6.6—6.8 have been evaluated with the EHLQ parameterisation of the quark distributions [15], and with the simple fragmentation function in (6.14). Any difference between the various structure function parameterisations manifests itself only in the small-x region, where all of the $R^{\nu(\bar{\nu})}(x)$ curves differ by an overall factor of $N^{\nu(\bar{\nu})}$ (because of factorisation of the structure function dependence in the differential cross section, Eq.(6.11)). At large x there is higher sensitivity to fragmentation functions at $z \to 1$, as we have discussed above, and this can be seen in the difference between the curves in Fig.6.9 computed with the constant, Eq.(6.14), and quadratic,

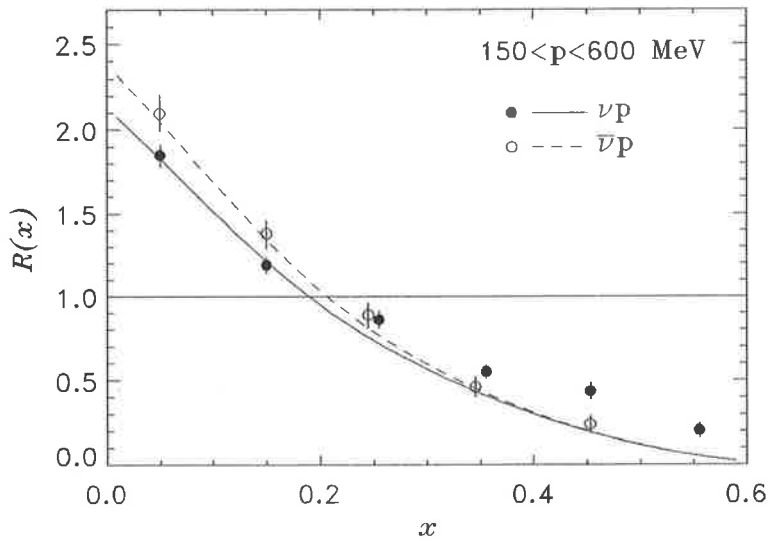

Figure 6.6: Ratio of normalised x-distributions for events with and without protons in the momentum range $150 < p < 600$ MeV. The data are from Ref.[239].

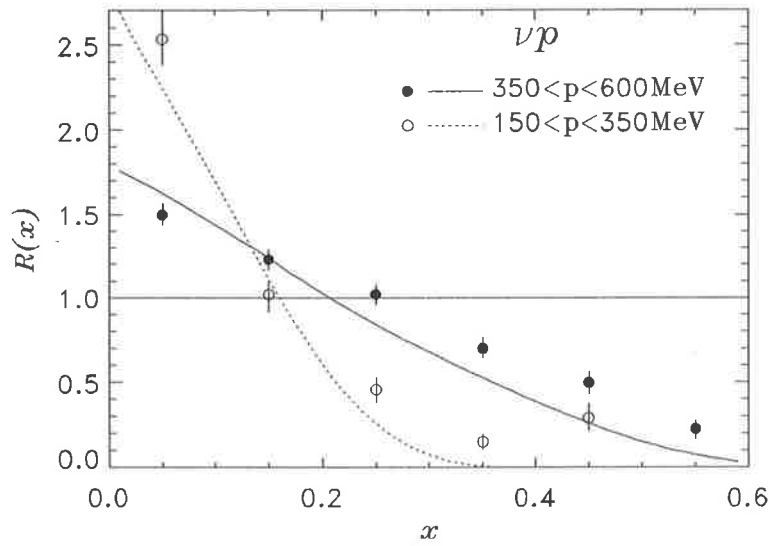

Figure 6.7: Ratio of normalised x-distributions for neutrino events with and without protons in momentum ranges $150 < |\mathbf{p}| < 350$ MeV, and $350 < |\mathbf{p}| < 600$ MeV. The data are from Ref.[227].

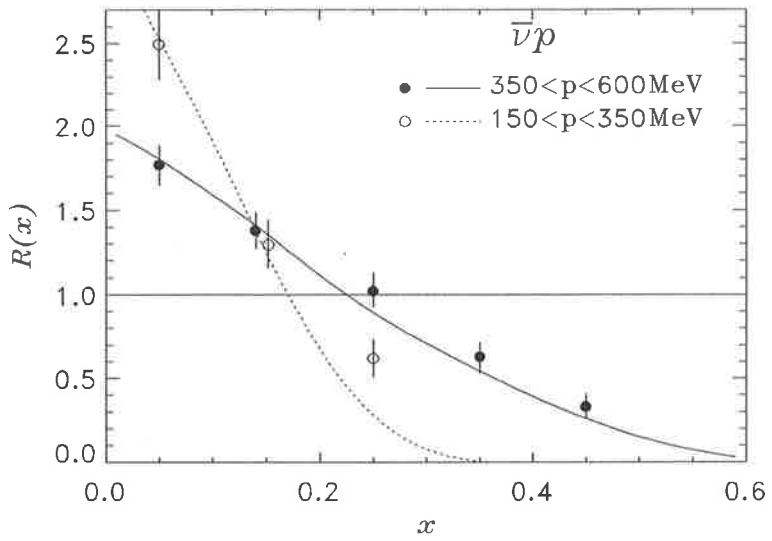

Figure 6.8: Same as in Fig.6.8, but for antineutrino events.

Eq.(6.15), fragmentation functions.

The curves for $R^{\nu(\bar{\nu})}(x)$ have also been smeared in x to correct for possible kinematic uncertainty in the experimental reconstruction of x. The need for this arises from the fact that only charged particles are measured in BEBC, while the momentum of neutral particles needed to reconstruct ν and Q^2, and then x, is reconstructed from the transverse momentum balance. On an event-by-event basis one thus has an inherent uncertainty in the determination of x. The impact of this uncertainty is estimated by smearing the calculated cross sections,

$$\frac{d\sigma_{sm}^{\nu(\bar{\nu})p}(x)}{dx} = \int d\xi\, \mathcal{S}(\xi)\, \frac{d\sigma^{\nu(\bar{\nu})p}(x/\xi)}{dx}. \tag{6.19}$$

For simplicity, we take a step-like smearing function, $\mathcal{S}(\xi) = 1$ for $1 - \Delta\xi \leq \xi \leq 1 + \Delta\xi$, and use $\Delta\xi \approx 0.5$ in Figs.6.6—6.8. (Using a Gaussian distribution instead, $\mathcal{S}(\xi) \propto \exp[-(\xi-1)^2]$, has little effect on the final results). The curves with no smearing tend to lie systematically below the data points at $x \gtrsim 0.3$, for all stub momentum cuts, as seen in Fig.6.9, where (for a constant fragmentation function) the curves have been evaluated with $\Delta\xi = 0, 0.25$ and 0.5. For larger x, corresponding to smaller values of s, the uncertainty in x should be bigger, but the effect can only be quantified by a careful analysis of the actual data.

Another possible source of error is that associated with the precision of the momentum cuts themselves, the lower 150 MeV limit especially will have a sizeable uncertainty. For larger (smaller) momentum intervals the ratio $R^{\nu(\bar{\nu})}(x)$ will be flatter (steeper). Assuming a (rough) ± 50 MeV error for both the upper and lower limits, an extended interval of $100 < |\mathbf{p}| < 650$ MeV brings the $R^{\nu(\bar{\nu})}(x)$ curve to better agreement with the large-x data, while the opposite is true for the more restricted, $200 < |\mathbf{p}| < 550$, interval. However, the effect of this on $R^{\nu(\bar{\nu})}(x)$ is numerically small.

In all, we have good quantitative agreement of our simple model with the normalised cross sections for (anti)neutrino events with and without slow protons. The description of the x dependence

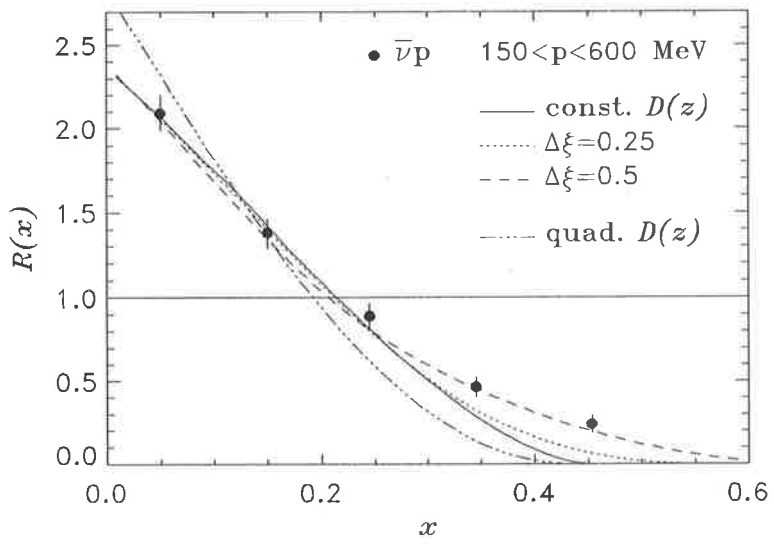

Figure 6.9: Ratio of normalised x-distributions for antineutrino events with and without protons in momentum ranges $150 < |\mathbf{p}| < 600$ MeV, for a constant and quadratic fragmentation function, and smearing corrections for the former.

of the ratios $R^{\nu(\bar{\nu})}(x)$ is virtually parameter free, which therefore unambiguously demonstrates the dominance of kinematics in this process. Therefore the fragmentation bias follows essentially from four-momentum conservation, and additional dynamical effects are likely to be of minor importance.

One such dynamical effect that one might suggest could play a role is that due to DIS from the non-perturbative pion (or other meson) cloud of the target proton (as in Chapter 3), leaving a low-momentum proton (or Δ, with subsequent decay to $p\pi$) exclusive final state. The main virtue of the pion model is its very specific predictions for the target fragmentation into protons. In particular, the x and z distributions in this case no longer factorise. Since the pion cloud of the proton is known to contribute only at small x ($x \sim 0.1$), the effect upon the cross section ratio will be restricted to this region only. However, as was shown in [240], the kinematics dominate this process so much that effects due pion exchange on $R^{\nu(\bar{\nu})}(x)$ are of minor significance. Where pions may play a more important role is in polarised semi-inclusive DIS, which we discuss next.

6.2 Spin-Dependent Fragmentation

The process under investigation involves an *unpolarised* beam scattering from a *polarised* target, so that we are not sensitive to the polarised proton structure functions $g_{1,2}(x)$, measurement of which requires both lepton and target polarisation. For simplicity, we consider charged-lepton scattering from a polarised proton, with subsequent production of a polarised Δ^{++}. We require the target proton to be initially longitudinally polarised with respect to the photon direction, with the spin of the produced Δ quantised along its direction of motion. The polarisation of such Δs can be reconstructed in a straightforward manner from their decay into $N\pi$ with an invariant mass near the Δ resonance mass. Detecting polarised final state protons, for example, would be more

difficult experimentally as one would need to remove additional backgrounds from $\Delta \to p\pi$ decays. Furthermore, because of the simple valence flavour structure of the Δ^{++}, the diquark $\to \Delta^{++}$ fragmentation functions are easier to model compared with multi-flavoured baryons.

Assuming factorisation of the x and z (or ζ) dependence, the semi-inclusive cross section for deep inelastic charged-lepton Δ-production from a polarised proton can be generically written in the quark parton model (QPM) as [241]

$$\frac{d^4\sigma^{QPM}}{dxdQ^2dzdp_T^2} \propto \mathcal{F}_{p\uparrow}(x,Q^2)\ \tilde{D}^{\Delta^{++}}_{p\uparrow - q\uparrow\downarrow}(z,p_T^2). \tag{6.20}$$

Here, the fragmentation function $\tilde{D}(z,p_T^2)$ gives the probability for the polarised ($p^\uparrow$ minus $q^{\uparrow\downarrow}$) spectator system to fragment into the polarised baryon. The function $\mathcal{F}_{p\uparrow}(x,Q^2)$ is proportional to the spin-weighted interacting-quark momentum distribution functions, $q^{\uparrow\downarrow}(x)$, where $^{\uparrow\downarrow}$ denote quark spins parallel or antiparallel to the spin of the target proton.

In one of the earliest models for the spin-dependence of the momentum density functions, Carlitz and Kaur [242] worked under the assumption that the contribution to the proton polarisation from sea quarks is negligible. In their model, the limiting behaviours as $x \to 0$ and $x \to 1$ were used to parameterise the polarised valence distributions as

$$\begin{aligned} u_V^{\uparrow\downarrow}(x) &= \frac{1}{2}\left(u_V(x)(1 \pm \cos\theta_D(x)) \mp \frac{2}{3}d_V(x)\cos\theta_D(x)\right) \\ d_V^{\uparrow\downarrow}(x) &= \frac{1}{2}\left(1 \mp \frac{1}{3}\cos\theta_D(x)\right) d_V(x). \end{aligned} \tag{6.21}$$

The spin dilution factor, $\cos\theta_D(x)$, was introduced to model interactions between valence quarks and the unpolarised sea quarks and gluons, with the constraint of satisfying the Bjorken sum rule [19]. In the limit as $x \to 0$, interactions with sea partons would become significant, so that if we assume that the valence quark spin is transferred equally among the sea quarks and gluons, $\cos\theta_D(x) \to 0$. The SU(6) limit, where only valence quarks are present, is recovered with $\cos\theta_D(x) \to 1$ as $x \to 1$.

Schafer [243] extended this idea by allowing for additional flavour dependence of the spin dilution factor, taking into account the spin dependence of one-gluon exchange, and hence the $\Delta - p$ mass difference (see also Close and Thomas [48]). For convenience, the quantities $A_0^p(x) = u_V(x) - \frac{1}{2}d_V(x)$ and $A_1^p(x) = \frac{3}{2}d_V(x)$ are defined to be the interacting quark distributions in the proton when accompanied by a diquark system in an isospin 0 and 1 state, respectively. In terms of these, the SU(6) wavefunction for the target proton is written [242–244]

$$\begin{aligned} p^\uparrow &= u(ud)_0\ (\uparrow(\uparrow\downarrow)_0)\ \sqrt{A_0^p(x)} \\ &+ \left(\sqrt{\frac{2}{3}}d\ (uu)_1 - \sqrt{\frac{1}{3}}u\ (ud)_1\right)\left(\sqrt{\frac{2}{3}}\downarrow(\uparrow\uparrow)_1 - \sqrt{\frac{1}{3}}\uparrow(\uparrow\downarrow)_1\right)\ \sqrt{A_1^p(x)} \end{aligned} \tag{6.22}$$

where the spectator diquark state has total spin and isospin equal to 0 and 1 in the first and second terms, respectively. The polarised valence quark distributions were then parameterised in [243] as

$$
\begin{aligned}
u_V^{\uparrow}(x) &= \left(u_V(x) - \frac{1}{3}d_V(x)\right) f_u(0;x) \\
u_V^{\downarrow}(x) &= \frac{1}{3}d_V(x) f_u(1;x) \\
d_V^{\uparrow}(x) &= \frac{1}{3}d_V(x) f_d(0;x) \\
d_V^{\downarrow}(x) &= \frac{2}{3}d_V(x) f_d(1;x)
\end{aligned}
\tag{6.23}
$$

where $f_q(j_z;x)$ denotes the spin dilution factor for scattering from quark q with the spectator diquark having spin projection j_z. Again, the SU(6) limit is obtained when $f_q(j_z;x) \to 1$ as $x \to 1$. (Note that the starting distributions q_V in (6.23) do not correspond exactly to the valence distributions defined as $q_V = q_V^{\uparrow} + q_V^{\downarrow}$.)

We should also add a note of caution that in both of these models the effects of the U(1) axial anomaly are neglected [219]. For comparison with (future) high-precision data a more rigorous theoretical treatment may indeed be needed. For now, in the absence of such data, we seek only a broad estimate of the QPM polarisation cross section, and in particular to contrast this with the predictions of the pion exchange model which will be discussed in Section 6.2.2.

6.2.1 Fragmentation Functions

In Section 6.1 we assumed for simplicity that the fragmentation into unpolarised baryons, given by the fragmentation function $\widetilde{D}(z, p_T^2)$, could be factorised into unpolarised transverse and longitudinal components. Furthermore, for the fragmentation function we took some very simple parameterisations, primarily because our concern was the ratio of cross sections, and because the effect illustrated there was so dominated by kinematics. On the other hand, if one is trying to calculate absolute cross sections then clearly more sophisticated fragmentation functions are needed.

Because the fragmentation functions describe soft, non-perturbative parton physics, and since a reliable calculation from first principles in QCD is some time away, a number of phenomenological models have been developed. Many of these [245, 246] have followed the basic approach that was originally formulated by Field and Feynman [117, 241], whose quark jet fragmentation model involved recursive $q\bar{q}$ pair creation (cascade) out of the colour field between the scattered and spectator partons, and subsequent recombination into colour neutral hadrons. In the original analysis of [117] only quark $\to$ meson fragmentation functions were modelled. Later this approach was extended by Bartl et al. [245] by also allowing for $q \to B$ and $qq \to B$ decays. Another approach was pioneered by the Lund group [247], who considered additional fragmentation into hadrons of the gluon string connecting the coloured partons. (The experimental observation of the subsequent 3-jet events was one of the prime pieces of evidence in favour of QCD.) Analytic expressions for the fragmentation functions can be obtained by constraining their limiting behaviour at the asymptotic limits. The $z \to 0$ limit requires a $1/z$ behaviour for $D(z)$ in order to reproduce

the observed logarithmic increase in hadron multiplicity as $s \to \infty$,

$$< n_B > \;=\; \int_{z_{min}}^{1} dz\; D(z) \;\sim\; \ln s \tag{6.24}$$

where $z_{min} \propto 1/s$ (see below). A common practice [248] for the $z \to 1$ limit is to apply dimensional counting rules, using essentially the same arguments as for the $x \to 1$ limit of the structure functions [103]. In all cases, however, the overall normalisation of the fragmentation functions has had to be fixed by the data.

The above models are all specific to the valence quark fragmentation functions, $D^B_{q_V q_V}(z)$, which describe the spectator system $\to$ baryon B fragmentation for scattering from valence quarks. At small x, where the probability of interaction with a sea quark or antiquark is large, we also need to know how systems such as $q_V q_V q_V q_S$ or $q_V q_V q_V \bar{q}$ fragment to baryons. In general, there is no reason why these more complicated systems should decay at the same rate as the valence diquark. In our region of interest, however, the fragment baryon is required to carry most of the parent system's momentum ($z \to 1$), and for this to occur the baryon must contain all of the spectator valence quarks of the appropriate flavour. At large z ($z \gtrsim 0.6$) model calculations [245] indicate that by far the most important contributions to the fragmentation functions come from the process whereby the baryon is formed after only one $q\bar{q}$ pair creation. In the case of the Δ^{++}, all of the valence u quarks in the spectator system must be present in the final state baryon. For interactions with d_S and $\bar{d}$ quarks, we would therefore expect that $D^{\Delta^{++}}_{u_V u_V d_V \bar{d}}(z) \simeq D^{\Delta^{++}}_{u_V u_V d_V d_S}(z) \simeq D^{\Delta^{++}}_{u_V u_V}(z)$. Similarly for scattering from u_S and $\bar{u}$ quarks, we have $D^{\Delta^{++}}_{u_V u_V d_V \bar{u}}(z) \simeq D^{\Delta^{++}}_{u_V u_V d_V u_S}(z) \simeq D^{\Delta^{++}}_{u_V u_V}(z)$. Note that if a u_V quark is struck, the probability of producing a Δ^{++} is smaller than if it is a u_S quark, $D^{\Delta^{++}}_{u_V d_V}(z) \ll D^{\Delta^{++}}_{u_V u_V}(z)$. Numerically, at $Q^2 \simeq 4$ GeV^2 the sea constitutes at most $\sim 20\%$ of the cross section at $x \sim 0.1$.

Usually, in semi-inclusive experiments [225] the longitudinal momentum dependence is measured as a function of the Feynman variable x_F, defined as the ratio of the centre of mass longitudinal momentum to its maximum allowed value, $x_F = p^*_L/p^*_{Lmax} \simeq 2|\mathbf{p}^*|/s \simeq 1 - M_X^2/s$, where M_X is the mass of the inclusive hadronic debris, and the asterisk (*) denotes centre of mass momenta. This variable can be related to the light-cone variable z via

$$z \;=\; \frac{\sqrt{M_B^2 + p_T^2 + s\; x_F^2/4} - \sqrt{s}\; x_F/2}{\sqrt{s}}. \tag{6.25}$$

Note that for $z \to 1$, $x_F \simeq z$ if $s \gg M_B^2 + p_T^2$. The TFR (CFR) corresponds to $x_F < 0$ ($x_F > 0$), and the boundary between the regions at $x_F = 0$ corresponds to $\zeta_{min} = \sqrt{M_B^2 + p_T^2}/s$.

For the fragmentation of quark systems with net polarisation into polarised baryons we need to know how the polarised spectator system (diquark for $z \to 1$) transfers its polarisation to the produced baryon. While there exists a small quantity of literature on polarised quark $\to$ polarised baryon fragmentation [249, 250], the spectator (diquark) $\to$ baryon process has received almost no attention. (One early calculation was made by Bigi [251] who, however, considered only spin-dependent fragmentation in polarised baryon production via the scattering of polarised leptons

from unpolarised protons.) We follow the approach taken by Bartl et al. in their study of polarised quark $\rightarrow$ baryon fragmentation [250], by assuming that the diquark retains its helicity during its decay. We also assume that the $q\bar{q}$ pair creation probability is independent of the helicity state of the quark q. This means that at leading order the produced baryon will contain the helicity of the diquark, so that, for example, a $\Delta^{\Uparrow}$ or $\Delta^{\uparrow}$ can emerge from a $q^{\uparrow}q^{\uparrow}$ diquark, whereas a $\Delta^{\Downarrow}$ cannot.

For $p_T^2 = 0$ we define the spin quantisation axes of the target proton and fragment Δ to be collinear, for which the calculation of the leading spin-dependent fragmentation functions is relatively straightforward. The overall normalisation of the spin-dependent fragmentation functions is fixed by the condition

$$\begin{aligned} q(x)\, D_{p-q}^{\Delta^{++}}(z) \;+\; \bar{q}(x)\, D_{p-\bar{q}}^{\Delta^{++}}(z) \;&=\; q^{\uparrow}(x)\, D_{p\uparrow-q\uparrow}^{\Delta^{++}}(z) \;+\; q^{\downarrow}(x)\, D_{p\uparrow-q\downarrow}^{\Delta^{++}}(z) \\ &+\; \bar{q}^{\uparrow}(x)\, D_{p\uparrow-\bar{q}\uparrow}^{\Delta^{++}}(z) \;+\; \bar{q}^{\downarrow}(x)\, D_{p\uparrow-\bar{q}\downarrow}^{\Delta^{++}}(z) \end{aligned} \tag{6.26}$$

where

$$D^{\Delta^{++}}(z) \;=\; \sum_{s=-3/2}^{+3/2} D^{\Delta^{++}s}(z). \tag{6.27}$$

In relating the production rates for various polarised Δ^{++} we employ simple SU(6) spin-flavour wavefunctions,

$$\begin{aligned} \Delta^{++\Uparrow} &\sim u^{\uparrow}\,(uu)_{1(+1)} \\ \Delta^{++\uparrow} &\sim \sqrt{\frac{2}{3}}u^{\uparrow}\,(uu)_{1(0)} + \sqrt{\frac{1}{3}}u^{\downarrow}\,(uu)_{1(+1)} \\ \Delta^{++\downarrow} &\sim \sqrt{\frac{2}{3}}u^{\downarrow}\,(uu)_{1(0)} + \sqrt{\frac{1}{3}}u^{\uparrow}\,(uu)_{1(-1)} \\ \Delta^{++\Downarrow} &\sim u^{\downarrow}\,(uu)_{1(-1)}. \end{aligned} \tag{6.28}$$

where the diquark $qq_{j(j_z)}$ is in a spin j (spin projection j_z) state. Note that this is true only when the spin projections of the diquark and Δ are in the same direction.

From these wavefunctions we can deduce simple relations among the valence spectator diquark $\rightarrow \Delta$ (spin projection s) fragmentation functions, $D_{qq_{j(j_z)}}^{\Delta^{++}s}(z)$. Clearly the leading functions will be those which can form the correct spin and flavour quantum numbers (to form a $\Delta^{++\ s}$) by picking up a single quark from a $q\bar{q}$ pair in the vacuum, and these are related by

$$D_{uu_{1(1)}}^{\Delta^{++}\Uparrow}(z) = 3\; D_{uu_{1(1)}}^{\Delta^{++}\uparrow}(z) = \frac{3}{2}D_{uu_{1(0)}}^{\Delta^{++}\uparrow}(z) = \frac{3}{2}D_{uu_{1(0)}}^{\Delta^{++}\downarrow}(z) \tag{6.29}$$

with normalisation determined from (6.26)–(6.27):

$$D_{uu_{1(1)}}^{\Delta^{++}\Uparrow}(z) \;=\; \frac{3}{4}D_{uu}^{\Delta^{++}}(z). \tag{6.30}$$

The non-leading fragmentation functions are those which require at least two $q\bar{q}$ pairs, namely $D_{uu_{1(0)}}^{\Delta^{++}\Uparrow/\Downarrow}$, $D_{uu_{1(1)}}^{\Delta^{++}\downarrow/\Downarrow}$, $D_{ud_{0(0)}}^{\Delta^{++}\Uparrow/\uparrow/\downarrow/\Downarrow}$, $D_{ud_{1(0)}}^{\Delta^{++}\Uparrow/\uparrow/\downarrow/\Downarrow}$, and $D_{ud_{1(1)}}^{\Delta^{++}\Uparrow/\uparrow/\downarrow}$, and those which require 3 such pairs, $D_{uu_{1(1)}}^{\Delta^{++}\Downarrow}$ and $D_{ud_{1(1)}}^{\Delta^{++}\Downarrow}$. Except at very small z ($\lesssim 0.2$) the fragmentation functions requiring 3

$q\bar{q}$ pairs are consistent with zero in the model of Ref.[245]. Since our region of interest is that in which there is a high yield of slow Δ baryons in the TFR, namely $z \gtrsim 0.6$, we can safely neglect the latter functions. For the 2 $q\bar{q}$ pair fragmentation functions, we also expect that $D^{\Delta^{++}\Uparrow}_{uu_{1(0)}}(z) = D^{\Delta^{++}\Downarrow}_{uu_{1(0)}}(z)$. For $z \gtrsim 0.2$ the unpolarised model fragmentation functions of [245] requiring 2 $q\bar{q}$ pairs (e.g. $D^{\Delta^{++}}_{ud}(z)$) were quite small compared with the leading fragmentation functions, and related approximately by $D^{\Delta^{++}}_{ud}(z) \simeq 0.1\ D^{\Delta^{++}}_{uu}(z)$. For larger z ($\gtrsim 0.6$) we expect that these non-leading fragmentation functions are also negligible compared with the leading functions. For the spin-dependent fragmentation functions, we therefore expect a similar behaviour for those decay probabilities requiring two $q\bar{q}$ pairs created in order to form the final state with the correct spin quantum numbers. This then allows for a complete description of the spin fragmentation at large z in terms of only the 4 fragmentation functions of (6.29).

As mentioned above, the spin-dependent $qq \to \Delta$ transition probabilities, $D^{\Delta^{++}s}_{qq_{j(j_z)}}(z)$, can be related via the SU(6) wavefunctions of the Δ only if the spins of the diquark and Δ are quantised along the same axis. For Δs produced in the target rest frame with $p_T^2 = 0$ (relative to the z-axis as defined by the γ^* direction) the analysis in terms of the above spin-dependent fragmentation functions is valid as long as the proton spin is also along the z-axis. This is no longer the case for specific polarised baryons with non-zero transverse momentum, $p_T^2 \neq 0$. We can see this more clearly by considering the $qq_{j(j_z)} \to \Delta^{++s}$ transition amplitudes, $A^s_{qq_{j(j_z)}}(\alpha)$, where the Δ momentum direction α (relative the the z-axis) is also the angle between the diquark and Δ spins (for longitudinally polarised Δs). Then $D^{\Delta^{++}s}_{qq_{j(j_z)}} \sim |A^s_{qq_{j(j_z)}}(0)|^2$. However, to describe the fragmentation into a Δ with polarisation at angle $\alpha \neq 0$ in terms of the amplitudes $A^s_{qq_{j(j_z)}}(\alpha)$, we must begin the fragmentation process from a diquark with spin in the α direction. Thus we need to know the spin projection of the diquark onto the axis given by angle α. This can be done by taking a linear combination of qq states with spin quantised along the z-axis, weighted by the spin rotation functions $d^{j=1}_{j_\alpha,j_z}(\alpha)$, where j_α is the diquark spin projection in the α-direction, and $j = 1$ is the total spin of the uu diquark in the Δ: $\sum_{j_z} d^{j=1}_{j_\alpha,j_z}(\alpha) A^s_{qq_{j(j_z)}}$. However, in this case the square of the transition amplitude will contain 'non-diagonal' terms, for which an interpretation in terms of fragmentation functions will no longer be possible. For the spin-dependent fragmentation of quarks to baryons with $p_T^2 \neq 0$ an ansatz was made in Ref.[250] in which the 'non-diagonal' functions were expressed as products of an empirical transverse momentum distribution and some unknown function of z. Only simple guesses were made for the z-dependence of these functions, and without accurate measurements of final state Δ polarisation, which would enable these to be determined, such prescriptions must remain speculative.

This problem will simplify somewhat because we have some knowledge of the spin state of the diquark from the spin of the struck quark. For example, with the SU(6) proton and Δ wavefunctions in (6.22) and (6.23), a photon striking a $d^\downarrow$ quark will leave a uu diquark with $j(j_z) = 1(1)$. Then to make a $\Delta^\Uparrow$ in the α direction, only the amplitude $A^\Uparrow_{uu_{1(1)}}$ will contribute, so that the fragmentation function in this case will be $\propto \left(d^1_{1,1}(\alpha)\right)^2 D^{\Delta^{++}\Uparrow}_{uu_{1(1)}}$. However, for a $\Delta^\uparrow$ there will be two transition

amplitudes, $A^{\uparrow}_{uu_{1(0)}}$ and $A^{\uparrow}_{uu_{1(1)}}$, and therefore two unknown terms for the fragmentation function into $\Delta^{\uparrow}$ at angle α. A possible way around this could be to approximate, for small laboratory angles α (since the production cross section in strongly peaked around $\alpha \approx 0$), the fragmentation function by the same function, $D^{\Delta^{++}s}_{qq_{j(jz)}}(z)$, as given by SU(6) symmetry. Our approach, however, will be to work in a frame of reference in which the target proton has large momentum, and to consider only the longitudinal momentum dependence of the fragmentation functions — that is, we will assume, as in the unpolarised case, that the transverse momentum distribution of the polarised Δ can also be factored, $\widetilde{D}^{s}_{p\uparrow - q\uparrow\downarrow}(z, p_T^2) = D^{s}_{p\uparrow - q\uparrow\downarrow}(z)\ \varphi(p_T^2)$. This then will enable us to use the model described above (Eqs.(6.26)—(6.30)) without ambiguity.

We therefore write the p_T-integrated QPM differential cross section for the leptoproduction of a Δ^{++} with spin s as

$$\begin{aligned}\frac{d^3\sigma^{QPM}}{dx dQ^2 d\zeta} &= \left(\frac{2\pi\alpha^2}{M^2E^2x(1-x)}\right)\left(\frac{1}{2x^2} + \frac{4M^2E^2}{Q^4}\left(1 - \frac{Q^2}{2MEx} - \frac{Q^2}{4E^2}\right)\right) \\ &\times \left[\frac{4x}{9}\left(u_V^{\uparrow} D^{\Delta^{++}s}_{ud_{1(0)}} + 2\bar{u}^{\uparrow}\left(\frac{2}{3}D^{\Delta^{++}s}_{uu_{1(1)}} + \frac{1}{3}D^{\Delta^{++}s}_{uu_{1(0)}}\right) + u_V^{\downarrow} D^{\Delta^{++}s}_{ud_{1(1)}} + 2\bar{u}^{\downarrow}\left(\frac{2}{3}D^{\Delta^{++}s}_{uu_{1(1)}} + \frac{1}{3}D^{\Delta^{++}s}_{uu_{1(0)}}\right)\right)\right. \\ &\left. + \frac{x}{9}\left(d_V^{\uparrow} D^{\Delta^{++}s}_{uu_{1(0)}} + 2\bar{d}^{\uparrow}\left(\frac{2}{3}D^{\Delta^{++}s}_{uu_{1(1)}} + \frac{1}{3}D^{\Delta^{++}s}_{uu_{1(0)}}\right) + d_V^{\downarrow} D^{\Delta^{++}s}_{uu_{1(1)}} + 2\bar{d}^{\downarrow}\left(\frac{2}{3}D^{\Delta^{++}s}_{uu_{1(1)}} + \frac{1}{3}D^{\Delta^{++}s}_{uu_{1(0)}}\right)\right)\right]\end{aligned} \tag{6.31}$$

where the fragmentation functions $D^{\Delta^{++}s}_{qq_{j(jz)}}$ are evaluated at $z = \zeta/(1-x)$. In our calculations we parameterise the (very limited) available data obtained by the EM Collaboration [225] in a recent analysis of (unpolarised) Δ^{++} muon production in the TFR for $z \to 1$. We further assume that the large z limit is dominated by the fragmentation $uu \to \Delta^{++}$, and parameterise the leading unpolarised function as $D^{\Delta^{++}}_{uu}(z \to 1) = a(1-z)^b$. Converting from the x_F dependence of the observed normalised hadron distribution, $(1/N_{total})\ dN^{\Delta^{++}}/dx_F$, we obtain $a \approx 0.68$ and $b \approx 0.3$, albeit with large uncertainty. From (6.29) and (6.30) we can then finally obtain the polarised fragmentation functions necessary to calculate the polarised Δ production cross section in (6.31).

An alternative description of this semi-inclusive process can be made in terms of the one pion exchange model discussed in Chapter 3. Since the production of final state Δs involves small four-momentum transfers t, one might expect that the t-channel exchange of pions could be used to describe the process, in at least part of the kinematic range.

6.2.2 Δ^{++} Leptoproduction via One Pion Exchange

Despite the various phenomenological successes of nucleon models which incorporate pionic degrees of freedom (see the discussion in Chapter 3), as yet there has been no direct experimental evidence to unambiguously point to the existence of a pion cloud in high energy reactions. It is part of our purpose to investigate the possibility of obtaining a clear signature in semi-inclusive DIS, which would be distinct from the QPM background described in the previous section.

The relevant process is illustrated in Fig.6.10, where the dissociation of a physical nucleon into a pion and a Δ is explicitly witnessed by the probing photon. Following our earlier discussions of the pion model, we can write down the one pion exchange (OPE) differential cross section for the

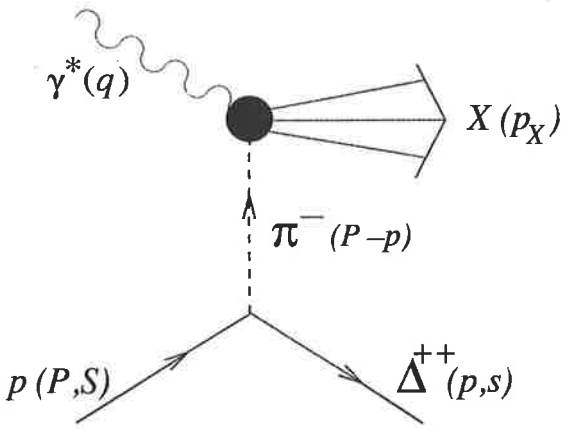

Figure 6.10: Semi-inclusive leptoproduction of polarised Δ^{++} baryons via one pion exchange.

reaction $lp \to l\Delta^{++}X$ as [66, 252]

$$\frac{d^5\sigma^{OPE}}{dx dQ^2 d\zeta dp_T^2 d\phi} = \left(\frac{\alpha^2}{M\ E^2\ x^2\ Q^4\ \zeta}\right) \frac{f^2_{\pi N\Delta}}{16\pi^2 m_\pi^2} \frac{\mathcal{T}^{S\ s}(t)\ \mathcal{F}^2_{\pi\Delta}}{(t-m_\pi^2)^2}\ L_{\mu\nu}(l,q)\ W_\pi^{\mu\nu}(k,q) \quad (6.32)$$

where $t \equiv (p-P)^2 = \left(-p_T^2 - (1-\zeta)(M_\Delta^2 - \zeta M^2)\right)/\zeta$, and ϕ is the azimuthal angle. The tensors $L_{\mu\nu}$ and $W_\pi^{\mu\nu}$, describing the leptonic and hadronic vertices, are given in (2.2) and (3.9).

For the $\pi N\Delta$ form factor, $\mathcal{F}_{\pi\Delta}$, we may use a dipole function

$$\mathcal{F}_{\pi\Delta}(t) = \left(\frac{\Lambda^2_{\pi\Delta} - m_\pi^2}{\Lambda^2_{\pi\Delta} - t}\right)^2 \quad (6.33)$$

as in (3.11). Alternatively, we can also take a form suggested in our earlier analysis of the proton's pion cloud in the infinite momentum frame (Section 3.1.2), in which we used the time-ordered (non-covariant) kinematics to evaluate only the diagram in which the exchanged meson travelled forwards in time. A similar analysis of the semi-inclusive DIS process in the IMF would yield the same results, but would allow us to take the form factor as

$$\mathcal{F}_{\pi\Delta}(p_T^2,\zeta) = \left(\frac{\Lambda^2 + M^2}{\Lambda^2 + s_{\pi\Delta}}\right)^2 \quad (6.34)$$

where $s_{\pi\Delta} \equiv (m_\pi^2 + p_T^2)/(1-\zeta) + (M_\Delta^2 + p_T^2)/\zeta$. Furthermore, as discussed at length in Chapter 3, the formulation in the IMF would remove some of the ambiguities associated with using the experimental structure function of the pion [101, 102] for the virtual pion structure function $F_{2\pi}$ in Eq.(6.32). (In addition, the form factors could be different for different polarisation states of the proton and Δ, however, we neglect such differences here.)

The function $\mathcal{T}^{S\ s}(t)$ is obtained by evaluating the trace over the target nucleon spinor and the Rarita-Schwinger spinor-vector u_α for the recoil Δ,

$$\mathcal{T}^{S\ s}(t) = \mathrm{Tr}\ [u(P,S)\bar{u}(P,S)\ u_\alpha(p,s)\bar{u}_\beta(p,s)]\ (p-P)^\alpha\ (p-P)^\beta \quad (6.35)$$

where the Rarita-Schwinger spinor-vector $u_\alpha(p,s)$ was given in (3.12). We define, as before, the target nucleon polarisation vector to lie in the z-direction (parallel to the γ^* direction), and the spin

of the produced Δ is quantised along its direction of motion. Because the Δ is emitted collinearly with the pion, production of Δ baryons with spin projection $\pm 3/2$ is forbidden, $\mathcal{T}^{S\,\pm\frac{3}{2}}(t) = 0$. This is confirmed by explicit evaluation of the trace in (6.35), if we recall that for polarised fermion spinors the spin projection is $u(P,S)\bar{u}(P,S) = (1+\gamma_5 \not{S})\,(\not{P}+M)/2$. It can also be shown that the yield of spin projection $\pm 1/2$ Δs is given by

$$\mathcal{T}^{+\frac{1}{2}\,\pm\frac{1}{2}}(t) \;=\; \frac{1}{12M_\Delta^2}\left[(M-M_\Delta)^2 - t\right]\,\left[(M+M_\Delta)^2 - t\right]^2\,(1 \pm \cos\alpha) \qquad (6.36)$$

where α is the angle between the polarisation vectors S and s. Furthermore, because the production of Δ baryons is limited to forward laboratory angles, the presence of the $(1\pm\cos\alpha)$ factor associated with the final state polarisation will significantly suppress the $s = -1/2$ yield relative to that of $s = +1/2$ final states. As will be seen in the next section when we discuss the numerical results, this suppression leads to strikingly different predictions for the polarisation asymmetry compared with those of the QPM.

6.2.3 Numerical Results and Discussion

Since the OPE contribution to the inclusive nucleon structure function peaked at $x \sim 0.05 - 0.1$ (see Fig.3.12 for example), this will be the region in which any direct pion exchange mechanism for Δ production is most likely to be visible.

The ζ-dependence of the p_T-integrated unpolarised differential cross section, $Q^2 d^3\sigma/dx dQ^2 d\zeta$, is plotted in Fig.6.11, for $x = 0.1$, $Q^2 = 4$ GeV^2 and $E = 100$ GeV. (Note the kinematic boundary at $\zeta = 1 - x$.) Clearly, the model predictions are dramatically different, with the OPE cross section being dominant at large ζ, while the quark parton models are rather more flat and tend to rise at smaller ζ (see Eq.(6.24)). Using the fragmentation functions extracted from the EMC data [225] on muon induced Δ^{++} production, the QPM model prediction is shown by the dashed curve. For estimation purposes, for the QPM calculation we use the polarised quark distributions of Carlitz & Kaur [242], with the input unpolarised distributions from Ref.[51]. For comparison, we also show the results of the fragmentation model of Bartl et al. [245], which predicts significantly smaller yields of Δ^{++} baryons. (However, in that analysis the flavour coefficients in the parameterisation of the $qq \rightarrow$ baryon fragmentation functions appear to be inconsistent with those expected from SU(3) flavour symmetry, so that this model may not be reliable.)

For the OPE model, we show in Fig.6.11 the predictions with two different form factors, namely the t-dependent dipole form factor (dotted curve), Eq.(6.33), and the p_T- and ζ-dependent form factor (solid curve) in Eq.(6.34). The two curves for each of these form factors correspond to different form factor cut-offs, namely $\Lambda_{\pi\Delta} = 700$ and 1000 MeV for the t-dependent form factor, and $\Lambda = 535$ and 675 MeV for the ζ-dependent form factor, with the cut-offs chosen to give the same value of $< n >_{\pi\Delta}$ (≈ 0.017 and 0.037, respectively). With the t-dependent form factor the cross section peaks at higher ζ, while for the ζ-dependent form it is quite a bit broader. This is consistent with the y dependence of the function $f_{\pi\Delta}(y)$ observed in Fig.3.6 for these form factors.

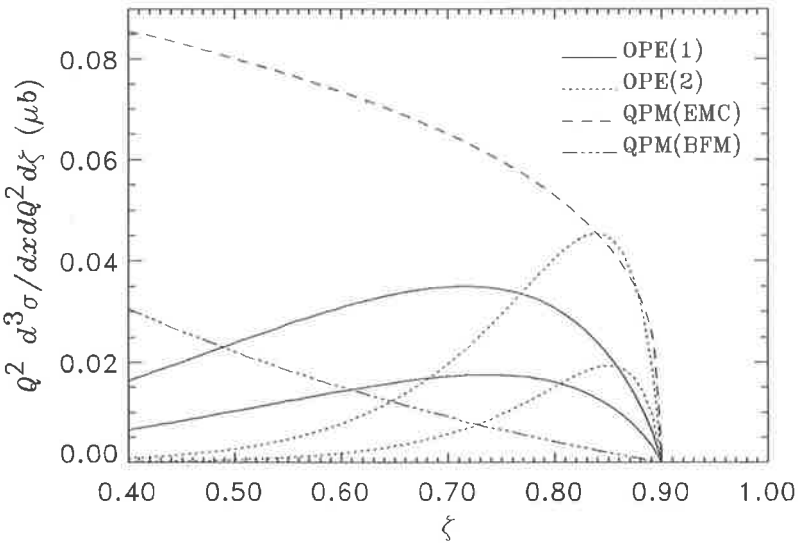

Figure 6.11: Differential cross section for leptoproduction of (unpolarised) Δ^{++}, for $x = 0.1$, $Q^2 = 4$ GeV^2 and initial lepton energy $E = 100$ GeV. OPE(1) is the one π exchange model with the ζ-dependent form factor in Eq.(6.34), with $\Lambda = 700$ (lower curve) and 1000 MeV (higher curve). OPE(2) is the π exchange model with the t-dependent form factor in Eq.(6.33), with $\Lambda_{\pi\Delta} = 535$ and 675 MeV chosen to give the same values of $< n >_{\pi\Delta}$. The QPM curves use fragmentation functions extracted from the EMC data [225], and from the model of Ref.[245].

Nevertheless, it appears that the unpolarised cross sections for both OPE curves lie below the QPM 'background' for the range of Λ considered. In such a case it would be difficult to observe the OPE contribution above this background. Of course with larger Λ the OPE cross section could be made to exceed that of the QPM, although this would bring us into conflict with the upper limits on Λ obtained in Section 3.1.4.

The predictions for the individual polarisation states of the produced Δ^{++} (for DIS from a proton with $S = +1/2$) are shown in Fig.6.12. As mentioned in Section 6.2.2, the spectrum of Δs in the OPE model is one in which the polarisations of the target proton and recoil Δ^{++} are highly correlated, and this is clearly visible in the figure (the OPE cross sections are evaluated using the form factor in Eq.(6.34) with $\Lambda = 700$ MeV). In particular, there are no $s = \pm 3/2$ states, and mostly $s = +1/2$ states. The QPM model shown in Fig.6.12 uses the fragmentation function extracted from the EMC data [225]. Note that there are no baryons with $s = -3/2$ predicted in the leading fragmentation function approximation at $z \to 1$ ($\zeta \to 1 - x$). In fact, the ratio of polarised Δs in the QPM is $s = +3/2 : +1/2 : -1/2 : -3/2 \approx 3 : 2 : 1 : 0$.

The dramatic difference between the OPE and QPM predictions for the polarised Δ spectra can be utilised by taking differences of cross sections for Δs with different polarisations. In Fig.6.13 we show the difference $\sigma^+ - \sigma^-$, where $\sigma^\pm \equiv Q^2 d^3/dxdQ^2d\zeta(s = \pm 1/2)$, for the different models (the OPE models have t- and ζ-dependent form factors, with $\Lambda_{\pi\Delta} = 535$ MeV and $\Lambda = 700$ MeV, respectively). Contrary to the situation for the unpolarised case, here the OPE cross sections are clearly discernible above the QPM background, even for the relatively small cut-offs used.

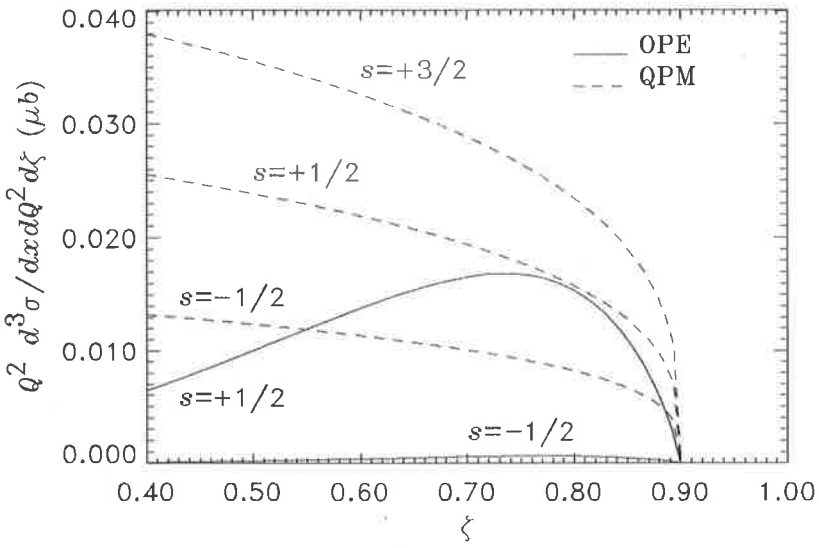

Figure 6.12: Differential leptoproduction cross section for various polarisation states of the Δ^{++}. The OPE curve is the prediction of the one π exchange model, with the form factor given in Eq.(6.34), with cut-off mass $\Lambda = 700$ MeV. The QPM curve is the quark parton model prediction with the fragmentation function extracted from the EMC data, as in Fig.6.11.

The spin asymmetry is even more dramatic when one looks at the ratio of polarisation cross sections. In Fig.6.14 the difference $\sigma^+ - \sigma^-$ is divided by the total predicted unpolarised cross section. The resulting ζ distribution is almost flat, but strikingly different for the quark model of Section 6.2.1 and the pion exchange mechanism (the latter is almost independent of the form factor, or of the cut-off mass). A measurement of this ratio would thus be particularly useful in testing the relevance of pions in the DIS process. Such experiments can in principle be performed, as all that is required is a several GeV lepton beam, of sufficiently high luminosity, and detectors capable of observing final state protons and π^+ mesons.

We may also ask whether there will be fragmentation into baryons from the hadronic debris (X) in Fig.6.10, in addition to the Δ produced at the hadronic vertex. What we know from the ideas in Section 6.2.1 is that large-ζ baryons originate from two (or more) quark systems. The CFR of the pion will be dominated by meson production. However, the TFR of the pion will also contain mostly mesons, in contrast to the TFR of baryons. Thus the only significant source of low-momentum baryons, with pion-exchange, will be from the purely hadronic vertex in Fig.6.10.

Note that we can also calculate the yield of pions resulting from the scatter off the virtual nucleon or Δ components of the physical proton, with an on-shell meson in the final state. The ζ dependence of this process would be somewhat different to the baryon recoil case, namely the peak in the cross section would occur for small ζ, so that both the TFR and CFR would be populated by such pions. As a possible extension of this work it may be useful to compare the predictions of the nucleon (or Δ) exchange process for pion production with the much more abundant data on meson leptoproduction.

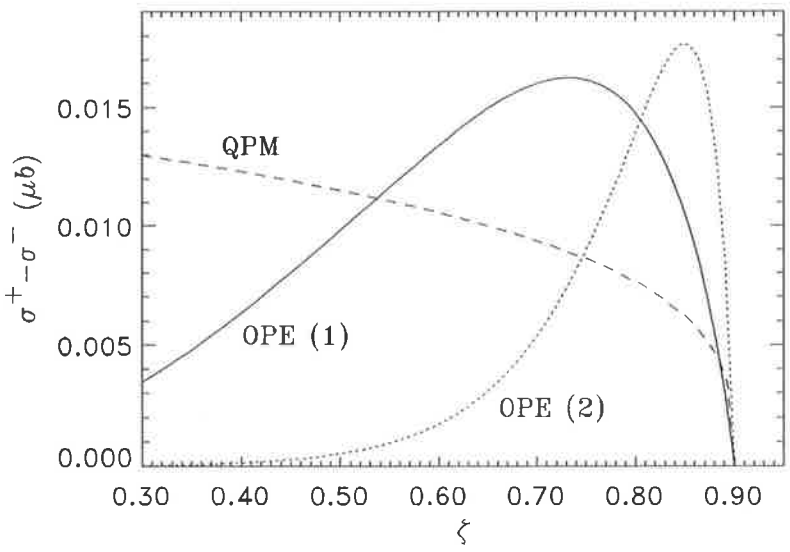

Figure 6.13: Difference between the differential cross sections $\sigma^{\pm} \equiv Q^2 d^3\sigma/dx dQ^2 d\zeta (s = \pm 1/2)$ for semi-inclusive Δ^{++} production. The OPE(1) and OPE(2) curves are as in Fig.6.11, with form factor cut-offs $\Lambda = 700$ and $\Lambda_{\pi\Delta} = 535$ MeV, respectively. The QPM curve is as in Fig.6.12.

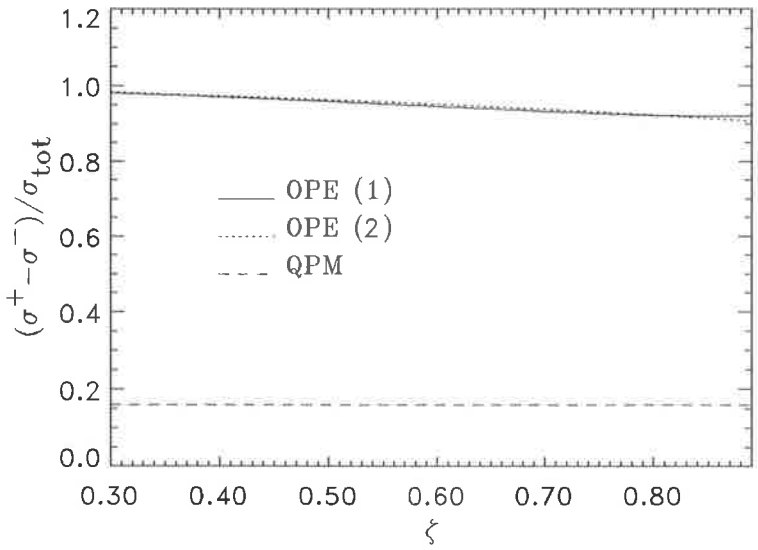

Figure 6.14: Polarisation asymmetry for semi-inclusive Δ^{++} production, with $\sigma^{\pm}$ as defined in Fig.6.13 and $\sigma_{\rm tot}$ is the sum over all polarisation states. The model curves are as in Fig.6.13.

Chapter 7

CONCLUSION AND OUTLOOK

In this thesis we have investigated aspects of the deep inelastic scattering of leptons from hadronic targets, with a view of obtaining a consistent description of the internal structure of nucleons and nuclei. In the context of QCD, deep inelastic scattering is only a partially understood process, since only the hard scattering of the photon (or W-boson) from partons can be analysed perturbatively. DIS therefore provides an opportunity to study the non-perturbative regime of QCD. Our emphasis has been on the region of intermediate momentum transfers, Q^2, where the transition takes place from hadronic to partonic variables as those appropriate to describe the strong interactions.

As a first step we would like to have an accurate description of deep inelastic scattering from nucleons, in particular to use it to probe the soft part of the interaction, between the partons and the parent nucleon. Progress in this direction has already been made by connecting quark distributions in DIS with low-energy models of the nucleon. Unfortunately, most of these models have been non-relativistic, and one would naturally like to include relativistic corrections. We have seen that a relativistic description of the nucleon quark distributions is possible if one constructs the scattering amplitude from the truncated nucleon tensor, $\widehat{W}_{\mu\nu}$, which itself can be determined from relativistic quark—nucleon vertices. At this stage it is not clear how the relativistic vertex functions can be related to the ordinary quark wavefunctions obtained from the non-relativistic models. For this reason we have used phenomenological input to parameterise the momentum dependence in the vertex functions. With a minimum of parameters (essentially the high momentum cut-offs and the spectator diquark masses) quite excellent agreement with the valence quark distribution data can be achieved.

The advantage of working with the truncated nucleon tensor is made apparent when one considers nuclear DIS. Specifically, incorporating the off-mass-shell dependence of the virtual nucleon structure functions, $\widehat{W}^i$, becomes straightforward. The only additional input necessary to completely determine the nuclear structure functions are the functions giving the four-momentum (p) dependence in the relativistic nucleon—nucleus vertices. Although relativistic calculations of nuclear structure functions have previously been attempted, these have all relied on specific on-shell approximations for the virtual nucleon tensor in order to formulate the problem in terms of the

convolution model. Within the present method, it has been possible to systematically derive the conditions under which the convolution approach could possibly be justified, and to demonstrate that in general these are not satisfied. Hence we have established that the convolution model is incompatible with the covariant formalism when the full off-shell structure of the nucleon tensor is retained. From a more general perspective, our new formalism can be seen as a positive development since it makes clear the necessity of using both quark and nuclear degrees of freedom within a single framework.

An obvious extension of this formalism would be to calculate the polarised structure functions of nucleons and nuclei. As in the spin averaged case, we would expect the factorisation (convolution) hypothesis to break down here as well. This could then have potentially significant consequences for the extraction of the polarised neutron structure function from the polarised deuterium and helium data, and to the whole argument about the proton spin.

Unfortunately, for practical applications, the relativistic nucleon—nucleus vertex functions are as yet unknown, save for the lightest nuclei like deuterium. As could be expected for the deuteron, we found that the results of the full, p^2-dependent calculation differ little from those obtained by making on-shell approximations, when the results are normalised to conserve baryon number. Of greater interest, however, and especially for understanding the nuclear EMC effect, are the off-shell corrections in heavy nuclei. An estimate of the size of the off-shell deviations was made by considering a nucleon immersed in nuclear matter. Here, the off-shell effects were parameterised in the form of an effective nucleon mass for the interacting nucleon. In addition, we found non-negligible consequences arising from final state interactions between the spectator diquarks and the nuclear medium. Combined, these effects give some 20-30% harder structure functions for interacting nucleons at $x \gtrsim 0.4$ compared with the free nucleon results.

Although we have modelled only the valence component of the nucleon (and nuclear) structure functions, it should be possible in future to extend the analysis to the sea quark sector. This will require additional model-dependent input for the sea-quark—nucleon vertex functions and for the four- (or more) quark spectator state. Alternatively, we can simply assume that the entire sea can be generated perturbatively. The only flaw in this approach is the possibility that there exists in addition an intrinsic, non-perturbative sea in the nucleon. We have investigated this component by taking a model in which part of the sea originates through interactions of the high energy probe with the extended virtual meson and baryon structure of the nucleon. This model warrants study not only as a possible source of the nucleon sea, but also for its prediction of a flavour asymmetry in the sea of the proton — a topic of much recent debate, especially since the experimental determination of the Gottfried sum rule by the NMC. Our technical treatment of this process has been to use the infinite momentum frame formulation of the the instant form of dynamics. This approach, contrary to the covariant formalism, enables the consistent use of the convolution formula, and ensures that ambiguities in the structure functions of virtual particles can be avoided.

An important parameter in this model is the relative size of the meson cloud surrounding the

nucleon. Within the limits imposed on the mesonic contributions by the experimental antiquark distributions (namely, a fairly soft meson—nucleon form factor, with a cut-off $\Lambda \approx 700$ MeV), we found that typically less than about half of the apparent discrepancy between the measured and quark parton model values for the Gottfried sum rule can be accommodated. It is likely that other mechanisms, such as Pauli blocking, do play at least as important a role in generating the flavour asymmetry. In fact, careful examination of the shape of the proton—neutron structure function difference as a function of Bjorken-x suggests the presence of both the mesonic and Pauli effects.

The inherent model-dependence in the extraction of the neutron structure function from deuteron DIS data introduces the largest uncertainty in the interpretation of the Gottfried sum rule data. Although generally small, the nuclear effects in deuterium could be magnified when one is considering differences of cross sections, especially at small x. With this in mind, we have calculated the shadowing corrections to the total virtual photon—deuteron cross section, using a model which incorporates both vector meson (which are important at low Q^2) and parton (high Q^2) degrees of freedom. We found subsequent corrections of the order of $1-2\%$ to the neutron structure function for $x \lesssim 0.01$, with the biggest uncertainty arising from the model deuteron wavefunction. Consequently, one should expect $\sim 5-10\%$ reduction of the value of the Gottfried sum rule due to shadowing. It would be quite valuable for the resolution of the question of shadowing in deuterium (and of SU(2) sea flavour symmetry) to have high quality data at smaller x on the proton structure functions from neutrino scattering, since this would enable the individual flavour distributions to be determined and the neutron structure function deduced from charge symmetry.

To check the consistency of our model of shadowing we also calculated the corrections to the structure functions of heavy nuclei at small x. Using realistic nuclear density parameters, we found good agreement of the model with the latest high-precision data from muon scattering experiments at CERN. In particular, what can be learned is that the rescattering of vector mesons plays an important role at small Q^2, where much of the small x data is taken. (Of course the approximate scaling property of shadowing at large Q^2 is accounted for by the Pomeron exchange mechanism.) A future refinement of the model may come from a better determination of the inelastic diffractive scattering cross section, parameterised in the form of the Pomeron 'structure function'. Progress in this direction is sure to be made shortly when new data at small x ($x \lesssim 10^{-4}$ at $Q^2 \sim 10$ GeV^2) from HERA becomes available.

As an extension of the present calculation, it would be useful to model the region of very small x and small Q^2 [253]. A recent Fermilab experiment [254] measured the deuteron to proton structure function ratio down to $x \approx 2 \times 10^{-5}$ (at $Q^2 \gtrsim 0.01$). Shadowing corrections to the deuteron data should therefore be estimated in this region. Also, data from the E665 Collaboration [255] observed what appeared to be saturation at very low x of the shadowing in the cross section ratio of Xe and deuterium. From the Q^2 dependence of the shadowing corrections discussed in Section 4.3 such saturation will be accommodated within the present model so long as there is a smooth extrapolation to the photoproduction limit.

In addition, the nucleon off-shell effects should also be included in the shadowing calculations. For this it will be necessary to have a relativistic description of the sea component of the nucleon structure functions, which is another reason to extend the model of Chapters 2 & 5. However, a rigorous and self-consistent treatment of the off-shell effects may be challenging if one is to use the Glauber scattering formalism, since the derivation of the multiple scattering expansion relies critically on the on-shell approximation for the bound nucleons. Also, despite the uncertainties in the model parameters, it may be useful to obtain an estimate of the effects due to meson exchange currents in heavy nuclei.

Finally, as another potentially rich source of information on the long-distance quark dynamics, we have studied the process of semi-inclusive hadron leptoproduction. In particular, we found that the fragmentation into polarised Δ^{++} baryons in the target fragmentation region offers a striking contrast between the predictions of the one-pion-exchange model, and a formulation in terms of diquark $\rightarrow$ baryon fragmentation functions. Furthermore, this reaction is experimentally feasible, and some input from our experimental colleagues in the near future would be very valuable.

Bibliography

[1] H.Yukawa, *Proc.Phys.Math.Soc.Japan* **17** (1935) 48.

[2] G.C.Wick, *Nature* **142** (1938) 993.

[3] M.Gell-Mann, *Phys.Lett.* **8** (1964) 214.

[4] G.Zweig, CERN preprint 8419/TH 412 (1964).

[5] M.Y.Han and Y.Nambu, *Phys.Rev.* **139** (1965) B1006.

[6] H.Fritzsch and M.Gell-Mann, in *Proceedings of the 16th. International Conference on High Energy Physics*, ed. J.P.Jackson and A.Roberts (National Accelerator Lab., Batavia, Illinois, 1972);

H.Fritzsch, M.Gell-Mann and H.Leutwyler, *Phys.Lett.* **B47** (1973) 365;

D.J.Gross and F.Wilczek, *Phys.Rev.* **D8** (1973) 3633;

F.J.Yndurain, *Quantum Chromodynamics* (Springer-Verlag, Berlin, 1983).

[7] H.D.Politzer, *Phys.Rev.Lett.* **30** (1973) 1346.

[8] D.J.Gross and F.Wilczek, *Phys.Rev.Lett.* **30** (1973) 1343.

[9] F.Wilczek, *Int.J.Mod.Phys.* **A8** (1993) 1359.

[10] E.D.Bloom et al., *Phys.Rev.Lett.* **23** (1969) 930;

M.Breidenbach et al., *Phys.Rev.Lett.* **23** (1969) 935.

[11] H.W.Kendall, *Rev.Mod.Phys.* **63** (1991) 597;

J.I.Friedman, H.W.Kendall and R.E.Taylor, *Rev.Mod.Phys.* **63** (1991) 629.

[12] R.P.Feynman, *Phys.Rev.Lett.* **23** (1969) 1415.

[13] J.J.Aubert et al. (EM Collaboration), *Phys.Lett.* **123B** (1983) 275.

[14] A.J.Buras, *Rev.Mod.Phys.* **52** (1980) 199.

[15] E.Eichten, I.Hinchliffe, K.Lane and C.Quigg, *Rev.Mod.Phys.* **56** (1984) 579.

[16] E.Leader and E.Predazzi, *An Introduction to Gauge Theories and the 'New Physics'* (Cambridge University Press, 1982);

F.E.Close, *An Introduction to Quarks and Partons* (Academic Press, 1979);

R.G.Roberts, *The Structure of the Proton* (Cambridge University Press, 1990).

[17] P.J.Mulders, A.W.Schreiber and H.Meyer, *Nucl.Phys.* **A549** (1992) 498.

[18] F.J.Gilman, *Phys.Rev.* **167** (1967) 1365.

[19] J.D.Bjorken, *Phys.Rev.* **148** (1966) 1467.

[20] J.D.Bjorken, *Phys.Rev.* **179** (1969) 1547.

[21] C.G.Callan,Jr. and D.J.Gross, *Phys.Rev.Lett.* **22** (1969) 156.

[22] R.P.Feynman, *Photon Hadron Interactions* (Benjamin, Reading, Massachusetts, 1972).

[23] J.D.Bjorken and E.A.Paschos, *Phys.Rev.* **185** (1969) 1975.

[24] S.D.Drell and T.M.Yan, *Ann.Phys.(New York)* **66** (1971) 578.

[25] T.Muta, *Foundations of Quantum Chromodynamics* (World Scientific, Singapore, 1987).

[26] K.Wilson, *Phys.Rev.* **179** (1969) 1499.

[27] R.A.Brandt and G.Preparata, *Nucl.Phys.* **B27** (1971) 541.

[28] O.Nachtmann, *Nucl.Phys.* **63** (1973) 237.

[29] D.J.Gross, S.B.Treiman and F.A.Wilczek, *Phys.Rev.* **D15** (1977) 2486.

[30] D.J.Gross, in *Methods in Field Theory*, Les Houches 1975, ed. R.Balin and J.Zinn-Justin (North-Holland, Amsterdam, 1976).

[31] H.Georgi and H.D.Politzer, *Phys.Rev.* **D9** (1974) 416.

[32] D.J.Gross and F.Wilczek, *Phys.Rev.* **D9** (1974) 920.

[33] E.G.Floratos, C.Kounnas and R.Lacaze, *Nucl.Phys.* **B192** (1981) 417.

[34] R.L.Jaffe, *Phys.Rev.* **D11** (1975) 1953.

[35] R.L.Jaffe and G.G.Ross, *Phys.Lett.* **93B** (1980) 313.

[36] A.Le Yaouanc, L.Oliver, O.Pène and J.C.Reynard, *Phys.Rev.* **D9** (1974) 2636.

[37] N.Cabbibo and R.Petronzio, *Nucl.Phys.* **B137** (1978) 395.

[38] A.I.Signal and A.W.Thomas, *Phys.Rev.* **D40** (1989) 2832.

[39] A.W.Schreiber, A.W.Thomas and J.T.Londergan, *Phys.Lett.* **B237** (1989) 120.

[40] C.J.Benesh and G.A.Miller, *Phys.Rev.* **D36** (1987) 1344.

[41] C.J.Benesh, T.Goldman and G.J.Stephenson, Jr., Los Alamos preprint LA-UR-93-1320 (1993).

[42] M.Glück and E.Reya, *Z.Phys.* **C43** (1989) 679.

[43] G.Altarelli and G.Parisi, *Nucl.Phys.* **126** (1977) 298.

[44] G.Parisi and R.Petronzio *Phys.Lett.* **62B** (1976) 331.

[45] V.M.Belayev and B.L.Ioffe, *Nucl.Phys.* **B310** (1988) 548.

[46] H.Meyer and P.J.Mulders, *Nucl.Phys.* **A528** (1991) 589.

[47] A.I.Signal, A.W.Schreiber and A.W.Thomas, *Mod.Phys.Lett.* **A6** (1991) 271.

[48] F.E.Close and A.W.Thomas, *Phys.Lett.* **B212** (1988) 227.

[49] M.Glück, E.Reya and A.Vogt, *Z.Phys.* **C48** (1990) 471.

[50] J.G.Morfin and W.K.Tung, *Z.Phys.* **C52** (1991) 13.

[51] J.F.Owens, *Phys.Lett.* **B266** (1991) 126.

[52] R.L.Jaffe, in *Relativistic Dynamics and Quark-Nuclear Physics*, ed. M.B.Johnson and A.Pickleseimer (Wiley, New York, 1985).

[53] G.E.Brown and M.Rho, *Phys.Lett.* **82B** (1979) 177.

[54] A.W.Thomas, *Adv.Nucl.Phys.* **13** (1984) 1.

[55] S.Theberge, G.A.Miller A.W.Thomas, *Can.J.Phys.* **60** (1982) 59.

[56] R.F.Alvarez-Estrada and A.W.Thomas, *J.Phys.* **G9** (1983) 161.

[57] J.D.Sullivan, *Phys.Rev.* **D5** (1972) 1732.

[58] A.W.Thomas, *Phys.Lett.* **126B** (1983) 97.

[59] L.L.Frankfurt, L.Mankiewicz, and M.I.Strikman, *Z.Phys.* **A334** (1989) 343.

[60] E.M.Henley and G.A.Miller, *Phys.Lett.* **B251** (1990) 497.

[61] S.Kumano and J.T.Londergan, *Phys.Rev.* **D44** (1991) 717.

[62] W.-Y.P.Hwang, J.Speth and G.E.Brown, *Z.Phys.* **A339** (1991) 383.

[63] W.Melnitchouk, A.W.Thomas and A.I.Signal, *Z.Phys.* **A340** (1991) 85.

[64] K.Gottfried, *Phys.Rev.Lett.* **18** (1967) 1174.

[65] P.Amaudruz et al. (New Muon Collaboration), *Phys.Rev.Lett.* **66** (1991) 2712.

[66] M.Lusignoli and Y.Srivastava, *Nucl.Phys.* **B138** (1978) 151.

[67] G.G.Arakelyan, K.G.Boreskov and A.B.Kaidalov, *Sov.J.Nucl.Phys.* **33** (1981) 247.

[68] M.T.Jeong and Il-T.Cheon, *Phys.Rev.* **D43** (1991) 3725.

[69] A.Szczurek and J.Speth, Jülich preprint KFA-IKP(TH)-1992-1 (1992).

[70] A.W.Thomas, *Prog.Theor.Phys.Supp.* **91** (1987) 204.

[71] S.Kumano, *Phys.Rev.* **D43** (1991) 59; 3067.

[72] W.Rarita and J.Schwinger, *Phys.Rev.* **60** (1941) 61.

[73] M.Benmerrouche, R.M.Davidson and N.C.Mukhopadhyay, *Phys.Rev.* **C39** (1989) 2339.

[74] M.Benmerrouche, private communication.

[75] V.Dmitrašinović and R.Tegen, *Phys. Rev.* **C46** (1992) 1108.

[76] E.L.Berger, F.Coester and R.B.Wiringa, *Phys.Rev.* **D29** (1984) 398.

[77] T.Hippchen, J.Haidenbauer, K Holinde and V.Mull, *Phys.Rev.* **C44** (1991) 1323.

[78] B.Kämpfer, A.I.Titov and E.L.Bratkovskaya, *Phys.Lett.* **B301** (1993) 123.

[79] A.Bodek and J.L.Ritchie, *Phys.Rev.* **D23** (1981) 1070.

[80] G.Dunne and A.W.Thomas, *Phys.Rev.* **D33** (1986) 2061.

[81] F.Güttner, G.Chanfray, H.J.Pirner and B.Povh, *Nucl.Phys.* **A429** (1984) 389.

[82] V.R.Zoller, *Z.Phys.* **C54** (1992) 425.

[83] S.Weinberg, *Phys.Rev.* **150** (1966) 1313.

[84] S.D.Drell, D.J.Levy and T.M.Yan, *Phys.Rev.* **D1** (1970) 1035.

[85] W.Melnitchouk and A.W.Thomas, *Phys.Rev.* **D47** (1993) 3794.

[86] R.Machleidt, K.Holinde and Ch.Elster, *Phys.Rep.* **149** (1987) 1.

[87] G.N.Khachatryan and Yu.G.Shakhnazaryan, *Sov.J.Nucl.Phys.* **29** (1979) 73;
G.I.Gakh and A.P.Korzh, *Ukr.J.Phys.* **26** (1981) 480.

[88] R.V.Reid, Jr., *Ann.Phys.* **50** (1968) 411.

[89] M.M.Nagels, Th.A.Rijken and J.J.de Swart, *Phys.Rev.* **12** (1975) 744.

[90] M.Lacombe et al., *Phys.Rev.* **D12** (1975) 1495;
M.Lacombe et al., *Phys.Rev.* **C21** (1980) 861;
M.Lacombe et al., *Phys.Lett.* **101B** (1981) 139.

[91] A.D.Jackson, D.O.Riska and B.Verwest, *Nucl.Phys.* **A249** (1975) 397.

[92] G.E.Brown and A.D.Jackson, *The Nucleon-Nucleon Interaction* (North-Holland, Amsterdam, 1976).

[93] S.Deister, M.F.Gari, W.Krumpelmann and M.Mahlke, *Few Body Systems* **10** (1991) 1.

[94] A.W.Thomas and K.Holinde, *Phys.Rev.Lett.* **63** (1989) 2025.

[95] K.Holinde and A.W.Thomas, *Phys.Rev.* **C42** (1990) R1195.

[96] U.G.Meissner, N.Kaiser and W.Weise, *Nucl.Phys.* **A466** (1987) 685;
C.Schuren, E.Ruiz Arriola and K.Goeke, Ruhr University preprint RUB-TPII-01-92 (1992).

[97] We thank K.Holinde for a discussion relating to this point.

[98] T.Uematsu and T.F.Walsh, *Nucl.Phys.* **B199** (1982) 93;
P.Hoodbhoy, R.L.Jaffe and A.Manohar, *Nucl.Phys.* **B312** (1989) 571;
F.E.Close and S.Kumano, *Phys.Rev.* **D42** (1990) 2377.

[99] D.Allasia et al. (BEBC Collaboration), *Z.Phys.* **C28** (1985) 321.

[100] A.I.Signal and A.W.Thomas, *Phys.Lett.* **B191** (1987) 205.

[101] B.Betev et al. (NA10 Collaboration), *Z.Phys.* **C28** (1985) 15.

[102] M.Gluck, E.Reya and A.Vogt, *Z.Phys.* **C53** (1992) 651.

[103] S.J.Brodsky and R.Blankenbecler, *Phys.Rev.* **D10** (1974) 2973;
S.J.Brodsky and G.Farrar, *Phys.Rev.Lett.* **31** (1975) 1193.

[104] P.D.B.Collins, *An Introduction to Regge Theory and High Energy Physics* (Cambridge University Press, 1977).

[105] J.Badier et al., *Phys.Lett.* **93B** (1980) 354.

[106] J.R.Bergervoet et al., *Phys.Rev.* **C41** (1990) 1435;
R.Machleidt and F.Sammarruca, *Phys.Rev.Lett.* **66** (1991) 564;
R.L.Workman, R.A.Arndt and M.M.Pavan, *Phys.Rev.Lett.* **68** (1992) 1653; 2712.

[107] R.Koch and E.Pietarinen, *Nucl.Phys.* **A336** (1980) 331.

[108] G.Hohler and E.Pietarinen, *Nucl.Phys.* **B95** (1975) 210.

[109] W.Grein and P.Kroll, *Nucl.Phys.* **A338** (1980) 332.

[110] O.Dumbrajs et al., *Nucl.Phys.* **B216** (1983) 277.

[111] P.M.M.Maessen, Th.A.Rijken and J.J.de Swart, *Phys.Rev.* **C40** (1989) 2226; B.Holzenkamp, K.Holinde and J.Speth, *Nucl.Phys.* **A500** (1989) 485.

[112] G.E.Brown and W.Wiese, *Phys.Rep.* **C22** (1975) 281.

[113] M.Diemoz, F.Ferroni, E.Longo and G.Martinelli, *Z.Phys.* **C39** (1988) 21.

[114] A.W.Schreiber, P.J.Mulders, A.I.Signal and A.W.Thomas, *Phys.Rev.* **D45** (1992) 3069.

[115] H.Abramowicz, et al. (CDHS Collaboration), *Z.Phys* **C15** (1982) 19; **C17** (1983) 1283.

[116] D.A.Ross and C.T.Sachrajda, *Nucl.Phys.* **B149** (1979) 497.

[117] R.D.Field and R.P.Feynman, *Phys.Rev.* **D15** (1977) 2590.

[118] J.F.Donoghue and E.Golowich, *Phys.Rev.* **D15** (1977) 3421.

[119] A.D.Martin, W.J.Stirling and R.G.Roberts, *Phys.Rev.* **D47** (1993) 867.

[120] B.-Q.Ma, *Phys.Lett.* **B274** (1992) 111.

[121] A.D.Martin, W.J.Stirling and R.G.Roberts, *Phys.Lett.* **B252** (1990) 653.

[122] S.Leone et al. (CDF Collaboration), presented at Rencontres de Moriond, Les Arcs, 1991, in *Moriond 1991: Electroweak*, p.13.

[123] A.S.Ito et al., *Phys.Rev.* **D23** (1981) 604.

[124] G.G.Arakelyan and K.G.Boreskov, *Sov.J.Nucl.Phys.* **41** (1985) 267.

[125] M.Ericson and A.W.Thomas, *Phys.Lett.* **148B** (1984) 191.

[126] E.J.Eichten, I.Hinchliffe and C.Quigg, *Phys.Rev.* **D47** (1993) R747.

[127] S.D.Ellis and W.J.Stirling, *Phys.Lett.* **B256** (1991) 258.

[128] S.Kumano and J.T.Londergan, *Phys.Rev.* **D46** (1992) 457.

[129] G.T.Garvey et al., *Measurement of* $\bar{d}(x)/\bar{u}(x)$ *in the Proton*, Fermilab Proposal P866.

[130] J.Levelt, P.J.Mulders and A.W.Schreiber, *Phys.Lett.* **B263** (1991) 498.

[131] M.Gronau, F.Ravndal and Y.Zarmi, *Nucl.Phys.* **B51** (1973) 611.

[132] M.Arneodo et al. (EM Collaboration) *Nucl.Phys.* **B321** (1989) 541.

[133] G.Preparata, P.G.Ratcliffe and J.Soffer, *Phys.Rev.Lett.* **66** (1991) 687.

[134] H.Walliser and G.Holzwarth, *Phys.Lett.* **B302** (1993) 377.

[135] M.R.Adams et al. (E665 Collaboration), Fermilab preprint (Sep., 1991).

[136] L.P.Kaptari and A.Yu.Umnikov, *Phys.Lett.* **B272** (1991) 359.

[137] J.Ashman et al. (EM Collaboration), *Phys.Lett.* **B202** (1988) 603;
M.Arneodo et al. (EM Collaboration), *Phys.Lett.* **B211** (1988) 493;
M.Arneodo et al. (EM Collaboration), *Nucl.Phys.* **B333** (1990) 1.

[138] P.Amaudruz et al. (NM Collaboration), *Z.Phys.* **C51** (1991) 387.

[139] N.N.Nikolaev and V.R.Zoller, *Z.Phys.* **C56** (1992) 623.

[140] B.Badelek and J.Kwiecinski, *Nucl.Phys.* **B370** (1992) 278.

[141] J.S.Bell, *Phys.Rev.Lett.* **13** (1964) 57.

[142] L.Stodolsky, *Phys.Rev.Lett.* **18** (1967) 135.

[143] R.J.Glauber, *Phys.Rev.* **100** (1955) 242.

[144] A.G.Sitenko, *Ukr.J.Phys.* **4** (1959) 152.

[145] V.N.Gribov, *JETP* **29** (1969) 483.

[146] S.J.Brodsky and J.Pumplin, *Phys.Rev.* **182** (1969) 1794.

[147] K̇.Gottfried and D.R.Yennie, *Phys.Rev.* **182** (1969) 1595.

[148] G.Grammar and J.D.Sullivan, in *Electromagnetic Interactions of Hadrons, Vol.2* ed. A.Donnachie and G.Shaw (Plenum Press, New York, 1978).

[149] V.Franco and R.J.Glauber, *Phys.Rev.* **142** (1966) 1195;

[150] T.H.Bauer, R.D.Spital, D.R.Yennie and F.M.Pipkin, *Rev.Mod.Phys.* **50** (1978) 261.

[151] A.Donnachie and G.Shaw, in *Electromagnetic Interactions of Hadrons, Vol.2* ed. A.Donnachie and G.Shaw (Plenum Press, New York, 1978).

[152] G.Schuler and T.Sjöstrand, CERN preprint CERN-TH-6796-93 (1993).

[153] R.J.M.Covolan and E.Predazzi, presented at Les Houches Winter School on Hadronic Physics with Multi-GeV Electrons, Les Houches, 1990, in *Les Houches Sch.Theo.Phys.* (1991) 199;
R.J.M.Covolan and E.Predazzi, *Nuov.Cim.* **103A** (1990) 773.

[154] D.Schildknecht, *Nucl.Phys.* **B66** (1973) 398.

[155] C.L.Bilchak, D.Schildknecht and J.D.Stroughair, *Phys.Lett.* **B214** (1988) 441.

[156] G.Piller and W.Weise, *Phys.Rev.* **C42** (1991) R1834.

[157] G.Shaw, *Phys.Rev.* **D47** (1993) R3676.

[158] N.N.Nikolaev and V.I.Zakharov, *Phys.Lett.* **55B** (1975) 397.

[159] F.E.Low, *Phys.Rev.* **D12** (1975) 163.

[160] S.Nussinov, *Phys.Rev.* **D14** (1976) 246.

[161] L.V.Gribov, E.M.Levin and M.G.Ryskin, *Phys.Rep.* **100** (1983) 1.

[162] G.Ingelman and P.E.Schlein, *Phys.Lett.* **152B** (1985) 256;
J.Bartels and G.Ingelman, *Phys.Lett.* **B235** (1990) 175.

[163] K.H.Streng, *Phys.Lett.* **166B** (1986) 443.

[164] A.Donnachie and P.V.Landshoff, *Phys.Lett.* **B185** (1987) 403;
A.Donnachie and P.V.Landshoff, *Phys.Lett.* **B191** (1987) 309.

[165] N.N.Nikolaev and B.G.Zakharov, *Z.Phys.* **C53** (1992) 331;
N.N.Nikolaev and B.G.Zakharov, *Z.Phys.* **C49** (1991) 607;
N.N.Nikolaev, Torino preprint DFTT-32/91 (1991).

[166] A.Donnachie and P.V.Landshoff, *Nucl.Phys.* **B244** (1984) 322.

[167] Particle Data Group, *Phys.Lett.* **B239** (1990) 1.

[168] P.N.Harriman, A.D.Martin, R.G.Roberts and W.J.Stirling, *Phys.Rev.* **D42** (1990) 798.

[169] V.Barone, M.Genovese, N.N.Nikolaev, E.Predazzi and B.G.Zakharov, Torino preprint DFTT-14/92 (1992).

[170] K.Goulianos, *Phys.Rep.* **101** (1983) 169.

[171] R.L.Cool et al., *Phys.Rev.Lett.* **47** (1981) 701;
T.J.Chapin et al., *Phys.Rev.* **D31** (1985) 17.

[172] A.Brandt et al., CERN preprint PPE/92-179 (1992).

[173] D.M.Alde et al. (E772 Collaboration), *Phys.Rev.Lett.* **64** (1990) 2479;
P.L.McGaughey et al. (E772 Collaboration), *Phys.Rev.Lett.* **69** (1992) 1726.

[174] J.J.Sakurai and D.Schildknecht, *Phys.Lett.* **40B** (1972) 121.

[175] J.Kwiecinski and B.Badelek, *Z.Phys.* **C43** (1989) 251.

[176] A.Donnachie and P.V.Landshoff, *Phys.Lett.* **B296** (1992) 227.

[177] V.Z.Jankus, *Phys.Rev.* **102** (1956) 1586;
M.Gourdin, *Nuov.Cim.* **28** (1963) 533.

[178] V.Franco and G.K.Varma, *Phys.Rev.* **C12** (1975) 225.

[179] L.P.Kaptari, A.I.Titov, E.L.Bratkovskaya and A.Yu.Umnikov, *Nucl.Phys.* **A512** (1990) 684;
L.P.Kaptari and A.Yu.Umnikov, *Phys.Lett.* **B259** (1991) 155.

[180] W.Melnitchouk and A.W.Thomas, *Phys.Rev.* **D47** (1993) 3783.

[181] D.Allasia et.al. (NM Collaboration), *Phys.Lett.* **B249** (1990) 366.

[182] A.H.Mueller and J.Qiu, *Nucl.Phys.* **B268** (1986) 427;
J.Qiu, *Nucl.Phys.* **B291** (1987) 746.

[183] E.L.Berger and J.Qui, *Phys.Lett.* **206B** (1988) 141;
F.E.Close, J.Qui and R.G.Roberts, *Phys.Rev.* **D40** (1989) 2820.

[184] J.Kwiecinski, A.D.Martin, W.J.Stirling and R.G.Roberts, *Phys.Rev.* **D40** (1990) 3645.

[185] L.P.Kaptari, K.Yu.Kazakov and A.Yu.Umnikov, *Phys.Lett.* **B293** (1992) 219.

[186] J.Kwiecinski and B.Badelek, *Phys.Lett.* **208** (1988) 508.

[187] L.L.Foldy and J.D.Walecka, *Ann.Phys.(N.Y.)* **54** (1969) 447.

[188] J.Kwiecinski, *Z.Phys.* **C45** (1990) 461.

[189] A.Donnachie and P.V.Landshoff, Manchester preprint M/C-TH 93/11 (1993).

[190] H.Abramowicz, E.M.Levin, A.Levy and U.Maor, *Phys.Lett.* **B269** (1991) 465.

[191] P.Amaudruz et al. (NM Collaboration), *Phys.Lett.* **B295** (1992) 159.

[192] L.Whitlow et al., *Phys.Lett.* **B282** (1992) 475.

[193] A.C.Benvenuti et al. (BCDMS Collaborations), *Phys.Lett.* **B237** (1990) 592.

[194] W.N.Cottingham and D.A.Greenwood, *An Introduction to Nuclear Physics* (Cambridge University Press, 1986).

[195] W.Melnitchouk, A.W.Schreiber and A.W.Thomas, Adelaide preprint ADP-93-210/T128, PSI-PR-93-13 (1993), submitted to *Phys.Rev.* **D**.

[196] D.Kusno and M.J.Moravcsik, *Phys.Rev.* **D20** (1979) 2734.

[197] F.E.Close, R.G.Roberts and G.G. Ross, *Phys.Lett.* **142B** (1984) 202.

[198] O.Nachtmann and H.J.Pirner, *Z.Phys.* **C21** (1984) 277.

[199] H.Jung and G.A.Miller, *Phys.Lett.* **B200** (1988) 351.

[200] K.Nakano, *Nucl.Phys.* **A511** (1990) 664.

[201] F.Gross and S.Liuti, *Phys.Rev.* **C45** (1992) 1374.

[202] M.B.Johnson and J.Speth, *Nucl.Phys.* **A470** (1987) 488.

[203] L.Heller and A.W.Thomas, *Phys.Rev.* **C41** (1990) 2756.

[204] B-Q.Ma, *Int.J.Mod.Phys.* **E1** (1993) 809.

[205] R.P.Bickerstaff and A.W.Thomas, *J.Phys.* **G15** (1989) 1523.

[206] U.Oelfke, P.U.Sauer, and F.Coester, *Nucl.Phys.* **A518** (1990) 593.

[207] R.Blankenbecler and L.F.Cook, Jr., *Phys.Rev.* **119** (1960) 1745.

[208] R.G.Arnold, C.E.Carlson and F.Gross, *Phys.Rev.* **C21** (1980) 1426.

[209] W.W.Buck and F.Gross, *Phys.Rev.* **D20** (1979) 2361.

[210] D.Allasia et al., *Z.Phys.* **C28** (1985) 321.

[211] D.Plümper and M.Gari, *Z.Phys.* **A343** (1992) 343.

[212] D.Kusno and M.J.Moravcsik, *Nucl.Phys.* **B184** (1981) 283; *Phys.Rev.* **C27** (1983) 2173.

[213] K.Nakano and S.S.M.Wong, *Nucl.Phys.* **A530** (1991) 555.

[214] B.D.Serot and J.D.Walecka, *Adv.Nucl.Phys.* **16** (1986) 1.

[215] P.A.M.Guichon, *Phys.Lett.* **B200** (1988) 235.

[216] K.Saito, A.Michels and A.W.Thomas, *Phys.Rev.* **C46** (1992) R2149;
A.W.Thomas, K.Saito and A.Michels, *Aust.J.Phys.* **46** (1993) 3.

[217] S.Fleck, W.Bentz, K.Shimizu and K.Yazaki, *Nucl.Phys.* **A510** (1990) 731.

[218] J.Ashman et al. (EM Collaboration), *Phys.Lett.* **B206** (1988) 364.

[219] R.L.Carlitz, J.C.Collins and A.H.Mueller, *Phys.Lett.* **B214** (1988) 229;
R.L.Jaffe and A.Manohar, *Nucl.Phys.* **B337** (1990) 509;
M.Takizawa and W.Weise, *Phys.Lett.* **B268** (1991) 323;
S.D.Bass, B.L.Ioffe, N.N.Nikolaev and A.W.Thomas, *J.Mosc.Phys.Soc.* **1** (1991) 317.

[220] P.V.Landshoff and J.C.Polkinghorne, *Nucl.Phys.* **B33** (1971) 221.

[221] J.Ellis, *Phys.Lett.* **35B** (1971) 537.

[222] J.D.Stack, *Phys.Rev.Lett.* **28** (1972) 57.

[223] C.J.Bebek et al., *Phys.Rev.* **D15** (1977) 3077.

[224] M.Arneodo et al. (EM Collaboration), *Phys.Let.* **B150** (1985) 458.

[225] M.Arneodo et al. (EM Collaboration), *Nucl.Phys.* **B264** (1986) 739.

[226] T.Kitagaki et al. (E745 Collaboration), *Phys.Lett.* **B214** (1988) 281.

[227] J.Guy et al. (BEBC Collaboration), *Phys.Lett.* **B229** (1989) 421.

[228] J.J.Aubert et al., *Phys.Lett.* **B123** (1983) 275.

[229] S.Kumano and F.E.Close, *Phys.Rev.* **C41** (1990) 1855.

[230] P.Castorina and A.Donnachie, *Z.Phys.* **C49** (1991) 481.

[231] T.Sloan, G.Smadja and R.Voss, *Phys.Rep.* **162** (1980) 45.

[232] C.Ishii, K.Saito and F.Takagi, *Phys.Lett.* **B216** (1989) 409.

[233] M.I.Strikman and L.L.Frankfurt, *Sov.J.Nucl.Phys.* **25** (1977) 625.

[234] G.D.Bosveld, A.E.L.Dieperink and O.Scholten, *Phys.Lett.* **B264** (1991) 11;
O.Scholten and G.D.Bosveld, *Phys.Lett.* **B265** (1991) 35.

[235] R.Renton and W.S.C.Williams, *Ann.Rev.Nucl.Part.Sci.* **31** (1981) 193.

[236] J.F.Martin et al., *Phys.Rev.* **D20** (1979) 5.

[237] A.E.Brenner et al., *Phys.Rev.* **D26** (1982) 1497.

[238] H.Ackermann et al., *Nucl.Phys.* **B120** (1977) 365.

[239] M.Aderholz et al. (WA21 Collaboration), *Phys.Lett.* **B173** (1986) 211.

[240] W.Melnitchouk, A.W.Thomas and N.N.Nikolaev, *Z.Phys.* **A342** (1992) 215.

[241] R.D.Field and R.P.Feynman, *Nucl.Phys.* **B136** (1978) 1.

[242] R.Carlitz and J.Kaur, *Phys.Rev.Lett.* **D38** (1977) 674; 1102;
J.Kaur, *Nucl.Phys.* **B128** (1977) 219.

[243] A.Schafer, *Phys.Lett.* **B208** (1988) 175.

[244] F.E.Close, *Phys.Lett.* **43B** (1973) 422.

[245] A.Bartl, H.Fraas and W.Majoretto, *Phys.Rev.* **D26** (1982) 1061.

[246] U.P.Sukhatme, K.E.Lassila and R.Orava, *Phys.Rev.* **D25** (1982) 2975.

[247] B.Andersson, G.Gustafson, G.Ingelman and T.Sjostrand, *Phys.Rep.* **97** (1983) 31.

[248] M.Fontannaz, B.Pire and D.Schiff, *Phys.Lett.* **77B** (1978) 315;
D.Beavis and B.R.Desai, *Phys.Rev.* **D23** (1981) 1967.

[249] J.F.Donoghue, *Phys.Rev.* **D17** (1978) 2922;
J.F.Donoghue, *Phys.Rev.* **D19** (1979) 2806.

[250] A.Bartl, H.Fraas and W.Majoretto, *Z.Phys.* **C6** (1980) 335;
A.Bartl, H.Fraas and W.Majoretto, *Z.Phys.* **C9** (1981) 181.

[251] I.I.Y.Bigi, *Nuov.Cim.* **41A** (1977) 43, 581.

[252] M.Lusignoli, P.Pistilli and F.Rapuano, *Nucl.Phys.* **B155** (1979) 394;
M.Lusignoli and P.Pistilli, *Nuov.Cim.Lett.* **24** (1979) 81;
N.S.Craigie and G.Schierholz, *Nucl.Phys.* **B100** (1975) 125.

[253] W.Melnitchouk and A.W.Thomas, work in progress.

[254] M.R.Adams et al. (E665 Collaboration), Fermilab preprint 93/065-E.

[255] M.R.Adams et al. (E665 Collaboration), *Phys.Rev.Lett.* **68** (1992) 3266.

LIST OF PUBLICATIONS

- W.Melnitchouk, A.W.Thomas and A.I.Signal,
Z.Phys. **A340** (1991) 85.
Gottfried Sum Rule and the Shape of $F_{2p} - F_{2n}$.

- W.Melnitchouk, A.W.Thomas and N.N.Nikolaev,
Z.Phys. **A342** (1992) 215.
Proton Production Bias in Neutrino-Hydrogen Interactions.

- W.Melnitchouk and A.W.Thomas,
Phys.Rev. **D47** (1993) 3783.
Shadowing in Deuterium.

- W.Melnitchouk and A.W.Thomas,
Phys.Rev. **D47** (1993) 3794.
Role of Vector Mesons in High-Q^2 *Lepton-Nucleon Scattering.*

- W.Melnitchouk, A.W.Schreiber and A.W.Thomas,
Adelaide preprint ADP-93-210/T128, PSI-PR-93-13, submitted to *Phys.Rev.* **D**.
Deep Inelastic Scattering From Off-Shell Nucleons.

Melnitchouk, W., Thomas, A. W. & Signal, A. I. (1991). Gottfried sum rule and the shape of F_{2p}-F_{2n}. *Zeitschrift für Physik A Hadrons and Nuclei, 340*(1), 85-92.

Melnitchouk, W., Thomas, A. W. & Nikolaev, N. N. (1992). Proton production bias in neutrino-hydrogen interactions. *Zeitschrift für Physik A Hadrons and Nuclei, 342*(2), 215-221.

Shadowing in deuterium

W. Melnitchouk and A. W. Thomas
Department of Physics and Mathematical Physics, University of Adelaide, Box 498 G.P.O., Adelaide, South Australia 5001, Australia
(Received 31 August 1992)

We calculate nuclear shadowing in lepton-deuteron deep-inelastic scattering, which arises from the double scattering of the virtual photon from both nucleons in the deuteron. The total correction to the deuteron structure function is found to be $\lesssim 1\%$ at small x, but dependent on the model deuteron wave function. The resulting increase in the corrected neutron structure function is $\sim 1-2\%$ for $x \approx 0.004$, which leads to a 4–10% decrease in the value of the Gottfried sum obtained recently by the New Muon Collaboration.

PACS number(s): 13.60.Hb, 12.40.Gg, 12.40.Vv

I. INTRODUCTION

The quark structure of the nucleon is one of the most fundamental aspects of hadron physics. Deep-inelastic scattering (DIS) of leptons from hydrogen has yielded a wealth of information on the deep-inelastic structure of the proton. However, the absence of free neutron targets has forced one to use deuterium in order to extract data on the neutron structure functions. Traditionally in DIS on the deuteron, in which the proton and neutron are held together very weakly, nuclear effects have been ignored, and the total lepton-deuteron cross section assumed to be the sum of the lepton-proton and lepton-neutron cross sections. It is the deviation from this simple relation in the region of small Bjorken x ($x \lesssim 0.1$) which is known as shadowing.

Experimentally, a deviation from linearity has been observed [1] in the so-called nuclear European Muon Collaboration (EMC) effect for the ratio of DIS cross sections (or structure functions) for lepton scattering from a nucleus and from deuterium. A dramatic decrease in the nuclear structure function per nucleon in the region of small x confirmed earlier predictions [2] that shadowing should be present in DIS. Furthermore, the shadowing was found to be only weakly dependent on Q^2. The extraction of information about the difference between nuclear structure functions and those for the free nucleon from the observed nucleus/deuterium ratios is sensitive to any nuclear effects in the deuteron. Conclusions made about nucleon parton distributions based on the nuclear/deuteron structure function ratios (e.g., for the proton antiquark distributions in the Drell-Yan process [3]) at small x may have to be modified once shadowing is taken into account.

A precise knowledge of the neutron structure function F_{2n} is essential for the determination of the Gottfried sum rule, and the corresponding resolution of the question of flavor symmetry violation in the proton sea. It is necessary therefore to check for nuclear shadowing effects in deuterium and include this correction in the extraction of F_{2n} from the deuteron structure function, F_{2D}. Some recent estimates [4,5] have suggested a significant amount of shadowing in deuterium (up to 4%) for $x \lesssim 0.1$. Other calculations [6] have predicted a less dramatic effect ($\approx 2\%$).

The cross section for lepton-deuteron DIS, Fig. 1, is related to the forward $\gamma^* D$ scattering amplitude. In the impulse approximation, Fig. 2, the virtual photon interacts with one of the nucleons in the nucleus. The double scattering diagram, Fig. 3, in which both nucleons participate in the interaction, is the origin of the shadowing in a nucleus.

II. VECTOR MESON DOMINANCE

A. Hadron-deuteron Glauber scattering

Glauber theory [7,8] for hadron-deuteron scattering gives the total hD cross section as a sum of the hN cross sections, and a screening term arising from the double scattering of both nucleons:

$$\sigma_{hD} = 2\sigma_{hN} + \delta\sigma_{hD} , \tag{1}$$

where

$$\delta\sigma_{hD} = -\frac{\sigma_{hN}^2}{8\pi^2} \int d^2\mathbf{k}_T S_D(\mathbf{k}^2) = -\frac{\sigma_{hN}^2}{4\pi} \int dk k S_D(\mathbf{k}^2) , \tag{2}$$

with $k \equiv |\mathbf{k}|$. In deriving $\delta\sigma_{hD}$, the assumption is made that the hadron-nucleon scattering amplitude $\mathcal{F}_{hN}$ is primarily imaginary, $\mathrm{Re}\mathcal{F}_{hN} \ll \mathrm{Im}\mathcal{F}_{hN}$, and approximately independent of $\mathbf{k}^2$ for small $\mathbf{k}^2$. [Contributions to $\delta\sigma_{hD}$ from large $\mathbf{k}^2$ will be suppressed by the deuteron form factor $S_D(\mathbf{k}^2)$.] Then from the forward double scattering amplitude [9]

$$\delta\mathcal{F}_{hD} = \frac{i}{2\pi|\mathbf{q}|} \int d^2\mathbf{k}_T S_D(\mathbf{k}^2) \mathcal{F}_{hp}(\mathbf{k}^2) \mathcal{F}_{hN}(\mathbf{k}^2) , \tag{3}$$

where $\mathbf{q}$ is the momentum of the projectile, Eq. (2) follows via the optical theorem:

$$\sigma = \frac{4\pi}{|\mathbf{q}|} \mathrm{Im}\mathcal{F} .$$

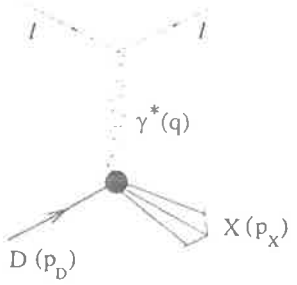

FIG. 1. Lepton-deuteron deep-inelastic scattering.

FIG. 2. Virtual photon-deuteron scattering in the impulse approximation.

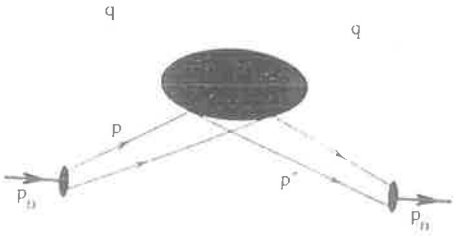

FIG. 3. Double scattering of virtual photons from the deuterons in which both nucleons take part in the interaction.

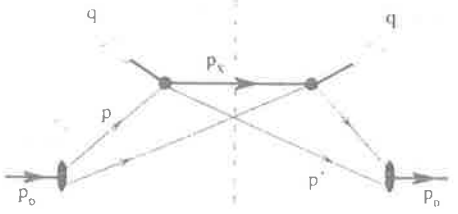

FIG. 4. Double scattering mechanism in the vector meson dominance model. The virtual photon dissociates into a vector meson which then scatters from the nucleon.

B. $\gamma^* D$ scattering

Assuming that the Glauber formalism can be applied to γ^*D scattering, the shadowing correction to the γ^*D cross section was originally calculated in terms of the vector meson dominance (VMD) model, where the virtual photon dissociates into its hadronic components (vector mesons) before interacting with the nucleon—see Fig. 4. In this model the shadowing cross section is given by [10]

$$\delta^{(V)}\sigma_{\gamma^* D}=\sum_v \frac{e^2}{f_v^2}\frac{1}{(1+Q^2/M_v^2)^2}\delta\sigma_{vD} , \tag{4}$$

where $v=\rho^0$, ω, ϕ, and the photon–vector-meson coupling constants are [11]

$$\frac{f_v^2}{4\pi}=\frac{\alpha^2 M_v}{3\Gamma_{v\to e^+e^-}} \tag{5}$$

(equal to 2.28, 26.14, and 14.91 for ρ^0, ω, and ϕ, respectively[1]). Writing (4) in terms of the deuteron structure function[2] F_{2D} we have

$$\delta^{(V)}F_{2D}(x)=\frac{Q^2}{\pi}\sum_v \frac{\delta\sigma_{vD}}{f_v^2(1+Q^2/M_v^2)^2} , \tag{6}$$

where now

$$\delta\sigma_{vD}=-\frac{\sigma_{vN}^2}{8\pi^2}\int d^2\mathbf{k}_T S_D(\mathbf{k}^2) . \tag{7}$$

The total vector meson-nucleon cross sections σ_{vN} are related to the total πN and KN cross sections via the quark model, and are set to 24 mb for $v=\rho^0$ and ω, and 14.5 mb for $v=\phi$ (see [10,12]). The deuteron form factor $S_D(\mathbf{k}^2)$ is given by the electric monopole body form factor [13]

$$S_D(\mathbf{k}^2)=\int_0^\infty dr[u^2(r)+w^2(r)]j_0(kr) , \tag{8}$$

where $u(r)$, $w(r)$ are the S, D-wave deuteron wave functions, normalized such that $\int dr[u^2(r)+w^2(r)]=1$, and where j_0 is the spherical Bessel function. The square of the three-momentum transfer to the interacting nucleon is $\mathbf{k}^2=\mathbf{k}_T^2+k_L^2$, where $k_L^2=m_N^2x^2(1+M_v^2/Q^2)^2$, and $x=Q^2/2p\cdot q$.

---

[1]Note that the fine-structure constant evaluated at $Q^2\sim 1$ GeV^2 is $\alpha=e^2/4\pi\approx 1/130$, although the error introduced by this is probably less than that associated with using f_v^2, which is obtained from the decay of meson v with timelike Q^2, for the coupling to a photon with spacelike Q^2.

[2]In terms of the total cross section for the photoabsorption of virtual photons on an unpolarized deuteron, $\sigma_{\gamma^* D}$, the deuteron structure function is

$$W_{2D}=\frac{K}{4\pi^2\alpha}\frac{Q^2}{Q^2+\nu^2}\sigma_{\gamma^* D} ,$$

where $K=\sqrt{\nu^2+Q^2}$ is the flux of incoming virtual photons (in the Gilman convention), so that in the Bjorken limit

$$F_{2D}=\frac{Q^2}{4\pi^2\alpha}\sigma_{\gamma^* D} .$$

From Eq. (6) it can be seen that the VMD shadowing correction to the deuteron structure function decreases as $1/Q^2$ for $Q^2 \to \infty$.

At $Q^2=4$ GeV^2 the VMD model shadowing predictions are given in Fig. 5 for deuteron form factors obtained from several different NN potential models. By far the largest contribution ($\approx 80\%$) to $\delta^{(V)}F_{2D}$ comes from the ρ^0 meson. The magnitude of $\delta^{(V)}F_{2D}(x)$ decreases with x because the lower limit of the k integration in Eq. (7), $k_{\min}=k_L$, is an increasing function of x, and the integrand peaks at small values of $k(\approx 0.7$ fm$^{-1})$. The model dependence arises from the differences in the large-$k(\gtrsim 2$ fm$^{-1})$ behavior of the form factor, Fig. 6, which itself is determined by the small-r behavior of $u(r), w(r)$. All of the deuteron wave functions obtained from realistic NN potential modes [namely Paris [14], Bonn [one-boson-exchange potential in q space (OBEPQ)] [15], and Bochum [16]] produce a trough in $kS_D(\mathbf{k}^2)$ at $k \approx 3.5$ fm^{-1} (because the Bessel function is negative at large kr), and a rapid falloff with k for $k \gtrsim 6$ fm^{-1}. Also shown is the model of Franco and Varma [17], which was used in [4,5], for which the form factor, parametrized by a sum of Gaussians, has no large-k tail at all. The form factor with the Paris wave function, which has the "deepest" trough, leads to $\delta^{(V)}F_{2D}$ which is $\approx 25\%$ smaller for $x \lesssim 0.01$ than with the Franco and Varma form factor. The trough is also responsible for the antishadowing in the region $x \gtrsim 0.2$.

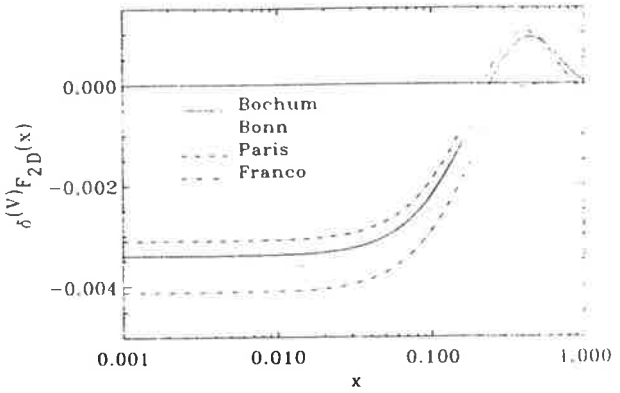

FIG. 5. VMD contribution to the total deuteron structure function at $Q^2=4$ GeV^2, for different model deuteron form factors.

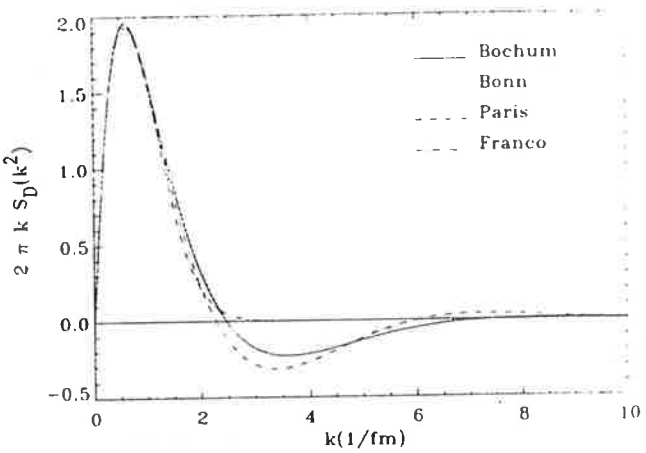

FIG. 6. Deuteron form factor, as defined by Eq. (8).

III. DIFFRACTIVE SCATTERING FROM PARTONS

At low Q^2, it is most natural to evaluate the γ^*D shadowing in terms of the VMD model. At higher energies a parton picture may be more relevant. An alternative description of the double interaction mechanism in Fig. 3 in the high-energy limit is in terms of Pomeron ($\mathcal{P}$) exchange, Fig. 7. If the momentum transfer between the photon and nucleon is small, the nucleon will most likely remain intact, in which case there will only be exchange of vacuum quantum numbers. Although there is as yet no QCD-based derivation of the properties of the reactions described by Pomeron exchange (e.g., constant hadronic cross sections), there have been suggestions [18,19,20] that the Pomeron represents a system of gluons. (In Ref. [18] hadron-hadron scattering is modeled in terms of gluon exchange between MIT bags, while in Ref. [20] gluon-ladder techniques are used to calculate deep-inelastic structure functions of hadrons at low x.)

In Fig. 7 the virtual photon probes the parton structure of the Pomeron, which is parametrized by the Pomeron structure function $F_{2\mathcal{P}}$ [21,22] (defined in terms of the cross section for γ^*-Pomeron diffraction scattering):

$$F_{2\mathcal{P}}(x) \equiv \frac{Q^2}{4\pi^2\alpha}\sigma_{\gamma^*\mathcal{P}} . \tag{9}$$

The contribution to the F_{2D} structure function from multiple diffractive scattering with $\mathcal{P}$ exchange can be written as a convolution of an exchange-$\mathcal{P}$ distribution function

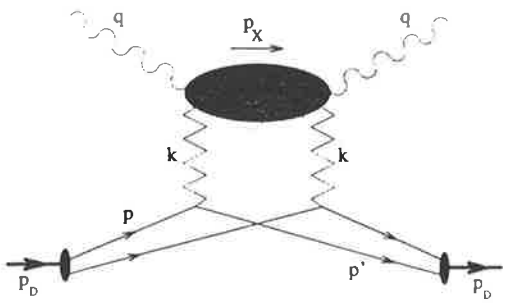

FIG. 7. Pomeron exchange contribution to the double scattering mechanism (the Pomeron is denoted by the zig zag).

$f_{\mathcal{P}}(y)$ with the $\mathcal{P}$ structure function:

$$\delta^{(\mathcal{P})}F_{2D}(x)=\int_{y_{\min}}^{2} dy\, f_{\mathcal{P}}(y)\,F_{2\mathcal{P}}(x_{\mathcal{P}})\ , \tag{10}$$

where

$$f_{\mathcal{P}}(y)=-\frac{\sigma_{pp}}{8\pi^2}\frac{1}{y}\int d^2\mathbf{k}_T S_D(\mathbf{k}^2) \tag{11}$$

is expressed as a function of the momentum fraction of the nucleon carried by the Pomeron, $y=k\cdot q/p\cdot q=x(1+M_X^2/Q^2)\approx M_X^2/s$ [$M_X^2=p_X^2, s=(p+q)^2$], and we define $x_{\mathcal{P}}\equiv x/y$. Figure 8 illustrates the y dependence of $f_{\mathcal{P}}(y)$, including the $1/y$ divergence for $y\to 0$. The rapid falloff with y is testament to the very small contribution coming from the large-y region.

In formulating a complete description of shadowing which includes more than one mechanism care must be taken to avoid possible double counting. Because of this concern some authors [6] have restricted the Pomeron exchange process to the region of M_X^2 above the highest mass of the vector mesons contributing to the VMD process: $M_X^2\geq M_{X_0}^2\simeq 1.5$ GeV^2, and consequently have taken the lower bound on the integral in Eq. (10) to be $y_{\min}=x(1+M_{X_0}^2/Q^2)$. The VMD contribution, which is essentially a higher twist ($1/Q^2$) effect, may compete with that part of the diagram in Fig. 7 which contains low-M_X single particle intermediate states. By keeping only the leading twist piece of the structure function $F_{2\mathcal{P}}$, we can exclude this contribution since it involves extra factors of $1/Q^2$ from the electromagnetic form factors. Nevertheless, we have tested the sensitivity of our numerical results to the cutoff procedure by varying $M_{X_0}^2$ from 0 to 2 GeV^2. For low x we find a difference over this range of only some 5% of the total $\mathcal{P}$ exchange contribution to F_{2D}. For larger Q^2 the separation into separate M_X regions becomes irrelevant since $y_{\min}\to x$ in the Bjorken limit.

For the Pomeron structure function we include contributions from the quark-antiquark box diagram, Fig. 9(a), and from the triple Pomeron interaction, Fig. 9(b) (see Refs. [23,24]):

$$F_{2\mathcal{P}}(x_{\mathcal{P}})=F_{2\mathcal{P}}^{(\mathrm{box})}(x_{\mathcal{P}})+F_{2\mathcal{P}}^{(3\mathcal{P})}(x_{\mathcal{P}}) \tag{12}$$

normalized such that

$$F_{2\mathcal{P}}=\left[\frac{16\pi y}{\sigma_{pp}}\right]\left.\frac{d^2F_2^{\mathrm{diff}}}{dt\,dy}\right|_{t=0}\ , \tag{13}$$

where $t\approx -\mathbf{k}^2$, and F_2^{diff} is the diffractive structure function, describing semi-inclusive diffractive lepton-nucleon DIS, in which the recoil nucleon and the hadronic state X X are separated by a large rapidity [22].

The Pomeron structure function arising from the quark box diagram, $F_{2\mathcal{P}}^{(\mathrm{box})}$, has been calculated by Donnachie and Landshoff [22]:

$$F_{2\mathcal{P}}^{(\mathrm{box})}(x_{\mathcal{P}})=\frac{(12\Sigma_{q^2}N_{\mathrm{sea}})\beta_0^2}{\sigma_{pp}}x_{\mathcal{P}}(1-x_{\mathcal{P}})\ . \tag{14}$$

The quark-Pomeron coupling constant is $\beta_0^2=3.4$ GeV^{-2}

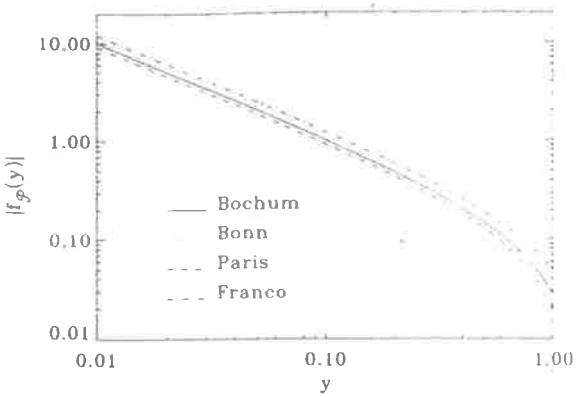

FIG. 8. Exchange-Pomeron distribution function, $|f_{\mathcal{P}}(y)|$.

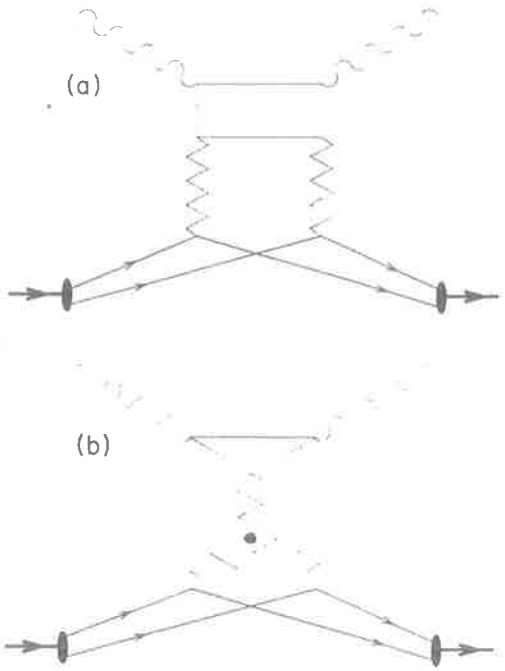

FIG. 9. (a) Quark-antiquark box contribution to the Pomeron structure function, where the Pomeron couples to the virtual photon via a quark-antiquark pair. (b) Triple Pomeron contribution to the Pomeron structure function.

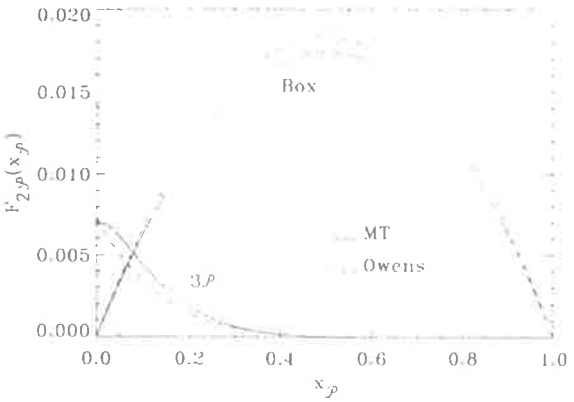

FIG. 10. $x_{\mathcal{P}}$ dependence of the "box" and $3\mathcal{P}$ contributions to $F_{2\mathcal{P}}(x_{\mathcal{P}})$ for the quark distribution function parametrizations of Owens [27] and Morfin and Tung [28] at $Q^2=4$ GeV^2.

[25], and we assume the same strength for u,d quark and antiquark-Pomeron couplings, but a weaker coupling to the strange quarks: $\Sigma_{q2}=(10+2\lambda_s)/9$ with $\lambda_s \simeq 0.5$. According to the Particle Data Group [11], the proton-proton total cross section σ_{pp} is approximately 40 mb. The parameter $N_{\rm sea}$ is determined by the $x \to 0$ behavior of the nucleon sea distribution, $xq_{\rm sea}(x \to 0) \to N_{\rm sea} x^a$. Recent parametrizations of world DIS, Drell-Yan, and prompt photon data [26,27,28] give $N_{\rm sea} \simeq 0.15$, and a approximately 0. Note that the overall normalization of the right-hand side of Eq. (14) is slightly smaller than in [6] due to our smaller sea parameter $N_{\rm sea}$ (cf. $N_{\rm sea}=0.17$ in [6]) and suppression of strange-Pomeron couplings. More recently, Nikolaev and Zakharov [24] have calculated the box diagram contribution to $F_{2\mathcal{P}}$, based on a perturbative QCD analysis of $q\bar{q}$ fluctuations of the virtual photon. The $x_{\mathcal{P}}$ dependence of their $F_{2\mathcal{P}}^{(\rm box)}$ parametrization is the same as that in Eq. (14): $M_X^2/(Q^2+M_X^2)^3$ (since $Q^2+M_X^2=Q^2/x_{\mathcal{P}}$ from the definition of $x_{\mathcal{P}}$), providing the same normalization is used (the normalizations in [22] and [24,29] differ by an overall factor $1-x_{\mathcal{P}}$).

The triple Pomeron part of the $\mathcal{P}$ structure function,

$$F_{2\mathcal{P}}^{(3\mathcal{P})}(x_{\mathcal{P}})=\frac{16\pi}{\sigma_{pp}}\left[\frac{y}{\sigma_{hp}}\frac{d^2\sigma_{hp\to hX}}{dt\,dy}\bigg|_{t=0}\right]F_{2N}^{\rm sea}(x_{\mathcal{P}},Q^2) \tag{15}$$

follows from

$$\frac{1}{F_{2N}^{\rm sea}}\frac{d^2F_2^{\rm diff}}{dt\,dy}\bigg|_{t=0}=\frac{1}{\sigma_{hp}}\frac{d^2\sigma_{hp\to hX}}{dt\,dy}\bigg|_{t=0} \tag{16}$$

and the Regge theory expression for the diffractive differential cross section [30],

$$\frac{d^2\sigma_{hp\to hX}}{dt\,dy}=\frac{\beta_{h\mathcal{P}}(t)\beta_{p\mathcal{P}}^2(t)g_{3\mathcal{P}}(t)}{16\pi}y^{1-2\alpha_{\mathcal{P}}(t)}, \tag{17}$$

where $\alpha_{\mathcal{P}}(t)\approx 1+0.25t$. In the Regge model the total hp cross section is also given in terms of the hadron-Pomeron couplings; $\beta_{h\mathcal{P}}$: $\sigma_{hp}=\beta_{h\mathcal{P}}(0)\beta_{p\mathcal{P}}(0)$. It is then evident that the combination

$$\frac{1}{\sigma_{hp}}\frac{d^2\sigma_{hp\to hX}}{dt\,dy}\bigg|_{t=0}=\frac{\beta_{p\mathcal{P}}(0)g_{3\mathcal{P}}(0)}{16\pi y} \tag{18}$$

is independent of hadron h. From experiments on the diffractive dissociation of $\pi^{\pm}$, $K^{\pm}$, p, and $\bar{p}$ on hydrogen, the triple Pomeron coupling constant was found to be $g_{3\mathcal{P}}(0)\simeq 0.364$ mb$^{1/2}$ [31], independent of t, and indeed of the hadron type h.

For the sea part of the nucleon structure function, $F_{2N}^{\rm sea}=5x[u_s+\bar{u}+d_s+\bar{d}+2(s+\bar{s})/5]/18$, we use recent parametrizations of the data at $Q^2=4$ GeV^2 [27,28]. In the calculation of Ref. [6], a constant value of 0.3 was used for $F_{2N}^{\rm sea}$ together with an empirical low-Q^2 dependence [22]. With the above triple Pomeron coupling constant, Eq. (15) gives a $3\mathcal{P}$ component which is about 40% smaller than that obtained in [4]. However, this is not very significant for the total Pomeron structure function, since $F_{2\mathcal{P}}^{(3\mathcal{P})}$ is very much smaller than the quark-antiquark "box" contribution $F_{2\mathcal{P}}^{(\rm box)}$, Fig. 10.

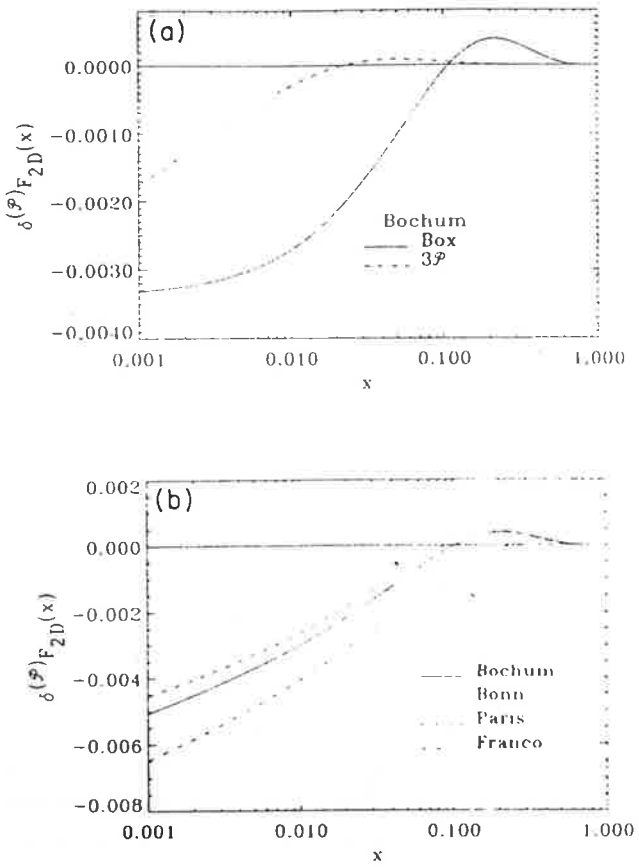

FIG. 11. (a) Quark-antiquark box and $3\mathcal{P}$ contributions to the total deuteron structure function. The deuteron form factor is given by the Bochum model wave function. (b) Deuteron form-factor dependence of the Pomeron exchange contribution to the deuteron structure function.

The scaling behavior of the $\mathcal{P}$-exchange mechanism is determined by the scaling behavior of the $\mathcal{P}$ structure function, and from Eqs. (14)–(18) it is clear that $\delta^{(\mathcal{P})}F_{2D}$ will scale as $Q^2 \to \infty$. At $Q^2=4$ GeV^2, Fig. 11(a) shows the individual "box" and $3\mathcal{P}$ contributions to $\delta^{(\mathcal{P})}F_{2D}$, with the deuteron form factor obtained from the Bochum wave function. The dependence of $\delta^{(\mathcal{P})}F_{2D}$ on $S_D(\mathbf{k}^2)$ is illustrated in Fig. 11(b). Again, as in the case of the VMD model, the large-k negative tail of the form factor produces a large (some 30–40%) difference between different models for $x \lesssim 0.05$. For $x \gtrsim 0.2$ the presence or absence of antishadowing will be determined by the model deuteron wave function.

IV. SHADOWING BY MESONS

Another potential source of shadowing arising from the double scattering mechanism is one which involves the exchange of mesons, Fig. 12. It has previously been suggested [32] that this leads to substantial antishadowing corrections to $F_{2D}(x)$. The total contribution to the

deuteron structure function from meson exchange is written

$$\delta^{(M)}F_{2D}(x)=\sum_{\mu}\int_{x}^{m_D/m_N}dy\ f_\mu(y)\ F_{2\mu}(x_\mu)\ , \qquad (19)$$

where $\mu=\pi,\rho,\omega,\sigma$, $y=k\cdot q/p\cdot q=(k_0+k_L)/m_N$ and $x_\mu=x/y$. For the virtual meson structure function $F_{2\mu}$ we take the parametrization of the (real) pion structure function from Drell-Yan production [33]. The exchange-meson distribution functions $f_\mu(y)$ are obtained from the nonrelativistic reduction of the nucleon-meson interaction:

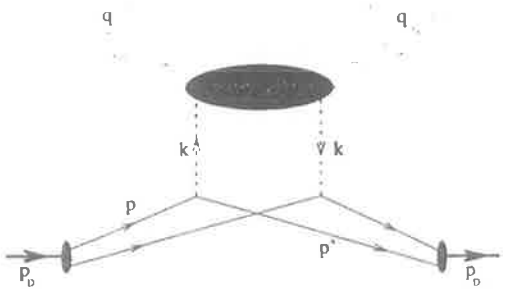

FIG. 12. Double scattering mechanism with meson exchange. The dotted line represents mesons π, ρ, ω, σ.

$$f_\mu(y)=4c_\mu m_N\int\frac{d^3\mathbf{p}\,d^3\mathbf{p}'}{(2\pi)^3}\frac{\mathcal{F}^2_{\mu NN}(k^2)}{(k^2-m_\mu^2)^2}y\left\{\frac{1}{3}\sum_{J_z}\Psi^\dagger(\mathbf{p},J_z)\mathcal{V}_{\mu NN}\Psi(\mathbf{p}',J_z)\right\}\delta\left[y-\frac{k_0+k_L}{m_N}\right]. \qquad (20)$$

The deuteron wave function is defined by

$$\Psi(\mathbf{p},J_z)=\frac{1}{\sqrt{4\pi}}\left[u(p)-w(p)\frac{S_{12}(\hat{p})}{\sqrt{8}}\right]\chi_1^{J_z}\ , \qquad (21)$$

where $u(p)$ and $w(p)$ are its S- and D-wave components, normalized so that $\int dp\,p^2[u^2(p)+w^2(p)]=1$, with $\hat{p}\equiv\mathbf{p}/p$ and $p\equiv|\mathbf{p}|$, and S_{12} is the tensor operator: $S_{12}(\hat{p})=3\sigma_1\cdot\hat{p}\,\sigma_1\cdot\hat{p}-\sigma_1\cdot\sigma_2$. The deuteron spin wave function is denoted by $\chi_1^{J_z}$, where J_z is the total angular momentum projection. In Eq. (20), $k^2=k_0^2-\mathbf{k}^2$, where $k_0=m_D-\sqrt{m_N^2+\mathbf{p}^2}-\sqrt{m_N^2+\mathbf{p}'^2}$ is the energy of the off-shell meson, and $\mathbf{k}=\mathbf{p}-\mathbf{p}'$ is its 3-momentum. The nucleon-meson interactions are given by [15]

$$\mathcal{V}_{\pi NN}=-\frac{f^2_{\pi NN}}{m_\pi^2}\sigma_1\cdot\mathbf{k}\ \sigma_2\cdot\mathbf{k}\ , \qquad (22)$$

$$\mathcal{V}_{\rho NN}=g^2_{\rho NN}\left[1+\frac{3q^2}{2m_N^2}-\frac{\mathbf{k}^2}{8m_N^2}-\sigma_1\cdot\sigma_2\frac{\mathbf{k}^2}{4m_N^2}+\frac{\sigma_1\cdot\mathbf{k}\,\sigma_2\cdot\mathbf{k}}{4m_N^2}\right]+\frac{g_{\rho NN}f_{\rho NN}}{2m_N}\left[-\frac{\mathbf{k}^2}{m_N}-\sigma_1\cdot\sigma_2\frac{\mathbf{k}^2}{m_N}+\frac{\sigma_1\cdot\mathbf{k}\,\sigma_2\cdot\mathbf{k}}{m_N}\right] \qquad (23)$$

$$+\frac{f^2_{\rho NN}}{4m_N^2}[-\sigma_1\cdot\sigma_2\mathbf{k}^2+\sigma_1\cdot\mathbf{k}\,\sigma_2\cdot\mathbf{k}]\ ,$$

$$\mathcal{V}_{\omega NN}=g^2_{\omega NN}\left[1+\frac{3q^2}{2m_N^2}-\frac{\mathbf{k}^2}{8m_N^2}-\sigma_1\cdot\sigma_2\frac{\mathbf{k}^2}{4m_N^2}+\frac{\sigma_1\cdot\mathbf{k}\,\sigma_2\cdot\mathbf{k}}{4m_N^2}\right], \qquad (24)$$

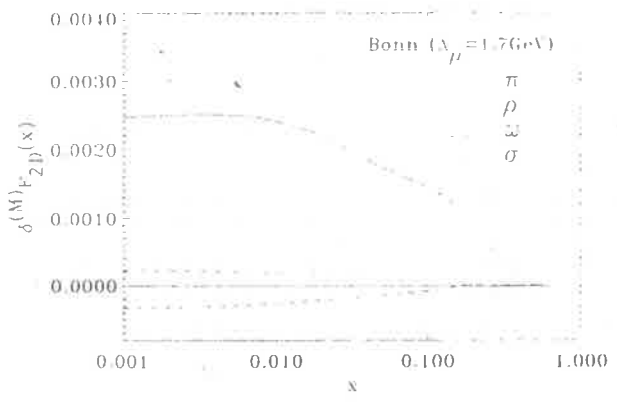

FIG. 13. Individual meson exchange contributions to the deuteron structure function, for the wave function of the Bonn (OBEPQ) model with a universal form-factor cutoff $\Lambda_\mu=1.7$ GeV. Note the mass of the effective σ meson is ≈ 800 MeV.

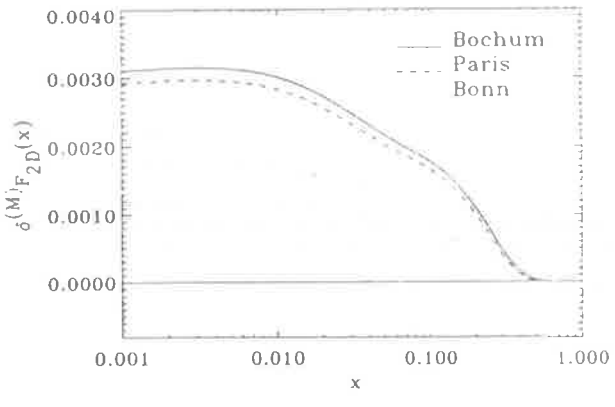

FIG. 14. Deuteron wave function and μNN form-factor dependence of the total meson exchange correction. The Bochum (solid) and Paris (dashed) curves are evaluated with $\Lambda_\mu=1.3$ GeV, while the Bonn (dotted) curves have $\Lambda_\mu=1.0$, 1.3, and 1.7 GeV, with the larger cutoff giving more overall antishadowing.

$$\mathcal{V}_{\sigma NN}=-g^2_{\sigma NN}\left[1-\frac{\mathbf{q}^2}{2m_N^2}+\frac{\mathbf{k}^2}{8m_N^2}\right], \tag{25}$$

Evaluation of Eq. (20) requires the identities

$$\frac{1}{3}\sum_{J_z}\Psi^\dagger(\mathbf{p},J_z)\Psi(\mathbf{p}',J_z)=\frac{1}{4\pi}[u(p)u(p')+w(p)w(p')P_2(\cos\theta)P_2(\cos\theta')]+\phi\text{-dependent terms}$$
$$=\frac{1}{3}\sum_{J_z}\Psi^\dagger(\mathbf{p},J_z)\sigma_1\cdot\sigma_2\Psi(\mathbf{p}',J_z)\,, \tag{26}$$

$$\frac{1}{3}\sum_{J_z}\Psi^\dagger(\mathbf{p},J_z)\sigma_1\cdot\mathbf{k}\sigma_2\cdot\mathbf{k}\Psi(\mathbf{p}',J_z)$$
$$=\frac{1}{4\pi}\left\{\frac{1}{3}[\mathbf{k}^2-2pp'\sin\theta\sin\theta']u(p)u(p')\right.$$
$$-\frac{1}{\sqrt{2}}\left[4pp'\cos\theta\cos\theta'\sin^2\theta'+4\mathbf{p}'^2\cos^2\theta'\sin^2\theta'-\frac{2}{3}(\mathbf{p}^2+\mathbf{p}'^2)P_2(\cos\theta')\right.$$
$$\left.+2(\mathbf{p}^2\cos^2\theta+\mathbf{p}'^2\cos^2\theta')P_2(\cos\theta')+\frac{8}{3}pp'\cos\theta\cos\theta'P_2(\cos\theta')\right]u(p)w(p')$$
$$-\frac{1}{\sqrt{2}}\left[4p'p\cos\theta'\cos\theta\sin^2\theta+4\mathbf{p}^2\cos^2\theta\sin^2\theta-\frac{2}{3}(\mathbf{p}'^2+\mathbf{p}^2)P_2(\cos\theta)+2(\mathbf{p}'^2\cos^2\theta'+\mathbf{p}^2\cos^2\theta)P_2(\cos\theta)\right.$$
$$\left.+\frac{8}{3}p'p\cos\theta'\cos\theta P_2(\cos\theta)\right]w(p)u(p')$$
$$-\frac{1}{3}\left[(p\cos\theta+p'\cos\theta')^2P_2(\cos\theta)P_2(\cos\theta')-2(\mathbf{p}^2\sin^2\theta+\mathbf{p}'^2\sin^2\theta')P_2(\cos\theta)P_2(\cos\theta')\right.$$
$$+3(\mathbf{p}^2\cos^2\theta\sin^2\theta+pp'\cos\theta\cos\theta'\sin^2\theta)P_2(\cos\theta')+3(\mathbf{p}'^2\cos^2\theta'\sin^2\theta'+p'p\cos\theta'\cos\theta\sin^2\theta')P_2(\cos\theta)$$
$$\left.\left.+\frac{9}{2}pp'\cos\theta\cos\theta'\sin^2\theta\sin^2\theta'\right]w(p)w(p')\right\}+\phi\text{ dependent terms}\,. \tag{27}$$

The terms in Eqs. (26) and (27) which depend on the azimuthal angle (ϕ) vanish after integration. The factors c_μ are due to isospin: $c_\pi=c_\rho=3$, $c_\omega=c_\sigma=-1$. The μNN vertex form factors $\mathcal{F}_{\mu NN}(k^2)$ are parametrized by a dipole form

$$\mathcal{F}_{\mu NN}(k^2)=\left[\frac{\Lambda_\mu^2-m_\mu^2}{\Lambda_\mu^2-k^2}\right]^2, \tag{28}$$

with the high-momentum cutoffs Λ_μ ranging from ~ 1 GeV in models with soft form factors [34,16] to $\sim 1.7-2$ GeV when hard form factors are employed [15].

Figure 13 shows the individual meson exchange contributions to $\delta^{(M)}F_{2D}$, for the wave function of the Bonn model, and with a universal dipole cutoff of $\Lambda_\mu=1.7$ GeV. As could be expected, pion exchange is the dominant process. We also include the fictitious σ meson, but with a mass (≈ 800 MeV) that is larger than that used to represent 2π exchange in NN scattering. Both of these produce antishadowing for small x. The exchange of vector mesons (ρ,ω) cancels some of this antishadowing, although the magnitude of these contributions is smaller. In fact, for $\Lambda_\mu \lesssim 1.3$ GeV all contributions other than that of the pion are totally negligible.

Figure 14 shows the dependence of the total $\delta^{(M)}F_{2D}$ on Λ_μ for the Bonn model wave function. There is approximately a factor of 2 difference between the amount of shadowing with soft ($\Lambda_\mu=1$ GeV, lower dotted line) and hard ($\Lambda_\mu=1.7$ GeV, upper dotted line) form factors. In lepton-nucleon DIS it is well known [35] that the meson cloud of the nucleon, with a hard μNN form factor, gives nucleon sea distributions that are several times larger than the empirical ones. In fact, to be consistent with the lepton-nucleon DIS data Λ_μ must be $\lesssim 0.8-0.9$ GeV. We also consider the effect of the model momentum-space deuteron wave function on $\delta^{(M)}F_{2D}$. Although the model wave functions differ substantially at large momenta ($p \gtrsim 2$ fm^{-1}), this variation will be largely suppressed by the μNN form factor. The Bochum and Paris wave functions are generally larger than the Bonn wave function, and this is reflected in a larger $\delta^{(M)}F_{2D}$.

We also comment here on the issue raised in the previous section, namely, double counting, this time between the meson exchange and the other mechanisms. It should be clear that since the $\mathcal{P}$ contribution involves the exchange of vacuum quantum numbers, there will be no interference between this and the exchange of pseudoscalar pions or vector mesons. The scalar σ meson, introduced as an effective description of two-pion $N\Delta$ excitations, does not correspond to actual exchange of a spin-0 particle. By restricting the meson structure function to only the leading twist component (our F_{2M} is determined

at $Q^2=25$ GeV^2 where this assumption is reasonable) we may view the VMD process as a description of higher twist effects. Still, imposing any low-M_X cut on the meson exchange term has numerically insignificant consequences, largely because $F_{2\mu}(x/y)\to 0$ as $y\to x$.

V. COMBINED SHADOWING EFFECTS AND THE GOTTFRIED SUM RULE

The total deuteron structure function is defined by

$$F_{2D}(x)=F_{2p}(x)+F_{2n}(x)+\delta F_{2D}(x)\ , \tag{29}$$

where the shadowing correction is a sum of the VMD, Pomeron, and meson exchange contributions:

$$\delta F_{2D}(x)=\delta^{(V)}F_{2D}(x)+\delta^{(\mathcal{P})}F_{2D}(x)+\delta^{(M)}F_{2D}(x)\ . \tag{30}$$

In Fig. 15 we compare the contributions to $\delta F_{2D}(x)$ from the three mechanisms considered. For $x\lesssim 0.1$ the magnitude of the (negative) Pomeron/VMD shadowing is larger than the (positive) meson-exchange contribution, so that the total δF_{2D} is negative. The fact that shadowing is present in this region of x does not depend on the model deuteron wave function. For larger $x(\approx 0.1-0.2)$ there is a small amount of antishadowing, which is due mainly to the VMD contribution. The dependence of the total shadowing correction on the deuteron wave function and on the μNN form factor is shown in Fig. 16 for $Q^2=4$ GeV^2. We point out that the magnitude of $\delta F_{2D}(x)$ is about 4 times smaller than that obtained in Ref. [4], and about 2 times smaller compared with the result of Ref. [6]. The most important reasons for our smaller results are the inclusion of meson exchange contributions which produce antishadowing at small x, and the use of realistic deuteron wave functions which lead to smaller $\mathcal{P}$ exchange and VMD contributions.

Recently the New Muon Collaboration (NMC) has measured F_{2p} and F_{2D} [36,37] down to very small values of $x(=x_{\min}=0.004)$. The neutron structure function was then extracted from F_{2D} in order to test the Gottfried sum rule [38]. However, by assuming that

$$\frac{F_{2D}(1-(F_{2D}/F_{2p}-1))}{1+(F_{2D}/F_{2p}-1)}=2F_{2p}-F_{2D}\equiv(F_{2p}-F_{2n})_{\rm NMC} \tag{31}$$

the NMC ignored any nuclear shadowing effects in D which may alter the F_{2n} values. The actual difference between the p and n structure functions should be

$$F_{2p}-F_{2n}=(F_{2p}-F_{2n})_{\rm NMC}+\delta F_{2D}\ , \tag{32}$$

and this is shown in Fig. 17. The dotted line is a best fit to the NMC data, and includes the small-x extrapolation used in [37]:

$$F_{2p}(x)-F_{2n}(x)\underset{x\to 0}{\sim}\alpha x^{\beta} \tag{33}$$

with $\alpha=0.21$, $\beta=0.62$. The other curves include the shadowing corrections to the NMC data parametrization. It is not clear whether $F_{2p}-F_{2n}$ will become negative at $x\lesssim 0.004$, and it will be interesting to see whether this crossover occurs when additional data at smaller x become available.

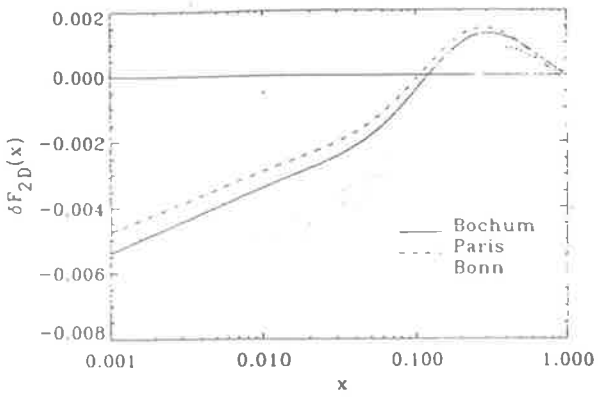

FIG. 16. Deuteron wave function and μNN form-factor dependence of the total shadowing correction. For the Bochum and Paris curves $\Lambda_\mu=1.3$ GeV, while the Bonn curves are calculated with $\Lambda_\mu=1.0$, 1.3, and 1.7 GeV, with the larger cutoff giving less overall shadowing.

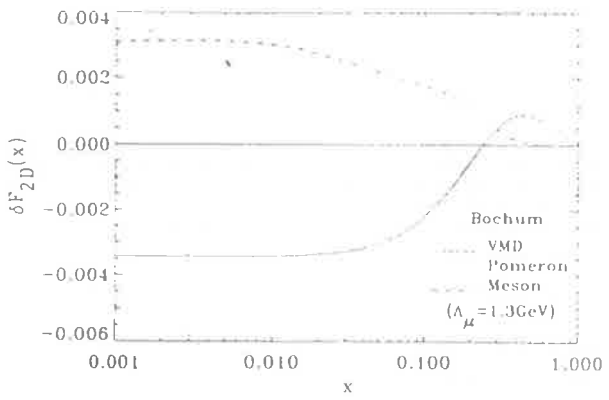

FIG. 15. Comparison between the VMD, Pomeron, and meson exchange corrections to the deuteron structure function at $Q^2=4$ GeV^2 (for the Bochum wave function, and a form factor cutoff $\Lambda_\mu=1.3$ GeV for the meson exchange process).

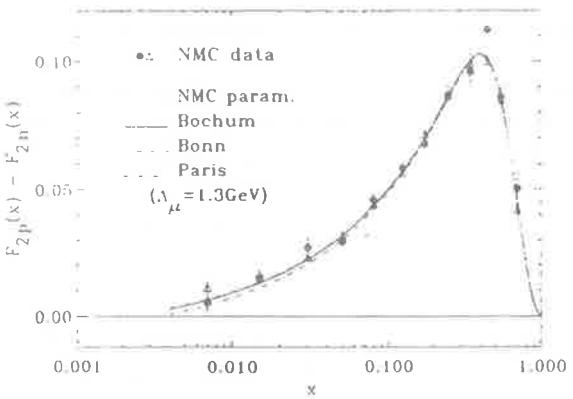

FIG. 17. Difference between the proton and neutron structure functions, with shadowing corrections to the NMC data at $Q^2=4$ GeV.^{2}

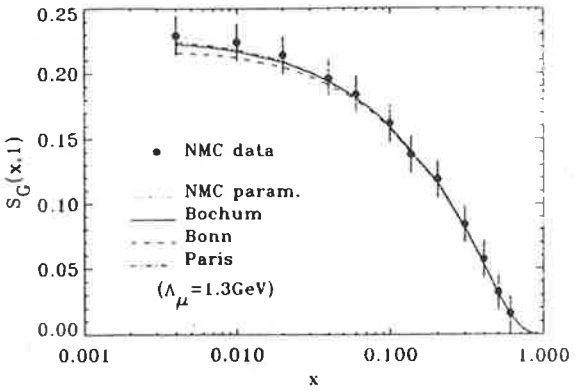

FIG. 18. Gottfried sum, with shadowing corrections to the NMC data.

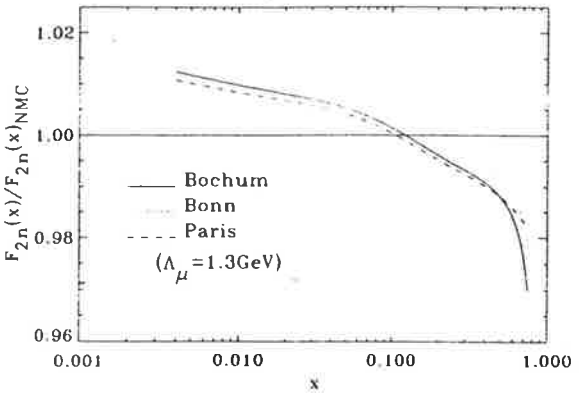

FIG. 19. Neutron structure function ratio, with and without shadowing corrections (at $Q^2=4$ GeV^2).

The Gottfried integral

$$S_G(x,1)=\int_x^1 dx'\frac{F_{2p}(x')-F_{2n}(x')}{x'}$$
$$=\int_{x'=x}^1 d(\ln x')[F_{2p}(x')-F_{2n}(x')] \qquad (34)$$

is given in Fig. 18 for x down to 0.004. In the naive quark model, $S_G(0,1)=1/3$. Ignoring nuclear effects, the NMC obtained $S_G(x_{\min},1)=0.229$. From the unmeasured region ($x<0.004$), using the above extrapolation, the contribution was found to be $S_G(0,x_{\min})=(\alpha/\beta)x_{\min}^{\beta}=0.011$. With the conventional Regge theory assumption that $\beta=0.5$, $S_G(0,x_{\min})$ would be 0.014. In Table I we give the values of S_G including shadowing corrections, and also the $x<x_{\min}$ extrapolation parameters. For simplicity we take $\beta=0.5$, and adjust α to achieve a smooth transition between the $x>x_{\min}$ and $x<x_{\min}$ regions. The overall correction to the NMC value for $S_G(0,1)$ is found to be between -0.010 and -0.026. This is to be compared with -0.07 to -0.088 obtained in [4,5,29].

As a fraction of the total $F_{2D}(x)$ [37], the shadowing correction amounts to (0.5–1.0 %,0.4–0.8 %, 0.0–0.3 %) at $x=(0.004,0.01,0.1)$, while the antishadowing is less than 0.2% of F_{2D} at $x\approx 0.2$.

In Fig. 19 we show the ratio of neutron structure functions with and without shadowing corrections:

$$\frac{F_{2n}}{(F_{2n})_{NMC}}=1-\frac{\delta F_{2D}}{F_{2D}}\left[\frac{1+(F_{2n}/F_{2p})_{NMC}}{(F_{2n}/F_{2p})_{NMC}}\right], \qquad (35)$$

where the NMC neutron/proton ratio was defined as $(F_{2n}/F_{2p})_{NMC}\equiv F_{2D}/F_{2n}-1$. There is an overall 1–2 % increase in the neutron structure function due to shadowing for $x\lesssim 0.01$.

Finally, we illustrate in Fig. 20 the dependence upon Q^2 of the total shadowing correction $\delta F_{2D}(x,Q^2)$. As expected, the VMD term vanishes rapidly with increasing Q^2, leaving the two scaling contributions from $\mathcal{P}$ and meson exchange to largely cancel each other for $Q^2\simeq 25$ GeV^2. However, we should add a note of caution about comparing shadowing corrections at very large values of Q^2. In the parton recombination model [2,39,40] the fusion of quarks and gluons from different nucleons introduces additional terms [39] in the Altarelli-Parisi equations governing the QCD evolution of the parton distributions. At very small x and large Q^2, such as those attainable at energies reached at the DESY ep collider HERA, this can lead to significant corrections [6] to the $\delta F_{2D}(x,Q^2)$ evolved without these terms, although the exact magnitude of these is sensitive to the small-x behavior of the input nucleon gluon distribution. For the moderate range of Q^2 and not too low x values in Fig. 20, however, we expect the indicated Q^2 behavior to be reliable.

VI. CONCLUSION

In summary, we have estimated the nuclear shadowing in lepton-deuteron DIS from the double scattering mechanism in Fig. 3. Our approach is similar to that of Refs. [5] and [6], in describing the interaction in terms of the

TABLE I. Small-x extrapolation parameters for $F_{2p}-F_{2n}(=\alpha x^{\beta})$ and the contributions to the Gottfried sum from different x regions.

Model	α	β	$S_G(0,x_{\min})$	$S_G(x_{\min},1)$	$S_G(0,1)$
NMC [37]	0.21	0.62	0.011	0.229	0.240±0.016
	0.109	0.5	0.014		0.243
Bochum (Λ_μ=1.3 GeV)	0.043	0.5	0.005	0.222	0.227
Paris (Λ_μ=1.3 GeV)	0.052	0.5	0.007	0.224	0.230
Bonn (Λ_μ=1.3 GeV)	0.011	0.5	0.001	0.215	0.217
Bonn (Λ_μ=1.0 GeV)	0.002	0.5	0.000	0.214	0.214
Bonn (Λ_μ=1.7 GeV)	0.019	0.5	0.002	0.217	0.219

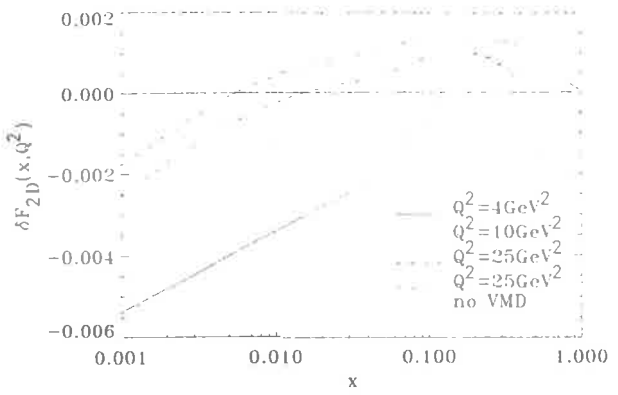

FIG. 20. Q^2 dependence of the total shadowing correction to F_{2D}. Curves represent the shadowing corrections at 4, 10, and 25 GeV^2, with the Bochum model wave function and with $\Lambda=1.3$ GeV. Also shown is the correction at $Q^2=25$ GeV^2 without the VMD contribution.

VMD model, together with Pomeron ($\mathcal{P}$) exchange. However we have also included contributions from the exchange of mesons which effectively cancel as much as half of the shadowing from the VMD/$\mathcal{P}$-exchange mechanisms alone. Numerically, there is some dependence on the model deuteron wave function, and also on the meson-nucleon form factor for the meson-exchange process. The net effect is a $\lesssim 1\%$ reduction of F_{2D} for $x\sim 0.004$, or equivalently a $\lesssim 2\%$ increase in the neutron structure function over the uncorrected F_{2n}. Consequently, the shadowing correction to the Gottfried sum $S_G(0,1)$ is between -0.010 and -0.026 (or about 4 and 10% of the NMC value), which is about 5 times smaller than in previous estimates.

To accurately test the descriptions of shadowing in the deuteron it is necessary to obtain model-independent information on the neutron structure function at low x. Even at HERA energies this is not possible with electron scattering alone. However, when combined with high-precision data from neutrino-proton experiments the individual flavor distributions can be determined, and the neutron structure function inferred from charge symmetry. For this to happen, however, the statistics on the neutrino data need to be improved, and the range extended into the smaller-x region.

ACKNOWLEDGMENTS

We would like to thank M. Gari, J. Haidenbauer, B. Loiseau, and N. Nikolaev for helpful discussions. This work was supported by the Australian Research Council.

[1] EMC, J. Ashman *et al.*, Phys. Lett. B **202**, 603 (1988); EMC, M. Arneodo *et al.*, *ibid.* **211**, 493 (1988).
[2] N. N. Nikolaev and V. I. Zakharov, Phys. Lett. **55B**, 397 (1975).
[3] E772 Collaboration, D. M. Alde *et al.*, Phys. Rev. Lett. **64**, 2479 (1990); E772 Collaboration, P. L. McGaughey *et al.*, *ibid.* **69**, 1726 (1992).
[4] V. R. Zoller, Z. Phys. C **54**, 425 (1992).
[5] N. N. Nikolaev and V. R. Zoller, Z. Phys. C **56**, 623 (1992).
[6] B. Badelek and J. Kwiecinski, Nucl. Phys. **B370**, 278 (1992).
[7] R. J. Glauber, Phys. Rev. **100**, 242 (1955).
[8] V. N. Gribov, Zh. Eksp. Teor. Fiz. **56**, 892 (1969) [Sov. Phys. JETP **29**, 483 (1969)].
[9] V. Franco and R. J. Glauber, Phys. Rev. **142**, 1195 (1966); E. S. Abers, H. Burkhardt, V. L. Teplitz, and C. Wilkin, Nuovo Cimento **42**, 365 (1966).
[10] J. J. Sakurai and D. Schildknecht, Phys. Lett. **40B**, 121 (1972); T. H. Bauer, R. D. Spital, D. R. Yennie, and F. M. Pipkin, Rev. Mod. Phys. **50**, 261 (1978).
[11] Particle Data Group, J. J. Hernández *et al.*, Phys. Lett. B **239**, 1 (1990).
[12] J. Kwiecinski and B. Badelek, Z. Phys. C **43**, 251 (1989).
[13] V. Z. Jankus, Phys. Rev. **102**, 1586 (1956); M. Gourdin, Nuovo Cimento **28**, 533 (1963).
[14] A. Lacombe *et al.*, Phys. Rev. C **21**, 861 (1980); M. Lacombe *et al.*, Phys. Lett. **101B**, 139 (1981).
[15] R. Machleidt, K. Holinde, and Ch. Elster, Phys. Rep. **149**, 1 (1987).
[16] S. Deister, M. F. Gari, W. Krumpelmann, and M. Mahlke, Few-Body Systems **10**, 1 (1991); D. Pluemper and M. Gari, Z. Phys. A **343**, 343 (1992).
[17] V. Franco and G. K. Varma, Phys. Rev. C **12**, 225 (1975).
[18] F. E. Low, Phys. Rev. D **12**, 163 (1975).
[19] S. Nussinov, Phys. Rev. D **14**, 246 (1976).
[20] L. V. Gribov, E. M. Levin, and M. G. Ryskin, Phys. Rep. **100**, 1 (1983).
[21] G. Ingelman and P. E. Schlein, Phys. Lett. **152B**, 256 (1985); K. H. Streng, *ibid.* **166B**, 443 (1986); J. Bartels and G. Ingelman, Phys. Lett. B **235**, 175 (1990).
[22] A. Donnachie and P. V. Landshoff, Phys. Lett. B **185**, 403 (1987); **191**, 309 (1987).
[23] J. Kwiecinski and B. Badelek, Phys. Lett. B **208**, 508 (1988).
[24] N. N. Nikolaev and B. G. Zakharov, Z. Phys. C **53**, 331 (1992); **49**, 607 (1991); N. N. Nikolaev, in *Proceedings of the Fourth International Conference on Elastic and Diffractive Scattering*, La Biodola, Elba, Italy, 1991, edited by F. Cervelli and S. Zuechelli [Nucl. Phys. B (Proc. Suppl.) **25B**, 152 (1992)].
[25] A. Donnachie and P. V. Landshoff, Nucl. Phys. **B244**, 322 (1984).
[26] P. N. Harriman, A. D. Martin, R. G. Roberts, and W. J. Stirling, Phys. Rev. D **42**, 798 (1990).
[27] J. F. Owens, Phys. Lett. B **266**, 126 (1991).
[28] J. G. Morfin and W. K. Tung, Z. Phys. C **52**, 13 (1991).
[29] V. Barone, M. Genovese, N. N. Nikolaev, E. Predazzi, and B. G. Zakharov, "Structure functions of bound nucleons: From the EMC effect to nuclear shadowing," Torino Report No. DFTT 14/92, DFUPG 53-92 (unpublished).
[30] K. Goulianos, Phys. Rep. **101**, 169 (1983).
[31] R. L. Cool *et al.*, Phys. Rev. Lett. **47**, 701 (1981); T. J. Chapin *et al.*, Phys. Rev. D **31**, 17 (1985).
[32] L. P. Kaptari and A. Yu. Umnikov, Phys. Lett. B **272**, 359 (1991).
[33] B. Betev *et al.*, Z. Phys. C **28**, 15 (1985).

[34] K. Holinde and A. W. Thomas, Phys. Rev. C **42**, R1195 (1990).
[35] A. W. Thomas, Phys. Lett. **126B**, 97 (1983); L. L. Frankfurt, L. Mankiewicz, and M. I. Strikman, Z. Phys. A **334**, 343 (1989); S. Kumano, Phys. Rev. D **43**, 59 (1991); W. Melnitchouk, A. W. Thomas, and A. I. Signal, Z. Phys. A **340**, 85 (1991).
[36] NMC, D. Allasia *et al.*, Phys. Lett. B **249**, 366 (1990).
[37] NMC, P. Amaudruz *et al.*, Phys. Rev. Lett. **66**, 2712 (1991).
[38] K. Gottfried, Phys. Rev. Lett. **18**, 1174 (1967).
[39] A. H. Mueller and J. Qiu, Nucl. Phys. **B268**, 427 (1986); J. Qiu, *ibid.* **B291**, 746 (1987).
[40] E. L. Berger and J. Qui, Phys. Lett. B **206**, 141 (1988); F. E. Close, J. Qui, and R. G. Roberts, Phys. Rev. D **40**, 2820 (1989); J. Kwiecinski, A. D. Martin, W. J. Stirling, and R. G. Roberts, *ibid.* **40**, 3645 (1990); S. Kumano, Indiana University IU/NTC-92-20 (unpublished).

Role of vector mesons in high-Q^2 lepton-nucleon scattering

W. Melnitchouk and A. W. Thomas
Department of Physics and Mathematical Physics, University of Adelaide, Box 498 G.P.O., Adelaide, 5001 Australia
(Received 14 December 1992)

The possible role played by vector mesons in inclusive deep-inelastic lepton-nucleon scattering is investigated. In the context of the convolution model, we calculate self-consistently the scaling contribution to the nucleon structure function using the formalism of time-ordered perturbation theory in the infinite momentum frame. Our results indicate potentially significant effects only when the vector-meson–nucleon form factor is very hard. Agreement with the experimental antiquark distributions, however, requires relatively soft form factors for the πN, ρN, and ωN vertices.

PACS number(s): 13.60.Hb, 12.38.Lg, 12.40.Aa

I. INTRODUCTION

In the context of meson-exchange models of the NN force in nuclear physics, it has long been realized that vector mesons play a vital role [1,2]. For example, the isovector ρ meson is needed to provide sufficient cancellation of the tensor force generated by π meson exchange, which would otherwise be too large. On the other hand, the isoscalar ω meson, through its large vector coupling, is responsible for the short range NN repulsive force, and also provides most of the spin-orbit interaction. Traditionally it has been necessary to use hard vector-meson–nucleon form factors in order to fit the NN phase shifts [2]. However, alternative approaches have recently been developed in which the NN data can be fitted with quite soft form factors [3,4].

From another direction, the vector-meson dominance model of the elastic electromagnetic nucleon form factors, in which an isovector photon couples to the nucleon via a ρ meson, provides a natural explanation of the dipole Q^2 behavior of the γNN vertex function. Recent analyses [3] have shown that a ρNN vertex parameterized by a soft monopole form factor ($\Lambda_1 \sim 800$ MeV) provides a good description of the Q^2 dependence of the Dirac and Pauli form factors. The effect of vector mesons upon nucleon electromagnetic form factors has also been explored [5] in the cloudy bag model [6], and in various soliton models [7].

In this paper we investigate the possible role played by vector mesons in high-Q^2 inelastic inclusive scattering of leptons from nucleons, in the context of the so-called convolution model, in which the deep-inelastic process is described in terms of both quark and explicit meson-baryon degrees of freedom. More specifically, the scaling property of the meson- and baryon-exchange contributions to the inclusive cross section allows us to probe the extended mesonic structure of nucleons.

Quite naturally the pion, being by far the lightest meson, was the first meson whose contributions to the nucleon structure function were investigated [8]. It was later noticed [9] that the pion cloud could be responsible for generating an asymmetry between the $\bar{u}$- and $\bar{d}$-quark content of the proton sea, through the preferred proton dissociation into a neutron and π^+. Furthermore, deep-inelastic scattering (DIS) data on the momentum fractions carried by antiquarks were used to obtain an upper limit on this nonperturbative pionic component [9,10]. An enhancement of $\bar{d}$ over $\bar{u}$ resulting from this process was also postulated as one explanation for the slope of the rapidity distribution in p-nucleus Drell-Yan production [11]. More recently it has been hypothesized that this asymmetry could account for some of the apparent discrepancy between the naive parton model prediction for the Gottfried sum rule [12] and its recently determined experimental value [13], and indeed this has resulted in the greater attention that the convolution model of lepton-nucleon scattering has received [14–21].

In a model in which the nucleon has internal meson and baryon degrees of freedom, the physical nucleon state in an infinite momentum frame can be expanded (in the one-meson approximation) in a series involving bare nucleon and two-particle meson-baryon states:

$$|N\rangle_{\text{phys}} = \sqrt{Z}\left\{|N\rangle_{\text{bare}} + \sum_{MB}\int dy\, d^2\mathbf{k}_T\, g_{0_{MBN}}\,\phi_{MB}(y,\mathbf{k}_T)\,|M(y,\mathbf{k}_T);B(1-y,-\mathbf{k}_T)\rangle\right\}. \quad (1)$$

Here, $\phi_{MB}(y,\mathbf{k}_T)$ is the probability amplitude for the physical nucleon to be in a state consisting of a meson M and baryon B, having transverse momenta $\mathbf{k}_T$ and $-\mathbf{k}_T$, and carrying longitudinal momentum fractions y and $1-y$, respectively. Z is the bare nucleon probability. Although we work in the one-meson approximation, we will include higher-order vertex corrections to the bare coupling constants $g_{0_{MBN}}$. Illustrated in Fig. 1 is the deep-inelastic scattering of the virtual photon from the two-particle state $|M;B\rangle$. In Fig. 1(a) the photon interacts with a quark or antiquark inside the exchanged meson, while in Fig. 1(b) the scattering is from a quark in the baryon component of the physical nucleon.

According to Eq. (1), the probability to find a meson inside a nucleon with momentum fraction $y\,(=k\cdot q/p\cdot q)$ is (to leading order in the coupling constant)

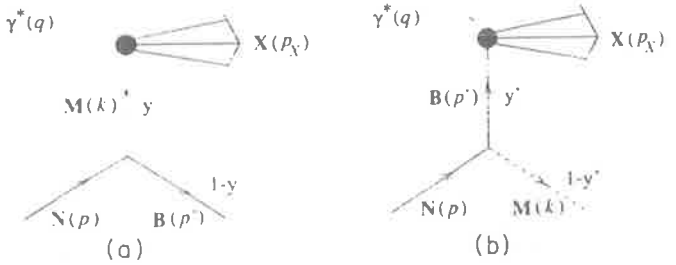

FIG. 1. Deep-inelastic scattering from the virtual (a) meson and (b) baryon components of a physical nucleon.

$f_{MB}(y) \equiv Z g^2_{0_{MBN}} \int d^2\mathbf{k}_T |\phi_{MB}(y,\mathbf{k}_T)|^2$. This must also be the probability to find a baryon inside a nucleon with momentum fraction $1-y$. The baryon distribution function $f_{BM}(y')$, where $y' = p'\cdot q / p\cdot q$, is probed directly through the process in Fig. 1(b), and should be related to the meson distribution function by

$$f_{MB}(y) = f_{BM}(1-y) \tag{2}$$

for all y, if the above interpretation is valid. We also demand equal numbers of mesons emitted by the nucleon, $\langle n \rangle_{MB} = \int_0^1 dy\, f_{MB}(y)$, and virtual baryons accompanying them, $\langle n \rangle_{BM} = \int_0^1 dy' f_{BM}(y')$:

$$\langle n \rangle_{MB} = \langle n \rangle_{BM} \ . \tag{3}$$

This is just a statement of charge conservation. Momentum conservation imposes the further requirement that

$$\langle y \rangle_{MB} + \langle y \rangle_{BM} = \langle n \rangle_{MB} \tag{4}$$

where $\langle y \rangle_{MB} = \int_0^1 dy\, y\, f_{MB}(y)$ and $\langle y \rangle_{BM} = \int_0^1 dy' y' f_{BM}(y')$ are the average momentum fractions carried by meson M and the virtual baryon B, respectively. Equations (3) and (4), and in fact similar relations for all higher moments of $f(y)$, follow automatically from Eq. (2).

In what follows we shall explicitly evaluate the functions f_{MB} and f_{BM}, and examine the conditions under which Eq. (2) is satisfied. The results will be used to calculate the contributions to the nucleon structure function from the extended mesonic structure of the nucleon, which are expressed as convolutions of the functions $f(y)$ with the structure functions of the struck meson or baryon:

$$\delta^{(MB)} F_{2N}(x) = \int_x^1 dy\, f_{MB}(y) F_{2M}(x/y) \ , \tag{5}$$

$$\delta^{(BM)} F_{2N}(x) = \int_x^1 dy' f_{BM}(y') F_{2B}(x/y') \ , \tag{6}$$

with $x = -q^2/2p\cdot q$ being the Bjorken variable. Note that Eqs. (5) and (6) are correct when physical (renormalized) meson-baryon coupling constants are used in the functions f_{MB} and f_{BM} (see Sec. IV for details). By comparing against the experimental structure functions, we will ultimately test the reliability of the expansion in Eq. (1), and in particular the relative importance of the states involving vector mesons compared with the pion states.

II. THE PION-NUCLEON CONTRIBUTION

A. Covariant formulation

Traditionally the effects upon $F_{2N}(x)$ of the π meson cloud have been studied most intensely. The distribution function of a virtual pion accompanied by a recoiling nucleon has been calculated in a covariant framework [8,9] as

$$f_{\pi N}(y) = \frac{3g^2_{\pi NN}}{16\pi^2} y \int_{-\infty}^{t^N_{\max}} dt \frac{(-t)\mathcal{F}^2_{\pi N}(t)}{(t-m_\pi^2)^2} \ . \tag{7}$$

Here, $t \equiv k^2 = t^N_{\max} - k_T^2/(1-y)$ is the four-momentum squared of the virtual pion, with a kinematic maximum given by $t^N_{\max} = -m_N^2 y^2/(1-y)$, and k_T^2 is the pion transverse momentum squared. In a covariant formulation the form factor $\mathcal{F}_{\pi N}$ parametrizing the πNN vertex, at which only the pion is off-mass-shell; can only depend on t.

Contributions from processes in which the virtual nucleon (accompanied by a recoiling pion) is struck have been calculated by several authors [18,20,22], although not all agree. Partly because there is less phenomenological experience with so-called sideways form factors (where the nucleon, rather than the pion, is off-mass-shell), some early work [23,15,17] simply defined $f_{N\pi}(y')$ through Eq. (2). However, this is unsatisfactory from a theoretical point of view, and ideally we would like to verify explicitly that the functions $f_{\pi N}$ and $f_{N\pi}$ satisfy Eq. (2).

Clearly the treatment of deep-inelastic scattering from an interacting nucleon is considerably more involved than that from a real nucleon, which is described by the usual hadronic tensor

$$W^{\mu\nu}_N(p,q) = \tilde{g}^{\mu\nu} W_{1N}(p,q) + \tilde{p}^\mu \tilde{p}^\nu W_{2N}(p,q) \ , \tag{8}$$

where $\tilde{g}^{\mu\nu} = -g^{\mu\nu} + q^\mu q^\nu/q^2$ and $\tilde{p}^\mu = p^\mu - q^\mu p\cdot q/q^2$. The hadronic vertex factor for the diagram of Fig. 1(b) in this case will be

$$\mathrm{Tr}[(\not p + m_N) i\gamma_5 (\not p' + m_N) \hat{W}^{\mu\nu}_N(p',q) (\not p' + m_N) i\gamma_5] \ , \tag{9}$$

where $\hat{W}^{\mu\nu}_N(p',q)$ is a matrix in Dirac space representing the hadronic tensor for an interacting nucleon, and is related to the hadronic tensor for real nucleons by [24]

$$W^{\mu\nu}_N(p,q) = \tfrac{1}{2}\mathrm{Tr}[(\not p + m_N)\hat{W}^{\mu\nu}_N(p,q)] \ . \tag{10}$$

If the struck nucleon is treated as an elementary fermion [25] the relevant operator in $\hat{W}^{\mu\nu}_N(p',q)$ is $\not q/2p'\cdot q$, which leads to [22]

$$f_{N\pi}(y') = \frac{3g^2_{\pi NN}}{16\pi^2} y' \int_{-\infty}^{t'^\pi_{\max}} dt' \left[-m_\pi^2 - \frac{1-y'}{y'}(t' - m_N^2) \right] \times \frac{\mathcal{F}^2_{N\pi}(t')}{(t'-m_N^2)^2} \ , \tag{11}$$

where $t' \equiv p'^2 = t'^\pi_{\max} - p'^2_T(1-y')$ is the four-momentum squared of the virtual nucleon, with the upper limit now given by $t'^\pi_{\max} = m_N^2 y' - m_\pi^2 y'/(1-y')$, and p'^2_T denotes the nucleon's transverse momentum squared. Apart from

the form factors, Eqs. (7) and (11) are clearly related by an interchange $y' \leftrightarrow 1-y$.

Note that choosing a different operator form for $\hat{W}_N^{\mu\nu}$ may lead to unphysical results. For example, with an operator involving I rather than $\not{q}$ the trace factor in Eq. (11) is proportional to $-m_\pi^2$. Problems also arise for the emission of scalar or vector mesons [26]. A full investigation of the off-mass-shell effects in deep-inelastic structure functions of composite objects will be the subject of a future publication [27].

The large-t' suppression for the $N\pi N$ vertex is introduced by the form factor $\mathcal{F}_{N\pi}$, which is usually parametrized by a monopole or dipole function

$$\mathcal{F}_{N\pi}(t') = \left(\frac{\Lambda_{N\pi}^2 - m_N^2}{\Lambda_{N\pi}^2 - t'} \right)^n$$

for $n=1$ and 2, respectively. However, to satisfy Eq. (3), the cutoff parameter $\Lambda_{N\pi}$ will in general have to be different from the cutoff $\Lambda_{\pi N}$ regulating the πNN vertex form factor in Eq. (7):

$$\mathcal{F}_{\pi N}(t) = \left(\frac{\Lambda_{\pi N}^2 - m_\pi^2}{\Lambda_{\pi N}^2 - t} \right)^n .$$

In general a different $\Lambda_{\pi N}$ would be required to satisfy Eq. (4), and it would not be possible to guarantee Eq. (2).

Another important assumption in the covariant convolution model is that the dependence of the virtual meson and baryon structure functions in Eqs. (5) and (6) on the invariant mass squared is negligible. The argument usually made is that the vertex form factor suppresses contributions from the far off-mass-shell configurations (i.e., for $|t| \gtrsim 10 m_N^2$ [17]). However, in this approach even the identification of the off-shell structure functions themselves is not very clear. Some suggestions about how to relate the off-shell functions to the on-shell ones were made [28] in the context of DIS from nuclei, although these were more *ad hoc* prescriptions rather than theoretical derivations. Attempts to simplify this situation were made in Ref. [29], where it was proposed that the instant form of dynamics, where only on-mass-shell particles are encountered, be used to calculate the nuclear structure functions. Along similar lines was the light-front approach of Berger *et al.* [23]. Actually these two techniques are the same if one works in the infinite momentum frame. The instant form of dynamics was previously used by Güttner *et al.* [30] in the calculation of the function $f_{\pi N}(y)$ for the case of pion electroproduction, and more recently by Zoller [20] in the DIS of charged leptons from nucleons.

B. Infinite momentum frame states

An alternative to the use of covariant Feynman diagrams, in the form of "old-fashioned" time-ordered perturbation theory in the infinite momentum frame (IMF), was proposed some time ago by Weinberg [31] for scalar particles. This was later extended by Drell, Levy, and Yan [32] to the πN system in deep-inelastic scattering. The main virtues of this approach are that off-mass-shell ambiguities in the structure functions of virtual particles can be avoided, and that the meson and baryon distribution functions can be shown to satisfy Eq. (2) exactly.

In the time-ordered theory the analogue of Fig. 1(a) will now involve two diagrams in which the π moves forwards and backwards in time, Fig. 2. However, in a frame of reference where the target nucleon is moving fast along the z direction with longitudinal momentum $p_L (\to \infty)$, only that diagram involving a forward moving pion gives a nonzero contribution. In the IMF the target nucleon has energy

$$p_0 = p_L + \frac{m_N^2}{2p_L} + O\left(\frac{1}{p_L^2} \right) .$$

Following Weinberg [31] we write the pion three-momentum as

$$\mathbf{k} = y\mathbf{p} + \mathbf{k}_T ,$$

where $\mathbf{k}_T \cdot \mathbf{p} = 0$, and conservation of momentum demands that the recoil nucleon momentum be

$$\mathbf{p}' = (1-y)\mathbf{p} - \mathbf{k}_T .$$

Since all particles are on their mass shells the energies of the intermediate π and N must be

$$k_0 = |y| p_L + \frac{k_T^2 + m_\pi^2}{2|y| p_L} + O\left(\frac{1}{p_L^2} \right) ,$$

$$p_0' = |1-y| p_L + \frac{k_T^2 + m_N^2}{2|1-y| p_L} + O\left(\frac{1}{p_L^2} \right) .$$

For forward moving particles [Fig. 2(a)] y and $1-y$ are positive, and according to the rules of the time-ordered perturbation theory the energy denominator appearing in the calculation of $f_{\pi N}(y)$ is $(p_0 - p_0' - k_0)$

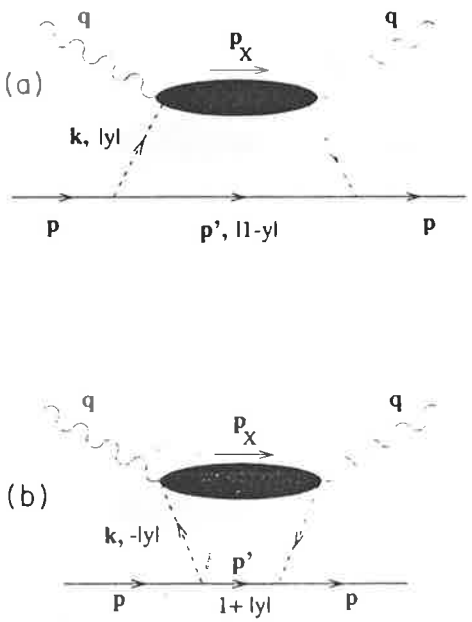

FIG. 2. Time-ordered diagrams for pions moving (a) forwards and (b) backwards in time. Time is increasing from left to right.

$=(m_N^2-s_{\pi N})/2p_L$, where

$$s_{\pi N}=s_{\pi N}(k_T^2,y)=(p_0'+k_0)^2-(\mathbf{p}'+\mathbf{k})^2 = \frac{k_T^2+m_\pi^2}{y}+\frac{k_T^2+m_N^2}{1-y} \tag{12}$$

is the center-of-mass energy squared of the intermediate πN state. Changing the variables of integration from $d^3\mathbf{k}$ to dy and dk_T^2, all powers of p_L are seen to cancel when combined with the appropriate vertex factors $(2p_0')^{-1}$ and $(2k_0)^{-2}$. However, for a backward moving pion [Fig. 2(b)] y is negative, and the energy denominator becomes $(p_0-p_0'-k_0)=2yp_L+O(1/p_L)$. Therefore in the $p_L\to\infty$ limit this time ordering does not contribute, and the result of Eq. (7) is reproduced, form factor aside.

For an interacting nucleon with π recoil, Fig. 3, the kinematics are similar to the above, namely the nucleon and pion move with three-momenta

$$\mathbf{p}'=y'\mathbf{p}-\mathbf{k}_T\ ,$$

$$\mathbf{k}=(1-y')\mathbf{p}+\mathbf{k}_T\ ,$$

and have energies

$$p_0'=|y'|p_L+\frac{k_T^2+m_N^2}{2|y'|p_L}+O\left[\frac{1}{p_L^2}\right]\ ,$$

$$k_0=|1-y'|p_L+\frac{k_T^2+m_\pi^2}{2|1-y'|p_L}+O\left[\frac{1}{p_L^2}\right]\ ,$$

respectively. The general structure of the tensor describing a nonelementary interacting nucleon can be written as

$$\hat{W}_N^{\mu\nu}(p,q)=\bar{g}^{\mu\nu}(\hat{W}_0+\not{p}\hat{W}_1+\not{q}\hat{W}_2)+\cdots\ , \tag{13}$$

where we have omitted terms proportional only to $p^{\mu,\nu}$ and $q^{\mu,\nu}$. The functions $\hat{W}_{0,1,2}$ are related to the on-mass-shell structure function W_{1N} by Eq. (10):

$$W_{1N}(p,q)=2(m_N\hat{W}_0+m_N^2\hat{W}_1+p\cdot q\hat{W}_2)\ . \tag{14}$$

Then direct evaluation of the trace in Eq. (9) gives

$$4(2p\cdot p'-2m_N^2)[\bar{g}^{\mu\nu}(m_N\hat{W}_0+m_N^2\hat{W}_1+p'\cdot q\hat{W}_2)+\cdots] = 2(2p\cdot p'-2m_N^2)\bar{g}^{\mu\nu}W_{1N}(p',q)+\cdots$$

where now the exact on-shell nucleon structure function appears, and there is no off-shell ambiguity.

For a backward moving nucleon [Fig. 3(b)] y' is negative, and $2p\cdot p'-2m_N^2=-4y'p_L^2+O(1/p_L)$, so that the numerator becomes large in the $p_L\to\infty$ limit. Technically this is due to the "badness" of the operator γ_5, which mixes upper and lower components of the nucleon spinors. The energy denominator here is $(p_0-p_0'-k_0)=2y'p_L+O(1/p_L)$, and when squared and combined with the $1/p_L^2$ from the integration and vertex factors, the contribution from this diagram vanishes when p_L is infinite.

Therefore we need only evaluate the diagram with the forward moving nucleon, Fig. 3(a), which gives the result of Eq. (11):

$$f_{N\pi}(y')=\frac{3g_{\pi NN}^2}{16\pi^2}\int_0^\infty dk_T^2\left[\frac{k_T^2+(1-y')^2m_N^2}{y'}\right] \times\frac{\mathcal{F}_{N\pi}^2(k_T^2,y')}{y'(1-y')(m_N^2-s_{N\pi})^2}\ , \tag{15}$$

with $s_{N\pi}(k_T^2,y')=s_{\pi N}(k_T^2,1-y')$, except that the form factor is now unknown. It is quite natural to choose the form factor to be a function of the center-of-mass energy squared of the πN system, $s_{N\pi}$, as was done by Zoller [20]. The only difference between our treatment and that in Ref. [20] is that we follow the conventional normalization so that the coupling constant $g_{\pi NN}$ has its standard value at the pole:

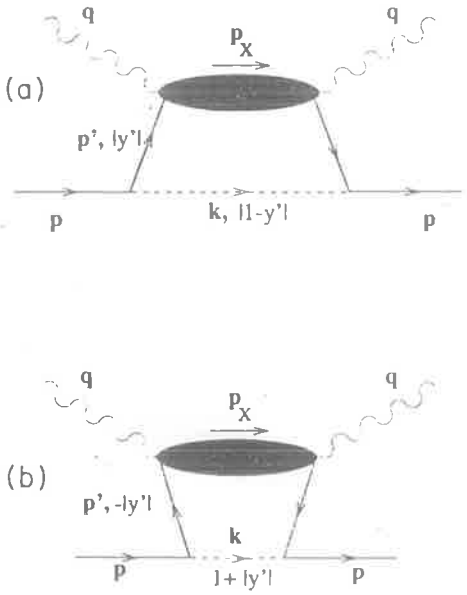

FIG. 3. Time-ordered diagrams for nucleons moving (a) forwards and (b) backwards in time.

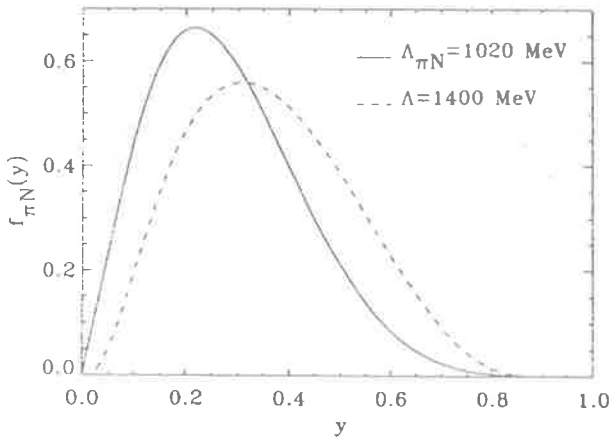

FIG. 4. πN distribution function for a dipole form factor and that given in Eq. (17). The cutoffs are chosen so that $\langle n\rangle_{\pi N}\simeq 0.25$ in both cases.

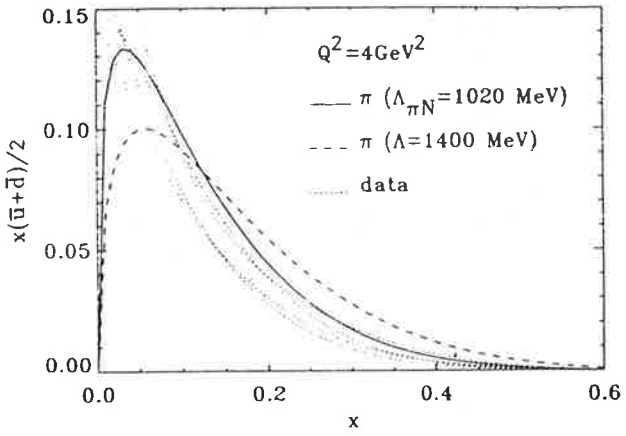

FIG. 5. Proton SU(2) antiquark distributions from DIS on the πN component of the nucleon, evaluated for the different πN form factors, as in Fig. 4. The data (dotted curves) are the parametrizations of Owens, Morfin and Tung, Eichten *et al.*, and Diemoz *et al.* [38].

$$\mathcal{F}_{N\pi}(k_T^2,y')=\exp\left[\frac{m_N^2-s_{N\pi}}{\Lambda^2}\right] . \tag{16}$$

Within this approach there is an explicit symmetry between the processes in which the intermediate pion and the intermediate nucleon are struck, provided we take the form factor in $f_{\pi N}$ as

$$\mathcal{F}_{\pi N}(k_T^2,y)=\mathcal{F}_{N\pi}(k_T^2,1-y) . \tag{17}$$

Then as long as the same mass parameter Λ is used in both vertex functions, Eq. (2) is automatically satisfied.

In Fig. 4 we compare $f_{\pi N}(y)$ with a dipole form factor and with the form factor in Eq. (17). In order to make the comparison meaningful the cutoffs have been chosen to yield the same value of $\langle n\rangle_{\pi N}(\simeq 0.25)$. With the y-dependent form factor in Eq. (17) $f_{\pi N}(y)$ is a little broader and peaks at around $y=0.3$, compared with $y\simeq 0.2$ for the covariant formulation with a dipole form factor. Consequently, the convolution of $f_{\pi N}(y)$ with $F_{2\pi}$ for the y-dependent form factor will have a slightly smaller peak and extend to marginally larger x. This is evident in Fig. 5, where we show the calculated SU(2) antiquark contribution to $\delta^{(\pi N)}F_{2p}(x)$, compared with some recent empirical data at $Q^2=4$ GeV^2.

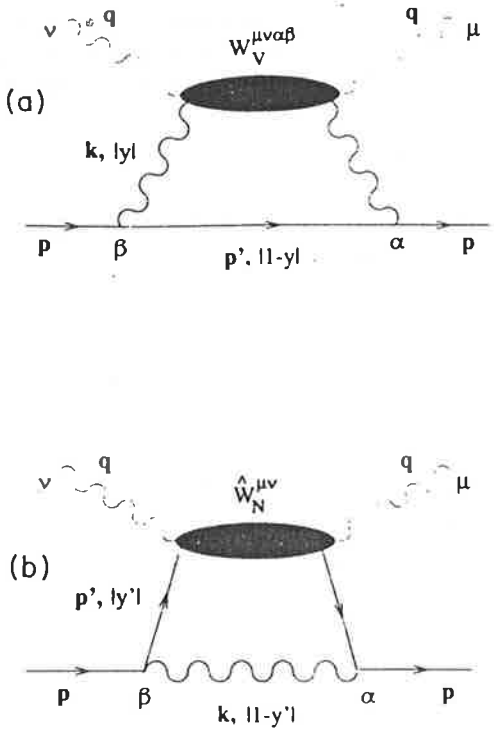

FIG. 6. Time-ordered diagrams for the DIS from (a) vector mesons and (b) nucleons with recoil vector mesons, that are nonzero in the IMF.

III. VECTOR MESON CONTENT OF THE NUCLEON

In this section we extend the convolution model analysis to the vector-meson sector. Our approach is similar to that described in Sec. II B, namely we use time-ordered perturbation theory to evaluate those diagrams which are nonzero in the IMF. Previous calculations [18,19] of the vector-meson contributions were made in a covariant framework, but with the assumption that the vector-meson and nucleon intermediate states were on-mass-shell. In our approach we self-consistently calculate both the contribution from a struck vector meson [Fig. 6(a)] and from a struck nucleon with a vector-meson recoil [Fig. 6(b)], and show explicitly that the distribution functions for these obey the relation in Eq. (2) exactly.

Starting from the effective VNN interaction (see, e.g., Ref. [2]), where $V=\rho$ or ω, we write in full the vector-meson contribution (with a nucleon recoil) to the nucleon hadronic tensor:

$$\delta^{(VN)}W^{\mu\nu}(p,q)=c_V\int\frac{d^3\mathbf{k}}{(2\pi)^3(2p_0')(2k_0)^2}\left[g_{VNN}^2A_{\alpha\beta}+\frac{f_{VNN}^2}{(4m_N)^2}B_{\alpha\beta}+g_{VNN}\frac{f_{VNN}}{4m_N}C_{\alpha\beta}\right]\frac{\mathcal{F}_{VN}^2(k_T^2,y)}{(p_0-p_0'-k_0)^2}W_V^{\mu\nu\alpha\beta}(k,q) , \tag{18}$$

where

$$\begin{aligned}
A_{\alpha\beta}&=2(m_N^2-p\cdot p')g_{\alpha\beta}+2p_\alpha p'_\beta+2p'_\alpha p_\beta ,\\
B_{\alpha\beta}&=\tfrac{1}{2}[(m_V^2m_N^2-2p\cdot k\,p'\cdot k+m_V^2p\cdot p')g_{\alpha\beta}-(m_N^2+p\cdot p')k_\alpha k_\beta\\
&\quad -m_V^2(p_\alpha p'_\beta+p_\beta p'_\alpha)+p'\cdot k(p_\alpha k_\beta+p_\beta k_\alpha)+p\cdot k(p'_\alpha k_\beta+p'_\beta k_\alpha)] ,\\
C_{\alpha\beta}&=2(p\cdot k-p'\cdot k)g_{\alpha\beta}-(p_\alpha k_\beta+p_\beta k_\alpha)+(p'_\alpha k_\beta+p'_\beta k_\alpha)
\end{aligned} \tag{19}$$

are the VNN vertex trace factors for the vector, tensor, and vector-tensor interference couplings, respectively. The isospin factor c_V is equal to 3 and 1 for isovector and isoscalar mesons, respectively. For an on-mass-shell vector meson, the spin-1 tensor $W^{\mu\nu\alpha\beta}$, symmetric under the interchange of $\mu\leftrightarrow\nu$ and $\alpha\leftrightarrow\beta$, is given by

$$W_V^{\mu\nu\alpha\beta}(k,q)=[\tilde{g}^{\mu\nu}W_{1V}(k,q)+\tilde{k}^{\mu}\tilde{k}^{\nu}W_{2V}(k,q)]\tilde{g}^{\alpha\beta} . \tag{20}$$

This form guarantees that the vector current is conserved, $k_{\alpha,\beta}W^{\mu\nu\alpha\beta}=0=q_{\mu,\nu}W^{\mu\nu\alpha\beta}$. Furthermore, it reproduces the correct unpolarized on-shell spin-1 tensor when contracted with the meson polarization vectors ($\epsilon_{\alpha,\beta}$) and summed over the V helicity, λ [33]:

$$W_V^{\mu\nu}(k,q)=\sum_{\lambda}\epsilon_{\alpha}^{*}(\lambda,k)\epsilon_{\beta}(\lambda,k)W_V^{\mu\nu\alpha\beta}(k,q)=\left[-g_{\alpha\beta}+\frac{k_\alpha k_\beta}{k^2}\right]W_V^{\mu\nu\alpha\beta}(k,q)$$
$$\propto\tilde{g}^{\mu\nu}W_{1V}(k,q)+\tilde{k}^{\mu}\tilde{k}^{\nu}W_{2V}(k,q) . \tag{21}$$

In the case of DIS from a vector particle emitted by a nucleon, Fig. 6(a), contracting the spin-1 tensor $W^{\mu\nu\alpha\beta}$ with the VNN vertex trace factors in Eq. (19), and equating coefficients of $\tilde{g}^{\mu\nu}$ gives

$$\delta^{(VN)}W_{1N}(p,q)=c_V\int\frac{d^3\mathbf{k}}{(2\pi)^3(2p_0')(2k_0)^2}\left\{g_{VNN}^2\left[-6m_N^2+\frac{4p\cdot k\,p'\cdot k}{m_V^2}+2p\cdot p'\right]-\frac{f_{VNN}^2}{2}\left[-3m_V^2+\frac{4p\cdot k\,p'\cdot k}{m_N^2}-\frac{m_V^2p\cdot p'}{m_N^2}\right]\right.$$
$$\left.-6g_{VNN}f_{VNN}[p\cdot k-p'\cdot k]\right\}\frac{\mathcal{F}_{VN}^2(k_T^2,y)}{(m_N^2-s_{VN})^2}W_{1V}(k,q) . \tag{22}$$

Using the IMF kinematics (which are similar to those for the πN system, except that $m_\pi\to m_V$), together with the Callan-Gross relation for the nucleon and vector meson, enables the contribution to F_{2N} from vector mesons to be written as a convolution of the vector-meson distribution function $f_{VN}(y)$ with the on-shell vector-meson structure function $F_{2V}(x/y)$, as in Eq. (5), where now

$$f_{VN}(y)=\frac{c_V}{16\pi^2}\int_0^{\infty}dk_T^2\left\{g_{VNN}^2\left[\frac{[k_T^2+y^2m_N^2+m_V^2][k_T^2+y^2m_N^2+(1-y)^2m_V^2]}{y^2(1-y)m_V^2}+\frac{k_T^2+y^2m_N^2}{1-y}-4m_N^2\right]\right.$$
$$+f_{VNN}^2\left[\frac{[k_T^2+y^2m_N^2+m_V^2][k_T^2+y^2m_N^2+(1-y)^2m_V^2]}{2y^2(1-y)m_N^2}-\frac{m_V^2[k_T^2+(2-y)^2m_N^2]}{4(1-y)m_N^2}-m_V^2\right]$$
$$\left.+3g_{VNN}f_{VNN}\left[\frac{k_T^2+y^2m_N^2-(1-y)m_V^2}{1-y}\right]\right\}\frac{\mathcal{F}_{VN}^2(k_T^2,y)}{y(1-y)(m_N^2-s_{VN})^2} . \tag{23}$$

The VNN form factor is defined analogously to Eq. (17),

$$\mathcal{F}_{VN}(k_T^2,y)=\exp\left[\frac{m_N^2-s_{VN}}{\Lambda^2}\right] , \tag{24}$$

and the VN center-of-mass energy squared is

$$s_{VN}=s_{VN}(k_T^2,y)=\frac{k_T^2+m_V^2}{y}+\frac{k_T^2+m_N^2}{1-y} . \tag{25}$$

Suppression of backward moving vector mesons is achieved in the IMF by the energy denominators, as for pions. The vector-meson structure function F_{2V} is not known experimentally, so in our numerical calculations we assume that its x dependence resembles that of the π meson structure function, which has been determined experimentally [34].

For the vector-meson recoil process, Fig. 6(b), we evaluate the distribution function $f_{NV}(y')$ using the full spinor structure of $\hat{W}_N^{\mu\nu}$ in Eq. (13):

$$\delta^{(NV)}W_{1N}(p,q)=c_V\int\frac{d^3\mathbf{p}'}{(2\pi)^3(2p_0')^2(2k_0)}\left[g_{VNN}^2A_{\alpha\beta}+\frac{f_{VNN}^2}{(4m_N)^2}B_{\alpha\beta}+g_{VNN}\frac{f_{VNN}}{4m_N}C_{\alpha\beta}\right]$$
$$\times\sum_{\lambda}\epsilon_{\alpha}^{*}(\lambda,k)\epsilon_{\beta}(\lambda,k)\frac{\mathcal{F}_{NV}^2(k_T^2,y')}{(p_0-p_0'-k_0)^2}(2m_N\hat{W}_0+2m_N^2\hat{W}_1+2p'\cdot q\hat{W}_2) , \tag{26}$$

where the tensors A, B, and C are as in Eq. (19). Performing the contractions over the indices α,β leads to the convolution integral of Eq. (6), with the nucleon distribution function with a vector-meson recoil given by

$$f_{NV}(y')=\frac{c_V}{16\pi^2}\int_0^\infty dk_T^2\left\{g_{VNN}^2\left[\frac{[k_T^2+(1-y')^2m_N^2+m_V^2][k_T^2+(1-y')^2m_N^2+y'^2m_V^2]}{y'(1-y')^2m_V^2}+\frac{k_T^2+(1-y')^2m_N^2}{y'}-4m_N^2\right]\right.$$
$$+f_{VNN}^2\left[\frac{[k_T^2+(1-y')^2m_N^2+m_V^2][k_T^2+(1-y')^2m_N^2+y'^2m_V^2]}{2y'(1-y')^2m_N^2}-\frac{m_V^2[k_T^2+(1+y')^2m_N^2]}{4y'm_N^2}-m_V^2\right]$$
$$\left.+3g_{VNN}f_{VNN}\left[\frac{k_T^2+(1-y')^2m_N^2-y'm_V^2}{1-y'}\right]\right\}\frac{\mathcal{F}_{NV}^2(k_T^2,y')}{y'(1-y')(m_N^2-s_{NV})^2}\,, \tag{27}$$

and where $s_{NV}(k_T^2,y')=s_{VN}(k_T^2,1-y')$. Again, we have evaluated only the diagram with forward moving nucleons which is nonzero in the IMF. It is clear therefore from Eqs. (23) and (27) that the probability distributions for the VN intermediate states are related by $f_{NV}(y')=f_{VN}(1-y')$.

Our numerical results, which are discussed below, rely upon the physical vector-meson–nucleon coupling constants whose values are taken at the poles, as obtained from analyses of πN scattering data: $g_{\rho NN}^2/4\pi=0.55, f_{\rho NN}/g_{\rho NN}=6.1$ [35], and $g_{\omega NN}^2/4\pi=8.1, f_{\omega NN}/g_{\omega NN}=0$ [36].

IV. RESULTS AND DISCUSSION

Figure 7 shows the meson distribution functions $f_{\rho N}$, $f_{\omega N}$, and $f_{\pi N}$ (scaled by a factor $\frac{1}{3}$) for the same vertex cutoff parameter Λ ($=1.4$ GeV). The vector-meson component will only be relevant when very hard form factors are employed. To make this point more explicit, we plot in Fig. 8 the average multiplicities $\langle n\rangle_{VN}$ and $\langle n\rangle_{\pi N}$ as a function of Λ. The dependence on Λ is much stronger for the ρ than for π mesons. For $\Lambda\lesssim 1.4$ GeV, $\langle n\rangle_{\rho N}$ is considerably smaller than $\langle n\rangle_{\pi N}$, and it is only with much larger cutoffs ($\Lambda\gtrsim 1.8$ GeV) that the ρ multiplicity becomes comparable with that of the π. Note that $\Lambda=(1000,1400,1800)$ MeV corresponds to a dipole $\Lambda_{\pi N}\simeq(650,1020,1410)$ MeV for the same $\langle n\rangle_{\pi N}$.

One should observe that the trace factor inside the braces in $f_{VN}(y)$ is divergent in the limit $y\to 0$, so that use of a form factor $\propto\exp[y(m_N^2-s_{VN})]$, which corresponds to a t-dependent covariant form factor $\exp[t-m_V^2]$, would make $\delta^{(VN)}F_{2N}(x)$ approach a finite value as $x\to 0$, much like for a perturbative sea distribution. However, there are several problems with accepting such a result, the most obvious of which is that it would violate charge and momentum conservation very badly, since $f_{NV}(y')\to 0$ for $y'\to 1$ and $\to$const as $y'\to 0$ for a form factor $\propto\exp[y'(m_N^2-s_{NV})]$, which in the covariant formalism corresponds to $\exp[t'-m_N^2]$. Furthermore, it would lead to a gross violation of the Adler sum rule, which integrates the flavor combination $u-\bar u-d+\bar d$, and such a violation has not been observed in the range $1<Q^2<40$ GeV^2 [37]. This gives further evidence for the preference of the IMF approach together with the form factor in Eq. (24). Note, however, that because the baryon recoil contributions to the quark and antiquark distributions are related by

$$\delta^{(MB)}u(x)=\delta^{(MB)}\bar d(x)\,,$$
$$\delta^{(MB)}d(x)=\delta^{(MB)}\bar u(x) \tag{28}$$

the divergent contributions would cancel for the Gottfried (which depends on the combination $u+\bar u-d-\bar d$) and Gross–Llewellyn-Smith ($u-\bar u$

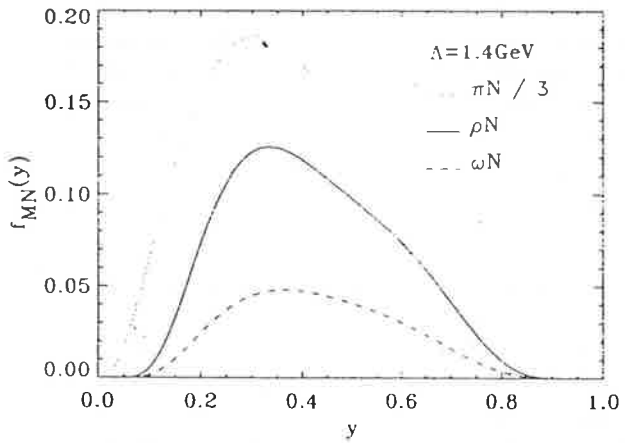

FIG. 7. Meson distribution functions $f_{\rho N}(y)$, $f_{\omega N}(y)$, and $f_{\pi N}(y)$, for $\Lambda=1.4$ GeV. Note the pion distribution is scaled by a factor of $\frac{1}{3}$.

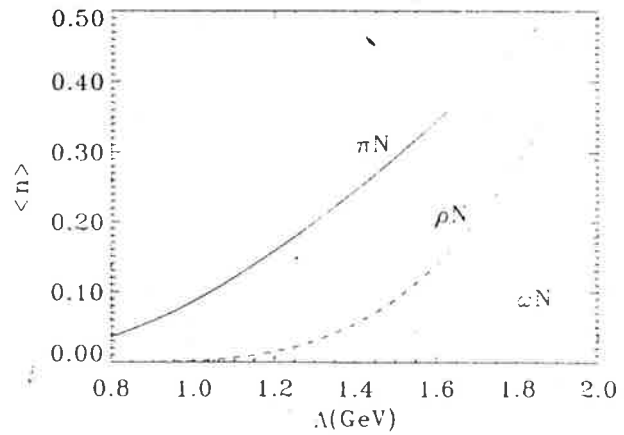

FIG. 8. Average number densities for the π, ρ, and ω mesons in a nucleon, as a function of the meson-nucleon form factor cutoff.

$+d-\bar{d}$) sum rules.

In previous studies [9,10] restrictions have been obtained on the magnitude of the form factor cutoffs by comparing $\langle y \rangle_{MB}$ with the measured momentum fractions carried by the antiquarks. Even more stringent constraints can be achieved by also demanding that the shape of the meson-exchange contributions to $\bar{q}(x)$,

$$\delta^{(MB)}\bar{q}(x)=\int_x^1 \frac{dy}{y} f_{MB}(y)\bar{q}_M(x/y) , \tag{29}$$

be consistent with the shape of the experimental antiquark distribution [10,16]. Figure 9 shows the calculated antiquark distributions from the π component of the nucleon alone and from the pion plus vector-meson structure of the nucleon, for $\Lambda=1.2$ and 1.4 GeV. Clearly the SU(2) $\bar{q}$ content of the nucleon (as parametrized by Owens, Morfin and Tung, Eichten *et al.*, and Diemoz *et al.* [38]) is saturated for $\Lambda\approx 1.2$ GeV in the intermediate-x region. For the πNN vertex this corresponds to a dipole form factor cutoff $\Lambda_{\pi N}\approx 830$ MeV—considerably smaller than that used by many authors. We can conclude therefore that for the range of form factor cutoffs allowed by the data, vector mesons play only a marginal role in the DIS process. The maximum value of Λ would have to be even smaller with the inclusion of $\pi\Delta$ states in the nucleon, as it has been shown previously [15–18] that these give non-negligible contributions to the nucleon structure function. The $\pi\Delta$ states would also be of relevance to the calculated $\bar{d}-\bar{u}$ difference (and to the Gottfried sum rule) resulting from DIS from the πN and ρN components, which will be partly canceled by this contribution.

At this point we would like to clarify an issue that has been the cause of some confusion recently in the literature. The meson- and baryon-exchange diagrams in Fig. 1 describe physical processes (inclusive baryon and meson leptoproduction) whose cross sections involve physical (renormalized) coupling constants. When integrated over the recoil particles' momenta these yield the inclusive DIS cross sections, which are proportional to the total quark (and antiquark) distributions

$$q(x)=Zq_{\text{bare}}(x)+\sum_{MB}[\delta^{(MB)}q(x)+\delta^{(BM)}q(x)] . \tag{30}$$

Therefore $\delta q(x)$ and the convolution integrals in Eqs. (5), (6), and (29) are expressed in terms of renormalized coupling constants contained in the functions $f(y)$. From Eq. (30) we also determine the bare nucleon probability

$$Z=1-\sum_{MB}\langle n \rangle_{MB} \tag{31}$$

by demanding that the valence number and momentum sum rules are satisfied. We emphasize that all quantities in Eqs. (30) and (31) are evaluated using renormalized coupling constants.

We could, of course, choose to work at a given order in the bare coupling constant, and explicitly verify that the various sum rules are satisfied. For example, to lowest order (g_0^2) the total quark distributions would be [39]

$$q(x)=Z\left\{q_{\text{bare}}(x)+\sum_{MB}[\delta^{(MB)}q_{(0)}(x)+\delta^{(BM)}q_{(0)}(x)]\right\} \quad (\text{order } g_0^2) \tag{32}$$

with

$$Z=\left[1+\sum_{MB}\langle n_{(0)} \rangle_{MB}\right]^{-1} \quad (\text{order } g_0^2) , \tag{33}$$

where the subscript (0) indicates that the functions $f(y)$ here are evaluated using bare couplings. Equations (30) and (31) are easily recovered since the bare couplings, to this order, are defined by $g_0^2=g_{\text{ren}}^2/Z$. It would, however, be inconsistent to use Eqs. (32) and (33) with renormalized coupling constants, especially with large form factor cutoffs. As long as the form factors are soft, the difference between the bare and renormalized couplings is quite small. However, with large cutoff masses the bare couplings would need to be substantially bigger than the physical ones. (In fact, the form factor cutoff dependence of the bare πN coupling constant in the cloudy bag model [40] showed some 40% difference for very hard form factors—or small bag radii, ~0.6 fm.) In addition, with large values of Λ, the higher-order diagrams involving more than one meson in the intermediate state would become non-negligible, and the initial assumption that the series in Eq. (1) can be truncated at the one-meson level would be seriously in doubt. Fortunately, we need not consider the multiple-meson contributions, since Fig. 9 clearly demonstrates the difficulty in reconciling the empirical data with quark distributions calculated with such large cutoffs.

Finally, we make some additional comments regarding this justification of our calculation in terms of an incoherent summation of cross sections for the various meson-exchange processes. Because of the pseudoscalar (or pseudovector) nature of the πNN vertex, there is no interference between π meson and vector-meson exchange. Furthermore, there will be no mixing between

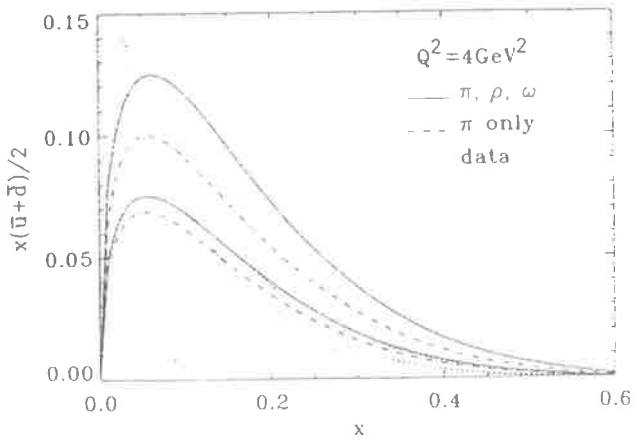

FIG. 9. Proton SU(2) antiquark distributions, calculated with π and $\pi+\rho+\omega$ components in the nucleon. The lower (upper) solid and dashed curves correspond to $\Lambda=1.2$ (1.4) GeV. The data are from Ref. [38].

the ω and ρ exchange configurations due to their different isospins. In fact, all of the processes considered in this analysis can be added incoherently. The question remains, however, whether it will be possible to identify an explicit vector-meson contribution to $F_{2N}(x)$ in an unambiguous way in deep-inelastic scattering experiments. While it may be feasible to search for one-pion exchange by observing the distribution of the produced low-momentum baryon spectrum [41], because of the smaller absolute vector-meson cross section it will be difficult to separate this component from both the perturbative background and from that due to other mesons.

ACKNOWLEDGMENTS

We would like to thank E. M. Henley for his friendly assistance and continued interest in this problem, as well as S. D. Bass, C. A. Hurst, W.-Y. P. Hwang, N. N. Nikolaev, A. W. Schreiber, J. Speth, and V. R. Zoller for useful comments and discussions related to this work. W.M. would like to thank the Institute for Nuclear Theory at the University of Washington for its hospitality during a recent visit, where part of this work was carried out. This work was supported by the Australian Research Council.

[1] R. V. Reid, Jr., Ann. Phys. (N.Y.) **50**, 411 (1968); M. M. Nagels, T. A. Rijken, and J. J. de Swart, Phys. Rev. **12**, 744 (1975); M. Lacombe *et al.*, Phys. Rev. D **12**, 1495 (1975); A. J. Jackson, D. O. Riska, and B. Verwest, Nucl. Phys. **A249**, 397 (1975); G. E. Brown and A. D. Jackson, *The Nucleon-Nucleon Interaction* (North-Holland, Amsterdam, 1976).

[2] R. Machleidt, K. Holinde, and Ch. Elster, Phys. Rep. **149**, 1 (1987).

[3] S. Deister, M. F. Gari, W. Krumpelmann, and M. Mahlke, Few Body Systems **10**, 1 (1991); M. Gari and W. Krumpelmann, Z. Phys. A **322**, 689 (1985).

[4] A. W. Thomas and K. Holinde, Phys. Rev. Lett. **63**, 2025 (1989); K. Holinde and A. W. Thomas, Phys. Rev. C **42**, R1195 (1990).

[5] M. T. Jeong and Il-T. Cheon, Phys. Rev. D **43**, 3725 (1991).

[6] A. W. Thomas, Adv. Nucl. Phys. **13**, 1 (1984); R. F. Alvarez-Estrada and A. W. Thomas, J. Phys. G **9**, 161 (1983).

[7] U. G. Meissner, N. Kaiser, and W. Weise, Nucl. Phys. **A466**, 685 (1987); C. Schuren, E. Ruiz Arriola, and K. Goeke, Phys. Lett. B **287**, 283 (1992).

[8] J. D. Sullivan, Phys. Rev. D **5**, 1732 (1972); M. Lusignoli and Y. Srivastava, Nucl. Phys. **B138**, 151 (1978); G. G. Arakelyan, K. G. Boreskov, and A. B. Kaidalov, Yad. Fiz. **33**, 471 (1981) [Sov. J. Nucl. Phys. **33**, 247 (1981)].

[9] A. W. Thomas, Phys. Lett. **126B**, 97 (1983).

[10] L. L. Frankfurt, L. Mankiewicz, and M. I. Strikman, Z. Phys. A **334**, 343 (1989).

[11] A. S. Ito *et al.*, Phys. Rev. D **23**, 604 (1981); M. Ericson and A. W. Thomas, Phys. Lett. **148B**, 191 (1984); G. G. Arakelyan and K. G. Boreskov, Yad. Fiz. **41**, 416 (1985) [Sov. J. Nucl. Phys. **41**, 267 (1985)].

[12] K. Gottfried, Phys. Rev. Lett. **18**, 1174 (1967).

[13] New Muon Collaboration, P. Amaudruz *et al.*, Phys. Rev. Lett. **66**, 2712 (1991).

[14] E. M. Henley and G. A. Miller, Phys. Lett. B **251**, 497 (1990).

[15] A. I. Signal, A. W. Schreiber, and A. W. Thomas, Mod. Phys. Lett. A **6**, 271 (1991).

[16] S. Kumano, Phys. Rev. D **43**, 59 (1991); S. Kumano and J. T. Londergan, *ibid.* **44**, 717 (1991).

[17] W. Melnitchouk, A. W. Thomas, and A. I. Signal, Z. Phys. A **340**, 85 (1991).

[18] W.-Y. P. Hwang, J. Speth, and G. E. Brown, Z. Phys. A **339**, 383 (1991).

[19] A. Szczurek and J. Speth, Jülich Report No. KFA-IKP(TH)-1992-1 (unpublished).

[20] V. Zoller, Z. Phys. C **53**, 443 (1992).

[21] V. Dmitrašinović and R. Tegen, Phys. Rev. C **46**, 1108 (1992).

[22] P. J. Mulders, A. W. Schreiber, and H. Meyer, Nucl. Phys. **A549**, 498 (1992).

[23] E. L. Berger, F. Coester, and R. B. Wiringa, Phys. Rev. D **29**, 398 (1984).

[24] V. M. Belayev and B. L. Ioffe, Nucl. Phys. **B310**, 548 (1988).

[25] R. L. Jaffe, in *Relativistic Dynamics and Quark-Nuclear Physics*, Proceedings of the Workshop, Los Alamos, New Mexico, 1985, edited by M. B. Johnson and A. Picklesimer (Wiley, New York, 1985).

[26] For scalar mesons, the trace factor in $f_{N\sigma}(y')$ for the structure $\not{q}/2\not{p}'q$ is $4m_N^2-m_\sigma^2+(m_N^2-t')(1-y')/y'$, which is clearly related to the trace in $f_{\sigma N}(y)$, namely, $-t+4m_N^2$ when written in terms of the transverse momentum squared (with $m_\pi \to m_\sigma$), and which thereby satisfies Eq. (2), apart from the form factor. For an operator $I/(2m_N)$ the trace factor in $f_{N\sigma}(y')$ is $2t'+2m_N^2-m_\sigma^2$, but this not only violates baryon-number conservation, it also leads to an unphysical (negative) cross section. Similar problems appear in $f_{NV}(y')$ with such an operator.

[27] A. W. Schreiber, W. Melnitchouk, and A. W. Thomas (in preparation).

[28] A. Bodek and J. L. Ritchie, Phys. Rev. D **23**, 1070 (1981); G. Dunne and A. W. Thomas, *ibid.* **33**, 2061 (1986).

[29] L. Heller and A. W. Thomas, Phys. Rev. C **41**, 2756 (1990); M. B. Johnson and J. Speth, Nucl. Phys. **A470**, 488 (1987); L. Kisslinger and M. B. Johnson, Phys. Rev. C **36**, 1081 (1987).

[30] F. Güttner, G. Chanfray, H. J. Pirner, and B. Povh, Nucl. Phys. **A249**, 389 (1984).

[31] S. Weinberg, Phys. Rev. **150**, 1313 (1966).

[32] S. D. Drell, D. J. Levy, and T. M. Yan, Phys. Rev. D **1**, 1035 (1970).

[33] T. Uematsu and T. F. Walsh, Nucl. Phys. **B199**, 93 (1982); P. Hoodbhoy, R. L. Jaffe, and A. Manohar, *ibid.* **B312**, 571 (1989); F. E. Close and S. Kumano, Phys. Rev. D **42**, 2377 (1990).

[34] NA10 Collaboration, B. Betev *et al.*, Z. Phys. C **28**, 15 (1985).

[35] G. Hohler and E. Pietarinen, Nucl. Phys. **B95**, 210 (1975).

[36] W. Grein and P. Kroll, Nucl. Phys. **A338**, 332 (1980).

[37] BEBC Collaboration, D. Allasia *et al.*, Z. Phys. C **28**, 321 (1985).

[38] J. F. Owens, Phys. Lett. B **266**, 126 (1991); J. G. Morfin

and W. K. Tung, Z. Phys. C **52**, 13 (1991); E. Eichten, I. Hinchliffe, K. Lane, and C. Quigg, Rev. Mod. Phys. **56**, 579 (1984); M. Diemoz, F. Ferroni, E. Longo, and G. Martinelli, Z. Phys. C **39**, 21 (1988).

[39] A. W. Schreiber, P. J. Mulders, A. I. Signal, and A. W. Thomas, Phys. Rev. D **45**, 3069 (1992).

[40] S. Théberge, G. A. Miller, and A. W. Thomas, Can. J. Phys. **60**, 59 (1982).

[41] W. Melnitchouk and A. W. Thomas (in preparation).

ADP-93-210/T128

PSI-PR-93-13

Deep Inelastic Scattering from Off-Shell Nucleons

W.Melnitchouk*
Department of Physics and Mathematical Physics, University of Adelaide, South Australia, 5005.

A.W.Schreiber
Paul Scherrer Institut, Würenlingen und Villigen, CH-5232 Villigen PSI, Switzerland.

A.W.Thomas
Department of Physics and Mathematical Physics, University of Adelaide, South Australia, 5005.
(June 29, 1993)

We derive the general structure of the hadronic tensor required to describe deep-inelastic scattering from an off-shell nucleon within a covariant formalism. Of the large number of possible off-shell structure functions we find that only four contribute in the Bjorken limit. In our approach the usual ambiguities which are encountered when discussing problems related to off-shellness in deep-inelastic scattering are not present. The formulation therefore provides a clear framework within which one can discuss the various approximations and assumptions which have been used in earlier work. As examples, we investigate scattering from the deuteron, nuclear matter and dressed nucleons. The results of the full calculation are compared with those where various aspects of the off-shell structure are neglected, as well as with those of the convolution model.

PACS numbers: 13.60.Hb, 12.38.Lg, 25.30.Fj

I. INTRODUCTION

The general structure of the hadronic tensor relevant to deep-inelastic scattering (DIS) from an on-mass-shell particle ($p^2 = M^2$) which transforms correctly under proper Lorentz transformations, the parity transformation and which is gauge invariant is well known. In the Bjorken limit the two possible structure functions collapse to one, so that, in the case of one flavour, deep-inelastic scattering may be expressed in terms of just one quark distribution which is a function of only one variable. (All these statements refer to spin independent scattering, to which we restrict ourselves throughout this paper.)

The situation is considerably more complex if one is considering, in a covariant formulation, DIS from an off-mass-shell ($p^2 \neq M^2$) hadronic constituent within a composite target. This situation arises, for example, in many calculations relevant to the EMC effect, where an off-shell nucleon contained in a nucleus interacts with a high energy probe. Another application of interest is the scattering from a nucleon dressed by a meson cloud. Indeed, because of the added complexity, many calculations ignore the issue completely in the hope that the effects are not large. Typically one neglects not only the possible p^2 dependence in the structure functions, but also assumes no change in the structure of the off-shell hadron tensor. Only in this case can the structure function of the target be written as a one-dimensional convolution between a constituent (nucleon) distribution function within the target and a quark distribution within the constituent [1].

We shall consider scattering from an off-mass-shell nucleon without making these approximations. The purpose is to develop a theoretical framework which is exact, thus keeping the model-dependent approximations to as late a stage as possible. It is important to realise that the change in the structure of the off-shell tensor is by no means a trivial matter. There are several distinct differences from the on-shell tensor:

I Most obviously, the dependence on the four-momentum squared of the nucleon is no longer trivial, as it is in the case where the target is on-shell.

II In a covariant formalism the off-shell fermion tensor is a 4×4 matrix in the external fermion legs. This corresponds to the fact that in a relativistic theory it is necessary to consistently incorporate the antiparticle degrees of freedom. Because of this matrix structure the tensor involves, at least in principle, many more independent functions than in the on-shell case.

---

*Address after 1 September 1993: Institut für Theoretische Physik, Universität Regensburg, D-93040 Regensburg, Germany.

III Because the incoming particles are off-mass-shell the gauge invariance condition for this tensor is not the same as in the on-shell case.

To show this last point, consider the truncated forward virtual Compton amplitude, $\widehat{T}_{\mu\nu}(p,q)$, which satisfies the well-known generalised Ward identity [2]

$$q^\mu \, \widehat{T}_{\mu\nu}(p,q) = -e \left\{ S^{-1}(p) S(p+q) \Gamma_\nu(p+q,p) \; - \; \Gamma_\nu(p,p-q) S(p-q) S^{-1}(p) \right\}, \tag{1}$$

where $\Gamma_\nu(p+q,p)$ is the γNN vertex function and $S(p)$ is the fermion propagator. For an on-shell nucleon, the full Compton amplitude is

$$T_{\mu\nu}(p,q) = \overline{u}(p) \widehat{T}_{\mu\nu} u(p) \tag{2}$$

so that inserting Eq.(1) into Eq.(2), and using the Dirac equation, leads to

$$q^\mu T_{\mu\nu}(p,q) = 0. \tag{3}$$

Note that the same equation does not hold for the off-shell tensor $\hat{T}_{\mu\nu}$ (ie. the right hand side of Eq.(1) is non-zero) — even for the case where the target is a free pointlike fermion.

Although in calculations of nuclear structure functions the off-shell aspects of the nucleon structure function have usually been ignored, a few partial attempts have been made to try to account for these effects. Unfortunately, these calculations are not without ambiguities [3,4]. Kusno and Moravcsik [5] used the so-called 'off-shell kinematics — on-shell dynamics' scheme, in which the off-shell nucleon tensor is evaluated at the same energy transfer ν and four-momentum transfer q^2 as the on-shell one, independent of the virtuality of the nucleon. Bodek and Ritchie [6] used a similar scheme, however they suggested that the off-shell structure functions could be identified with the on-shell ones, evaluated for the same values of q^2 and centre of mass energy squared $s = (p+q)^2$, and hence a different value of energy transfer, $\nu \to \nu + (p^2 - M^2)/2$. Dunne and Thomas [7], on the other hand, used an ansatz in which the matrix elements of the hadronic operators in the operator product expansion were assumed to be independent of p^2. The result was a nucleon structure function that was to be evaluated at a shifted value of $q^2 (\to \xi(p^2,q^2) q^2$, where ξ is the q^2 rescaling parameter). This result was mathematically equivalent to the dynamical rescaling model of Close, Roberts and Ross [8] and Nachtmann and Pirner [9], in which the shift in q^2 was attributed to a change in confinement radius for nucleons bound inside a nucleus.

All of the above treatments use, in one form or other, the familiar convolution formula [1], which amounts to folding the quark momentum distribution in the off-shell constituent with the constituent momentum distribution in the target. In order to derive this formula it is assumed that the form of the off-shell nucleon tensor (i.e. the structure in its Dirac indices) is the same as the on-shell one [10,11]. However, as we show in Sections II and III, more than one operator contributes in the Bjorken limit, so there is no *a priori* reason for this to be a valid assumption. The appearance of these other operator structures is closely connected with the antiparticle degrees of freedom arising in any relativistic treatment and constitutes an important part of the off-shell effects. Relativistic calculations have been attempted in the past by Nakano [12] and Gross and Liuti [13], however their derivations of the convolution model also rely critically on assumptions about the off-shell tensor, and the relativistic bound nucleon density matrix, respectively. In fact, to our knowledge, all attempts to derive the simple covariant convolution model have ultimately resorted to some prescription to account for the fact that the nucleon has $p^2 \neq M^2$. Without performing a full calculation which self-consistently accounts for the nucleon virtuality, all such *ad hoc* approximations must remain in doubt. In short, the naive convolution formula is not a sound starting point for discussing off-shell effects and we make no use of it.

There exist alternative approaches to these just described which do not suffer from off-mass-shell ambiguities. For the nuclear EMC effect, Berger et al. [14] used light-front dynamics to calculate the nuclear structure functions. Here all particles are on-mass-shell, the transverse momentum and the light-cone variable $p_+ = p_0 + p_L$ are conserved at each vertex, while $p_- = p_0 - p_L$ is not. Alternatively, Johnson and Speth [3] and Heller and Thomas [4] used old-fashioned perturbation theory with the instant form of dynamics, where particles are on-mass-shell, three-momentum is conserved, but not necessarily energy. Unfortunately, in both of these approaches, the off-mass-shell ambiguities in the definition of the off-shell structure functions are simply replaced by off-energy-shell ambiguities [15]. A review of some of the problems with these approaches may be found in Refs. [16,17].

The advantage of the covariant method in nuclear calculations is that Lorentz invariance is manifest. However, for a consistent treatment within this framework one has to include the antiparticle degrees of freedom, which has not been done up to now. We will set up the formalism in such a way that the structure functions of the physical target are expressed in terms of fully relativistic quark–nucleon and nucleon–target vertex functions. This will enable us to ensure gauge invariance, the Callan-Gross relation and an unambiguous identification of the scaling variables.

All model approximations will be contained entirely in the vertex functions themselves, which, of course, we cannot calculate from first principles.

This paper is organised as follows: In Section II we define the general structure of the off-shell tensor in terms of a suitable set of structure functions. In Section III we explicitly calculate the scaling properties of these functions. As we shall see, only 4 of 22 possible functions contribute in the Bjorken limit. In Section IV we discuss how our formalism can be used to calculate structure functions of composite particles and discuss the limits in which the conventional convolution model may be obtained. In Section V we use some simple parameterisations of the relativistic vertex functions to calculate the nucleon valence quark distributions. Using these same vertex functions we then calculate in Section VI the structure functions of composite targets containing off-shell nucleons.

II. GENERAL STRUCTURE OF THE OFF-SHELL NUCLEON TENSOR

The process in which we are interested is depicted in Fig.1, with the photon momentum q and the off-shell nucleon momentum p marked. The corresponding off-shell tensor $\chi_{\mu\nu}$ with the correct transformation properties under proper Lorentz and parity transformations is a 4×4 matrix depending on p and q, and may in general be written in terms of 22 functions:

$$\begin{aligned}\chi_{\mu\nu}(p,q) = \chi^0_{\mu\nu}(p,q) &+ \not{p}\,\chi^1_{\mu\nu}(p,q) + \not{q}\,\chi^2_{\mu\nu}(p,q) + \gamma_{\{\mu}p_{\nu\}}\,\chi^3(p,q) + \gamma_{\{\mu}q_{\nu\}}\,\chi^4(p,q)\\ &+ \sigma_{\alpha\beta}p^\alpha q^\beta\,\chi^5_{\mu\nu}(p,q) + \sigma_{\alpha\{\mu}\,p_{\nu\}}p^\alpha\,\chi^6(p,q) + \sigma_{\alpha\{\mu}\,p_{\nu\}}q^\alpha\,\chi^7(p,q)\\ &+ \sigma_{\alpha\{\mu}\,q_{\nu\}}p^\alpha\,\chi^8(p,q) + \sigma_{\alpha\{\mu}\,q_{\nu\}}q^\alpha\,\chi^9(p,q),\end{aligned} \tag{4}$$

where the braces $\{...\}$ around the subscripts indicate the symmetric $\mu\nu$ combination. Here, $\chi^i_{\mu\nu}(p,q)$ are the most general tensors of rank two which may be constructed out of q and p,

$$\begin{aligned}\chi^i_{\mu\nu}(p,q) = &P_{T\mu\nu}(p,q)\,\chi^i_T(p,q) + P_{L\mu\nu}(p,q)\,\chi^i_L(p,q)\\ &+ P_{Q\mu\nu}(p,q)\,\chi^i_Q(p,q) + P_{QL\mu\nu}(p,q)\,\chi^i_{QL}(p,q), \qquad i=0,1,2,5.\end{aligned} \tag{5}$$

The χ^i's on the right hand side of Eq.(5), as well as χ^3, χ^4 and χ^6—χ^9 in Eq.(4), are scalar functions of q and p. The tensors $P^{\mu\nu}$ are defined by

$$\begin{aligned}P^{\mu\nu}_T(p,q) &= \tilde{g}^{\mu\nu} + \frac{\tilde{p}^\mu\tilde{p}^\nu}{\tilde{p}^2}, & P^{\mu\nu}_L(p,q) &= \frac{\tilde{p}^\mu\tilde{p}^\nu}{\tilde{p}^2},\\ P^{\mu\nu}_Q(p,q) &= \frac{q^\mu q^\nu}{q^2}, & P^{\mu\nu}_{QL}(p,q) &= \frac{1}{\sqrt{-q^2\tilde{p}^2}}\left(\tilde{p}^\mu q^\mu + \tilde{p}^\nu q^\mu\right),\end{aligned} \tag{6}$$

where $\tilde{g}_{\mu\nu} = -g_{\mu\nu} + q_\mu q_\nu/q^2$ and $\tilde{a}_\mu = a_\mu - q_\mu\, a\cdot q/q^2$, with a_μ being any four-vector.

The above decomposition of the off-shell tensor is of course not unique. It is written in this convenient form because the tensors $P^{\mu\nu}$ turn out to be projection operators [11] and satisfy

$$\begin{aligned}P^{\mu\nu}_T(p,q)\,P_{T\mu\nu}(p,q) &= 2, & P^{\mu\nu}_L(p,q)\,P_{L\mu\nu}(p,q) &= 1,\\ P^{\mu\nu}_Q(p,q)\,P_{Q\mu\nu}(p,q) &= 1, & P^{\mu\nu}_{QL}(p,q)\,P_{QL\mu\nu}(p,q) &= -2,\end{aligned} \tag{7}$$

with all other combinations vanishing. It is important to note that in the Bjorken limit these relations are also true for projectors involving different momenta. That is, the projectors are still orthogonal in this limit and

$$P^{\mu\nu}_T(p_1,q)\,P_{T\mu\nu}(p_2,q) = 2 \quad \text{etc.} \tag{8}$$

In general, Fig.1 is a subdiagram of Fig.2, where $\mathcal{P}$ is the on-shell momentum of the composite target (labelled A). As will be discussed more fully in Sections IV and V, the hadron tensor for the complete process, $W^A_{\mu\nu}(\mathcal{P},q)$, involves an integral over the nucleon momentum p of the tensor $\chi_{\mu\nu}(p,q)$, traced with another 4×4 matrix originating in the soft target-constituent part of the diagram. Hence no experiment measures the off-shell tensor by itself, so it is not possible to measure all the functions χ^i separately. Only combinations thereof give rise to observable experimental quantities. Using the above projectors, we can determine which combinations of off-shell structure functions contribute to the physical ones. In particular, the operators $P^{\mu\nu}_T(\mathcal{P},q)$, $P^{\mu\nu}_L(\mathcal{P},q)$, $P^{\mu\nu}_Q(\mathcal{P},q)$ and $P^{\mu\nu}_{QL}(\mathcal{P},q)$ project from the composite target tensor $W^A_{\mu\nu}(\mathcal{P},q)$ the transverse, longitudinal and the two possible gauge non-invariant contributions, respectively, in terms of the scalar functions $\chi^i(p,q)$.

Not all of the functions χ^i will in fact be independent, as the gauge invariance of the theory requires that the latter two contributions vanish. Furthermore, the longitudinal function must also be zero in the Bjorken limit ($\mathcal{P}\cdot q,\ Q^2 \equiv -q^2 \to \infty,\ x = Q^2/2\mathcal{P}\cdot q$ fixed), if the Callan-Gross relation is to be satisfied. That this is indeed the case is shown explicitly in the Appendix. For the remaining physical (transverse) contribution we obtain for the coefficients of the χ^i's:

$$\begin{aligned}\frac{1}{2}P_T^{\mu\nu}(\mathcal{P},q)\ \chi_{\mu\nu}(p,q) = {}& \chi_T^0(p,q) + \not{p}\ \chi_T^1(p,q) + \not{q}\ \chi_T^2(p,q) + \sigma_{\alpha\beta}p^\alpha q^\beta\ \chi_T^5(p,q)\\ &+ \frac{q^2}{2(p\cdot q)^2}\ (p - y\mathcal{P})^2\ [\chi_L^0(p,q) + \not{p}\ \chi_L^1(p,q) + \not{q}\ \chi_L^2(p,q) + \sigma_{\alpha\beta}p^\alpha q^\beta\ \chi_L^5(p,q)\ ]\\ &+ \left[-\not{p} + y\not{\mathcal{P}} + \frac{1}{\mathcal{P}\cdot q}\left(\mathcal{P}\cdot p - y\mathcal{P}^2\right)\not{q}\right]\chi^3(p,q)\\ &- \left[y\,\mathcal{P}^\alpha + \frac{\mathcal{P}\cdot(p - y\,\mathcal{P})}{\mathcal{P}\cdot q}q^\alpha\right]\sigma_{\alpha\beta}p^\beta\ \chi^6(p,q) + [p^\alpha - y\mathcal{P}^\alpha]\sigma_{\alpha\beta}q^\beta\ \chi^7(p,q)\ ,\end{aligned} \tag{9}$$

where $y = p\cdot q/\mathcal{P}\cdot q = p_+/\mathcal{P}_+$ is the constituent's light-cone momentum fraction. In the next Section we derive the scaling behaviour of the functions χ^i using the parton model, by separating the hard, q^2 dependent, part of the truncated amplitude $\chi_{\mu\nu}(p,q)$ from the soft, non-perturbative component. We will see that Eq.(9) simplifies considerably, as many terms do not contribute in the Bjorken limit.

A special case of the above formalism is DIS from an on-shell nucleon, described by the tensor which we denote by $W_{\mu\nu}^N(p,q)$. In this case the contribution to the nucleon tensor is given by Eq.(9) traced with $(\not{p} + M)/2$, where $\mathcal{P}{=}p$ and no integration over p is performed:

$$M\ W_{\mu\nu}^N(p,q;p^2 = M^2) = \frac{1}{2}\mathrm{Tr}\left[(\not{p} + M)\ \chi_{\mu\nu}(p,q)\right]. \tag{10}$$

This gives the transverse unpolarised on-shell structure functions in terms of the on-shell limits of the functions χ^i ($\tilde{\chi}^i(p,q) \equiv \chi^i(p,q;p^2 = M^2)$):

$$\frac{M}{2}W_T^N(p,q) = M\ \tilde{\chi}_T^0(p,q) + M^2\ \tilde{\chi}_T^1(p,q) + p\cdot q\ \tilde{\chi}_T^2(p,q). \tag{11}$$

Similar expressions can also be found for the other functions (i.e. longitudinal and non gauge-invariant), but again these vanish in the Bjorken limit.

III. SCALING BEHAVIOUR OF THE OFF-SHELL FUNCTIONS χ

We shall now calculate the leading twist contribution to the off-shell structure functions in the quark-parton model. This is given by the imaginary part of the forward scattering amplitude depicted in Fig.3, i.e.

$$[\chi_{\mu\nu}(p,q)]_{ab} = \mathcal{I}\cdot[r_{\mu\nu}(k,q)]_{cd}\,[H(k,p)]_{dcab} \tag{12}$$

where $\mathcal{I}$ is the integral operator

$$\mathcal{I} = \int\frac{d^4k}{(k^2 - m^2)^2}\delta([q+k]^2 - m^2) \tag{13}$$

and the Dirac matrix structure has been made explicit. (The complete forward scattering amplitude in addition contains the crossed photon diagram, which we do not explicitly take into account. All the formal results of Sections I to IV remain valid upon inclusion of this diagram. Numerically, it can make a small contribution in the small x region, however in the subsequent model calculation in which we consider only two-quark intermediate states there will be no contribution.) In Eq.(13) k is the parton's four-momentum and m its (current) mass. In the following we will drop quark mass terms as the difference between the $m = 0$ results and those for $m \sim$ few MeV is negligible. (We shall return to the question of quark masses in Section V.) The non-perturbative part of the structure function is contained in the function H, while the perturbative, calculable part is contained in $r_{\mu\nu}$,

$$r_{\mu\nu}(k,q) = k^2\left(q_\alpha g_{\mu\nu} - \left(k_{\{\mu} + q_{\{\mu}\right)g_{\nu\}\alpha}\right)\gamma^\alpha + \not{k}\left(q^2 g_{\mu\nu} + 4k_\mu k_\nu + 2k_{\{\mu}q_{\nu\}}\right). \tag{14}$$

The trace over the indices c, d in Eq.(12) may be performed and the results written as

$$\mathrm{Tr}\left[r_{\mu\nu}[H]_{ab}\right] = \left[k^2\left(q_\alpha g_{\mu\nu} - \left(k_{\{\mu} + q_{\{\mu}\right) g_{\nu\}\alpha}\right) + k_\alpha\left(q^2 g_{\mu\nu} + 4k_\mu k_\nu + 2k_{\{\mu}q_{\nu\}}\right)\right][G^\alpha(p,k)]_{ab}. \tag{15}$$

As G^α is a 4×4 matrix which transforms like a vector and must be even under parity transformations, its most general form is

$$\begin{aligned} G^\alpha = {} & (p^\alpha f_1 + k^\alpha f_2)\,\mathbf{I} + (p^\alpha f_3 + k^\alpha f_5)\,\not{k} + (p^\alpha f_4 + k^\alpha f_6)\,\not{p} + \gamma^\alpha f_7 \\ & + \sigma^{\beta\alpha} p_\beta\, f_8 \;+\; \sigma^{\beta\alpha} k_\beta\, f_9 \;+\; p^\beta k^\delta \sigma_{\beta\delta}\, p^\alpha\, f_{10} \;+\; p^\beta k^\delta \sigma_{\beta\delta}\, k^\alpha\, f_{11}, \end{aligned} \tag{16}$$

where the functions f_i are scalar functions of p and k.

The integrals over k can be done in a standard way. For example, for an integrand containing one free k^α, contracting with p_α and q_α enables us to make the replacement

$$\mathcal{I}\cdot k^\alpha \to \mathcal{I}\cdot\{\rho_1\, p^\alpha + \rho_2\, q^\alpha\} \tag{17}$$

Similarly for $k^\alpha k^\beta$ terms,

$$\mathcal{I}\cdot k^\alpha k^\beta \to \mathcal{I}\cdot\left\{\rho_3\; P_T^{\alpha\beta}(p,q) + \tilde{p}^2\rho_1^2\; P_L^{\alpha\beta}(p,q) + \frac{(k\cdot q)^2}{q^2} P_Q^{\alpha\beta}(p,q) - \frac{\tilde{k}\cdot\tilde{p}\;\, k\cdot q}{\sqrt{-q^2\;\tilde{p}^2}} P_{QL}^{\alpha\beta}(p,q)\right\} \tag{18}$$

and for $k^\alpha k^\beta\, \not{k}$ terms,

$$\begin{aligned} \mathcal{I}\cdot k^\alpha k^\beta\, \not{k} \to \mathcal{I}\cdot\Big\{ & -\rho_3\left(\rho_1 p^{\{\alpha} + \rho_2 q^{\{\alpha}\right)\gamma^{\beta\}} + \rho_3\left(\rho_1\,\not{p} + \rho_2\,\not{q}\right)\, P_T^{\alpha\beta}(p,q) \\ & + \rho_1\left(\left[2\rho_3 + \tilde{p}^2\rho_1^2\right]\left[\not{p} - \frac{p\cdot q}{q^2}\,\not{q}\right] + \frac{k\cdot q}{q^2}\tilde{p}^2\rho_1\,\not{q}\right)\, P_L^{\alpha\beta}(p,q) \\ & + \frac{(k\cdot q)}{q^2}\left(k\cdot q\rho_1\,\not{p} + \left[k\cdot q\rho_2 + 2\rho_3\right]\not{q}\right)\, P_Q^{\alpha\beta}(p,q) \\ & - \frac{1}{\sqrt{-q^2\;\tilde{p}^2}}\left(\left[k\cdot q\rho_3 + \tilde{p}^2\rho_1^2\right]\not{p} + \left[\tilde{p}^2\rho_1(\rho_3 + k\cdot q\rho_2) - \frac{p\cdot q\;\, k\cdot q}{q^2}\rho_3\right]\not{q}\right) P_{QL}^{\alpha\beta}(p,q)\Big\}, \end{aligned} \tag{19}$$

where

$$\begin{aligned} \rho_1 &= \frac{\tilde{k}\cdot\tilde{p}}{\tilde{p}^2} \\ \rho_2 &= \frac{k\cdot q}{q^2} - \frac{p\cdot q\;\tilde{k}\cdot\tilde{p}}{q^2\;\tilde{p}^2} \\ \rho_3 &= \frac{1}{2}\left(-\tilde{k}^2 + \tilde{p}^2\rho_1^2\right). \end{aligned} \tag{20}$$

The χ^i's are then completely defined in terms of the functions f_1–f_{11}, and as all the dependence on the photon momentum q is now explicit, their scaling behaviour may be derived in a straightforward manner. We find that χ_T^0 and χ_T^1 are of order 1, while all other χ^i's are of order $1/\nu$, with the exception of χ^7 and χ^9, which are of order $1/\nu^2$. Hence we find that deep-inelastic scattering from an off-shell nucleon may be expressed in terms of just four functions,

$$\frac{1}{2}P_T^{\mu\nu}(\mathcal{P},q)\;\chi_{\mu\nu}(p,q) = \chi_T^0(p,q) + \not{p}\,\chi_T^1(p,q) + \not{q}\,\chi_T^2(p,q) \;+\; \sigma_{\alpha\beta}p^\alpha q^\beta\;\chi_T^5(p,q). \tag{21}$$

The complete expressions for the functions χ_T^i are

$$\chi_T^0(p,q) = \mathcal{I}\cdot\left\{-\left(k^2 p\cdot q + q^2 k\cdot p\right) f_1(k,p) - \frac{q^2k^2}{2} f_2(k,p)\right\} \tag{22a}$$

$$\begin{aligned} \chi_T^1(p,q) = \mathcal{I}\cdot\Big\{ & -\left(k^2 p\cdot q + q^2 k\cdot p\right)\left(f_4(k,p) - \frac{q^2}{2p\cdot q} f_3(k,p)\right) \\ & -\frac{q^2k^2}{2}\left(f_6(k,p) - \frac{q^2}{2p\cdot q} f_5(k,p)\right) + \frac{q^4}{2p\cdot q} f_7(k,p)\Big\} \end{aligned} \tag{22b}$$

$$\chi_T^2(p,q) = \mathcal{I}\cdot\Big\{-\left(\frac{p^2q^2}{2p\cdot q}+k\cdot p\right)\left(\left[k^2+\frac{k\cdot p\,q^2}{p\cdot q}\right]f_3(k,p)+\frac{q^2}{2p\cdot q}\left[k^2\ f_5(k,p)+2\ f_7(k,p)\right]\right) - k^2\ f_7(k,p)\Big\} \tag{22c}$$

$$\chi_T^5(p,q) = \mathcal{I}\cdot\Big\{-\left(\frac{p^2q^2}{2p\cdot q}+p\cdot k\right)\left(\frac{q^2}{p\cdot q}f_8(k,p)+\left[k^2+\frac{p\cdot kq^2}{p\cdot q}\right]f_{10}(k,p)+\frac{k^2q^2}{2p\cdot q}f_{11}(k,p)\right) + k^2\left(f_8(k,p)-\frac{q^2}{2p\cdot q}f_9(k,p)\right)\Big\}. \tag{22d}$$

For the other χ's it can be easily demonstrated (see the Appendix for details) that for each of the arbitrary functions f_i, there are cancellations at leading order in ν in the expressions for $P_L^{\mu\nu}(\mathcal{P},q)\chi_{\mu\nu}(p,q)$, $P_Q^{\mu\nu}(\mathcal{P},q)\chi_{\mu\nu}(p,q)$ and $P_{QL}^{\mu\nu}(\mathcal{P},q)\chi_{\mu\nu}(p,q)$ in the Bjorken limit. Hence the Callan-Gross relation, as well as gauge invariance ($q^\mu W^A_{\mu\nu}=0$), are assured, independent of the nature of the target-constituent part of the diagram. This result is completely general, so that model dependent approximations for the vertex functions do not affect these results.

IV. CONVOLUTION MODEL

Before we move on to making model dependent assumptions for the vertex functions, we need to write down the on-shell tensor $W^A_{\mu\nu}(\mathcal{P},q)$ for the target A in terms of the off-shell tensor $\chi_{\mu\nu}(p,q)$. The full tensor for the composite target is given by

$$M_T\ W^A_{\mu\nu}(\mathcal{P},q) = \int\frac{d^4p}{(2\pi)^4}\frac{2\pi\delta\left([\mathcal{P}-p]^2-M_R^2\right)}{(p^2-M^2)^2}\mathrm{Tr}\left[\Big(IA_0(p,\mathcal{P})+\gamma_\alpha A_1^\alpha(p,\mathcal{P})+\sigma_{\alpha\beta}A_2^{\alpha\beta}(p,\mathcal{P})\Big)\ \chi_{\mu\nu}(p,q)\right], \tag{23}$$

where A_0, A_1 and A_2 are functions describing the target—constituent part of the complete diagram in Fig.2, and M_T and M_R are the masses of the target and target recoil systems, respectively. Implicit in the functions A_0-A_2 is a sum over all excited target recoil states, or equivalently an integration over the masses M_R weighted by some target recoil spectral function.

For most vertices only A_0 and A_1 will contribute, while A_2 will arise typically as an interference term when more than one type of vertex is used. Using the transverse projection operator defined in Eq.(6), we get

$$\begin{aligned} M_T\ W_T^A(\mathcal{P},q) &= \frac{M_T}{2}P_T^{\mu\nu}(\mathcal{P},q)\ W^A_{\mu\nu}(\mathcal{P},q) \\ &= \int\frac{dy\ d^2\mathbf{p}_T}{(2\pi)^3(1-y)(p^2-M^2)^2}\left\{A_0(p,\mathcal{P})\ \chi_T^0(p,q)\ +\ p\cdot A_1(p,\mathcal{P})\ \chi_T^1(p,q)\ +\ q\cdot A_1(p,\mathcal{P})\ \chi_T^2(p,q)\right. \\ &\qquad \left.+\ (p_\alpha\ q_\beta\ -\ p_\beta\ q_\alpha)A_2^{\alpha\beta}(p,\mathcal{P})\ \chi_T^5(p,q)\right\}, \end{aligned} \tag{24}$$

where $p^2 = p_+p_- - \mathbf{p}_T^2$, $p_+ = y\mathcal{P}_+$, and we have used the δ function to fix $p_- = M_T\ +\ (M_R^2-\mathbf{p}_T^2)/(p_+ + M_T)$.

The convolution model may only be derived from Eq.(24) if we make some additional assumptions. First of all, we need to assume that the target structure function can be written in factorised form, in terms of the nucleon structure function, W_T^N, and some nucleon distribution function, φ:

$$W_T^A(x,Q^2) = \int dy\ \int d^2\mathbf{p}_T\ \ \varphi(A_0,A_1,A_2)\ \ W_T^N(x/y,Q^2,\mathbf{p}_T). \tag{25}$$

Furthermore, to obtain the usual one-dimensional convolution formula [1,11] we must assume that W_T^N is independent of $\mathbf{p}_T$ (or equivalently p^2):

$$W_T^A(x,Q^2) = \int dy\ \tilde{\varphi}(y)\ \ W_T^N(x/y,Q^2), \tag{26}$$

where now the integral over $\mathbf{p}_T$ has been absorbed into the definition of $\tilde{\varphi}$.

There are several ways in which the first assumption might be valid:

CASE (a): If all but one of the functions χ_T^i ($i=0-2,5$) are zero in the Bjorken limit. Most authors (see for example Refs. [1,10,11]) adopt this choice, as this is the case for a pointlike fermion (where only χ_T^2 contributes). However, as was shown in Section III, all four functions χ_T^i in principle contribute in the Bjorken limit, so that one

would require that some of the functions f in Eqs.(22) vanish or cancel. We know of no reason why this should be the case — indeed even the extremely simple quark-nucleon vertex functions which we consider in the next Section give rise to more than one nonvanishing χ_T^i.

CASE (b): If more than one of the χ_T^i's is non-zero, but the non-zero ones are proportional to each other. For example, $f_1 = Mf_4$ and all other f's equal to zero would imply $\chi_T^0 = M\chi_T^1$, and so Eq.(25) is obtained. Again, in general there doesn't seem to be any reason to expect this behaviour.

CASE (c): If the non-zero nucleon — target functions $A_0 - A_2$ multiplying the functions χ_T^i are proportional to each other. An example of this would be if A_0 and A_1 were non-zero and if $A_0 = p \cdot A_1/M = q \cdot A_1\ M/p \cdot q$, which would then give Eq.(25). In general this will not be true unless the $p^2 = M^2$ limit is taken inside the functions $A_0 - A_2$.

In short, none of the above conditions are generally satisfied in a self-consistent, fully covariant (relativistic) calculation. Consequently the convolution model interpretation, Eq.(26), of the nuclear structure function in terms of bound nucleon structure functions is inconsistent within this formalism. This difficulty is intrinsically related to the presence of antinucleon degrees of freedom, which are not accounted for in the traditional convolution model. Furthermore, in the absence of the convolution model, the common practice of extracting *nucleon* structure functions from nuclear DIS data is not valid. Indeed, the very concept of a structure function of a nucleon bound within a nucleus looses its utility. One is *forced* to consider quark and nuclear degrees of freedom side by side in the calculation of the *nuclear* structure functions.

Using Eq.(24) directly we may compare, for some simple vertex functions, the exact result with those obtained by making the convolution model approximation, Eq.(26). This we will do in the next Section. As a final comment, it should be noted that, within the physical assumptions made by the use of the model in the first place (i.e. no final state interactions), the functions χ_T^i are independent of the physical target, and depend only on the nucleon constituent. By selecting various targets (i.e. by varying $A_0 - A_2$) the relative contributions from the functions χ_T^i could in principle be probed, provided, of course, we know the target—constituent functions $A_0 - A_2$ sufficiently well. Conversely, once the χ's have been determined for one process, they may be used for all other processes.

V. CALCULATION OF THE NUCLEON STRUCTURE FUNCTION

To calculate the transverse structure function of the complete target requires two sets of functions describing the soft, non-perturbative physics, namely the quark—nucleon functions $f_1 - f_{11}$, and the nucleon—target functions $A_0 - A_2$. Here we concentrate on the former set.

We observe that because both the constituent nucleon and struck quark inside the nucleon have spin 1/2, the intermediate spectator state will have either spin 0 or 1. In order to make an overall Lorentz scalar, we therefore need only consider quark—nucleon vertices that transform as a scalar or vector under Lorentz transformations. It is straightforward to identify the form of the vertices that are allowed by Lorentz, parity and time-reversal invariance, however the specific momentum dependence has to be determined within a model. There will be 15 independent scalar ($\Phi^S_{1-4}(k,p)$) and vector ($\Phi^V_{1-11}(k,p)$) vertex functions appearing in the general expression

$$\mathcal{V}^S = I\ \Phi_1^S + \not{p}\ \Phi_2^S + \not{k}\ \Phi_3^S + \sigma_{\alpha\beta}p^\alpha k^\beta\ \Phi_4^S \tag{27}$$

for a scalar vertex, and

$$\begin{aligned}\mathcal{V}^V_\alpha = {} & \gamma_\alpha\ \Phi_1^V + p_\alpha\ I\ \Phi_2^V + k_\alpha\ I\ \Phi_3^V + \sigma_{\alpha\beta}p^\beta\ \Phi_4^V + \sigma_{\alpha\beta}k^\beta\ \Phi_5^V \\ & + p_\alpha\ \not{p}\ \Phi_6^V + p_\alpha\ \not{k}\ \Phi_7^V + k_\alpha\ \not{p}\ \Phi_8^V + k_\alpha\ \not{k}\ \Phi_9^V \\ & + \sigma_{\beta\delta}p^\beta k^\delta\ p^\alpha\ \Phi_{10}^V + \sigma_{\beta\delta}p^\beta k^\delta\ k^\alpha\ \Phi_{11}^V\end{aligned} \tag{28}$$

for a vector vertex.

The functions $f_1 - f_{11}$ in Eq.(16) can be uniquely determined from these vertex functions. To see this, let us firstly consider the scalar vertex. The general target—constituent function from Section III, $(H(k,p))_{dcab}$, will be proportional to $(\mathcal{V}^S)_{ac}(\mathcal{V}^S)_{db}$. Using the Fierz theorem the Dirac indices can be rearranged into a form that enables the connection with the functions f_i to be explicit:

$$\begin{aligned}
f_1 &= 2\ \Phi_1^S\ \Phi_2^S\ \delta, & f_2 &= 2\ \Phi_1^S\ \Phi_3^S\ \delta, \\
f_3 &= 2\ \left(\Phi_2^S\ \Phi_3^S + p\cdot k\ (\Phi_4^S)^2\right)\ \delta, & f_4 &= 2\ \left((\Phi_2^S)^2 - k^2\ (\Phi_4^S)^2\right)\ \delta, \\
f_5 &= 2\ \left((\Phi_3^S)^2 - p^2\ (\Phi_4^S)^2\right)\ \delta, & f_6 &= 2\ \left(\Phi_2^S\ \Phi_3^S + p\cdot k\ (\Phi_4^S)^2\right)\ \delta, \\
f_7 &= \left((\Phi_1^S)^2 - (p\ \Phi_2^S + k\ \Phi_3^S)^2 + (p^2k^2 - (p\cdot k)^2)\ (\Phi_4^S)^2\right)\ \delta,
\end{aligned} \tag{29}$$

$$f_8 = -4\,k\cdot(p\,\Phi_2^S\;+\;k\,\Phi_3^S)\,\Phi_4^S\,\delta, \qquad f_9 \;=\; 4\,p\cdot(p\,\Phi_2^S\;+\;k\,\Phi_3^S)\,\Phi_4^S\,\delta,$$
$$f_{10} = 8\,\Phi_2^S\,\Phi_3^S\,\delta, \qquad f_{11} \;=\; 8\,\Phi_3^S\,\Phi_4^S\,\delta,$$

where $\delta \equiv \delta\left([p-k]^2 - m_S^2\right)$ and m_S is the mass of the scalar spectator system.

Calculating the functions Φ_{1-4}^S from first principles amounts to solving the relativistic, many-body bound state problem. As this is presently not possible one could resort to models such as the MIT bag model. It is not our aim to do this in this paper. Rather, we shall choose a single scalar vertex, say $\mathcal{V}^S = I\,\Phi_1^S$, and use phenomenological input to constrain its functional form. From Eq.(29) we find that the $I\,\Phi_1^S$ vertex contributes only to f_7:

$$f_7 = (\Phi_1^S)^2\,\delta\left([p-k]^2 - m_S^2\right) \qquad \text{[scalar vertex]}. \tag{30}$$

Similarly we choose for the vector vertex a single form, $\mathcal{V}^V = \gamma_\alpha \Phi_1^V$, and find that this makes the following contributions:

$$f_3 = -f_4 \;=\; -f_5 \;=\; f_6 \;=\; -\frac{2\,f_7}{m_V^2} \;=\; -\frac{2\,(\Phi_1^V)^2\,\delta\left([p-k]^2 - m_V^2\right)}{m_V^2} \qquad \text{[vector vertex]} \tag{31}$$

where m_V is the mass of the vector spectator state. In writing Eq.(31) we have assumed that the intermediate vector state has a Lorentz structure $-g_{\alpha\beta} + (p_\alpha - k_\alpha)(p_\beta - k_\beta)/m_V^2$. For the sake of simplicity we further assume that only valence quarks are present, so that the scalar or vector spectator may be identified with a diquark. In a more refined calculation one could, for example, integrate over diquark masses using some diquark spectral function.

From Eqs.(30) and (31) we see that even the simplest vertex functions lead to a large number of non-zero functions f_i. This in turn implies that there are scaling contributions to both of the functions χ_T^1 and χ_T^2 in Eqs.(22), thereby failing to satisfy scenarios (a) and (c) in Section IV for the derivation of the convolution model. For more complicated $N-q$ vertices, even more of the f's (and hence χ_T^0 and χ_T^5 as well) will be non-zero.

The k^2 dependence of the functions $\Phi_1^{S,V}$ can be most easily modelled by considering the on-shell nucleon structure function (i.e. we shall approximate the quark's off-shell dependence to be the same in on- and off-shell nucleons. We discuss this point further in Section VI.A.) The large-x limit is known to be dominated by valence u quarks, which implies that the scalar vertex dominates at large x [19]. Now note that, as the spectator state is on-mass-shell, the quark four-momentum will behave as $k^2 \sim (-m_S^2 - \mathbf{k}_T^2)/(1-x)$ at large x. In order to obtain the correct large-x behaviour of the structure function, namely $W_T^N \sim (1-x)^3$, the k^2 dependence in the scalar vertex function must be $1/k^2$, after we also take into account the two quark propagators, as well as the factor $(1-x)$ arising from the delta function $\delta\left([p-k]^2 - m_R^2\right)$ for the on-shell diquark state of mass m_R ($= m_S$ or m_V) [18].

We fix the large k^2 behaviour of the vector vertex function in a similar way, this time by requiring that we obtain the correct valence d_V/u_V ratio at large x, namely $\sim (1-x)$. This means that the vertex function for DIS from valence d_V quarks has to go like $(1-x)^4$ for large x, i.e. like $(k^2)^{-5/2}$ (there is an additional $(1-x)^{-2}$ factor arising from the trace for the vector diquark).

It may now seem reasonable to choose a simple monopole form for the scalar vertex function, and an equivalent one for the vector vertex as was done, for example, in Refs. [18,11]. We do not do this, however, for the following reason. The quark propagator, $(k^2-m^2)^{-2}$, in Eq.(13) contains a pole. Because the kinematic maximum for k^2 is $(M-m_R)^2$, this pole is in the physical region of k^2 when $m_R + m < M$. The origin of this pole is clear — the model, so far, is not confining and the proton may dissociate into its quark and diquark constituents. One solution would be to make the sum of the quark and diquark masses so large that this cannot occur. However, we do not believe that this is desirable — confinement occurs not because the quark mass is large (it is only a few MeV), but in a dynamical way associated with the nature of the colour interaction. The only place where the information about colour confinement can enter in this model is through the relativistic quark—nucleon vertex function. A convenient way to ensure that the contribution from a deconfined quark is excluded is to choose a numerator in $\Phi_1^{S,V}$ so that the integrand in the structure function remains finite at the on-shell point, $k^2 = m^2$.

For the masses of the scalar and vector diquark, m_S and m_V, the only information available to us is that from low energy models, such as the bag model or the non-relativistic quark model. There, at a scale (Q^2) of order a few hundred MeV^2, the diquark masses are expected to be somewhere within the range of 600 to 1100 MeV [19,20]. Furthermore, from the nucleon—$\Delta(1232)$ mass splitting we also anticipate that m_V would be some 200 MeV larger than m_S.

The p^2 dependence of the vertex functions is of course more difficult to obtain, since for this purpose data on nuclear structure functions must be used. In this case the p^2 dependence will not be restricted to the quark—nucleon vertex function alone, but will also be present in the nucleon—nucleus vertices, which introduces an inherent uncertainty in the determination of the former. Nevertheless, the functions $\Phi_1^{S,V}(k,p)$ do not depend on the nuclear target — that information is contained entirely in the functions $A_0 - A_2$. Since for the deuteron the p^2 dependence of the relativistic

DNN vertex can be related to known deuteron wavefunctions [21–23], we may use deuteron DIS data to constrain this universal p^2 dependence of the quark—nucleon vertex functions.

In order to obtain the valence quark distribution for the deuteron, we will use data obtained from muon scattering for $x > 0.3$, where valence quarks are known to dominate. Because of isospin symmetry ($u^D = d^D$) only a single experimental quantity for the deuteron (compared with two — $u + d$ and d/u — for the nucleon) is meaningful, namely $F_{2D} = x(4u^D + d^D)/9 = 5x(u + d)/9$, where u^D, d^D and u, d are the up and down quark distributions in the deuteron and proton, respectively. Hence we cannot differentiate between the p^2 dependence in Φ_1^S and that in Φ_1^V. We therefore choose a simple monopole form and use the same cut-off mass, Λ_p, in both functions. A detailed comparison between the model and data for $x \lesssim 0.3$ would require separation of the valence and sea components of F_{2D}. Although in principle this could be done by analysing the $\nu - D$ and $\bar{\nu} - D$ DIS data, in practice those data suffer from poor statistics. Furthermore, typically only the extracted quark distributions in the nucleon are presented [24], and these depend on the theoretical assumptions made to treat binding and Fermi motion corrections.

To summarise, the vertex functions that we use are given by

$$\Phi_1^S(p,k) \propto \frac{(k^2 - m^2)}{(k^2 - \Lambda_S^2)^2} \frac{(M^2 - \Lambda_p^2)}{(p^2 - \Lambda_p^2)} \tag{32a}$$

$$\Phi_1^V(p,k) \propto \frac{(k^2 - m^2)}{(k^2 - \Lambda_V^2)^{7/2}} \frac{(M^2 - \Lambda_p^2)}{(p^2 - \Lambda_p^2)}. \tag{32b}$$

We find the best fit to the experimental nucleon distributions at $Q^2 = 4\text{GeV}^2$ (we evolve the curves from $Q_0^2 = 0.15$ GeV^2 using leading order QCD evolution, with $\Lambda_{QCD} = 250$ MeV [25]) for masses $m_S = 850$ MeV and $m_V = 1050$ MeV, and cut-offs $\Lambda_S = 1.2$ GeV and $\Lambda_V = 1.0$ GeV, which we fit to the recent parameterisations by Morfin and Tung [26] and Owens [27]. The fits to the $u_V + d_V$ valence quark distribution as well as the valence d_V/u_V ratio are shown in Figs.4 and 5 respectively. It is remarkable that such simple forms for the vertex functions reproduce the data so well.

Having parameterised the free nucleon vertices, we are now ready to consider the specific cases of DIS from the deuteron, from nuclear matter, and from dressed nucleons. Throughout, we consider the isoscalar valence structure function, $xW_T \propto x(u_V + d_V) = 3/2\ x(q_0 + q_1)$, where q_0 and q_1 are the quark distributions arising in connection with the scalar and vector diquarks, respectively, normalised so that their first moments are unity (from the spin-flavour wavefunction of the proton we have $d_V = q_1$ and $u_V = (q_1 + 3q_0)/2$).

VI. CALCULATION OF COMPOSITE TARGET STRUCTURE FUNCTIONS

A. DIS from the Deuteron

We examine nuclear DIS from a deuteron for several reasons. Firstly, it is critical to know the size of the off-mass-shell corrections to the deuteron structure function if ultimately the EMC data (which usually measures the ratio of nuclear to deuterium structure functions) is to be used to draw conclusions about the differences between quark distributions in free nucleons and those bound in nuclei. Secondly, in the absence of high-statistics neutrino data, the neutron structure function is often inferred from the deuteron structure function using the naive assumption of additivity of the bound proton and neutron structure functions. Apart from the off-mass-shell effects which we consider here, several other effects spoil this simple assumption. For example, nuclear shadowing is important as $x \to 0$ [28–31], and of course the deuteron structure function extends beyond $x_N = 1$ ($x_N \equiv (M_D/M)\ x$) to $x_N = M_D/M$. Hence deviations from additivity occur over much of the range of x. For a reliable extraction of the neutron structure function a systematic computation of these effects is clearly valuable.

The calculation of DIS from the deuteron is more straightforward and reliable than for heavier nuclei, since the relativistic deuteron–nucleon vertex is reasonably well understood. The treatment of the deuteron recoil state is simplified by the fact that most of the time this will be an on-shell nucleon, as this can be expected to dominate the contributions from processes with a recoil Δ or Roper resonance, or a higher mass state.

The structure of the general DNN vertex, with one nucleon on-shell, was first derived by Blankenbecler and Cook [32], $\langle N|\psi_N|D\rangle \propto (\not{p} - M)^{-1}\Gamma_\alpha^D\ \epsilon^\alpha\ \mathcal{C}\bar{u}^T(\mathcal{P} - p)$, where the DNN vertex function is [33]

$$\Gamma_\alpha^D(p^2) = \gamma_\alpha\ F(p)\ +\ \left(\frac{1}{2}\mathcal{P}_\alpha - p_\alpha\right)\ G(p)\ +\ \frac{\not{p} - M}{M}\left[H(p)\gamma_\alpha\ +\ \frac{J(p)}{M}\left(\frac{1}{2}\mathcal{P}_\alpha - p_\alpha\right)\right], \tag{33}$$

and $\mathcal{C}$ is the charge conjugation operator. The functions F, G, H and I are related to the $^3S_1$,$^3D_1$,$^1P_1$ and $^3P_1$ deuteron wavefunctions, u, w, v_s and v_t, respectively, by

$$F(p) = \pi\sqrt{2M_D}\,(2E_p - M_D)\left(u(|\mathbf{p}|) - \frac{w(|\mathbf{p}|)}{\sqrt{2}} + \sqrt{\frac{3}{2}}\frac{M}{|\mathbf{p}|}v_t(|\mathbf{p}|)\right) \tag{34a}$$

$$G(p) = \pi\sqrt{2M_D}\,(2E_p - M_D)\left(\frac{M}{E_p+M}u(|\mathbf{p}|) + \frac{M\,(2E_p+M)}{\mathbf{p}^2}\frac{w(|\mathbf{p}|)}{\sqrt{2}} + \sqrt{\frac{3}{2}}\frac{M}{|\mathbf{p}|}v_t(|\mathbf{p}|)\right) \tag{34b}$$

$$H(p) = \pi\sqrt{2M_D}\,\frac{E_p M}{|\mathbf{p}|}\,\sqrt{\frac{3}{2}}\,v_t(|\mathbf{p}|) \tag{34c}$$

$$J(p) = -\pi\sqrt{2M_D}\,\frac{M^2}{M_D}\left(\frac{2E_p - M_D}{E_p+M}u(|\mathbf{p}|) - \frac{(2E_p - M_D)(E_p+2M)}{\mathbf{p}^2}\frac{w(|\mathbf{p}|)}{\sqrt{2}} + \frac{\sqrt{3}M_D}{|\mathbf{p}|}\,v_s(|\mathbf{p}|)\right) \tag{34d}$$

where $E_p = \sqrt{M^2+\mathbf{p}^2}$. For the deuteron wavefunctions we use the model of Buck and Gross [21], with a pseudovector π exchange interaction.

For the spin-averaged deuteron hadronic tensor we therefore need to evaluate the trace

$$\sum_\lambda \epsilon^{*\alpha}(\lambda,\mathcal{P})\,\epsilon^{\beta}(\lambda,\mathcal{P})\,\mathrm{Tr}\left[(\not{\mathcal{P}}^T - \not{p}^T + M)\,\mathcal{C}\bar{\Gamma}^D_\beta(p^2)\,(\not{p}+M)\,\chi_{\mu\nu}(p,q)\,(\not{p}+M)\,\mathcal{C}\Gamma^D_\alpha(p^2)\right], \tag{35}$$

where $\epsilon^\alpha(\lambda,\mathcal{P})$ is the polarisation vector for a deuteron with helicity λ, and $\bar{\Gamma}^D_\beta = \gamma_0\,\Gamma^{D\dagger}_\beta\,\gamma_0$. This yields the following deuteron—nucleon functions:

$$\begin{aligned}
A^D_0(p^2) = M\Bigg\{ & 4\,F^2\left[4\,M^2 + 2\,M_D^2 - (p^2-M^2)\left(-2+\frac{p^2-M^2}{M_D^2}\right)\right] \\
& - 8\,F\,G\left[4\,M^2 - M_D^2 + \frac{(p^2-M^2)}{4M^2}\left(10\,M^2 - M_D^2 + 2\,p^2 + \frac{3\,M^4 - 2\,M^2p^2 - p^4}{M_D^2}\right)\right] \\
& + \frac{G^2}{M^2}\left[\left(4\,M^2 - M_D^2\right)^2 - (p^2-M^2)\left(4\,M_D^2 - 5\,p^2 - 11\,M^2 + \frac{2p^4 - 2M^4}{M_D^2}\right)\right] \\
& - \frac{(p^2-M^2)}{M^2}\Bigg[-12\,H^2\,(p^2-M^2) + 4\,F\,H\left(-5M^2 - 2M_D^2 + p^2 + \frac{(p^2-M^2)^2}{M_D^2}\right) \\
& \qquad + \left(p^2 - \frac{(\mathcal{P}\cdot p)^2}{M_D^2}\right)\left(\frac{(p^2-M^2)}{M^2}\left(-4\,J^2 + 8\,H\,J\right) + 16\,F\,J\right. \\
& \qquad \left. +16\,G\,H + 8\,G\,J\,\frac{(\mathcal{P}\cdot p - M^2 - p^2)}{M^2}\right)\Bigg]\Bigg\}
\end{aligned} \tag{36a}$$

$$\begin{aligned}
A^D_{1\alpha}(p^2) = {} & 4\,F^2\left[\left(4\,M^2 + 2\,M_D^2\right)p_\alpha - (p^2-M^2)\left(\frac{(p^2-M^2)}{M_D^2}p_\alpha + \left(2 - \frac{(p^2-M^2)}{M_D^2}\right)\mathcal{P}_\alpha\right)\right] \\
& - 8\,F\,G\left[\left(4\,M^2 - M_D^2\right)p_\alpha + \left(\left(1 - \frac{(p^2-M^2)}{M_D^2}\right)p_\alpha + \frac{\mathcal{P}\cdot p}{M_D^2}\right)\right] \\
& + \frac{G^2}{M^2}\left[\left(4\,M^2 - M_D^2\right)^2 p_\alpha - (p^2-M^2)\left(\left(M_D^2 - 4\,M^2\right)\left(2 - \frac{p^2-M^2}{M_D^2}\right)p_\alpha\right.\right. \\
& \qquad \left.\left. -4\left(p^2 - \frac{(\mathcal{P}\cdot p)^2}{M_D^2}\right)\mathcal{P}_\alpha\right)\right] \\
& - \frac{(p^2-M^2)}{M^2}\Bigg\{4\,H^2\,(p^2-M^2)\left[p_\alpha - \left(2 - \frac{p^2-M^2}{M_D^2}\right)\mathcal{P}_\alpha\right] \\
& \quad - 4\,J^2\,\frac{p^2-M^2}{M^2}\left(p^2 - \frac{(\mathcal{P}\cdot p)^2}{M_D^2}\right)[p_\alpha - \mathcal{P}_\alpha] + 8\,H\,J\,(p^2-M^2)\left[p_\alpha - \frac{\mathcal{P}\cdot p}{M_D^2}\mathcal{P}_\alpha\right] \\
& \quad - 8\,F\,H\,M^2\left[2\,p_\alpha + \left(2 - \frac{p^2-M^2}{M_D^2}\right)\mathcal{P}_\alpha\right] \\
& \quad + 4\,F\,J\left[\left(3M^2 + p^2 - \frac{(p^2-M^2)^2}{M_D^2}\right)p_\alpha - \left(p^2 + M^2 - \frac{(p^2-M^2)^2}{M_D^2}\right)\mathcal{P}_\alpha\right]
\end{aligned}$$

$$+ 8\,G\,H\left[\left(M^2+p^2-\mathcal{P}\cdot p\right)p_\alpha+\left(p^2-\frac{p^2+M^2}{M_D^2}\mathcal{P}\cdot p\right)\mathcal{P}_\alpha\right]$$
$$+ 8\,G\,J\left(p^2-\frac{(\mathcal{P}\cdot p)^2}{M_D^2}\right)[-2p_\alpha+\mathcal{P}_\alpha]\Big\} \tag{36b}$$
$$A^D_{2\alpha\beta}(p^2)=0. \tag{36c}$$

As mentioned in the previous section, we constrain the cut-off parameter Λ_p in the quark—(off-shell) nucleon vertex functions defined in Eqs.(32) by fitting our full, p^2 dependent calculated distribution to the experimental deuteron structure function, using the lepton—deuteron data from NMC, BCDMS and SLAC [34]. However, we still need to fix the normalisation constants in Eqs.(32). Naturally, these will be functions of the cut-off Λ_p. Actually, if the exact nucleon—quark vertex functions were known, they would be the same for the off-shell as for the on-shell nucleon. We do not assume this, however, as the vertex functions which we use are only approximations to the exact results. For example, the arguments given in Section V, relating to the counting rules which give the k^2 dependence of the vertex functions, are based on quark distributions in an on-shell nucleon. In an off-shell nucleon the connection between x and k^2 is given by the modified expression

$$k^2=k_+k_--k_T^2 \;=\; xM_D\left(p_- - \frac{(\mathrm{p}_T-\mathrm{k}_T)^2+m_R^2}{M_D(y-x)}\right) \;-\; k_T^2, \tag{37}$$

with p_- now constrained by the δ function for the on-shell nuclear recoil state (see Section IV). In principle, the asymptotic k^2 dependence for the off-shell nucleon—quark vertices expected from counting rules could be determined after integration over the nucleon's momentum. Clearly this is a much more complicated task than was the case for the on-shell nucleon, and we do not believe our simple ansatz for the vertices warrants such a treatment, in which case we shall simply normalise by comparing with the data.

In Fig.6 we compare the experimental F_{2D} at $Q^2=10$ GeV^2 with the calculated total valence quark distribution in the deuteron, $5/9x(u_V+d_V)$, evolved from the same value of $Q_0^2=0.15$ GeV^2 (since we use the same diquark masses) as for the free nucleon distributions in Section V. The result of the full calculation is almost independent of the value of Λ_p used, after the normalisation constants for the vertex functions have been determined by the charge conservation condition. This is because the p_T distribution is strongly peaked at small transverse momenta, $p_T\sim 25$ MeV, so that modification of the large p_T (or large $|p^2|$) behaviour by altering the form factor cut-off has negligible consequences. Clearly there is very good agreement between the model calculation and the data for $x\gtrsim 0.3$.

From the discussion in Sections IV and V it should be clear that it is not possible to justify the convolution model for deuteron deep-inelastic scattering. Still, it is of interest to compare our results with those of previous calculations that have made use of convolution-like formulas. Firstly we can notice that by taking the on-shell limit ($p^2\to M^2$) for the kinematic factors in A_0^D and A_1^D in Eqs.(36), we obtain $A_0^D/M=p\cdot A_1^D/M^2=q\cdot A_1^D/p\cdot q$, thereby satisfying condition (c) in Section IV for the convolution model (although this approximation need not be taken in the functions F,G,H,J themselves). Such an approximation is in the spirit of that used in Ref. [13] for the nuclear structure functions. The result of this approximation is shown in the dashed curve of Fig.6, where we have used the same normalisation constants in Eqs.(32) (for $\Lambda_p=\infty$) as those determined in the full calculation. The effect is a reduction in the absolute value of the structure function, without much affect on the shape. By artificially normalising the new distribution so that the final result conserves baryon number, this curve becomes almost indistinguishable from the full result. However, there is no good reason for using different normalisation constants in this approximation, since the $p^2=M^2$ limit is taken in the nuclear part of the diagram and thus should not in principle affect the quark—off-shell nucleon vertex.

In other calculations using the convolution model for deuterium, the most common prescription has been to drop all terms but $I\chi_T^0$ in the expansion of $\chi_{\mu\nu}$ (in Eq.(35)), and to replace χ_T^0 by the experimental, on-shell structure function of the nucleon [5,35], In Fig.6 the dotted curve shows the result after renormalisation to ensure baryon number two for the deuteron. It is somewhat surprising that the difference in shape between the full result and this ansatz is as small as it is. Still, a discrepancy of $\sim 20\%$ is quite significant in a system as loosely bound as the deuteron.

A numerically significant difference between the convolution approach and the exact calculation is of particular importance if one recalls that the neutron structure function is extracted from structure functions of light nuclei, such as deuterium, using the convolution model. Indeed, in view of the problems which we have just described, it is rather worrying than our knowledge of F_{2n} is based on this. As seen in Fig.6, depending on the approximation or ansatz taken in calculating F_{2D}, the deviation from the correct, p^2-dependent result, will vary. Still, although unsatisfactory from a theoretical point of view, by artificially re-normalising the deuteron structure function by hand so that it respects baryon number conservation, the differences can be reduced.

A similar situation arises in calculations of the nuclear EMC effect, in which differences between nuclear and deuteron structure functions are explored. Clearly for any accurate description of this effect we need firstly to have a reliable method of calculating the deuteron structure function. As we have seen, the off-shell effects that are ignored in the deuteron may be compensated for by suitably renormalising the final result. Whether this can also be done in other, heavier, nuclei is not clear. Certainly in heavy nuclei we would expect off-shell effects to play some role. To date these have not been adequately accounted for, and this is what we turn to next.

B. Nuclear Matter

For any nucleus we can easily repeat the above calculation if we know the relativistic nucleon—nucleus vertex functions. Unfortunately, at the present time these are not at all well known for heavy nuclei. A solution to this problem would be to simply parameterise the vertex functions, and to make some assumptions for the nuclear recoil state. Alternatively, if one tried to use non-relativistic nuclear models as an approximation, it would be difficult to incorporate the off-shell nucleon structure. The best way is to consider first the simpler case of a nucleon embedded in nuclear matter. In this type of calculation the off-shell effects are parameterised in the effective nucleon mass, $M \to M^*$.

Experimentally, the effective nucleon mass at nuclear matter density (~ 0.15 fm^{-3}) is found to be $\sim 0.7\ M$ [36]. Theoretically, there is a large number of models for nuclear matter, which predict a wide range of effective nucleon masses. The Quantum Hadrodynamics model of Walecka and Serot [36], in which pointlike nucleons (in the mean field approximation) are bound by the exchange of scalar (σ) and vector (ω) mesons, predicts rather small effective masses, $M^*/M \simeq 0.56 - 0.6$. Somewhat larger masses are obtained when explicit quark degrees of freedom are introduced. For example, in the Guichon model [37], where the σ and ω mesons are allowed to couple directly to quarks inside the nucleons, the value of M^* is typically $\sim 0.9\ M$. Even larger values are obtained if one includes centre-of-mass corrections and self-coupling of the scalar fields [38,39]. Rather than choose a specific nuclear model, we let M^* be a parameter and examine the effect of its variation upon the nucleon structure function, defined in Eq.(11).

Because the quark—nucleon vertex function will now also depend on the effective mass, it would be inappropriate to use the same normalisation constants in Eqs.(32) as those determined by normalising the on-shell nucleon distributions. Therefore the normalisation constants in this case must be determined by normalising the calculated quark distributions in nuclear matter, for $p^2 = M^{*2}$, so that their first moments are unity.

Fig.7 shows the isoscalar valence nucleon structure function, $x\left(u_V(x, p^2 = M^{*2}) + d_V(x, p^2 = M^{*2})\right)$, for a range of effective masses, $M^*/M \sim 0.5 - 1$. There is clearly quite significant softening of the structure function, with the most prominent effects appearing for $0.2 \lesssim x \lesssim 0.6$.

However, it should be remembered that our formalism neglects interactions between the spectator quarks and the surrounding nucleons in the nuclear medium (i.e. it assumes the impulse approximation). This has been found to be quite a poor approximation [38] for nuclear matter. A simple way to estimate the importance of final state interactions is to assume that the strength of the interaction of the spectator diquark with the nuclear medium is 2/3 that of the nucleon interaction, and that it is independent of the mass of the diquark. In that case the diquark mass is modified by $m_R \to m_R^*$, where

$$m_R^* = m_R - \frac{2}{3}\left(M - M^*\right) \tag{38}$$

for both scalar and vector diquarks. The effect of this is shown in Fig.8. As can be seen, interactions of the spectator diquark lead to a hardening of the quark distribution, typically of the same order of magnitude as the nucleon off-shell effects. Combined with the off-shell effects, this gives a structure function which (for $M^*/M \approx 0.7$) is $\sim 20 - 30\%$ larger than the on-shell result for $x \gtrsim 0.4$. For quantitative comparison against deep-inelastic scattering data on nuclear structure functions it would therefore be very valuable to develop a consistent formalism incorporating both effects.

C. DIS From Dressed Nucleons

Models of the nucleon which incorporate PCAC by including a pion cloud have been used in DIS, among other things, to estimate the size of the πNN form factor [40,41], and to calculate the flavour symmetry breaking in the proton sea — the possibility of which was recently suggested by the result of the New Muon Collaboration's measurement of the Gottfried sum rule [42]. Previous covariant calculations [43–46] have all relied upon the same assumptions as for the nuclear calculations, namely the validity of the convolution formula in the first place, and the

lack of any dependence of the bound nucleon structure function on p^2 and $\mathbf{p}_T$. In this Section we apply the formalism we have developed for dealing with off-shell effects to the part of this problem where the virtual photon hits the virtual nucleon, with its spectator pion left on-mass-shell.

In order to calculate this contribution the only additional ingredient which we need is the 'sideways' πNN form factor, $\Gamma_{\pi NN}(p^2)$, where one nucleon is off-mass-shell. For this we use the same monopole form that is usually used in the literature [11] (see also [47,48])

$$\Gamma_{\pi NN}(p^2) \propto \left(p^2 - \Lambda_{\pi N}^2\right)^{-1}, \tag{39}$$

with $\Lambda_{\pi N} \sim 1.4$ GeV and a pseudoscalar πN coupling. With this, we can rearrange the relevant trace in Eq.(23),

$$\mathrm{Tr}\left[(\not{\mathcal{P}} + M)\; i\gamma_5 \Gamma_{\pi NN}(p^2)\; (\not{p} + M)\; \chi_{\mu\nu}(p,q)\; (\not{p} + M)\; i\gamma_5 \Gamma_{\pi NN}(p^2)\right], \tag{40}$$

to obtain the nucleon–pion functions $A_{0-2}^{\pi N}$,

$$A_0^{\pi N}(p,\mathcal{P}) = \left(-m_\pi^2\; M\right) \Gamma_{\pi NN}^2(p^2) \tag{41a}$$

$$A_{1\;\alpha}^{\pi N}(p,\mathcal{P}) = \left(-m_\pi^2\; p_\alpha \;+\; (p^2 - M^2)(p_\alpha - \mathcal{P}_\alpha)\right) \Gamma_{\pi NN}^2(p^2) \tag{41b}$$

$$A_{2\;\alpha\beta}^{\pi N}(p,\mathcal{P}) = 0. \tag{41c}$$

Again, as was the case for the deuteron, by inserting $p^2 \to M^2$ in $A_{1\alpha}^{\pi N}$ we can satisfy the conditions of case (c) in Section IV. However, the structure function this time is proportional to $-m_\pi^2$ (i.e. negative), which is clearly unphysical. This illustrates the fact that even though the one dimensional convolution formula may indeed be obtained from the exact result by certain approximations (e.g. on-shell limit), there is no guarantee that these approximations are physically meaningful.

As was shown in [11], the convolution model may be derived if, amongst other things, one assumes that the off-shell nucleon structure is the same as that of a point-like fermion [1], in which case the relevant operator in $\chi_{\mu\nu}$ is $\not{q}\chi_T^2(p,q)$. As we have seen above, this is only part of the complete expression in the Bjorken limit if one assumes the nucleon quark vertex to be of the form in Section V. Nevertheless, the model of [11] can be obtained using these vertices if the following steps are taken: firstly the trace in Eq.(40) evaluated with the $\not{q}\chi_T^2$ structure; then to obtain factorisation the limits $\mathbf{p}_T = 0$ and $p^2 = M^2$ taken in the 'nucleon structure function' (i.e. k dependent) parts; and finally the full structure of the on-shell nucleon function used, as in Eq.(11), rather than just keeping the χ_T^2 term. The necessity of the last point is clear, since for the on-shell structure function the *individual* functions χ_T^i are not necessarily positive definite, although the sum of course is positive.

Other authors [49] have implicitly assumed that the relevant operator to be used in the $\chi_{\mu\nu}$ of Eq.(40) is $I\chi_T^0$, similar to what was done in the convolution model calculation for the deuteron discussed in Section VI A. However, even with the subsequent replacement of χ_T^0 by the full on-shell nucleon structure function in the convolution expression, the result will be proportional to $-m_\pi^2$ since the coefficient of χ_T^0 is $A_0^{\pi N}$. Thus it appears that the result of [49] can only be obtained by taking the modulus of a negative structure function.

Clearly, the above procedures are somewhat arbitrary. It is a reflection of the fact that none of the scenarios described in Section IV (namely cases (a)—(c)) for obtaining the convolution model are applicable. As in the deuteron case, the convolution model for dressed nucleons is not derivable from the exact result.

In Fig.9 we show the result of the convolution model of [11]. This is compared with the result of the calculation including the full p^2 dependence, with the quark—nucleon vertex function evaluated with $\Lambda_p = \infty$, as for the deuteron. For the full calculation we use the same normalisation constants for the quark—nucleon vertices as determined from the on-shell nucleon calculation in Section V. The results indicate that the full, p^2 dependent calculation gives somewhat smaller results compared with those of the convolution model (although the shapes are quite similar, as can be seen from the dotted curve, where we normalise the scalar and vector vertex functions to give the same first moments as in the convolution model). Such a difference might have been surprising had the convolution expression been a simple approximation to the full result, in which case we may well have expected small off-shell corrections. Unfortunately, this calculation is more difficult to check since there is no clear normalisation condition for the structure function. Comparing the first moment of the calculated distributions with the average number of pions in the intermediate state, which can be calculated by considering DIS from the virtual pion, is ambiguous due to the presence of antiparticles in the covariant formulation. (A convolution formula such as Eq.(25) can be written for DIS from virtual pions, since there are no spinor degrees of freedom to spoil this factorisation. However, ambiguities in the p^2 dependence of the 'off-shell pion structure function' would still remain.) We therefore believe that this fact illustrates the absence of a firm foundation for the covariant convolution model for DIS from dressed nucleons (see [50,51] for an alternative approach to this calculation).

VII. CONCLUSION

We have investigated within a covariant framework the deep-inelastic scattering from composite particles containing virtual nucleon constituents. The scattering has been treated as a two-step process, in which the off-shell nucleon in the target interacts with the high energy probe. The treatment amounts to neglecting final state interactions. We have constructed the truncated photon—nucleon amplitude from 22 general, independent functions, and used the parton model to show that only 4 of these are relevant in describing the deep-inelastic structure functions in the Bjorken limit. The calculation explicitly ensures current conservation and the Callan-Gross relation.

Within this framework we can unambiguously examine under what conditions the conventional convolution model breaks down. Furthermore, we use some simple models of the relativistic nucleon–quark and nucleus–nucleon vertex functions to investigate this breakdown numerically. While the failure of the convolution model may appear to be an unwelcome complication, it is clear that in any theoretically self-consistent calculation which takes off-mass-shell effects into account it is an inevitable one. Indeed, the 'bound nucleon structure function' is an ill-defined quantity within a covariant formulation. This has wide-ranging consequences, as almost all calculations of composite target structure functions (e.g. nuclei, for the EMC effect) have relied upon the validity of the simple convolution model.

We have been able to calculate the deuteron structure function without making any assumptions about the p^2 dependence of the structure functions, and find excellent agreement with the data in the region of x where our model is applicable ($x \gtrsim 0.3$). Making various assumptions for the off-shell nucleons naturally introduces deviations from the exact result. However, by suitably renormalising the approximated curves by hand to ensure baryon number conservation (as was done in most previous calculations) the differences between the exact results and those of the convolution ansatz are minimised. Although this is most unsatisfactory from a theoretical point of view, phenomenologically the consequences of neglecting the nucleon off-shell effects in the deuteron may not be too great.

To understand the consequences of the off-shell effects in heavy nuclei, we considered a simple model of a nucleon embedded in nuclear matter. We found quite a significant softening of the structure function at intermediate x when the nuclear medium acts to decrease the effective nucleon mass. However, interactions of the spectator diquark state with the surrounding medium tend to make the overall structure function some $20-30\%$ harder at large x ($x \gtrsim 0.4$), for $M^*/M \approx 0.7$, compared with the on-shell result.

The other application which has been examined is DIS from the virtual nucleon component of a physical, or dressed, nucleon, where we also find quite significant differences between the full result and the convolution model. A detailed quantitative understanding of this effect is needed in order to be able to describe the x distributions for all processes where the nucleon's dissociation into a virtual nucleon and meson is expected to be of importance, such as in the measurement of the asymmetry in the light sea quark sector of the proton and neutron, as well as the neutron spin structure function $g_{1n}(x)$.

ACKNOWLEDGMENTS

This work was supported by the Australian Research Council. One of us (AWS) would like to acknowledge the kind hospitality extended to him by the theory group during his visit to Adelaide, where this work was commenced.

APPENDIX: GAUGE INVARIANCE AND THE LONGITUDINAL STRUCTURE FUNCTION

Here we give the full details regarding the vanishing of the longitudinal and non gauge-invariant structure functions.

Using the projection operators defined in Section II we project from the truncated nucleon tensor $\chi_{\mu\nu}$ the contributions to the longitudinal (W_L^A) and non gauge-invariant ($W_Q^A, W_{Q_L}^A$) functions:

$$\begin{aligned} P_L^{\mu\nu}(\mathcal{P},q)\,\chi_{\mu\nu}(p,q) = {} & \chi_L^0(p,q) + \not{p}\,\chi_L^1(p,q) + \not{q}\,\chi_L^2(p,q) + \sigma_{\alpha\beta}p^\alpha q^\beta\,\chi_L^5(p,q) \\ & + \frac{q^2}{(p\cdot q)^2}\,(p-y\mathcal{P})^2\,[\chi_T^0(p,q) + \not{p}\,\chi_T^1(p,q) + \not{q}\,\chi_T^2(p,q) \\ & \qquad + \sigma_{\alpha\beta}p^\alpha q^\beta\,\chi_T^5(p,q)\,] \\ & - \frac{2\,p\cdot q}{q^2}\not{q}\,\chi^3(p,q) - \frac{2\,p\cdot q}{q^2}\sigma_{\alpha\beta}p^\alpha q^\beta\,\chi^6(p,q) - 2\,y\,\sigma_{\alpha\beta}\mathcal{P}^\alpha q^\beta\,\chi^7(p,q) \qquad \text{(A1a)} \\ P_Q^{\mu\nu}(\mathcal{P},q)\,\chi_{\mu\nu}(p,q) = {} & \chi_Q^0(p,q) + \not{p}\,\chi_Q^1(p,q) + \not{q}\,\chi_Q^2(p,q) + \frac{2\,p\cdot q}{q^2}\not{q}\,\chi^3(p,q) + 2\not{q}\,\chi^4(p,q) \end{aligned}$$

$$+\sigma_{\alpha\beta}p^\alpha q^\beta\left[\chi_Q^5(p,q)+\frac{2p\cdot q}{q^2}\chi^6(p,q)+2\chi^8(p,q)\right] \tag{A1b}$$

$$-\frac{1}{2}P_{QL}^{\mu\nu}(\mathcal{P},q)\,\chi_{\mu\nu}(p,q)=\chi_{QL}^0(p,q)+\not{p}\,\chi_{QL}^1(p,q)+\not{q}\,\chi_{QL}^2(p,q)+\frac{2\,p\cdot q}{q^2}\not{q}\,\chi^3(p,q)+\not{q}\,\chi^4(p,q)$$
$$+\sigma_{\alpha\beta}p^\alpha q^\beta\left[\chi_{QL}^5(p,q)+\frac{2p\cdot q}{q^2}\chi^6(p,q)+\chi^8(p,q)\right]$$
$$+\sigma_{\alpha\beta}\mathcal{P}^\alpha q^\beta\left[y\,\chi^7(p,q)+\frac{q^2}{\mathcal{P}\cdot q}\chi^9(p,q)\right]. \tag{A1c}$$

Following the procedure described in Section III we find that all the $\chi(p,q)$'s in Eqs.(A1) are of order $1/\nu$, with the exception of $\chi^7(p,q)$ and $\chi^9(p,q)$, which are of order $1/\nu^2$. Hence in the Bjorken limit Eqs.(A1) becomes

$$P_L^{\mu\nu}(\mathcal{P},q)\chi_{\mu\nu}(p,q)=\not{q}\left(\chi_L^2(p,q)-\frac{2\,p\cdot q}{q^2}\chi^3(p,q)\right)$$
$$+\sigma_{\alpha\beta}p^\alpha q^\beta\left(\chi_L^5(p,q)-\frac{2p\cdot q}{q^2}\chi^6(p,q)\right) \tag{A2a}$$

$$P_Q^{\mu\nu}(\mathcal{P},q)\,\chi_{\mu\nu}(p,q)=\not{q}\left(\chi_Q^2(p,q)+\frac{2\,p\cdot q}{q^2}\chi^3(p,q)+2\,\chi^4(p,q)\right)$$
$$+\sigma_{\alpha\beta}p^\alpha q^\beta\left(\chi_Q^5(p,q)+\frac{2\,p\cdot q}{q^2}\chi^6(p,q)+2\,\chi^8(p,q)\right) \tag{A2b}$$

$$-\frac{1}{2}P_{QL}^{\mu\nu}(\mathcal{P},q)\,\chi_{\mu\nu}(p,q)=\not{q}\left(\chi_{QL}^2(p,q)+\frac{2\,p\cdot q}{q^2}\chi^3(p,q)+\chi^4(p,q)\right)$$
$$+\sigma_{\alpha\beta}p^\alpha q^\beta\left(\chi_{QL}^5(p,q)+\frac{2\,p\cdot q}{q^2}\chi^6(p,q)+\chi^8(p,q)\right). \tag{A2c}$$

Furthermore, for the functions $\chi(p,q)$ we find that at leading order in ν,

$$\begin{aligned}
\chi_L^2(p,q)&=\frac{2\,p\cdot q}{q^2}\chi^3(p,q), & \chi_L^5(p,q)&=\frac{2\,p\cdot q}{q^2}\chi^6(p,q),\\
\chi_Q^2(p,q)&=-\frac{2\,p\cdot q}{q^2}\chi^3(p,q)-2\,\chi^4(p,q), & \chi_Q^5(p,q)&=-\frac{2\,p\cdot q}{q^2}\chi^6(p,q)-2\,\chi^8(p,q),\\
\chi_{QL}^2(p,q)&=\chi_Q^2(p,q)+\chi^4(p,q), & \chi_{QL}^5(p,q)&=\chi_Q^5(p,q)+\chi^8(p,q),\\
\chi_{L,Q,QL}^i(p,q)&=0, \quad i=0,1
\end{aligned} \tag{A3}$$

Substituting these expressions into Eqs.(A2) therefore leads to vanishing results for each of the longitudinal and non gauge-invariant functions. This result is true independent of the production mechanism of the off-shell particle, that is, independent of the functions A_0-A_2 as defined in Section IV. For the special case of an on-shell nucleon the longitudinal and gauge non-invariant structure functions are

$$\frac{M}{2}W_L^N(p,q)=M\,\tilde{\chi}_L^0(p,q)+M^2\,\tilde{\chi}_L^1(p,q)+p\cdot q\,\tilde{\chi}_L^2(p,q)-\frac{2\,(p\cdot q)^2}{q^2}\,\tilde{\chi}^3(p,q)\to 0 \tag{A4a}$$

$$\frac{M}{2}W_Q^N(p,q)=M\,\tilde{\chi}_Q^0(p,q)+M^2\,\tilde{\chi}_Q^1(p,q)+p\cdot q\,\tilde{\chi}_Q^2(p,q)+\frac{2\,(p\cdot q)^2}{q^2}\,\tilde{\chi}^3(p,q)+2\,p\cdot q\,\tilde{\chi}^4(p,q)\to 0 \tag{A4b}$$

$$\frac{M}{2}W_{QL}^N(p,q)=M\,\tilde{\chi}_{QL}^0(p,q)+M^2\,\tilde{\chi}_{QL}^1(p,q)+p\cdot q\,\tilde{\chi}_{QL}^2(p,q)+\frac{2\,(p\cdot q)^2}{q^2}\tilde{\chi}^3(p,q)+p\cdot q\,\tilde{\chi}^4(p,q)\to 0 \tag{A4c}$$

where the zero results follow directly from (A3).

[1] R. L.Jaffe, in M. B.Johnson and A.Pickleseimer, editors, *Relativistic Dynamics and Quark-Nuclear Physics*, pages 1–82, Wiley New York, 1985.
[2] E.Kazes, Il Nuovo Cimento, **8** (1959) 1226.
[3] M.B.Johnson and J.Speth, Nucl.Phys. **A470** (1987) 488.
[4] L.Heller and A. W.Thomas, Phys.Rev. **C41** (1990) 2756.
[5] D.Kusno and M. J.Moravcsik, Phys.Rev. **D20** (1979) 2734; Nucl.Phys. **B184** (1981) 283; Phys.Rev. **C27** (1983) 2173.
[6] A.Bodek and J. L.Ritchie, Phys.Rev. **D23** (1981) 1070.
[7] G. V.Dunne and A. W.Thomas, Nucl.Phys. **A455** (1986) 701; Phys.Rev. **D33** (1986) 2061.
[8] F.E.Close, R.G.Roberts and G.G. Ross, Phys.Lett. **142B** (1984) 202.
[9] O.Nachtmann and H.J.Pirner, Z.Phys. **C21** (1984) 277.
[10] H.Jung and G. A.Miller, Phys.Lett. **B200** (1988) 351.
[11] P. J.Mulders, A. W.Schreiber, and H.Meyer, Nucl.Phys. **A549** (1992) 498.
[12] K.Nakano, Nucl.Phys. **A511** (1990) 664.
[13] F.Gross and S.Liuti, Phys.Rev. **C45** (1992) 1374.
[14] E. L.Berger, F.Coester, and R. B.Wiringa, Phys.Rev. **D29** (1984) 398.
[15] B-Q.Ma, Int.J.Mod.Phys. **E1** (1993) 809.
[16] R. P.Bickerstaff and A. W.Thomas, J.Phys. **G15** (1989) 1523.
[17] U.Oelfke, P. U.Sauer, and F.Coester, Nucl.Phys. **A518** (1990) 593.
[18] H.Meyer and P.J.Mulders, Nucl.Phys. **A528** (1991) 589.
[19] F.E.Close and A.W.Thomas, Phys.Lett. **B212** (1988) 227.
[20] A.W.Schreiber, A.I.Signal and A.W.Thomas, Phys.Rev. **D44** (1991) 2653.
[21] W.W.Buck and F.Gross, Phys.Rev. **D20** (1979) 2361.
[22] M.P.Locher and A.Svarc, Z.Phys. **A338** (1991) 89.
[23] D.Plümper and M.Gari, Z.Phys. **A343** (1992) 343.
[24] D.Allasia et al., Z.Phys. **C28** (1985) 321.
[25] M.Glück, E.Reya and A.Vogt, Z.Phys. **C48** (1990) 471.
[26] J.G.Morfin and W-K.Tung, Z.Phys. **C52** (1991) 13.
[27] J.F.Owens, Phys.Lett. **B266** (1991) 126.
[28] V.R.Zoller, Z.Phys. **C54** (1992) 425;
N.N.Nikolaev and V.R.Zoller, Z.Phys. **C56** (1992) 623.
[29] B.Badelek and J.Kwiecinski, Nucl.Phys. **B370** (1992) 278.
[30] L.P.Kaptari and A.Yu.Umnikov, Phys.Lett. **B272** (1991) 359;
JINR preprint E2-92-170, Dubna, 1992 (to be published).
[31] W.Melnitchouk and A.W.Thomas, Phys.Rev. **D47** (1993) 3783.
[32] R.Blankenbecler and L.F.Cook, Jr., Phys.Rev. **119** (1960) 1745.
[33] R.G.Arnold, C.E.Carlson and F.Gross, Phys.Rev. **C21** (1980) 1426.
[34] NMC Collaboration, Phys.Lett. **B295** (1992) 159.
[35] K.Nakano and S.S.M.Wong, Nucl.Phys. **A530** (1991) 555.
[36] B.D.Serot and J.D.Walecka, Adv.Nucl.Phys. **16** (1986) 1.
[37] P.A.M.Guichon, Phys.Lett. **B200** (1988) 235.
[38] K.Saito, A.Michels and A.W.Thomas, Phys.Rev. **C46** (1992) R2149;
A.W.Thomas, K.Saito and A.Michels, Aust.J.Phys. **46** (1993) 3.
[39] S.Fleck, W.Bentz, K.Shimizu and K.Yazaki, Nucl.Phys. **A510** (1990) 731.
[40] A.W.Thomas, Phys.Lett. **126B** (1983) 97.
[41] L.L.Frankfurt, L.Mankiewicz and M.Strikman, Z.Phys. **A334** (1989) 343.
[42] NMC Collaboration, Phys.Rev.Lett. **66** (1991) 2712.
[43] E.M.Henley and G.A.Miller, Phys.Lett. **B251** (1990) 453.
[44] A.I.Signal, A.W.Schreiber and A.W.Thomas, Mod.Phys.Lett. **A6** (1991) 271.
[45] S.Kumano, Phys.Rev. **D43** (1991) 59, *ibid* 3067.
[46] W.Melnitchouk, A.W.Thomas and A.I.Signal, Z.Phys. **A340** (1991) 85.
[47] T. Hippchen, J. Haidenbauer, K. Holinde and V. Mull, Phys. Rev. **C44** (1991) 1323.
[48] B.Kämpfer, A.I.Titov and E.L.Bratkovskaya, Phys.Lett. **B301** (1993) 123.
[49] V.Dmitrašinović and R.Tegen, Phys. Rev.**C46** (1992) 1108.
[50] V.R.Zoller, Z.Phys. **53** (1992) 443.
[51] W.Melnitchouk and A.W.Thomas, Phys.Rev. **D47** (1993) 3794.

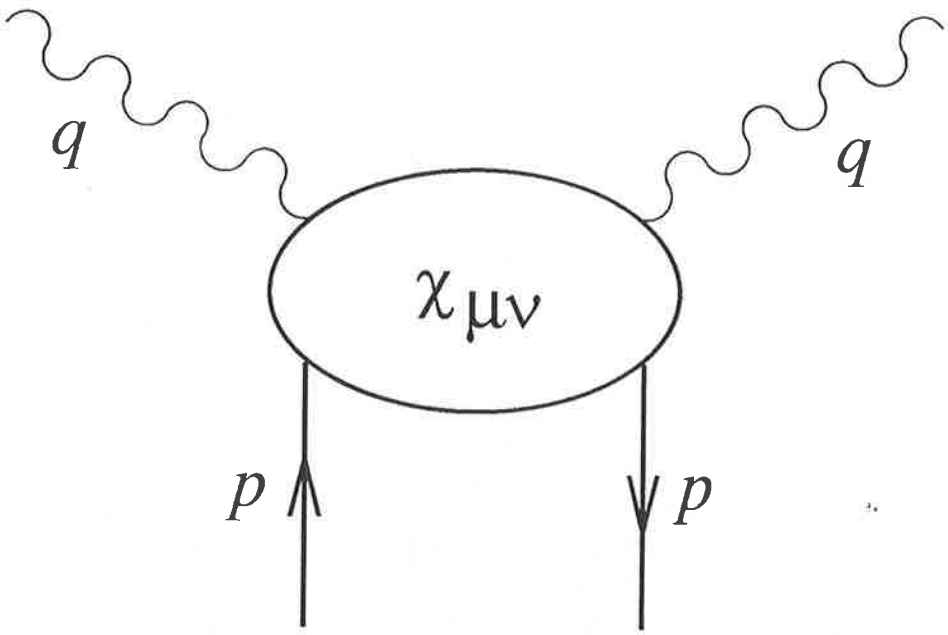

FIG. 1. The truncated nucleon tensor $\chi_{\mu\nu}$.

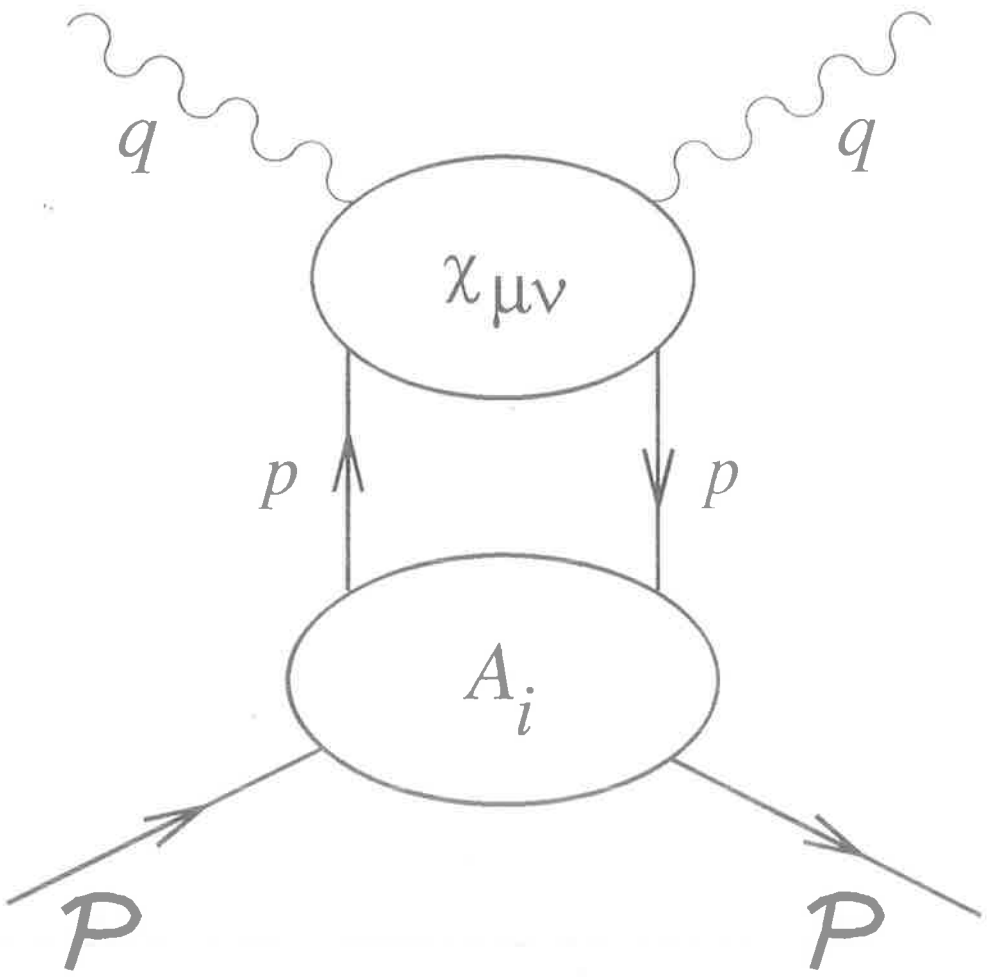

FIG. 2. Scattering from an off-shell nucleon in a composite target. The functions A_i describe the nucleon – composite target interaction.

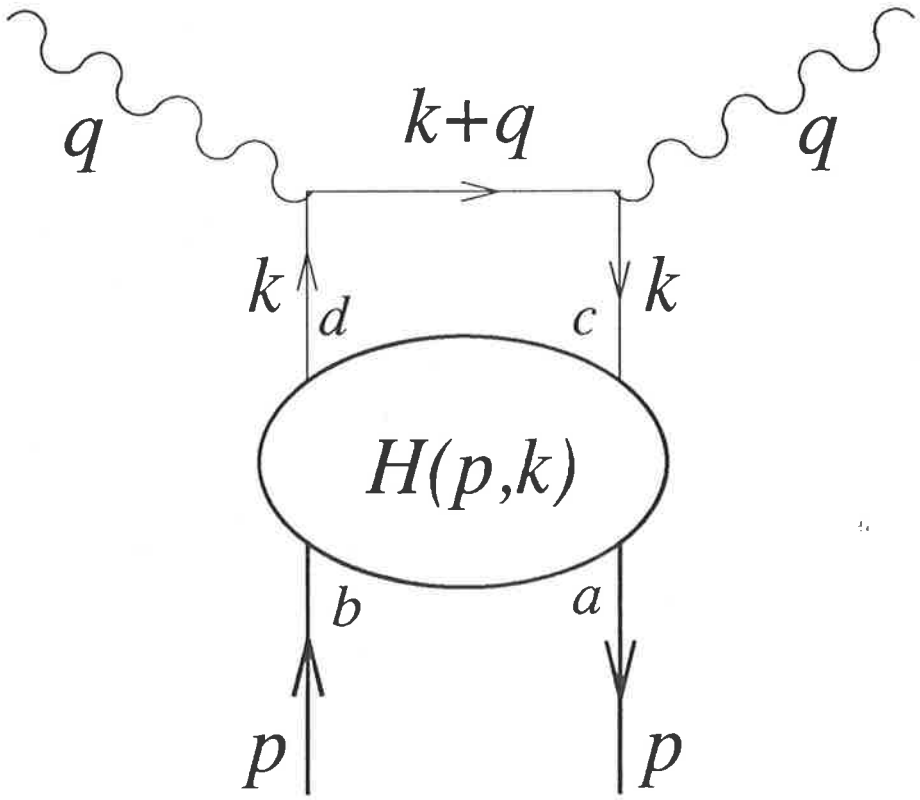

FIG. 3. Leading twist contribution to the off-shell tensor $\chi_{\mu\nu}$. The function $H(p,k)$ describes the soft, non-perturbative physics.

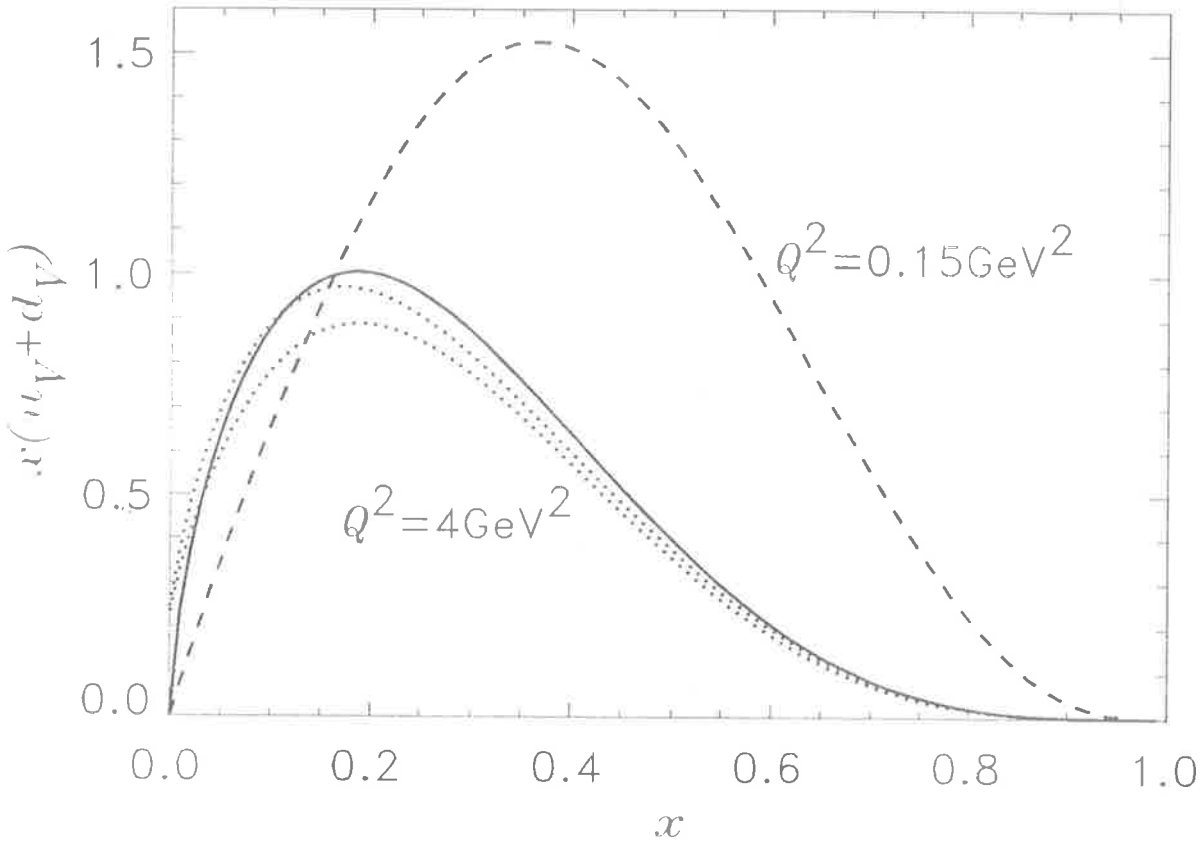

FIG. 4. Valence $u_V + d_V$ quark distribution in the nucleon, evolved from $Q_0^2 = 0.15$ GeV^2 (dashed curve) to $Q^2 = 4$ GeV^2 (solid curve), and compared against parameterisations (dotted curves) of world data [26,27].

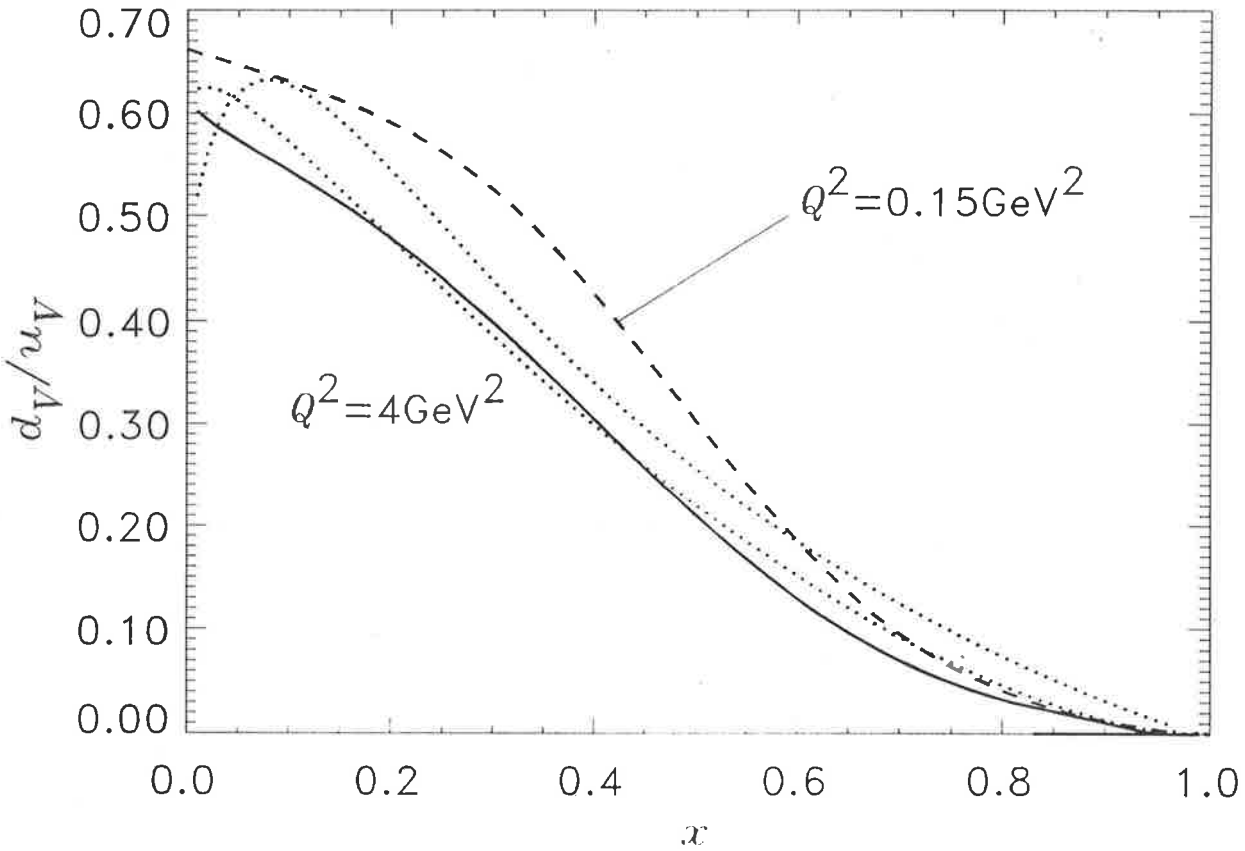

FIG. 5. Valence d_V/u_V ratio, evolved from $Q_0^2 = 0.15$ GeV^2 (dashed curve) to $Q^2 = 4$ GeV^2 (solid curve), and compared against parameterisations (dotted curves) of world data [26,27].

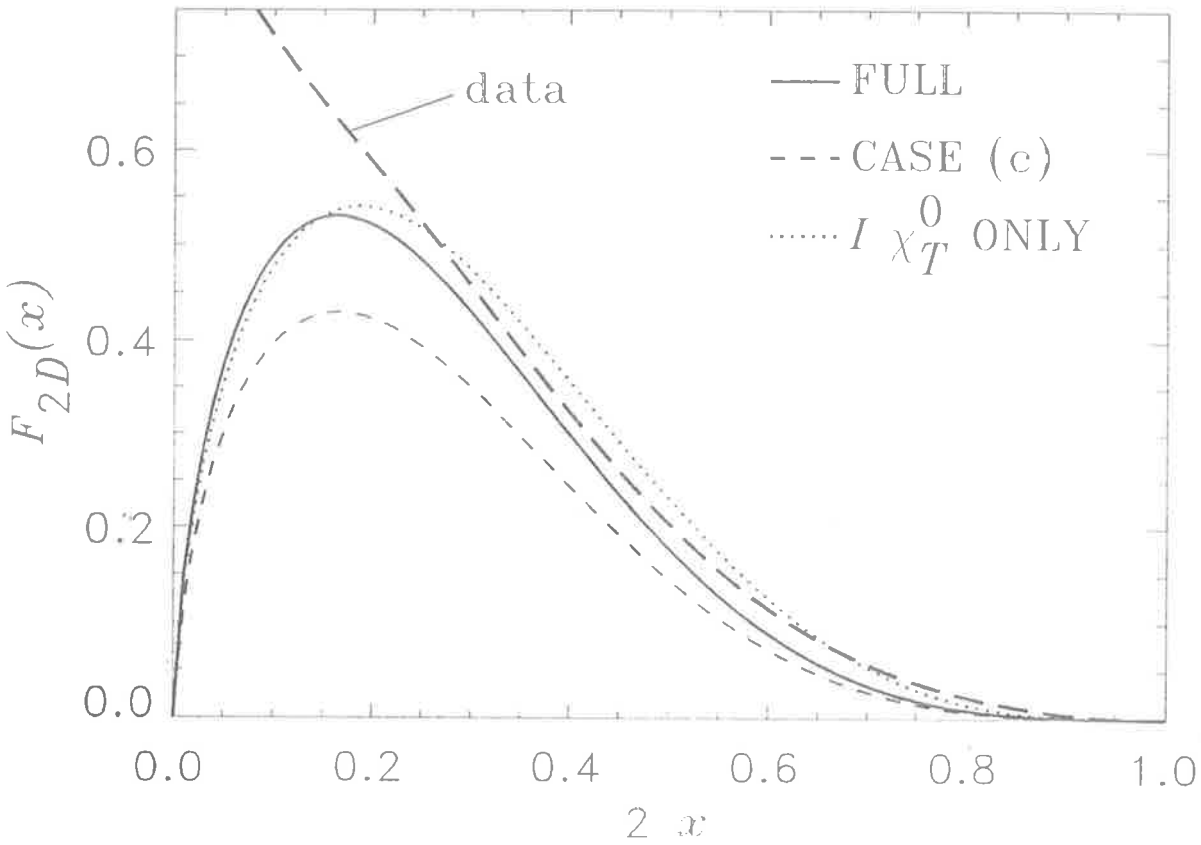

FIG. 6. Valence part of the deuteron structure function: the solid line is the full calculation (with $\Lambda_p = \infty$); the dashed line is with the $p^2 = M^2$ approximation in A_0, A_1 (case (c) in Section IV), with the same normalisation constants as in the full curve; the dotted line is the convolution model using only the $\chi_T^0(p,q)$ operator, together with the full nucleon structure function, normalised to baryon number one. The curves have been evolved from $Q_0^2 = 0.15$ GeV^2 to $Q^2 = 10$ GeV^2 for comparison against the experimental $F_{2D}(x, Q^2 = 10\text{GeV}^2)$ [34].

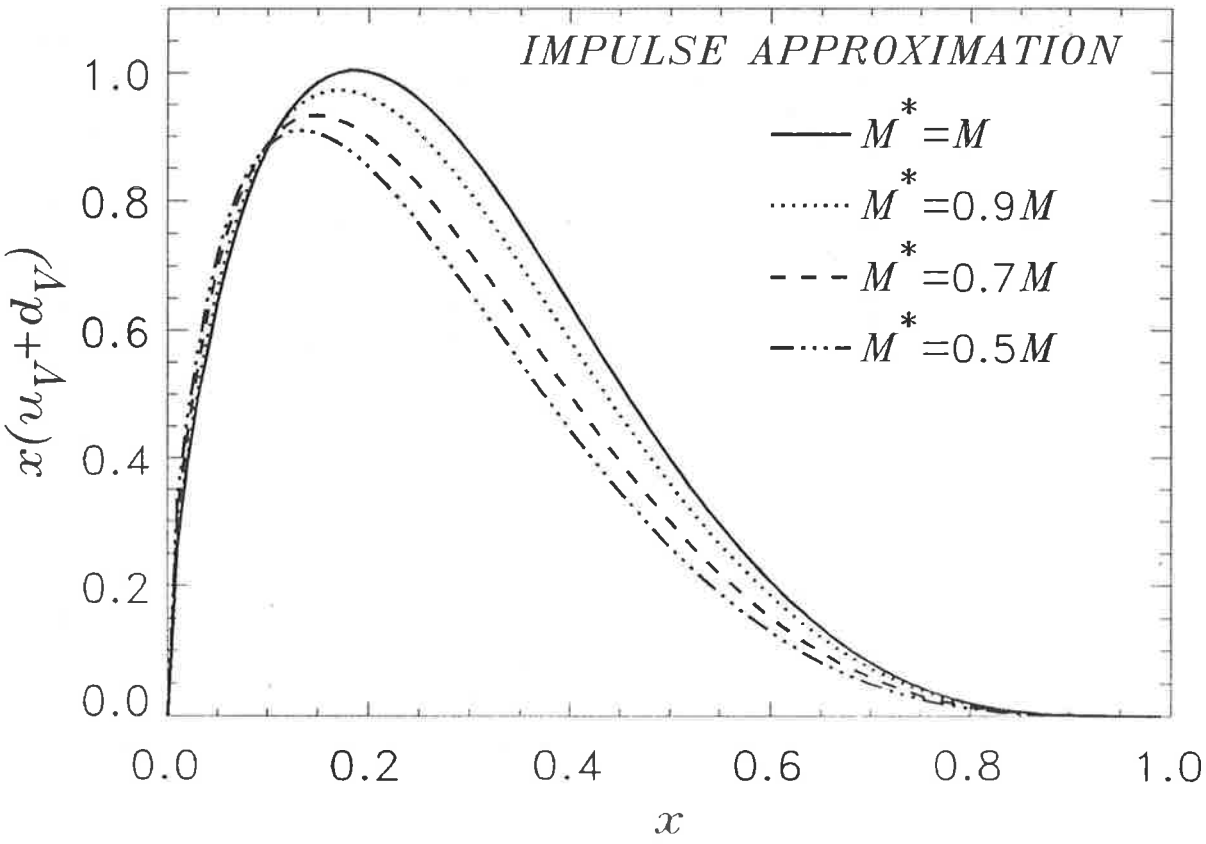

FIG. 7. Nucleon structure function in nuclear matter, in the impulse approximation, for a range of effective nucleon masses, evolved from $Q_0^2 = 0.15$ GeV^2 to $Q^2 = 4$ GeV^2.

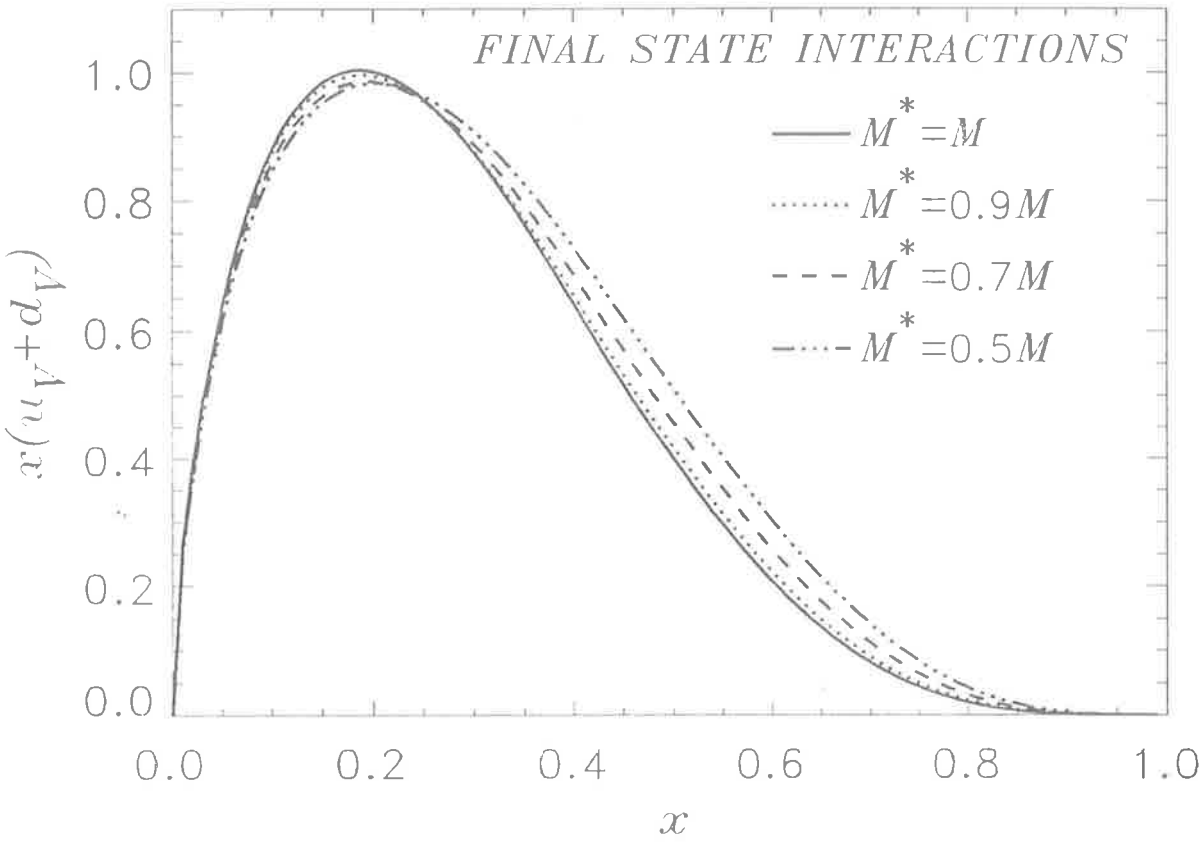

FIG. 8. As in Fig.7, but including the effects of interaction of the spectator diquark with the nuclear medium.

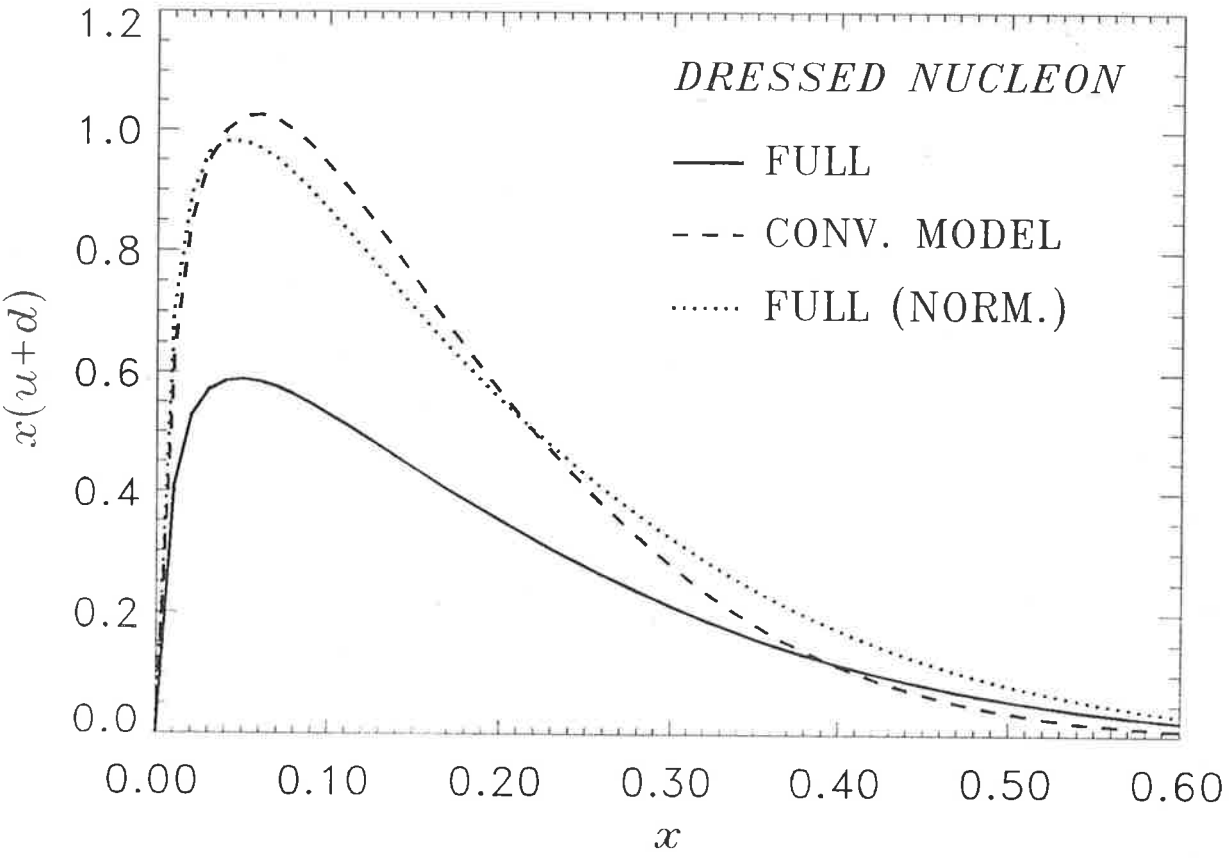

FIG. 9. Contribution to the structure function of a nucleon from DIS off a virtual nucleon dressed by pions. The convolution model of Ref. [11] (dashed) is compared with the full calculation (for $\Lambda_p = \infty$), using the same normalisation for the off-shell $N - q$ vertices as for the on-shell vertices (solid), and normalising the full result (dotted) to give the same first moment as for the convolution curve. All curves are evolved from $Q_0^2 = 0.15$ GeV^2 to $Q^2 = 4$ GeV^2.